PERFORMANCE EVALUATION OF CORROSION PROTECTION SYSTEMS FOR REINFORCED CONCRETE

By

Omid Farshadfar

Submitted to the graduate degree program in Civil Engineering
and the Graduate Faculty of the University of Kansas in partial fulfillment
of the requirements for the degree of Doctor of Philosophy.

_____
Chairperson: Dr. Matt O'Reilly

_____
Dr. David Darwin

_____
Dr. Andres Lepage

_____
Dr. Remy Lequesne

_____
Dr. Reza Barati

Date Defended: 1/06/2017

The dissertation committee for **Omid Farshadfar**
certifies that this is the approved version of the following dissertation:

PERFORMANCE EVALUATION OF CORROSION PROTECTION SYSTEMS FOR REINFORCED CONCRETE

_____
Chairperson: Dr. Matt O'Reilly

Date Approved:_____

ABSTRACT

In this study the performance of corrosion protection systems for reinforced concrete is evaluated. Conventional bare and epoxy-coated reinforcement are compared with alternative forms of reinforcement–galvanized steel, MMFX steel containing 9% and 4% chromium (ASTM A1035 Type CS and CM steel), and epoxy-coated MMFX steel containing 4% and 2% chromium (epoxy-coated ASTM A1035 Type CM and CL steel). Furthermore, corrosion performance of reinforced concrete with partial replacement of cement by 20% fly ash, 40% fly ash, 5% silica fume, 10% silica fume, 20% slag cement, and 40% slag cement in bridge decks containing uncoated conventional steel as well as 40% fly ash, 10% silica fume, and 40% slag cement in bridge decks containing conventional epoxy-coated reinforcement are compared with the concrete bridge decks containing only portland cement along with epoxy-coated and uncoated reinforcement. The corrosion performance of systems are evaluated using bench-scale specimens (Southern Exposure, cracked beam, and beam specimens) and rapid macrocell tests. Macrocell corrosion rates, corrosion potential, and total corrosion rates, which are measured by Linear Polarization Resistance test, are used to monitor the corrosion performance of specimens. Critical corrosion loss required to crack concrete cover in specimens containing galvanized bars and conventional steel are investigated and compared with the results of predictive equations introduced in the literature. The critical chloride threshold of conventional reinforcement in concrete containing different supplementary cementitious materials (fly ash, silica fume, and slag cement) are compared. The chloride contents are measured based on the free chloride content (water soluble chloride) of concrete samples at the level of bar. The life-expectancy and cost effectiveness of a bridge deck constructed with each system are estimated for a 75-year design period based on the obtained results.

Results show that galvanized steel exhibits better performance than conventional bars against corrosion; galvanized steel requires over twice the corrosion loss and has an expected-life about three times as long as conventional steel. The average critical corrosion loss to crack concrete with 1-in. cover is found to be approximately 25 μm, very close to the value obtained by O'Reilly's (2011) predictive equation.

While MMFX bare bars show higher corrosion resistance than conventional bars, those with 9% chromium exhibit better corrosion performance than MMFX bars containing 4% chromium; however, critical chloride threshold of both MMFX bars are about three times of that for conventional steel. Although use of galvanized steel and uncoated MMFX bars are more cost effective than conventional steel, they are not as cost effective as epoxy-coated bars. Epoxy-coated MMFX bars containing 2% chromium do not show significant better performance against corrosion compared to conventional epoxy-coated bars; however, those with 4% chromium have an appreciably higher corrosion resistance and life-expectancy than conventional ECR.

Using supplementary cementitious materials in concrete enhances the corrosion resistance of the systems; with increasing the amount of SCM, the time to initiation increased and the corrosion rates decreased. Chloride ingress rate is significantly lower in concrete containing SCM compared to those without it, with the lowest rate in concrete with silica fume. Most specimens containing 40% fly ash, 20% slag, 40% slag, and 10% silica fume repassivate after initiation, with corrosion re-initiating at a higher chloride threshold. The initial critical chloride thresholds for slag cement and 40% fly ash specimens are similar to that for 100% ordinary portland cement, but the secondary CCCT values are significantly higher. For 10% silica fume specimens, the initial CCCT value is lower, but the secondary CCCT value is similar to the critical chloride threshold of conventional steel in specimens with 100% portland cement. While using epoxy-coated

reinforcement and supplementary cementitious materials separately, increases the life-expectancy and cost effectiveness of a corrosion protection system, using them together exponentially increases the effects.

ACKNOWLEDGMENTS

I would like to sincerely thank my advisor Dr. Matthew O'Reilly for his indefinite advice and guidance, and also Dr. David Darwin for his unending support, help, and patience in the way of completing this research. I very much appreciate my other committee members, Dr. Andres Lepage, Dr. Remy Lequesne, and Dr. Reza Barati for all their helpful comments and suggestions. I also want to thank my coworkers in the lab for their warm friendship and support during this project.

Part of funding for this research comes from MMFX Technologies Corporation and material support is provided by Midwest Concrete Materials.

Finally, I am so grateful for my family, especially my mother and father, for all of their love, patience and support throughout my Ph.D. study.

CONTENTS

LIST OF FIGURES

LIST OF TABLES

CHAPTER 1: INTRODUCTION

1.1 GENERAL

Corrosion is a natural phenomenon that occurs due to a reaction between a metal and its environment that usually results in deterioration of the metal. Corrosion-related damage affects nearly all industries, from automobiles to pipelines, bridges, and buildings. Between 1999 and 2001 (Koch et al. 2002), the total direct cost of corrosion was estimated at $276 billion per year, 3.1% of the 1998 U.S gross domestic product. The indirect costs of corrosion, including loss of time and productivity, were estimated to be a similar magnitude. The transportation system is one of the categories most affected by corrosion. As of 2014, there are 610,749 bridges in the United States. About 10% of the total number of bridges, 61,365, are classified as structurally deficient bridges (FHWA 2014), many of them due to corrosion. The annual direct cost of corrosion for highway bridges is estimated to be $8.3 billion; the indirect costs due to traffic delays and loss of productivity are estimated to be more than 10 times of the direct cost of corrosion (Koch et al. 2002).

1.2 CORROSION MECHANISMS OF REINFORCING STEEL IN CONCRETE

The corrosion process for steel is a series of chemical reactions involving iron, oxygen, and water. These reactions are spontaneous electrochemical processes that require four components to occur: an anode, a cathode, an electrical connection, and an electrolyte or ionic connection.

The anode, where oxidation of iron releases electrons and ferrous ions, is the site where corrosion products are accumulated. The anodic reaction is the process of oxidation of iron which leads to the release of two electrons:

$$Fe \rightarrow Fe^{2+} + 2e^{-} \quad (1.1)$$

The released electrons flow to another part of steel, the cathode, where they will be consumed in a reaction with water and oxygen to yield hydroxyl ions. The cathodic reaction is the process of reduction of oxygen in presence of water to produce hydroxyl ions:

$$2H_2O + O_2 + 4e^{-} \rightarrow 4OH^{-} \quad (1.2)$$

For electrons to flow from anode to cathode, an electrical connection, the third mandatory component of corrosion, is required. This electrical path can be provided by metal within the concrete between anode and cathode, such as reinforcing bars or tie wires. Flow of electrons from anode to cathode can be measured and presented as current density (*i*), usually expressed as $\mu A/cm^2$, and is directly proportional to corrosion rate.

The forth necessary component of corrosion, the electrolyte or ionic connection, is the path that lets the hydroxyl ions formed at the cathode migrate to the anode, where ferrous ions are present, and produce ferrous hydroxide:

$$Fe^{2+} + 2OH^{-} \rightarrow Fe(OH)_2 \quad (1.3)$$

The pore solution in concrete acts as the electrolyte to complete the corrosion process. Ferrous hydroxide, in turn, can produce two different products depending on the concrete pH. In a pH above 11.5 (non-carbonated concrete typically has a pH above 13), ferrous hydroxide forms an oxide layer, which surrounds the steel as a passive layer and prevents further corrosion from occurring (Verbeck 1975). Ghods et al. (2012) by analyzing the passive layer with X-ray photoelectron spectroscopy (XPS) technique showed that the oxide film around the embedded steel in an intact concrete pore solution approximately has a thickness of 2×10^{-4} mil (5 nm), and is comprised of two layers. The inner layer close to the underlying steel is mainly comprised of Fe(II) oxides including Fe_3O_4/FeO, and the outer layer consists of Fe(III) oxides including

Fe_2O_3/FeOOH. Ghods et al. showed that the inner layer containing Fe(II) oxides has more passive properties compared to the outer layer. γ-ferric oxyhydroxide which is present in the outer layer is produced by the reaction of ferrous hydroxide and oxygen:

$$4Fe(OH)_2 + O_2 \rightarrow 4\ \gamma\text{-}FeOOH + 2H_2O \quad (1.4)$$

This passive layer, however, can be disrupted by carbonation or chlorides. Carbonation in concrete reduces the pH of the pore solution. When the pH of concrete drops below 11.5, the passive layer destabilizes (Verbeck 1975). Instead, in the presence of oxygen and moisture, ferrous hydroxide forms ferric oxide, rust, through the following reactions:

$$4Fe(OH)_2 + 2H_2O + O_2 \rightarrow 4Fe(OH)_3 \quad (1.5)$$

$$4Fe(OH)_3 \rightarrow 4Fe_2O_3 \cdot H_2O + 4H_2O \quad (1.6)$$

Another process besides carbonation that can disrupt the passive layer is chloride ingress. Ghods et al. (2012) showed that chloride ions decrease the passive layer thickness and change its stoichiometry such that in the vicinity of passive inner layer-steel interface, Fe (II)/Fe(III) oxides ratio decreases; that is, concentration of Fe(II) oxides, which are more protective, decreases with respect to Fe (III) oxides, which has less passive effect. Chloride ingress can destroy the passive layer even in concrete with a high pH. Chloride ions react with the passive layer of iron to form a Fe-Cl complex. This complex, in turn, reacts with water and yields ferric oxide:

$$Fe^{2+} + 4Cl^- \rightarrow (FeCl_4)^{2-} \quad (1.7)$$

$$(FeCl_4)^{2-} + 2H_2O \rightarrow Fe(OH)_2 + 2H^+ + 4Cl^- \quad (1.8)$$

The reaction then proceeds in a manner similar to that seen in carbonation.

As seen in Equations (1.7) and (1.8), chloride ions become free after the reactions, and can continue to depassivate the protective layer by reacting with other iron ions. Furthermore,

hydrogen ion production in reaction (1.8) lowers the pH of the surrounding pore solution, making the depassivation of the protective layer easier and increasing the corrosion rate.

In addition to the general corrosion mechanism listed above, coated reinforcement, such as epoxy-coated reinforcement, can undergo crevice corrosion (Weyers et al. 1998, Draper et al. 2009). Crevice corrosion usually takes place in disbonded portions of the epoxy layer, where chloride ions reach the underlying steel and react with ferrous ions and water (in the absence of oxygen) to produce ferrous hydroxide:

$$[Fe^{2+}Cl_2^{2-}] + 2H_2O \rightarrow Fe(OH)_2 + 2[H^+Cl^-] \quad (1.9)$$

Hydrogen ions produced in this reaction makes the environment acidic which, in turn, accelerates the corrosion rate (Weyers et al. 1998).

There are two distinct phases in the corrosion duration–the initiation period and the propagation period (Browne 1980, Tuutti 1980). The initiation period is the time for a sufficient quantity of aggressive substances to diffuse through the concrete to the steel to cause corrosion initiation via the reactions described above. The propagation period is the time from initiation of corrosion to loss of the serviceability of the structure. Although chlorides have a significant role in corrosion initiation, they don't appreciably affect the corrosion rate after initiation (Redaelli et al. 2013). The primary factors that control the corrosion rate and propagation period are concrete properties such as resistivity, moisture content, temperature, pH, and oxygen availability. The corrosion rate increases as oxygen availability on the surface of the steel increases and resistivity of the concrete decreases (Redaelli et al. 2013). The maximum corrosion rate occurs in concrete with moisture content at equilibrium with a relative humidity in the atmosphere of about 95%. Concrete with a low water content has a higher resistivity, which will reduce corrosion rate. On

the other hand, concrete with a water content near the saturation point has a low resistivity, but slow oxygen diffusion, which also decreases the corrosion rate (Redaelli et al. 2013).

The initiation and propagation periods will be discussed in detail in the following sections.

1.3 CHLORIDE INGRESS AND CRITICAL CHLORIDE CORROSION THRESHOLD

Chloride ingress through concrete consists of two mechanisms, diffusion of chloride ions through pore liquid and absorption. Diffusion occurs due to a chloride concentration gradient and is a relatively slow and continuous process. However, it is generally accepted that the dominant mechanism in uncracked concrete is diffusion and governed by Fick's second law:

$$\frac{\partial C(x,t)}{\partial t} = D_c \frac{\partial^2 C(x,t)}{\partial x^2} \tag{1.10}$$

Where C(x,t) is chloride concentration at depth x and time t, and D_c is the diffusion coefficient.

Absorption, the other chloride ingress mechanism, occurs whereas bulk solution containing chloride ions is absorbed into concrete pores (Hong & Hooton 1999). Concrete exposed to cycles of wetting and drying has shown to be more vulnerable to corrosion damage compared to concrete which experiences continuous exposure. In concrete exposed to wet-dry cycles, chloride initially enters the concrete by periodic absorptions, creating a reservoir of chloride ions near the concrete surface. This reservoir becomes the chloride source when concrete dries out. Subsequent wetting cycles can carry the chloride from the reservoir to deeper depths, creating a new reservoir. These repeated drying-wetting cycles can accelerate the rate of chloride ingress through the absorption mechanism (Hong & Hooton 1999).

The chloride ion concentration that is needed to depassivate the protective film around steel embedded in concrete and initiate corrosion is defined as the critical chloride threshold. This concentration, however, depends on many factors and varies significantly based on reinforcing bar

type, cement content and type, pH of concrete, availability of oxygen and moisture, presence of air voids around the steel, and other factors (Bertolini et al. 2004).

The chloride content of a sample can be measured based on either the free chloride content (water-soluble chloride) or the total chloride content (acid-soluble chloride). The total chloride content in concrete is acid-soluble, but not all of this chloride is able to contribute to corrosion process. A portion of the chloride ions binds with tricalcium aluminate, $3(Cao)Al_2O_3$ abbreviated by C_3A, in the cement matrix and is not able to depassivate the protective layer of the steel. This chloride binding can remove some of the free chlorides, which are capable of triggering corrosion, from the pore solution. In theory, chloride ions removed from the pore solution by the binding reaction with the cement matrix do not contribute to corrosion. Therefore, many studies measure and report the free chloride content as the critical chloride threshold (Ann & Song 2007). However, this theory has been challenged, as local drops of pH result in the release of bound chlorides, which are then able to contribute to the corrosion process (Glass 2000). Reporting the critical chloride threshold values by the total chloride concentration (acid-soluble), containing both free and bound chlorides, can cover the deficiency measuring the water-soluble chloride content has in ignoring the effect of released bound chlorides due to the local pH drops. However, some researchers argue that reporting the acid-soluble chloride content as the critical chloride threshold is excessively conservative; although some bound chlorides are released and contribute to corrosion due to the local pH drop, the majority of bound chlorides do not participate in corrosion.

Balma et al. (2005) tested 45 chloride samples and compared free chloride content (water-soluble) with total chloride content (acid-soluble). Results were divided into two categories; samples with chloride content greater than and less than 1 lb/yd^3 (0.6 kg/m^3). For samples with chloride content greater than 1 lb/yd^3 (0.6 kg/m^3), the ratio of water-soluble to acid-soluble

chloride ranged between 0.9 and 1.0 with the average of 0.96. For samples with chloride content lower than 1 lb/yd^3 (0.6 kg/m^3), however, the ratio range was not as consistent and ranged from 0.52 to 1.31 with an average of 0.8.

Entrapped air voids surrounding the embedded steel bar is another factor that influences the critical chloride threshold. Air voids due to bleeding or settlement beneath the steel bars are the spots that corrosion tends to initiate regardless of the presence of chlorides (Yonezawa 1988, Castel et al. 2003, Soylev & Francois 2003). In the vicinity of steel, air voids saturated with pore solution potentially have more tendency for electrochemical reactions rather than the cement matrix, where the resistivity is higher (Ann & Song 2007). Absence of cement hydration products at air voids will cause a localized decrease in pH, which in turn, accelerates the corrosion initiation and rate. Other factors that have been reported to influence the critical chloride threshold are relative humidity, temperature, moisture level and composition of embedded steel. Moisture level can influence the mobility and concentration of chloride ions in the pore solution, which in turn, can influence the chloride threshold (Ann & Song 2007). The chemical composition of steel also can affect the critical chloride threshold. For instance, increasing chromium and nickel content in alloyed steel can increase the critical chloride threshold (Trejo & Pillai 2004). Hussain et al. (1995) reported that increasing temperature would reduce critical chloride threshold, lower the percentage of bound chloride and reduce the pore solution pH.

Chloride content in concrete is not constant at a particular depth, as chlorides do not ingress through concrete uniformly. Since most aggregates are impermeable, chloride ions have to move around the aggregates to continue advancing (Yu 2007b). Therefore, aggregate distribution may affect the results of chloride sampling. Moreover, reinforcing steel acts as a barrier against chloride transport and causes chloride concentration to build up, resulting in much higher chloride

concentrations over the reinforcement than in adjacent concrete (Kranc et al. 2002, Yu 2007a). Chloride concentration over the embedded steel bars can be 1.9 to 3.8 times greater than chloride levels of adjacent concrete (Yu 2007a). Despite this discrepancy in chloride concentrations over bar surface and in clear concrete at the same depth, sampling concrete away from bars is a common and accepted method of measuring critical chloride threshold and provides appreciable information about the condition of concrete at the bar level. Alternate methods of measuring critical chloride threshold, such as using bare bars in simulated pore solution or chloride internally mixed into concrete, usually report values higher than tests with chlorides externally added and diffused through concrete, since the latter methods do not account for accumulation of chlorides over the reinforcement (Ann & Song 2007).

Chloride content of a sample can be expressed in terms of $[Cl^-]/[OH^-]$ ratio, chloride content per unit mass of cement, chloride content per unit volume of concrete, and $[Cl^-]/[H^+]$ ratio. Free chloride content has been expressed by $[Cl^-]/[OH^-]$ ratio in some studies. This method assumes that bound chlorides do not contribute to the corrosion process and that hydroxyl ion concentration reflects the potential of inhibiting corrosion by sustaining the pH of the pore solution (Ann & Song 2007). Ann and Song investigated the $[Cl^-]/[OH^-]$ ratio reported as the critical chloride threshold from various studies and found that the values varied widely between 0.3 and 40. This wide range of results could be due to the ignoring the effect of local pH drops on binding chlorides and the inability of hydroxide ions to resist the pH drop at all pH values (Ann & Song 2007). Critical chloride content can also be presented as the total chloride content as a percentage of cement weight, which recognizes the inhibitive effect of cement hydration products in the corrosion mechanism, or in terms of mass per unit volume of concrete.

Chloride contents presented in this report are measured in terms of free chloride content (water-soluble) and expressed as mass of chloride per unit volume of concrete.

1.4 EFFECT OF CORROSION ON CONCRETE CRACKING

The various corrosion products in the vicinity of the embedded steel in concrete have a volume from 1.7 to 6.15 times that of the uncorroded steel (Youping & Richard 1998, Oh et al. 2009). Suda et al. (1993) proposed a model for corrosion products and estimated that the equivalent volume expansion ratio to be between 2.9 and 3.2. The buildup of corrosion products around the reinforcing bar induces tensile stresses in the surrounding concrete. Because of concrete's low tensile strength, these continuous tensile stresses eventually cause cracking. The amount of thickness of steel, which corrodes and builds up corrosion products, is defined as corrosion loss of steel and presented in terms of mils (μm). The tensile stress caused by accumulation of corrosion products in concrete is related to the corrosion loss of steel. The amount of corrosion loss required to cause cracking is defined as critical corrosion loss. Critical corrosion loss, is an important factor to predict the service life of structures. Critical corrosion loss depends on factors such as concrete cover, strength (Oh et al. 2009), the reinforcement diameter, bar spacing, elastic modulus of concrete, (Cady & Weyers 1992) and the length of the corroding region (Torres-Acosta & Sagues 2004). Oh et al. (2009) investigated the effects of concrete strength and cover thickness on critical corrosion loss of various concrete specimens and found that critical corrosion loss increases as cover increases. This increase was approximately proportional to the square of cover thickness of concrete. Oh et al. also reported that for reinforcement with more than 1.6 in. concrete cover, increasing the concrete strength increased the critical corrosion loss. However, concrete compressive strength had no significant effect when the cover was less than 0.8 in. (Oh et al. 2009).

A study by O'Reilly et al. (2011) on specimens with various concrete covers containing conventional and intentionally damaged epoxy-coated reinforcement showed that for general corrosion, the critical corrosion loss is linearly proportional to the concrete cover; for localized corrosion, however, critical corrosion loss is proportional to the square of cover thickness. Rasheeduzzafar et al. (1992) found that the ratio of concrete cover to bar diameter was a better predictor for critical corrosion loss than either parameter alone.

Xu and Shayan (2016) considered the combination of concrete cover and its embedded steel as a thick-wall concrete cylinder which surrounds the embedded steel, and the expansion of corroded steel exerts an internal pressure to the concrete cylinder. Available equations for calculating stress and strain in the thick-wall cylinders were used to propose an equation for calculating critical corrosion loss of conventional reinforcement based on factors such as, concrete cover, concrete tensile strength, concrete modulus of elasticity, and bar diameter:

$$x_{crit} = \frac{f_t c(c+d)(1+\upsilon)}{E_{eff} d \beta} \tag{1.11}$$

where

x_{crit} = corrosion loss at crack initiation, μm

c = concrete cover, mm (in.)

d = bar diameter, mm (in.)

f_t = concrete tensile strength, MPa (psi)

υ = concrete poison's ratio

β = relative volume change ($\Delta V/V_{steel}$) due to conversion of steel to rust

E_{eff} = E/(1+φ) = effective elastic modulus, MPa (psi)

E= elastic modulus, MPa (psi)

φ = concrete creep coefficient

In the study by Xu and Shayan, 15 × 12 × 7 in. (380 × 300 × 180 mm) concrete prismatic specimens with two distinct compressive strength, 4351 psi (30 MPa) and 7252 psi (30 MPa), containing three different bar diameters , 0.24 in. (6 mm), 0.47 in. (12 mm), and 0.94 in. (24 mm) with three different concrete clear covers of 1 in. (25 mm), 2 in. (50 mm), and 2.8 in. (70 mm) were used. Three different levels of chlorides 1.35, 5.31, and 10.62 lb/yd^3 (0.8, 3.15, 6.3 kg/m^3) in terms of mass of chloride ions per unit volume of concrete were introduced to the concrete mix to accelerate corrosion. Slabs were kept in containers filled with 60% concentration salt solution up to 1 in. (25 mm) below reinforcement for five years. To measure the corrosion rates, linear polarization resistance (LPR) test was carried out during the experiment. The predicted critical corrosion loss based on the introduced formula was found four or greater as much as the calculated values based on the measured corrosion rates from LPR test in their research. Although investigators did not mention any reason for this difference, it can be attributed to the fact that upon cracking the concrete, the whole surface of embedded steel is not corroding, but it is the limited regions of the bar that corrodes and cause cracking. This fact is in controversy with the assumption of considering the whole surface of the bar corroding in the calculation of corrosion loss from LPR test. Therefore, the calculated corrosion loss from LPR tests should be modified based on the actual corroded area of the embedded steel to present the real values.

Alonso et al. (1998) and El Maaddawy and Soudki (2003) have investigated the effects of cover to diameter ratio, cement content, w/c ratio, cast position of the bar, transverse reinforcement, and corrosion rate on the critical corrosion loss, and introduced two steps for crack development – crack generation and crack propagation. It was reported that corrosion rate is a basic parameter that influences crack propagation, but has little effect on crack generation (Alonso

et al. 1998, El Maaddawy & Soudki 2003). The observation that corrosion rate did not affect crack initiation may be due to the fact that tensile stress needed to crack the concrete is a function of the amount of the buildup of corrosion products, not the rate of their formation.

To determine the effect of corrosion rate on crack propagation, El Maaddawy tested twelve 5.9 × 5.9 × 11.8 in. (150 × 250 × 300 mm) reinforced-concrete prismatic specimens containing No. 10 reinforcing bars. Corrosion was induced in the specimens by applying 100-500 $\mu A/cm^2$ by means of electric power supplies. To disturb the passive layer, 5% sodium chloride by weight of cement was added to the concrete mix. El Maaddawy reported that crack width increased as current density (and therefore, corrosion rate) increased. In similar research by Alonso et al., corrosion was accelerated in specimens by applying a current density of 3-100 $\mu A/cm^2$. To depassify the steel, 3% by cement weight of calcium chloride was added during mixing the concrete. Alonso et al., contrary to the results found by El Maddawy et al., showed that after crack initiation, crack width increases more rapidly with lower corrosion rates. However, the current density range used by Maddawy et al. (100-500 $\mu A/cm^2$) was higher than that used by Alonso et al. (3-100 $\mu A/cm^2$), which might explain the differing results. Alonso et al. also studied the effect of concrete quality and reported that an increase of porosity from an increase in w/c ratio leads to a delay in the generation of the crack. This can be attributed to the higher available void space to accommodate the corrosion products around the rebar without exerting any tensile stress to the surrounding concrete (Alonso et al. 1998). Similarly, in air-entrained concrete, existence of microscopic voids around steel may prolong generation of the crack. On the other hand, although these microscopic voids may increase porosity of concrete, previous studies showed that it is the pore size distribution, rather than total porosity, which affects the permeability and chloride ingress rate of concrete (Hooton 1986, Bijen 1996, Chindaprasirt et al. 2005); therefore, existence of these

microscopic voids in air-entrained concrete can have significant lower effect on chloride diffusivity of concrete, compared to large pores in concrete with high w/c ratio.

Alonso et al. showed the corrosion loss required to generate the first visible crack is linearly proportional to the cover-rebar diameter ratio (c/d):

$$x_{crit} = 7.53 + 9.32\, c/d \tag{1.12}$$

where

x_{crit} = corrosion loss at crack initiation, μm

c = concrete cover, mm (in.)

d = bar diameter, mm (in.)

In Alonso's study, specimens with cover-bar diameter ratios between 2 and 3, which is the most likely range of ratios for structures, required 15 to 35 μm of corrosion loss for crack generation in the experimental tests; the derived equation predicted 26 to 35 μm, a reasonable match between the results. However, this equation is derived based on the assumption that general corrosion in steel will cause the concrete to crack, and in cases when corrosion is limited to small locations, such as when corrosion occurs at damaged sites of epoxy-coated bars, cannot predict the critical corrosion loss. To investigate the effects of localized steel corrosion on the critical corrosion loss, Torres-Acosta and Sagues tested two series of specimens. The first series tested cylindrical specimens with a 0.875 in. (21 mm) test bar along the axis of the cylinder, localized exposed metal lengths between 0.75 and 13.5 in. (19.1 and 346 mm), and cover between 1.1 and 2.6 in. (27.6 and 65.7 mm). The second series tested 5.5 in. × 5.5 in. × 16 in. (140 mm × 140 mm × 406 mm) prismatic specimens with 0.25 in or 0.5 in. (6 mm or 13 mm) test bars, an exposed metal length between 0.3 and 15.4 in. (8 and 390 mm), and cover between 0.5 and 1.75 in. (13 and 45 mm). An applied current density of 100 μA/cm^2 was used to drive the corrosion. According to

the results from the 36 specimens in their study as well as 31 specimens from other researchers, in cases that preferential chloride penetration initiates local corrosion in small regions, Torres and Sagues derived an equation which relates the length of corroded steel and cover-bar diameter ratio to the critical corrosion loss (Torres-Acosta & Sagues 2004):

$$x_{crit} = 11.0 \frac{c}{d}\left(\frac{c}{l}+1\right)^2 \tag{1.13}$$

where

x_{crit} = corrosion loss at crack initiation, μm

c = cover, mm

d = bar diameter, mm

l = length of exposed steel, mm

For very cases approximating uniform corrosion, equation (1.13) can be simplified to:

$$x_{crit} = 11.0\, c/d \tag{1.14}$$

For cover-bar diameter ratios between 2 and 3 the critical corrosion losses obtained from equation (1.14) and (1.12) are 22-33 μm and 26-35 μm, respectively, showing both equations give similar predictions for general corrosion.

In a study by O'Reilly et al. (2011), the corrosion loss required to crack the concrete cover for conventional, galvanized and intentionally damaged epoxy-coated reinforcement was investigated. 2% chloride by weight of cement was dissolved into the mix water of concrete prior to casting to destabilize the passive layer of the reinforcement and increase the ionic conductivity of the specimens. A current density of 100-500 μA/cm^2 was also applied to the test bar to drive corrosion. To derive a relationship between corrosion loss and cracking, specimens with 0.5, 1 and

2 in. concrete covers containing bare bars and 1 in. concrete cover containing epoxy-coated bars were tested. In addition to experimental specimens, finite element models for multiple combinations of cover thickness for bare bars as well as cover thickness and exposed area of bar for damaged epoxy-coated bars were analyzed in ABAQUS and compared with the experimental results. Equation 1.15 represents the derived relationship between corrosion loss at crack initiation, concrete cover, and bar diameter for localized corrosion as well as general corrosion.

$$x_{crit} = 0.53\left(\frac{C^{2-A_f}}{D^{0.38}L_f^{\ 0.1}A_f^{\ 0.6}} + 0.6\right)\times 3^{A_f-1} \tag{1.15}$$

where

x_{crit} = corrosion loss at crack initiation, mil

C = cover, in.

D = bar diameter, in.

L_f = fractional length of bar corroding, $L_{\text{corroding}}/L_{\text{bar}}$

A_f = fractional area of bar corroding, $A_{\text{corroding}}/A_{\text{bar}}$

For general corrosion, as fractional area and length of bar corroding are equal to 1 ($A_f = 1$, $L_f = 1$), equation (1.15) can be simplified to:

$$x_{crit} = 0.53\left(\frac{C}{D^{0.38}} + 0.6\right) \tag{1.16}$$

where

x_{crit} = corrosion loss at crack initiation, mil

C = cover, in.

D = bar diameter, in.

By comparing Eq. (1.16) and (1.14), it can be inferred that both equations perform comparably for the bars that require less than 50 μm corrosion loss to crack concrete. However,

the equation derived by Torres-Acosta is less conservative based on the both finite element and experimental results for corrosion loss greater than 50 μm (O'Reilly et al. 2011).

1.5 EFFECT OF CRACKS IN CONCRETE ON CORROSION

Cracks in concrete can be oriented coincidental with reinforcing steel or intersect the reinforcement. The presence of moisture, oxygen, and chlorides on the surface of the steel plays an important role in its corrosion. The existence of a longitudinal crack through the concrete cover to the surface of the embedded steel can provide a path for oxygen, moisture, and chloride ions to reach the bar surface significantly faster than they would in uncracked concrete. Therefore, longitudinal concrete cracks play an important role in the corrosion process, and in turn, the durability of reinforced concrete. As shown in Figure 1.1 (Lindquist et al. 2006), chloride content at the depth of the reinforcing steel, 3 in. (76.2 mm), in uncracked regions of bridge decks was below the most conservative estimates of the chloride threshold for conventional steel, 1 lb/yd^3 (0.6 kg/m^3), after 12 years, whereas, as presented in Figure 1.2, at cracked locations the chloride content reached the threshold after one winter (Lindquist et al. 2006).

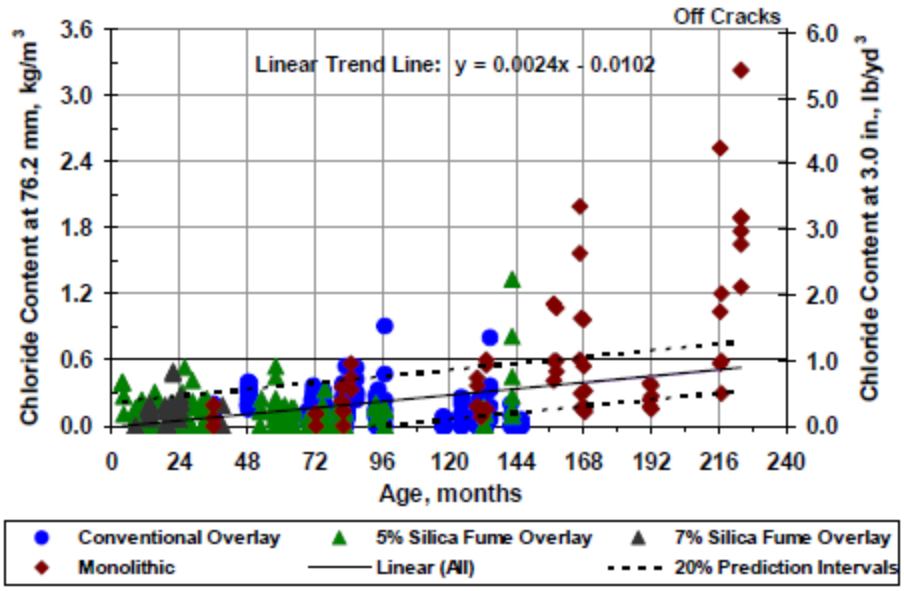

Figure 1.1— Chloride content taken away from cracks interpolated at depth of 3 in. vs. placement age (Lindquist et al. 2006)

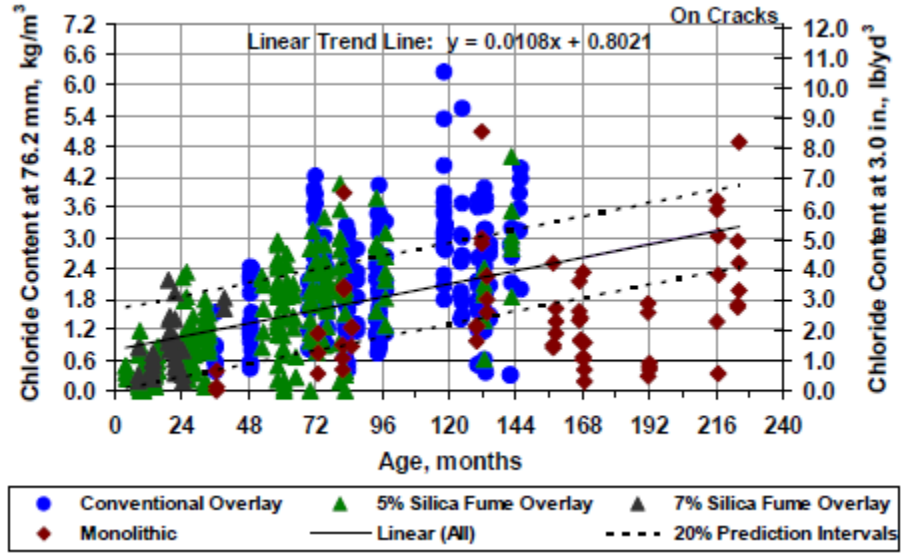

Figure 1.2— Chloride content taken on cracks interpolated at depth of 3 in. vs. placement age (Lindquist et al. 2006)

Although transverse cracks at the regions, where they intersect the steel, may provide a direct path for chloride, moisture, and oxygen to reach the bar surface and form a localized anodic site, their impact on the corrosion process mostly depends on the presence of oxygen and moisture in cathodic regions. If the cathodic sites are remained between transverse cracks, in crack-free

non permeable concrete, where moisture and oxygen is not present, corrosion may not occur (Arya & Wood 1995, Bentur et al. 1997). Settlement, plastic shrinkage, drying shrinkage, thermal changes, and loading can all cause cracks in concrete; therefore, most concrete structures will have some degree of cracking (Lindquist et al. 2006).

Some studies have examined the effects of crack width on corrosion rate and corrosion initiation with mixed results. Some researchers (Beeby 1983, Arya & Wood 1995, Bentur et al. 1997) found that although cracks may accelerate corrosion initiation, there is no direct relationship between crack width and corrosion rate. Beeby investigated several studies in the literature about the effect of crack width on corrosion rate and concluded that the width of cracks has far less importance than concrete cover and quality on the corrosion rate of steel (Beeby 1983). A study carried out by Technical University in Munich created crack widths of up to 0.016 in. (0.4 mm) in reinforced concrete beams and exposed them to three different environments: a normal urban environment, a heavily polluted atmosphere, and a marine environment. Concrete cover ranged from 0.9 to 1.38 in. (23 to 35 mm). Beams from each type of environment were autopsied after one, two, four, and ten years, and the depth of corrosion was measured and related to the crack width at each crack. Although at earlier ages (up to 2 years) a considerable influence of crack width was detectable, after ten years the influence of crack width was found to be small (Beeby 1983). However, other studies by Petterson et al (1996), and Scott and Alexander (2007) showed that cracks accelerate both corrosion initiation and propagation. Otieno et al. (2010) investigated the influence of 0.028 in. (0.7 mm), 0.016 in. (0.4 mm), and less than 0.016 in. (0.4 mm) wide cracks on the corrosion rate of concrete containing 100% ordinary portland cement and 50% slag and found that for 1.6 in. (40 mm) constant concrete cover over 31 weeks, increasing the crack width increased the corrosion rate; up to 40% for binary cement and 210% for ordinary portland cement.

Otieno et al. showed that incipient cracks with crack widths less than 0.016 in. (0.4 mm) may significantly affect both corrosion initiation and propagation based on concrete quality and type. For concrete contained 100% portland cement, it was shown that specimens with incipient cracks have higher corrosion rate compared to uncracked ones. Considering the relative difference between corrosion rates, the impact of crack width was noticeably higher between uncracked and incipient-cracked specimens than between 0.4 and 0.7 mm cracked specimens. However, this effect was reduced in concrete containing 50% slag compared to 100% ordinary portland cement due to the higher resistivity of the concrete (Otieno et al. 2010). Rodrigues and Hooton (2003) showed that for the parallel-wall cracks with crack widths ranging from 0.003 to 0.027 in. (0.08 mm to 0.68 mm), chloride diffusion rate is independent of crack width or roughness, which implies that even narrow cracks can accelerate corrosion if they reach the bar surface (Rodriguez & Hooton 2003). Francois and Arliguie (1999) studied effect of width of transverse cracks on corrosion of reinforced concrete under loading condition. Two groups of 3 m long reinforced beams were kept in a confined salt fog chamber for 12 years and loaded to create transverse cracks along the beams at location of stirrups. Two distinct magnitude of loads were applied to create cracks ranging from 2 to 8 mils (0.05 to 0.2 mm) and from 2 to 20 mils (0.05 to 0.5 mm). Specimens were autopsied and degree of corrosion evaluated after five years. Although crack widths were twice as much in group two compared to group one, degree of corrosion was similar in both groups after five years; therefore, results showed that variation in transverse crack widths for crack widths less than 0.02 in. (0.5 mm) do not affect the corrosion development of embedded steel. Furthermore, it was showed that tensile microcracking in concrete due to service loading increases the penetration of chloride ions and affects the development of corrosion in reinforcement.

1.6 CORROSION PROTECTION SYSTEMS

In highway bridges in snow-belt states, the main cause of corrosion is the deicing salts used during winters. These salts can diffuse through concrete, reach the bar surface and cause corrosion. The most common deicing salt used is sodium chloride, which can significantly contribute to corrosion. The use of alternate deicing chemicals, such as magnesium chloride, calcium chloride, and calcium magnesium acetate, can be less corrosive to steel but cause severe deterioration to the concrete itself (Cody et al. 1996, Darwin et al. 2007, Lee et al. 2000). Therefore, designing bridge deck components to be more resistant to corrosion remains a critical corrosion control method.

To improve the durability of concrete against corrosion, there are four different methods, which can be used, based on the way of protection they provide (Kepler et al. 2000): 1- Methods that use more corrosion resistant steels. 2- Barrier methods that protect reinforced concrete by preventing water, oxygen and chloride ions from reaching the reinforcement. 3- Electrochemical methods including cathodic protection and electrochemical chloride extraction. 4- Corrosion inhibitors which can provide protection by raising the critical chloride threshold, reducing the permeability of the concrete, or by doing both. Barrier methods involve the concrete itself by increasing concrete cover and decreasing permeability of concrete. These methods usually slow the corrosion initiation by increasing the transition time for the chloride ions, oxygen, and moisture to reach the reinforcement surface and provide the necessary components for corrosion initiation. Using more corrosion resistant reinforcement is another way that can be used to extend the corrosion initiation time or the propagation period. Epoxy-coated and stainless steel bars are the two most common corrosion resistant bars frequently used in bridge decks. Using a combination of different methods; that is, enhancing the concrete properties such as increasing the concrete cover or decreasing its permeability along with using the more corrosion resistant bars, such as

epoxy-coated reinforcement is another option that frequently used in concrete decks. Although epoxy-coated reinforcement and stainless steel bars are the most common resistant reinforcing bars, there are some concerns with their use. The potential for damage to epoxy coatings and the cost of stainless steel result in continued investigation into better protection systems against corrosion. Using different types of bars, such as galvanized bars, MMFX bars, duplex coating bars, and stainless steel clad bars in combination with other protective systems against corrosion, are some options being considered. A detailed description of these corrosion protection systems is presented in the following sections.

1.6.1 Epoxy-Coated Reinforcement (ECR)

One of the most common methods of corrosion protection for reinforcing steel is coating conventional bars with a corrosion resistant epoxy coating. Epoxy-coated reinforcement was first developed in the early 1970s (Manning 1996). When epoxy-coated reinforcement was first introduced, concrete bridge decks with uncoated rebar often required repair every seven to ten years (Clifton et al. 1994). After using epoxy-coated reinforcement in construction of over 100,000 structures, only a few problems have been documented (McHattie et al. 1996). Several studies showed that epoxy-coated reinforcement significantly increased the durability and service life of concrete compared to conventional bars (Treadaway & Davies 1989, McDonald et al. 1996, Fanous & Wu 2005). Epoxy coatings prevent corrosion through two methods: by forming a barrier against moisture, chlorides, and oxygen, and by acting as an electrical insulator between bars, which prevents electrical connections between anodes and cathodes located on separate bars (macrocell corrosion).

Although the use of epoxy-coated reinforcement has been favorable in many cases, some poor performance and problems also have been documented. Poor performance of epoxy-coated bars when concrete remains saturated, such as in bridge piers in salt water, and the tendency of epoxy to lose its adhesion to the underlying steel over time, are problems observed with the use of epoxy-coated bars (Darwin et al. 2011). One of the first uses of epoxy-coated reinforcement in the substructure of bridges in the Florida Keys showed severe corrosion damage after only six years in service. Local corrosion damage sites and disbondment of the epoxy coating layers from the underlying steel aggravated by bending of the bars resulted in severe corrosion damage (Zayed & Sagues 1989, Smith et al. 1993). Some of the reasons that may cause poor performance of epoxy-coated bars are imperfections and damage on the epoxy coating and loss of adhesion of the epoxy layer. Epoxy coating contains some very small imperfections (holidays); epoxy coatings are also prone to damage during shipment, placement, fabrication, and casting concrete. An investigation of holiday testing has showed that handling, placing, and casting concrete over epoxy-coated reinforcement induces an average of 12.2 holidays per foot (40 holidays per meter) (Samples 1998). Under-film and crevice corrosion can occur in these holidays. Migration of water, oxygen, and chlorides to the surface of the steel would cause under-film corrosion, and in the regions that oxygen is not available, crevice corrosion. Without the presence of oxygen, the pH of the environment under the epoxy can drop to as low as 5, accelerating crevice corrosion (Weyers et al. 1998). Adhesion loss in epoxy-coated reinforcement is another problem that can result in disbondment of epoxy layer from the underlying steel (Manning 1996, Weyers et al. 1998, Draper et al. 2009). Cathodic disbondment or blistering can also occur when the hydroxide ions produced at the cathodic sites build up in the region between the coating and the steel, resulting in disbondment of the epoxy coating.

In spite of these imperfections, an overall comparison between epoxy-coated and conventional bare bars show significant improvement in the service life of the structures by using epoxy-coated bars. Draper et al. (2009) compared the corrosion loss of epoxy-coated reinforcement with damaged coating and conventional bars and showed that the epoxy-coated bars had 1 percent of the corrosion loss of conventional reinforcement. Darwin et al. (2011) investigated 11 systems in which epoxy-coated bars were combined with another corrosion protection system. Multiple corrosion systems included conventional epoxy-coated reinforcement with three distinct corrosion inhibitors; bars that were treated with a primer coating containing microencapsulated calcium nitrite (a corrosion inhibitor) prior to coating with conventional epoxy; bars with improved adhesion between the epoxy and the underlying steel, obtained via use of either zinc chromate pretreatment or special epoxies with increased adhesion from DuPont™ and Valspar®; bars with an improved adhesion epoxy combined with addition of calcium nitrite to the concrete; and bars with multiple coatings consist of a 2 mil (50 μm) layer of 98% zinc and 2% aluminum coated with a conventional epoxy. Darwin et al. showed that the conventional fusion-bonded epoxy coatings significantly improve the corrosion resistance, life expectancy, and cost effectiveness of reinforcing steel compared to conventional bars. For epoxy-coated bars critical chloride threshold were several times greater and corrosion rates were typically two orders of magnitude below those showed by conventional bars. The differences in the costs over a 75-year design life were shown relatively small for coated bars. Reinforcement with higher adhesion to the underlying steel showed no advantage in terms of improved corrosion performance or improved adhesion when used in concrete (Darwin et al. 2011). Erdogdu et al. (2001) exposed concrete slabs containing undamaged epoxy-coated bars as well as bars with 1 % and 2% intentionally damaged area to the coating to synthetic seawater and a 3% salt solution. It was found that undamaged epoxy-coated

bars exhibited no sign of corrosion and the bars with damaged coating, regardless of the degree of the damage, showed significant reductions in corrosion activity compared to the bare bars. However, the importance of preventing damage to the epoxy layer and its effectiveness on the corrosion loss was obvious during the study.

1.6.2 Zinc Coated (Galvanized) Reinforcement

Zinc coating is another method of increasing the corrosion resistance of reinforcement and has been used since the early 1940s. Zinc coatings can protect the underlying steel through two ways. Like epoxy coatings, zinc coatings act as a barrier against oxygen, moisture, and chloride ions. Furthermore, zinc provides protection by serving as a sacrificial anode. The half-cell potential of zinc, –1.004 V versus saturated calomel electrode (SCE), is more negative than that of iron (–0.681 V versus SCE); that is, zinc is a more active metal. In a homogenous environment, where zinc and steel are in contact, the more active metal (zinc) will corrode and protect the less active metal (steel) from corrosion (Jones 1996). This protection continues even if the coating is damaged and the underlying steel exposed.

Hot-dip galvanizing is the most common method for coating a bar with zinc. In the hot-dipping method, steel is immersed in a molten bath of zinc at a temperature of 860 ˚F (460 ˚C), forming a metallurgical bond between the steel and zinc.

Zinc in contact with air forms zinc hydroxide ($Zn(OH)_2$), which in turn reacts with available carbon dioxide in air and produces a protective layer called zinc carbonate ($ZnCO_3$), preventing further corrosion. In concrete with pH between 11 and 12.3 isolated crystals of ZnO and ε-$Zn(OH)_2$ will form due to localized corrosion of zinc (Andrade & Macias 1988). In concrete

with pH between 12.2 and 13.3, zinc reacts with water of alkaline pore solution to form zinc hydroxide and hydrogen gas:

$$Zn + 2H_2O \rightarrow Zn(OH)_2 + H_2 \quad (1.17)$$

Zinc hydroxide then reacts with calcium ions in the pore solution to form calcium hydroxyzincate (Andrade & Macias 1988):

$$2Zn(OH)_2 + 2H_2O + Ca(OH)_2 \rightarrow Ca(Zn(OH)_3)_2 \cdot 2H_2O \quad (1.18)$$

The sequence of reactions that leads to formation of calcium hydroxyzincate is:

$$Zn + 4OH^- \rightarrow Zn(OH)_4^{2-} + 2e^- \quad (1.19)$$

$$Zn + 2OH^- \rightarrow ZnO + H_2O + 2e^- \quad (1.20)$$

$$ZnO + H_2O + 2OH^- \rightarrow Zn(OH)_4^{2-} \quad (1.21)$$

$$Zn(OH)_4^{2-} + 2H_2O + Ca^{2+} \rightarrow Ca(Zn(OH)_3)_2 \cdot 2H_2O + 2OH^- \quad (1.22)$$

In environments with pH above 12.2 calcium hydroxyzincate produces small compact crystals, which in turn, forms a stable passive layer on the surface of the bar. With increase of pH, crystals become larger and due to the formation of tiny gaps in between, they are not able to seal the surface completely. For environments with pH above 13.3, calcium hydroxyzincate produces large isolated crystals that cannot seal the surface at all, and are not able to protect the underlying layer against corrosion (Andrade & Macias 1988). Furthermore, hydrogen gas produced in equation (1.17) can increase the permeability of the surrounding concrete. Thus, ASTM A767 requires galvanized bars to be submerged in a chromate bath after coating to passivate the zinc surface and prevent reaction of hydroxide ions in fresh concrete with zinc (Virmani & Clemeña 1998). This passive layer can be broken down with the presence of chlorides in a manner similar to that of iron. Concrete carbonation also can destroy the passive layer of calcium hydroxyzincate and form amorphous products of $ZnCO_3$ and $Zn_5(CO_3)_2(OH)_6$, which have limited passivating

properties (Roventi et al. 2014). This carbonation process, however, lowers the critical chloride threshold of the galvanized bar in concrete (Roventi et al. 2014).

Studies about the effectiveness of galvanized bars against corrosion showed mixed results. Treadaway and Davis (1989) compared epoxy-coated, galvanized, and conventional bar corrosion resistance after 5 years of exposure to a sodium chloride environment and showed that concrete slabs with galvanized bars corroded heavily and demonstrated more cracking than slabs with conventional bars. Sarawathy and Song (2005) investigated the performance of four types of galvanized bars under macrocell corrosion conditions and found that only one type of galvanized bar was more corrosion resistant than conventional steel bars. A study by Hime and Machin (1993) showed that in addition to formation of ZnO, the zinc layer of the galvanized bar can form zinc hydroxychloride II ($Zn[OH]_8Cl_2.H_2O$). Unlike ZnO, which occupies only 50% more volume than uncorroded metal, zinc hydroxychloride occupies 260% more space than uncorroded zinc and exerts a greater expansive force than most forms of rust, resulting in more rapid cracking than in cases where ZnO forms. This finding may explain the variation in the results of some studies about the corrosion resistance of galvanized bars (Hime & Machin 1993). Conversely, O'Reilly et al. (2011) compared the critical corrosion loss required to crack concrete containing galvanized bars with concrete containing conventional steel bars for 0.5, 1, and 2 in. concrete cover and showed that the average critical corrosion loss for galvanized steel was approximately four times that of conventional steel in specimens with 0.5 in. concrete cover, and twice that of conventional reinforcement for specimens with 1 in. and 2 in. concrete cover. Another study (Yeomans 1994) investigated concrete samples containing galvanized steel, conventional steel, and epoxy-coated steel exposed to a cyclic salt water wetting and drying or to a continuous salt fog. Results showed the critical chloride threshold of the zinc bars was about 2.5 times that of conventional steel, with

a time to initiation four to five times greater than that of conventional steel (Yeomans 1994). A study by Haran et al. (2000) showed that although zinc corrodes at a much faster rate in the presence of chloride ions compared to conventional steel, it sacrificially delays the onset of corrosion of underlying steel. Rasheeduzzafar et al. (1992) compared the resistance of galvanized reinforcing steel with other corrosion resistant bars, and showed that galvanized steel in concrete containing less than 2 lb/yd^3 (1.2 kg/m^3) chlorides results in a delay in the onset of cracking and reduction in the metal loss compared to conventional steel. Rasheeduzzafar claimed, however, that in concrete with a higher chloride content severe corrosion along with concrete cracking was observed in specimens with galvanized steel. Darwin et al. (2009) compared the critical chloride threshold of concrete specimens containing zinc bars with conventional steel and showed that while the average critical chloride threshold of conventional steel was 1.63 lb/yd^3 (0.97 kg/m^3), it was 2.57 lb/yd^3 (1.52 kg/m^3) for galvanized steel exposed to the same conditions.

1.6.3 MMFX Reinforcing Steel

Alloying of ferrous metals to improve their resistance against corrosion has a long history. Stainless steel reinforcement, steel that is alloyed with more than 11% chromium and often with the addition of nickel, has been investigated and showed significantly greater resistance against corrosion compared to conventional reinforcing bars. There are four types of stainless steel: ferritic, ferritic-austenitic, austenitic, and martensitic (Kepler et al. 2000). Ferritic steels are low carbon steels with less than 17% chromium. Austenitic steels are low carbon steels with approximately 18% chromium and 8% nickel. Ferritic-austenitic steels (duplex steels) typically contain 22-28% chromium and 4-8% nickel (Kepler et al. 2000). The improved resistance to pitting and general corrosion in stainless steel is due to the decrease in chromium depletion and chromium

carbide ($Cr_{23}C_6$) formation (Presuel-Moreno et al. 2010). Upon production of stainless steel, chromium on the surface of steel reacts with oxygen in the air to produce a passive layer of chromium oxide around steel. This passive layer is chemically stable and can self-repair in cases that get damaged as long as sufficient oxygen is available at its surface. Stainless steel passive layer is often stabilized by washing the steel surface with particular acid solutions such as nitric acid (HNO_3) and hydrofluoric acid (HF), in a process called pickling. Usually in the manufacturing process before delivering steel, a thick visible dark oxide scale would be removed by a process called descaling. Afterwards, in the pickling process, by use of acids, the impurities on the surface of the bar, where chromium tends to react with oxygen, would be removed and oxidation of chromium would be assisted. Pickling is required for many types of stainless steels, including the duplex stainless steel often used in reinforcement, to obtain a high degree of corrosion resistance. Balma et al. (2005) compared the corrosion resistance of pickled 2205 (22% Cr, 5% Ni) and 2101 (21% Cr, 1% Ni) stainless steel bars with unpickled bars. Without pickling, the 2205 stainless steel bars performed slightly worse than pickled 2205 steel, while the 2101 stainless steel bars performed significantly worse than pickled 2101 bars. Tests showed that in the pickled state, average corrosion losses for 2205 and 2101 stainless steel were 0.3% and 1.3%, respectively, of those for conventional steel, while in the unpickled state, 2101 stainless steel showed corrosion losses between 6.5% and 8.5% of those observed in conventional steel.

Research on stainless steel reinforcement indicates that it may remain free of corrosion in chloride contaminated concrete for more than 75 years (Kepler et al. 2000). Although a high level of corrosion resistance is obtained through the use of stainless steel, the high chromium and nickel content has made stainless steel a much more expensive alternative than other corrosion resistant bars. Microcomposite steel, reinforcing steel with a lower level of chromium content (4% or 9%

chromium), which was first introduced by MMFX Steel Corporation of America, has received increasing attention, since this type of steel has a significantly lower cost than stainless steel. Manufacturers claim that due to the chemical composition and production process of MMFX steel, the formation of microgalvanic cells, which occurs between ferrites and carbides in conventional steel, would be minimized (Ji et al. 2005).

MMFX bar was first used in 2001 in a bridge in Iowa (Wipf et al. 2006). The westbound lane of the deck was reinforced with epoxy-coated bars and the eastbound lane with uncoated MMFX bars. To monitor the corrosion activity over a 12 month period, reference electrodes were installed throughout the bridge. The initial corrosion current of the epoxy-coated bars was six times that of the MMFX bars. The corrosion current in the epoxy-coated bars, however, stabilized after 150 days. This initial higher corrosion current might have occurred due to defects in the coating of the epoxy-coated bars (Wipf et al. 2006). In addition to the field test, Wipf et al. tested the bars in accelerated laboratory conditions (ASTM G109) and showed that after 40 weeks, MMFX and undamaged epoxy-coated reinforcement exhibited no signs of corrosion. Epoxy-coated reinforcement with intentionally induced defects, however, exhibited signs of corrosion within 15 to 30 weeks (Wipf et al. 2006).

Gong et al. (2003) studied and compared the corrosion performance of MMFX bars with that of epoxy-coated and uncoated conventional bars. Reinforcement was evaluated using the rapid macrocell test and two bench-scale techniques-southern exposure and cracked beam tests. The combination of MMFX bars with conventional bars was also tested in both rapid macrocell and bench-scale tests to determine the potential for galvanic corrosion if the steels were mixed. The study found the macrocell corrosion rate of MMFX bars was between one-third and two-thirds that of conventional steel. The epoxy-coated reinforcement with the coating penetrated, however,

exhibited corrosion rates between 5% and 25% that of conventional steel and provided superior corrosion performance compared to MMFX steel. Combining MMFX bars with conventional steel showed significantly lower corrosion rates (2.2 μm/yr) compared to using conventional bars alone (5.6 μm/yr) after 40 weeks while MMFX bars were used as anode, and showed slightly lower corrosion rates (5.1 μm/yr) while MMFX bars were used as cathode. No significant differences were found in the composition of corrosion products on conventional and MMFX bars. Gong et al. found that although MMFX steel is more corrosion resistant than conventional uncoated steel, it is not as resistant as epoxy-coated steel unless it is used with a supplementary corrosion protection system (Gong et al. 2003).

Darwin et al. (2002) compared corrosion resistance of MMFX Microcomposite steel with conventional mild steel and epoxy-coated reinforcement. Corrosion performance of the bars were evaluated using rapid macrocell tests of bare and mortar-wrapped reinforcement as well as Southern Exposure and cracked beam tests. Based on experience and costs in South Dakota in conjunction with laboratory results, life expectancy and cost effectiveness of the various reinforcement was evaluated. Results showed that bridge decks containing MMFX steel will require repair approximately 30 years after construction, compared to 10 to 25 years for conventional steel and 40 years for epoxy-coated reinforcement under typical conditions in South Dakota. However, time to first repair for epoxy-coated reinforcement was estimated based on the observation that no bridges built with epoxy-coated have required repair. A comparison of the expenses showed that bridge decks containing MMFX steel do not appear to be cost effective compared to bridge decks containing epoxy-coated reinforcement (Darwin et al. 2002).

A study by Clemana and Virmani (2004) compared the corrosion resistance of MMFX, stainless steel, and conventional bars. Results showed that MMFX bars had high corrosion rates

from the start of exposure of the concrete specimens to the salt solution, which might have been due to the presence of mill scale on the bar surfaces. However, the corrosion rate of MMFX bars was one-third that of conventional steel. Clemana and Virmani reported a time for corrosion of MMFX bars almost 2.6 times greater than conventional steel reinforcement.

A study by Ji et al. compared the corrosion resistance of MMFX microcomposite steel with epoxy-coated and uncoated bars (Ji et al. 2005). Results showed that MMFX steel exhibited a critical chloride threshold ranging from 4.72 to 6.86 lb/yd^3 (2.8 to 4.07 kg/m^3), three to four times that of uncoated conventional steel (1.53 to 2.05 lb/yd^3 (0.91 to 1.22 kg/m^3)). The corrosion loss of MMFX bars ranged from 16% to 66% that of uncoated conventional bars. However, corrosion loss of the epoxy-coated bars with the coating which was intentionally penetrated to simulate damage ranged from 0.4% to 6% of the corrosion loss for conventional steel, significantly lower than the value for MMFX bars. Ji et al estimated the service life of the bridge decks including the time to corrosion initiation and the time to concrete cracking for decks containing MMFX and conventional bars as 35 and 12 years, respectively (Ji et al. 2005). Similarly, Akhoondan and Sagues (2012) investigated the cathodic behavior of 9% chromium steel and showed that the 9% chromium alloy was a considerably weaker cathode than conventional steel, and therefore more corrosion resistant.

Previous studies investigated the corrosion resistance of MMFX bars containing 9% chromium; however, the behavior of newer alloys with 2% and 4% chromium has not been studied.

1.6.4 SUPPLEMENTARY CEMENTITIOUS MATERIALS (SCM)

Supplementary cementitious materials are finely ground solid materials which can be added to concrete for a variety of purposes such as replacing cement, improving workability of

fresh concrete, and enhancing its strength and durability (Mindess et al. 2002). Two main categories of supplementary cementitious materials widely used are pozzolanic and cementitious materials. Four major components of cement are: tricalcium silicate ($3CaO.SiO_2$ or C_3S), dicalcium silicate (2CaO.SiO2 or C_2S), tricalcium aluminate ($3CaO.Al_2O_3$ or C_3A), and tetracalcium aluminoferrite ($4Cao.Al_2O_3.Fe_2O_3$ or C_4AF). In the presence of water, calcium silicates (C_3S and C_2S) are hydrated to produce calcium silicate hydrate (C-S-H), which in turn contributes to the strength of cement paste, and calcium hydroxide ($Ca(OH)_2$). Pozzolanic materials, such as fly ash and silica fume, contain amorphous or glassy silica which reacts with calcium hydroxide ($Ca(OH)_2$) formed from the hydration of the calcium silicates (C_3S and C_2S) in portland cement and produces calcium silicate hydrate (C-S-H). The more calcium hydroxide consumed in the reaction with the pozzolan, the more effective the pozzolan is in improving long term strength and concrete durability. Fly ash is an inorganic, noncombustible residue of powdered coal after burning in power plants, and silica fume is a by-product in the manufacture of silicon metal (Mindess et al. 2002). Besides pozzolans, other cementitious materials such as slags are frequently used in concrete mixtures. Slag is the residue of metallurgical processes in the blast furnace production of iron from ore. Blast furnace slag (slag cement) contains lime (CaO), silica (SiO_2), and alumina (Al_2O_3). These components in the presence of an alkaline activator such as calcium hydroxide in concrete can produce calcium silicate hydrate (C-S-H) and contribute to concrete compressive strength (Mindess et al. 2002).

Supplementary cementitious materials affect the critical chloride threshold, time for chloride ingress, and corrosion rate of concrete through several distinct ways. Supplementary cementitious materials can increase the time required for corrosion initiation by creating a denser and less permeable concrete matrix. Some researchers believe that reduction in permeability of

concrete by use of supplementary cementitious materials can reduce the corrosion rate through controlling the diffusion of chloride, oxygen, and moisture in concrete (Mangat & Molloy 1992), though other studies contradict this finding. Supplementary cementitious materials also have a significant impact on chloride binding and pore solution composition. Arya and Xu (1995) compared the amount of bound chlorides and corrosion rate in concrete containing ordinary portland cement as well as concrete with cement partially replaced by 65% slag cement, 35% fly ash, and 10% silica fume. Salt was introduced to the concrete by 1% and 3% of cement weight during mixing to depassivate the reinforcing steel. Chloride binding was greatest for the mixture containing slag cement, with decreasing binding for mixtures containing fly ash, ordinary portland cement, and silica fume. Other reports also suggest that binding decreases with the use of silica fume (Page & Vennesland 1983, Rasheeduzzafar et al. 1991). However, corrosion rates did not line up with binding capacity. Arya and Xu reported that for mixtures containing 1% chloride content, the fly ash mixture had the greatest corrosion rate, followed by silica fume, slag cement, and ordinary portland cement. For mixtures containing 3% chloride content, the fly ash mixture again had the greatest corrosion rate, followed by ordinary portland cement, slag cement, and silica fume. The higher corrosion rates of mixtures containing fly ash, silica fume, and slag compared to ordinary portland cement with 1% chloride content was attributed to the lower OH^- concentration, or in other words, the lower pH in these concrete due to the consumption of hydroxide ions (Arya & Xu 1995). Bouteiller et al (2012) showed that concrete containing 70% slag cement with w/c ratios as of 0.45 and 0.65 have lower chloride diffusion rate than concrete with ordinary portland cement only. This lower chloride ingress rate in concrete containing slag cement was attributed to transport properties rather than chloride binding capacity of slag cement (Bouteiller et al 2012). For slag cement, other studies (Tromans 1980) reported that sulfides present in the pore solution

may incorporate into the oxide layer of steel, reducing its stability and increasing the corrosion rate. Oxidation of sulfides in concrete containing slag cement can drop corrosion potentials to the values, which according to ASTM C876, show over 90% probability of corrosion, without any actual chloride induced corrosion occurring on the bar surface (Holloway & Sykes 2005, Bouteiller et al. 2012, Garcia et al. 2014).

Sirivivatnanon et al. (1994) compared effects of silica fume, fly ash, and slag cement on the corrosion of machined and polished steel in mortar. Because of variation in the diffusion characteristics of the blended cement (and therefore, the chloride content on the surface of the steel), comparing corrosion rates was difficult in their study. However, the reported macrocell corrosion rates after 6 months were in order of portland cement > 5% silica fume > 20% fly ash > 40% fly ash > 40% slag cement > 60% slag cement > 60% fly ash > 80% slag cement > 10% silica fume. Scott and Alexander investigated the influence of supplementary cementitious materials on specimens with crack widths of 0.008 in. (0.2 mm) and 0.028 in. (0.7 mm) (Scott & Alexander 2007). Ordinary portland cement concrete and mixtures with cement partially replaced by 25% slag cement, 50% slag cement, 75% slag cement, 30% fly ash, 7% silica fume, and a ternary blend of 50% portland cement, 43% slag cement, and 7% silica fume were tested. Inclusion of any of the supplementary cementitious materials resulted in at least a 50% reduction in corrosion rate compared to ordinary portland cement. While resistivity had the greatest impact on the corrosion rate of concrete containing supplementary cementitious materials, concrete cover variation (or in other words, availability of oxygen) controlled the corrosion rate of ordinary portland cement concrete (Scott & Alexander 2007).

Research on the effect of supplementary cementitious materials on the critical chloride threshold has also yielded mixed results. The consumption of hydroxide ions in the pore solution

by supplementary cementitious materials lowers the pH of concrete, which in turn can lead to destabilizing the protective passive layer around the steel. Thomas (1996) showed that although the mass loss of the steel embedded in the concrete containing fly ash exposed to a marine environment decreased with increasing fly ash content, the critical chloride threshold was also decreased. Likewise, (Oh & Jang 2003) found that increasing the content of fly ash from 15% to 30% resulted in a decrease in the total chloride threshold content from 0.90% to 0.68% and free chloride threshold content from 0.11% to 0.07% by binder weight of concrete. It was also found that using 30% of slag cement had a negligible effect on critical chloride threshold compared to ordinary portland cement concrete. Thomas and Matthews (2004) showed that although critical chloride threshold decreased in specimens in which cement was partially replaced by fly ash, the rate of chloride ingress and corrosion rate also decreased. In a study by Presuel-Moreno and Moreno (2015) critical chloride threshold and time to initiation of concrete specimens containing 20%, 35%, and 50% cement replacement by fly ash as well as 6%, 15%, and 27% cement replacement by silica fume were investigated. Specimens were cast with and without reinforcement with w/c ratio as of 0.37 and were exposed to natural seawater for over 17 years on weekly wetting-drying cycles. Among specimens containing fly ash, those with 50% fly ash had the lowest critical chloride threshold value and specimens with 35% fly ash had the highest; specimens with 20% and 50% fly ash showed lower critical chloride threshold than specimens containing portland cement only. Among specimens containing silica fume, specimens with 6% silica fume had comparable critical chloride threshold to specimens containing only portland cement; increasing silica fume content resulted in decrease of critical chloride threshold values (Presuel-Moreno and Moreno 2015). On the other hand, Breit and Schiessl (1997) reported that in a test that chloride ions were added to the mixing water of concrete, specimens containing 25% fly

ash and 50% slag cement had almost as 1.5 times the critical chloride threshold as the specimens without supplementary cementitious materials. Monticelli et al. (2016) evaluated corrosion behavior of steel in fly ash mortars, which were activated by NaOH and sodium silicate solutions. Results showed that for specimens with the ratio of Na_2O/SiO_2 as low as 0.12 and 0.14 (most compact pozzolanic products), the critical chloride threshold (about 1% to 1.7% with respect to binder weight) was higher than that for specimens containing cement (about 0.5% versus binder weight).

Despite the variations in performance for mixtures containing supplementary cementitious materials on critical chloride threshold, most research has shown that the partial replacement of cement with supplementary cementitious material will increase the time to corrosion initiation. This delay in initiation is the result of several mechanisms such as an improved microstructure, a lower degree of interconnected voids, and improvement to the interfacial transition zone between the cement matrix and aggregates (Mackechnie & Alexander 1996, Mangat et al. 1994). Hussain and Rasheeduzzafar (1994) reported that the partial replacement of cement with 30% fly ash approximately doubled the time to corrosion initiation. Partial cement replacement by fly ash caused significant reduction in permeability to water and chloride ions, and increased electrical resistivity (Hussain & Rasheeduzzafar 1994). These improvements in physical characteristics of fly ash concrete offset the moderate increase in unbound chloride concentration in the pore solution (Hussain & Rasheeduzzafar 1994).

1.7 CORROSION MONITORING AND MEASUREMENTS

Corrosion-induced failure in critical structures is a threat to human life and safety. Even in situations where corrosion does not result in failure, significant maintenance costs are incurred every year. Therefore, corrosion monitoring has become important for scheduling structure maintenance, predicting structural life, and ensuring health and safety. Monitoring of concrete

structures can be as simple as periodic visual inspection. This level of monitoring, however, can only detect damage in a late stage when rust stains the surface of concrete; additional methods are needed to monitor corrosion at earlier stages. Some methods of corrosion monitoring used in this study are described below.

1.7.1 Corrosion Potential

In the corrosion process, corrosion potential is a value correlated to the electrochemical energy at equilibrium, which shows the tendency of the corrosion reaction to occur. In other words, the potential difference between a metal and the surrounding environment represents the driving force for corrosion. The higher the negative value of the potential difference is for a given metal, the greater the tendency of corrosion. Although the corrosion potential indicates the tendency for the reaction to occur, it does not measure the rate of corrosion; thus, it should be used in combination with other techniques to evaluate the corrosion performance of the embedded steel in concrete.

Corrosion potential is measured with respect to a reference electrode using a high-impedance voltmeter. There are several reference electrodes with known properties that can be used including the standard hydrogen electrode (SHE), saturated calomel electrode (SCE), and copper-copper sulfate electrode (CSE). The standard hydrogen electrode is comprised of purified hydrogen gas bubbled over platinum foil in a 0.5 molar sulfuric acid solution. Components of this standard electrode make it impractical for measurements in the field, so its use is limited. The saturated calomel electrode consists of mercurous chloride (Hg_2Cl_2, calomel) in contact with liquid mercury within a compartment surrounded by saturated potassium chloride (KCl) solution. The potential of the calomel electrode is +0.241 V with respect to standard hydrogen electrode; that is,

potentials read with SCE are 0.241 V more negative compared to the readings taken with SHE. The copper-copper sulfate electrode is comprised of a copper rod submerged in a saturated copper sulfate solution within a plastic tube that has a porous plug at one end which allows contact with the copper sulfate electrolyte. Because of its simple and durable design, this electrode usually is favored in the field tests (Jones 1996). Potentials taken with this electrode are 0.312 volts more negative compared to that taken with a standard hydrogen electrode.

ASTM C876 has provided guidelines and interpretation for likelihood of corrosion of uncoated conventional reinforcing steel in concrete, which are summarized in Table 1.1 below.

Table 1.1: ASTM C876 corrosion potential interpretation

Measured Potential (V)		**Corrosion Activity**
SCE	**CSE**	
> –0.125	> –0.200	>90% probability corrosion is not occurring
–0.125 to –0.275	–0.200 to –0.350	corrosion activity uncertain
<–0.275	<–0.350	>90% probability corrosion is occurring

Concrete resistance, humidity, oxygen, chloride concentration, stray currents, and carbonation are some of the factors that affect interpreting half-cell potential data. The heterogeneous water and chloride content can result in shifting the potential up to 150 mV (Schiegg et al. 2009). A decrease in oxygen concentration at the surface of the embedded steel can result in more negative potential readings (Gu & Beaudoin 1998). That is, epoxy-coated steel bars or the bars embedded in very high concrete cover or in low permeability concrete would have a more negative corrosion potential which is not necessarily indicative of a high probability of corrosion. Because of this, ASTM C876 has reported that half-cell potential interpretation is not valid for concrete with epoxy-coated bars. In addition, ASTM C876 indicates that the half-cell potential

interpretation is not suitable for measurements involving galvanized steel, since the potential reading is no longer the corrosion potential of steel, but the mixed potential of steel and zinc (Gu & Beaudoin 1998). Potential readings are also affected by concrete resistivity. The potential reading from a voltmeter is the potential difference between the two ends of the internal voltmeter resistance, and is accurate when this voltmeter internal resistance is significantly higher than concrete resistance. Thus, in order to obtain accurate potential readings, concrete resistance must be decreased as much as possible. For instance, wetting the concrete surface prior to measurement can lower the concrete resistivity and increase the accuracy of the potential readings (Gu & Beaudoin 1998).

1.7.2 Macrocell Corrosion Rate

For corrosion mechanism to occur, an electrical connection is necessary to provide a path for electrons to flow from anode to cathode. The corrosion rate depends on the measurement of the electron flow from anode to cathode in a corrosive environment and can provide meaningful data for evaluating the corrosion in a system. If the anode and cathode are located on the same bar, the resulting corrosion is termed microcell corrosion; if the anode and cathode are on different bars it is termed macrocell corrosion. In practice, microcell and macrocell corrosion occur simultaneously, and electrical connections between reinforcing bars connected by steel tie wires or bar chairs make direct measurement of the macrocell corrosion rate infeasible. In the laboratory, however, by separating the anode and cathode region (either by keeping the anode in a corrosive environment and the cathode in an inert environment or electrically isolating the bars in concrete) these complications can be minimized. If the bars are then connected in a series circuit across a

resistor, the voltage drop across the resistor can be measured by voltmeter and the current density between anode and cathode calculated according to Ohm's Law:

$$i_{\text{corr}} = 10^6 \times \frac{V}{RA} \tag{1.23}$$

where

i_{corr} = current density, μA/cm^2

V = measured voltage drop across resistor, volts

R = resistance, ohms

A = surface area of anode, cm^2

Current density can be shown as the first representative value of corrosion rate between anode and cathode. In addition to the current density, corrosion rate can be presented in terms of thickness loss per unit time. The relationship between these two is shown below per Faraday's Law:

$$r = k \frac{ia}{nF\rho} \tag{1.24}$$

where

r = corrosion rate, μm/year

k = conversion factor, $315360 \frac{\text{A} \cdot \mu\text{m} \cdot \text{s}}{\mu\text{A} \cdot \text{cm} \cdot \text{yr}}$

i = current density, μA/cm^2

a = atomic weight of the corroding metal, g/mol

n = number of electrons lost per atom of metal oxidized

F = Faraday's constant, 96,485 Coulombs/equivalent

ρ = density of metal, g/cm^3

For iron, a = 55.85 g/mol, n = 2, and ρ = 7.87 g/cm^3. Eq. (1.24) simplifies to

$$R = 11.6i \tag{1.25}$$

For zinc, a = 65.38 g/mol, n = 2, and ρ = 7.13 g/cm^3. Eq. (1.24) simplifies to

$$R = 15.0i \tag{1.26}$$

There are several ways to separate anode and cathode regions to measure the macrocell corrosion rate in the laboratory. One of the most common ways is the method used in ASTM G109 and similar test methods. In this method, anode bars are placed as the top mat of a concrete slab section and chloride is applied through the top surface of the slab, while cathode bars are located as the bottom mat of the slab and remain intact from the chloride ingress. This method, however, does not account for microcell corrosion with anode and cathode on the same bar.

1.7.3 Linear Polarization Resistance (LPR)

To obtain the total corrosion rate (macrocell and microcell corrosion) of a bar, more complicated electrochemical methods are used. Without any external applied voltage, the current density and potential of a metal in a corrosion reaction are i_{cor} and E_{cor}, respectively. By applying external voltage (polarization) to the system, the potential of the metal can be shifted by an amount $\Delta\varepsilon$, and as a result, the current shifted by Δi. The linear polarization curve can be obtained and plotted by applying several external voltages ($\Delta\varepsilon$) and measuring the shifts in currents (Δi), or vice versa. The linear polarization resistance (LPR) test is a nondestructive method for measuring the total corrosion rate (microcell and macrocell) of a metal based on the fact that the potential-current polarization curve is approximately linear in the vicinity of E_{cor}. The slope of this approximately linear curve is called the polarization resistance, R_p, and is defined as follows (Jones 1996):

$$R_p = \left[\frac{\Delta\varepsilon}{\Delta i}\right]_{\varepsilon\to 0} \tag{1.27}$$

where

R_p = polarization resistance

$\Delta\varepsilon$ = imposed potential change

Δi = current density change caused by $\Delta\varepsilon$

The linear polarization resistance is inversely proportional to the corrosion current density according to Stern-Geary equation:

$$i_{corr} = \frac{B}{R_p} \tag{1.28}$$

Where, B is the Stern-Geary constant and equals to:

$$B = \frac{\beta_a \beta_c}{2.3(\beta_a + \beta_c)} \tag{1.29}$$

Where

β_a, β_c = anodic and cathodic Tafel constants, V/decade

R_p = polarization resistance

Using values of 0.12 V/decade for both anodic and cathodic Tafel constants (β_a, β_c) and applying those in Eq. (1.29), the Stern-Geary constant becomes 0.026 V. Using these values, which are recommended for reinforcing steel in concrete by several studies (Lambert et al. 1991, McDonald et al. 1998), will result in a linear region for the polarization curve over an interval of ±10 mV with respect to E_{corr}. Using these values, the current density in Eq. (1.28) is simplified to:

$$i_{corr} = \frac{0.026}{R_p} \tag{1.30}$$

In order to perform LPR measurements, a working electrode (the corroding reinforcing steel), a counter electrode (usually a platinum rod), and a reference electrode (such as a calomel electrode or a copper-copper sulfate electrode) are necessary.

Eq. (1.30) is used to calculate the current densities for all linear polarization tests accomplished in this report.

1.8 OBJECTIVE AND SCOPE

The objective of this study is to evaluate the corrosion performance of several different protection systems. The following investigations are included in this report:

1- Investigating the critical corrosion loss required to crack the concrete containing conventional and galvanized steel. This will continue the research by O'Reilly et al. (2011). In this study, six specimens containing conventional reinforcement and six specimens with galvanized reinforcement are exposed to chlorides without the application of an external current to drive corrosion. The total number of galvanized bar test specimens in this study is listed in Table 1.2.

Table 1.2: Galvanized bar test specimens

Steel Designation[a]	**B[b]**
Conv.	6
Zinc	6
Total	**12**

[a]Conv. = Conventional steel
Zinc = Galvanized reinforcement
[b]B = Beam specimen

2- Evaluating the corrosion performance of MMFX bare bars containing 4% and 9% chromium, and MMFX epoxy-coated bars containing 2% and 4% chromium. The performance of this corrosion system is evaluated using Southern Exposure, cracked beam, and rapid macrocell tests (to be described in Chapter 3). Since the pickling process stabilizes the formed passive layer of chromium oxides around stainless steel bars (typically with >20% chromium) and significantly improves their resistivity against corrosion, MMFX bare bars containing 4% and 9% chromium

are also pickled and tested with the rapid macrocell test to investigate the effect of pickling on MMFX bars. The total number of MMFX test specimens in this study is listed in Table 1.3.

Table 1.3: MMFX bar test specimens

Steel Designation[a]	SE[b]	CB[c]	B[d]	RM[e]	Total
MMFX(4%)	8	6	-	6	20
MMFX(9%)	8	6	-	6	20
PMMFX(4%)	-	-	-	6	6
PMMFX(9%)	-	-	-	6	6
MMFX-ECR(2%)	6	6	6	6	24
MMFX-ECR(4%)	6	6	6	6	24
Total	**28**	**24**	**12**	**36**	**100**

[a]MMFX(4%) = MMFX steel containing 4% chromium
MMFX(9%) = MMFX steel containing 9% chromium
PMMFX(4%) = Pickled MMFX steel containing 4% chromium
PMMFX(9%) = Pickled MMFX steel containing 9% chromium
MMFX-ECR(2%) = Epoxy-coated MMFX steel containing 2% chromium
MMFX-ECR(4%) = Epoxy-coated MMFX steel containing 4% chromium
[b]SE = Sothern Exposure specimen
[c]CB = Cracked beam specimen
[d]B = Beam specimen
[e]RM = Rapid macrocell

3- Studying the effect of supplementary cementitious materials on the critical chloride threshold and corrosion performance of conventional and epoxy-coated reinforcement. The replacing cementitious materials in terms of volume of cement were 5% and 10% of silica fume, 20% and 40% of Class C fly ash, and 20% and 40% of slag cement. The total number of supplementary cementitious materials test specimens in this study is listed in Table 1.4.

Table 1.4: Supplementary cementitious materials (SCM) test specimens

Specimen Designation[a]	B[b]
PC	6
PC-ECR	6
FA(20)	6
FA(40)	6
FA-ECR(40)	6
Slag(20)	6
Slag(40)	6
Slag-ECR(40)	6
SF(5)	6
SF(10)	6
SF-ECR(10)	6
Total	**66**

[a]PC = Conventional bar in concrete containing 100% portland cement
PC-ECR = Epoxy-coated bar in concrete containing 100% portland cement
FA(20) = Conventional bar in concrete containing 20% fly ash and 80% Portland cement by volume
FA(40) = Conventional bar in concrete containing 40% fly ash and 60% portland cement by volume
FA-ECR(40) = Epoxy-coated bar in concrete containing 40% fly ash and 60% portland cement by volume
Slag(20) = Conventional bar in Concrete containing 20% slag cement and 80% portland cement by volume
Slag(40) = Conventional bar in Concrete containing 40% slag cement and 60% portland cement by volume
Slag-ECR(40) = Epoxy-coated bar in concrete containing 40% slag cement and 60% portland cement by volume
SF(5) = Conventional bar in Concrete containing 5% silica fume and 95% portland cement by volume
SF(10) = Conventional bar in Concrete containing 10% silica fume and 90% portland cement by volume
SF-ECR(10) = Epoxy-coated bar in Concrete containing 10% silica fume and 90% portland cement by volume
[b]B = Beam specimen

CHAPTER 2: A COMPARISON BETWEEN CRITICAL CORROSION LOSS OF GALVANIZED AND CONVENTIONAL STEEL

2.1 INTRODUCTION

Corrosion-resistant reinforcement is often used to improve the durability of reinforced concrete. Although epoxy-coated reinforcement is the most common alternative to conventional reinforcement, concerns about potential damage to epoxy-coated reinforcement have led investigators to study the use of other alternatives, such as galvanized reinforcement. Galvanizing protects the underlying steel through two ways. The outer galvanizing can act as a barrier, preventing moisture, oxygen, and chloride ions from reaching the underlying steel. Furthermore, zinc provides protection by serving as a sacrificial anode. The more active metal (zinc) in contact with steel in a homogenous environment will become an anode, corrode, and protect the underlying steel (Jones 1996).

In concrete, zinc reacts with the alkaline pore solution to form zinc hydroxide and hydrogen gas. In concrete with a pH higher than 12.2, zinc hydroxide reacts with calcium hydroxide ($Ca(OH)_2$) to form calcium hydroxyzincate ($Ca(Zn(OH)_3)_2.2H_2O$). In environments with a pH near 12.2, calcium hydroxyzincate produces small compact crystals, which in turn, form a stable passive layer on the surface of the bar. As the pH increases, however, these crystals become larger and more porous; in environments with a pH above 13.3, calcium hydroxyzincate produces large isolated crystals that provide no significant protection, and are not able to protect the underlying layer against corrosion (Andrade & Macias 1988). The passive layer formed by calcium hydroxyzincate can be destroyed in the presence of chloride ions in a manner similar to steel. Carbonation also can destroy the passive layer of calcium hydroxyzincate and form amorphous products of $ZnCO_3$ and $Zn_5(CO_3)_2(OH)_6$ with more limited passivating properties (Roventi et al.

2014). ASTM A767 requires galvanized bars to be submerged in a chromate bath after coating to passivate the zinc surface and prevent reaction of hydroxide ions in fresh concrete with zinc.

Mixed results have been observed about the effectiveness of galvanized bars against corrosion. Teadaway and Davis (1989) showed that concrete containing galvanized bars, after five years of exposure to a sodium chloride environment, were corroded and cracked much more than the specimens containing conventional bars. Sarawathy and Song (2005) investigated the performance of four types of galvanized bars under macrocell corrosion conditions and found that only one type of galvanized bar was more corrosion resistant than conventional steel bars. Conversely, Darwin et al. (2009) compared the critical chloride threshold of concrete specimens containing galvanized bars with conventional steel and showed that the average critical chloride threshold for galvanized reinforcement was 2.57 lb/yd^3 (1.52 kg/m^3), compared to 1.63 lb/yd^3 (0.97 kg/m^3) for conventional reinforcement exposed to the same conditions. Furthermore, O'Reilly et al. (2011) compared the critical corrosion loss required to crack concrete containing galvanized bars with that required for conventional steel bars. No. 5 (No. 16) bars were tested with 0.5 in. (12.7 mm), 1 in. (25.4 mm), and 2 in. (51 mm) concrete cover. A current density of 100-500 μA/cm^2 was applied to the test bars to drive corrosion, while specimens were continuously ponded with deionized water. Results showed that the average critical corrosion loss for galvanized steel was approximately four times that of conventional steel in specimens with 0.5 in. concrete cover, and twice that of conventional reinforcement for specimens with 1 in. and 2 in. concrete cover.

The variation in performance of galvanized reinforcement may be explained by the behavior of oxidized zinc. Hime and Machin (1993) showed that in concrete containing a high concentration of chloride ions, in addition to ZnO (which occupies only 50% more space than zinc

itself), another corrosion product, zinc hydroxychloride II ($Zn[OH]_8Cl_2.H_2O$) (which occupies 260% more space) can form. This expansive corrosion product can exert a greater tensile force on surrounding concrete and cause cracking (Hime & Machin 1993).

The following study continues the research carried out by O'Reilly et al. (2011), and compares the critical corrosion loss required to crack concrete containing galvanized steel with conventional steel, but without applying any external current to accelerate corrosion to further simulate realistic field conditions.

2.2 EXPERIMENTAL PROCEDURE

In this study the critical corrosion loss required to crack concrete containing galvanized bars was investigated and compared with the critical corrosion loss of conventional steel. Six concrete specimens containing galvanized bars and six concrete specimens containing conventional steel (ASTM A615) were cast. Zinc coating in galvanized steel had an average thickness of 6 mil (0.15 mm), and galvanized steel met the requirements of ASTM A767, with the exception that no chromate treatment was applied. Salt equivalent to 2% chloride by weight of cement was introduced to the concrete mix; in addition, specimens were ponded with a 15% salt solution during testing to accelerate corrosion and provide a chloride gradient. Corrosion rates of the specimens were monitored, and upon observation of a crack on the concrete surface, specimens were autopsied to evaluate the actual corroded area of the steel that caused the crack. Finally, the measured critical corrosion loss needed to crack specimens with conventional bars was calculated and compared to the critical loss when galvanized steel bars were used.

2.2.1 Preparation of Concrete Specimens

The concrete mix used in this study contained type I/II portland cement with water-cement ratio (w/c) of 0.45, an air content of 5.1%, and a slump of 3 in. (76 mm). The unit weight of mixed concrete was 144.1 pcf (2308 kg/m^3), and the average 28-day concrete compressive strength was 4490 psi (31 MPa). Aggregate properties and mixture proportions are shown in Table 2.1. To destabilize the passive layer of reinforcement and increase the ionic conductivity of concrete, equivalent amount of sodium chloride to provide 2% chloride with respect to cement weight was added to the mixture by dissolving it in the mix water prior to casting.

Table 2.1: Mix proportions (SSD basis)

Water lb/yd^3 (kg/m^3)	**Cement lb/yd^3 (kg/m^3)**	**Coarse Aggregate lb/yd^3 (kg/m^3)**	**Fine Aggregate lb/yd^3 (kg/m^3)**	**Air-entraining Agent oz/yd^3 (mL/m^3)**	**NaCl, lb/yd^3 (kg/m^3)**
269 (160)	598 (355)	1484 (880)	1435 (851)	4.73 (183)	19.8 (11.7)

Bulk specific gravity of fine aggregate = 2.63
Bulk specific gravity of Coarse aggregate = 2.59

The specimens used in this study were identical to those used by O'Reilly et al. (2011), with the exception that no external current was applied to the specimens. Six prismatic test specimens containing galvanized bars as well as six specimens containing conventional steel with dimensions 6 × 7 × 12 in. (152 × 178 × 305 mm), shown in Figure 2.1, were used in this study. To allow the specimens to be ponded with salt solution, a 0.75 in. (19 mm) concrete dam was cast integrally with the specimens. Specimens were fabricated and cast in an inverted position. Concrete was placed in two layers, and each layer was consolidated by internal vibration. Two mats of 12-in. (305 mm) long No. 5 (No. 16) bars were used in each specimen, with one bar as the top mat and two bars as the bottom mat. The clear concrete cover to the bars was 1 in. (25.4 mm), and bars were centered within the prism. The top bar was electrically connected to the bottom bars

through external wiring across a 10-ohm resistor placed in a terminal box for the macrocell corrosion rate measurement. After casting, specimens were wet cured for 3 days and air cured for 25 days thereafter. Ponding and lab tests began 28 days after casting; a linear polarization resistance (LPR) test was performed after 14 days to monitor any early corrosion from the admixed salt.

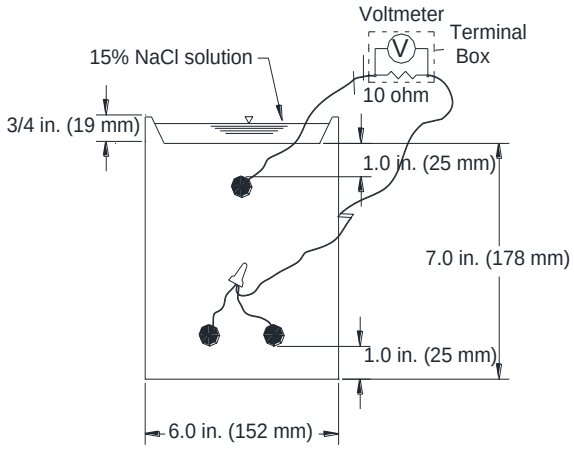

Figure 2.1— Beam specimens

2.2.2 Test Procedure

The test procedure consisted of 12 weeks of wet-dry cycles followed by 12 weeks of continuously wet cycles. These two regimes were alternated and repeated until cracking was visually observed on the surface of the concrete. During wet-dry cycles, specimens were ponded with 15% NaCl solution and maintained at ambient room temperature for four days. At this point, corrosion measurements including macrocell corrosion rate, corrosion potentials, and linear polarization resistance (LPR) test were taken, the salt solution was vacuumed off from the surface of the concrete specimens, and specimens were placed under a heat tent at 100 ± 3 °F (38 ± 2 °C) for three days. This procedure was repeated for 12 weeks. At this point, specimens entered a continuously wet cycle, where specimens were ponded continuously with 15% NaCl solution and

kept covered at ambient room temperature for 12 weeks. Readings were taken every week during wet cycles similar to that of wet-dry cycles. Deionized water was added to the concrete surfaces as needed, to replace water lost due to evaporation.

2.2.3 Corrosion Measurements

The following measurements were taken on each specimen on a weekly basis. To obtain a macrocell corrosion rate, which depends on the current or the electron flow from anode to cathode, the voltage drop between the top and bottom mat of each specimen was taken across a 10-ohm resistor. The current density per unit area between two mats can be obtained by Ohm's Law:

$$i_{corr} = 10^6 \times \frac{V}{RA} \tag{2.1}$$

where i_{corr} is current density (μA/cm^2); V is the measured voltage drop across the resistor (volts); R is the resistance of resistor (10 ohms); and A is the surface area of anode, the top mat in this test, (cm^2). Corrosion rate can be expressed as the thickness loss of steel per time. The relationship between current density and thickness loss is shown below per Faraday's Law:

$$r = k\frac{ia}{nF\rho} \tag{2.2}$$

where r is the corrosion rate (μm/year); k is a conversion factor (315360 (A.μm.s)/(μA.cm.yr)); a is the atomic weight of the corroding metal (g/mol); n is the number of electrons lost per atom of metal oxidized (2 for iron or zinc); F is Faraday's constant (96485 Coulombs/equivalent); and ρ is the density of metal (g/cm^3). By substituting proper values, for iron Eq. (2.2) simplifies to $r = 11.6i$ in μm/yr ($0.457i$ in mils/yr), and for zinc Eq. (2.2) simplifies to $r = 15.0i$ in μm/yr ($0.591i$ in mils/yr).

After measuring the voltage drop, the connection between the top and bottom mat across the resistor was disconnected for at least two hours to allow the potentials to stabilize, and then the corrosion potential of the top and bottom mat was measured.

In addition to the weekly corrosion potential measurements, linear polarization resistance (LPR) was measured on a monthly basis for each specimen. Linear polarization resistance is used to measure the total corrosion rate of the top mat bar of the specimen, including both macrocell corrosion rate, where the top mat is the anode and the bottom mat is the cathode, as well as microcell corrosion rate, where the anode and cathode are both located on the top mat. In a corroding specimen, both forms of corrosion are present simultaneously, and voltage drop readings will not measure microcell corrosion. The LPR test was accomplished using a computer-controlled corrosion measurement system connected to a potentiostat comprised of a working electrode (corroding reinforcement), a counter electrode (platinum rod), and a reference electrode (calomel electrode). The potentiostat controls the voltage difference between the working electrode and reference electrode in a system, and the counter electrode is used to apply current to that system. By applying external voltage, corrosion potential of the system can be shifted by ($\Delta\varepsilon$) with respect to E_{corr} (-20 mV to 20 mV for this test), resulting in a change in the current density (Δi). The obtained data are plotted as a potential-current curve via software in the connected computer. In the vicinity of the equilibrium potential (in a range from -10 mV to 10 mV with respect to E_{corr}), the potential-current curve is linear and the slope of the curve is defined as the linear polarization resistance (R_p). The linear polarization resistance is inversely proportional to the corrosion current density according to Stern-Geary equation:

$$i_{corr} = \frac{\beta_a \beta_c}{2.3 R_p (\beta_a + \beta_c)} \tag{2.3}$$

Where β_a and β_c are anodic and cathodic Tafel constants, taken as 0.12 V/decade for reinforcing steel in concrete ((Lambert et al. 1991, McDonald et al. 1998). By using these values, the current density in Eq. (2.3) is simplified to:

$$i_{corr} = \frac{0.026}{R_p} \tag{2.4}$$

2.3 TEST RESULTS

Macrocell corrosion rates calculated from voltage drops for galvanized and conventional steel are shown in Figures 2.2 and 2.3, respectively. As mentioned before, testing terminated for a specimen upon observation of a crack on its surface; the specimen was then autopsied to estimate the corroded area of the top bar. For galvanized bars, the average macrocell corrosion rate increased from 7 μm/yr at week 1 to 15 μm/yr at week 25, and then became roughly steady until week 56, after which the rate decreased to values between approximately 5 and 10 μm/yr. The highest macrocell corrosion rate before cracking for specimens with galvanized steel was 33.9 μm/yr at week 25 for Specimen Zn-5. Specimens containing conventional steel generally had a corrosion rate ranging from 3 to 5 μm/yr before cracking. For Specimen Conv-4, the corrosion rate increased after week 20 up to 21.3 μm/yr at week 25. Specimens 1 through 6 containing conventional steel cracked at week 16, 21, 19, 27, 22, and 22, respectively, with an average age at cracking of 21 weeks. Specimens containing galvanized bars took approximately four times as long to crack. Specimens with galvanized reinforcement cracked after week 84, 78, 75, 82, 78, and 78, with an average age at cracking of 79 weeks.

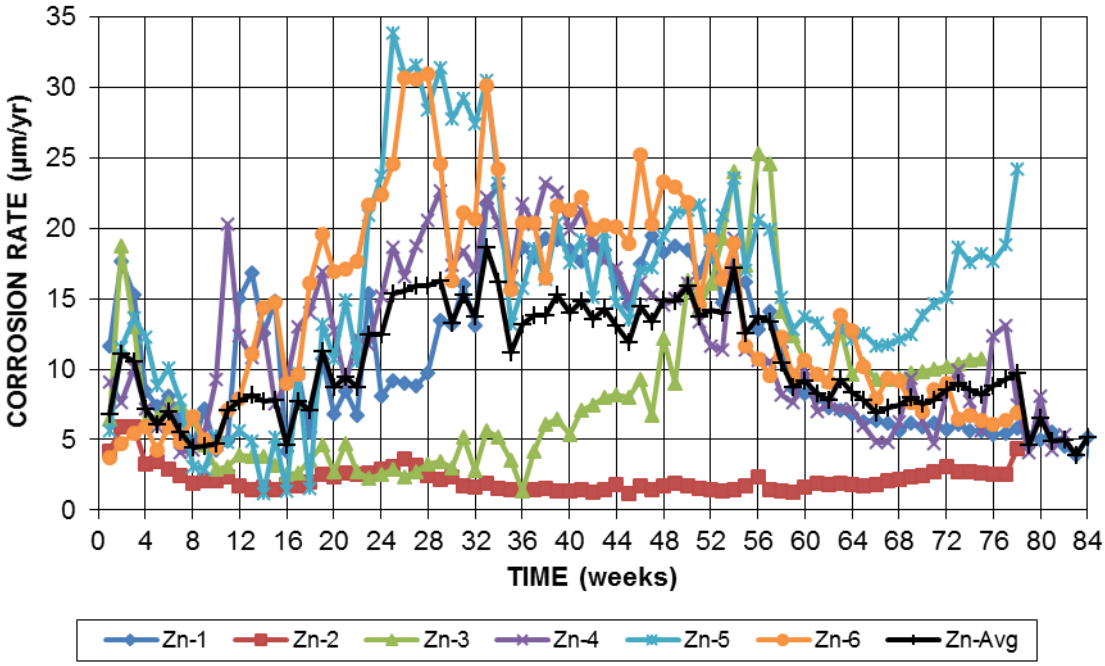

Figure 2.2— Macrocell corrosion rates (µm/yr) for beam specimens containing galvanized steel

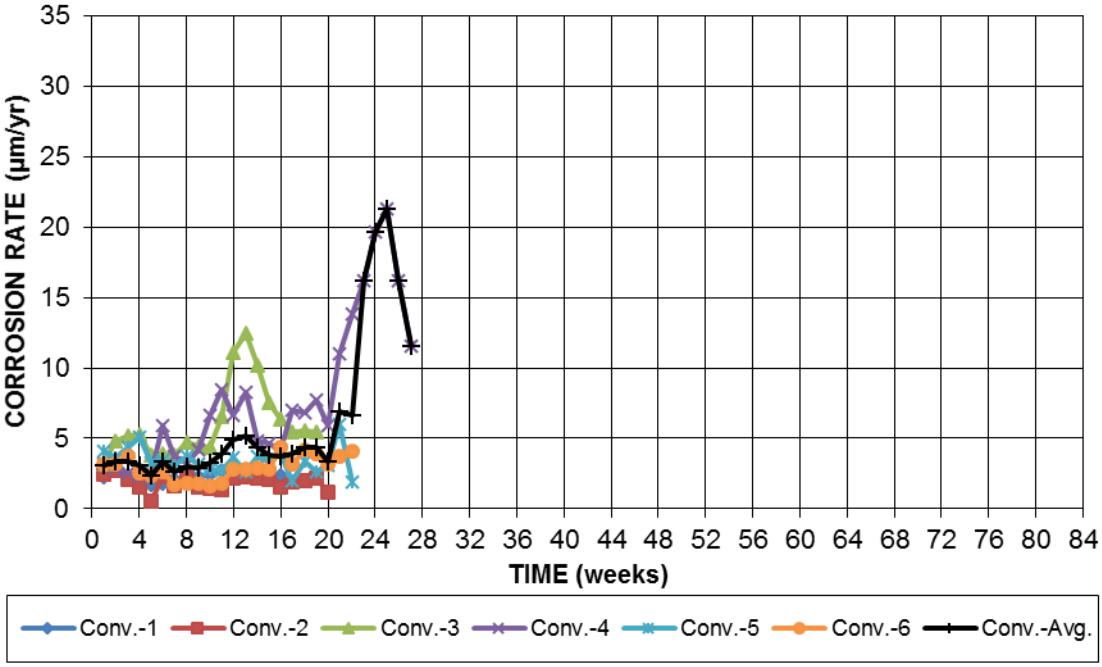

Figure 2.3— Macrocell corrosion rates (µm/yr) for beam specimens containing conventional steel

Figures 2.4 and 2.5 show the corrosion loss for specimens containing galvanized and conventional steel, obtained by integrating their macrocell corrosion rates with respect to time. For galvanized steel critical corrosion losses ranged from 3.3 to 23.3 μm with the average, standard deviation, and coefficient of variation as 16.3 μm, 7.6 μm, and 0.465, respectively. For conventional steel, critical corrosion losses ranged from 0.7 to 4.1 μm with 1.7 μm, 1.3 μm, and 0.73, as the average, standard deviation, and coefficient of variation, respectively. For conventional bars, however, the obtained critical corrosion loss values needed to be modified based on the fact that corrosion was not uniform over the entire surface of the bar, as assumed in Eqs. (2.1) and (2.2), but rather it was localized to a portion of the bar. Critical corrosion loss obtained from macrocell corrosion rates for specimens containing conventional steel are modified based on the actual percent corroded surface area for each bar and tabulated in Table 2.2. The high coefficient of variation for critical corrosion loss obtained from macrocell corrosion rates for both specimens containing conventional and galvanized bars could be due to the fact that total critical corrosion loss includes microcell corrosion in addition to the measured macrocell corrosion. To account for the microcell corrosion (when anode and cathode are on the same bar), corrosion losses of galvanized and conventional bars were compared based on the corrosion rates obtained from the LPR test.

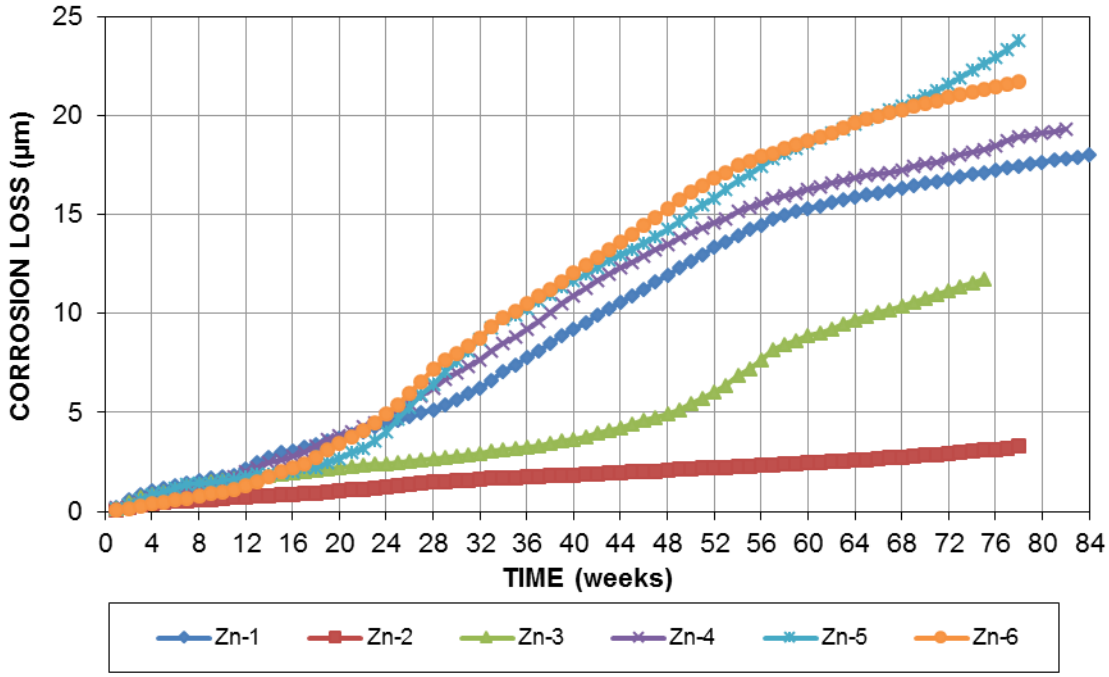

Figure 2.4— Corrosion loss (µm) for beam specimens containing galvanized steel

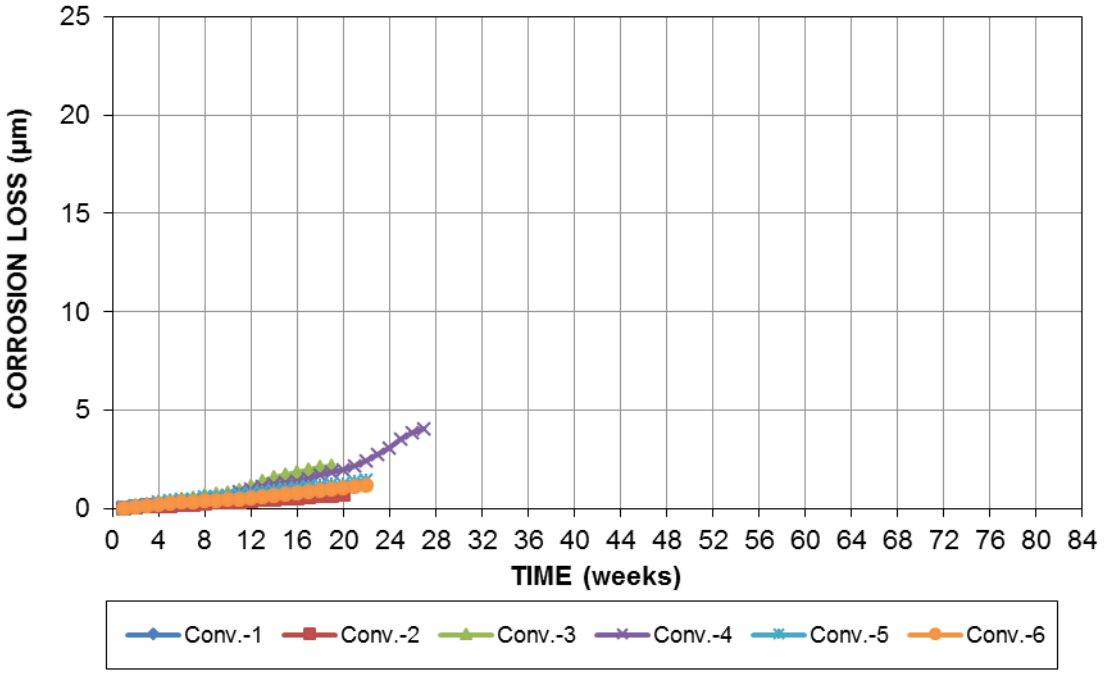

Figure 2.5— Corrosion loss (µm) for beam specimens containing conventional steel

Table 2.2: Modified critical corrosion loss of conventional steel based on actual corroded surface area from macrocell corrosion results.

Conventional steel	Specimen						Average	Standard Deviation
	1	2	3	4	5	6		
Corroded Area (%)	20	25	35	20	15	30	24	7
Uniform corrosion loss (µm)	0.72	0.72	2.2	4.1	1.5	1.2	1.7	1.3
Modified corrosion loss (µm)	3.6	2.9	6.3	20.3	9.7	4.1	7.8	6.6

The average top mat corrosion potentials (with respect to a copper-copper sulfate electrode) of specimens containing conventional and galvanized reinforcement are shown in Figure 2.6. For specimens containing conventional steel, the average top mat potential ranged from –0.525 V at the beginning of the test to –0.573 V at the end life. For galvanized steel, however, the average potential was more negative at the start of the test (–0.630 V) than conventional steel. By week 28, no significant difference in top mat potential was observed between conventional and galvanized reinforcement.

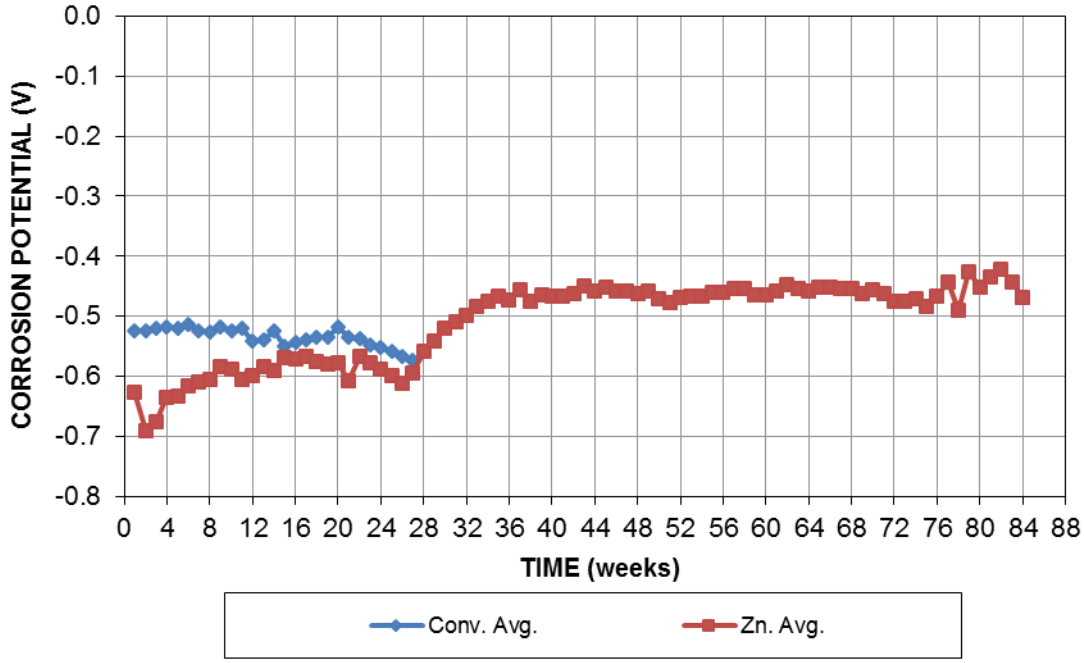

Figure 2.6— Average corrosion potentials (V) for top mat of beam specimens containing conventional and galvanized steel

Corrosion rates obtained from LPR test results on specimens with galvanized and conventional bars are shown in Figures 2.7 and 2.8, respectively. For specimens with galvanized reinforcement the average corrosion rate at week 0 (taken two weeks after casting and before the top and bottom mats were electrically connected) was 1.2 µm/yr; the corrosion rate for the specimens then increased to between 8 and 10 µm/yr by week 24 and generally remained constant until cracking. Specimen Zn-3, however, exhibited corrosion rates as high as 16 µm/yr. For conventional steel, the initial corrosion rates were greater (8 µm/yr) than galvanized reinforcement (1.2 µm/yr). The corrosion rate for the specimens increased approximately to 15 µm/yr after 12 weeks and generally remained constant until specimens cracked.

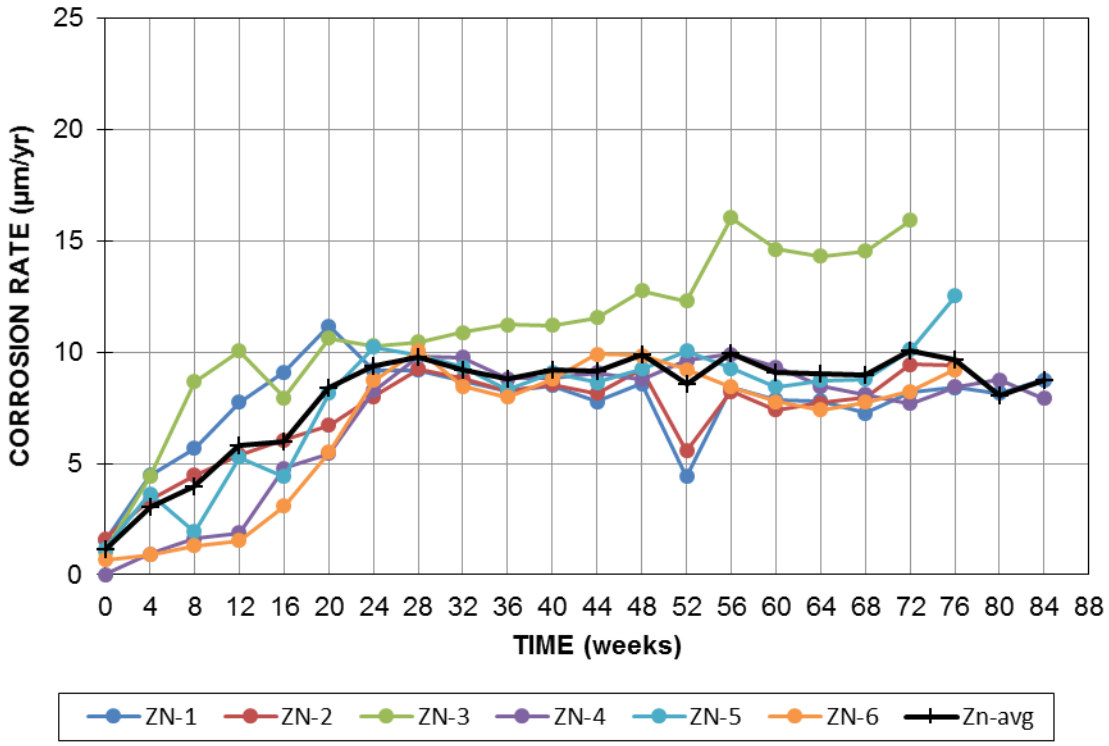

Figure 2.7— LPR test Corrosion rates (µm/yr) for beam specimens containing galvanized steel

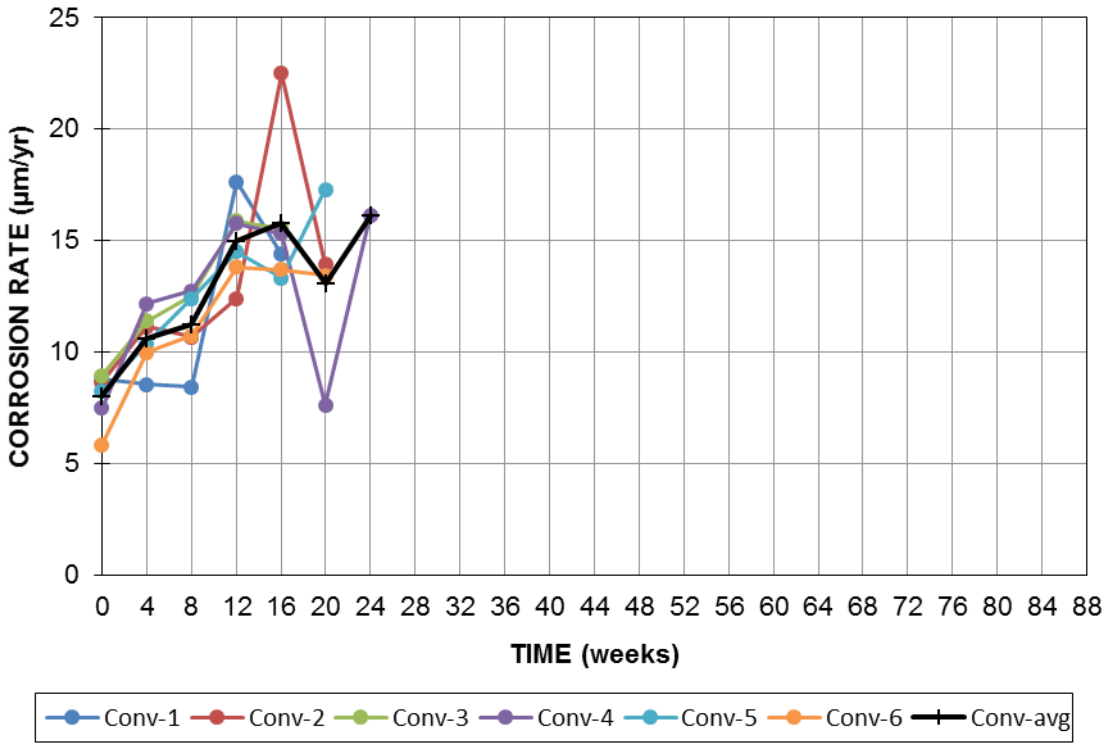

Figure 2.8— LPR test corrosion rates (µm/yr) for beam specimens containing conventional steel

By integrating corrosion rates from LPR tests with respect to time, the corrosion loss for each specimen can be obtained. Figures 2.9 and 2.10 present the amount of corrosion loss over time for specimens containing galvanized and conventional steel, respectively. Critical corrosion loss, the thickness loss of metal that is required to crack concrete, is tabulated in Table 2.3. The average, standard deviation, and coefficient of variation of critical corrosion loss of conventional steel are 5.5 µm, 0.8 µm, and 0.15, respectively. For galvanized steel, the average critical corrosion loss is 12.4 µm, 2.25 times as much for the one for conventional steel (The standard deviation and coefficient of variation were 2.0 µm and 0.16, respectively.).

Table 2.3: Critical corrosion loss based on LPR test results

Corrosion Loss (µm)	Specimen						Average	Standard Deviation
	1	2	3	4	5	6		
Conventional	4.4	6.1	4.9	6.7	5.9	5.2	5.5	0.8
Galvanized	13.0	11.0	16.1	12.0	12.1	10.4	12.4	2.0

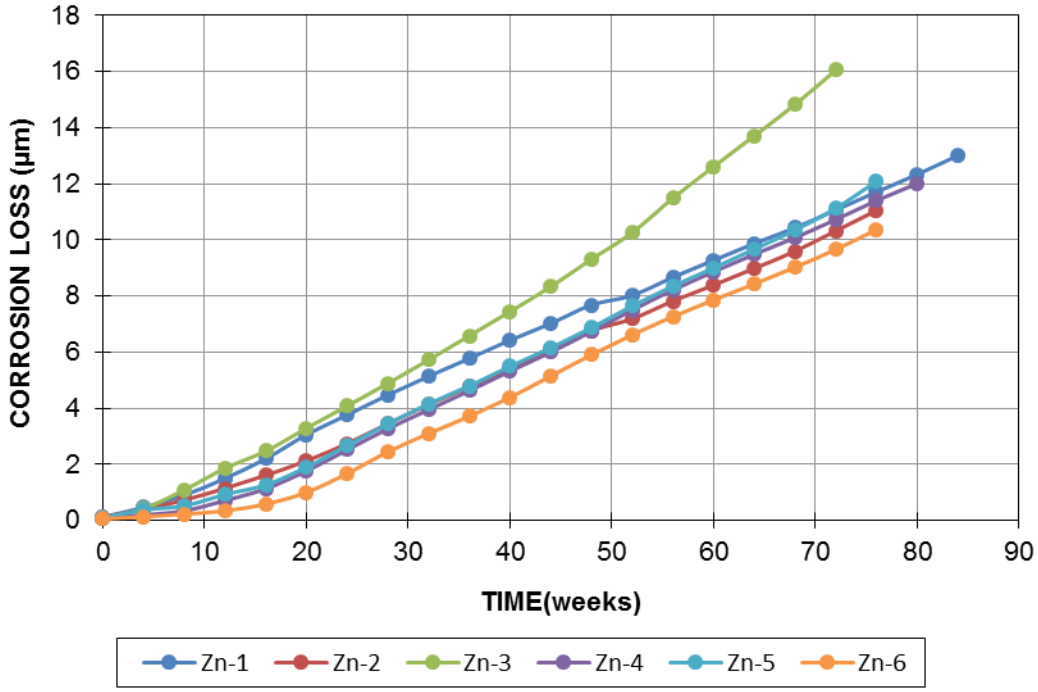

Figure 2.9— LPR test corrosion losses (µm) for beam specimens containing galvanized steel

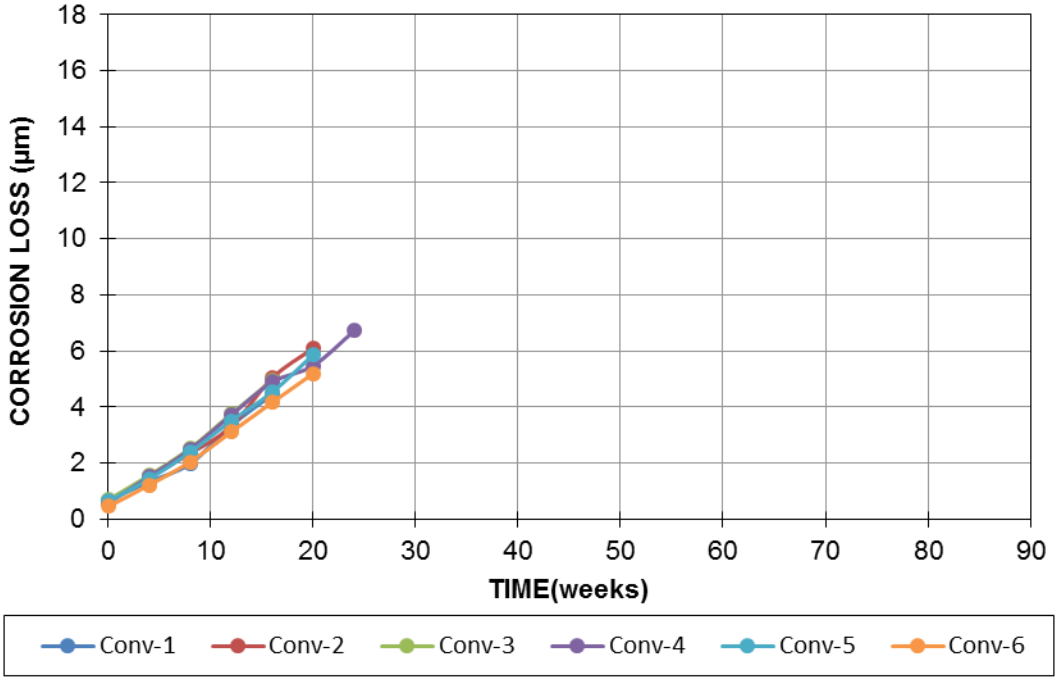

Figure 2.10— LPR test corrosion losses (µm) for beam specimens containing conventional steel

Upon observation of cracking, specimens were removed from testing and autopsied to evaluate and measure the corroded surface area of the top bar. The top and bottom face of a representative conventional bar is shown in Figures 2.11 and 2.12, and a galvanized bar in Figures 2.13 and 2.14, respectively. As mentioned before, for conventional anode bars, the corrosion was not uniform over the entire surface area, as assumed in Equations (2.1) and (2.2), but rather was limited to a portion of the bar. The actual partial corroded area and length of the conventional bars are tabulated in Table 2.4. Based on the percent corroded surface area, the critical corrosion loss obtained from LPR results was modified; these results are presented in Table 2.4. For conventional reinforcement, the average critical corrosion loss required to cause a crack in concrete specimens with 1 in. clear concrete cover based on corroded area of the bar was 25.1 µm. On the other hand, the galvanized bar exhibited corrosion over the entire surface area (Figures 2.13 and 2.14). The brown corrosion products seen on the bar surface are due to the corrosion of underlying steel. The estimated corroded area of underlying steel in galvanized bars were 5, 8, 10, 5, 5, and 10% respectively, with an average of 7%.

Table 2.4: Modified critical corrosion loss of conventional steel based on actual corroded surface area from LPR test results

Conventional steel	Specimen						Average	Standard Deviation
	1	2	3	4	5	6		
Corroded Length (%)	75	67	75	58	67	83	71	8.7
Corroded Area (%)	20	25	35	20	15	30	24	7
Uniform corrosion loss (µm)	4.4	6.1	4.9	6.7	5.9	5.2	5.5	0.8
Modified corrosion loss (µm)	22.0	24.4	14.0	33.5	39.3	17.3	25.1	9.7

Figure 2.11— Top conventional steel bar of specimen Conv-4 after autopsy (top face)

Figure 2.12— Top conventional steel bar of specimen Conv-4 after autopsy (bottom face)

Figure 2.13— Top galvanized bar of specimen Zn-5 after autopsy (top face)

Figure 2.14— Top galvanized bar of specimen Zn-5 after autopsy (bottom face)

2.4 DISCUSSION

The average time to crack initiation for galvanized bars was 79 weeks; almost 4 times greater than that of conventional reinforcement (21 weeks).

The average corrosion losses at crack initiation based on the LPR tests for specimens with galvanized and conventional reinforcement (Fig. 2.9 and 2.10, respectively) show that the loss to crack concrete for specimens with galvanized reinforcement, 12.4 μm, is 2.25 times greater than the ones with conventional steel (5.5 μm). These results, which are based on the assumption that the whole embedded surface area of the bar is corroding, suggest concrete containing galvanized reinforcement will exhibit a greater service life after initiation than concrete containing conventional reinforcement. While comparing losses based on total area is valid for comparing the relative performance of conventional and galvanized bars, establishing the accuracy of previously developed predictive equations requires correcting for the percent corroded area of the bars.

For conventional reinforcement, correcting for corroded area gives an average corrosion loss of 25.1 μm at crack initiation. For the galvanized bars, the observed average corroded area of the underlying steel was about 7%, in addition to the uniform corrosion of zinc coating, after autopsy. Since determining the proportional effect of corroded zinc and steel on the crack generation is not feasible in these bars, modification of the corrosion losses of galvanized bars based on the corroded surface area is not possible.

O'Reilly et al. (2011) compared the critical corrosion loss of galvanized reinforcement with conventional steel for concrete specimens with 0.5, 1, and 2 in. concrete cover, and showed that for 1 in. cover, similar to concrete cover used in this study, the critical corrosion loss for specimens with galvanized steel, 49.7 μm, is twice of that for conventional steel (22.4 μm). In O'Reilly's study, corrosion was driven by applying an external current, resulting in near uniform corrosion. However, in this study, no external current was applied to the specimens, and the observed corrosion was not uniform. However the critical corrosion loss for conventional steel for concrete with 1 in. clear cover based on O'Reilly's study (22.4 μm) is in close agreement with the modified critical corrosion loss based on the actual corroded area of the bar in this report (25.1 μm). In addition, the results of both studies show the ratio of critical corrosion loss of galvanized reinforcement with respect to conventional steel as about 2.

There are several equations that have been developed in the literature to predict the critical corrosion loss for conventional steel to crack concrete based on concrete cover-rebar diameter ratio. To compare the obtained critical corrosion loss for conventional steel with other studies, three equations introduced by other researchers to predict the critical corrosion loss are considered. Alonso et al. (1998) showed the corrosion loss required to generate the first visible crack is linearly proportional to the cover-rebar diameter ratio (c/d) and can be obtained by:

$$x_{crit} = 7.53 + 9.32\,c/d \tag{2.5}$$

where x_{crit} is corrosion loss at crack initiation, (μm), c is concrete cover, (mm), and d is bar diameter, (mm). This equation is only applicable for the cases where uniform corrosion occurs over the surface of embedded steel. Torres-Acosta and Sagues (2004) introduced a new equation that accounts for the corroded length of steel in addition to cover-bar diameter ratio:

$$x_{crit} = 11.0\frac{c}{d}\left(\frac{c}{l}+1\right)^2 \tag{2.6}$$

where l is length of the corroded region (mm) and other parameters are as described in Eq. (2.5). For cases approximating uniform corrosion, Eq. (2.6) can be simplified to:

$$x_{crit} = 11.0\,c/d \tag{2.7}$$

In the study by O'Reilly et al. (2011) a relationship between corrosion loss at crack initiation, concrete cover, and bar diameter for localized corrosion as well as general corrosion was introduced:

$$x_{crit} = 0.53\left(\frac{C^{2-A_f}}{D^{0.38}L_f{}^{0.1}A_f{}^{0.6}} + 0.6\right)\times 3^{A_f-1} \tag{2.8}$$

Where, x_{crit} is corrosion loss at crack initiation, (mil), C is concrete cover, (in.), D is bar diameter (in.), L_f is fractional length of corroded bar, ($L_{\text{corroding}}/L_{\text{bar}}$), and A_f is fractional area of corroded bar, ($A_{\text{corroding}}/A_{\text{bar}}$). For general corrosion, as fractional area and length of bar corroding are equal to 1 ($A_f = 1$, $L_f = 1$), Equation (2.8) can be simplified to:

$$x_{crit} = 0.53\left(\frac{C}{D^{0.38}} + 0.6\right) \tag{2.9}$$

By using the actual corroded length and area of the conventional steel upon crack initiation and applying those in Equations (2.6) and (2.8), the critical corrosion losses based on Torres-Acosta's and O'Reilly's equations were calculated and tabulated in Table 2.5. These obtained values are based on the actual localized corrosion visualized after autopsy, and not the uniform corrosion. There is only 5% difference between the average predicted critical corrosion loss obtained from Torres' (22 μm) and O'Reilly's (21 μm) equations; these values vary from the value obtained from testing (25.1 μm) by 12% and 16%, respectively.

Table 2.5: Critical corrosion loss of conventional steel based on actual corroded surface area and length from predictive equations and LPR test results

Conventional steel	Specimen						Avg[a]	SD[b]	COV[c]
	1	2	3	4	5	6			
Corroded Length (%)	75	67	75	58	67	83	71	8.7	0.12
Corroded Area (%)	20	25	35	20	15	30	24	7	0.29
Torres corrosion loss (μm)	21.7	22.3	21.7	23.0	22.3	21.3	22.0	0.59	0.03
O'Reilly corrosion loss (μm)	21.4	20.4	19.2	21.9	23.7	19.4	21.0	1.71	0.08
LPR test corrosion loss (μm)	22.0	24.4	14.0	33.5	39.3	17.3	25.1	9.7	0.39

[a]Avg = average
[b]SD = standard deviation
[c]COV = coefficient of variation

The critical corrosion losses obtained from predictive equations and presented in Table 2.5 were calculated based on the actual corroded surface area of bar; however, by assuming existence of uniform corrosion instead of localized corrosion along the corroded bar, Alonso's equation (Eq. 2.5) predicts 22.4 μm loss, Torres-Acosta's equation (Eq. 2.7) gives 17.6 μm, and O'Reilly's equation (Eq. 2.9) predicts 24 μm. Comparing these values with the critical corrosion loss obtained in this study (25.1 μm), Equations 2.5, 2.7, and 2.9 vary from experimental data by 11%, 30%, and 4%, respectively.

2.5 CONCLUSIONS

The following conclusions are drawn based on the results presented in this report:

1- Galvanized reinforcement required over twice the corrosion loss and took almost four times as long to crack concrete as specimens with conventional reinforcement. Thus, concrete with galvanized steel exhibits greater life expectancy compared to conventional steel in terms of crack generation on the concrete surface.

2- By accounting for actual localized corroded area and length on the conventional bars, the predicted critical corrosion loss obtained from Torres-Acosta's and O'Reilly's equations (22 and 21 μm, respectively) are in close agreement for 1 in. concrete cover specimens.

3- The modified average critical corrosion loss that is needed for conventional steel to crack a 1 in. concrete cover, based on the actual corroded area of the steel, is found to be approximately 25 μm, very close to the O'Reilly's test result (22.4 μm) and his predictive equation (21 μm taking localized corrosion into account, and 24 μm assuming general corrosion), as well as the equation developed by Torres-Acosta.

4- For galvanized bars at the time of crack generation, uniform corrosion of zinc and localized corrosion of underlying steel were observed on the surface of reinforcement.

CHAPTER 3: EVALUATION OF CORROSION PERFORMANCE OF MMFX BARE AND EPOXY-COATED BARS

3.1 INTRODUCTION

One method of improving the corrosion resistance of concrete structures is to use more corrosion resistant reinforcement, such as stainless steel or epoxy-coated reinforcement; the latter of which is one of the most common corrosion protection systems for reinforcing steel. Stainless steel reinforcement is a corrosion resistant steel that is alloyed with more than 11% chromium and often with the addition of nickel. The added chromium reacts with oxygen to produce a passive layer of chromium oxide that protects the reinforcement from corrosion. This passive layer is chemically stable and can self-repair as long as sufficient oxygen is available at its surface. Formation of chromium oxide around steel can be assisted and stabilized by washing the steel surface with particular acid solutions such as nitric acid (HNO_3) and hydrofluoric acid (HF) in a process called pickling. Epoxy coatings, on the other hand, prevent corrosion by forming a physical barrier against moisture, chlorides, and oxygen, as well as by acting as an electrical insulator.

Although stainless steel and epoxy-coated reinforcement have showed significantly greater resistance against corrosion compared to conventional reinforcing bars, there are still some concerns with their use. Epoxy-coated bars may contain holidays from the manufacturing process and also have the potential to get damaged during shipping, fabricating, and casting concrete. This damage can result in localized corrosion and disbondment of the coating. For stainless steel, the high chromium and nickel content results in a product with a greater initial cost than other systems.

These concerns have led investigators to look for other less expensive alternatives, such as microcomposite steel. Microcomposite steel is a duplex-phase steel (dislocated packet laths of

martensite surrounded by austenite films) containing chromium, but at a lower percentage than stainless steel. Microcomposite steel was first introduced by MMFX Steel Corporation of America and has been claimed to be more corrosion resistant than conventional steel by its manufacturers due to its different chemical composition and production process, which minimizes the formation of microgalvanic cells between ferrites and carbides in conventional steel (Ji et al. 2005).

ASTM A1035 has classified low carbon, chromium bars into three different categories based on their chromium content: type CL with 2 to 3.9% chromium, type CM with 4 to 7.9% chromium, and type CS with 8 to 10.9% chromium. Most of the research on MMFX has been performed on steel with a 9% chromium content (ASTM A1035 Type CS). This reinforcement was first used in 2001 in part of a bridge in Iowa with another section fabricated with conventional epoxy-coated reinforcement as a control (Wipf et al. 2006). The initial corrosion current of the epoxy-coated bars was six times that of the MMFX bars in the first 150 days of casting (the corrosion current in the epoxy-coated bars stabilized thereafter). The initial higher corrosion current was attributed to defects in coating of the epoxy-coated bars (Wipf et al. 2006). In addition to the field test, MMFX and conventional epoxy-coated bars were tested in accelerated laboratory conditions (ASTM G109) for 40 weeks. No signs of corrosion were observed for MMFX and undamaged conventional epoxy-coated bars, but intentionally damaged epoxy-coated bars exhibited signs of corrosion within 15 to 30 weeks (Wipf et al. 2006). Gong et al. (2003) compared the corrosion performance of 9% chromium MMFX bars (type CS) with that of conventional epoxy-coated and bare bars. Reinforcement was evaluated using the rapid macrocell test and two bench-scale techniques, the Southern Exposure and cracked beam tests. Gong et al. showed that although MMFX steel exhibited improved corrosion resistance–its corrosion rate was between one-third and two-thirds that of conventional uncoated steel–it is not as corrosion resistant as the

intentionally damaged conventional epoxy-coated steel (which exhibited corrosion rates between 5% and 25% that of conventional steel). In a study by Clemana and Virmani (2004), the corrosion rate of MMFX bars was reported to be one-third of conventional steel. Clemana and Virmani reported a time for corrosion of MMFX bars almost 2.6 times greater than conventional steel reinforcement. Akhoondan and Sagues (2012) investigated the cathodic behavior of 9% chromium steel and showed that the 9% chromium alloy was a considerably weaker cathode than conventional steel, and therefore more corrosion resistant.

Darwin et al. (2002) evaluated and compared the corrosion performance of 9% chromium MMFX bars with uncoated and epoxy-coated conventional reinforcement. Lab results and bridge replacement costs from South Dakota were used to evaluate the life expectancy and cost effectiveness of the reinforcement. Results showed that bridge decks containing MMFX steel will require repair approximately 30 years after construction, compared to 10 to 25 years for conventional steel and 40 years for epoxy-coated reinforcement. However, the time to first repair for epoxy-coated reinforcement was estimated based on the observation that no bridge built with epoxy-coated reinforcement in South Dakota has required repair. A cost comparison showed that bridge decks containing MMFX steel do not appear to be cost effective compared to bridge decks containing epoxy-coated reinforcement (Darwin et al. 2002). Ji et al. (2005) reported the critical chloride threshold of 9% MMFX bars ranging from 4.72 to 6.86 lb/yd^3 (2.8 to 4.07 kg/m^3), three to four times that of uncoated conventional steel (1.53 to 2.05 lb/yd^3 (0.91 to 1.22 kg/m^3)). Ji et al. showed that although the corrosion loss of MMFX bars ranged from 16% to 66% that of uncoated conventional bars it is not as low as intentionally damaged epoxy-coated bars, which ranged from 0.4% to 6% of the corrosion loss for conventional steel. Ji et al. estimated the service life of the

bridge decks (including the time to corrosion initiation and the time to concrete cracking) for decks containing MMFX and conventional bars as 35 and 12 years, respectively (Ji et al. 2005).

Although the corrosion resistance of MMFX bars containing 9% chromium (type CS of A1035) has been studied in the literature, corrosion performance of other types of A1035 steel (those with less than 9% chromium content) has not been well studied; nor has the performance of epoxy-coated MMFX bars of any type. This paper will evaluate the corrosion performance of uncoated A1035 type CM and CS bars containing 4% and 9% chromium, respectively, as well as epoxy-coated A1035 type CL and CM bars containing 2% and 4% chromium, respectively. The performance of these bars will be compared with that of conventional bare and epoxy-coated bars.

3.2 EXPERIMENTAL PROCEDURE

Four types of bars were tested in this study; uncoated MMFX bars containing 9% and 4% chromium (ASTM A1035 type CS and CM, respectively) and epoxy-coated MMFX bars containing 4% and 2% chromium (ASTM A1035 type CM and CL, respectively). The chemical composition of the bars is provided in Table 3.1.

Table 3.1: Chemical composition of MMFX bars

Specimen	Chemical Composition of Product (%Wt)										
	C	Si	Mn	P	S	Cr	Ni	Cu	Mo	V	N(PPM)
MMFX(9%)	0.072	0.244	0.82	0.023	0.0028	9.46	0.129	0.078	0.019	0.02	110
MMFX(4%)	0.143	0.243	0.66	0.02	0.0028	4.05	0.073	0.081	0.011	0.0093	110
MMFX-ECR(4%)	0.14	0.22	0.66	0.026	0.003	4.03	0.06	0.09	0.001	0.011	145
MMFX-ECR(2%)	0.264	0.242	0.73	0.02	0.0012	2.09	0.071	0.087	0.011	0.0064	68

Four tests were used to evaluate the reinforcement in this study; the rapid macrocell test, the cracked beam test, the Southern Exposure test, and a modified Southern Exposure test, referred to as a beam specimen.

3.2.1 Southern Exposure, Cracked Beam, and Beam Specimens

3.2.1.1 Description

Three types of prismatic concrete specimens were cast in this study. Southern Exposure (SE) specimens (shown in Figure 3.1) have dimensions of 12 × 12 × 7 in. (305 × 305 × 178 mm). Two layers of reinforcement were used in the specimens, top mat and bottom mat consisted of two and four No. 5 (No. 16) reinforcing bars, respectively. Bars were 12 in. (305 mm) long with 1 in. (25 mm) clear cover, spaced at 2.5 in. (64 mm) and centered within the prism. Top and bottom mats were electrically connected through a terminal box across a 10-ohm resistor via external wiring to allow for macrocell corrosion rate measurements. To allow the specimens to be ponded with salt solution, a 0.75 in. (19 mm) concrete dam was cast integrally with the specimens.

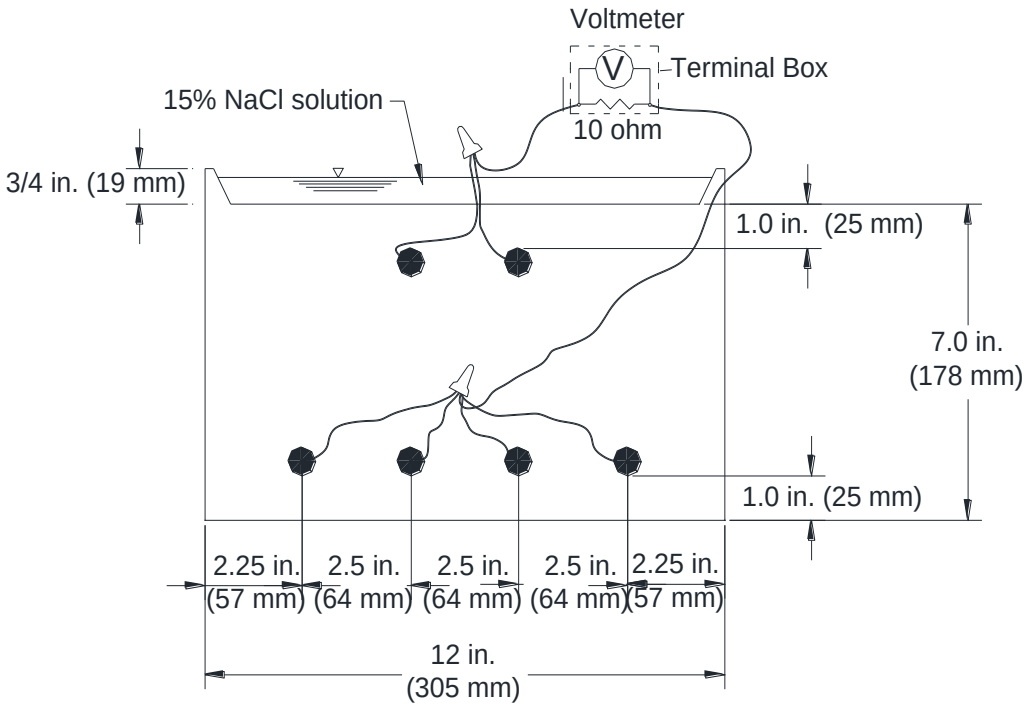

Figure 3.1– Southern Exposure (SE) specimen

Cracked beam (CB) and beam (B) specimens are half the width of Southern Exposure specimens and consist of two mats; the top mat is comprised of a single No. 5 (No. 16) bar and the

bottom mat consists of two No. 5 (No. 16) bars. For cracked beam specimens, a simulated crack was made by inserting a 12 mil (0.3 mm), 6 in. (151 mm) long stainless steel shim centered into the mold and in contact with the top bar prior to casting. The shim was removed 24 hours after casting. Beam specimens were similar to cracked beam specimens, but contained no crack. Cracked beam and beam specimens are shown in Figures 3.2 and 3.3, respectively.

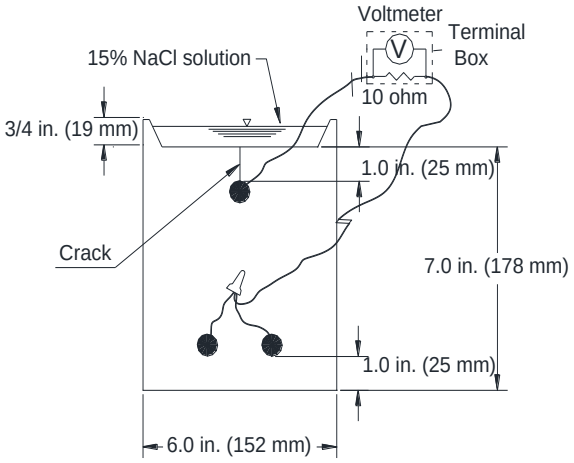

Figure 3.2— Cracked beam (CB) specimens

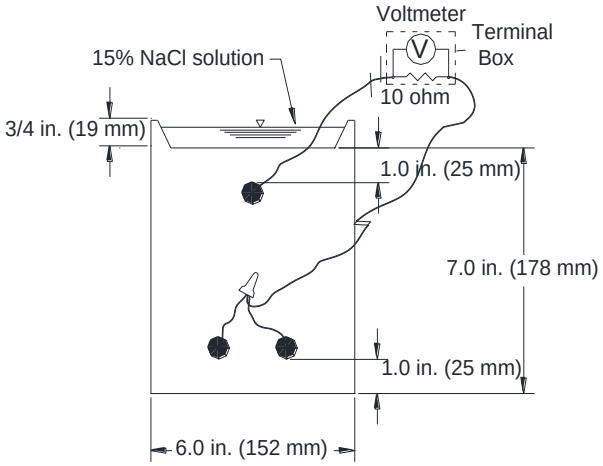

Figure 3.3— Beam (B) specimens

3.2.1.2 Test Procedure

To fabricate bench-scale specimens, first of all, reinforcing bars were cut to 12 in. (305 mm), and both ends of each bar were drilled and tapped to a 0.75 in. (19 mm) depth with 10-24 threading. To simulate the effects of damage, all epoxy-coated reinforcement used in Southern Exposure, beam, and cracked beam specimens, as shown in Figure 3.4, was intentionally damaged using a 0.125 in. (3 mm) diameter four-flute drill bit. The epoxy layer was penetrated to a depth of 15 mils (0.4 mm), deep enough just to expose the underlying steel. The epoxy layer was penetrated with a total of ten holes on each bar, with five holes spaced every 2 in. (51 mm) on each side of a bar.

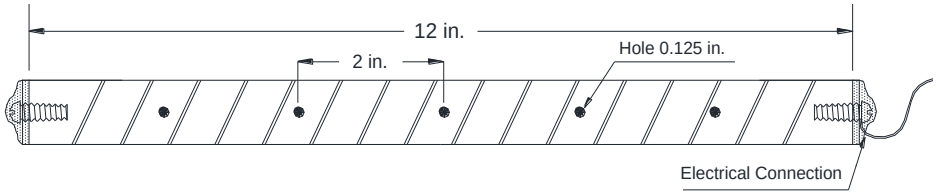

Figure 3.4— Damage pattern of epoxy-coated bar (plan view) in bench-scale tests

Epoxy-coated bars were rinsed with soapy water and uncoated bars were submerged in acetone for at least two hours to remove any oil from bar surface. Forms were built from 0.75 in. (19 mm) plywood and comprised of four sides and a base. Since specimens were cast upside down, to build the dam around the top surface of a specimen, a tapered 10.5 × 10.5 × 0.75 in. (267 × 267 × 19 mm) plywood was attached and centered to the base for Southern Exposure molds. Width of this attached plywood was half for cracked beam and beam molds. The forms were assembled, and reinforcement were placed into the molds. Epoxy-coated bars were aligned in a way that the intentionally damaged sites face the top and bottom side of the mold. All bars and molds were fabricated using 1.25 in. (32 mm) long 10-24 threaded stainless steel machine screws. Specimens

were fabricated and cast in an inverted position. Concrete was placed in two layers, and each layer was consolidated by internal vibration.

After casting, all specimens were wet cured for 3 days and air cured for 25 days thereafter. Ponding and lab tests began 28 days after casting. Prior to onset of testing, the test bars were wired by connecting wire leads through 10-24 × 0.5 in. (13 mm) stainless steel screws and a No. 10 stainless steel washer. The four sides of specimens were coated with an epoxy to protect the electrical connections and to prevent chloride ingress from the sides of the specimen. Both top and bottom mats of specimens were connected to a terminal box across a 10-ohm resistor.

The test duration of the Southern Exposure, cracked beam, and beam specimens was 96 weeks. The test procedure consisted of 12 weeks of wet-dry cycles followed by 12 weeks of continuously wet cycles. These two regimes were alternated and repeated until end of the test. During wet-dry cycles, specimens were ponded with 15% NaCl solution and maintained at ambient room temperature for four days. At this point, corrosion measurements including macrocell corrosion rate, corrosion potentials, and linear polarization resistance (LPR) test were taken, the salt solution was vacuumed off from the surface of the concrete specimens, and specimens were placed under a heat tent at 100 ± 3 °F (38 ± 2 °C) for 3 days. This procedure was repeated for 12 weeks. After 12 weeks of wet-dry cycles, specimens entered a continuously wet cycle, where specimens were ponded continuously with 15% NaCl solution and kept covered at ambient room temperature for 12 weeks. Deionized water was added to the concrete surfaces as needed, to replace water lost due to evaporation. Readings were taken on a weekly basis.

3.2.1.3 Chloride Sampling and Analysis

To evaluate the critical chloride threshold of reinforcement, Southern Exposure and beam specimens were sampled upon corrosion initiation. Corrosion initiation on an uncoated bar was defined as a measured macrocell corrosion rate exceeding 0.3 μm/yr or a corrosion potential became more negative than –0.275 V with respect to a saturated calomel electrode (SCE). However, these rules are not applicable for the coated bars, since corrosion initiation is restricted to the damaged sites and will exhibit lower corrosion rates upon corrosion initiation. Furthermore, epoxy-coated bars may show more negative corrosion potential values compared to bare bars due to a lack of oxygen. To determine the initiation of epoxy-coated bars, a combination of a jump in macrocell corrosion rate and a drop in potential were considered.

In addition to sampling at corrosion initiation, Southern Exposure and beam specimens were sampled at the end of the test life (96 weeks) to determine the final chloride content of specimens at the level of the bar. Samples were taken using a 0.25 in. (6.4 mm) masonry drill bit such that the top of the bit was level with the top of the top mat of reinforcing steel (as shown in Figures 3.5 and 3.6 for Southern Exposure and beam specimens, respectively). Six samples (three from each side) were taken upon onset of corrosion and six samples at the test end life. At each sample site, concrete was initially drilled to a depth of 0.5 in. (13 mm) and the powdered concrete discarded. The specimen was then drilled to a depth of 2.5 in. (63 mm); this powdered sample (about 3 g) was transferred to a plastic bag for analysis. After each sampling, the drill bit was cleaned with deionized water. If the specimen was to continue testing, the holes were filled with modeling clay.

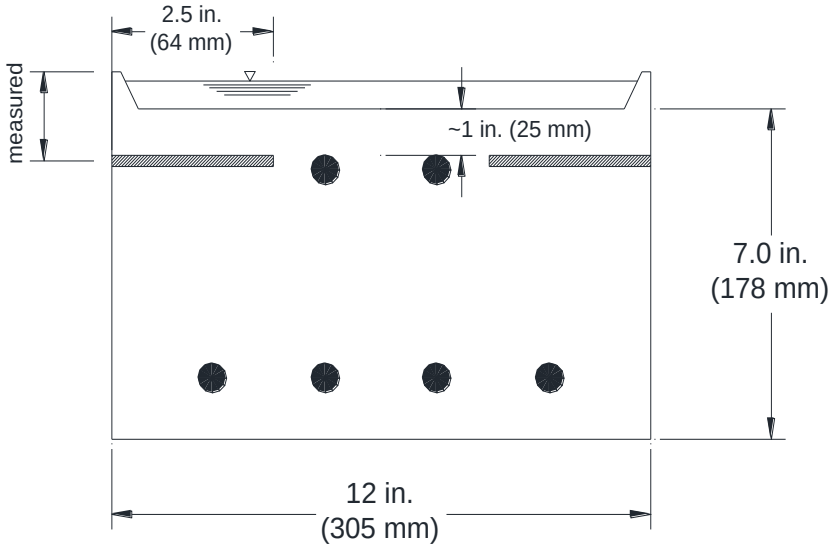

Figure 3.5— Southern Exposure specimen chloride sampling

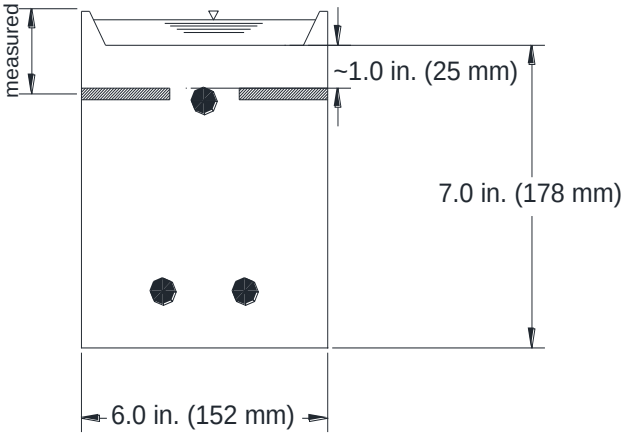

Figure 3.6— Beam specimen chloride sampling

The water-soluble chloride content of concrete samples were measured per AASHTO T 260-94, "Standard Method of Test for Sampling and Testing for Chloride Ion in Concrete and Concrete Raw Materials." First, samples were boiled with distilled water to release any water-soluble chlorides. Samples then were filtered and titrated. During titration, samples were acidified with nitric acid and then titrated with silver nitrate. During titration, potential of a chloride ion-

selective electrode was monitored and the change between potentials versus the incremental volume of added silver nitrate was plotted. The amount of added volume of silver nitrate in the inflection point of potential-volume curve (the point at which the highest potential difference for an incremental addition of silver nitrate is obtained) was recorded for calculating of chloride ion concentration in terms of percentage chloride by mass (weight) of concrete. Results then can be converted to weight of chloride content per volume of concrete in terms of lb/yd^3 (kg/m^3) by multiplying by the unit weight of concrete as 3786 lb/yd^3 (2246 kg/m^3).

3.2.1.4 Disbondment Test

To evaluate the integrity of the epoxy coatings, a disbondment test was performed after testing had been completed at sites of intentional damage. To accomplish this, two cuts were made at a 45° angle with the axis of the bar using a utility knife, creating the shape of an 'X' with its center at the center of each damaged site. The edge of the knife was then used to attempt to remove any coating. The area of disbondment, if any, was measured. If disbondment extended more than 0.5 in. (12.7 mm) from the hole in all directions (corresponding to an area of 1.05 in.^{2} (677 mm^2)) the specimen was said to have experienced total disbondment.

3.2.1.5 Corrosion Measurements

Macrocell Corrosion Rate:

To obtain the macrocell corrosion rate, the voltage drop between the anode and cathode of each specimen was taken across a 10-ohm resistor. The current density per unit area between two can be obtained by Ohm's Law:

$$i_{\text{corr}} = 10^6 \times \frac{V}{RA} \tag{3.1}$$

where i_{corr} is current density (μA/cm^2); V is the measured voltage drop across the resistor (volts); R is the resistance of resistor (10 ohms); and A is the surface area of anode (cm^2). The top mat of steel is the anode in the bench-scale tests (152 cm^2 for cracked beam and beam specimens and 304 cm^2 for Southern Exposure specimens).

The corrosion rate can be expressed as the thickness loss of steel per time. The relationship between current density and thickness loss is shown below per Faraday's Law:

$$r = k\frac{ia}{nF\rho} \tag{3.2}$$

where r is the corrosion rate (μm/year); k is a conversion factor (315360 (A.μm.s)/(μA.cm.yr)); a is the atomic weight of the corroding metal (g/mol); n is the number of electrons lost per atom of metal oxidized (2 for iron); F is Faraday's constant (96485 Coulombs/equivalent); and ρ is the density of metal (g/cm^3). By substituting proper values for iron, Eq. (3.2) simplifies to $r = 11.6i$ in μm/yr ($0.457i$ in mils/yr).

Corrosion Potential:

After measuring the voltage drop, the connection between anode and cathode across the resistor was disconnected for at least two hours to allow the potentials to stabilize, and then the corrosion potential of the top and bottom mat in bench-scale tests was measured using a saturated calomel electrode (SCE).

Linear Polarization Resistance:

In addition to the weekly voltage drop and corrosion potential measurements, linear polarization resistance (LPR) was measured on a monthly basis for bench-scale specimens. Linear polarization resistance is used to measure the total corrosion rate of reinforcement, including both macrocell corrosion (where the anode and cathode are on separate bars), and microcell corrosion, where the anode and cathode on the same bar. In a corroding specimen, both forms of corrosion

are present simultaneously, and voltage drop readings will not measure microcell corrosion. The LPR test consists of a working electrode (corroding reinforcement), a counter electrode (platinum rod), and a reference electrode (calomel electrode) connected to a potentiostat. The potentiostat controls the voltage difference between the working electrode and reference electrode in a system, and the counter electrode is used to apply current to that system. By applying external voltage, corrosion potential of the system can be shifted by ($\Delta\varepsilon$) with respect to E_{corr} (in a range of –20 mV to 20 mV for this test), resulting in a change in the current density (Δi). The obtained data are plotted as a potential-current curve. In the vicinity of the equilibrium potential (in a range from –10 mV to 10 mV with respect to E_{corr}), the potential-current curve is linear and the slope of the curve is defined as the linear polarization resistance (R_p). The linear polarization resistance is inversely proportional to the corrosion current density according to the Stern-Geary equation:

$$i_{corr} = \frac{\beta_a \beta_c}{2.3 R_p (\beta_a + \beta_c)} \tag{3.3}$$

Where β_a and β_c are anodic and cathodic Tafel constants, taken as 0.12 V/decade for reinforcing steel in concrete ((Lambert et al. 1991, McDonald et al. 1998). By using these values, the current density in Eq. (3.3) is simplified to:

$$i_{corr} = \frac{0.026}{R_p} \tag{3.4}$$

Current density then can be converted to thickness loss per Eq. (3.2).

3.2.2 Rapid Macrocell Test

3.2.2.1 Description

A rapid macrocell test set up is shown in Figure 3.7. This test exposes the bars to a simulated concrete pore solution environment and enables chloride ions to reach the bar surface immediately; thus, accelerating the corrosion process. This test was first developed at the University of Kansas and is listed in the Annex of ASTM A955 as a means of evaluating the corrosion resistance of stainless steel bars. The rapid macrocell test consists of two containers. One container, containing the cathode, consisted of two No. 5 (No. 16) bars in a simulated concrete pore solution at a depth of 3 in. (76 mm). One liter of pore solution consisted of 17.87 g of sodium hydroxide (NaOH) and 18.81 g of potassium hydroxide (KOH) dissolved in 974.8 g of deionized water (ASTM A955-14). The other container, containing the anode, contained a single No. 5 (No. 16) bar in a simulated pore solution with salt, created by adding 172.1 g of NaCl to one liter of pore solution. The anode and cathode bars were electrically connected through a terminal box across a 10-ohm resistor via external wiring to allow for electron flow and macrocell corrosion rate measurements. A salt bridge (ionic connection) was provided to allow ionic movement from cathode to anode. Air, scrubbed to remove any CO_2, was bubbled into the cathode. The test duration was 15 weeks, with pore solution changed every 5 weeks to maintain the pH. Macrocell corrosion rate and corrosion potential measurements were taken on a weekly basis; LPR was performed on a triweekly basis. For this test method, one set of six specimens were tested for each uncoated bar type, in both the as-received and pickled condition, as well as each coated bar type.

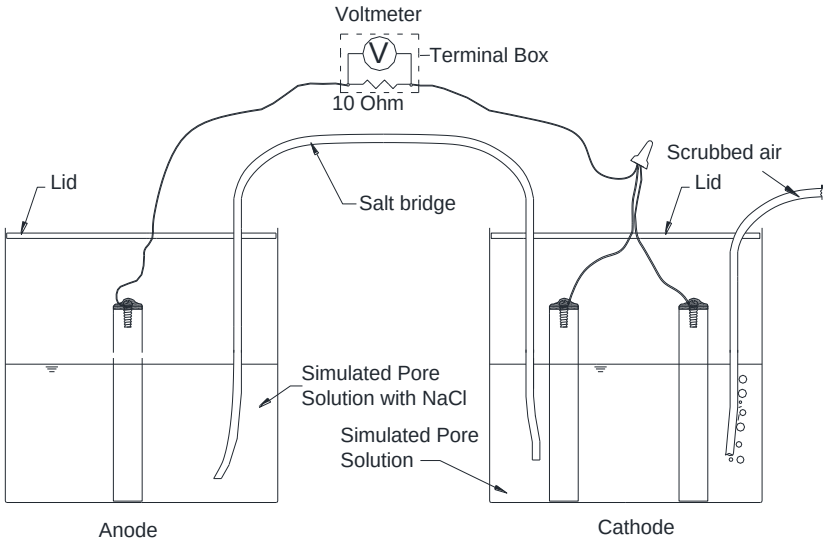

Figure 3.7— Rapid Macrocell Specimen

3.2.2.2 Test Procedure

To fabricate the rapid macrocell specimens, bars were first cut to 5 in. (127 mm) and one end of each bar was drilled and tapped to a 0.75 in. (19 mm) depth with 10-24 threading. Epoxy-coated bars were rinsed with soapy water and bare bar soaked in acetone for at least two hours to remove any oil and dirt. A wire was attached to the bar tapped end using a 0.5 in. (13 mm) 10-24 stainless steel machine screw and a No. 10 stainless steel washer. The electrical connection was epoxied with 3M Scotchkote^{TM} rebar patch kit. For the epoxy-coated bars the untapped bare end was capped and epoxied. All epoxy-coated bars, as shown in Figure 3.8, were intentionally damaged, using a 0.125 in. (3 mm) diameter four-flute drill bit, to a depth of 15 mils (0.4 mm), deep enough to expose the underlying steel with a total of four holes (two holes on each side, the first hole 1 in. (25 mm), and second hole 2 in. (51 mm) far from the bottom end). Bars were placed into the containers and electrically connected through a 10-ohm resistor via terminal box.

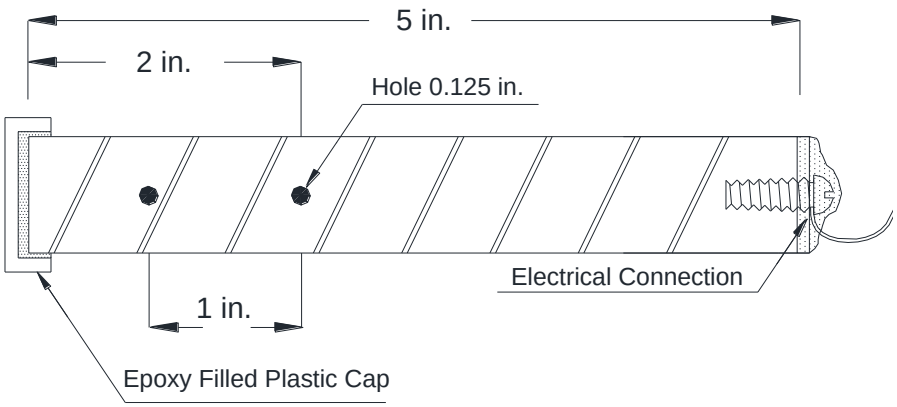

Figure 3.8— Damage pattern of epoxy-coated bar in rapid macrocell test

3.2.2.3 Disbondment Test

At the end of the test, specimens were removed from solutions, photographed, and epoxy-coated bars were tested for disbondment. The disbondment test procedure was similar to what was described in Section 3.2.1.4 for bench-scale tests.

3.2.2.4 Corrosion Measurements

The top mat in bench-scale test was considered as anode and the bottom as cathode, while for rapid macrocell test the anode and cathode bars were separated into two containers and corrosion potentials were measured between those two. Macrocell corrosion rate and LPR test measurements for rapid macrocell test were similar to that described in Section 3.2.1.5 for bench-scale tests except that anode bar surface area used in Eq. (3.1) to calculate the current density is the surface area of the bar in the salt solution (63 cm^2), and LPR was measured on a triweekly basis instead of monthly. All other corrosion measurements were similar to that for bench-scale tests.

3.3 TEST PROGRAM

For all four types of reinforcement (MMFX bare bars containing 4% and 9% chromium and MMFX epoxy-coated bars containing 2% and 4% chromium), six Southern Exposure specimens, six cracked beam specimens and six rapid macrocell tests were prepared. (For the Southern Exposure test, an additional two uncoated MMFX bare bar specimens were cast). For each MMFX epoxy-coated bar, six beam specimens were cast in addition to the specimens listed above to allow for a more accurate determination of the critical chloride threshold of the reinforcement. To investigate the effect of pickling on MMFX bars, uncoated bars containing 4% and 9% chromium (one set of six bars from each) were also pickled and evaluated with rapid macrocell test. To pickle the bars, they have been submerged into a solution containing 2.5% nitric acid (HNO_3) and 0.5% hydrofluoric acid (HF) at ambient room temperature (72 °F) for 15 minutes. The total number of MMFX test specimens in this study is listed in Table 3.2.

Table 3.2: MMFX Bar Test Specimens

Steel Designation[a]	SE[b]	CB[c]	B[d]	RM[e]	Total
MMFX(4%)	8	6	-	6	20
MMFX(9%)	8	6	-	6	20
PMMFX(4%)	-	-	-	6	6
PMMFX(9%)	-	-	-	6	6
MMFX-ECR(2%)	6	6	6	6	24
MMFX-ECR(4%)	6	6	6	6	24
Total	**28**	**24**	**12**	**36**	**100**

[a]MMFX(4%) = MMFX steel containing 4% chromium
MMFX(9%) = MMFX steel containing 9% chromium
PMMFX(4%) = Pickled MMFX steel containing 4% chromium
PMMFX(9%) = Pickled MMFX steel containing 9% chromium
MMFX-ECR(2%) = Epoxy-coated MMFX steel containing 2% chromium
MMFX-ECR(4%) = Epoxy-coated MMFX steel containing 4% chromium
[b]SE = Sothern Exposure specimen
[c]CB = Cracked beam specimen
[d]B = Beam specimen
[e]RM = Rapid macrocell

The bench-scale specimens were cast with six batches of concrete. For each of the first three batches, two Southern Exposure and two cracked beam specimens were cast for each bar type. One cracked beam specimen was cast in batch four to replace one of cracked beams since the inserted shim was not removed properly from specimen. Batch five consisted of four Southern Exposure specimens-two of each uncoated bar type. Batch six consisted of twelve beam specimens-six specimens of each coated bar type. The concrete mix used contained type I/II portland cement with a water-cement ratio (w/c) of 0.45, a target air content of 6 ± 1%, and target slump of 3 ± 1 in. (75 ± 25 mm). Aggregate properties and mixture proportions are shown in Table 3.3. The average 28-day concrete compressive strength for batches one through six were 5550, 4650, 4250, 4530, 4770, and 4850 psi (38.2, 32.1, 29.3, 31.2, 32.9, and 33.4 MPa).

Table 3.3: Mix Proportions (SSD basis)

Water lb/yd^3 (kg/m^3)	**Cement lb/yd^3 (kg/m^3)**	**Coarse Agg. lb/yd^3 (kg/m^3)**	**Fine Agg. lb/yd^3 (kg/m^3)**	**Air-entraining Agent oz/yd^3 (mL/m^3)**
269 (160)	598 (355)	1484 (880)	1435 (851)	4.73 (183)

Bulk specific gravity of fine aggregate = 2.63
Bulk specific gravity of Coarse aggregate = 2.59

3.4 TEST RESULTS

3.4.1 Southern Exposure Specimens

3.4.1.1 Macrocell Corrosion Rate

Macrocell corrosion rates of Southern Exposure specimens calculated from voltage drops for MMFX uncoated bars containing 9% chromium (SE-MMFX(9%)) and 4% chromium (SE-MMFX(4%)) are shown in Figures 3.9 and 3.10, respectively. For the SE-MMFX(9%) bars, Specimens 1 and 2 initiated corrosion at weeks 11 and 8, respectively. Specimens 3, 5, and 6 initiated at week 13 and Specimen 4 at week 31. Specimen 8 initiated corrosion at week 36 and

specimen 7 initiated corrosion at week 46. The average time to corrosion initiation for SE-MMFX(9%) specimens was 21.4 weeks. The maximum corrosion rates for specimens SE-MMFX(9%) through week 96 ranged from 9.2 to 16.9 µm/yr.

For bars containing 4% chromium, Specimen SE-MMFX-4%-3 initiated corrosion at week 4 and had a maximum corrosion rate of 13.9 µm/yr at week 32. The early initiation was likely due to corrosion at electrical connection; thus, this specimen was excluded from the average initiation age. Specimens 1, 2, 4, 5 and 6 exhibited corrosion initiation at weeks 19, 20, 24, 29 and 14, respectively. Specimen 7 and 8 have shown corrosion initiation at week 31 and 51, respectively. The average time to corrosion initiation for SE-MMFX(4%) specimens was 27 weeks. The maximum corrosion rates for the SE-MMFX(4%) specimens through week 96 ranged from 8.0 to 22.5 µm/yr.

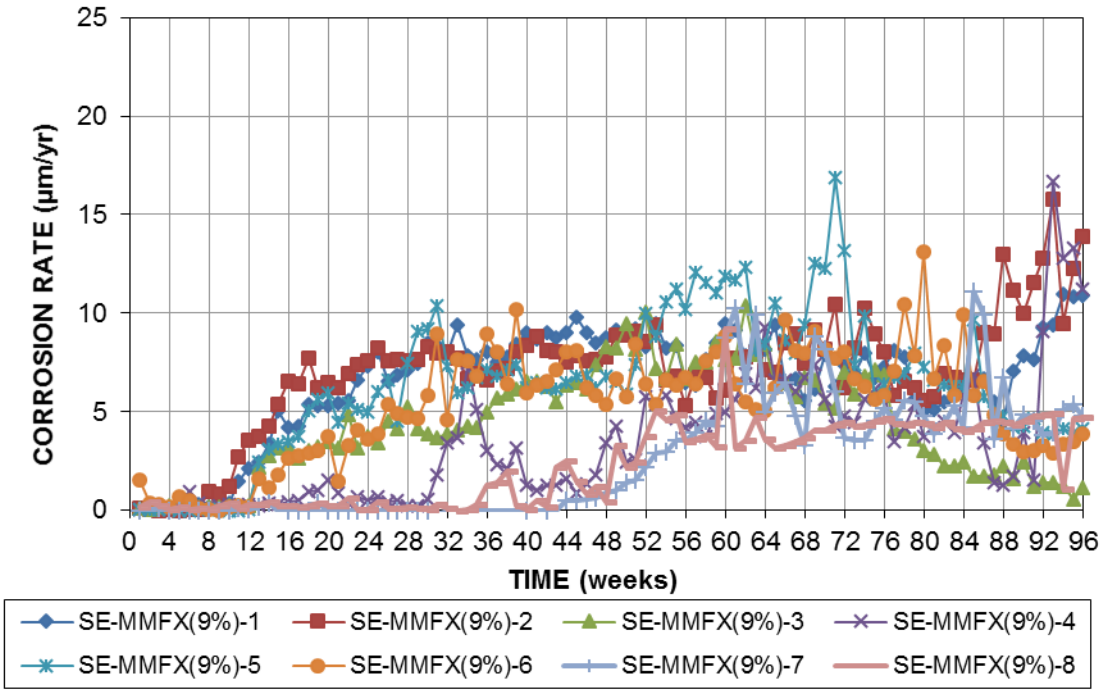

Figure 3.9— Macrocell corrosion rates (µm/yr) for Southern Exposure specimens containing MMFX(9%) bars

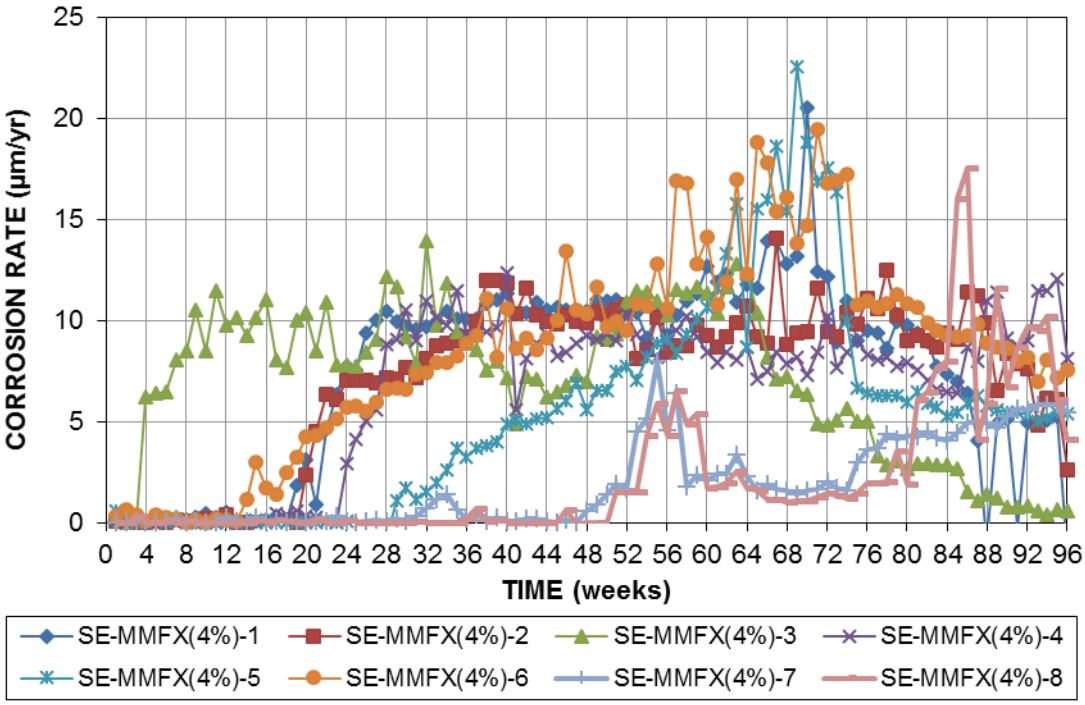

Figure 3.10— Macrocell corrosion rates (µm/yr) for Southern Exposure specimens containing MMFX(4%) bars

Macrocell corrosion rates of Southern Exposure specimens calculated from voltage drops for epoxy-coated MMFX bars containing 4% chromium (SE-MMFX-ECR(4%)) and 2% chromium (SE-MMFX-ECR(2%)) based on total area of the bar are shown in Figures 3.11 and 3.12, respectively. The maximum corrosion rates based on total area for the SE-MMFX-ECR(4%) and SE-MMFX-ECR(2%) specimens through week 96 ranged from 0.122 to 0.625 µm/yr and 0.187 to 0.918 µm/yr, respectively.

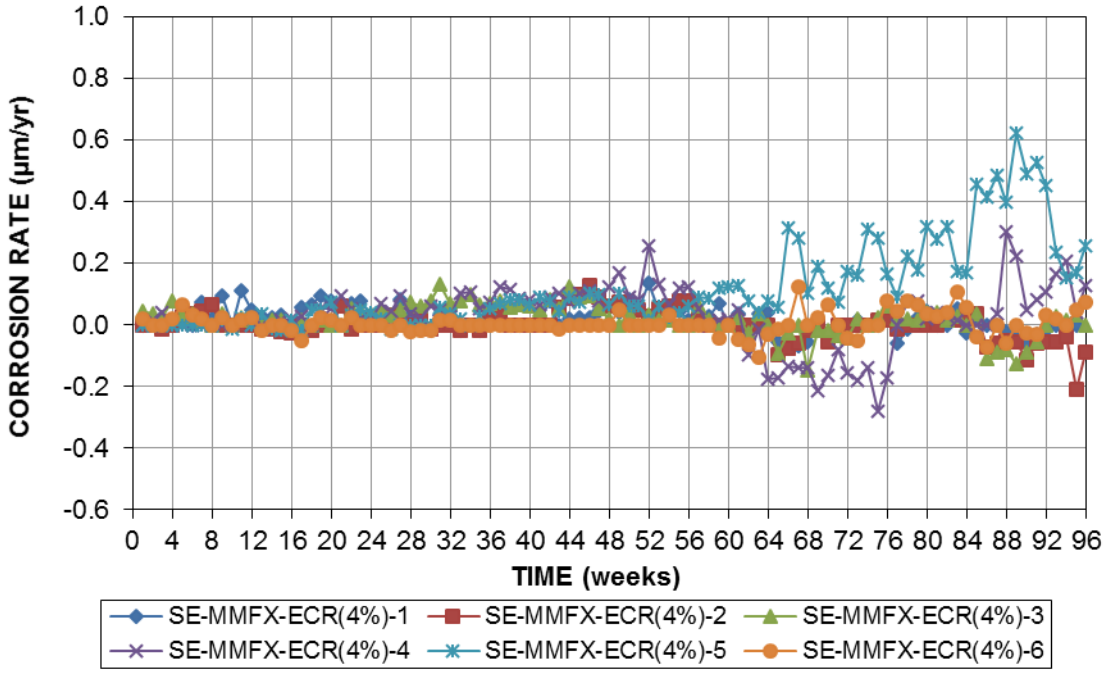

Figure 3.11— Macrocell corrosion rates (µm/yr) based on total area of reinforcement for Southern Exposure specimens containing MMFX-ECR(4%) bars

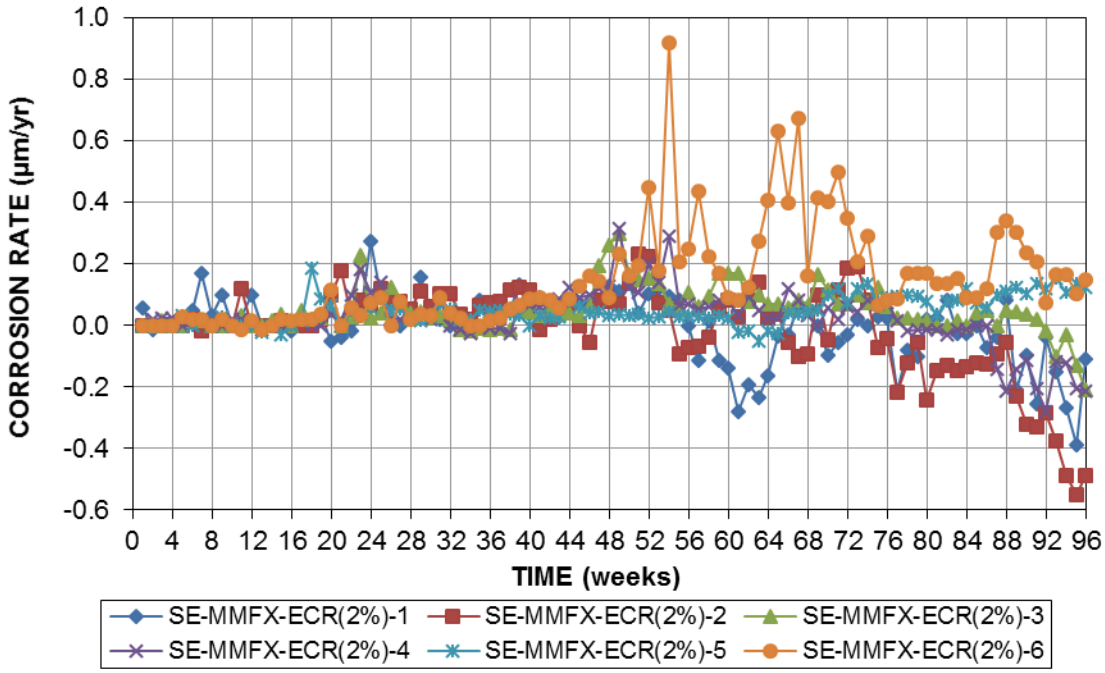

Figure 3.12— Macrocell corrosion rates (µm/yr) based on total area of the reinforcement for Southern Exposure specimens containing MMFX-ECR(2%) bars

Macrocell corrosion rates based on total area are calculated based on the assumption that the entire surface area of the bar is corroding. However, since for the epoxy-coated bars corrosion is more likely to occur on the damaged area of the bar, it is useful to calculate the corrosion rates based on the assumption that only damaged area of the bar is corroding. Figures 3.13 and 3.14 show macrocell corrosion rate for the SE-MMFX-ECR(4%) and SE-MMFX-ECR(2%) specimens, respectively, based on exposed area of the reinforcement. Corrosion rates based on the exposed area at the holes for bars with 10 penetrations through the epoxy on each bar are 192 times the corrosion rate based on total bar area. The maximum corrosion rates based on exposed area for the SE-MMFX-ECR(4%) and SE-MMFX-ECR(2%) specimens through week 96 ranged from 23.4 to 120 µm/yr and 35.8 to 176.3 µm/yr, respectively.

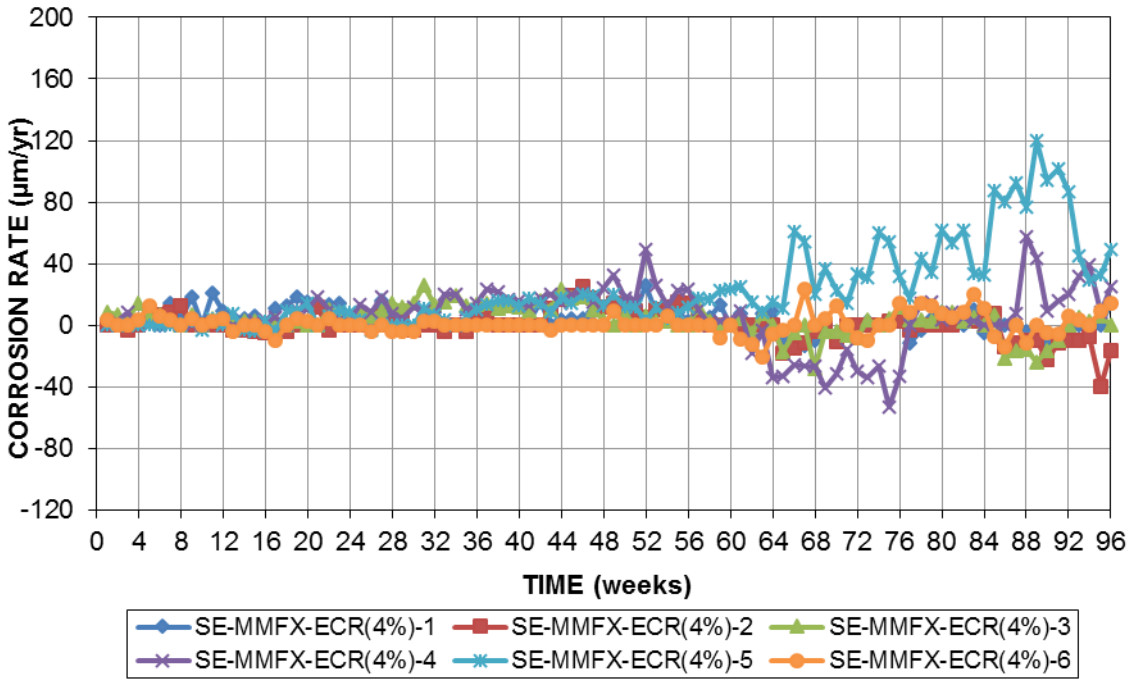

Figure 3.13— Macrocell corrosion rates (µm/yr) based on exposed area of the reinforcement for Southern Exposure specimens containing MMFX-ECR(4%) bars

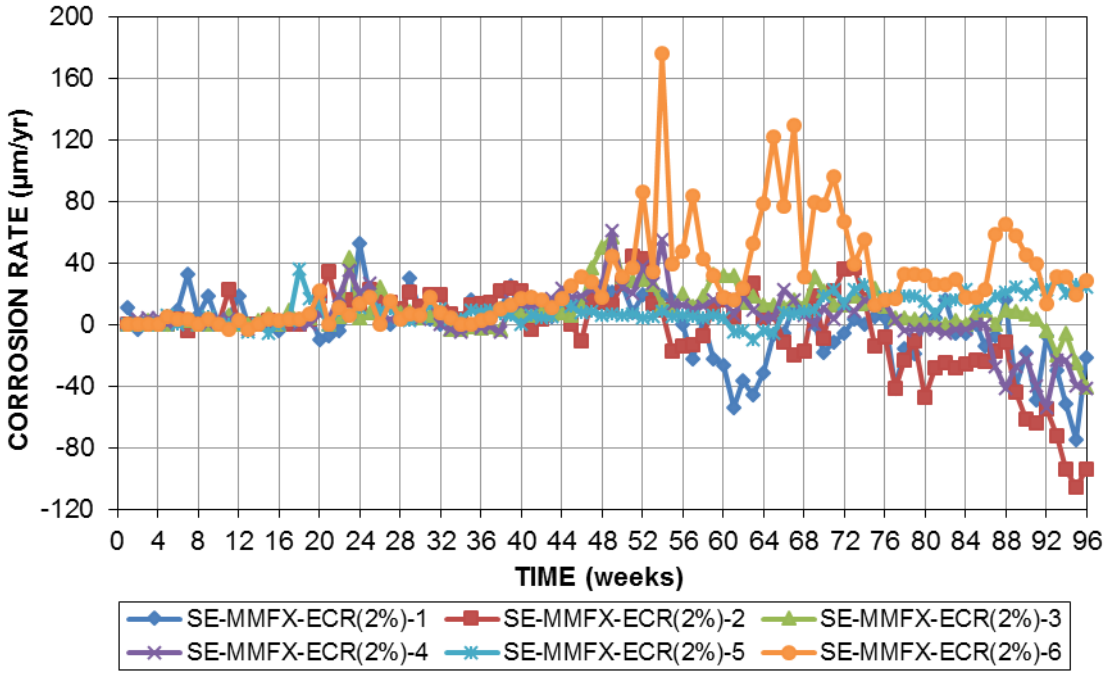

Figure 3.14— Macrocell corrosion rates (µm/yr) based on exposed area of the reinforcement for Southern Exposure specimens containing MMFX-ECR(2%) bars

Figure 3.15 shows the average corrosion rate for the Southern Exposure specimens based on total area. The epoxy-coated specimens present very low corrosion rates based on total area; less than 0.1 µm/yr for bars containing 4% chromium and less than 0.25 µm/yr for bars containing 2% chromium. The SE-MMFX(4%) and SE-MMFX(9%) specimens exhibited average corrosion rates less than 1 µm/yr through week 6 and 12 respectively. Average corrosion rates for SE-MMFX(4%) reached a maximum of 10 µm/yr at week 67, and then decreased to 4 µm/yr at week 96. SE-MMFX(9%) reached a maximum corrosion rate of 8.35 µm/yr at week 60, decreasing to 4.4 µm/yr at week 87 before increasing to about 7 µm/yr for the final five weeks of testing.

Figure 3.16 shows the average corrosion rate for the Southern Exposure specimens based on exposed area. Based on exposed area, the epoxy-coated bars with 2% nominal chromium content exhibited average corrosion rates of 10.0 µm/yr or less through week 22. From week 23 to 96, the corrosion rates on these specimens fluctuated between –33.0 and 46.9 µm/yr. The epoxy-

coated bars with 4% nominal chromium content exhibited a maximum average corrosion rate of 20.1 µm/yr at week 89.

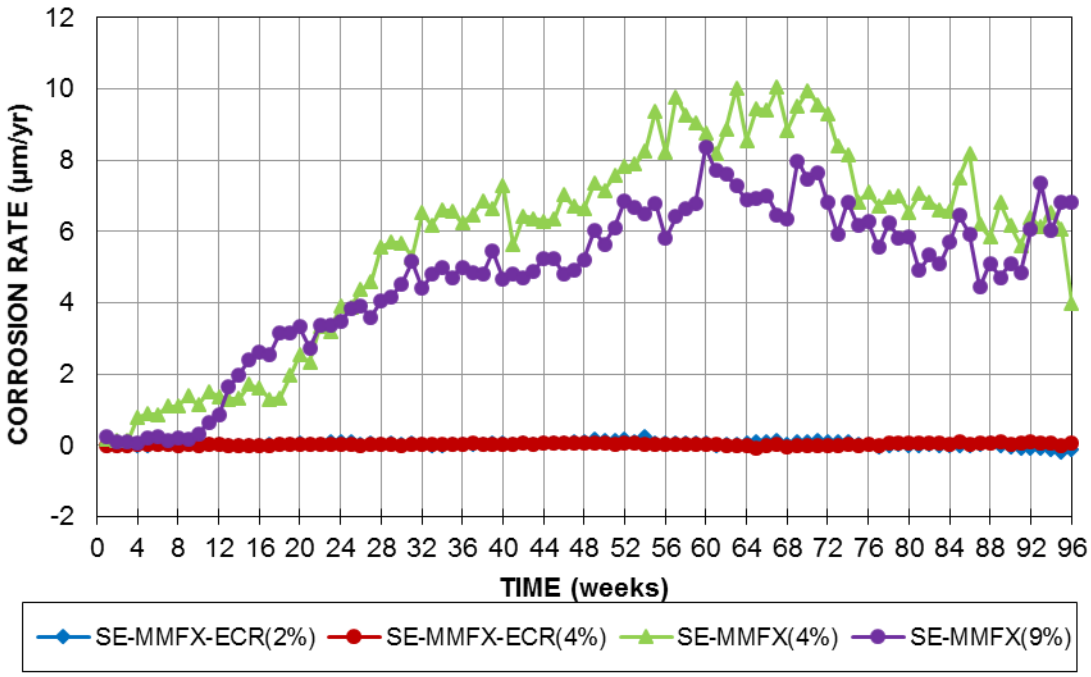

Figure 3.15— Average corrosion rate (µm/yr) based on total area versus time for Southern Exposure specimens containing bare and epoxy-coated MMFX bars

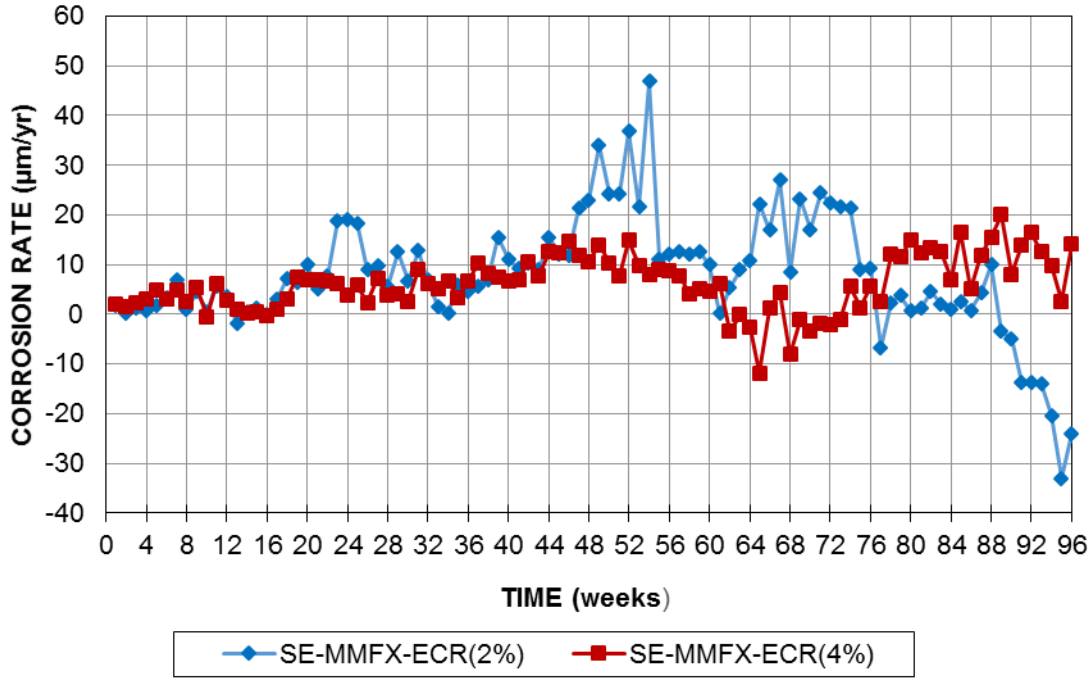

Figure 3.16— Average corrosion rate (µm/yr) based on exposed area versus time for Southern Exposure specimens containing epoxy-coated MMFX bars

The average and individual corrosion losses for the Southern Exposure specimens through end of the test (week 96) are tabulated in Table 3.4. Corrosion losses were obtained by integrating corrosion rates with respect to time; that is, corrosion loss is the accumulated amount of thickness of steel that is corroded with respect to time. Average corrosion losses for MMFX(4%) and MMFX(9%) specimens at week 96 were 10.3 and 8.73 µm, respectively. Based on total area, the greatest individual loss, 15.6 µm, was observed on specimen MMFX(4%)-6. The maximum corrosion loss for the MMFX-9% specimens was 13.0 µm for MMFX(9%)-2. Based on exposed area, the average corrosion losses for the MMFX-ECR(2%) and MMFX-ECR(4%) specimens were 14.7 and 11.4 µm, respectively.

Table 3.4: Corrosion loss (µm) for Southern Exposure specimens

Specimen	Corrosion Loss (µm)-Total Area								Average	Std. Dev.
	Week 96		Week 96		Week 96		Week 96			
	1	2	3	4	5	6	7	8		
MMFX-ECR(2%)	-0.007	-0.024	0.089	0.045	0.089	0.267			0.076	0.105
MMFX-ECR(4%)	0.037	0.002	0.036	0.055	0.217	0.01			0.059	0.080
MMFX(4%)	13.7	13.3	13.1	12.2	10.0	15.6	3.45	4.08	10.7	4.54
MMFX(9%)	12.1	13.0	8.05	6.34	11.7	9.73	4.73	4.23	8.73	3.41
	Corrosion Loss (µm)-Exposed Area									
MMFX-ECR(2%)	-1.3	-4.7	17	8.6	17.1	51.3			14.7	45.8
MMFX-ECR(4%)	7.1	0.4	6.9	10.6	41.7	1.8			11.4	22.3

3.4.1.2 Linear Polarization Resistance (LPR) Test

Corrosion rates obtained from LPR test results on Southern Exposure specimens with uncoated MMFX bars containing 9% and 4% chromium are shown in Figures 3.17 and 3.18, respectively. The maximum corrosion rates for specimens SE-MMFX(9%) and SE-MMFX(4%) through week 96 ranged from 3.7 to 21.6 µm/yr and 3.6 to 34.2 µm/yr, respectively.

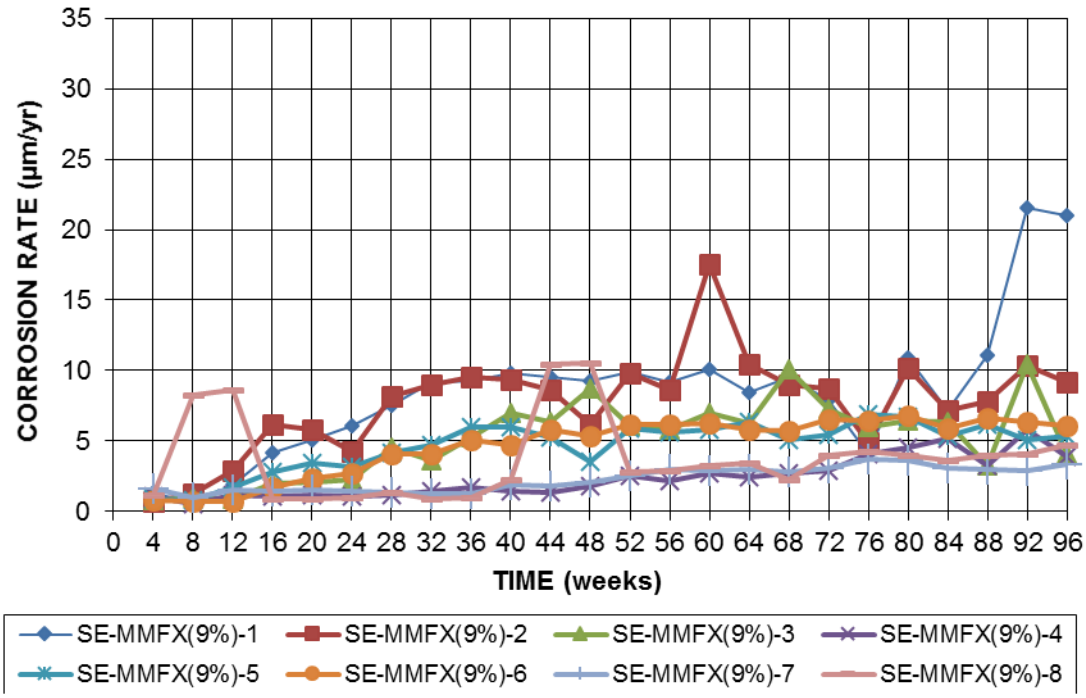

Figure 3.17— LPR test corrosion rates (µm/yr) for Southern Exposure specimens containing MMFX(9%) bars

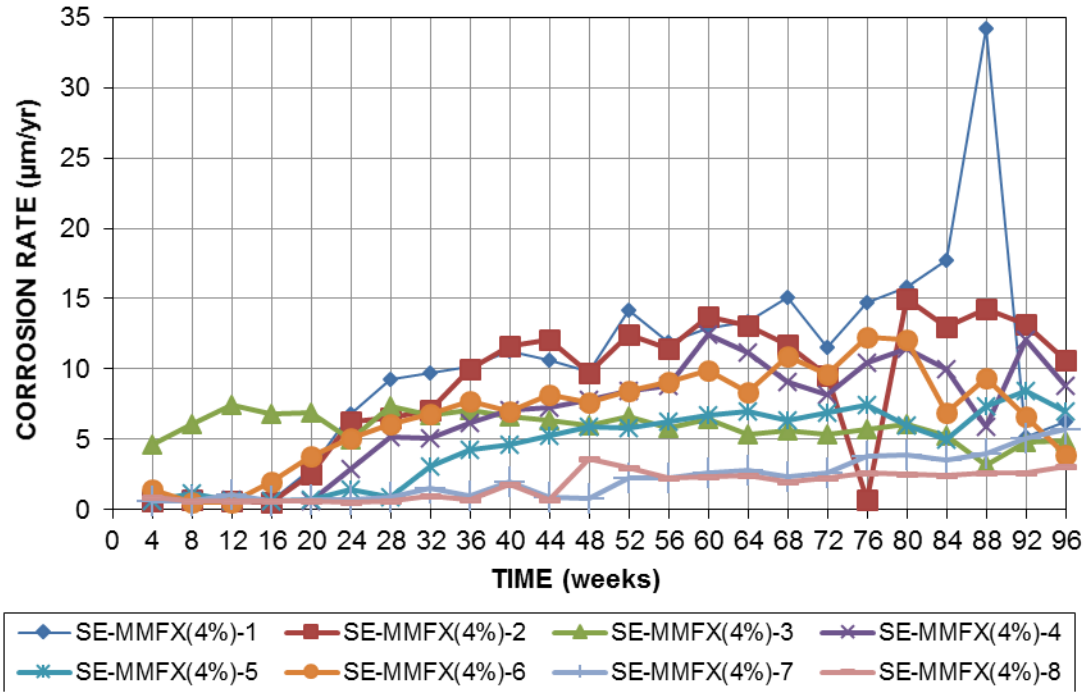

Figure 3.18— LPR test corrosion rates (µm/yr) for Southern Exposure specimens containing MMFX(4%) bars

Corrosion rates based on total area obtained from LPR test results on Southern Exposure specimens with MMFX epoxy-coated specimens containing 4% and 2% chromium are shown in Figures 3.19 and 3.20, respectively. Based on total area, the maximum corrosion rates for specimens SE-MMFX-ECR(4%) and SE-MMFX-ECR(2%) through week 96 ranged from 0.1 to 0.42 µm/yr and 0.22 to 0.72 µm/yr, respectively.

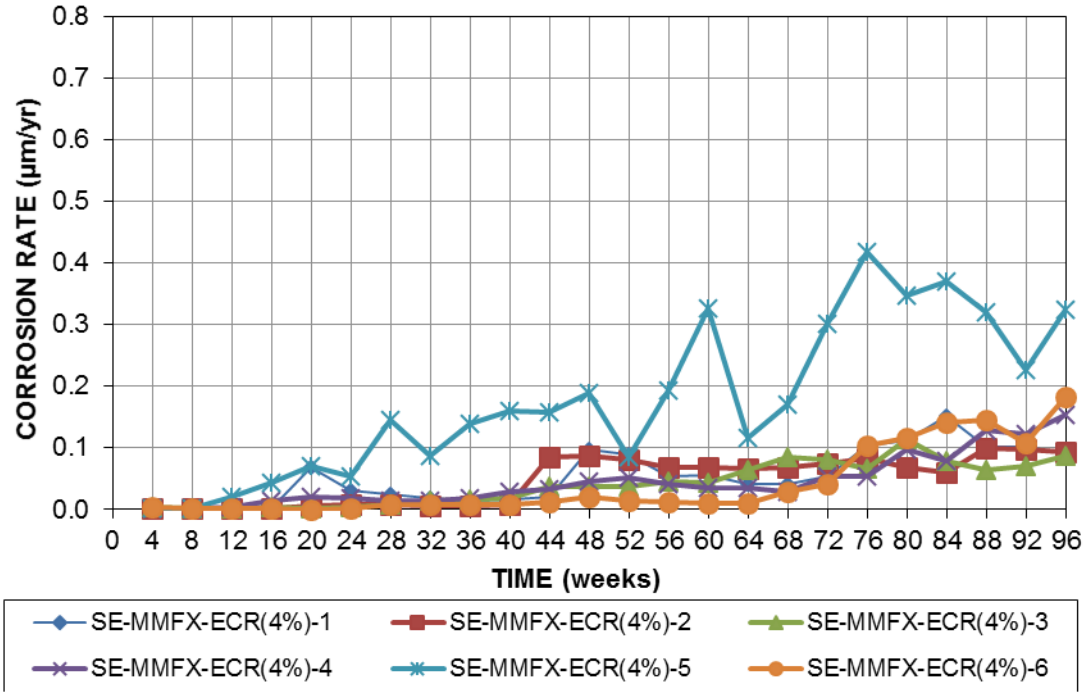

Figure 3.19— LPR test corrosion rates (µm/yr) based on total area of reinforcement for Southern Exposure specimens containing MMFX-ECR(4%) bars

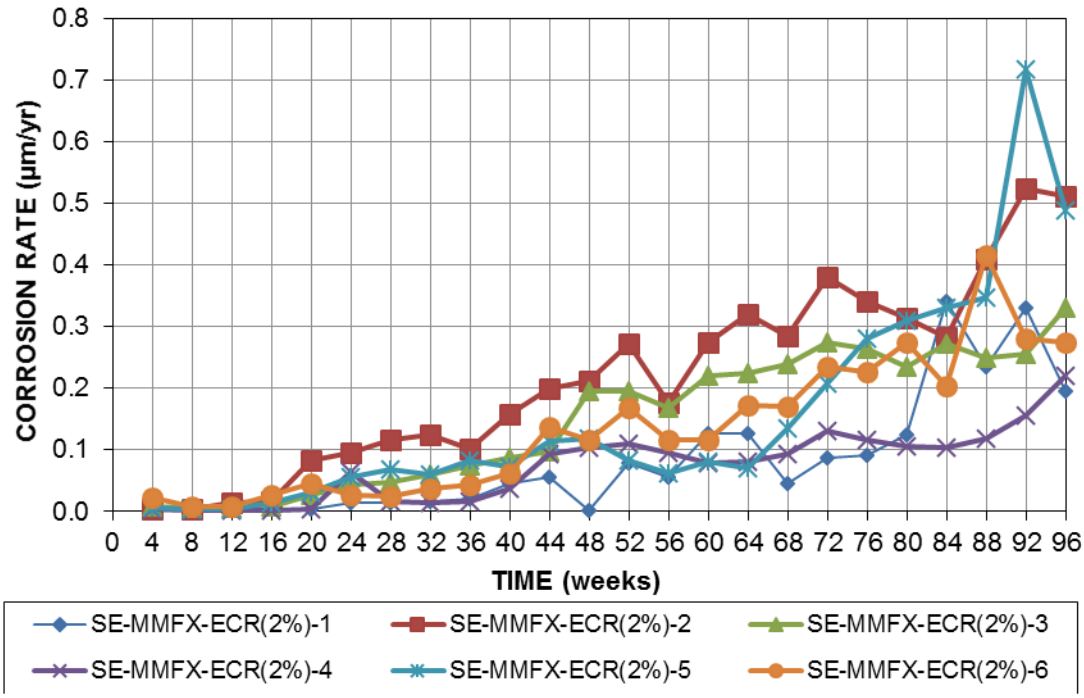

Figure 3.20— LPR test corrosion rates (µm/yr) based on total area of reinforcement for Southern Exposure specimens containing MMFX-ECR(2%) bars

Figure 3.21 shows the average corrosion rate for the Southern Exposure specimens based on total area obtained from LPR test results. For all specimens, average corrosion rates generally increased through the end life of the test (96 weeks). Compared to the uncoated bars, the epoxy-coated specimens present very low corrosion rates based on total area. The maximum average corrosion rate for epoxy-coated bars containing 4% and 2% chromium were 0.15 and 0.38 µm/yr, compared to 8.35 and 10 µm/yr for uncoated bars containing 9% and 4% chromium, respectively.

Figure 3.22 shows the average corrosion rate for the Southern Exposure specimens based on exposed area obtained from LPR test results. As was observed for uncoated bars, corrosion rates tended to increase throughout the test. Based on exposed area, the epoxy-coated bars with 2% nominal chromium content exhibited a maximum average corrosion rate of 72 µm/yr at week 88. The epoxy-coated bars with 4% nominal chromium content exhibited a maximum average corrosion rate of 29.7 µm/yr at week 96.

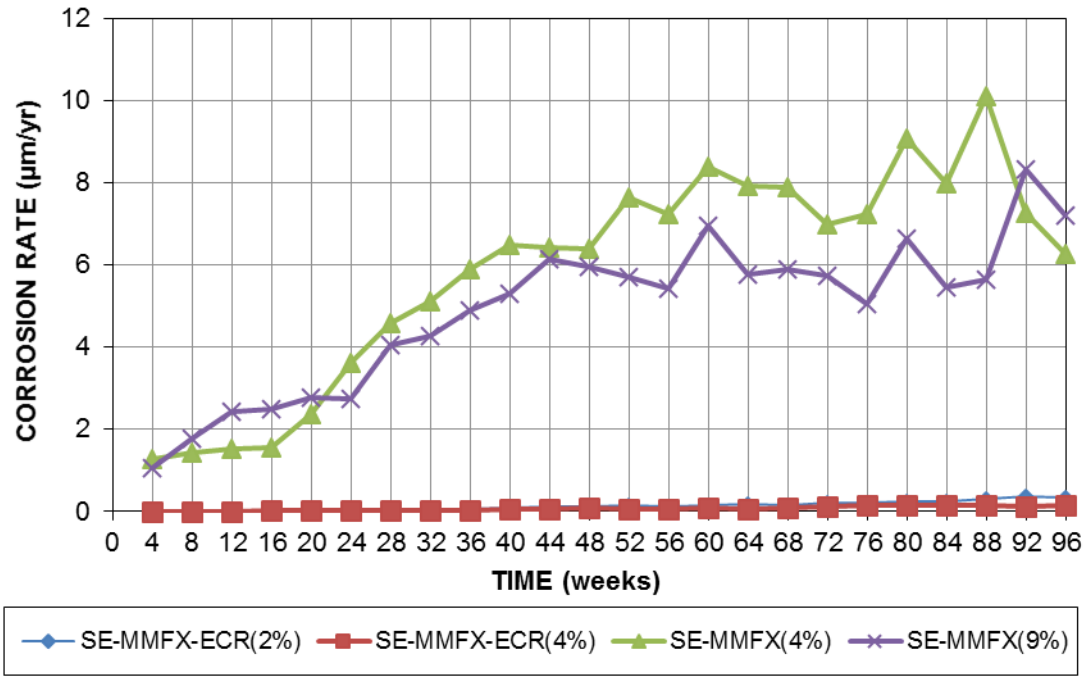

Figure 3.21— Average LPR test corrosion rate (µm/yr) based on total area versus time for Southern Exposure specimens containing bare and epoxy-coated MMFX bars

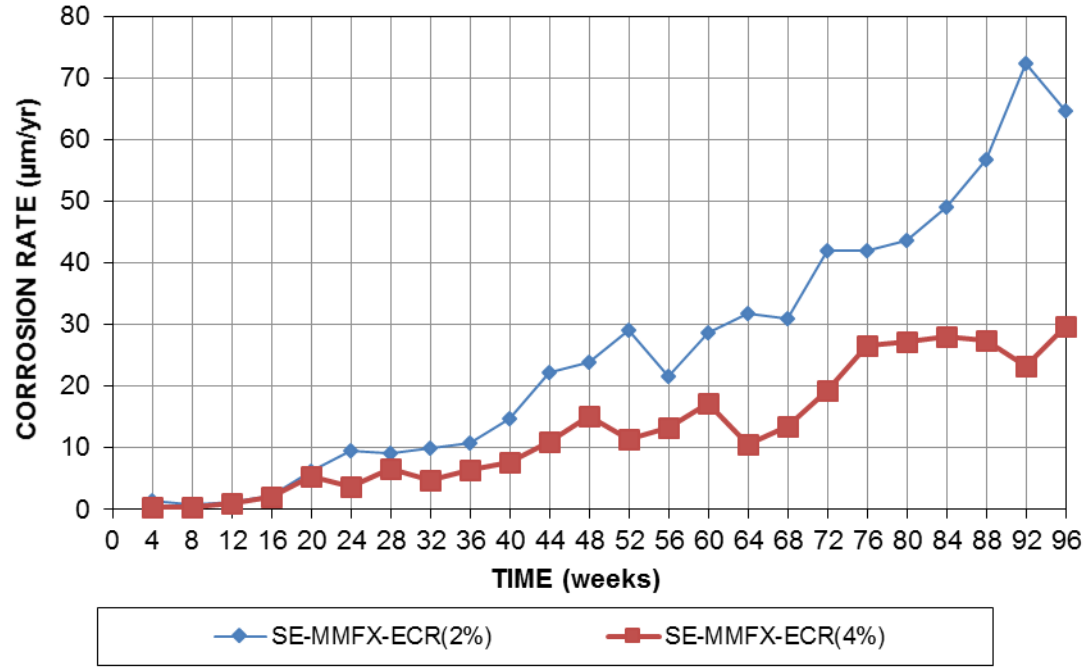

Figure 3.22— Average LPR test corrosion rate (µm/yr) based on exposed area versus time for Southern Exposure specimens containing epoxy-coated MMFX bars

The average and individual corrosion losses obtained from LPR test results for the Southern Exposure specimens through end of the test (week 96) are tabulated in Table 3.5. Average corrosion losses for MMFX(4%) and MMFX(9%) specimens at week 96 were 10.8 and 9.05 µm, respectively, about 1% more than that obtained from macrocell corrosion rates. Based on total area, the greatest individual loss, 18.9 µm, was observed on Specimen MMFX(4%)-1. The maximum corrosion loss for the MMFX(9%) specimens was 15.7 µm for MMFX(9%)-1. Based on exposed area, the average corrosion losses for the MMFX-ECR(2%) and MMFX-ECR(4%) specimens were 48 and 24 µm, more than three times and two times as much as obtained from macrocell corrosion rates, respectively.

Table 3.5: Corrosion loss (µm) for Southern Exposure specimens based on LPR test results

Specimen	Corrosion Loss (µm)-Total Area								Average	Std. Dev.
	Week 96		Week 96		Week 96		Week 96			
	1	2	3	4	5	6	7	8		
MMFX-ECR(2%)	0.155	0.400	0.275	0.135	0.288	0.246			0.250	0.097
MMFX-ECR(4%)	0.100	0.088	0.075	0.084	0.328	0.076			0.125	0.010
MMFX(4%)	18.9	15.9	10.9	12.4	8.42	12.6	4.03	3.27	10.8	5.43
MMFX(9%)	15.7	14.2	9.49	4.38	8.62	8.68	4.23	6.96	9.05	4.17
	Corrosion Loss (µm)-Exposed Area									
MMFX-ECR(2%)	29.8	77.0	52.9	26.0	55.2	47.3			48.0	18.6
MMFX-ECR(4%)	19.1	16.8	14.4	16.1	63.0	14.5			24.0	19.2

3.4.1.3 Corrosion Potential

The average top mat corrosion potentials (with respect to a copper-copper sulfate electrode) for the Southern Exposure specimens are shown in Figure 3.23. The average bottom mat corrosion potentials are exhibited in Appendix D. The average top mat potential for all specimens was between –0.23 V and –0.34 V at the start of the test. The potential of the MMFX (ECR)-2% specimens gradually increased to –0.28 V by week 9 and exhibited drops in potential thereafter, reaching –0.62 V at week 96. Likewise, the potential of the MMFX-ECR(4%) specimens gradually

increased to –0.24 V by week 7, but exhibited drops in potential after week 7 and decreased to –0.58 V through week 96. The MMFX(4%) specimens exhibited corrosion potentials near –0.25 V through week 13, after which the potential dropped to –0.62 V by week 96. The potential of the MMFX(9%) specimens gradually increased to –0.21 V by week 7, after which the potential decreased to –0.58 V by week 96. The drops in potential correspond to the initiation of corrosion for a specimen in the series.

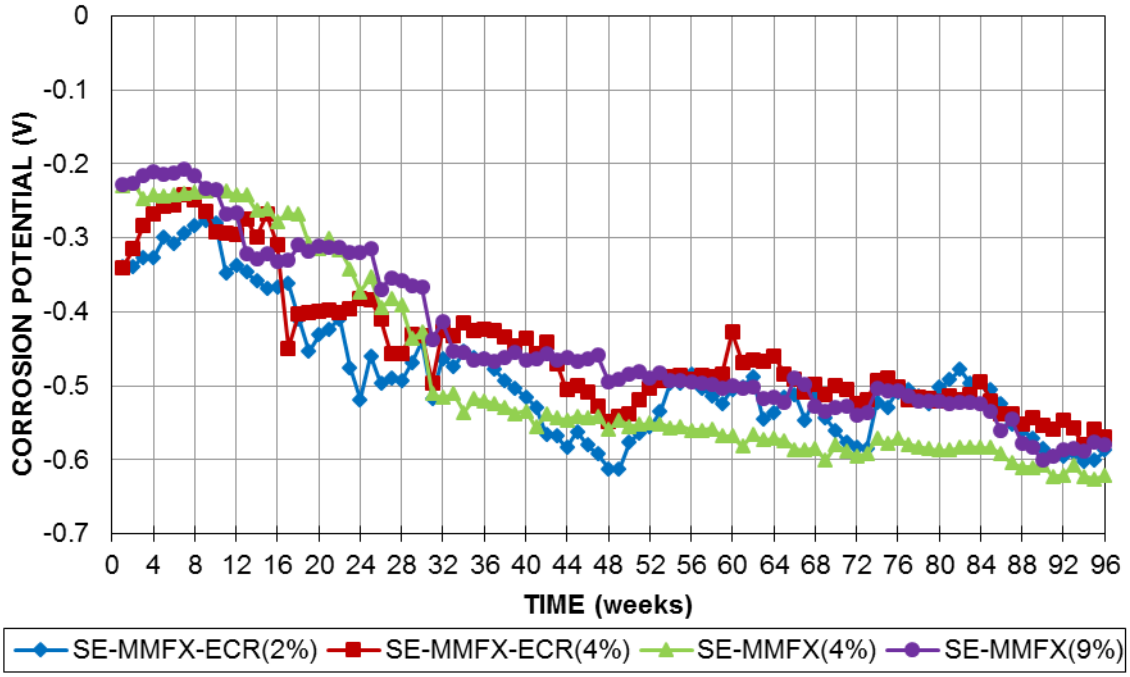

Figure 3.23—Top mat (anode) corrosion potential (CSE) versus time for Southern Exposure specimens containing bare and epoxy-coated MMFX bars

3.4.1.4 Autopsy

Upon completion of the test (96 weeks), Southern Exposure specimens were drilled to measure the final chloride content and then autopsied and photographed. Figures 3.24 and 3.25 show the top and bottom mats, respectively, of a representative Southern Exposure specimen containing bars with 4% chromium (SE-MMFX(4%)-6), after autopsy. Figures 3.26 and 3.27 show

the top and bottom mat of a representative specimen with MMFX reinforcement containing 9% chromium (SE-MMFX(9%)-5). Signs of corrosion can be observed on both top and bottom mat bars of specimens. On the top bars, corrosion was concentrated on the upper face of the bars, with as much as 50% of the surface area corroded. Corroded regions on the bottom mat bars were significantly less than the top mat (about 10% of one side of one or two bars). This indicates that the duration of the bench-scale tests (96 weeks) were long enough for chlorides to penetrate through the entire concrete section, reach the bottom bar surface, and initiate corrosion there. The corrosion initiation of bottom bars can be determined by the drop in corrosion potentials of bottom mat bars; this data is presented in Appendix D. The corroded area on the surface of bars with 9% chromium was generally lower than that on bars with 4% chromium.

Figure 3.24— Southern Exposure MMFX(4%)-6 top bars after 96 weeks

Figure 3.25— Southern Exposure MMFX(4%)-6 bottom bars after 96 weeks

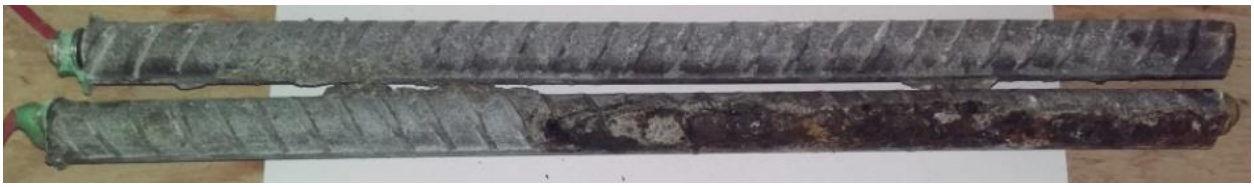

Figure 3.26— Southern Exposure MMFX(9%)-5 top bars after 96 weeks

Figure 3.27— Southern Exposure MMFX(9%)-5 bottom bars after 96 weeks

Figure 3.28 shows a representative top mat epoxy-coated reinforcement of Southern Exposure specimens (SE-MMFX-ECR(4%)-5) before disbondment. Corrosion products were visible on some of intentionally damaged sites of reinforcement after autopsy. However, corrosion products were more obvious on the underlying steel after the disbondment test. The top mat and a representative bar from the bottom mat of SE-MMFX-ECR(4%)-5 after the disbondment test are shown in Figures 3.29 and 3.30, respectively. Figures 3.31 and 3.32 present top bars and a bottom bar of SE-MMFX-ECR(2%)-5, respectively, after the disbondment test. Visible corrosion products, after the disbondment test, on the underlying steel of top mat bars in Figures 3.29 and 3.31 are indicated by ovals.

Figure 3.28— Southern Exposure MMFX-ECR(4%)-5 top bars before disbondment test after 96 weeks

Figure 3.29— Southern Exposure MMFX-ECR(4%)-5 top bars after disbondment test after 96 weeks

Figure 3.30— Southern Exposure MMFX-ECR(4%)-5 bottom bar after disbondment test after 96 weeks

Figure 3.31— Southern Exposure MMFX-ECR(2%)-5 top bars after disbondment test after 96 weeks

Figure 3.32— Southern Exposure MMFX-ECR(2%)-5 bottom bar after disbondment test after 96 weeks

The disbonded area for top bars from MMFX-ECR(4%) and MMFX-ECR(2%) Southern Exposure specimens are tabulated in Tables 3.6 and 3.7, respectively. For each bar, the disbondment test was performed at three intentionally damaged sites, two of which were chosen from the upper surface of the bar, as it was oriented in the specimen, and the third from the bottom surface. The average disbondment of MMFX-ECR(4%) top bars, 0.55 in^2 (358 mm^2), was 20% less than the disbondment for MMFX-ECR(2%), 0.69 in^2 (447 mm^2), however, a wide variation betweeen specimens was observed.

Table 3.6: Disbonded area and total corrosion loss at week 96 for the MMFX-ECR(4%) top bars in Southern Exposure specimens

Specimen	Total Corrosion Loss (µm)	Top side 1 (in^2)	Top side 2 (in^2)	Bottom side (in^2)	Average (in^2)
1	0.100	1.05	0.54	0.32	0.42
		0.19	0.21	0.22	
2	0.088	1.05	0.39	0.41	0.49
		0.25	0.28	0.31	
3	0.075	1.05	0.21	0.20	0.41
		0.61	0.25	0.15	
4	0.084	1.05	1.05	1.05	0.98
		0.62	1.05	1.05	
5	0.328	0.33	0.15	0.23	0.54
		1.05	1.05	0.43	
6	0.076	0.11	0.24	0.01	0.53
		0.95	0.36	0.29	
Average	0.125				0.55

Table 3.7: Disbonded area and total corrosion loss at week 96 for the MMFX-ECR(2%) top bars in Southern Exposure specimens

Specimen	Total Corrosion Loss (µm)	Top side 1 (in^2)	Top side 2 (in^2)	Bottom side (in^2)	Average (in^2)
1	0.155	0.79	0.26	0.17	0.73
		1.05	1.05	1.05	
2	0.4	0.39	0.17	0.59	0.41
		0.85	0.34	0.12	
3	0.275	0.73	0.50	0.22	0.67
		1.05	1.00	0.53	
4	0.135	0.27	1.05	0.87	0.63
		0.59	0.15	0.87	
5	0.288	0.91	1.05	1.05	1.03
		1.05	1.05	1.05	
6	0.246	1.05	0.59	0.41	0.70
		1.05	0.24	0.83	
Average	0.250				0.69

3.4.2 Cracked Beam Specimens

3.4.2.1 Macrocell Corrosion

Macrocell corrosion rates of cracked beam specimens calculated from voltage drops for MMFX uncoated bars containing 9% chromium (CB-MMFX(9%)) and 4% chromium (CB-MMFX(4%)) are shown in Figures 3.33 and 3.34, respectively. The maximum corrosion rates for the CB-MMFX(9%) and CB-MMFX(4%) specimens through week 96 ranged from 16.6 to 24.6 µm/yr and 23.5 to 29.1 µm/yr, respectively.

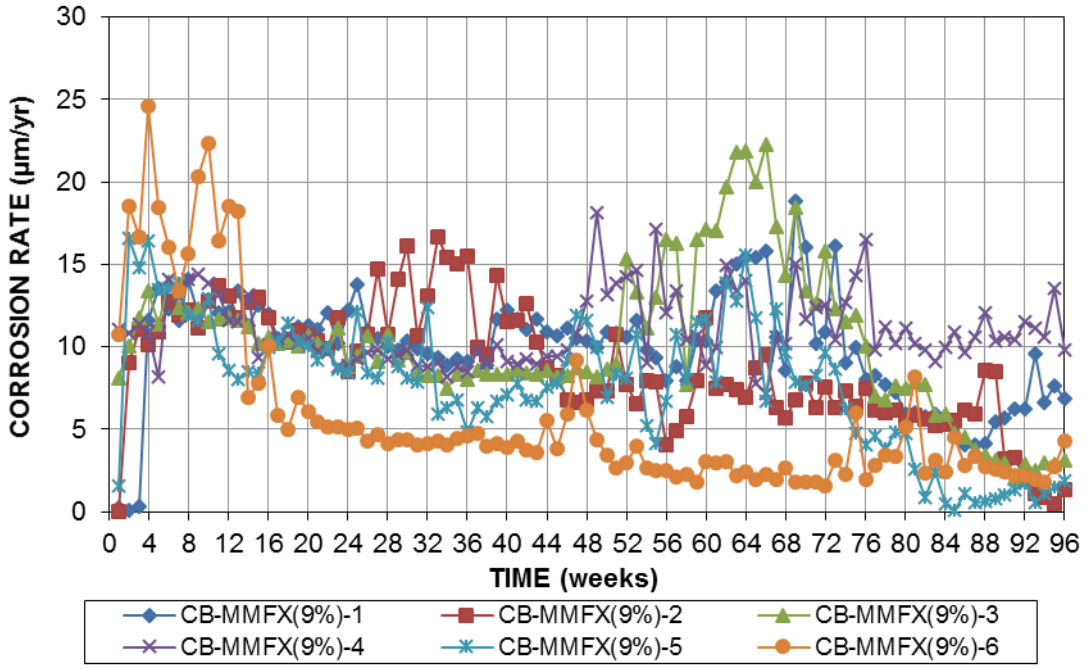

Figure 3.33— Macrocell corrosion rates (µm/yr) for cracked beam specimens containing MMFX(9%) bars

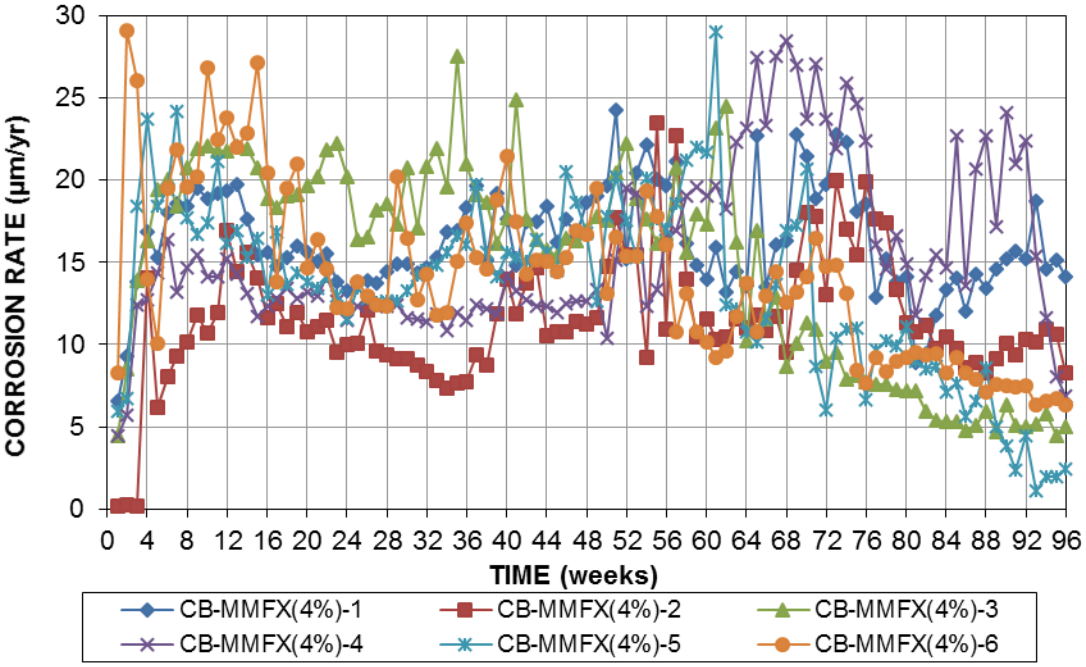

Figure 3.34— Macrocell corrosion rates (µm/yr) for cracked beam specimens containing MMFX(4%) bars

Macrocell corrosion rates of cracked beam specimens calculated from voltage drops for epoxy-coated MMFX bars containing 4% chromium (CB-MMFX-ECR(4%)) and 2% chromium (CB-MMFX-ECR(2%)) based on total area of the bar are shown in Figures 3.35 and 3.36, respectively. The maximum corrosion rates based on total area for the CB-MMFX-ECR(4%) and CB-MMFX-ECR(2%) specimens through week 96 ranged from 0.389 to 1.43 µm/yr and 0.602 to 2.08 µm/yr, respectively.

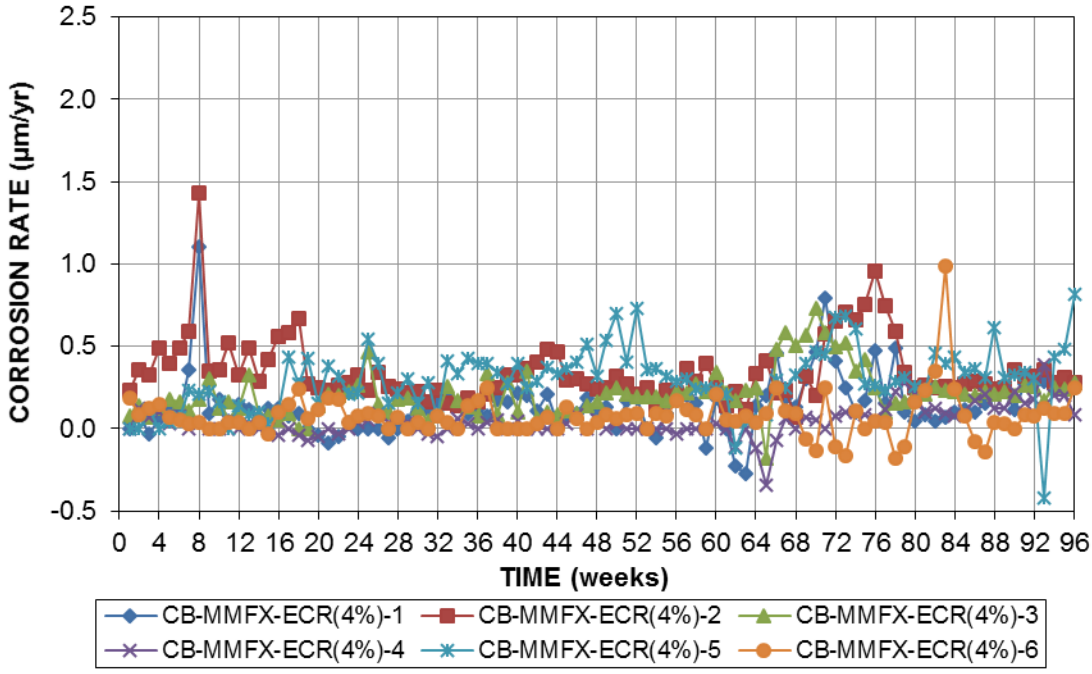

Figure 3.35— Macrocell corrosion rates based on total area (µm/yr) for cracked beam specimens containing MMFX-ECR(4%) bars

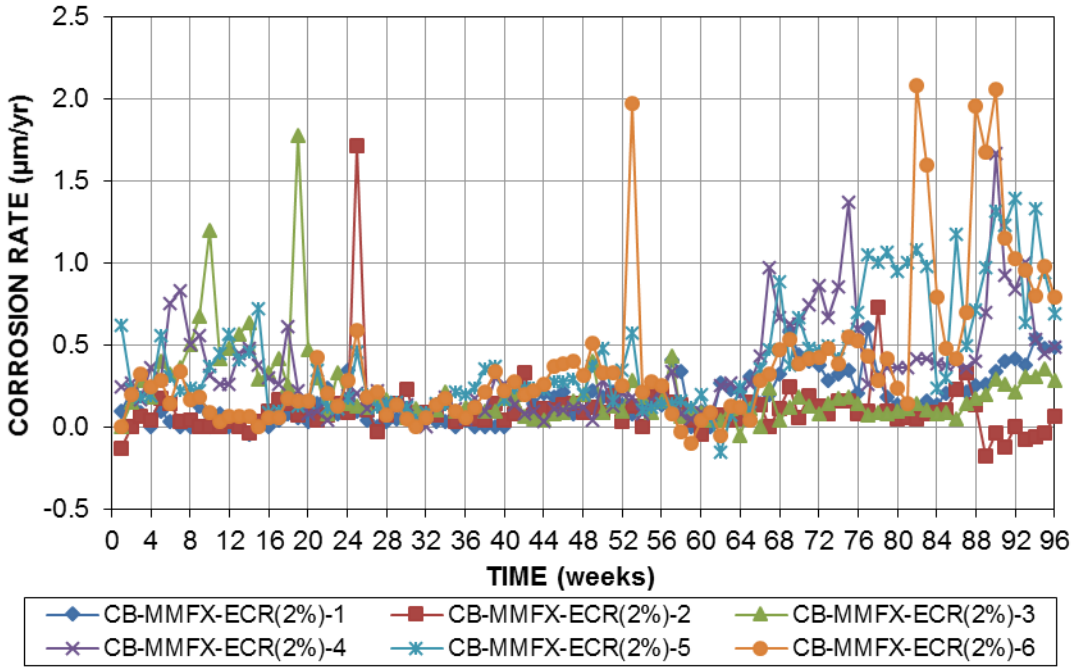

Figure 3.36— Macrocell corrosion rates based on total area (µm/yr) for cracked beam specimens containing MMFX-ECR(2%) bars

Figures 3.37 and 3.38 show macrocell corrosion rate for the CB-MMFX-ECR(4%) and CB-MMFX-ECR(2%) specimens, respectively, based on exposed area of the reinforcement. The maximum corrosion rates based on exposed area for the CB-MMFX-ECR(4%) and CB-MMFX-ECR(2%) specimens through week 96 ranged from 74.6 to 275 µm/yr and 116 to 399 µm/yr, respectively.

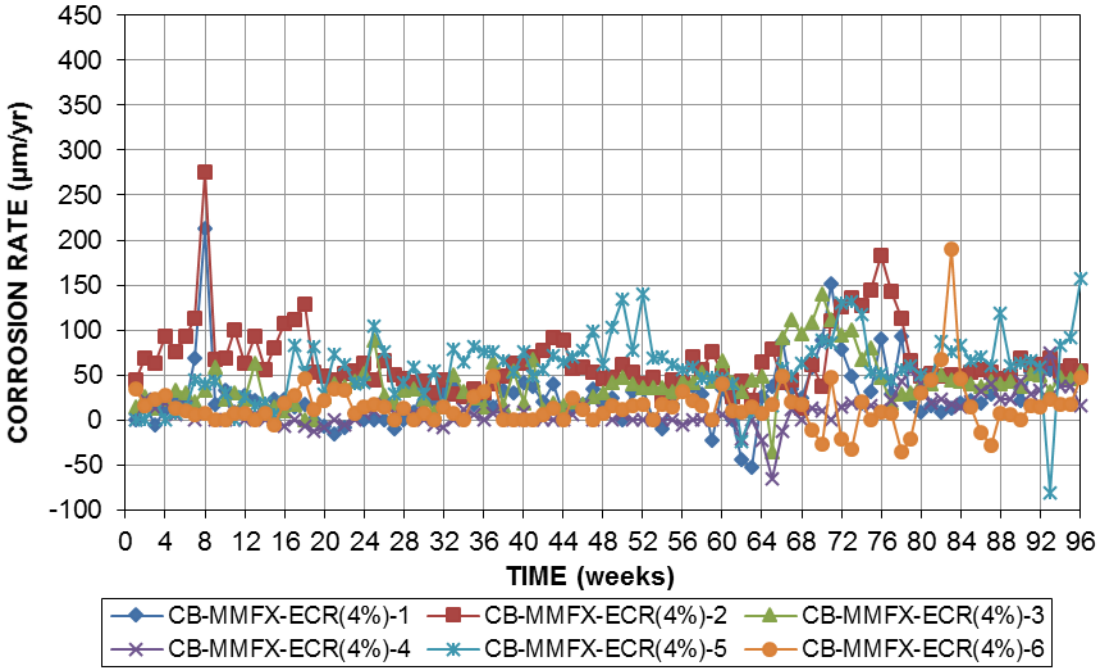

Figure 3.37— Macrocell corrosion rates based on exposed area (µm/yr) for cracked beam specimens containing MMFX-ECR(4%) bars

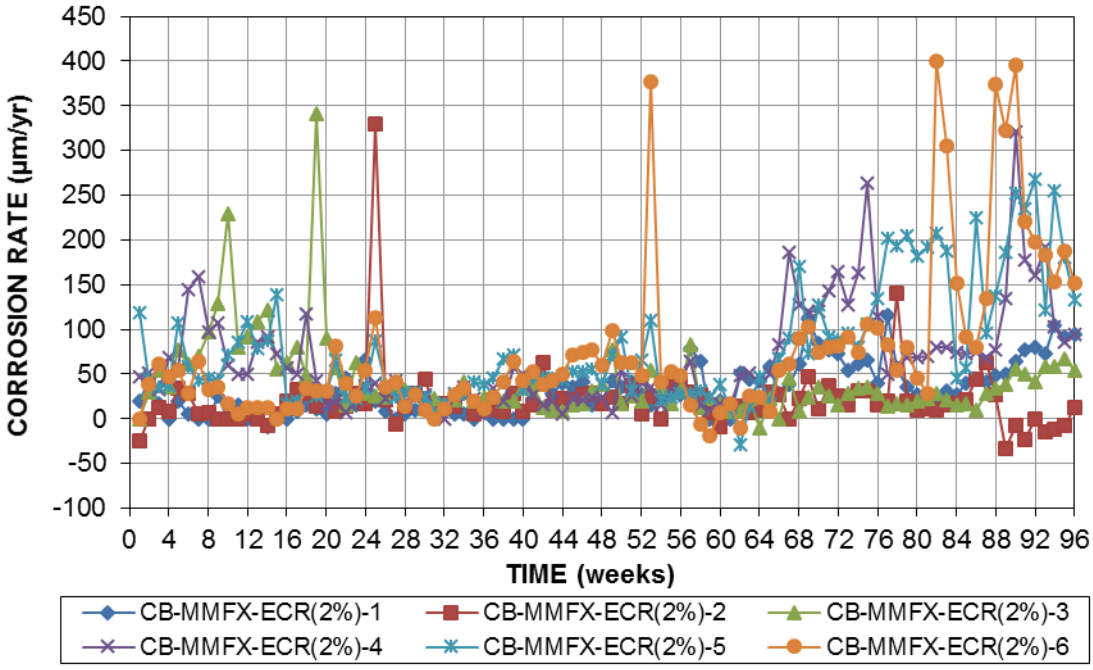

Figure 3.38— Macrocell corrosion rates based on exposed area (µm/yr) for cracked beam specimens containing MMFX-ECR(2%) bars

Figure 3.39 shows the average corrosion rates for the cracked beam specimens. The highest corrosion rate through week 96 has been observed on the CB-MMFX(4%) specimens, with an average corrosion rate of 19.1 µm/yr at week 51. The CB-MMFX(9%) specimens exhibited a maximum average corrosion rate of 14.5 µm/yr at week 4. Based on total area, the epoxy-coated bars with the 2% and 4% nominal chromium contents show corrosion rates less than 1 µm/yr over 96 weeks of testing. The epoxy-coated CB-MMFX-ECR(2%) and CB-MMFX-ECR(4%) specimens exhibited maximum corrosion rates of 0.94 µm/yr and 0.50 µm/yr at weeks 90 and 8, respectively. Based on exposed area (Figure 3.40), the corrosion rate of epoxy-coated bars with 2% nominal chromium content fluctuated between 0 and 180 µm/yr; bars with 4% chromium content had rates between 0 and 95 µm/yr.

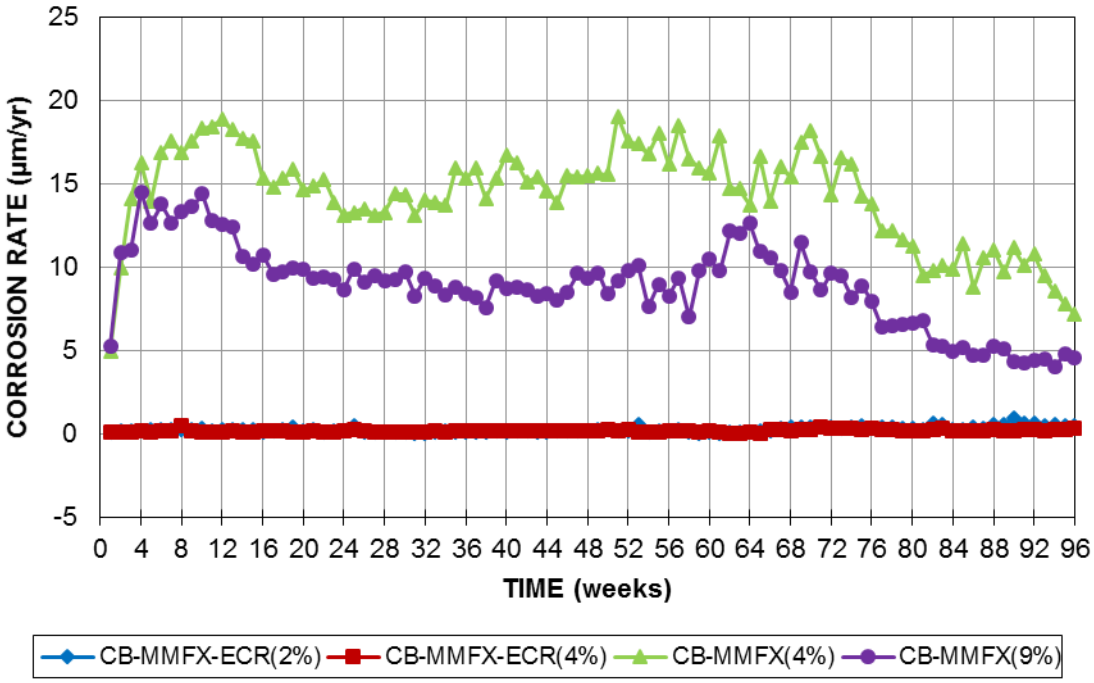

Figure 3.39— Average corrosion rate (µm/yr) based on total area versus time for cracked beam specimens containing bare and epoxy-coated MMFX bars

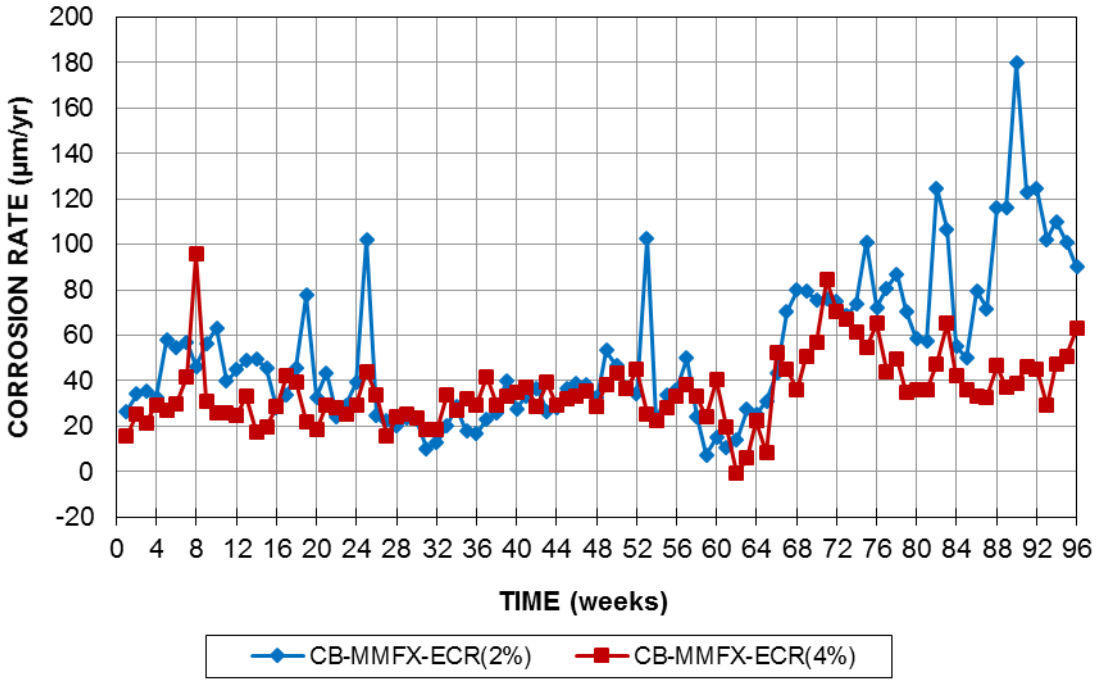

Figure 3.40— Average corrosion rate (µm/yr) based on exposed area versus time for cracked beam specimens containing epoxy-coated MMFX bars

The average and individual corrosion losses for the cracked beam specimens through end of the test (week 96) are tabulated in Table 3.8. Based on total area, the greatest individual loss, 30.1 µm was observed for Specimen MMFX(4%)-1. The average corrosion loss of the MMFX(4%) specimens was 26.5 µm. The corrosion losses for the MMFX-9% specimens ranged from 10.6 to 20.4 µm, with an average of 16.4 µm. Based on total area, the epoxy-coated bars exhibited losses approximately two orders of magnitude less than the uncoated bars. Based on exposed area, losses for the MMFX-ECR(2%) and MMFX-ECR(4%) specimens ranged from 37.0 to 147 µm, with an average of 97.1 µm, and 15.8 to 123 µm, with an average loss of 65.4 µm, respectively.

Table 3.8: Corrosion loss (µm) for cracked beam specimens

Specimen	Corrosion Loss (µm)-Total Area						Average	Std. Dev.
	Week 96		Week 96		Week 96			
	1	2	3	4	5	6		
MMFX-ECR(2%)	0.315	0.193	0.401	0.644	0.767	0.715	0.506	0.235
MMFX-ECR(4%)	0.262	0.638	0.390	0.082	0.546	0.127	0.341	0.224
MMFX(4%)	30.1	21.3	27.6	29.0	25.0	26.2	26.5	3.16
MMFX(9%)	18.3	16.1	18.9	20.4	14.2	10.6	16.4	3.59
	Corrosion Loss (µm)-Exposed Area							
MMFX-ECR(2%)	60.5	37.0	76.9	124	147	137	97.1	45.1
MMFX-ECR(4%)	50.3	123	74.9	15.8	105	24.4	65.4	43.1

3.4.2.2 Linear Polarization Resistance (LPR) Test

Corrosion rates obtained from LPR test results on cracked beam specimens with uncoated MMFX bars containing 9% and 4% chromium are shown in Figures 3.41 and 3.42, respectively. The maximum corrosion rates for specimens CB-MMFX(9%) and CB-MMFX(4%) through week 96 ranged from 10.2 to 45.9 µm/yr and 19.3 to 79.2 µm/yr, respectively.

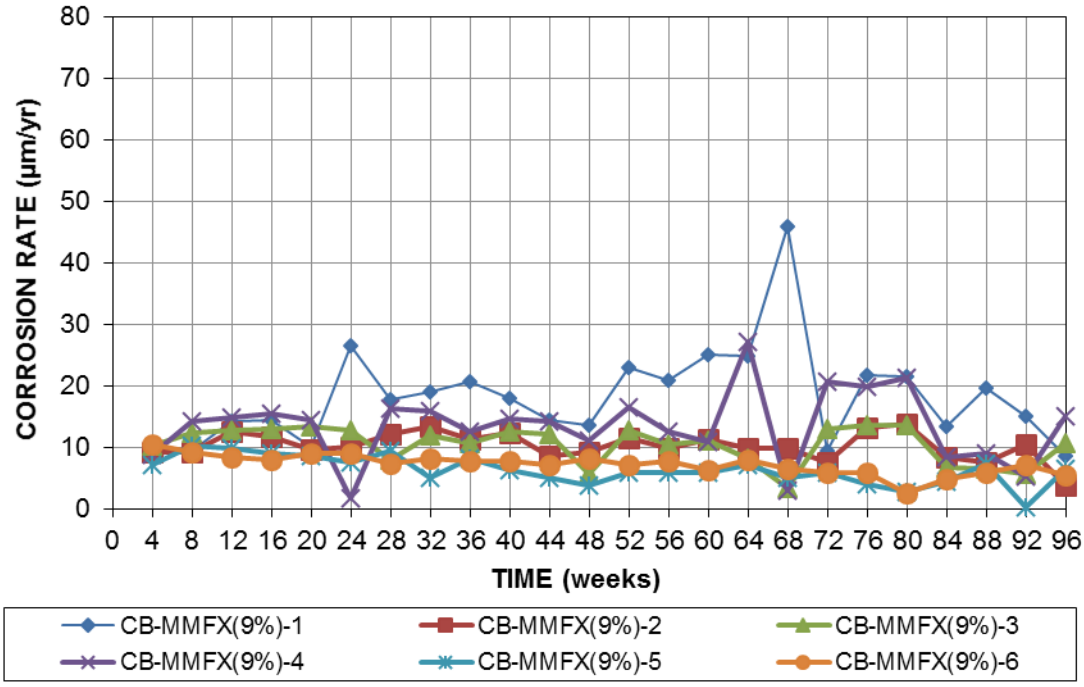

Figure 3.41— LPR test corrosion rates (µm/yr) for cracked beam specimens containing MMFX(9%) bars

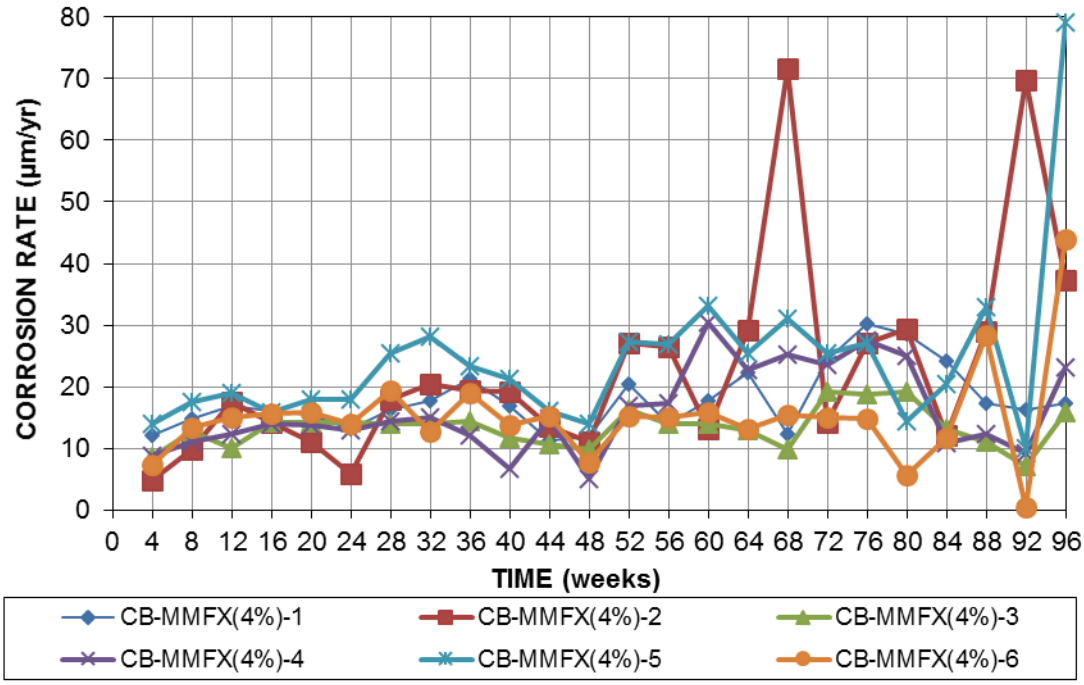

Figure 3.42— LPR test corrosion rates (µm/yr) for cracked beam specimens containing MMFX(4%) bars

Corrosion rates based on total area obtained from LPR test results on cracked beam specimens with MMFX epoxy-coated specimens containing 4% and 2% chromium are shown in Figures 3.43 and 3.44, respectively. Based on total area, the maximum corrosion rates for specimens CB-MMFX-ECR(4%) and CB-MMFX-ECR(2%) through week 96 ranged from 0.28 to 3.76 µm/yr and 0.66 to 9.95 µm/yr, respectively.

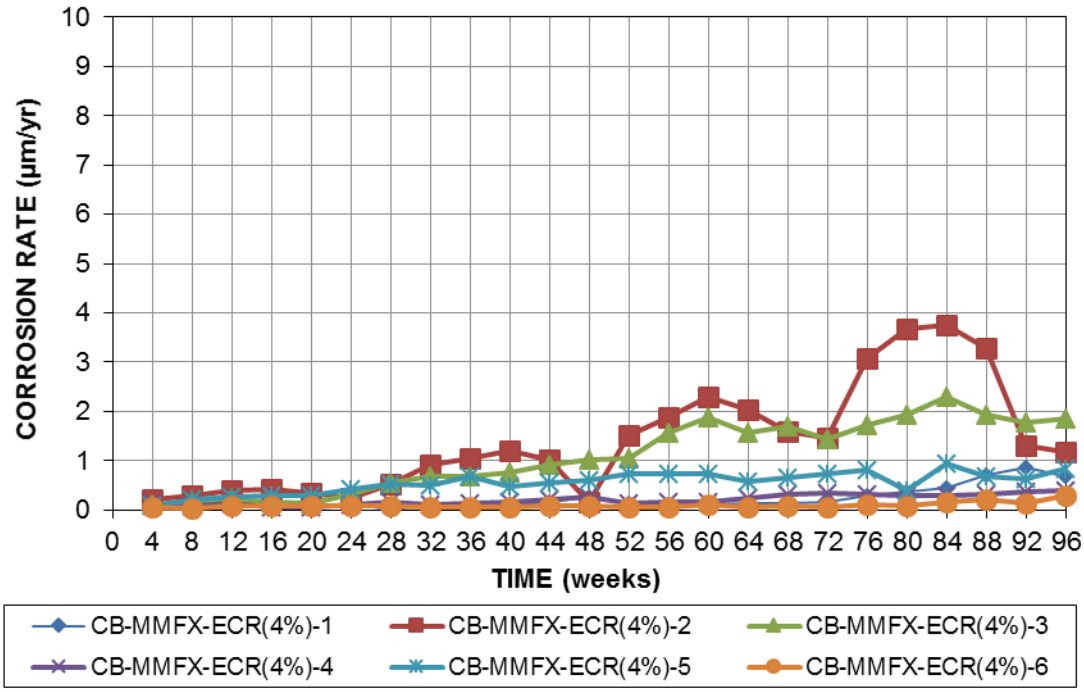

Figure 3.43— LPR test corrosion rates (µm/yr) based on total area of reinforcement for cracked beam specimens containing MMFX-ECR(4%) bars

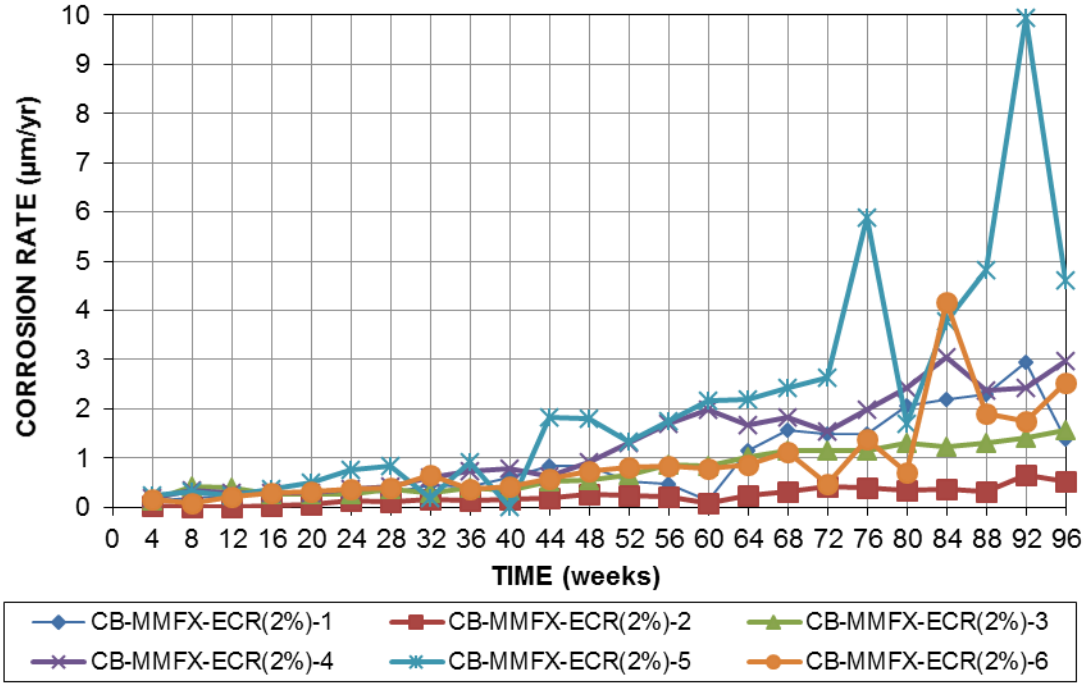

Figure 3.44— LPR test corrosion rates (µm/yr) based on total area of reinforcement for cracked beam specimens containing MMFX-ECR(2%) bars

Figure 3.45 shows the average corrosion rate for the cracked beam specimens based on total area obtained from LPR test results. For CB-MMFX(4%) specimens average corrosion rate generally increased throughout the test and reached the peak value (44 µm/yr) at the end of test, while the average corrosion rate for CB-MMFX(9%) remained relatively constant during the test and ranged from 7.3 to 14.2 µm/yr. The epoxy-coated specimens, compared to the uncoated bars, present lower corrosion rates based on total area. The maximum average corrosion rates for epoxy-coated bars containing 4% and 2% chromium were 1.31 and 3.19 µm/yr, respectively.

Figure 3.46 shows the average corrosion rate for the cracked beam specimens based on exposed area obtained from LPR test results. As shown, up to week 40 the average corrosion rate for CB-MMFX-ECR(2%) was similar to that of CB-MMFX-ECR(4%). After week 40, CB-MMFX-ECR(2%) exhibited greater corrosion rates than CB-MMFX-ECR(4%), and the difference between the two increased over time. Based on exposed area, the epoxy-coated CB-MMFX-ECR(2%) and CB-MMFX-ECR(4%) specimens exhibited maximum corrosion rates of 613 µm/yr and 253 µm/yr at weeks 92 and 84, respectively.

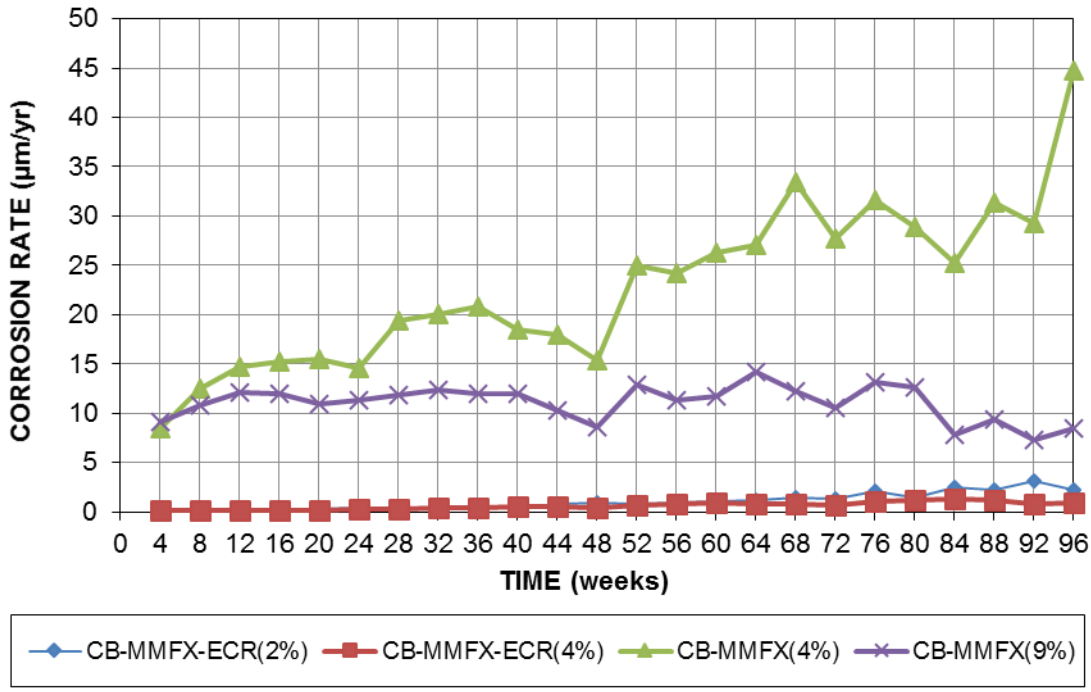

Figure 3.45— Average LPR test corrosion rate (µm/yr) based on total area versus time for cracked beam specimens containing bare and epoxy-coated MMFX bars

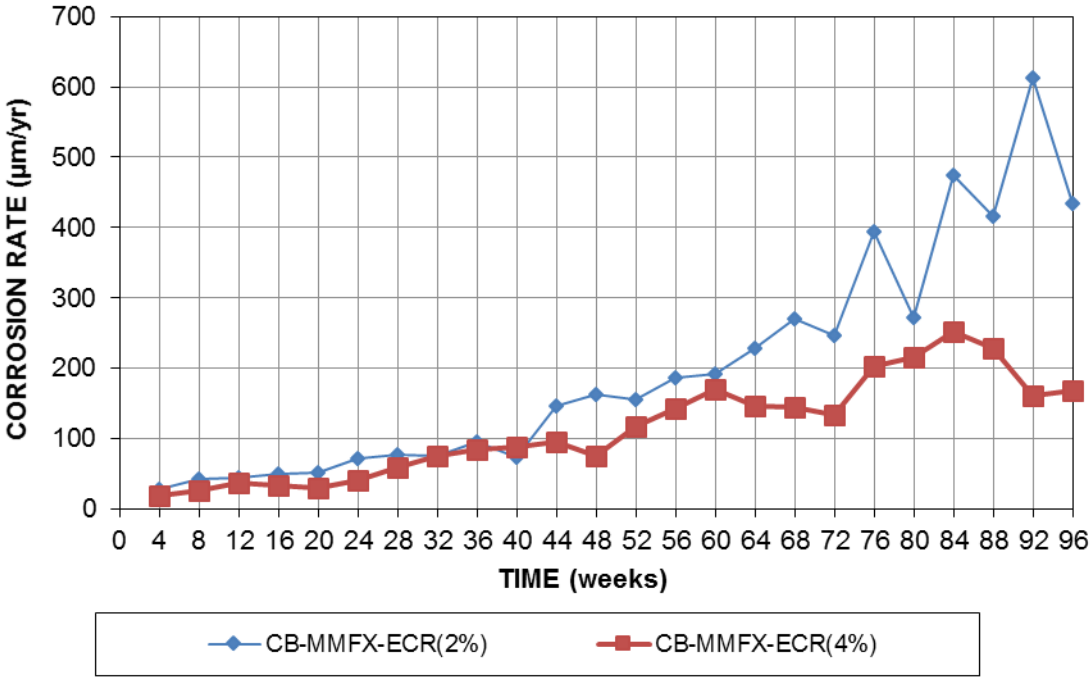

Figure 3.46— Average LPR test corrosion rate (µm/yr) based on exposed area versus time for cracked beam specimens containing epoxy-coated MMFX bars

The average and individual corrosion losses for the cracked beam specimens obtained from LPR test results through the end of test (week 96) are tabulated in Table 3.9. Based on total area, the greatest individual loss, 44.9 µm was observed for Specimen MMFX(4%)-5. The average corrosion loss of the MMFX(4%) specimens was 33.8 µm, about 28% higher than that obtained from macrocell corrosion rates. The corrosion losses for the MMFX(9%) specimens ranged from 11.7 to 33.6 µm, with an average of 20.4 µm, about 24% higher than that obtained from macrocell corrosion rates. Based on total area, the epoxy-coated bars exhibited losses approximately one order of magnitude less than the uncoated bars. Based on exposed area, losses for the MMFX-ECR(2%) specimens ranged from 79.2 to 756 µm, with an average of 370 µm, about 3.8 times the one obtained from macrocell corrosion rates. Corrosion losses for MMFX-ECR(4%) specimens ranged from 32.5 to 500 µm, with an average loss of 212 µm, about 3.2 times that obtained from macrocell corrosion rates.

Table 3.9: Corrosion loss (µm) for cracked beam specimens based on LPR test results

Specimen	Corrosion Loss (µm)-Total Area						Average	Std. Dev.
	Week 96		Week 96		Week 96			
	1	2	3	4	5	6		
MMFX-ECR(2%)	1.74	0.413	1.38	2.40	3.94	1.69	1.93	1.18
MMFX-ECR(4%)	0.397	2.60	2.03	0.385	1.03	0.170	1.10	1.00
MMFX(4%)	33.1	42.4	24.6	29.7	44.9	27.9	33.8	8.2
MMFX(9%)	33.6	19.0	19.4	24.97	11.7	13.5	20.4	8.0
	Corrosion Loss (µm)-Exposed Area							
MMFX-ECR(2%)	335	79.2	265	461	756	324	370	226
MMFX-ECR(4%)	76.2	500	390	74.0	198	32.5	212	192

3.4.2.3 Corrosion Potential

The average top mat corrosion potentials (with respect to a copper-copper sulfate electrode) for the cracked beam specimens are shown in Figure 3.47. The specimens with all four bar types exhibited potentials between –0.40 V and –0.47 V at the start of the test. The average potential of the MMFX-ECR(2%) specimens dropped to near –0.60 V up to week 11 and gradually increased

up to week 24. After week 24, potentials again decreased, ranging between –0.53 V and –0.70 V by week 96. The potentials of the MMFX-ECR(4%), MMFX(4%), and MMFX(9%) specimens dropped from the values at the start of testing to near –0.58 V, –0.53 V, and –0.52 V at weeks 2, 4, and 5, respectively, and exhibited potentials between –0.60 V and –0.70 V through week 96. The potential values indicate that the specimens initiated corrosion in the first week of testing.

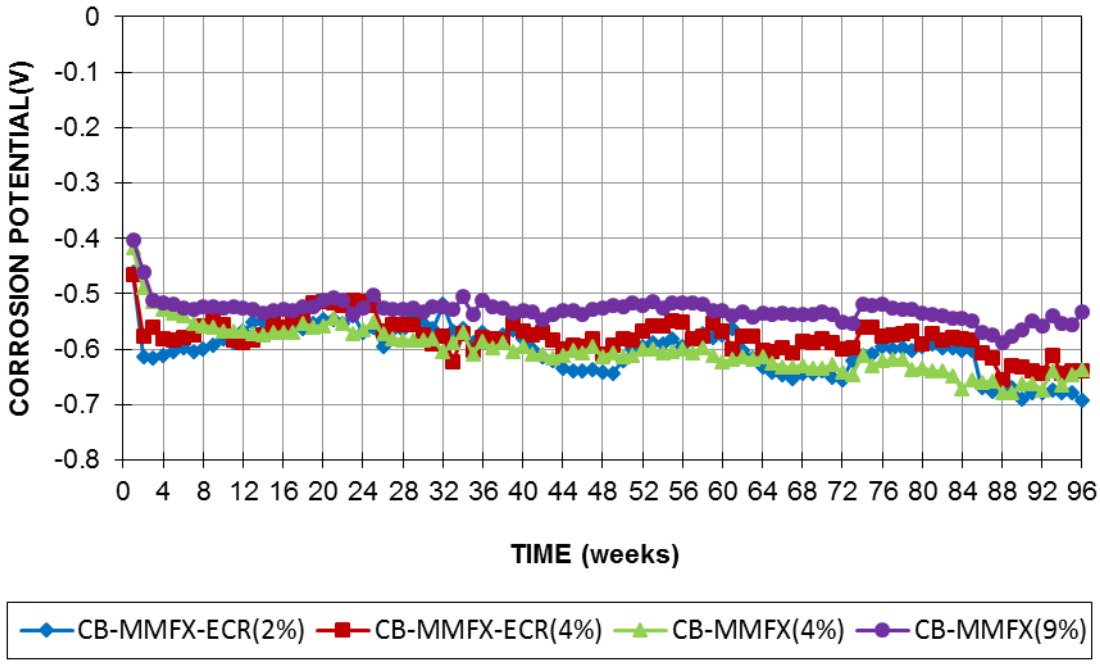

Figure 3.47— Top mat (anode) corrosion potential (CSE) versus time for cracked beam specimens containing bare and epoxy-coated MMFX bars

3.4.2.4 Autopsy Results

Upon completion of the test (96 weeks), cracked beam specimens were autopsied and photographed. Top and bottom bars from a representative cracked beam specimen with uncoated bars containing 4% chromium (CB-MMFX(4%)-5) are shown in Figures 3.48 and 3.49; a top bar from a specimen containing a bar with 9% chromium is shown in Figure 3.50. Corrosion products can be observed on the both top and bottom mat bars of the specimens with bars containing 4%

chromium. However, the corroded area on the top bar was significantly greater (70% of the top face and 30% of the bottom face) than the corroded area of the bottom bar (35% of the top face only). As shown in Figure 3.50, corrosion products were also visible on bars containing 9% chromium, but with a significantly lower corroded area than that on bars with 4% chromium.

Figure 3.48— Cracked beam MMFX(4%)-5 top bar after 96 weeks

Figure 3.49— Cracked beam MMFX(4%)-5 bottom bars after 96 weeks

Figure 3.50— Cracked beam MMFX(9%)-5 top bar after 96 weeks

Disbondment tests were performed on the epoxy-coated bars for the top bar as well as one representative bar from the bottom mat of each specimen. Top and bottom bars of representative cracked beam specimens containing 2% and 4% chromium (CB-MMFX-ECR(2%)-2 and CB-MMFX-ECR(4%)-5) are shown in Figures 3.51 through 3.53, respectively. Most of the top mat bars containing 2% chromium experienced total disbondment between the epoxy layer and the

underlying steel. Accumulated corrosion products under the disbonded epoxy were also widespread for these reinforcement (Figure 3.51). Bottom mat bars containing 2% chromium, however, did not exhibit significant disbondment or visible corrosion products (Figure 3.52). Top mat reinforcement of specimens with bars containing 4% chromium did not show as much disbondment as reinforcement with 2% chromium; however, corrosion products were still visible under the disbonded epoxy. For CB-MMFX-ECR(4%)-5 top and bottom bars, visible corrosion products are indicated by ovals in Figures 3.53 and 3.54, respectively.

Figure 3.51— Cracked beam MMFX-ECR(2%)-2 top bar after disbondment test after 96 weeks

Figure 3.52— Cracked beam MMFX-ECR(2%)-2 bottom bar after disbondment test after 96 weeks

Figure 3.53— Cracked beam MMFX-ECR(4%)-5 top bar after disbondment test after 96 weeks

Figure 3.54— Cracked beam MMFX-ECR(4%)-5 bottom bar after disbondment test after 96 weeks

The disbonded area for the top bar of MMFX-ECR(4%) and MMFX-ECR(2%) cracked beam specimens are tabulated in Tables 3.10 and 3.11, respectively. For bars that experienced total disbondment, the disbonded area was treated as 1.05 in^2 (677 mm^2). The average disbondment of MMFX-ECR(4%) top bars was 0.71 in^2 (454 mm^2). All but one tested site for top bars containing 2% chromium experienced total disbondment, resulting in an average disbondment of 0.98 in^2 (634 mm^2).

Table 3.10: Disbonded area at week 96 for the MMFX-ECR(4%) top bar in cracked beam specimens

Specimen	Top side 1 (in^2)	Top side 2 (in^2)	Bottom side (in^2)	Average (in^2)
1	1.05	1.05	0.85	0.98
2	1.05	1.05	1.05	1.05
3	1.05	1.05	0.61	0.90
4	1.05	0.11	0.31	0.49
5	0.80	0.58	0.62	0.67
6	0.17	0.13	0.11	0.14
Average				0.71

Table 3.11: Disbonded area at week 96 for the MMFX-ECR(2%) top bar in cracked beam specimens

Specimen	Top side 1 (in^2)	Top side 2 (in^2)	Bottom side (in^2)	Average (in^2)
1	1.05	1.05	1.05	1.05
2	1.05	1.05	1.05	1.05
3	1.05	0.62	1.05	0.91
4	1.05	1.05	0.77	0.96
5	1.05	1.05	1.05	1.05
6	1.05	1.05	0.55	0.88
Average				0.98

3.4.3 Rapid Macrocell (RM) Test

For all four types of reinforcement (MMFX bare bars containing 4% and 9% chromium and MMFX epoxy-coated bars containing 2% and 4% chromium) six rapid macrocell tests were prepared. In addition, to investigate the effect of pickling on MMFX bars, uncoated bars containing 4% and 9% chromium (one set of six bars from each) were also pickled and evaluated under the

rapid macrocell test. Macrocell corrosion, corrosion potential, LPR test, autopsy, and (for epoxy-coated bars) disbondment test results for these specimens are discussed in the following sections.

3.4.3.1 Macrocell Corrosion

The corrosion rates of the bare MMFX bar specimens with 4% and 9% nominal chromium content in the as-received and pickled conditions are shown in Figure 3.55. Over the 15 weeks of testing, the as-received MMFX(4%) specimens exhibited the greatest corrosion rate (42.34 µm/yr during first week of testing), whereas the pickled MMFX(9%) specimens exhibited the lowest corrosion rate (below 12.20 µm/yr). After the first week, the corrosion rates of the as-received MMFX(4%) specimens decreased gradually, to 35.20 µm/yr at week 15. The corrosion rates of as-received MMFX(9%) specimens was 20.25 µm/yr or less, except for the peak at week 4. The pickled MMFX(4%) corrosion rate fluctuated between 8.07 µm/yr at week 11 and 33.77 µm/yr at week 2, but generally decreased over time. For bars with both 9% and 4% chromium, pickling resulted in reductions in the average corrosion rate relative to unpickled bars.

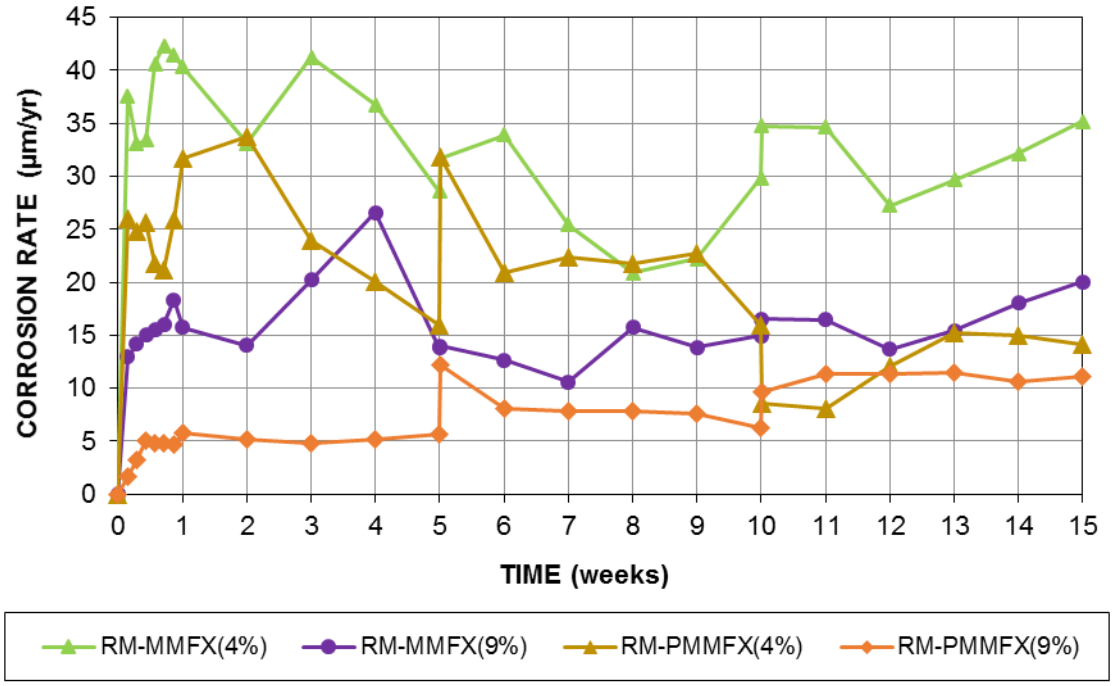

Figure 3.55—Average corrosion rates (µm/yr) versus time for rapid macrocell tests containing bare MMFX bars in as-received and pickled condition

The average corrosion rates of the epoxy-coated MMFX bars with 2% and 4% nominal chromium content is shown in Figure 3.56. Over 15 weeks of testing, the average corrosion rate of MMFX-ECR(4%) specimens was lower than that of MMFX-ECR(2%); however, all of the coated specimens exhibited average corrosion rates below 2.00 µm/yr, with the exception of the epoxy-coated MMFX-ECR(2%) specimens at week 5, which had an average corrosion rate of 2.33 µm/yr.

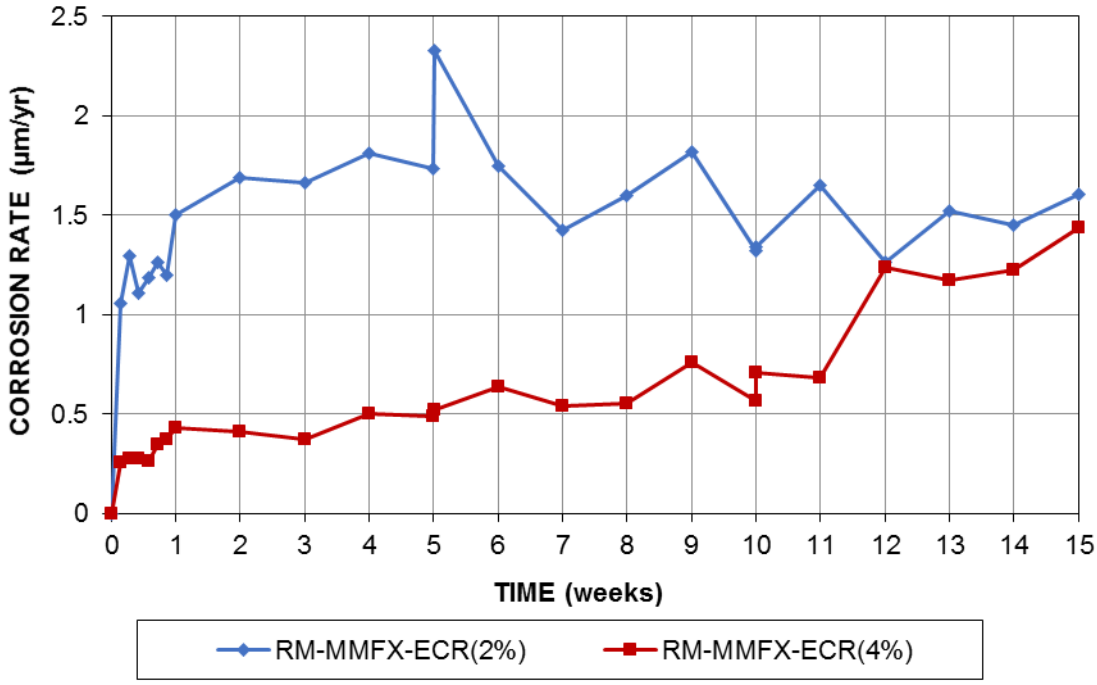

Figure 3.56— Average corrosion rates (µm/yr) versus time for rapid macrocell tests containing epoxy-coated MMFX bars based on total area

The individual corrosion losses at the end of the test (week 15) of the uncoated MMFX bar specimens with 4% and 9% nominal chromium content in the as-received and pickled conditions, and epoxy-coated bars containing 2% and 4% chromium are tabulated in Table 3.12. The average corrosion loss during the test for bare bars in the as-received and pickled condition and for the epoxy-coated bars (based on the total area) are shown in Figures 3.57 and 3.58, respectively. Corrosion losses were obtained by integrating the macrocell corrosion rates with respect to time. The corrosion losses of the as-received bars with 4% and 9% chromium after 15 weeks were 9 µm and 4.63 µm, respectively; whereas the pickled bars with 4% and 9% chromium exhibited lower corrosion losses (5.51 µm and 2.27 µm respectively). After 15 weeks, corrosion loss of MMFX-ECR(4%) was 0.21 µm, less than half of corrosion loss of MMFX-ECR(2%), 0.45 µm.

Table 3.12: Corrosion loss (µm) for rapid macrocell specimens

Specimen	Corrosion Loss (µm)-Total Area						Average	Std. Dev.
	Week 15		Week 15		Week 15			
	1	2	3	4	5	6		
MMFX-ECR(2%)	0.296	0.524	0.500	0.502	0.310	0.577	0.451	0.118
MMFX-ECR(4%)	0.378	0.175	0.212	0.189	0.145	0.156	0.209	0.086
MMFX(4%)	4.36	4.30	10.2	13.2	11.8	10.2	9.00	3.79
MMFX(9%)	4.90	2.44	4.03	5.99	6.53	3.90	4.63	1.50
PMMFX(4%)	5.78	4.96	6.39	4.56	5.21	6.15	5.51	0.72
PMMFX(9%)	2.54	3.10	1.74	2.27	2.16	1.83	2.27	0.50

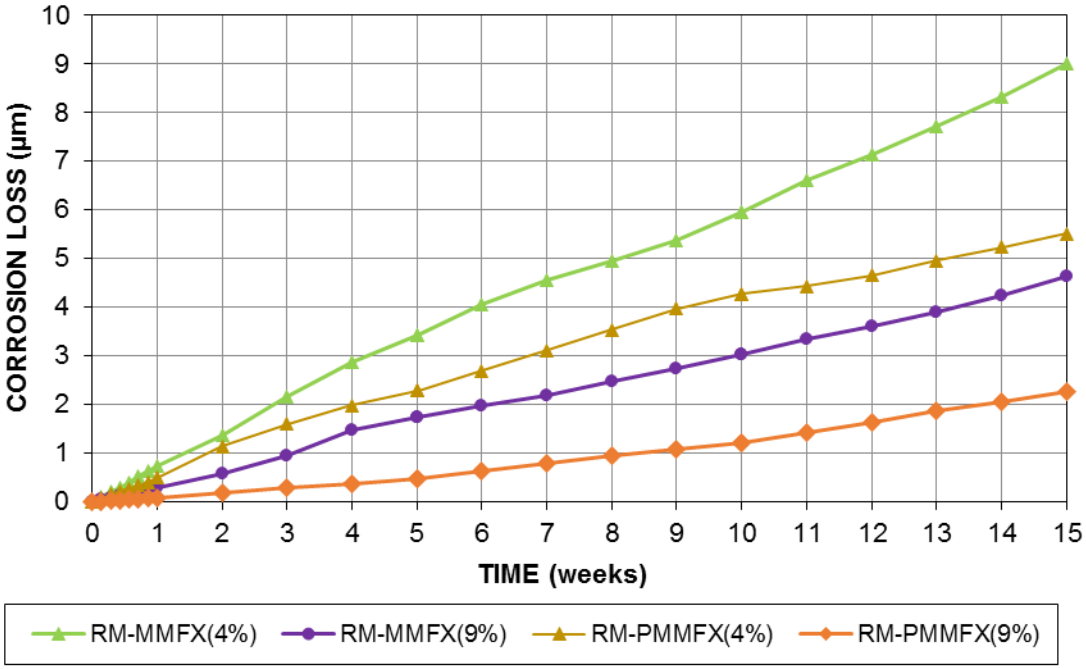

Figure 3.57—Average corrosion loss (µm) versus time for rapid macrocell tests containing bare MMFX bars in as-received and pickled condition

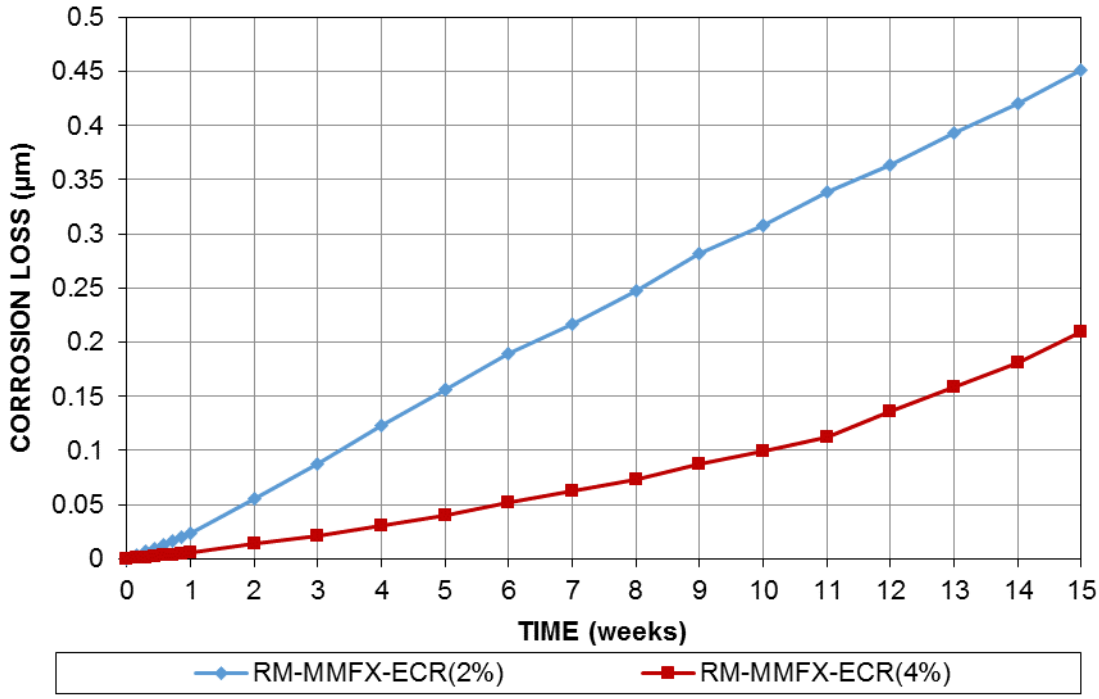

Figure 3.58— Average corrosion loss (µm) versus time for rapid macrocell tests containing epoxy-coated MMFX bars based on total area.

3.4.3.2 Linear Polarization Resistance (LPR) Test

Figures 3.59 and 3.60 show the average corrosion rate and loss, respectively, from LPR test results for the rapid macrocell specimens based on total area. Similar to results obtained from macrocell corrosion data, among bare bars, corrosion rate and loss decreased as chromium content increased. Although pickling reduced corrosion rate and loss of MMFX bars containing 9% chromium, it was not effective on the MMFX bars with 4% chromium.

The individual corrosion loss at the end of the test (week 15) of the uncoated MMFX bar specimens with 4% and 9% nominal chromium content in the as-received and pickled conditions, and epoxy-coated bars containing 2% and 4% chromium based on the LPR test results are tabulated in Table 3.13. Pickling MMFX bars containing 9% chromium approximately halved the corrosion loss (1.92 µm for PMMFX(9%) and 4.08 µm for MMFX(9%)) after 15 weeks of test. Pickling, however was not effective on reducing corrosion loss of MMFX bars containing 4% chromium

(8.28 µm for PMMFX(4%) and 8.73 µm for MMFX(4%)). For epoxy-coated bars, the corrosion loss of MMFX-ECR(4%), 0.33 µm, was about one third of the one for MMFX-ECR(2%), 1.07 µm. A comparison between the corrosion loss of reinforcement based on macrocell corrosion and LPR test results shows that for MMFX-ECR(4%) and MMFX-ECR(2%), corrosion losses based on LPR test results were two and 1.5 times greater than that based on macrocell corrosion, respectively. For bare bars the difference between LPR and macrocell corrosion losses was not significant.

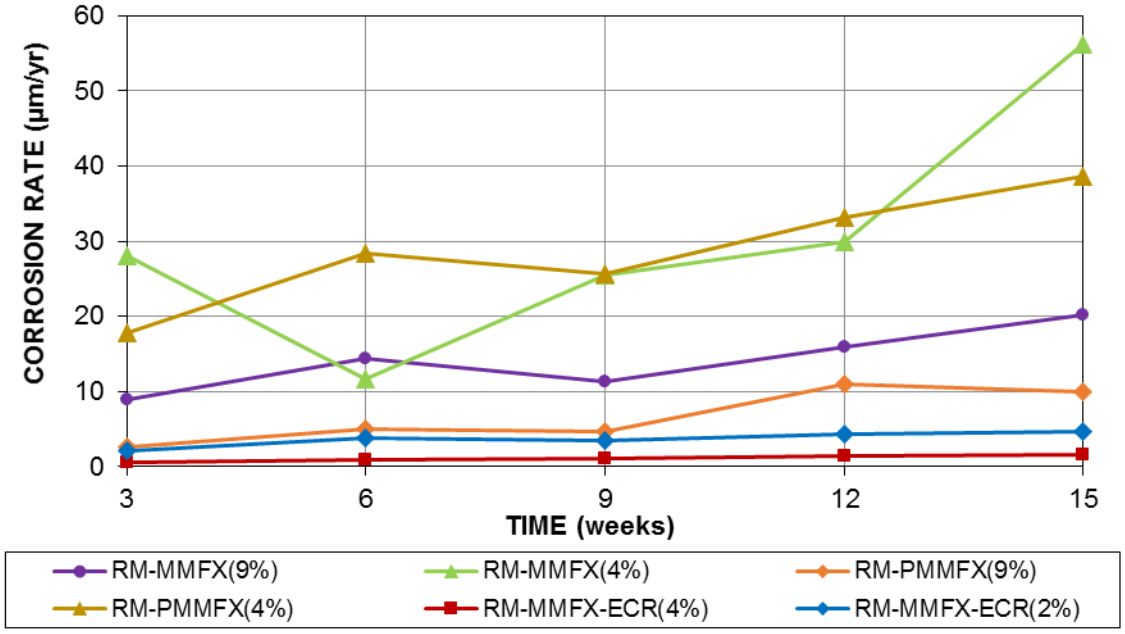

Figure 3.59— Average corrosion rates (µm/yr) versus time for rapid macrocell tests containing MMFX bars based on total area from LPR test results

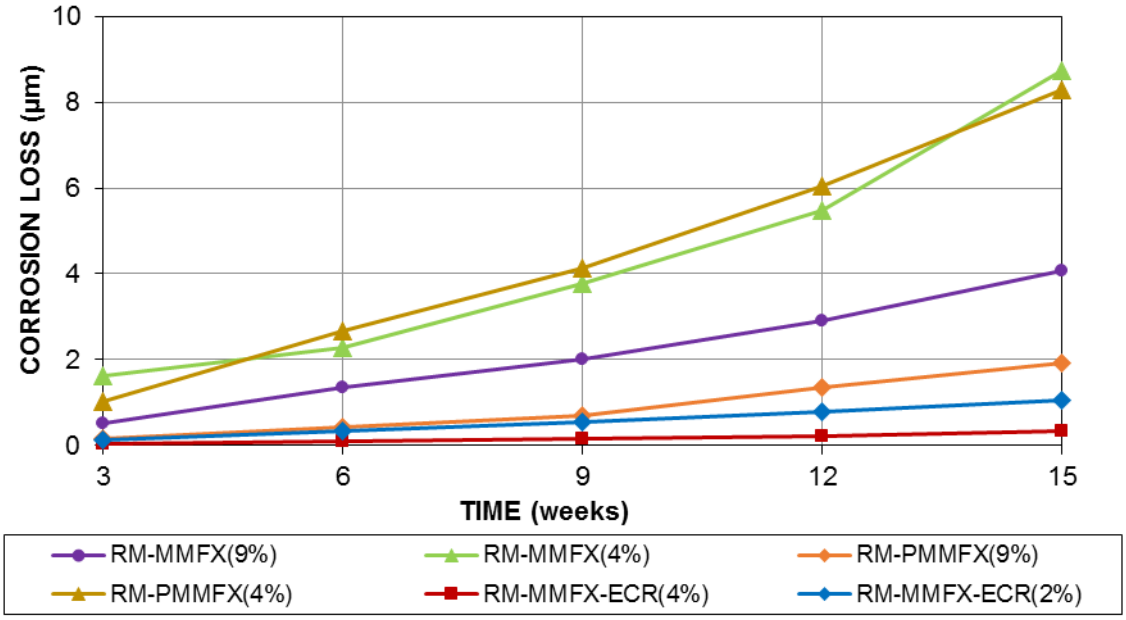

Figure 3.60— Average corrosion loss (µm) versus time for rapid macrocell tests containing MMFX bars based on total area from LPR test results

Table 3.13: Corrosion Loss (µm) for rapid macrocell specimens based on LPR test results

Specimen	Corrosion Loss (µm)-Total Area						Average	Std. Dev.
	Week 15		Week 15		Week 15			
	1	2	3	4	5	6		
MMFX-ECR(2%)	1.01	1.03	1.51	0.97	0.85	1.03	1.07	0.23
MMFX-ECR(4%)	0.56	0.20	0.07	0.35	0.42	0.35	0.33	0.17
MMFX(4%)	8.27	3.75	8.41	14.3	7.95	9.74	8.73	3.39
MMFX(9%)	2.48	3.62	4.46	3.32	5.95	4.64	4.08	1.21
PMMFX(4%)	7.01	6.92	10.8	6.00	7.96	11.1	8.28	2.13
PMMFX(9%)	1.64	2.52	1.81	1.55	2.50	1.50	1.92	0.47

3.4.3.3 Corrosion Potential

The average anode corrosion potentials taken with respect to a saturated calomel electrode (SCE) are shown in Figure 3.61. The anode potentials for the as-received and pickled MMFX(9%) specimens, ranged from –0.40 V to –0.46 V and –0.31 V to –0.51 V, respectively. Similarly, potentials ranged from –0.46 V to –0.55 V for the as-received and pickled MMFX(4%) specimens. As shown, the pickling process did not significantly affect the corrosion potential of bars with 9%

or 4% chromium. The potential of epoxy-coated MMFX-ECR(2%) and MMFX-ECR(4%) specimens decreased from –0.56 V to –0.61 V and –0.51 V to –0.57 V, respectively, during the first week of testing and remained there throughout the testing period.

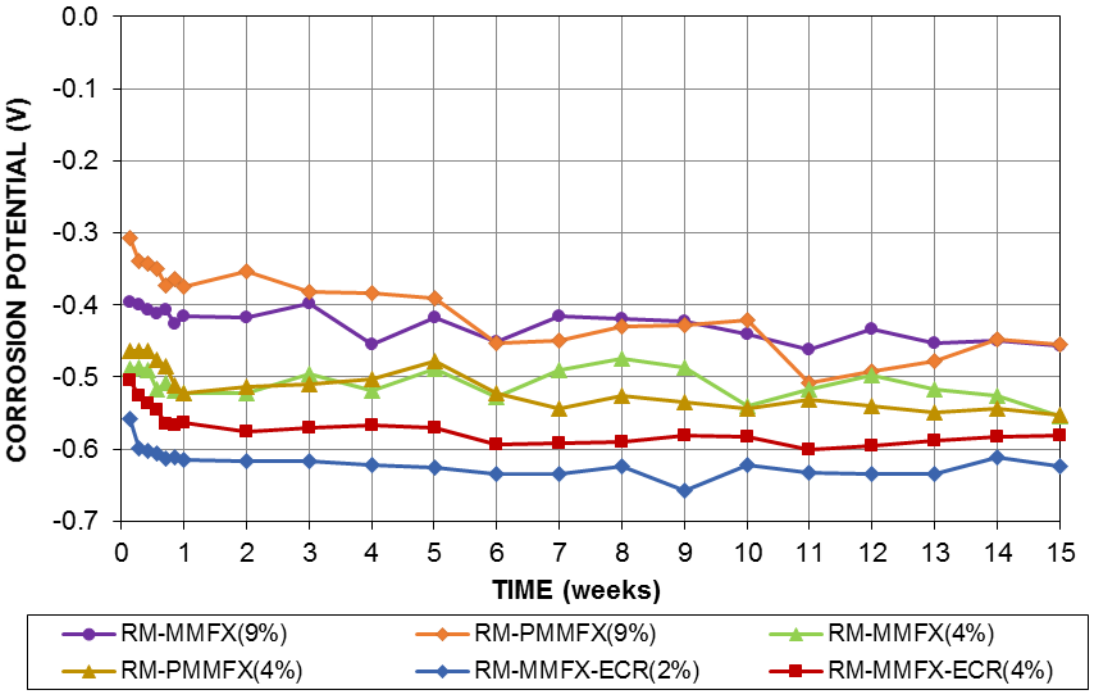

Figure 3.61— Average anode corrosion potentials (SCE) versus time for rapid macrocell tests containing MMFX bars

The average cathode corrosion potentials taken with respect to a saturated calomel electrode (SCE) are shown in Figure 3.62. The cathode potential of the bare MMFX bar specimens ranged from –0.17 V to –0.28 V at the first week of testing. The potentials of all, as-received and pickled, bare bars became more positive after the first week and ranged between –0.15 V and –0.17 V at week 5. After week 5, the potentials showed greater variation, with potentials between –0.15 V and –0.19 V at the end of 15 week testing.

The epoxy-coated bars showed more negative potentials compared to uncoated bars, likely due to the oxygen-blocking effect of the coating. After the first week of testing, the average

potential for both coated bar types was –0.33 V and remained near there through week 8. After week 8, the potential varied, and both the epoxy-coated MMFX-ECR(2%) and MMFX-ECR(4%) bars exhibited slightly increased potentials of –0.27 V at the end of 15 weeks of testing.

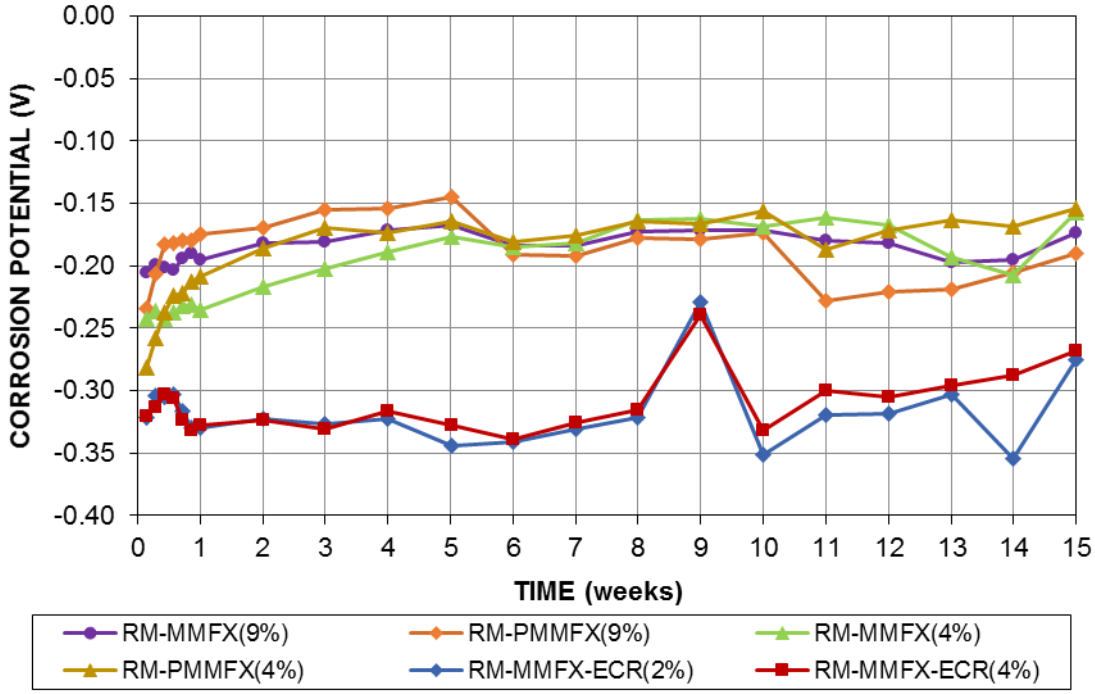

Figure 3.62— Average cathode corrosion potentials (SCE) versus time for rapid macrocell tests containing MMFX bars

3.4.3.4 Visual Observations

Upon completion of the rapid macrocell tests (15 weeks), all specimens were visually inspected and photographed. As shown in Figures 3.63 through 3.66, corrosion products were observed on the bars for all as-received and pickled uncoated MMFX steel, predominantly at and above the surface level of the solution.

Figure 3.63— Rapid macrocell test, anode bar of as-received MMFX(9%)-6 after 15 weeks

Figure 3.64 — Rapid macrocell test, anode bar of as-received MMFX(4%)-6 after 15 weeks

Figure 3.65— Rapid macrocell test, anode bar of pickled PMMFX(9%)-3 after 15 weeks

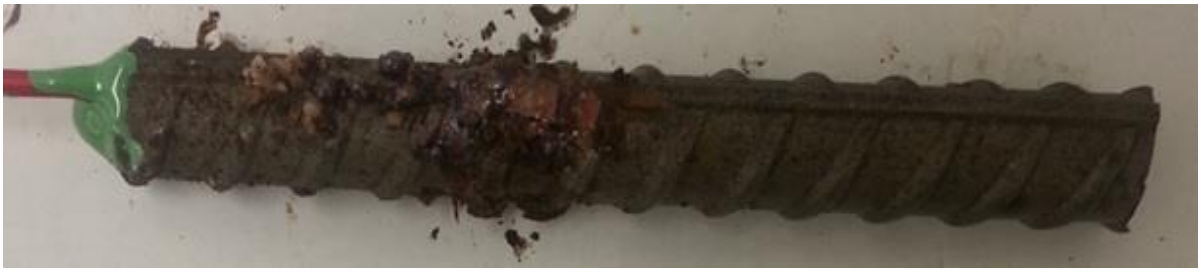

Figure 3.66— Rapid macrocell test, anode bar of pickled PMMFX(4%)-4 after 15 weeks

For the epoxy-coated bars, corrosion products were visible at the intentionally damaged sites. A disbondment test was performed at all four intentional damaged areas of the epoxy layer for each anode bar. If the tested site exhibited total disbondment, the disbonded area was

considered as 1.05 in^2 (677 mm^2). Representative bars with 4% and 2% chromium are shown in Figures 3.67 and 3.68, respectively. The disbonded area of anode bars of epoxy-coated MMFX bars containing 4% and 2% versus their total corrosion loss obtained from LPR test results are tabulated in Tables 3.14 and 3.15, respectively. The average corrosion loss (0.325 µm) and disbonded area (0.12 in^2 (78 mm^2)) of epoxy-coated MMFX bars containing 4% chromium were approximately 30% and 50% of those in epoxy-coated MMFX bars containing 2% chromium (1.07 µm as average corrosion loss and 0.23 in^2 (151 mm^2) as average disbonded area).

Figure 3.67— Rapid macrocell test, anode bar of MMFX-ECR(4%)-5 after disbondment test after 15 weeks

Figure 3.68— Rapid macrocell test, anode bar of MMFX-ECR(2%)-5 after disbondment test after 15 weeks

Table 3.14: Disbonded area and total corrosion loss at week 15 for the MMFX-ECR(4%) in rapid macrocell test

Specimen	Total Corrosion Loss (µm)	Site 1 (in^2)	Site 2 (in^2)	Site 3 (in^2)	Site 4 (in^2)	Average (in^2)	Average (mm^2)
1	0.56	0.24	0.13	0.24	0.07	0.17	110
2	0.2	0.06	0.04	0.33	0.04	0.12	76
3	0.07	0.04	0.27	0	0.09	0.10	65
4	0.35	0.11	0.09	0.07	0.12	0.10	63
5	0.42	0.16	0.26	0.06	0.11	0.15	95
6	0.35	0.11	0.24	0.01	0.02	0.10	61
Average	0.325					0.12	78

Table 3.15: Disbonded area and total corrosion loss at week 15 for the MMFX-ECR(2%) in rapid macrocell test

Specimen	Total Corrosion Loss (µm)	Site 1 (in^2)	Site 2 (in^2)	Site 3 (in^2)	Site 4 (in^2)	Average (in^2)	Average (mm^2)
1	1.01	0.06	0.25	0.13	0.26	0.18	113
2	1.03	0.25	0.09	0.25	0.22	0.20	131
3	1.51	0.25	0.14	0.26	0.33	0.25	158
4	0.97	0.36	0.45	0.13	0.10	0.26	168
5	0.85	0.37	0.27	0.19	0.19	0.26	165
6	1.03	0.42	0.23	0.29	0.12	0.27	171
Average	1.07					0.23	151

The disbonded area of the anode bars of rapid macrocell tests from this study for the epoxy-coated MMFX bars containing 4% and 2% chromium were compared with the results for rapid macrocell test of conventional epoxy-coated bars carried out in a study by Darwin et al. (2013) in Figure 3.69. As shown, MMFX-ECR(4%) specimens has the least disbonded area and total corrosion loss, and MMFX-ECR(2%) has the most, the corrosion loss was also greater than the conventional ECR bars. This is likely due to relatively low losses observed on the ECR bars used for comparison; previous tests on ECR bars exhibited greater losses (O'Reilly et al. 2011).

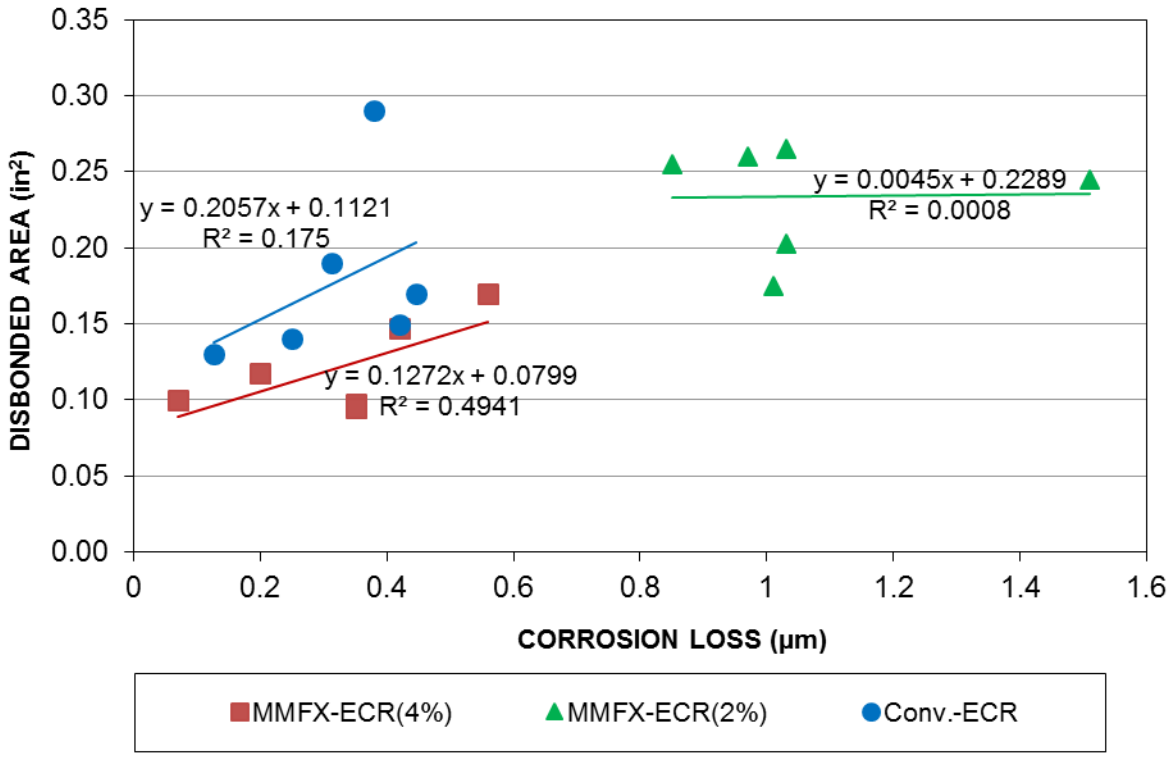

Figure 3.69— Disbonded area (in^2) versus total corrosion loss (µm) after 15 weeks for rapid macrocell tests containing epoxy-coated conventional (Darwin et al. 2013) and MMFX bars

3.3.5 Critical Chloride Threshold

For specimens with MMFX bare bars containing 9% and 4% chromium, Southern Exposure specimens were sampled for measuring critical chloride threshold at corrosion initiation. For epoxy-coated MMFX bars containing 4% and 2% chromium, to obtain a more accurate determination of the critical chloride threshold, beam specimens were cast and sampled for measuring chloride content upon initiation. The macrocell corrosion rates, total corrosion rates (LPR test results), and corrosion potentials for beam specimens containing epoxy-coated MMFX bars are shown in Appendix E.

Critical chloride thresholds of coated and uncoated MMFX bars are shown in Table 3.16. Southern Exposure specimens with uncoated MMFX reinforcement containing 9% chromium had

a similar critical chloride threshold (4.54 lb/yd^3 (2.69 kg/m^3)) to the MMFX bars containing 4% chromium (4.25 lb/yd^3 (2.52 kg/m^3)). The average time to corrosion initiation for MMFX(9%) and MMFX(4%) specimens was 21.4 and 27 weeks, respectively. The critical chloride threshold of beam specimens containing MMFX-ECR(2%) was 4.11 lb/yd^3 (2.44 kg/m^3) at 34 weeks. Epoxy-coated

MMFX bars containing 4% chromium in beam specimens initiated corrosion with an average critical chloride threshold of 5.16 lb/yd^3 (3.06 kg/m^3) at an average age of 45 weeks. The chloride content for individual samples of each specimen is presented in Appendix K.

Table 3.16: Critical chloride threshold (lb/yd3) of MMFX bars

Specimen	Water Soluble Chloride Content (lb/yd^3)*								Average	Std. Dev.
	1	2	3	4	5	6	7	8		
MMFX-ECR(2%)	4.44	5.41	3.93	4.26	3.69	2.96	-	-	4.11	0.63
MMFX-ECR(4%)	5.11	3.42	6.67	5.16	4.15	6.42	-	-	5.16	1.66
MMFX(4%)	3.05	3.46	5.51	3.03	3.78	2.34	5.35	7.46	4.25	1.81
MMFX(9%)	4.24	5.59	2.76	4.12	1.87	1.59	5.45	10.7	4.54	1.47

*1(lb/yd^3) = 0.593(kg/m^3)

3.5 DISCUSSION

By comparing the average corrosion rate of Southern Exposure specimens (Figures 3.15 and 3.21) and cracked beam specimens (Figures 3.39 and 3.45) containing MMFX bars with 4% and 9% chromium for both macrocell corrosion and LPR test results, it can be seen that MMFX bars containing 9% chromium exhibit greater corrosion resistance than MMFX bars containing 4% chromium.

The corrosion loss of conventional and MMFX steel for bench-scale tests and rapid macrocell tests are shown in Table 3.17 and 3.18 for bare bars and epoxy-coated bars, respectively. Corrosion losses presented in the tables for conventional (coated and uncoated) steel were obtained from research by Darwin et al. (2013) with all the test procedures and specifications identical to

the ones used for this study. Tabulated corrosion losses were obtained by integrating macrocell corrosion and LPR test corrosion rates with respect to time to express the macrocell and total corrosion losses, respectively.

Table 3.17: Average corrosion loss (μm) for uncoated conventional (Darwin et al. 2013) and MMFX bars

Steel Designation	Macrocell Corrosion (μm)			Total (LPR) Corrosion (μm)		
	SE	CB	RM	SE	CB	RM
Conv.	16.4	30.1	10.9	16.6	56.4	13.6
MMFX(9%)	8.70	16.4	4.63	9.05	20.4	4.08
MMFX(4%)	10.7	26.5	9.00	10.8	33.8	8.73

Macrocell and total corrosion losses tabulated in Table 3.17 are compared in Figures 3.70 and 3.71, respectively. For uncoated reinforcement, the corrosion loss decreases as chromium content increases. The corrosion losses of MMFX(9%) were 55%, 36%, and 30% of those for conventional bars for Southern Exposure, cracked beam, and rapid macrocell tests, respectively. These findings agree with the results of study by Gong et al. (2003) which showed that the macrocell corrosion rate of MMFX bars was between one-third and two-thirds of that for conventional steel. Total corrosion losses of MMFX(4%) obtained from Southern Exposure, cracked beam and rapid macrocell tests were 65%, 60%, and 64% of the ones for conventional bars, respectively, greater than that observed for MMFX(9%) but still about two-thirds of the losses for conventional steel.

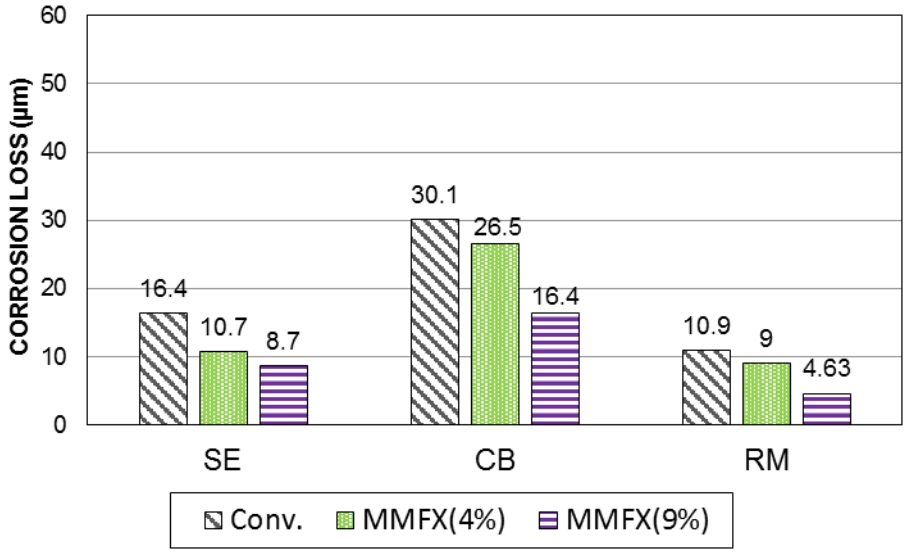

Figure 3.70— Corrosion loss (µm) for uncoated conventional (Darwin et al. 2013) and MMFX bars in bench-scale and rapid macrocell tests obtained from macrocell corrosion rates

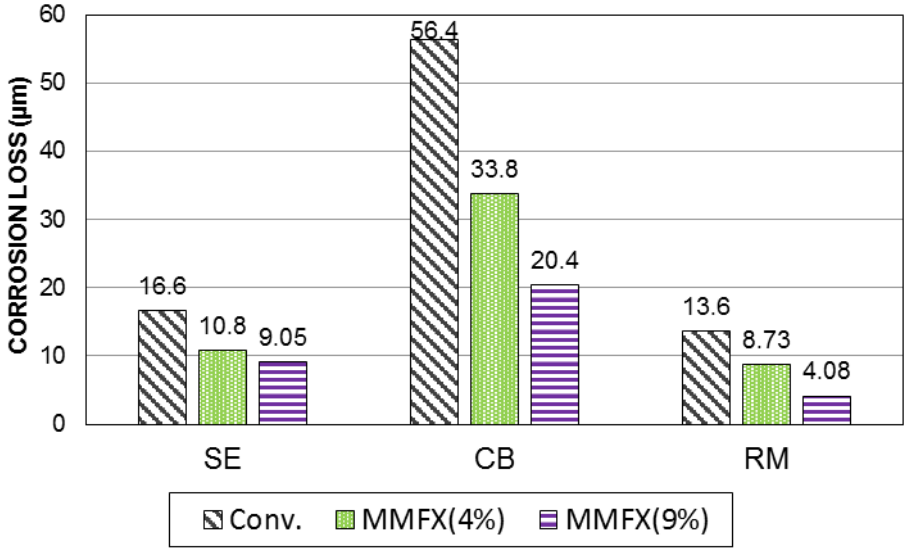

Figure 3.71— Corrosion loss (µm) for uncoated conventional (Darwin et al. 2013) and MMFX bars in bench-scale and rapid macrocell tests obtained from LPR test corrosion rates

Figures 3.72 and 3.73 present a comparison between macrocell and total corrosion loss of epoxy-coated MMFX bars with conventional epoxy-coated steel based on total area of the bar. The intentionally damaged area of the epoxy layer was identical for all bars in a given test method (10 holes for bench-scale tests and 4 holes for the rapid macrocell test). MMFX-ECR(4%) specimens

had the least macrocell and total corrosion losses in bench-scale tests. For the rapid macrocell test, conventional epoxy-coated bars had the least average macrocell corrosion loss compared to the others. (As discussed earlier, previous tests on conventional ECR exhibited greater losses than the ECR used for comparison in this study). Conventional ECR total corrosion loss (0.32 µm), however, was very close to that for MMFX-ECR(4%), 0.33 µm, but still one third of MMFX-ECR(2%) total corrosion loss (1.07 µm). The corrosion loss of MMFX epoxy-coated bars containing 4% chromium were 12%, 30%, and 100% that of conventional steel for Southern Exposure, cracked beam, and rapid macrocell test.

Table 3.18: Average corrosion loss (µm) for epoxy-coated conventional (Darwin et al. 2013) and MMFX bars

Steel Designation	Macrocell Corrosion (µm)			Total Corrosion (µm)		
	SE	CB	RM	SE	CB	RM
ECR	0.342	0.453	0.107	1.05	3.71	0.322
MMFX-ECR(4%)	0.059	0.341	0.2	0.125	1.10	0.33
MMFX-ECR(2%)	0.076	0.506	0.45	0.25	1.93	1.07

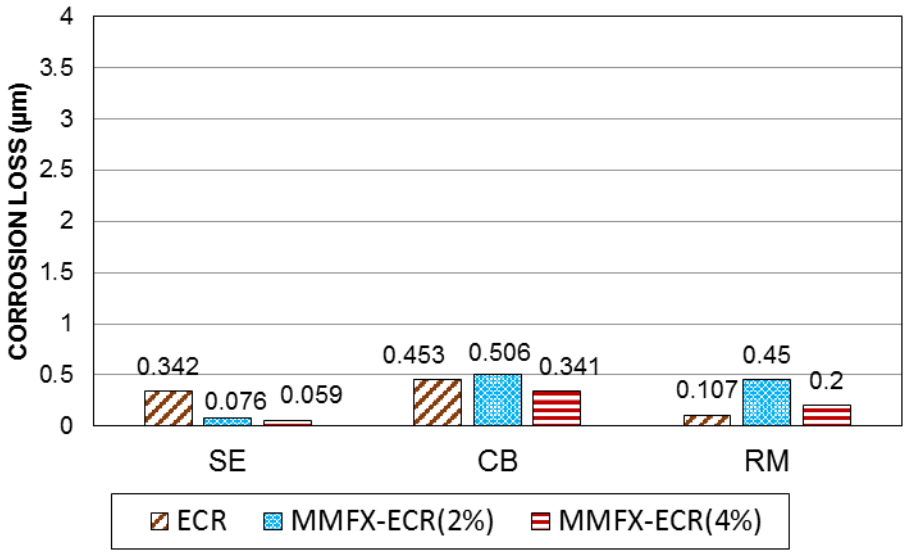

Figure 3.72— Corrosion loss (µm) for epoxy-coated conventional (Darwin et al. 2013) and MMFX bars in bench-scale and rapid macrocell tests obtained from macrocell corrosion rates

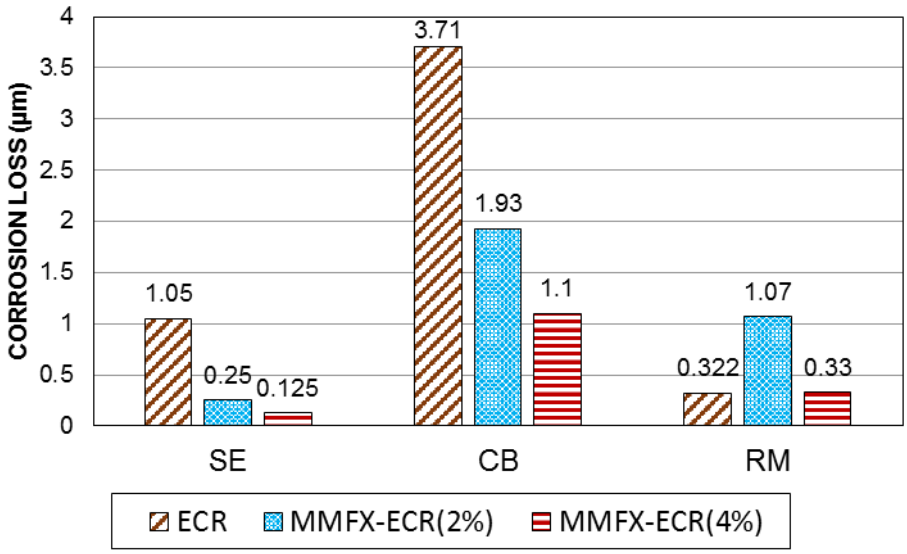

Figure 3.73— Corrosion loss (µm) for epoxy-coated conventional (Darwin et al. 2013) and MMFX bars in bench-scale and rapid macrocell tests obtained from LPR test corrosion rates.

To compare the significance of differences between mean values of corrosion loss of epoxy-coated bars, Student's t-test, a method of statistical analysis, was performed on the data sets. Student's t-test compares two data sets to determine the probability (*p*) that any difference between the two data sets is not significant; that is, the differences in the mean values of two data sets are due to natural variability, not the differences in the systems. Differences are considered statistically significant if the probability is less than 5% ($p < 0.05$) that the difference between the two data sets has resulted by chance. Student's t-test results (*p* values) for total corrosion loss of epoxy-coated conventional and MMFX bars are tabulated in Table 3.19. Comparison between data sets of MMFX-ECR(4%) and conventional epoxy-coated bars shows that for bench-scale specimens *p* is less than 5%; that is, the probability that the lower corrosion loss of MMFX-ECR(4%) than conventional epoxy-coated bars to be resulted by chance is less than 5%, so the difference is statistically significant. The *p* values of comparison between MMFX-ECR(2%) and conventional epoxy-coated bars in bench-scale tests are more than 5% (7.4% for Southern

Exposure and 9.4% for cracked beam); thus, the difference is not considered significant. For rapid macrocell tests the MMFX-ECR(2%) exhibited significantly greater losses than other bars.

Table 3.19: Student's t-test results (p values) for total corrosion loss of epoxy-coated bars

Steel Designation	**Southern Exposure**			**Cracked beam**			**Rapid macrocell**		
	ECR	MMFX-ECR(4%)	MMFX-ECR(2%)	ECR	MMFX-ECR(4%)	MMFX-ECR(2%)	ECR	MMFX-ECR(4%)	MMFX-ECR(2%)
ECR	-	**0.041**	0.074	-	**0.019**	0.094	-	0.97	**0.00003**
MMFX-ECR(4%)	**0.041**	-	**0.042**	**0.019**	-	0.22	0.97	-	**0.00008**
MMFX-ECR(2%)	0.074	**0.042**	-	0.094	0.22		**0.00003**	**0.00008**	-

The disbondment test results for top and bottom bars of Southern Exposure and cracked beam specimens and anode bars of rapid macrocell test of MMFX epoxy-coated reinforcement obtained from this study has been compared with the ones for conventional epoxy-coated bars obtained from Darwin et al. (2013) study and shown in Figures 3.74, 3.75 and 3.76, respectively. For anode bars, MMFX bars containing 4% chromium had the least disbonded area for all three tests. MMFX bars containing 4% chromium disbonded areas were 52%, 67%, and 67% of the ones for conventional epoxy-coated and 80%, 70%, and 50% of those for MMFX-ECR(2%) in Southern Exposure, cracked beam and rapid macrocell tests, respectively. Although MMFX bars containing 2% chromium had less disbonded area compared to conventional epoxy-coated bars in Southern Exposure specimens, the disbonded area was comparable to conventional ECR in cracked beam specimens and greater than conventional ECR in rapid macrocell specimens.

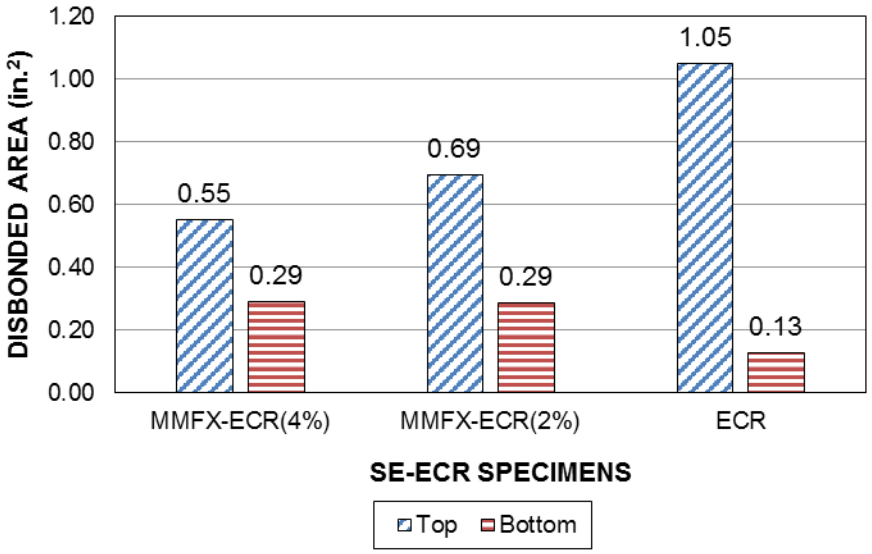

Figure 3.74— Comparison of disbondment test results of top and bottom bars in Southern Exposure specimens containing epoxy-coated conventional (Darwin et al. 2013) and MMFX bars

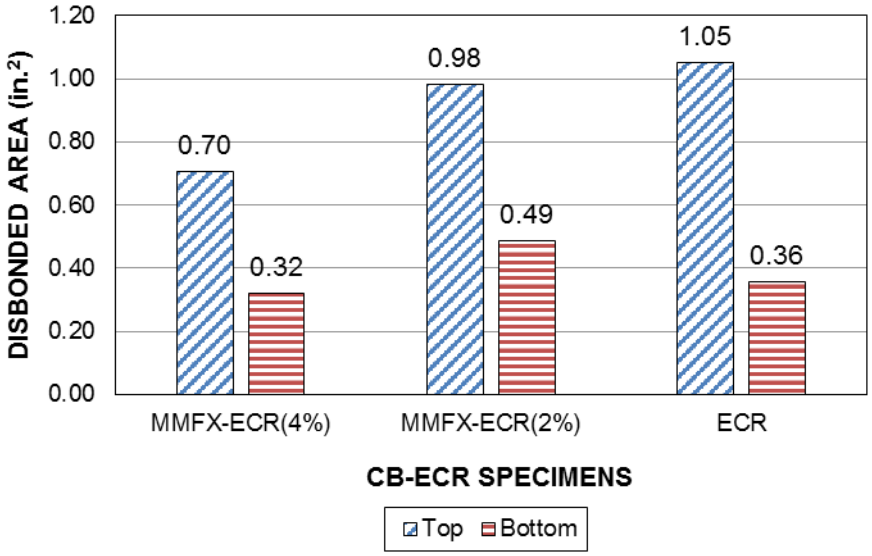

Figure 3.75— Comparison of disbondment test results of top and bottom bars in cracked beam specimens containing epoxy-coated conventional (Darwin et al. 2013) and MMFX bars

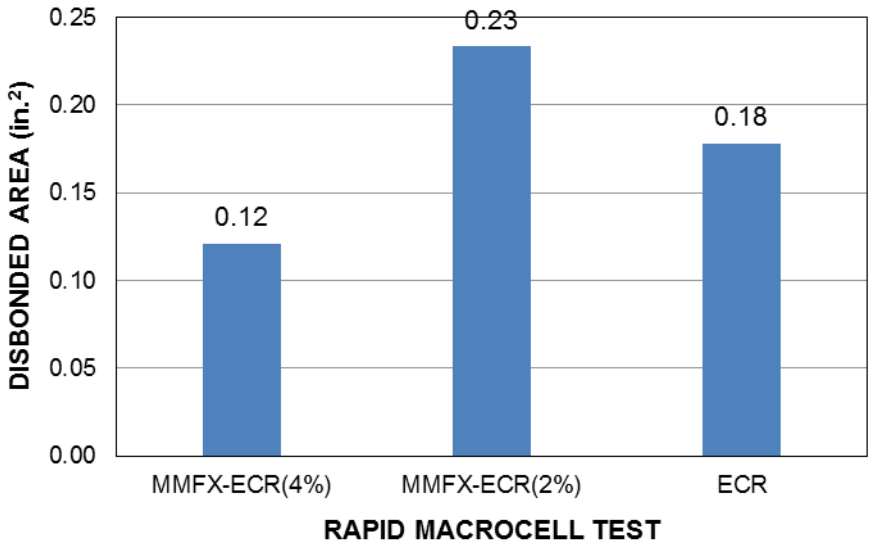

Figure 3.76— Comparison of disbondment test results of anode bars in rapid macrocell tests containing epoxy-coated conventional (Darwin et al. 2013) and MMFX bars

The critical chloride threshold of MMFX bars containing 9% chromium obtained in this study was 4.54 lb/yd^3 (2.69 kg/m^3), which is in agreement with the results of a study carried out by Ji et al. (2005) that showed the critical chloride threshold of the reinforcement ranged from 4.72 to 6.86 lb/yd^3 (2.8 to 4.07 kg/m^3). The critical chloride threshold of MMFX bars containing 4% chromium (4.25 lb/yd^3 (2.52 kg/m^3)) was close to that for MMFX(9%) bars (4.54 lb/yd^3 (2.69 kg/m^3)); as was the time to corrosion initiation (21.4 weeks for MMFX(9%) and 27 weeks for MMFX(4%)). These critical chloride thresholds were almost three times that of reported for uncoated conventional steel (1.53 to 2.05 lb/yd^3 (0.91 to 1.22 kg/m^3)) in prior research (Ji et al. 2005).

A comparison between total corrosion rates and losses of pickled and as-received MMFX bars in Figure 3.59 and Table 3.13 shows that pickling reduced total corrosion loss of MMFX(9%) bars to almost half; thus, was effective on improving the corrosion resistance of MMFX bars containing 9% chromium. However, pickling was not as effective on corrosion performance of MMFX bars containing 4% chromium.

3.6 CONCLUSIONS

The following conclusions are drawn based on the results presented in this chapter:

1- The critical chloride threshold of MMFX bars containing 4% and 9% chromium were similar and about three times greater than the critical chloride threshold of conventional steel (4.25 lb/yd^3 (2.52 kg/m^3) and 4.54 lb/yd^3 (2.69 kg/m^3), respectively).

2- The average corrosion loss of MMFX bars containing 9% chromium ranged from 30% to 55% that of conventional steel, while for MMFX bars containing 4% chromium the average corrosion loss was approximately two-thirds of that for conventional steel.

3- Pickling was effective on improving corrosion resistance of MMFX bars containing 9% chromium but not on MMFX bars containing 4% chromium.

4- The critical chloride threshold of epoxy-coated MMFX bars containing 2% and 4% chromium were 4.11 lb/yd^3 (2.44 kg/m^3) and 5.16 lb/yd^3 (3.06 kg/m^3), respectively.

5- Epoxy-coated MMFX bars containing 4% chromium had greater corrosion resistance than MMFX-ECR(2%) and conventional epoxy-coated bars. The average total corrosion rate of MMFX-ECR(4%) reinforcement ranged from 30% to 60% of that for MMFX reinforcement with 2% chromium, and from 15% to 30% of that for epoxy-coated conventional steel. The disbonded area of the epoxy layer for MMFX bars containing 4% chromium was half to two-thirds of that for conventional epoxy-coated bars and 50% to 80% of that for MMFX bars containing 2% chromium.

6- Epoxy-coated MMFX bars containing 2% chromium did not show significantly better performance against corrosion compared to conventional epoxy-coated bars.

CHAPTER 4: EVALUATION OF EFFECT OF SUPPLEMENTARY CEMENTITIOUS MATERIALS ON CORROSION PERFORMANCE OF REINFORCED CONCRETE

4.1 INTRODUCTION

Decreasing the permeability of the concrete is a commonly-used means of improving the durability of concrete structures against corrosion, as a lower permeability slows the rate at which oxygen, moisture, and chlorides reach the reinforcing steel. One way to achieve this is to use supplementary cementitious materials.

Supplementary cementitious materials are classified into two main categories: pozzolanic materials, which contain amorphous or glassy silica, and cementitious materials. Amorphous or glassy silica in pozzolanic materials reacts with calcium hydroxide ($Ca(OH)_2$) formed from the hydration of the calcium silicates (C_3S and C_2S) in portland cement and produces calcium silicate hydrate (C-S-H), which is the primary contributor to concrete strength. The more calcium hydroxide consumed in the reaction with the pozzolan, the more effective the pozzolan is in improving long term strength and concrete durability. Common pozzolanic materials include silica fume and fly ash; slag cement is the most commonly used cementitious material.

Silica fume is a pozzolan which is produced as a by-product in the manufacture of silicon metal. A good-quality silica fume contains up to 98% of amorphous silica (SiO_2) (Mindess et al. 2002). The fine nature of silica fume (the mean particle size of silica fume is about one-hundredth that of cement) is the reason for its high activity. Extremely fine particles of silica fume pack between cement particles and decrease the mean size of capillary pores and permeability of concrete. Fly ash, another pozzolan, is an inorganic, noncombustible residue of powdered coal after burning in power plants. Fly ash is categorized as Class C or Class F fly ash based on its composition. Class F Fly ash contains $SiO_2 > 50\%$, and $CaO < 5\%$ by weight, while Class C

contains SiO_2 > 30%, and 20% < CaO < 30% by weight; thus, because of the higher amorphous silica content, Class F has more pozzolanic characteristics (Mindess et al. 2002).

Besides pozzolanic materials, cementitious materials such as slag cement are used in concrete. Slag cement mainly contains lime (CaO), silica (SiO_2), and alumina (Al_2O_3). Slag in the presence of an alkaline activator such as calcium hydroxide in concrete can produce calcium silicate hydrate (C-S-H) and contribute to concrete compressive strength (Mindess et al. 2002).

Supplementary cementitious materials can increase the time required for corrosion initiation by creating a denser and less permeable concrete matrix. Most research has shown that the partial replacement of cement with supplementary cementitious materials will increase the time to corrosion initiation. Hussain and Rasheeduzzafar (1994) reported that the partial replacement of cement with 30% fly ash approximately doubled the time to corrosion initiation. This delay in initiation is the result of several mechanisms such as an improved microstructure, a lower degree of interconnected voids, and improvement to the interfacial transition zone between the cement matrix and aggregates (Mackechnie & Alexander 1996, Mangat et al. 1994). Bouteiller et al (2012) showed that concrete containing 70% slag cement with w/c ratio as of 0.45 and 0.65 are more chloride penetration resistant than concrete with ordinary portland cement only. This lower chloride ingress rate in concrete containing slag cement was attributed to transport properties rather than chloride binding capacity of slag cement (Bouteiller et al 2012). The effect of supplementary cementitious materials on corrosion rate, chloride binding, pore solution composition, and critical chloride threshold showed mixed results. A portion of the chloride ions in concrete bind with tricalcium aluminate (C_3A) in the cement matrix and are not able to depassivate the protective layer of the steel. Arya and Xu (1995) compared the amount of bound chlorides and corrosion rate in concrete containing ordinary portland cement as well as concrete with either 65% slag cement,

35% fly ash, or 10% silica fume as a partial replacement of cement. Salt was introduced to the concrete at a dosage of 1% and 3% of cement weight during mixing to depassivate the reinforcing steel. Chloride binding was greatest for the mixture containing slag cement, with decreasing binding for mixtures containing fly ash, ordinary portland cement, and silica fume. However, corrosion rates did not line up with binding capacity. For mixtures containing 1% chloride content, corrosion rates were the highest for specimens containing fly ash followed by specimens with silica fume, slag cement, and ordinary portland cement. For mixtures containing 3% chloride content, however, specimens containing fly ash had the highest corrosion rates followed by ordinary portland cement, slag cement, and silica fume. The higher corrosion rate of steel in concrete with supplementary cementitious materials compared with ordinary portland cement for mixtures containing 1% chloride content was attributed to the consumption of OH^- ions in concrete containing pozzolans, which results in a reduction of the concrete pore solution pH and depassivation of reinforcement (Arya & Xu 1995). Sirivivatnanon et al. (1994) compared effects of various partial replacements of cement by supplementary cementitious materials (5% and 10% silica fume, 20%, 40% and 60% fly ash, and 40%, 60%, and 80% slag cement) on the corrosion of machined and polished steel in mortar. After six months, steel in mortar containing SCM's exhibited lower corrosion rates than those in mortar containing only portland cement. Increasing the amount of SCM decreased the corrosion rate, with the lowest corrosion rates observed in mixtures containing 10% silica fume, followed by mixtures with slag cement and fly ash. Scott and Alexander (2007) investigated the influence of supplementary cementitious materials on corrosion in cracked concrete. Ordinary portland cement concrete and mixtures with cement partially replaced by 25% slag cement, 50% slag cement, 75% slag cement, 30% fly ash, 7% silica fume, and a ternary blend of 50% portland cement, 43% slag cement, and 7% silica fume were

tested. Inclusion of any of the supplementary cementitious materials resulted in at least a 50% reduction in corrosion rate compared to ordinary portland cement.

The chloride ion concentration that is needed to depassivate the protective film around steel embedded in concrete and initiate corrosion is defined as the critical chloride threshold. This threshold depends on many factors and varies significantly based on reinforcing bar type, cement content and type, pH of concrete, availability of oxygen and moisture, presence of air voids around the steel, and other factors (Bertolini et al. 2004). Research on the effect of supplementary cementitious materials on the critical chloride threshold, like corrosion rate, has also yielded mixed results. Thomas (1996) showed that although the mass loss of the steel embedded in the concrete containing fly ash exposed to a marine environment decreased with increasing fly ash content, the critical chloride threshold was also decreased. Likewise, Oh & Jang (2003) found that increasing the content of fly ash from 15% to 30% resulted in a decrease in the total chloride threshold content from 0.90% to 0.68% and free chloride threshold content from 0.11% to 0.07% (by cementitious material weight). It was also found that using 30% replacement with slag cement had a negligible effect on critical chloride threshold compared to ordinary portland cement concrete. Thomas and Matthews (2004) showed that although critical chloride threshold decreased in specimens in which cement was partially replaced by fly ash, the rate of chloride ingress and corrosion rate also decreased. Lower values of the critical chloride threshold of concrete using supplementary cementitious materials in the mentioned studies could be due to the consumption of hydroxide ions, which results in a decrease of pH in concrete pore solution. In a study by Presuel-Moreno and Moreno (2015) critical chloride threshold and time to initiation of concrete specimens containing 20%, 35%, and 50% cement replacement by fly ash as well as 6%, 15%, and 27% cement replacement by silica fume were investigated. Specimens were cast with and without

reinforcement with w/c ratio as of 0.37 and were exposed to natural seawater for over 17 years on weekly wetting-drying cycles. Among specimens containing fly ash, those with 50% fly ash had the lowest critical chloride threshold value and specimens with 35% fly ash had the highest; specimens with 20% and 50% fly ash showed lower critical chloride threshold than specimens containing portland cement only. Among specimens containing silica fume, specimens with 6% silica fume had comparable critical chloride threshold to specimens containing only portland cement; increasing silica fume content resulted in decrease of critical chloride threshold values (Presuel-Moreno and Moreno 2015). On the other hand, Breit and Schiessl (1997) reported that in a test that chloride ions were added to the mixing water of concrete, specimens containing 25% fly ash and 50% slag cement had almost as 1.5 times the critical chloride threshold as the specimens without supplementary cementitious materials. Monticelli et al. (2016) evaluated corrosion behavior of steel in fly ash mortars, which were activated by NaOH and sodium silicate solutions. Results showed that for specimens with the ratio of Na_2O/SiO_2 as low as 0.12 and 0.14 (most compact pozzolanic products), the critical chloride threshold (about 1% to 1.7% with respect to binder weight) was higher than that for specimens containing cement (about 0.5% versus binder weight). In a study by Angst et al. (2011) the initiation stage of chloride induced corrosion and CCCT value of several concrete mixes including mixes containing ordinary portland cement and sulfate resistant cement as well as these binders in combination with fly ash were evaluated. Specimens were exposed to chloride solutions during wetting/drying cycles and monitored with measuring potentials, electrical resistances, and LPR test. Corrosion potentials for different specimens showed three different cases corresponding to corrosion initiation: specimens with sudden drop in corrosion potential, specimens with slow potential decrease, and specimens with several depassivation and repassivation. Angst et al. (2011) showed that for many cases after the first signs of initiation, a marked increase in chloride content was required to prevent repassivation and to enable stable pit growth.

The mixed results about the effect of use of supplementary cementitious materials on critical chloride threshold and corrosion rate of reinforcement in concrete has raised the necessity of further study about these effects. This study examined the effect of using supplementary cementitious materials (Class C fly ash, silica fume, and slag cement) as a partial replacement of cement in concrete on the critical chloride threshold and corrosion rate of reinforcement. Corrosion performance of uncoated bars (ASTM A615) and epoxy-coated reinforcement in concrete containing these supplementary cementitious materials were evaluated and compared with concrete containing ordinary portland cement.

4.2 EXPERIMENTAL PROCEDURE

To investigate the effect of supplementary cementitious materials on corrosion performance of reinforcement, the ordinary portland cement was partially replaced by supplementary cementitious materials such that the total volume of cementitious materials remained constant. For instance, 20% and 40% of cement volume was replaced with an equal volume of Class C fly ash. Likewise, mixtures with 5% and 10% silica fume, and 20% and 40% slag cement was designed with the same procedure. The mixture proportions are provided in Table 4.1. All concrete mixes had a water-cement ratio (w/c) of 0.45, a target air content of 6 ± 1%, and a target slump of 3 ± 1 in. (75 ± 25 mm). Plastic and hardened concrete properties for each mix are tabulated in Table 4.2. For this study prismatic concrete specimens called beam specimens containing uncoated bars (ASTM A615) as well as epoxy-coated reinforcement were used.

Table 4.1: Mixture proportions (SSD basis)

Specimen	Mix type[a]	Cement lb/yd^3 (kg/m^3)	Fly Ash[b] lb/yd^3 (kg/m^3)	Silica Fume[b] lb/yd^3 (kg/m^3)	Slag Cement[b] lb/yd^3 (kg/m^3)	Water lb/yd^3 (kg/m^3)	Coarse Agg.[b] lb/yd^3 (kg/m^3)	Fine Agg. lb/yd^3 (kg/m^3)	Air-entraining Agent oz/yd^3 (mL/m^3)
PC	100% PC	598 (355)	-	-	-	269 (160)	1484 (880)	1435 (851)	5.63 (209)
FA(20)	20% FA	506.9 (301.1)	91.1 (54.1)	-	-	269 (160)	1484 (880)	1430 (849)	5.63 (209)
FA(40)	40% FA	404.3 (240.2)	193.7 (115.1)	-	-	269 (160)	1484 (880)	1397 (830)	5.63 (209)
SF(5)	5% SF	577.1 (342.8)	-	20.9 (12.4)	-	269 (160)	1484 (880)	1452 (862)	5.63 (209)
SF(10)	10% SF	555.5 (333)	-	42.5 (25.4)	-	269 (160)	1484 (880)	1446 (859)	6.33 (236)
Slag(20)	20% Slag	487.5 (290)	-	-	110.5 (65.6)	269 (160)	1484 (880)	1450 (861)	5.63 (209)
Slag(40)	40% Slag	372.8 (221.4)	-	-	225.2 (133.8)	269 (160)	1484 (880)	1397 (829)	5.63 (209)

[a] 100% PC = Mixture paste containing 100% portland cement
20% FA = Mixture paste containing 20% fly ash and 80% Portland cement by volume
40% FA = Mixture paste containing 40% fly ash and 60% portland cement by volume
20% Slag = Mixture paste containing 20% slag cement and 80% portland cement by volume
40% Slag = Mixture paste containing 40% slag cement and 60% portland cement by volume
5% SF = Mixture paste containing 5% silica fume and 95% portland cement by volume
10% SF = Mixture paste containing 10% silica fume and 90% portland cement by volume
[b] Specific gravity of fly ash = 2.3
Specific gravity of silica fume = 2.3
Specific gravity of slag cement = 2.9
Bulk specific gravity of fine aggregate = 2.63
Bulk specific gravity of Coarse aggregate = 2.59

Table 4.2: Mix properties

Specimen	Mix type	Slump in. (mm)	Unit weight lb/ft^3 (kg/m^3)	Air content	Comp. strength psi (Mpa)
PC	100% PC	3 (76)	144.2 (2310)	5.6%	4030 (27.8)
FA(20)	20% FA	2.5 (64)	143.6 (2300)	5.1%	4510 (31.1)
FA(40)	40% FA	3.5 (89)	143.2 (2293)	5.6%	4870 (33.6)
SF(5)	5% SF	2 (51)	145.6 (2332)	5.4%	4940 (34.1)
SF(10)	10% SF	3 (76)	142.6 (2284)	5%	4610 (31.8)
Slag(20)	20% Slag	4 (102)	139.8 (2239)	6.6%	4590 (31.6)
Slag(40)	40% Slag	4 (102)	140.2 (2245)	6.7%	4730 (32.6)

4.2.1 Beam Specimens

Figure 4.1 shows the beam specimens used in this study. Beam specimens have dimensions of 12 × 6 × 7 in. (305 × 152 × 178 mm) with two layers of reinforcement; a top mat and a bottom mat. The top mat and bottom mat consisted of one and two No. 5 (No. 16) reinforcing bars, respectively. Bars were 12 in. (305 mm) long with 1 in. (25 mm) clear cover. Bottom bars were spaced at 2.5 in. (64 mm), and the top bar was centered within the prism. To allow the specimens to be ponded with salt solution, a 0.75 in. (19 mm) concrete dam was cast integrally with the specimens. Top and bottom mats were electrically connected through a terminal box across a 10-ohm resistor via external wiring to allow for macrocell corrosion rate measurements.

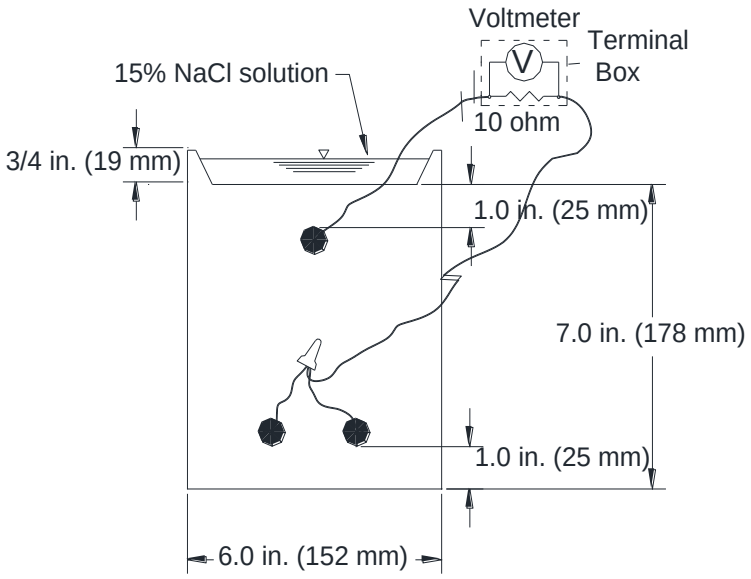

Figure 4.1— Beam (B) specimens

4.2.2 Test Procedure

To fabricate beam specimens, reinforcing bars were cut to 12 in. (305 mm), and both ends of each bar were drilled and tapped to a 0.75 in. (19 mm) depth with 10-24 threading. To simulate the effects of damage, the epoxy-coated reinforcement used was intentionally damaged using a 0.125 in. (3 mm) diameter four-flute drill bit. The epoxy layer was penetrated to a depth of 15 mils (0.4 mm), deep enough just to expose the underlying steel. The epoxy layer was penetrated with a total of ten holes on each bar, with five holes spaced every 2 in. (50 mm) on each side of a bar, as shown in Figure 4.2.

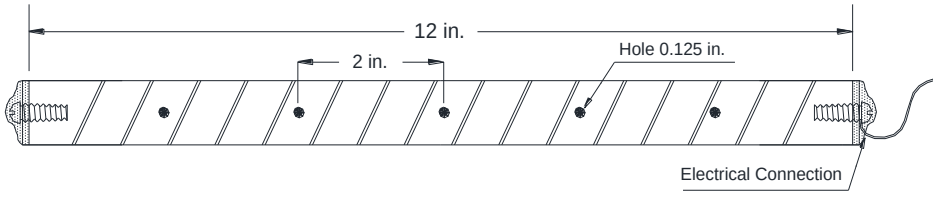

Figure 4.2— Damage pattern of epoxy-coated bar (plan view) in bench-scale tests

Epoxy-coated bars were rinsed with soapy water and uncoated bars were submerged in acetone for at least two hours to remove any oil from bar surface. Forms were built from 0.75 in. (19 mm) plywood and comprised of four sides and a base. Since specimens were cast upside down, to build the dam around the top surface of a specimen, a tapered 4.5 × 10.5 × 0.75 in. (114 × 267 × 19 mm) plywood was attached and centered to the base. To hold reinforcement and plywood in place, holes were drilled in the plywood, and 1.25 in. (32 mm) long 10-24 threaded stainless steel machine screws were used. Prior to placing reinforcement, all interior surfaces of molds were coated with mineral oil. Reinforcement was placed into the molds and epoxy-coated bars were aligned in a way that the intentionally damaged sites face the top and bottom sides of the mold. Specimens were fabricated and cast in an inverted position. Concrete was placed in two layers, and each layer was consolidated by internal vibration.

After casting, all specimens were wet cured for 3 days and air cured for 25 days thereafter. Ponding and lab tests began 28 days after casting. Prior to testing, the test bars were wired by connecting wire leads through 10-24 × 0.5 in. (13 mm) stainless steel screws and a No. 10 stainless steel washer. The four sides of the specimens were coated with an epoxy to protect the electrical connections and to prevent chloride ingress from the sides of the specimen. The top and bottom mats of specimens were connected to each other across a 10-ohm resistor via a terminal box.

The target test duration of the beam specimens was 96 weeks; for specimens that did not exhibit corrosion initiation, the test period was extended. The test procedure consisted of 12 weeks of wet-dry cycles followed by 12 weeks of continuously wet cycles. These two regimes were alternated and repeated until the end of test. During wet-dry cycles, specimens were ponded with 300 mL of 15% NaCl solution and maintained at ambient room temperature for four days. At this point, corrosion measurements including macrocell corrosion rate, corrosion potentials, and linear polarization resistance (LPR) were taken, the salt solution was vacuumed off from the surface of the concrete specimens, and specimens were placed under a heat tent at 100 ± 3 °F (38 ± 2 °C) for 3 days. This procedure was repeated for 12 weeks. After 12 weeks of wet-dry cycles, specimens entered a continuously wet cycle, where specimens were ponded continuously with 15% NaCl solution and kept covered at ambient room temperature for 12 weeks. Deionized water was added to the concrete surfaces as needed to replace water lost due to evaporation. All readings were taken on a weekly basis except for the LPR test, which was taken on a monthly basis.

4.2.3 Chloride Sampling and Analysis

The total chloride content in concrete is acid-soluble, but not all of this chloride is able to contribute to the corrosion process, as a portion of it binds with tricalcium aluminate (C_3A) in the

cement matrix and is not able to depassivate the protective layer of the steel. Therefore, many studies measure and report the free chloride content (water-soluble) as the critical chloride threshold (Ann & Song 2007). Chloride contents presented in this report are measured in terms of free chloride content (water-soluble) and expressed as mass of chloride per unit volume of concrete.

To evaluate the critical chloride threshold of reinforcement, beam specimens were sampled upon corrosion initiation. Corrosion initiation on an uncoated bar was defined as a measured macrocell corrosion rate exceeding 0.3 μm/yr and a corrosion potential more negative than –0.275 V with respect to a saturated calomel electrode (SCE). However, these rules are not applicable for the coated bars; corrosion initiation is restricted to the damaged sites, so epoxy-coated bars exhibit lower corrosion rates upon corrosion initiation. Furthermore, epoxy-coated bars may show more negative potential values compared to bare bars due to the lack of oxygen at the steel surface. To determine the initiation of epoxy-coated bars, a combination of a jump in macrocell corrosion rate, drop in potential, and a jump in total corrosion rate obtained from the LPR test was considered. In addition to sampling at initiation, half of the specimens from each series were sampled at the end of testing (96 weeks). This allowed for the chloride ingress over time to be compared between the mixtures and provides a lower bound for the chloride threshold in the case of specimens that did not initiate corrosion by week 96.

As shown in Figure 4.3, samples were taken using a 0.25 in. (6.4 mm) masonry drill bit such that the top of the bit was level with the top of the top mat of reinforcing steel. The chloride content in concrete is not constant at a particular depth, as chlorides do not ingress through concrete uniformly. Since most aggregates are significantly less permeable than cement paste, chloride ions have to move around the aggregates to continue advancing (Yu 2007b). Moreover, reinforcing

steel acts as a barrier against chloride transport and causes chloride concentration to build up, resulting in much higher chloride concentrations over the reinforcement than in adjacent concrete (1.9 to 3.8 times greater) (Kranc et al. 2002, Yu 2007a). Chloride samples are taken in concrete adjacent to the bar (as would be done in the field) as opposed to over the bar. Ten samples (five from each side) were taken upon onset of corrosion and six samples at the test end life. At each sample site, concrete was initially drilled to a depth of 0.5 in. (13 mm) and the powdered concrete discarded. The specimen was then drilled to a depth of 2.0 in. (51 mm); this powdered sample (about 3 g) was transferred to a plastic bag for analysis. After each sampling, the drill bit was cleaned with deionized water. If the specimen was to continue testing, the holes were filled with modeling clay.

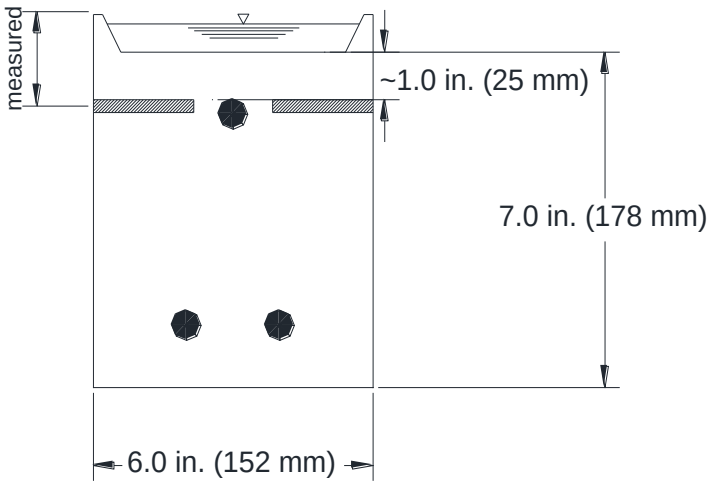

Figure 4.3— Beam specimen chloride sampling

The water-soluble chloride content of concrete samples were measured per AASHTO T 260-94, "Standard Method of Test for Sampling and Testing for Chloride Ion in Concrete and Concrete Raw Materials." First, samples were boiled with distilled water to release any water-

soluble chlorides. Samples then were filtered and titrated. During titration, samples were acidified with nitric acid and then titrated with silver nitrate. During titration, potential of a chloride ion-selective electrode was monitored and the change between potentials versus the incremental volume of added silver nitrate was plotted. The amount of added volume of silver nitrate in the inflection point of potential-volume curve (the point at which the highest potential difference for an incremental addition of silver nitrate is obtained) was recorded for calculating of chloride ion concentration in terms of percentage chloride by mass (weight) of concrete. Results then can be converted to weight of chloride content per volume of concrete in terms of lb/yd^3 (kg/m^3) by multiplying by the unit weight of concrete as 3786 lb/yd^3 (2246 kg/m^3).

4.2.4 Corrosion Measurements

4.2.4.1 Macrocell Corrosion Rate

To obtain the macrocell corrosion rate, the voltage drop between the anode and cathode of each specimen was taken across a 10-ohm resistor. The current density per unit area between two can be obtained by Ohm's Law:

$$i_{corr} = 10^6 \times \frac{V}{RA} \tag{4.1}$$

where i_{corr} is current density (μA/cm^2); V is the measured voltage drop across the resistor (volts); R is the resistance of resistor (10 ohms); and A is the surface area of anode (152 cm^2), surface area of the top mat of steel in beam specimens.

The corrosion rate can be expressed as the thickness loss of steel per time. The relationship between current density and thickness loss is shown below per Faraday's Law:

$$r = k\frac{ia}{nF\rho} \tag{4.2}$$

where r is the corrosion rate (μm/year); k is a conversion factor (315360 (A.μm.s)/(μA.cm.yr)); a is the atomic weight of the corroding metal (g/mol); n is the number of electrons lost per atom of metal oxidized (2 for iron); F is Faraday's constant (96485 Coulombs/equivalent); and ρ is the density of metal (g/cm^3). By substituting proper values for iron, Eq. (4.2) simplifies to $r = 11.6i$ in μm/yr ($0.457i$ in mils/yr).

4.2.4.2 Corrosion Potential

After measuring the voltage drop, the connection between anode and cathode across the resistor was disconnected for at least two hours to allow the potentials to stabilize, and then the corrosion potential of the top and bottom mat in beam specimens was measured using a saturated calomel electrode (SCE).

4.2.4.3 Linear Polarization Resistance

In addition to the weekly voltage drop and corrosion potential measurements, linear polarization resistance (LPR) was measured on a monthly basis for bench-scale specimens. Linear polarization resistance is used to measure the total corrosion rate of reinforcement, including both macrocell corrosion (where the anode and cathode are on separate bars), and microcell corrosion, where the anode and cathode on the same bar. In a corroding specimen, both forms of corrosion are present simultaneously, while voltage drop readings will not measure microcell corrosion. The LPR test consists of a working electrode (corroding reinforcement), a counter electrode (platinum rod), and a reference electrode (calomel electrode) connected to a potentiostat. The potentiostat controls the voltage difference between the working electrode and reference electrode in a system, and the counter electrode is used to apply current to that system. By applying external voltage,

corrosion potential of the system can be shifted by (Δε) with respect to E_{corr} (in a range of –20 mV to 20 mV for this test), resulting in a change in the current density (Δi). The obtained data are plotted as a potential-current curve. In the vicinity of the equilibrium potential (in a range from –10 mV to 10 mV with respect to E_{corr}), the potential-current curve is linear and the slope of the curve is defined as the linear polarization resistance (R_p). The linear polarization resistance is inversely proportional to the corrosion current density according to the Stern-Geary equation:

$$i_{corr} = \frac{\beta_a \beta_c}{2.3 R_p (\beta_a + \beta_c)} \tag{4.3}$$

Where β_a and β_c are anodic and cathodic Tafel constants, taken as 0.12 V/decade for reinforcing steel in concrete (Lambert et al. 1991, McDonald et al. 1998). By using these values, the current density in Eq. (4.3) is simplified to:

$$i_{corr} = \frac{0.026}{R_p} \tag{4.4}$$

Current density then can be converted to thickness loss per Eq. (4.2).

4.2.5 TEST PROGRAM

Seven distinct concrete mixes were cast in this study. In the first mix, ordinary portland cement was used as the only cementitious material; the other mixes were batched by three types of cementitious materials (fly ash, silica fume, and slag cement), which partially replaced the cement content volume in mixtures. The partial cement content volumes replaced by cementitious materials were as follows: 20% and 40% by fly ash, 5% and 10% by silica fume, and 20% and 40% by slag cement. Two kinds of reinforcement were used to make the specimens; conventional uncoated (ASTM A615) bars, and conventional epoxy-coated reinforcement. Uncoated bars were used to make beam specimens with all seven concrete mixtures (100% portland cement, 20% fly

ash, 40% fly ash, 5% silica fume, 10% silica fume, 20% slag cement, and 40% slag cement). However, epoxy-coated bars were only used in specimens containing 100% ordinary portland cement, 40% fly ash, 10% silica fume, and 40% slag cement; these specimens have an ECR added to their designation after the mixture type. For example, PC-ECR indicated a specimen with epoxy-coated reinforcement in 100% portland cement concrete. Six beam specimens were cast for each set. The total number of beam specimens cast in this study is listed in Table 4.3.

Table 4.3: Supplementary cementitious materials (SCM) test specimens

Specimen Designation[a]	Uncoated	ECR
PC	6	6
FA(20)	6	-
FA(40)	6	6
Slag(20)	6	-
Slag(40)	6	6
SF(5)	6	-
SF(10)	6	6
Total	**42**	**24**

[a]PC = Conventional bar in concrete containing 100% portland cement
PC-ECR = Epoxy-coated bar in concrete containing 100% portland cement
FA(20) = Conventional bar in concrete containing 20% fly ash and 80% Portland cement by volume
FA(40) = Conventional bar in concrete containing 40% fly ash and 60% portland cement by volume
FA-ECR(40) = Epoxy-coated bar in concrete containing 40% fly ash and 60% portland cement by volume
Slag(20) = Conventional bar in concrete containing 20% slag cement and 80% portland cement by volume
Slag(40) = Conventional bar in concrete containing 40% slag cement and 60% portland cement by volume
Slag-ECR(40) = Epoxy-coated bar in concrete containing 40% slag cement and 60% portland cement by volume
SF(5) = Conventional bar in concrete containing 5% silica fume and 95% portland cement by volume
SF(10) = Conventional bar in concrete containing 10% silica fume and 90% portland cement by volume
SF-ECR(10) = Epoxy-coated bar in concrete containing 10% silica fume and 90% portland cement by volume

4.3 TEST RESULTS

4.3.1 Macrocell Corrosion Rate and Corrosion Potential

4.3.1.1 Uncoated reinforcement

The macrocell corrosion rates calculated from voltage drops and the top mat corrosion potentials with respect to a saturated calomel electrode (SCE) of uncoated bars for specimens containing 100% portland cement (PC) are shown in Figures 4.4 and 4.5, respectively. Specimens 1 and 2 initiated corrosion at weeks 23 and 15, respectively. Specimens 3 and 4 initiated corrosion at week 12, and Specimens 5 and 6 initiated corrosion at weeks 13 and 20, respectively. Corrosion rates jumping above 0.3 μm/yr and sharp drops in corrosion potentials to below –0.275 V correspond to corrosion initiation. The average time to corrosion initiation for specimens containing 100% portland cement (PC) was 15.8 weeks. The maximum corrosion rates for specimens with 100% ordinary portland cement through week 96 ranged from 16.9 to 34.5 μm/yr. The top mat potentials for all specimens decreased over time and reached the maximum negative values ranging from –0.600 to –0.700 V at the final weeks of test. The bottom mat corrosion potentials with respect to SCE are presented in Appendix J.

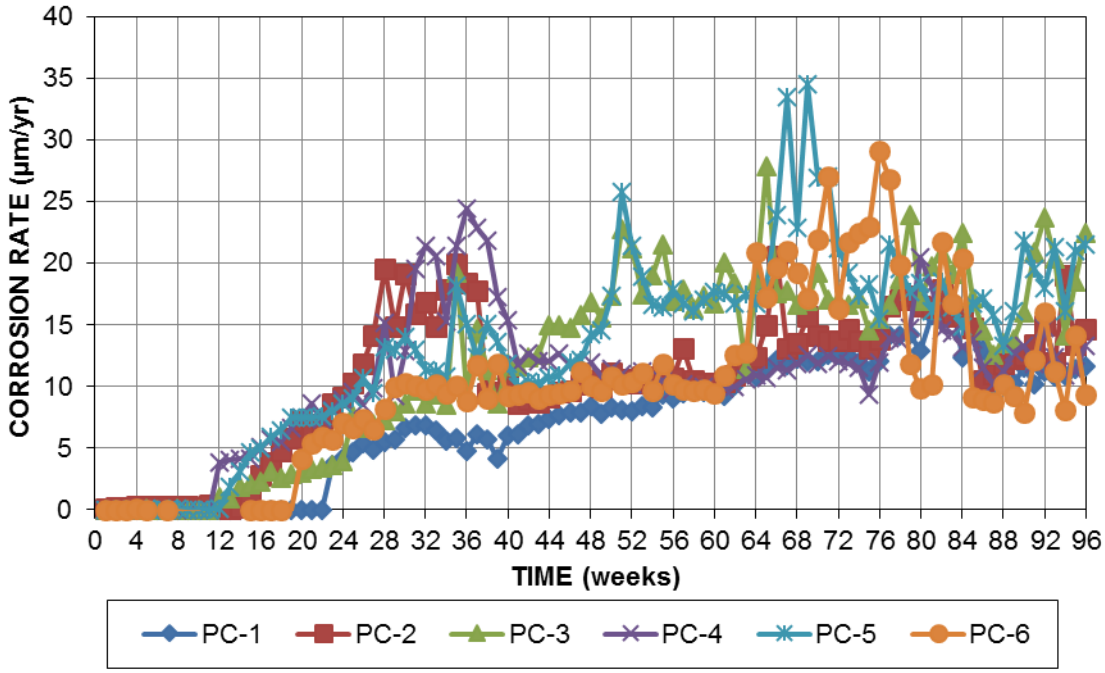

Figure 4.4— Macrocell corrosion rates (µm/yr) for specimens containing uncoated conventional reinforcement and 100% portland cement

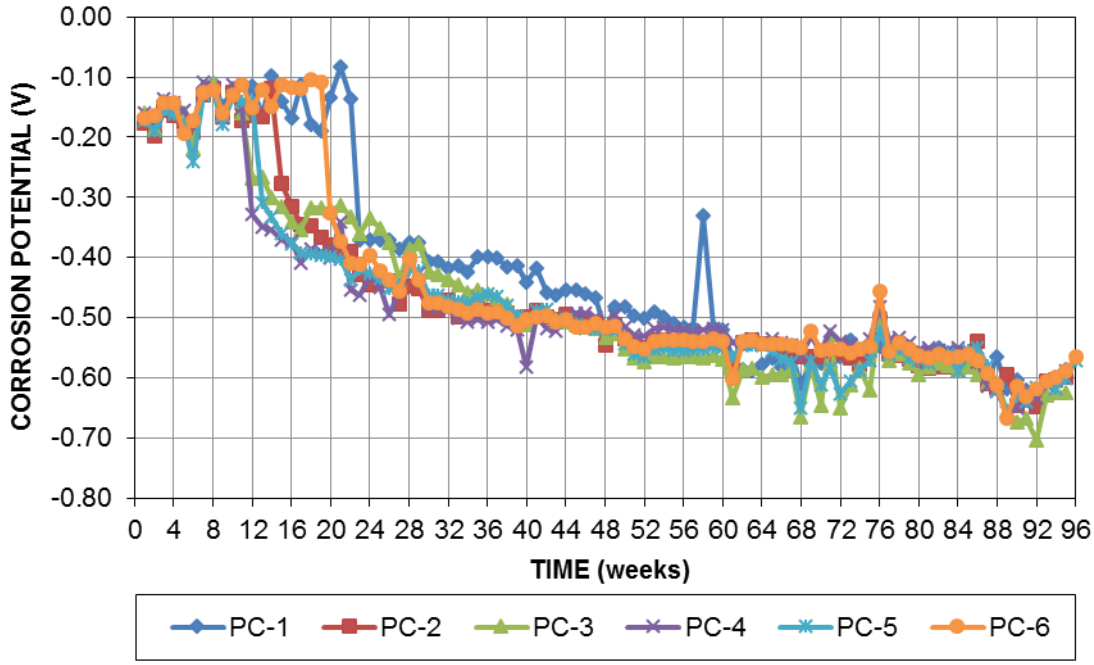

Figure 4.5—Top mat (anode) corrosion potential (SCE) versus time for specimens containing uncoated conventional reinforcement and 100% portland cement

The macrocell corrosion rates and top mat corrosion potentials with respect to SCE for specimens with uncoated bars, containing 20% fly ash (FA(20)), are shown in Figures 4.6 and 4.7, respectively. For specimens containing 20% fly ash, Specimens 1 and 2 initiated corrosion at weeks 30 and 23, respectively. Specimens 3 and 4 initiated corrosion at week 28, and Specimens 5 and 6 at weeks 47 and 8, respectively. The average time to corrosion initiation for specimens containing 20% fly ash was 27.3 weeks. The maximum corrosion rates for specimens containing 20% fly ash through week 96 was significantly lower than that for 100% ordinary portland cement, and ranged from 4.5 to 8.8 µm/yr. After dropping to below –0.275 V, the top mat potential for all specimens, except FA(20)-3, decreased over time, reaching –0.500 to –0.550 V at end of the test.

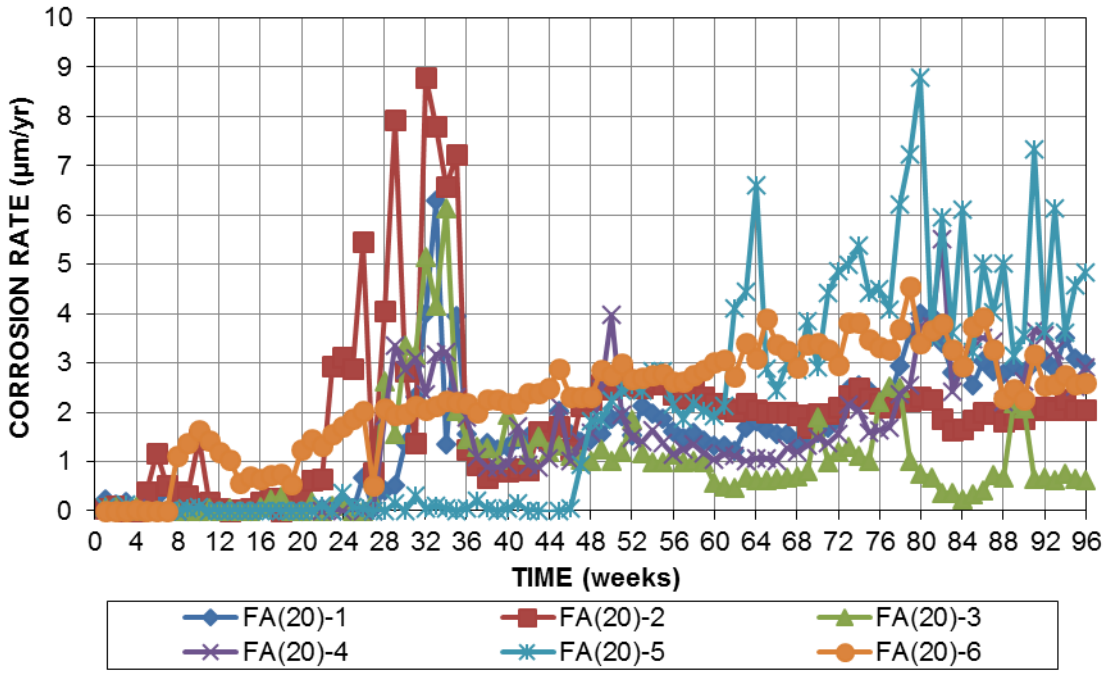

Figure 4.6— Macrocell corrosion rates (µm/yr) for specimens containing uncoated conventional reinforcement and 20% fly ash

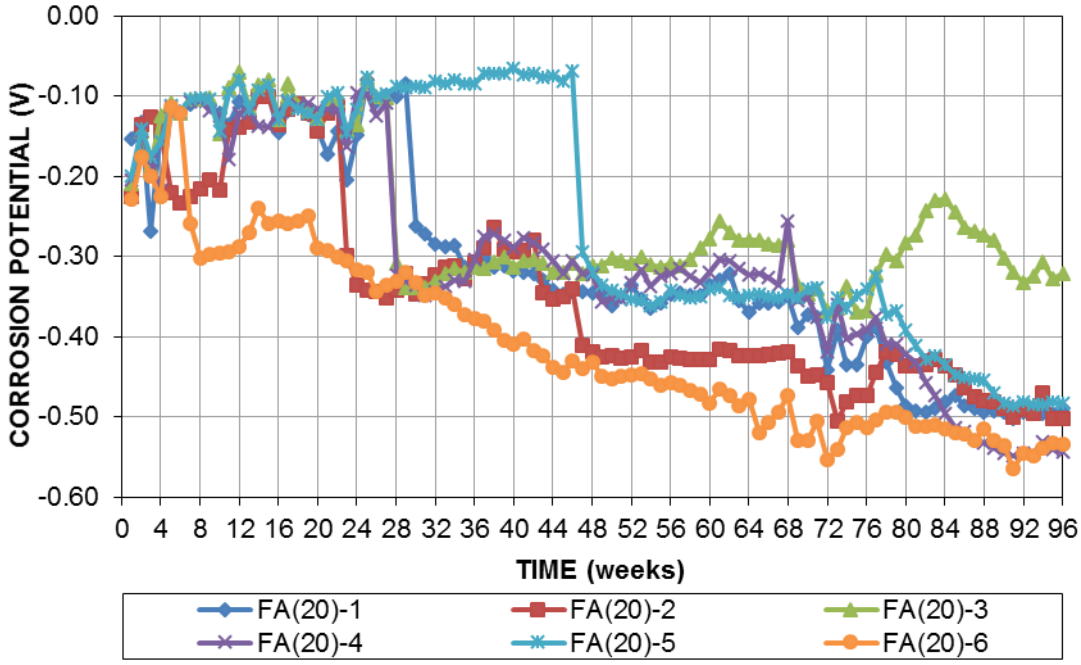

Figure 4.7—Top mat (anode) corrosion potential (SCE) versus time for specimens containing uncoated conventional reinforcement and 20% fly ash

The macrocell corrosion rates and top mat corrosion potentials versus SCE of uncoated bars for specimens containing 40% fly ash (FA(40)) are shown in Figures 4.8 and 4.9, respectively. For specimens containing 40% fly ash, tests were continued after week 96 to obtain further information about their corrosion performance. Specimens FA(40)-1, 3, 4, and 6 initiated corrosion at weeks 42, 49, 33, and 39 with an average of week 41; however, their corrosion rate and potential indicated repassivation of the reinforcement after a few weeks. These specimens re-initiated at weeks 87, 87, 92, and 81, respectively. Specimens 2 and 5 initiated corrosion at weeks 49 and 85, and did not repassivate afterwards. The average time to final corrosion initiation for all specimens containing 40% fly ash (FA(40)) was 80 weeks. The maximum corrosion rates for specimens containing 40% fly ash to date (week 124) ranged from 1.51 to 2.37 µm/yr, at least one order of magnitude lower than those for specimens with 100% portland cement. The corrosion potential of all specimens containing 40% fly ash after week 87 ranged from –0.230 V to –0.370 V.

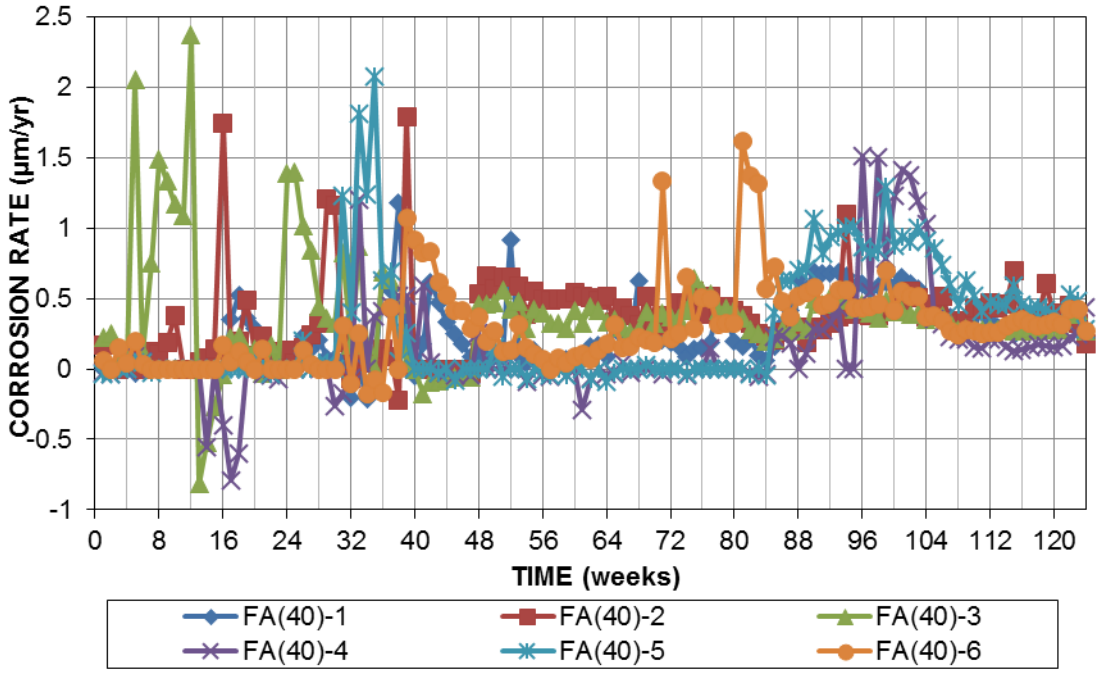

Figure 4.8— Macrocell corrosion rates (µm/yr) for specimens containing uncoated conventional reinforcement and 40% fly ash

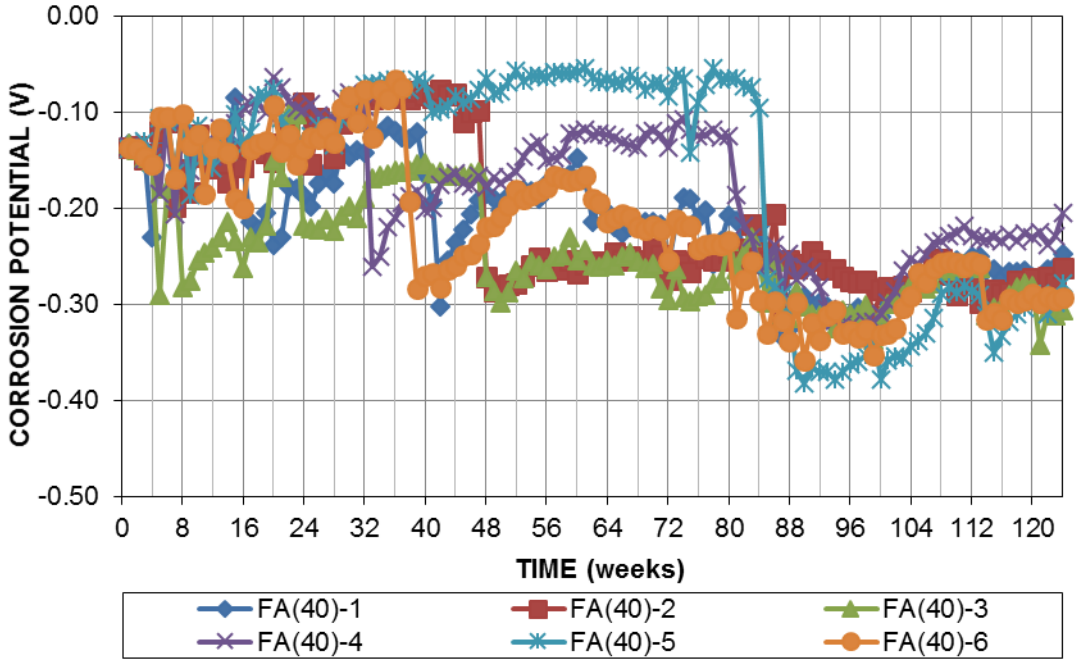

Figure 4.9—Top mat (anode) corrosion potential (SCE) versus time for specimens containing uncoated conventional reinforcement and 40% fly ash

The macrocell corrosion rates and corrosion potentials of beam specimens with uncoated bars, containing 5% silica fume (SF(5)), are shown in Figures 4.10 and 4.11, respectively. Although the corrosion rate of Specimens SF(5)-3, 5, and 6 exceeded 0.3 µm/yr for a few weeks prior to week 27, since no drop in corrosion potential or jump in LPR test results were observed, the jump was possibly due to corrosion in electrical connections, not corrosion on the test bar. The macrocell corrosion rate of Specimens 1, 2, and 3 exceeded 0.3 µm/yr at weeks 97, 82, and 97, respectively, and continued to increase through week 113. The corrosion potentials of other specimens remained above –0.200 V through week 113.

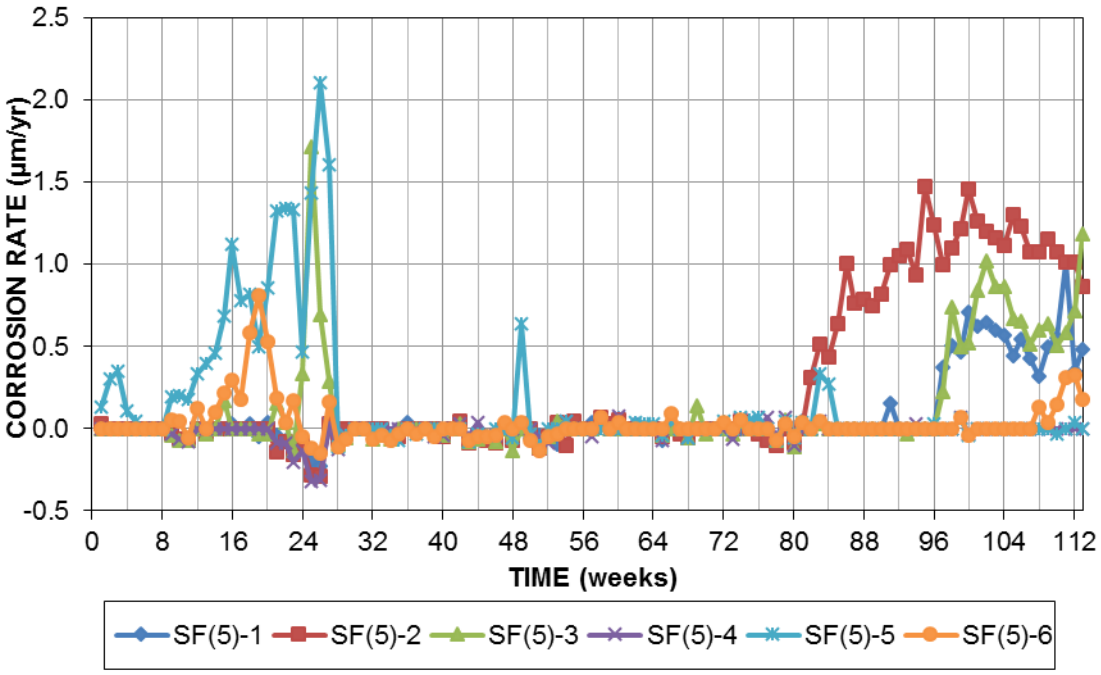

Figure 4.10— Macrocell corrosion rates (µm/yr) for specimens containing uncoated conventional reinforcement and 5% silica fume

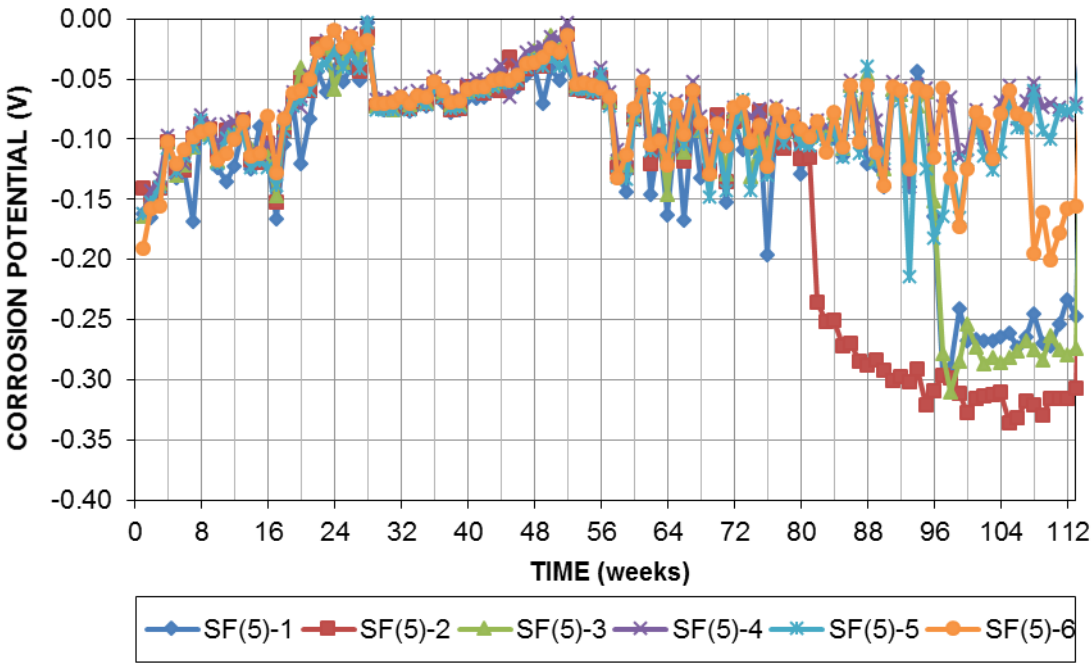

Figure 4.11—Top mat (anode) corrosion potential (SCE) versus time for specimens containing uncoated conventional reinforcement and 5% silica fume

The macrocell corrosion rates and corrosion potential versus SCE for specimens with uncoated bars and 10% silica fume (SF(10)) are shown in Figures 4.12 and 4.13, respectively. The corrosion rate and potential of Specimen SF(10)-2 showed corrosion initiation at week 19 and repassivating at week 41. Specimen 2 reinitiated at week 66, with a maximum macrocell corrosion rate of 4.74 µm/yr at week 73. The other specimens containing 10% silica fume did not exhibit corrosion initiation through week 110.

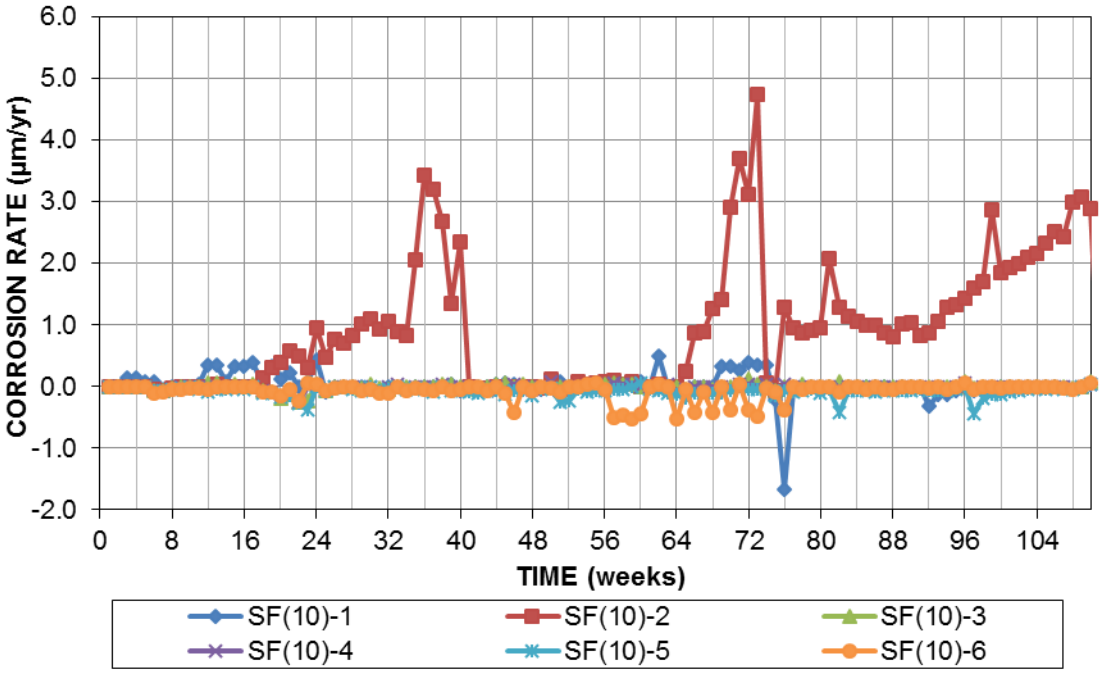

Figure 4.12— Macrocell corrosion rates (µm/yr) for specimens containing uncoated conventional reinforcement and 10% silica fume

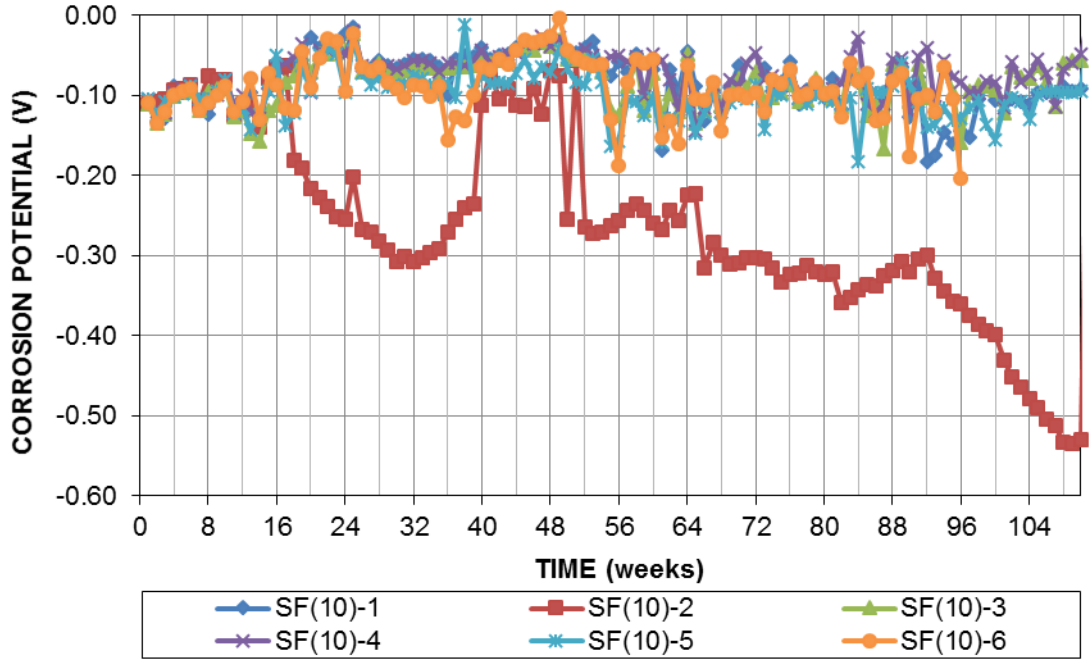

Figure 4.13—Top mat (anode) corrosion potential (SCE) versus time for specimens containing uncoated conventional reinforcement and 10% silica fume

The macrocell corrosion rates and top mat corrosion potentials versus SCE for specimens with uncoated bars, containing 20% slag cement (Slag(20)), are shown in Figures 4.14 and 4.15, respectively. For specimens containing 20% slag cement, Specimens 1, 2 and 6 initiated corrosion at weeks 56, 80, and 65, respectively. Specimens Slag(20)-1 and 2 exhibited one sharp drop in corrosion potential below –0.275 V at weeks 56 and 65, respectively, and remained below –0.275 V thereafter. The potential for Specimen Slag(20)-6 gradually decreased over time and dropped below –0.275 V at week 65. Specimens 3, 4, and 5 showed corrosion initiation at weeks 32, 12, and 6; however, repassivation occurred shortly thereafter. These specimens re-initiated at weeks 83, 76, and 46, respectively. The average time to corrosion initiation for specimens containing 20% slag cement was 67.7 weeks. The maximum corrosion rate of Specimen Slag(20)-5, 7.3 µm/yr, was significantly higher than the other specimens, which had corrosion rates ranging from 0.63 to 2.96 µm/yr.

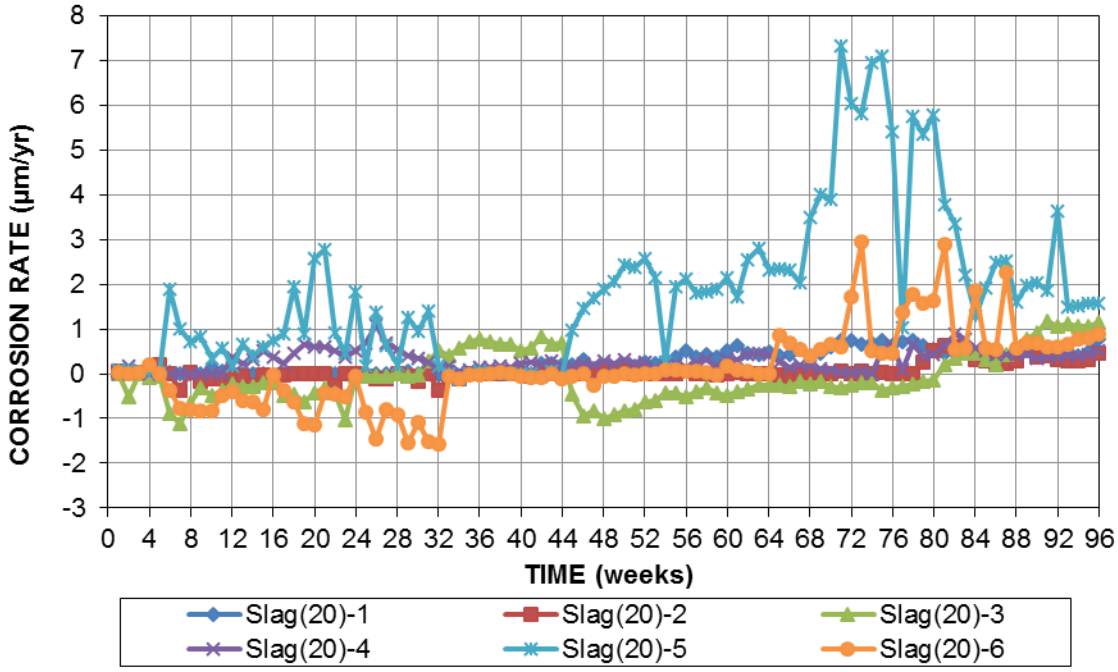

Figure 4.14— Macrocell corrosion rates (µm/yr) for specimens containing uncoated conventional reinforcement and 20% slag cement

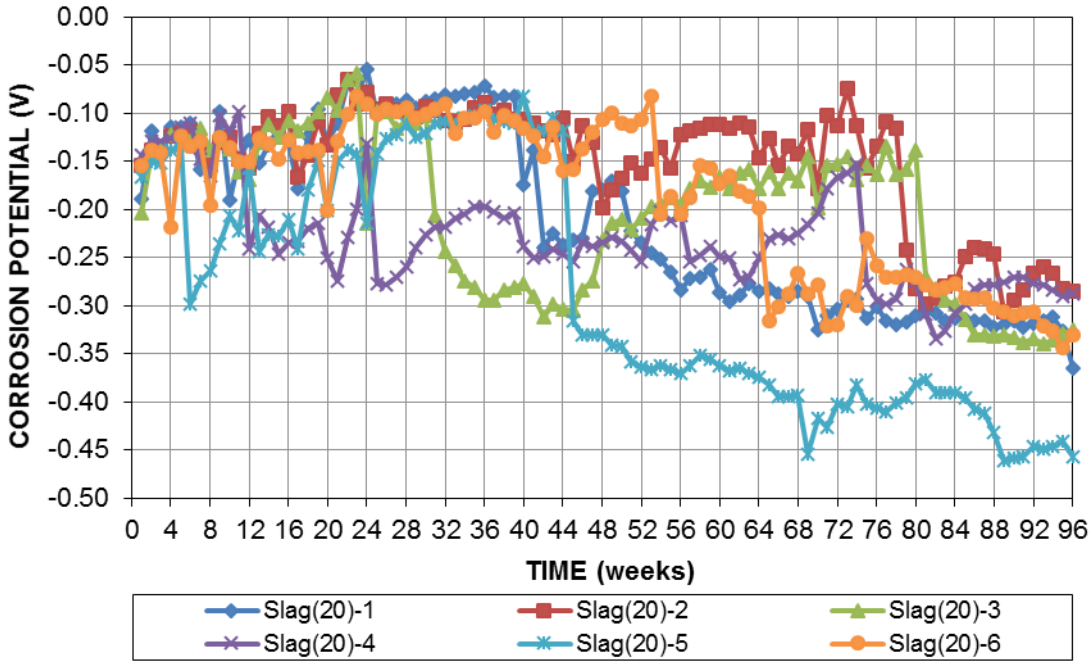

Figure 4.15—Top mat (anode) corrosion potential (SCE) versus time for specimens containing uncoated conventional reinforcement and 20% slag cement

The macrocell corrosion rates and top mat corrosion potentials versus SCE for specimens with uncoated bars containing 40% slag cement (Slag(40)), are shown in Figures 4.16 and 4.17, respectively. For specimens containing 40% slag cement, testing was extended beyond 96 weeks to obtain further information about their corrosion performance. Specimen Slag(40)-2 showed corrosion rates higher than 0.3 µm/yr after week 81; its potential gradually decreased below –0.275 V at week 87. Specimen Slag(40)-5 initiated corrosion at week 94. Specimen 3 showed corrosion rates above 0.3 µm/yr from week 19 to 23, re-initiating at week 50 when its potential decreased to below –0.275 V. Other specimens (Slag(40)-1, 4, and 6) have not initiated corrosion through week 118. The maximum corrosion rates for specimens containing 40% slag cement (to date) ranged from 0.37 to 2.78 µm/yr, at least one order of magnitude lower than those for specimens with 100% portland cement.

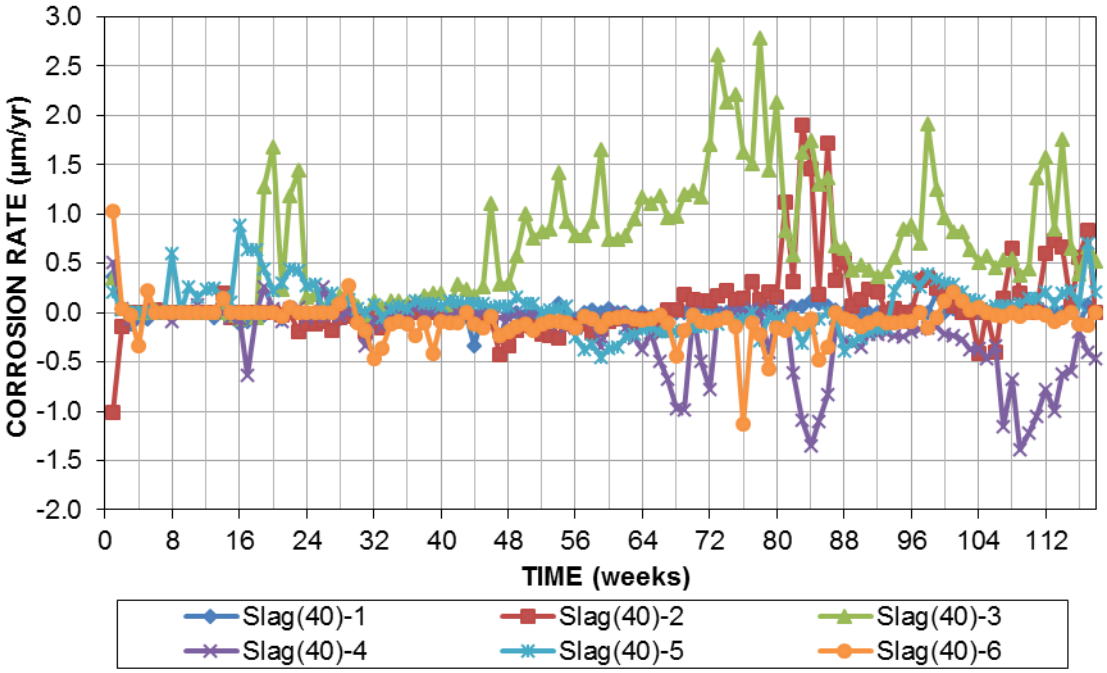

Figure 4.16— Macrocell corrosion rates (µm/yr) for specimens containing uncoated conventional reinforcement and 40% slag cement

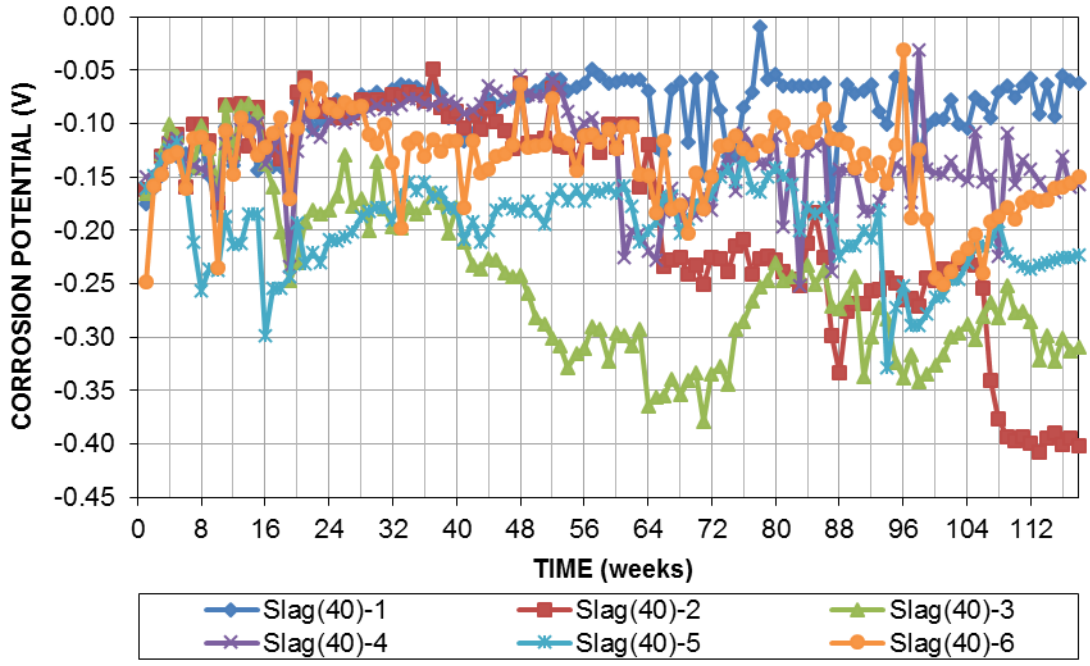

Figure 4.17—Top mat (anode) corrosion potential (SCE) versus time for specimens containing uncoated conventional reinforcement and 40% slag cement

Figures 4.18 and 4.19 compare the average corrosion rate of the uncoated conventional reinforcement in all beam specimens. As shown, specimens with supplementary cementitious materials exhibited an average corrosion rate about one order of magnitude less than the specimens with only ordinary portland cement. Among specimens with supplementary cementitious materials (SCM), increasing the amount of SCM decreased the corrosion rate, with the lowest corrosion rates observed in specimens containing silica fume, followed by slag cement, and fly ash. Among specimens containing SCMs, FA(20) specimens had the maximum average corrosion rate, 3.73 µm/yr, followed by Slag(20) with 1.56 µm/yr, and FA(40), Slag(40), SF(5), and SF(10) with less than 1 µm/yr.

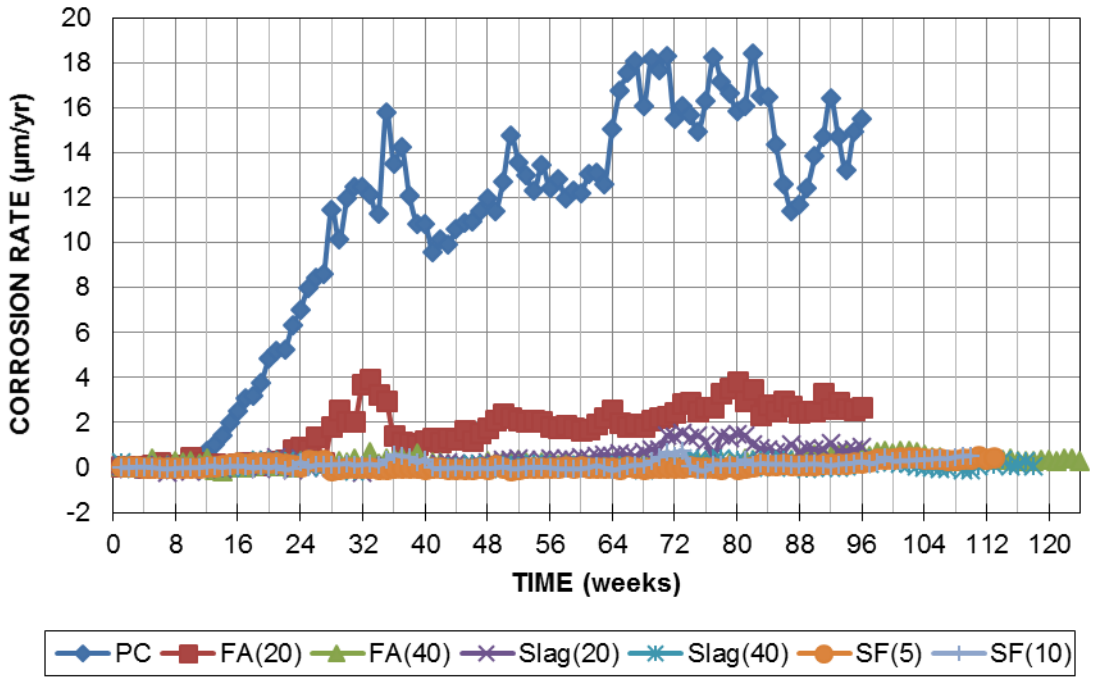

Figure 4.18— Average macrocell corrosion rates (µm/yr) for all specimens containing uncoated conventional reinforcement

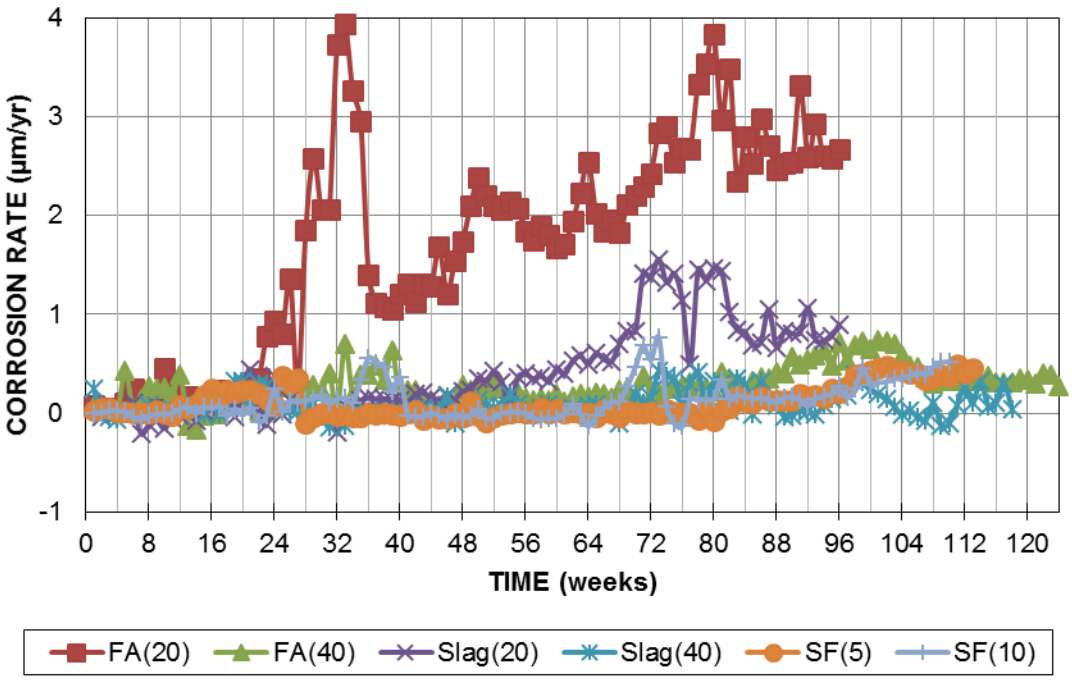

Figure 4.19— Average macrocell corrosion rates (µm/yr) for specimens containing supplementary cementitious materials and uncoated conventional reinforcement

The average top mat corrosion potentials versus SCE for the beam specimens containing ASTM A615 uncoated bars are shown in Figure 4.20. The average bottom mat corrosion potentials are shown in Appendix J. The average top mat potential for all specimens was between –0.100 V and –0.200 V at the start of the test. The PC specimens exhibited the most negative potential in the test, followed by FA(20), Slag(20), FA(40), Slag (40), SF(5) and SF(10), respectively.

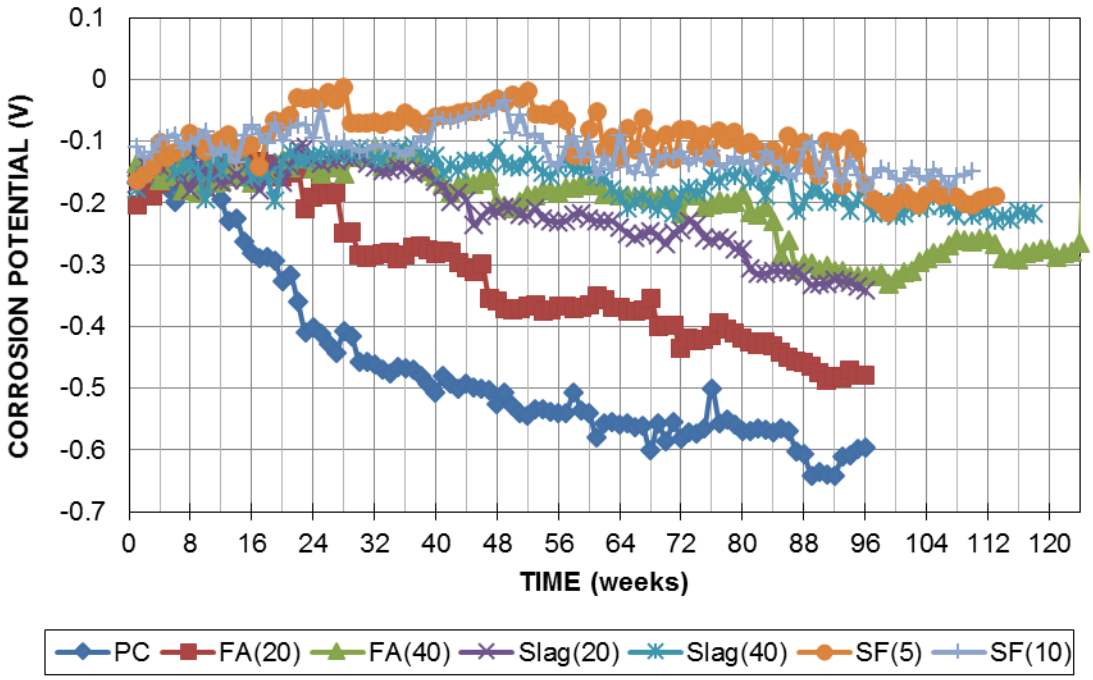

Figure 4.20—Top mat (anode) average corrosion potential (SCE) versus time for specimens containing uncoated conventional reinforcement

The individual and average corrosion losses for the beam specimens containing uncoated conventional bars through week 96 are tabulated in Table 4.4. Corrosion loss is obtained by integrating macrocell corrosion rates with respect to time; that is, corrosion loss is the accumulated amount of thickness of steel that is corroded with respect to time assuming uniform corrosion. Specimens containing 100% ordinary portland cement had the highest average corrosion loss, 19.7 µm followed by FA(20) specimens, which had an average corrosion loss of 3.17 µm. Specimens containing 20% slag, 40% fly ash, 40% slag, 5% silica fume, and 10% silica fume had average corrosion losses less than 1 µm, approximately 5% of that for specimens with 100% portland cement.

Table 4.4: Corrosion loss (µm) for all specimens containing uncoated conventional bars

Specimen	Week	Corrosion Loss (µm)-Total Area						Average	Std. Dev.
		1	2	3	4	5	6		
PC	96	13.5	19.6	22.6	19.5	24.8	18.3	19.7	3.87
FA(20)	96	2.90	3.63	1.81	2.69	3.76	4.23	3.17	0.88
FA(40)	96	0.394	0.598	0.736	0.081	0.345	0.518	0.445	0.227
SF(5)	96	-0.022	0.207	0.042	-0.030	0.346	0.049	0.107	0.140
SF(10)	96	0.067	1.33	-0.010	-0.014	-0.134	-0.149	0.233	0.539
Slag(20)	96	0.475	0.097	-0.093	0.559	3.367	0.215	0.786	1.28
Slag(40)	96	-0.022	0.087	1.25	-0.289	0.055	-0.172	0.232	0.500

4.3.1.2 Epoxy-coated Reinforcement (ECR)

The macrocell corrosion rates calculated from voltage drops based on the total area of reinforcement, and the top mat corrosion potentials of specimens with ECR containing 100% portland cement (PC-ECR) are shown in Figures 4.21 and 4.22. The bottom mat potentials are exhibited in Appendix J. Specimens PC-ECR-1 through 6 initiated corrosion at weeks 35, 47, 40, 40, 35, and 44 with an average of week 40. The maximum corrosion rates for specimens with 100% ordinary portland cement containing ECR through week 96 ranged from 0.14 to 0.64 µm/yr. The top mat potential for all specimens was between –0.150 V and –0.250 V at the start of the test, and then increased slightly until a sharp drop in corrosion potentials corresponding with corrosion initiation. The top mat potential for all specimens reached the maximum negative values near the end of testing, ranging from –0.450 to –0.570 V.

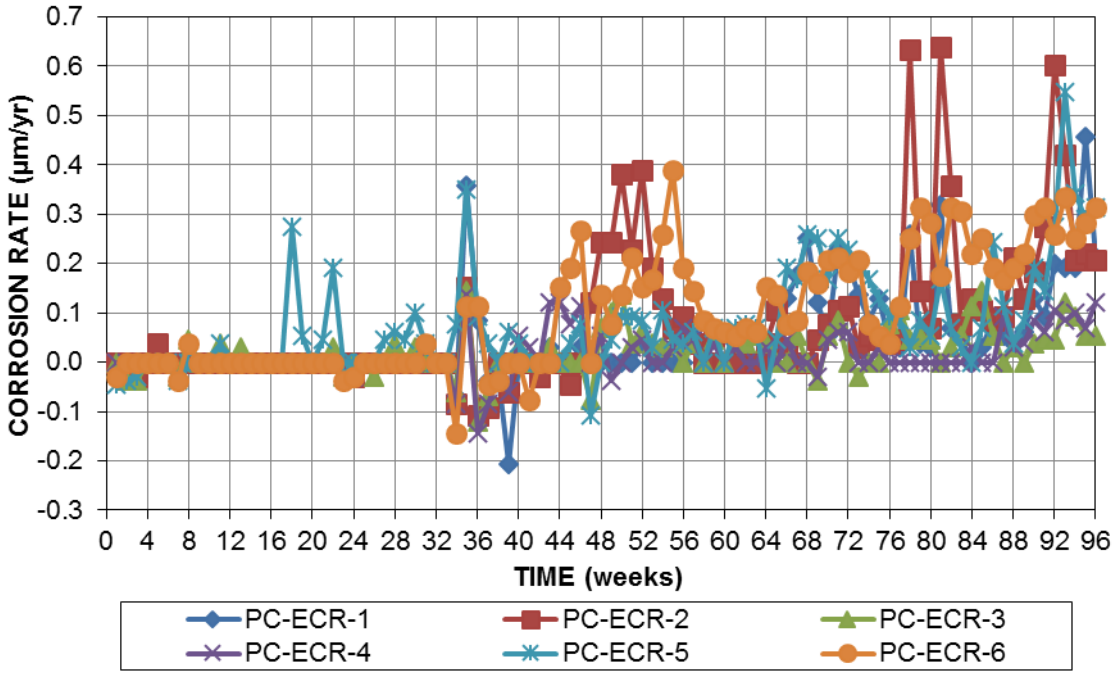

Figure 4.21— Macrocell corrosion rates (µm/yr) based on total area of reinforcement for specimens containing ECR and 100% portland cement

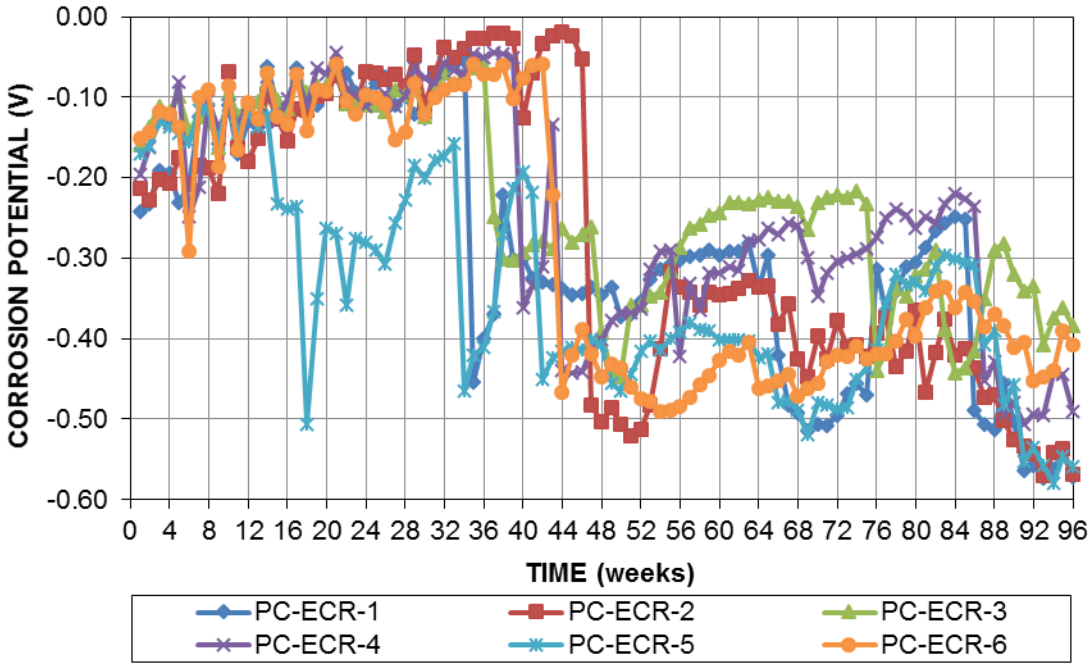

Figure 4.22—Top mat (anode) corrosion potential (SCE) versus time for specimens containing ECR and 100% portland cement

The macrocell corrosion rates based on the total area of reinforcement and corrosion potentials of specimens with epoxy-coated bars for specimens containing 40% fly ash (FA-ECR(40)) through week 124 are shown in Figures 4.23 and 4.24, respectively. Specimens FA-ECR(40)-2, 5 and 6 initiated corrosion at weeks 59, 102, and 101, respectively. Specimens FA-ECR(40)-1, 3 and 4 initiated corrosion at week 85. All specimens repassivated after a few weeks of corrosion; specimen FA-ECR(40)-2 re-initiated at week 85. The average time to final corrosion initiation for FA-ECR(40) specimens that initiated (to date) was 88 weeks. The maximum corrosion rates for specimens containing 40% fly ash through week 124 ranged from 0.05 to 0.27 µm/yr.

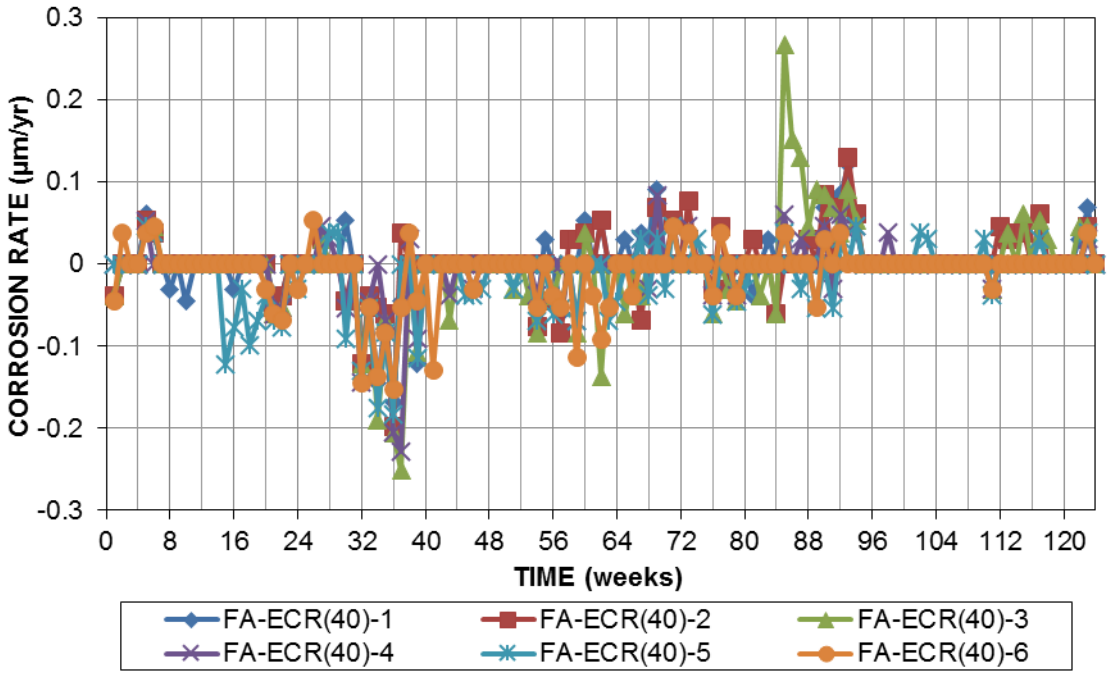

Figure 4.23— Macrocell corrosion rates (µm/yr) based on total area of reinforcement for specimens containing ECR and 40% fly ash

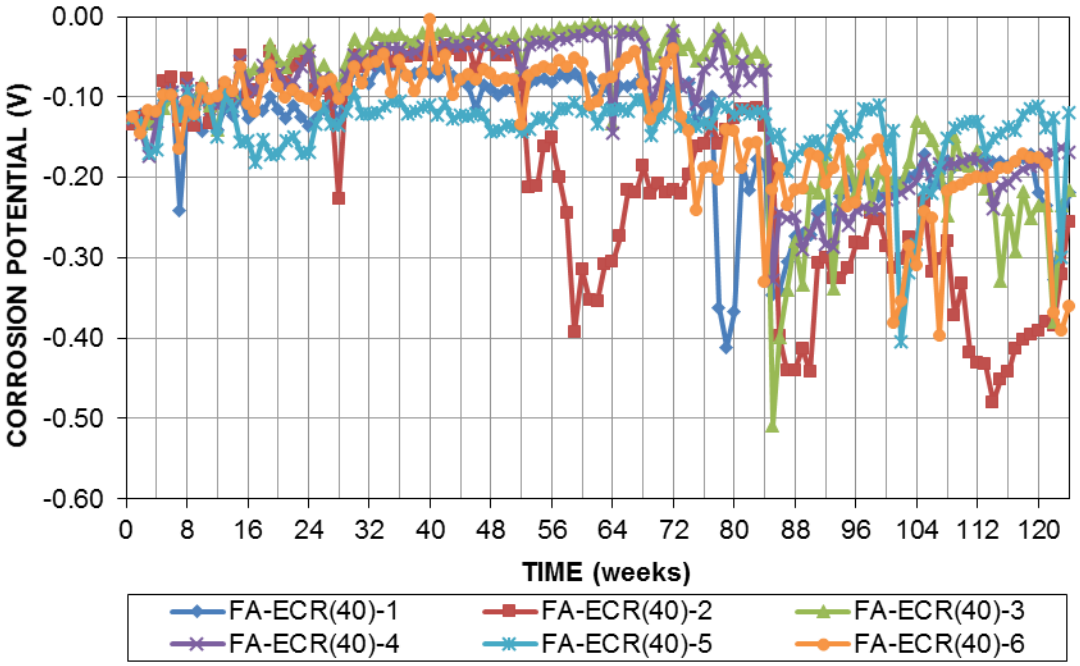

Figure 4.24—Top mat (anode) corrosion potential (SCE) versus time for specimens containing ECR and 40% fly ash

The macrocell corrosion rates based on the total area of bar and the top mat corrosion potential of epoxy-coated reinforcement in beam specimens containing 10% silica fume (SF-ECR(10)) through week 110 are shown in Figures 4.25 and 4.26, respectively. During the first six weeks, Specimen SF-ECR(10)-4 exhibited a corrosion rate up to 0.13 µm/yr and a corrosion potential near –0.400 V; however, the corrosion rates and potentials settled after the first six weeks. Specimen SF-ECR(10)-3 showed corrosion initiation at week 41, repassivated after several weeks, and reinitiated at week 97. Corrosion potential for Specimen 3 dropped to about –0.500 V at week 97, potential then gradually increased to near –0.270 V through week 110. Other specimens did not show any sign of corrosion initiation through week 110. The maximum corrosion rates for specimens containing 10% silica fume through week 110 ranged from 0.05 to 0.20 µm/yr. Except for Specimen 3, potentials ranged from –0.075 to –0.150 V during the final weeks, indicating no active corrosion.

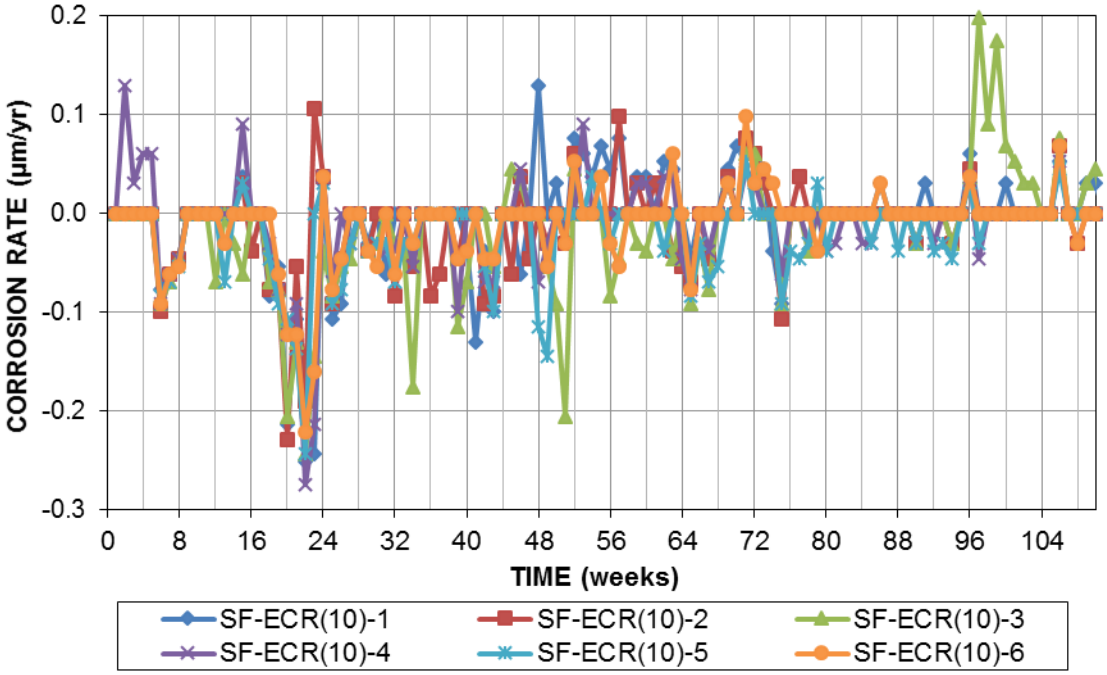

Figure 4.25— Macrocell corrosion rates (µm/yr) based on total area of reinforcement for specimens containing ECR and 10% silica fume

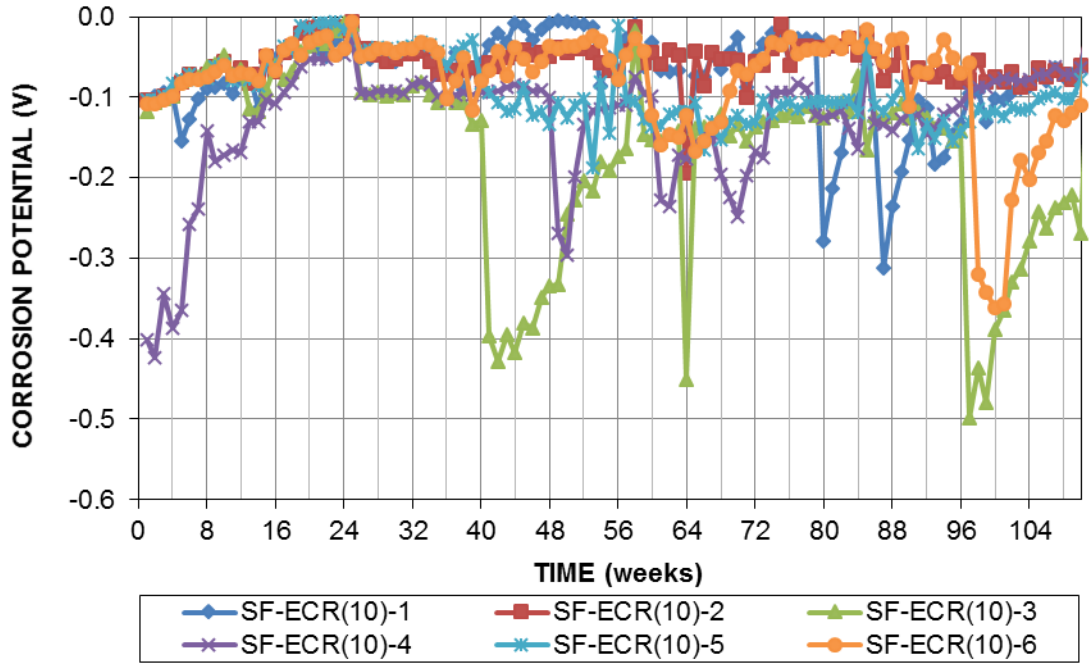

Figure 4.26—Top mat (anode) corrosion potential (SCE) versus time for specimens containing ECR and 10% silica fume

The macrocell corrosion rates of beam specimens calculated from voltage drops of epoxy-coated bars, based on their total area, and the top mat corrosion potentials for specimens containing 40% slag cement (Slag-ECR(40)) through week 118 are shown in Figures 4.27 and 4.28, respectively. Specimens Slag-ECR(40)-1, 2 and 5 exhibited corrosion initiation twice; each time, the bar repassivated shortly thereafter . A sharp drop in potentials occurred for these specimens at weeks 47, 5, and 40 that corresponds to corrosion initiation. These specimens then re-initiated at weeks 65, 50, and 70, respectively. Specimen Slag-ECR(40)-3 showed corrosion initiation at week 81 and repassivated after a few weeks; this specimen re-initiated at week 117. Specimens Slag-ECR(40)-4 and 6 have not showed corrosion initiation to date (week 118). The maximum corrosion rates for specimens containing 40% slag cement through week 118 ranged from 0.06 to 0.17 µm/yr.

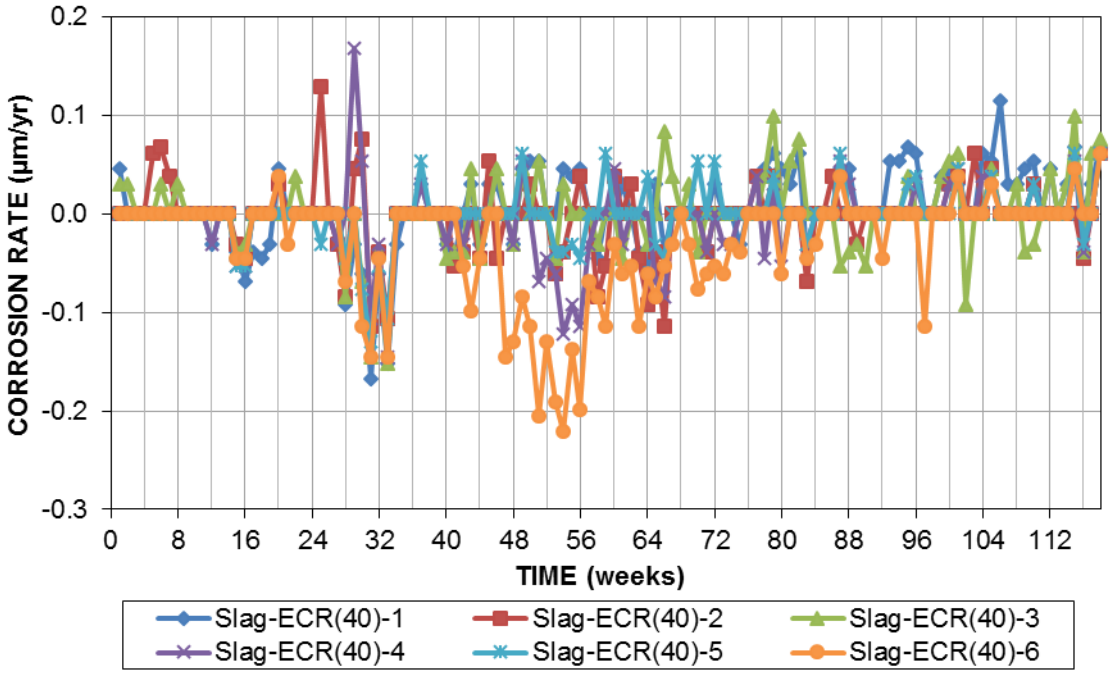

Figure 4.27— Macrocell corrosion rates (µm/yr) based on total area of reinforcement for specimens containing ECR and 40% slag cement

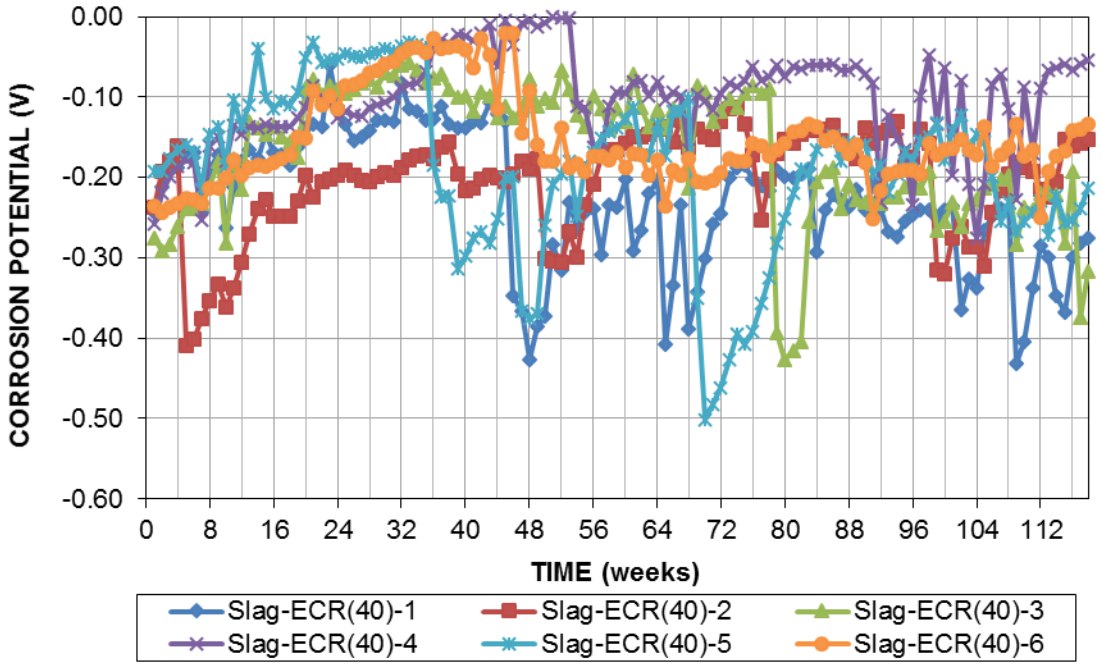

Figure 4.28—Top mat (anode) corrosion potential (SCE) versus time for specimens containing ECR and 40% slag cement

Figure 4.29 compares the average corrosion rate of the epoxy-coated reinforcement, based on their total area, for specimens containing 100% ordinary portland cement (PC-ECR), 40% fly ash (FA-ECR(40)), 10% silica fume (SF-ECR(10)), and 40% slag (Slag-ECR(40)). As shown in Figure 4.29, specimens with any supplementary cementitious materials exhibited average corrosion rate significantly lower than specimens with only ordinary portland cement. The maximum average corrosion rate of specimens with 100% portland cement was 0.28 µm/yr; specimens with fly ash, silica fume and slag cement exhibited maximum corrosion rates less than a quarter of that observed in the 100% portland cement mixture (0.07, 0.07, and 0.04 µm/yr, respectively).

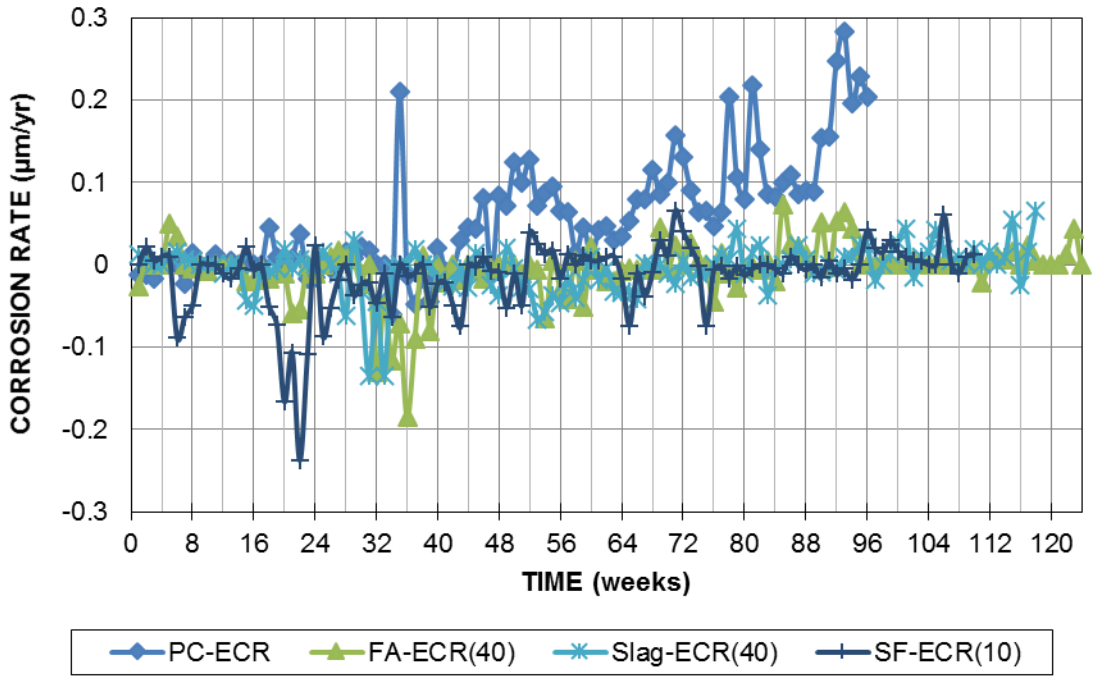

Figure 4.29— Average macrocell corrosion rates (µm/yr) based on total area of reinforcement for all specimens containing ECR

The average top mat corrosion potentials (with respect to a saturated calomel electrode) for the beam specimens containing conventional epoxy-coated bars are shown in Figure 4.30. The average bottom mat corrosion potentials are shown in Appendix J. The average top mat potential for all specimens was between –0.150 V and –0.250 V at the start of testing. Specimens with 100% portland cement exhibited a drop in potentials between weeks 32 and 48. Specimens with 40% fly ash showed a sharp drop in average potential after week 85. While the average corrosion potential for Slag-ECR(40) specimens is gradually decreasing over time, the average corrosion potential for SF-ECR(10) specimens has not shown significant drop in corrosion potential to date.

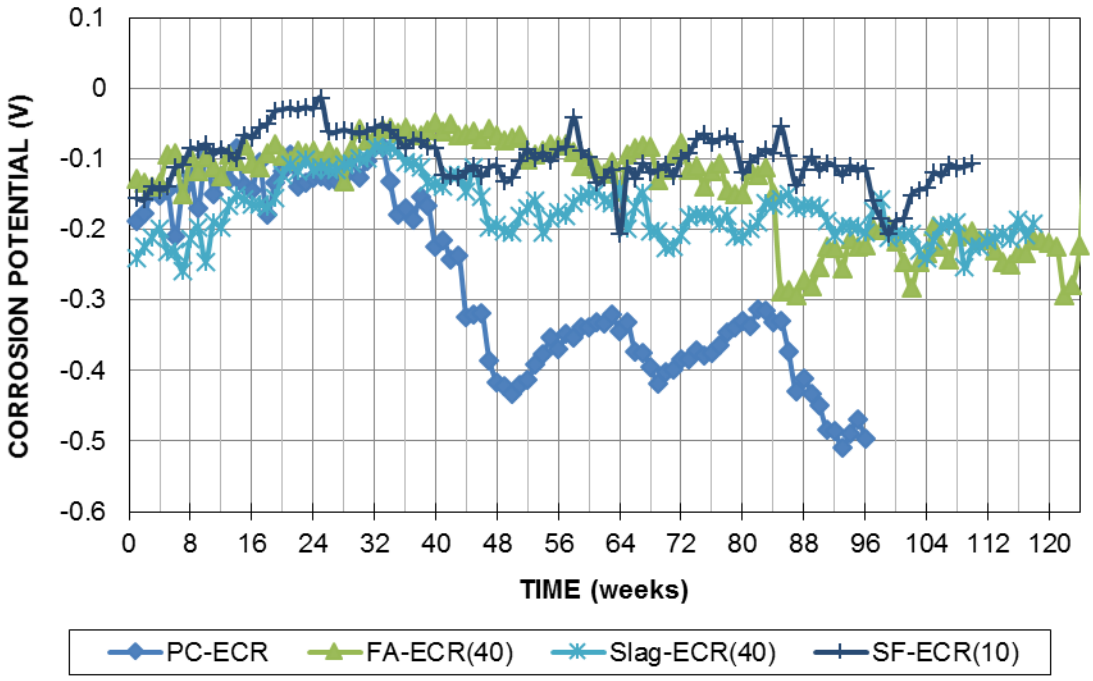

Figure 4.30—Top mat (anode) average corrosion potential (SCE) versus time for specimens containing epoxy-coated reinforcement

The individual and average corrosion losses for the beam specimens containing epoxy-coated bars through week 96 are tabulated in Table 4.5. Corrosion losses were obtained by integrating corrosion rates with respect to time, and presented based on both total and exposed area of epoxy-coated bars. Macrocell corrosion losses based on total area are calculated based on the assumption that the entire surface area of the bar is corroding. However, since for the epoxy-coated bars corrosion is more likely to occur on the damaged area of the bar, it is useful to calculate the corrosion losses based on the assumption that only damaged area of the bar is corroding. Corrosion loss based on the exposed area at the holes, for bars with 10 penetrations through the epoxy on each bar, are 192 times the corrosion loss based on total bar area. Specimens containing 100% ordinary portland cement had the highest average corrosion loss based on exposed area, 20.1 µm; while specimens with supplementary cementitious materials exhibited no significant corrosion losses. (The negative corrosion losses are caused by minor differences in oxidation rate between

the single anode bar and the two cathode bars in the absence of corrosion on the top bar, and are not indicative of chloride-induced corrosion.)

Table 4.5: Corrosion loss (µm) for specimens containing epoxy-coated bars

Specimen	Week	Corrosion Loss (µm)-Total Area						Average	Std. Dev.
		1	2	3	4	5	6		
PC-ECR	96	0.085	0.144	0.039	0.030	0.145	0.184	0.104	0.063
FA-ECR(40)	96	-0.005	-0.002	-0.015	-0.013	-0.036	-0.024	0	0
SF-ECR(10)	96	-0.017	-0.026	-0.051	-0.023	-0.044	-0.023	0	0
Slag-ECR(40)	96	-0.002	-0.010	-0.005	-0.018	-0.006	-0.069	0	0
		Corrosion Loss (µm)-Exposed Area							
PC-ECR	96	16.4	27.6	7.5	5.7	27.9	35.3	20.1	12.0
FA-ECR(40)	96	-0.98	-0.31	-2.87	-2.45	-6.92	-4.56	0	0
SF-ECR(10)	96	-3.18	-5.04	-9.88	-4.50	-8.44	-4.39	0	0
Slag-ECR(40)	96	-0.31	-2.00	-1.04	-3.52	-1.18	-13.31	0	0

4.3.2 Linear Polarization Resistance (LPR) Test

4.3.2.1 Uncoated Reinforcement

Figure 4.31 and 4.32 compare the average corrosion rates obtained from LPR test results for specimens with uncoated conventional reinforcement. Corrosion rates obtained from LPR tests for individual specimens of each series are presented in Appendix H. As shown in Figure 4.31, specimens with 100% portland cement had the greatest average corrosion rate, 24 µm/yr, whereas specimens with supplementary cementitious materials (SCM) exhibited an average corrosion rate about one order of magnitude less than the specimens with only ordinary portland cement. Increasing the amount of SCM decreased the total corrosion rate, with the lowest total corrosion rates observed in specimens containing silica fume. As shown in Figure 4.32, among specimens with supplementary cementitious materials, FA(20) specimens had the maximum average corrosion rate, 7.34 µm/yr, followed by Slag(20) with 2.57 µm/yr, FA(40) with 1.78 µm/yr, and Slag(40), SF(5), and SF(10) close to 1 µm/yr.

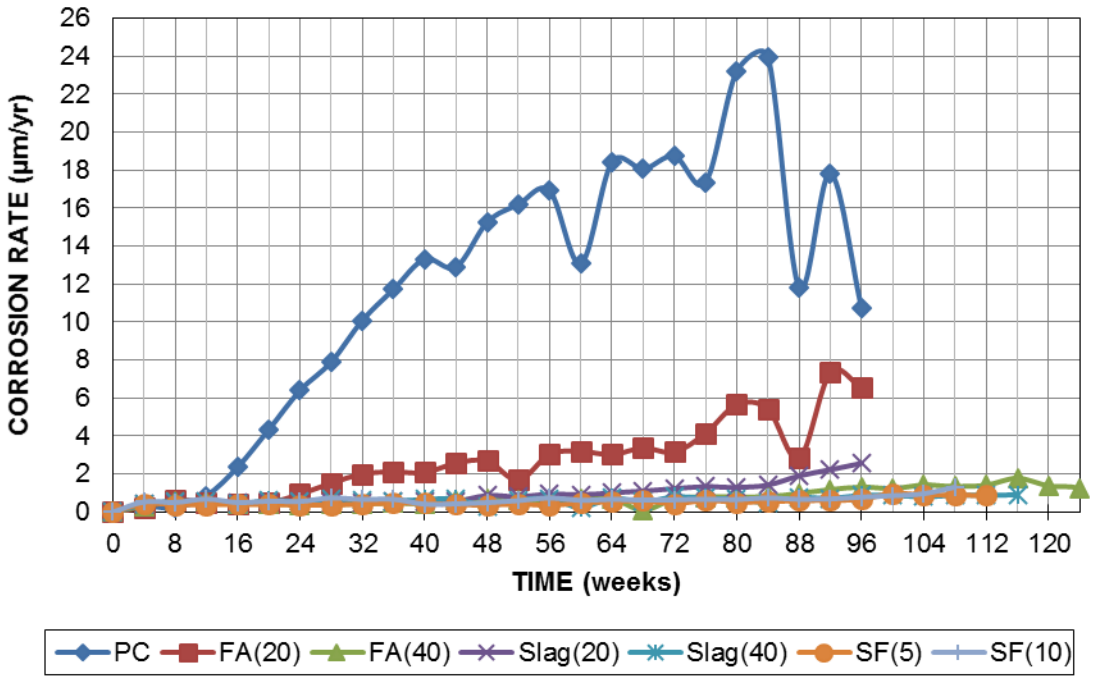

Figure 4.31— Average LPR test corrosion rates (µm/yr) for all specimens containing uncoated conventional reinforcement

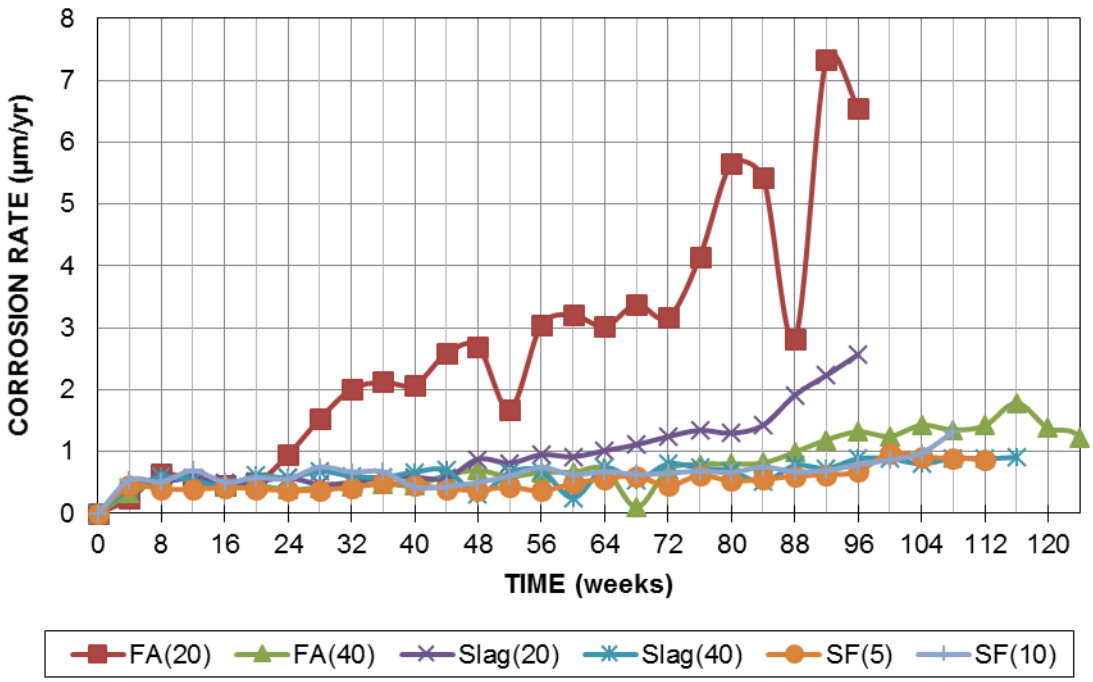

Figure 4.32— Average LPR corrosion rates (µm/yr) for specimens containing supplementary cementitious materials and uncoated conventional reinforcement

The individual and average total corrosion losses for all specimens containing uncoated conventional bars through week 96 are tabulated in Table 4.6. Total corrosion losses were obtained by integrating corrosion rates gained from LPR test results with respect to time. Generally, specimens with silica fume had the lowest total corrosion loss. Specimens with slag cement had a lower total corrosion loss than specimens with an equal percentage of fly ash; increasing the amount of SCM decreased the total corrosion loss. Specimens containing 100% ordinary portland cement had the highest average corrosion loss, 22.5 µm, followed by FA(20) specimens with a total corrosion loss of 5.05 µm, about a quarter of that for PC specimens. Specimens containing 40% fly ash, 40% slag, 5% silica fume, and 10% silica fume had average corrosion losses less than 2 µm, one order of magnitude less than that for specimens with 100% portland cement.

Table 4.6: Total corrosion loss (µm) for all specimens containing uncoated conventional bars based on LPR test results

Specimen	Week	Corrosion Loss (µm)-Total Area						Average	Std. Dev.
		1	2	3	4	5	6		
PC	96	16.8	25.0	25.7	24.4	22.7	20.2	22.5	3.42
FA(20)	96	4.09	5.54	3.76	5.21	3.39	8.33	5.05	1.81
FA(40)	96	1.05	1.22	1.66	0.97	0.86	1.16	1.15	0.28
SF(5)	96	0.888	1.00	0.848	0.846	0.791	0.896	0.878	0.071
SF(10)	96	0.998	1.90	0.827	1.09	1.08	1.05	1.16	0.376
Slag(20)	96	1.65	0.97	1.55	1.77	3.73	1.17	1.81	0.99
Slag(40)	96	0.784	1.01	1.64	1.16	1.25	0.934	1.13	0.301

4.3.2.2 Epoxy-coated Reinforcement (ECR)

Figure 4.33 compares the average corrosion rates obtained from LPR test results of the epoxy-coated reinforcement, based on their total area, in specimens containing 100% ordinary portland cement (PC-ECR), 40% fly ash (FA-ECR(40)), 10% silica fume (SF-ECR(10)), and 40% slag (Slag-ECR(40)). As shown in Figure 4.33, specimens with supplementary cementitious materials exhibited an average corrosion rate about one order of magnitude less than the specimens

with only ordinary portland cement. The maximum average corrosion rate of PC-ECR specimens was 0.54 µm/yr; for specimens with fly ash, silica fume and slag cement, the maximum average rate was 0.04, 0.03, and 0.05 µm/yr, respectively.

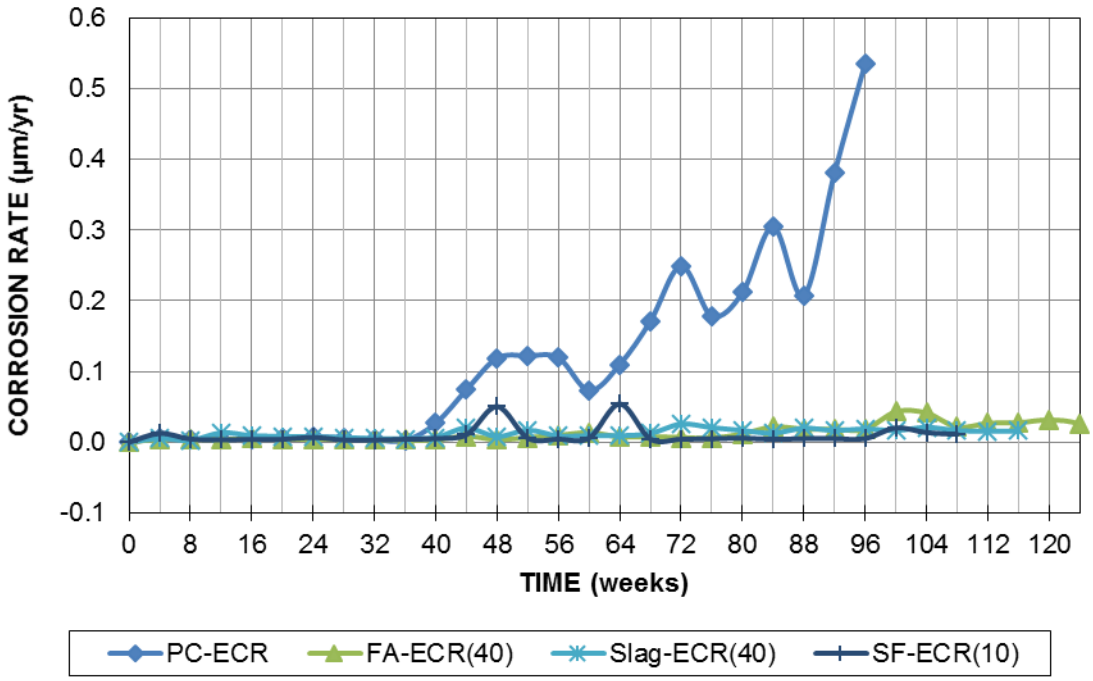

Figure 4.33— Average LPR test corrosion rates (µm/yr) based on total area of reinforcement for all specimens containing epoxy-coated reinforcement

The individual and average total corrosion losses through week 96 for the beam specimens containing epoxy-coated bars are tabulated in Table 4.7. Total corrosion losses were obtained by integrating corrosion rates gained from LPR test results with respect to time and are presented based on both total and exposed area of epoxy-coated bars. Specimens containing 100% ordinary portland cement had the highest average corrosion loss based on exposed area, 43.2 µm, while specimens with supplementary cementitious materials exhibited total corrosion losses one order of magnitude less: 2.95 µm for FA-ECR(40), 3.25 µm for SF-ECR(10), and 4.22 µm for Slag-ECR(40) specimens.

Table 4.7: Total corrosion loss (μm) for specimens containing epoxy-coated bars

Specimen	Week	Corrosion Loss (μm)-Total Area						Average	Std. Dev.
		1	2	3	4	5	6		
PC-ECR	96	0.207	0.285	0.183	0.221	0.277	0.178	0.225	0.046
FA-ECR(40)	96	0.026	0.015	0.010	0.014	0.013	0.013	0.015	0.005
SF-ECR(10)	96	0.014	0.013	0.021	0.026	0.016	0.010	0.017	0.006
Slag-ECR(40)	96	0.026	0.044	0.012	0.010	0.031	0.010	0.022	0.014
		Corrosion Loss (μm)-Exposed Area							
PC-ECR	96	39.7	54.6	35.1	42.5	53.3	34.2	43.2	8.80
FA-ECR(40)	96	4.98	2.82	2.00	2.73	2.58	2.59	2.95	1.04
SF-ECR(10)	96	2.75	2.56	4.09	5.06	3.16	1.90	3.25	1.15
Slag-ECR(40)	96	4.90	8.44	2.25	1.84	5.98	1.90	4.22	2.69

4.3.3 Critical Chloride Threshold

All specimens were sampled for measuring critical chloride threshold at corrosion initiation; three out of six specimens from each mixture were also sampled at 96 weeks to provide a comparison of chloride ingress over time. Some specimens exhibited corrosion initiation more than once; for these specimens ten samples were drilled upon the first initiation, and six samples thereafter. The critical chloride concentration upon corrosion initiation and chloride content at week 96 of beam specimens containing 100% portland cement with bare and epoxy-coated conventional bars are shown in Tables 4.8 and 4.9, respectively. For bare bars, specimens exhibited individual average critical chloride thresholds ranging from 0.70 to 2.50 lb/yd^3 (0.41 to 1.48 kg/m^3) with an average of 1.46 lb/yd^3 (0.86 kg/m^3). For Specimen PC-5 at corrosion initiation and PC-6 at week 96, one of the measured chloride contents (5.8 lb/yd^3 (3.43 kg/m^3) and 35.5 lb/yd^3 (21.0 kg/m^3), respectively) was more than two standard deviation far from the mean and was discarded as an outlier. The average time to corrosion initiation for PC specimens was 15.8 weeks.

Table 4.8: Critical chloride threshold for specimens containing 100% portland cement with uncoated bars

Specimen	Chloride Content (lb/yd^3)[a]										Avg.	Std. Dev.
	1	**2**	**3**	**4**	**5**	**6**	**7**	**8**	**9**	**10**		
PC-1	-	-	-	-	-	-	-	-	-	-	-	-
PC-2	0.48	1.50	4.64	0.48	0.41	0.70	0.46	0.73	0.34	0.88	1.06	1.3
PC-3	1.50	0.96	3.65	2.57	2.62	0.26	2.38	3.47	-	-	2.18	1.19
PC-4	1.09	0.19	0.40	2.96	0.22	0.27	-	-	-	-	0.86	1.08
PC-5	4.87	2.09	2.29	1.12	2.28	2.71	3.49	5.8[b]	2.08	1.55	2.50	1.11
PC-6	0.27	0.37	0.58	0.37	0.70	2.55	0.35	0.56	0.98	0.25	0.70	0.69
											1.46	**1.07**
	Chloride Content (lb/yd^3)[a] at week 96											
PC-1	35.5[b]	17.0	21.29	21.2	16.5	17.9	-	-	-	-	18.8	2.30
PC-4	29.7	23.1	24.4	19.3	24.9	18.7	-	-	-	-	23.3	4.06
PC-6	17.2	25.1	17.4	22.4	27.2	17.2	-	-	-	-	21.1	4.44
											21.1	**3.6**

[a]1 (lb/yd^3) = 0.592 (kg/m^3)
[b]Outlier; excluded from analysis

For epoxy-coated bars, specimens showed individual critical chloride thresholds ranging from 5.44 to 8.48 lb/yd^3 (3.22 to 5.02 kg/m^3) with an average of 7.05 lb/yd^3 (4.17 kg/m^3). The average time to corrosion initiation for PC-ECR specimens was 40 weeks. For Specimen PC-ECR-3, one of the measured chloride contents, 13.4 lb/yd^3 (7.93 kg/m^3), was more than two standard deviation far from the mean and excluded from the average as an outlier.

Table 4.9: Critical chloride threshold for specimens containing 100% portland cement with epoxy-coated bars

Specimen	Chloride Content (lb/yd^3)[a]										Avg.	Std. Dev.
	1	**2**	**3**	**4**	**5**	**6**	**7**	**8**	**9**	**10**		
PC-ECR-1	8.00	5.34	10.7	9.95	7.24	10.6	10.0	7.62	9.59	5.78	8.48	1.96
PC-ECR-2	8.31	5.98	7.09	6.56	6.05	-	7.10	10.9	10.25	9.17	7.93	1.82
PC-ECR-3	8.85	5.78	5.40	6.40	7.37	13.4[b]	8.50	6.50	9.64	9.16	7.51	1.57
PC-ECR-4	4.94	7.78	6.05	4.12	3.14	4.36	8.92	3.57	4.68	10.0	5.76	2.37
PC-ECR-5	6.26	9.46	9.93	6.62	6.79	4.11	-	-	-	-	7.20	2.17
PC-ECR-6	7.13	3.72	4.36	3.98	6.13	6.76	5.23	8.51	4.14	4.40	5.44	1.62
	Chloride Content (lb/yd^3)[a] at week 96										**7.05**	**1.92**
PC-ECR-1	21.0	15.4	21.0	16.9	14.0	18.9	-	-	-	-	17.8	2.91
PC-ECR-3	18.3	24.7	15.1	17.9	21.8	23.9	-	-	-	-	20.3	3.80
PC-ECR-6	13.3	9.13	8.81	7.48	14.9	12.4	-	-	-	-	11.0	2.94
											16.4	**3.2**

[a]1 (lb/yd^3) = 0.592 (kg/m^3)
[b]Outlier; excluded from analysis

The measured chloride content upon corrosion initiation and at week 96 versus time for specimens containing 100% portland cement with bare and coated reinforcement are shown in Figure 4.34. The chloride content rate (slope of trend line) at the bar level for specimens with bare bars 0.2149 (lb/yd^3)/week was slightly higher than that for specimens with coated bars (0.1713 (lb/yd^3)/week). Rate of chloride concentration at the bar level of specimens is proportional to the chloride ingress rate; that is, higher chloride ingress rate results in higher chloride content rate a certain level of concrete.

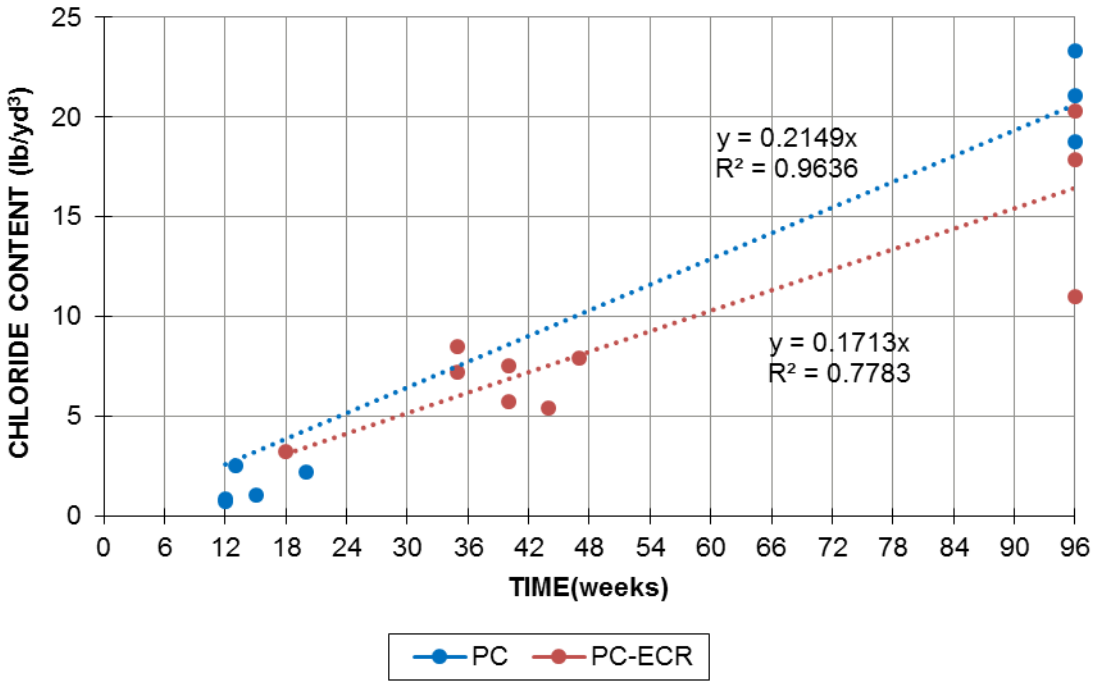

Figure 4.34—Water soluble chloride content versus time for specimens containing 100% portland cement and ECR

The critical chloride thresholds for specimens containing 40% fly ash with bare and epoxy-coated bars are tabulated in Table 4.10 and 4.11, respectively. For FA(40) specimens, four out of six specimens repassivated after initial initiation. The average time to final corrosion initiation (after which reinforcement did not repassivate) was 80 weeks. Table 4.10 shows two critical chloride corrosion thresholds (CCCT) for FA(40) specimens; the initial CCCT was 1.53 lb/yd^3 (0.91 kg/m^3) and the final critical chloride threshold was 2.70 lb/yd^3 (1.60 kg/m^3). For specimens with epoxy-coated bars (FA-ECR(40)), the final critical chloride threshold obtained (to date) was 3.47 lb/yd^3 (2.05 kg/m^3).

Table 4.10: Critical chloride threshold for specimens containing 40% fly ash with uncoated bars

Specimen	Chloride Content (lb/yd^3)[a]-First initiation										Avg.	Std. Dev.
	1	2	3	4	5	6	7	8	9	10		
FA(40)-1	0.36	0.43	3.41	1.49	0.84	2.78	0.92	0.69	3.87	0.76	1.56	1.30
FA(40)-3	0.56	1.35	1.36	0.74	2.08	0.70	-	-	-	-	1.13	0.58
FA(40)-4	1.51	3.75	1.35	1.50	2.21	0.83	1.43	1.51	6.64[b]	0.62	1.63	0.91
FA(40)-6	1.74	2.44	0.43	1.75	1.77	1.03	3.77	1.01	0.85	3.21	1.80	1.07
											1.53	**0.97**
	Chloride Content (lb/yd^3)[a]-Final initiation											
FA(40)-1	0.93	1.99	3.29	1.83	0.66	1.27	-	-	-	-	1.66	0.94
FA(40)-2	0.52	1.32	0.76	0.58	1.73	2.04	0.55	2.12	0.68	0.43	1.07	0.67
FA(40)-3	4.90	8.44	2.25	1.84	5.98	1.90	-	-	-	-	2.17	1.10
FA(40)-4	4.78	4.11	0.90	3.15	0.80	6.29	-	-	-	-	3.34	2.18
FA(40)-5	0.91	0.59	0.60	1.84	1.56	6.39	2.45	4.95	2.77	8.36	3.04	2.66
FA(40)-6	5.48	5.20	6.44	5.58	1.83	-	-	-	-	-	4.91	1.78
											2.70	**1.56**

[a]1 (lb/yd^3) = 0.592 (kg/m^3)
[b]Outlier; excluded from analysis

Table 4.11: Critical chloride threshold for specimens containing 40% fly ash with epoxy-coated bars

Specimen	Chloride Content (lb/yd^3)[a]-First initiation										Avg.	Std. Dev.
	1	2	3	4	5	6	7	8	9	10		
FA-ECR(40)-2	4.08	1.13	0.58	1.39	1.89	3.79	2.10	2.35	0.68	3.74	2.17	1.30
	Chloride Content (lb/yd^3)[a]-Final initiation											
FA-ECR(40)-1	2.66	7.68	7.09	7.90	1.42	1.59	1.67	-	3.82	4.94	4.31	2.69
FA-ECR(40)-2	2.15	5.07	4.78	1.99	1.04	1.97	-	-	-	-	2.83	1.67
FA-ECR(40)-3	2.74	2.61	2.80	1.94	4.71	2.04	1.51	3.63	0.38	0.53	2.29	1.32
FA-ECR(40)-4	5.19	2.72	2.75	2.73	4.84	2.13	0.67	1.77	3.40	5.07	3.13	1.50
FA-ECR(40)-5	-	-	-	-	-	-	-	-	-	-	-	-
FA-ECR(40)-6	5.69	2.36	6.61	2.90	5.58	5.66	-	-	-	-	4.80	1.73
											3.47	**1.78**

[a]1 (lb/yd^3) = 0.592 (kg/m^3)

The measured chloride content versus time for specimens containing 40% fly ash is shown in Figure 4.35. The slope of trend lines for bare and epoxy-coated bars, 0.0392 and 0.0308 (lb/yd^3)/week, respectively, show similar chloride content rates at bar level, or in other words, similar chloride ingress rates for both series, as expected.

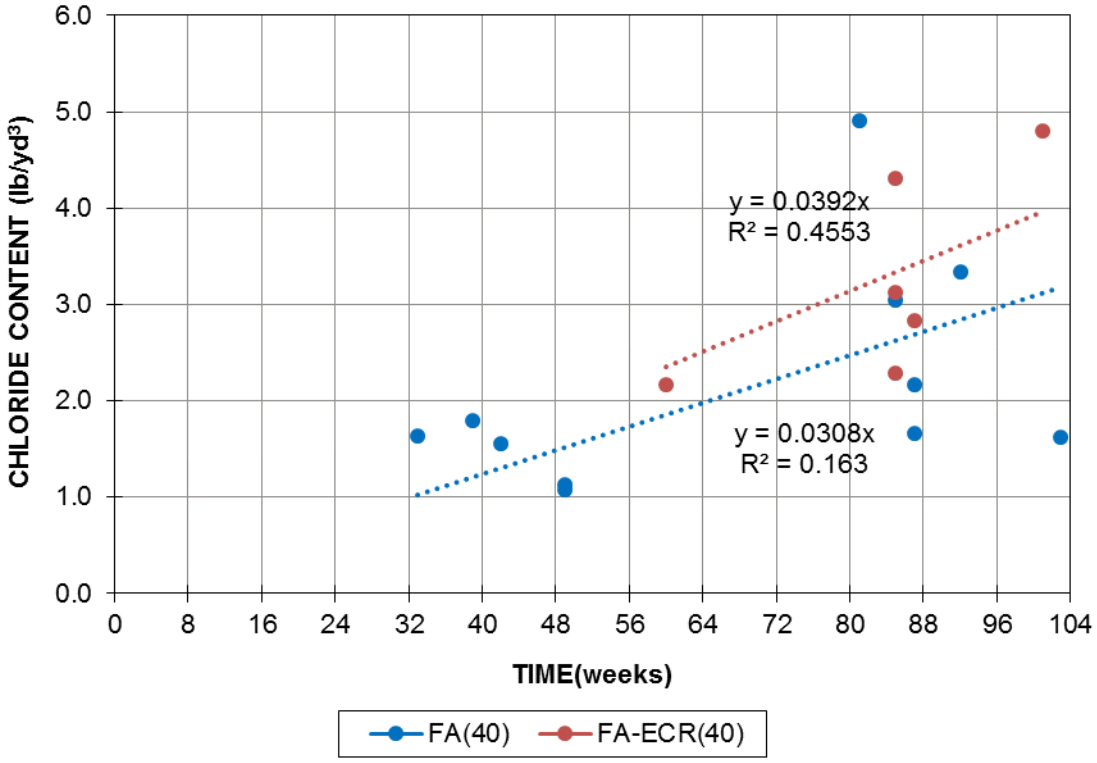

Figure 4.35—Water soluble chloride content versus time for specimens containing 40% fly ash

For specimens containing 5% silica fume, as of week 101, Specimens SF(5)-1, 2, and 3 initiated corrosion at weeks 97, 82, and 97, respectively. Three specimens were also sampled at week 96 to obtain a lower bound for the critical chloride threshold. Table 4.12 shows the individual and average critical chloride threshold for SF(5)-1, 2, and 3, along with the chloride content of Specimens SF(5)-4, 5, and 6 at week 96. The obtained average chloride content for Specimens SF(5)-4, 5, and 6 at week 96, 1.59 lb/yd^3 (0.94 kg/m^3), was below the CCCT value for Specimens SF(5)-1, 2, and 3 at initiation (1.86 lb/yd^3 (1.10 kg/m^3)).

Table 4.12: Critical chloride threshold for specimens containing 5% silica fume with uncoated bars

Specimen	Chloride Content (lb/yd^3)[a]-First initiation										Avg.	Std. Dev.
	1	2	3	4	5	6	7	8	9	10		
SF(5)-1	0.46	0.71	0.66	1.79	0.61	1.02	1.43	0.56	0.78	3.93[b]	0.89	0.45
SF(5)-2	3.21	1.00	3.14	3.67	1.20	1.95	4.15	0.61	0.87	0.89	2.07	1.34
SF(5)-3	1.80	1.83	2.27	1.57	4.63	1.48	4.50	2.80	2.59	5.69[b]	2.61	1.19
	Chloride Content (lb/yd^3)[a] at week 96										**1.86**	**0.99**
SF(5)-4	3.15	0.63	0.78	1.50	1.11	0.95	-	-	-	-	1.35	0.93
SF(5)-5	1.59	1.29	2.05	5.11[b]	1.37	3.12	-	-	-	-	1.88	0.75
SF(5)-6	1.11	2.06	1.10	1.98	2.40	0.45	-	-	-	-	1.52	0.74
											1.59	**0.81**

[a]1 (lb/yd^3) = 0.592 (kg/m^3)
[b]Outlier; excluded from analysis

The measured chloride content versus time for specimens containing 5% silica fume is shown in Figure 4.36. The chloride content rate (slope of trend line) at the bar level for these specimens is 0.0182 (lb/yd^3)/week.

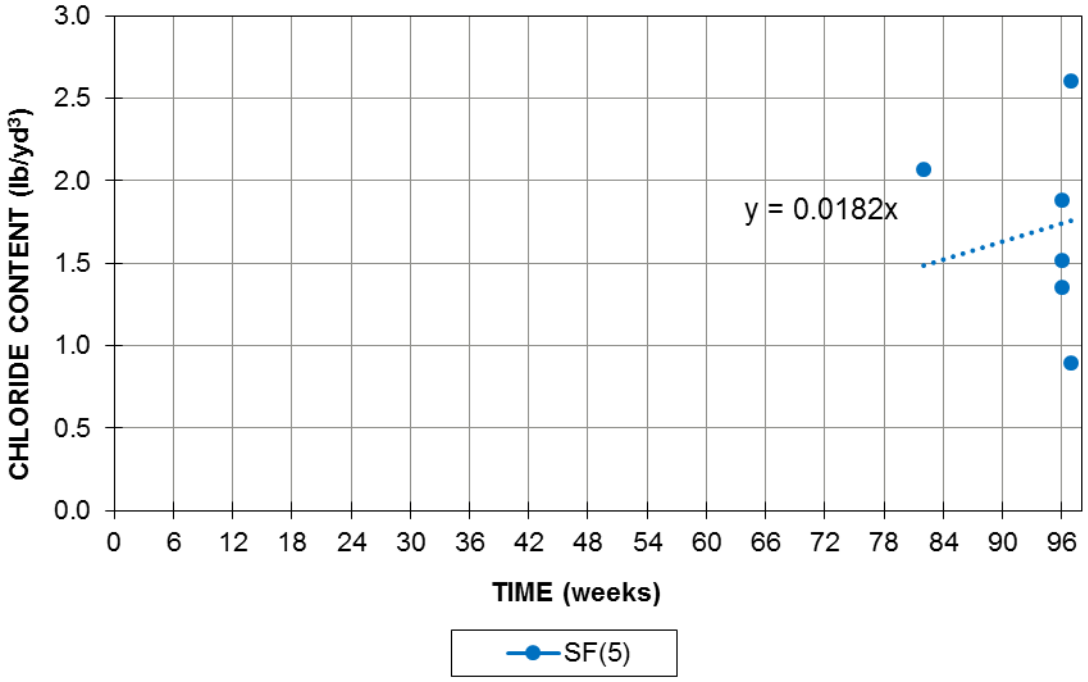

Figure 4.36—Water soluble chloride content versus time for specimens containing 5% silica fume

The critical chloride thresholds for specimens containing 10% silica fume with bare and epoxy-coated bars are tabulated in Tables 4.13 and 4.14, respectively. For specimens containing bare bars, as of week 110, only Specimen SF(10)-2 initiated corrosion; however, this specimen later repassivated and re-initiated thereafter. In addition to this specimen, Specimens SF(10)-1, 3, and 5 were sampled at week 96 to establish a lower bound for the critical chloride threshold. Table 4.13 shows the initial and final individual and average critical chloride threshold for SF(10)-2 as well as the chloride content of Specimens SF(10)-1, 3, and 5 at week 96. For Specimens 2 and 3, one of the measured chloride contents (11.0 lb/yd^3 (6.51 kg/m^3) and 4.29 lb/yd^3 (2.54 kg/m^3), respectively) was more than two standard deviation far from the mean and discarded as an outlier. For specimens containing epoxy-coated bars as of week 110, only Specimen SF-ECR(10)-3 initiated corrosion (at week 41), repassivated and re-initiated (at week 97) thereafter. Table 4.14 shows the initial and final critical chloride threshold for SF-ECR(10)-3 along with chloride contents of Specimens SF-ECR(10)-2, 4, and 6 at week 96 of the test. The obtained average chloride content for specimens containing bare and coated bars at week 96 (1.50 lb/yd^3 (0.89 kg/m^3) and 1.82 lb/yd^3 (1.08 kg/m^3), respectively) was below the CCCT values for these specimens (1.59 lb/yd^3 (0.94 kg/m^3) and 2.68 lb/yd^3 (1.59 kg/m^3), respectively) upon initiation.

Table 4.13: Critical chloride threshold for specimens containing 10% silica fume with uncoated bars

Specimen	**Chloride Content (lb/yd^3)[a]-First initiation**										**Avg.**	**Std. Dev.**
	1	**2**	**3**	**4**	**5**	**6**	**7**	**8**	**9**	**10**		
SF(10)-2	0.53	0.29	0.34	0.81	0.42	0.48	1.25	0.65	0.27	0.32	0.54	0.30
	Chloride Content (lb/yd^3)[a]-Final initiation											
SF(10)-2	1.06	3.82	2.18	11.0[b]	0.37	0.53	-	-	-	-	1.59	1.43
	Chloride Content (lb/yd^3)[a] at week 96											
SF(10)-1	1.38	0.81	2.24	0.47	1.04	0.50	-	-	-	-	1.07	0.67
SF(10)-3	2.36	1.59	3.25	2.58	0.96	4.29[b]	-	-	-	-	2.15	0.89
SF(10)-5	0.61	1.18	0.71	3.21	1.24	0.67	-	-	-	-	1.27	0.99
											1.50	**0.85**

[a]1 (lb/yd^3) = 0.592 (kg/m^3)
[b]Outlier; excluded from analysis

Table 4.14: Critical chloride threshold for specimens containing 10% silica fume with epoxy-coated bars

Specimen	Chloride Content (lb/yd^3)[a]-First initiation										Avg.	Std. Dev.
	1	2	3	4	5	6	7	8	9	10		
SF-ECR(10)-3	5.83	3.66	0.40	0.32	1.08	0.38	-	-	-	-	1.94	2.29
	Chloride Content (lb/yd^3)[a]-Final initiation											
SF-ECR(10)-3	3.18	2.18	2.23	0.56	4.21	3.71	-	-	-	-	2.68	1.31
	Chloride Content (lb/yd^3)[a] at week 96											
SF-ECR(10)-2	22.5[b]	2.93	0.67	4.11	0.97	5.03	-	-	-	-	2.74	1.91
SF-ECR(10)-4	1.16	1.62	0.41	0.61	4.09	4.53	-	-	-	-	2.07	1.79
SF-ECR(10)-6	0.78	4.08[b]	0.72	1.04	0.30	0.43	-	-	-	-	0.66	0.29
											1.82	**1.33**

[a]1 (lb/yd^3) = 0.592 (kg/m^3)

The measured chloride content versus time for specimens containing 10% silica fume is shown in Figure 4.37. The slope of the trend lines for bare and epoxy-coated bars, 0.0168 and 0.0223 (lb/yd^3)/week, respectively, show similar chloride concentration rates at the top bar level, or in other words, similar chloride ingress rates for both series, as expected. Chloride content rates for specimens containing 10% silica fume are one order of magnitude less than those for specimens with 100% portland cement.

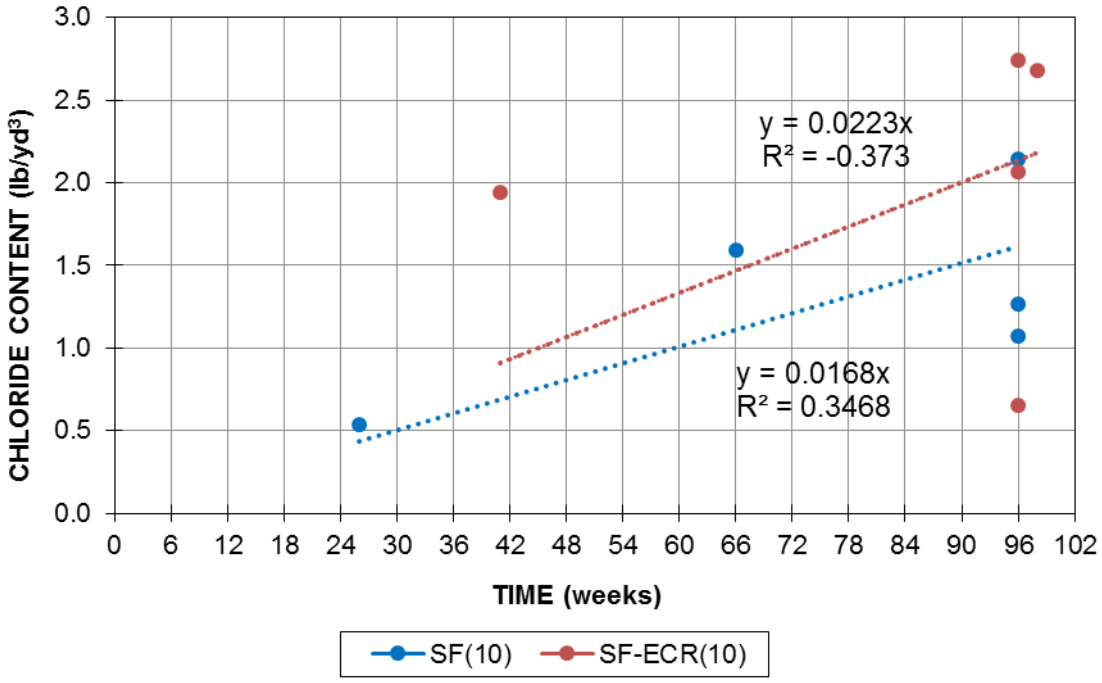

Figure 4.37—Water soluble chloride content versus time for specimens containing 10% silica fume

The critical chloride thresholds for specimens containing 20% slag cement with uncoated conventional bars are tabulated in Table 4.15. Three out of six specimens repassivated after initial initiation. The average time to final corrosion initiation (after which reinforcement did not repassivate) was 67.7 weeks. Table 4.13 shows two critical chloride corrosion thresholds (CCCT) for Slag(20) specimens; the initial CCCT was 1.72 lb/yd^3 (1.02 kg/m^3) and the final critical chloride threshold was 4.51 lb/yd^3 (2.67 kg/m^3). The average chloride content at week 96 was 6.73 lb/yd^3 (3.98 kg/m^3).

Table 4.15: Critical chloride threshold for specimens containing 20% slag cement with uncoated bars

Specimen	Chloride Content (lb/yd^3)[a]-First initiation										Avg.	Std. Dev.
	1	2	3	4	5	6	7	8	9	10		
Slag(20)-3	2.85	0.86	0.79	2.43	1.22	4.50	4.56	3.22	1.81	1.34	2.36	1.40
Slag(20)-4	4.87	2.07	3.17	0.97	2.72	1.67	0.72	0.80	0.61	1.79	1.94	1.35
Slag(20)-5	0.86	1.98	0.66	0.60	0.78	0.65	0.72	0.76	0.59	0.97	0.86	0.41
											1.72	**1.06**
	Chloride Content (lb/yd^3)[a]-Final initiation											
Slag(20)-1	5.46	1.96	2.34	1.93	0.99	-	-	-	-	-	2.53	1.71
Slag(20)-2	5.30	2.00	4.77	5.15	0.64	10.8	3.94	7.45	3.13	4.11	4.73	2.84
Slag(20)-3	4.40	2.55	5.28	2.75	4.37	2.77	-	-	-	-	3.69	1.14
Slag(20)-4	3.96	6.01	7.17	2.67	13.57	23.4[b]	-	-	-	-	6.68	4.23
Slag(20)-5	4.99	2.37	2.97	0.88	4.35	4.96	8.80	3.27	7.18	3.99	4.38	2.30
Slag(20)-6	9.16	2.82	3.03	1.61	5.90	17.4[b]	11.7	5.66	2.49	3.03	5.05	3.44
											4.51	**2.61**
	Chloride Content (lb/yd^3)[a] at week 96											
Slag(20)-1	3.46	15.41	9.42	9.22	9.83	9.31	-	-	-	-	9.44	3.79
Slag(20)-2	5.74	4.78	10.52	1.19	2.69	6.24	-	-	-	-	5.20	3.23
Slag(20)-6	4.79	6.14	9.99	2.56	2.74	7.13	-	-	-	-	5.56	2.82
											6.73	**3.28**

[a]1 (lb/yd^3) = 0.592 (kg/m^3)
[b]Outlier; excluded from analysis

Figure 4.38 shows the measured chloride contents versus time for Slag(20) specimens. The chloride content rate at the top bar level for specimens with 20% slag cement followed an approximately a linear trend line with an average rate of 0.0679 (lb/yd^3)/week.

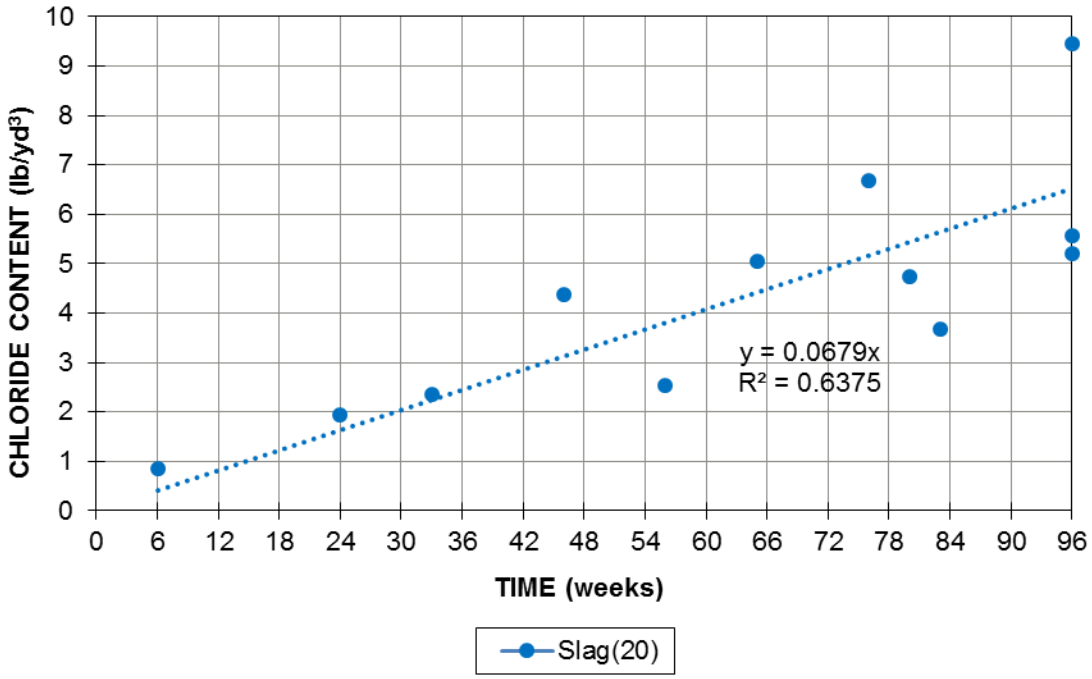

Figure 4.38—Water soluble chloride content versus time for specimens containing 20% slag cement with uncoated conventional steel

The critical chloride thresholds for specimens containing 40% slag cement with uncoated and coated conventional bars are tabulated in Tables 4.16 and 4.17, respectively. For uncoated reinforcement, as of week 118, three specimens had not initiated corrosion, and two specimens repassivated after the initial initiation. Table 4.16 shows two critical chloride corrosion thresholds (CCCT) for Slag(40) specimens; the initial CCCT was 1.89 lb/yd^3 (1.12 kg/m^3) and the final critical chloride threshold was 2.88 lb/yd^3 (1.70 kg/m^3). The final CCCT value will change upon initiation of the remaining specimens, but will likely would be higher than the initial CCCT values. The chloride content of Specimen Slag(40)-3 was measured at week 96 (3.97 lb/yd^3 (2.35 kg/m^3)). For specimens with epoxy-coated bars, two out of six specimens have not initiated corrosion to date (week 118), and three specimens repassivated after initial initiation. The final critical chloride threshold obtained to date for specimens containing 40% slag cement with epoxy-coated bars was 2.22 lb/yd^3 (1.31 kg/m^3).

Table 4.16: Critical chloride threshold for specimens containing 40% slag cement with uncoated bars

Specimen	Chloride Content (lb/yd^3)[a]-First initiation										Avg.	Std. Dev.
	1	2	3	4	5	6	7	8	9	10		
Slag(40)-3	2.85	0.86	0.79	2.43	1.22	4.50	4.56	3.22	1.81	1.34	2.36	1.40
Slag(40)-5	0.86	1.98	0.66	0.60	0.78	0.65	0.72	0.76	0.59	0.97	0.86	0.41
	Chloride Content (lb/yd^3)[a]-Final initiation										**1.89**	**1.11**
Slag(40)-1	-	-	-	-	-	-	-	-	-	-	-	-
Slag(40)-2	0.76	5.68	3.26	3.03	2.35	1.63	1.22	5.79	0.86	1.03	2.56	1.89
Slag(40)-3	1.10	3.70	3.14	3.85	4.68	1.14	-	-	-	-	2.94	1.49
Slag(40)-4	-	-	-	-	-	-	-	-	-	-	-	-
Slag(40)-5	9.46	1.40	1.46	4.36	0.77	1.51	-	-	-	-	3.16	3.34
Slag(40)-6	-	-	-	-	-	-	-	-	-	-	-	-
	Chloride Content (lb/yd^3)[a] at week 96										**2.88**	**2.24**
Slag(40)-3	1.25	5.30	5.32	5.48	5.32	1.18	-	-	-	-	3.97	2.14

[a]1 (lb/yd^3) = 0.592 (kg/m^3)
[b]Outlier; excluded from analysis

Table 4.17: Critical chloride threshold for specimens containing 40% slag cement with epoxy-coated bars

Specimen	Chloride Content (lb/yd^3)[a]-First initiation										Avg.	Std. Dev.
	1	2	3	4	5	6	7	8	9	10		
Slag-ECR(40)-1	0.72	0.87	0.88	0.84	1.03	0.95	3.50	1.20	2.54	1.56	1.41	0.91
Slag-ECR(40)-2	2.46	2.14	2.20	1.77	1.96	2.35	1.94	2.22	1.98	2.00	2.10	0.21
Slag-ECR(40)-5[c]	3.79	1.02	0.84	0.93	0.68	0.69	0.62	0.75	2.01	0.82	1.21	0.99
Slag-ECR(40)-5[c]	1.01	1.13	0.88	0.99	0.63	3.07	-	-	-	-	1.29	0.89
	Chloride Content (lb/yd^3)[a]-Final initiation										**1.50**	**0.75**
Slag-ECR(40)-1	1.55	2.89	1.33	0.62	0.77	0.61	-	-	-	-	1.30	0.87
Slag-ECR(40)-2	0.75	1.05	0.95	0.76	3.82	5.17	-	-	-	-	2.08	1.92
Slag-ECR(40)-3	2.68	2.70	2.36	3.39	3.07	1.77	9.9[b]	4.27	3.35	2.77	2.93	0.71
Slag-ECR(40)-4	-	-	-	-	-	-	-	-	-	-	-	-
Slag-ECR(40)-5[c]	0.39	0.38	0.79	9.27	2.06	-	-	-	-	-	2.58	3.80
Slag-ECR(40)-6	-		-	-	-	-	-	-	-	-	-	-
											2.22	**1.83**

[a]1 (lb/yd^3) = 0.592 (kg/m^3)
[b]Outlier; excluded from analysis
[c]Specimen #5 sampled three times at weeks 40, 47 and 70

Figure 4.39 shows the measured chloride content values versus time for specimens containing 40% slag cement. The chloride content rates at the top bar level for specimens with bare and epoxy-coated bars, 0.0386 and 0.0319 (lb/yd^3)/week, respectively, indicate similar chloride ingress rates for both series, as expected.

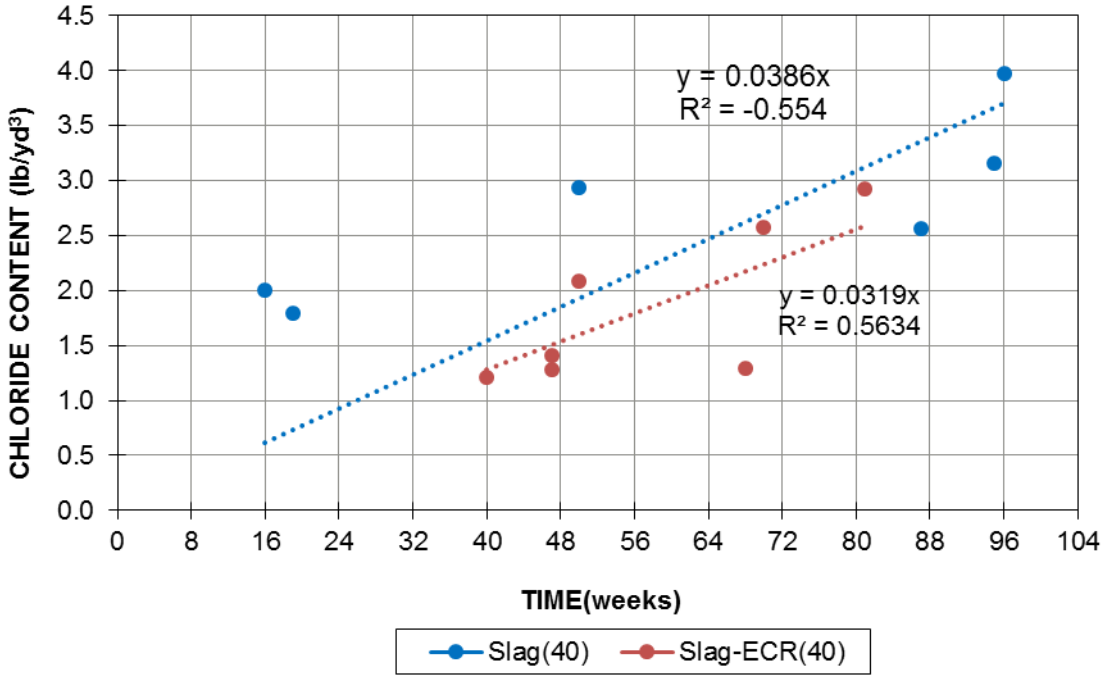

Figure 4.39—Water soluble chloride content versus time for specimens containing 40% slag cement

4.4 DISCUSSION

The macrocell corrosion losses and total corrosion losses after 96 weeks for all specimens are tabulated in Table 4.18. For specimens containing epoxy-coated reinforcement corrosion losses are presented based on both total and exposed area of bars.

Table 4.18: Macrocell and total corrosion losses based on total and exposed area of reinforcement

Specimen	Macrocell loss (μm)		Total loss (μm)	
	Total area	Exposed area	Total area	Exposed area
PC	19.7	-	22.5	-
FA(20)	3.17	-	5.05	-
FA(40)	0.445	-	1.15	-
SF(5)	0.107	-	0.878	-
SF(10)	0.233	-	1.16	-
Slag(20)	0.786	-	1.81	-
Slag(40)	0.232	-	1.13	-
PC-ECR	0.104	20.1	0.225	43.2
FA-ECR(40)	0	0	0.015	2.95
SF-ECR(10)	0	0	0.017	3.25
Slag-ECR(40)	0	0	0.022	4.22

Figure 4.40 compares the total corrosion loss after 96 weeks for specimens containing uncoated reinforcement and Figures 4.41 and 4.42 show total corrosion losses based on total area and exposed area of bars, respectively, for epoxy-coated reinforcement. For specimens containing uncoated bars, specimens with silica fume had the lowest total corrosion loss and specimens with only ordinary portland cement had the highest. Specimens with slag cement had lower corrosion losses than fly ash, and increasing the amount of SCM decreased the total corrosion loss. The difference between corrosion loss of SF(5) and SF(10) specimens was negligible since for each set only one out of six specimens initiated through week 96. For specimens with epoxy-coated reinforcement (Figures 4.41 and 4.42), specimens containing 40% fly ash, 40% slag, and 10% silica fume showed corrosion loss about one-tenth of that for specimens containing 100% portland cement. A comparison between Figures 4.40 and 4.41 shows that the use of epoxy-coated

reinforcement lowered the total corrosion loss as of two orders of magnitude in specimens with 100% ordinary portland cement. Specimens with supplementary cementitious materials and epoxy-coated reinforcement, however, showed the total corrosion loss as of three orders of magnitude less than specimens with uncoated conventional bars and 100% ordinary portland cement. These results show that use of a combination of ECR and supplementary cementitious materials in concrete significantly improves its performance against corrosion.

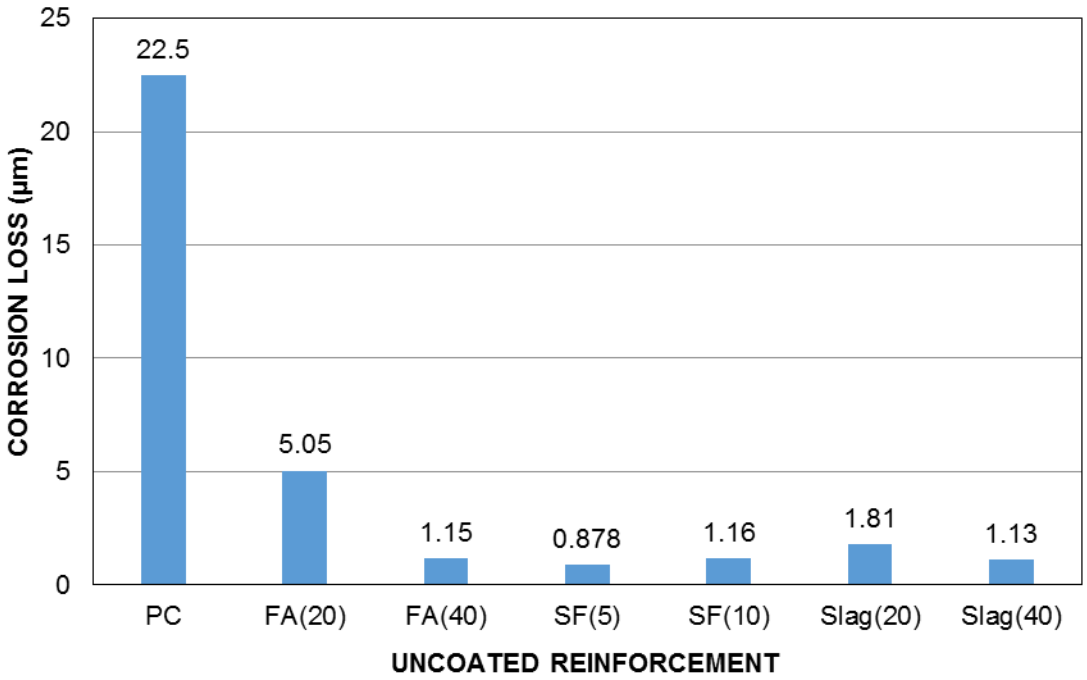

Figure 4.40—Comparison of total corrosion loss (based on LPR results) for specimens containing uncoated conventional reinforcement

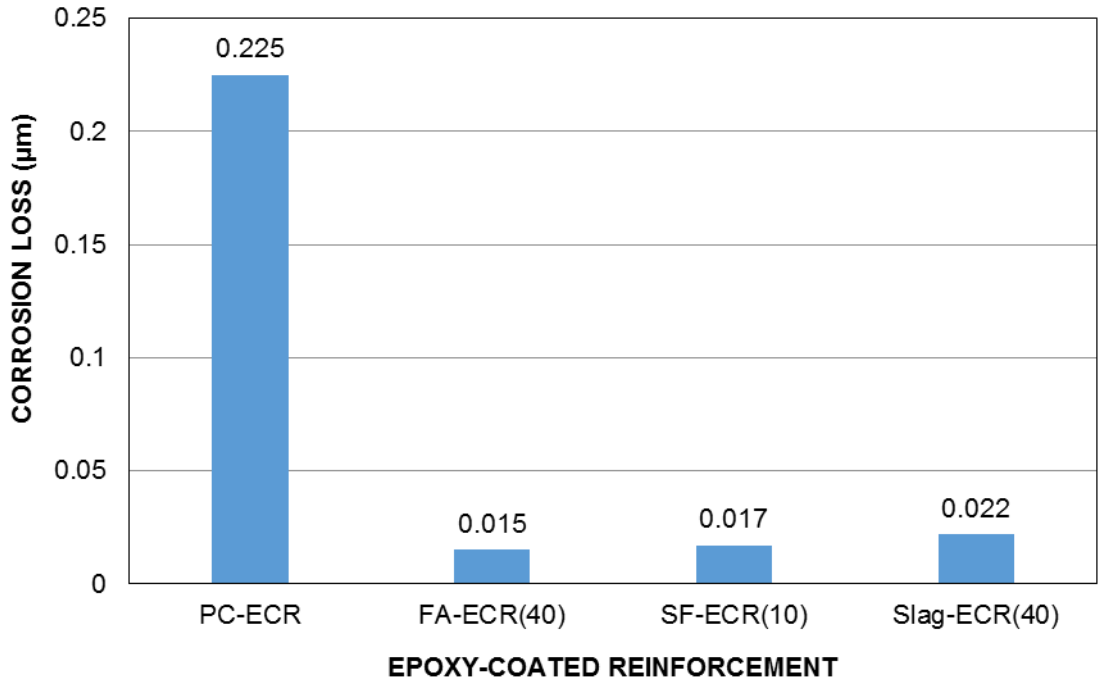

Figure 4.41—Comparison of total corrosion loss (based on LPR results) for specimens containing epoxy-coated reinforcement based on total area of bars

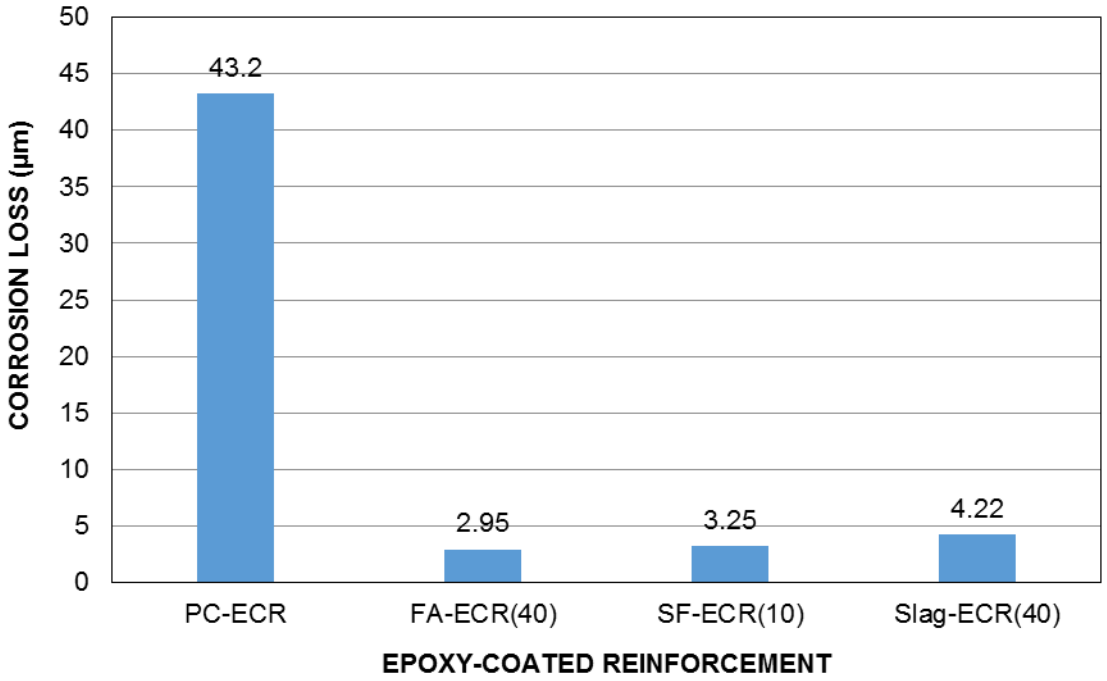

Figure 4.42—Comparison of total corrosion loss (based on LPR results) for specimens containing epoxy-coated reinforcement based on exposed area of bars

Most specimens containing 40% fly ash, 20% slag, and 40% slag showed corrosion initiation at least twice; that is, after a few weeks of initiation, specimens entered the passive state and again re-initiated after several weeks. This phenomenon also occurred for the only specimen out of six specimens containing 10% silica fume that initiated to date (week 98). This initiation and repassivation of specimens containing supplementary cementitious materials can be due to the fact that pozzolans react with the hydroxide ions (OH^-), leading to local pH drops in the vicinity of the bar which can initiate corrosion. However, this local pH reduction could be resisted by the buffering capacity of hydration products in the paste, which could explain why specimens containing supplementary cementitious materials re-enter the passive state after several weeks of corrosion. Repassivation of steel after corrosion initiation in specimens containing supplementary cementitious materials were observed in the literature (Angst et al. 2011, Presuel-Moreno and Moreno 2016). In a study by Angst et al. (2011) the initiation stage of chloride induced corrosion and CCCT value of several concrete mixes including mixes containing ordinary portland cement and sulfate resistant cement as well as these binders in combination with fly ash were evaluated. Specimens were exposed to chloride solutions during wetting/drying cycles and monitored with measuring potentials, electrical resistances and LPR test. Corrosion potentials for different specimens showed three different cases corresponding to corrosion initiation: specimens with sudden drop in corrosion potential, specimens with slow potential decrease, and specimens with several depassivation and repassivation. Angst et al. (2011) claimed that for specimens with depassivation-repassivation cases, chloride concentration at corrosion initiation can be sufficiently high to initiate pitting, but might not necessarily be able to sustain stable pit growth. In a study by Presuel-Moreno and Moreno (2015) critical chloride threshold and time to initiation of concrete specimens containing 20%, 35%, and 50% cement replacement by fly ash as well as 6%, 15%, and 27% cement replacement by silica fume were investigated. Specimens were exposed to natural seawater for over 17 years on weekly wetting-drying cycles. Corrosion potential and chloride

content of specimens were monitored during this investigation. Presuel-Moreno and Moreno (2015) showed that in some specimens corrosion potential increases and bar repassivate after potential drops showed corrosion initiation; the duration of repassivation lasted from a few months to a few years. The reason for recovery of potential to more positive values after first drop was attributed to a combination of environmental and electrochemical conditions, such as temperature, and seasonal changes, which did not allow the incipient corrosion to sustain. For concrete containing slag cement, some studies showed very low corrosion potentials, values that according to ASTM C876 indicate over 90% probability of corrosion; however, no or very small sign of corrosion was observed on the bar surface showing that no chloride induced corrosion was occurring (Holloway & Sykes 2005, Bouteiller et al. 2012, Garcia et al. 2014). Low values for corrosion potential was mainly attributed to the oxidation of sulfides (Holloway & Sykes 2005, Garcia et al. 2014). In a study by Garcia et al. (2014) CCCT values for concrete containing 60% slag cement was evaluated; corrosion initiation was determined by monitoring corrosion potential of steel. Low values of corrosion potentials and repetitive potential drops was observed for specimens containing slag cement, which was attributed to the oxidation of sulfides not chloride induced corrosion. These low values of corrosion potentials increased over time by consumption of sulfides to above –0.200 V with respect to saturated calomel electrode, showing that chloride induced corrosion was not occurring. Garcia et al. (2014) showed that in solutions containing sulfide ions, regardless of concentration of chlorides, corrosion potential drop from –0.200 V to –0.500 V with respect to saturated calomel electrode.

This repetitive corrosion initiation in specimens containing supplementary cementitious materials could explain the variation in the reported critical chloride corrosion thresholds (CCCT) in the literature. Some of the reported critical chloride threshold values in the literature that claim

the CCCT values for supplementary cementitious materials to be lower than ordinary portland cement could be the values for the first initiation of specimens, not accounting for repassivation. The primarily and final critical chloride corrosion threshold and initiation time for specimens that initiated corrosion to date are shown in Table 4.19. For series where not all specimens have initiated, the average reported corrosion initiation age and CCCT will increase upon initiation of new specimens.

Table 4.19: Critical chloride threshold and time to initiation

Specimen	First initiation		Final initiation		Chloride ingress rate (lb/week)
	CCCT[a]	Time (weeks)	CCCT[a]	Time (weeks)[b]	
PC			1.46	15.8	0.215
FA(20)			-	27.3	-
FA(40)	1.53	41	2.70	80	0.031
SF(5)			1.86	> 94[b]	0.018
SF(10)	0.54	26[a]	1.59	> 94[b]	0.017
Slag(20)	1.72	21	4.51	67.7	0.068
Slag(40)	1.89	18[a]	2.88	> 93[b]	0.039
PC-ECR			7.05	40	0.171
FA-ECR(40)	2.17	60[a]	3.47	> 97[b]	0.039
SF-ECR(10)	1.94	41[a]	2.68	> 97[b]	0.022
Slag-ECR(40)	1.50	35[a]	2.22	>100[b]	0.032

[a]Not all specimens initiated, average based on specimens that initiated corrosion
[b]Average is based on initiated specimens time and the maximum time that uninitiated specimens reached

The initial and final CCCT value for specimens containing uncoated bars are compared in Figure 4.43. The initial average CCCT value for FA(40), Slag(20), and Slag(40) (1.53 lb/yd^3 (0.91 kg/m^3), 1.72 lb/yd^3 (1.02 kg/m^3), and 1.89 lb/yd^3 (1.12 kg/m^3), respectively) were similar to that for specimens containing 100% portland cement (1.46 lb/yd^3 (0.86 kg/m^3)). However, the final CCCT values for FA(40), Slag(20), and Slag(40) (2.70 lb/yd^3 (1.60 kg/m^3), 4.51 lb/yd^3 (2.67 kg/m^3), and 2.88 lb/yd^3 (1.7 kg/m^3)) were significantly higher than the CCCT value for PC specimens. Although specimens containing slag had higher CCCT values than PC specimens, the CCCT value decreased as slag cement content increased from 20% to 40%. However, since three

out of six specimens with 40% slag cement have not initiated, the CCCT values for Slag(40) specimens should be taken as a lower bound. For SF(5) specimens, three out of six specimens initiated corrosion with a CCCT value of 1.86 lb/yd^3 (1.10 kg/m^3) (through week 113), close to that for portland cement. SF(10) specimens, however, showed lower critical chloride thresholds compared to other specimens with supplementary cementitious materials; the first CCCT value was lower than the CCCT value for PC specimens, and the final CCCT value was similar to specimens with ordinary portland cement; not all SF(10) specimens have initiated, however. An overall comparison of time to initiation for specimens showed that specimens with silica fume required the longest time to initiate corrosion followed by specimens with slag, fly ash, and ordinary portland cement, with an increase in the SCM content increasing the required time to initiate corrosion.

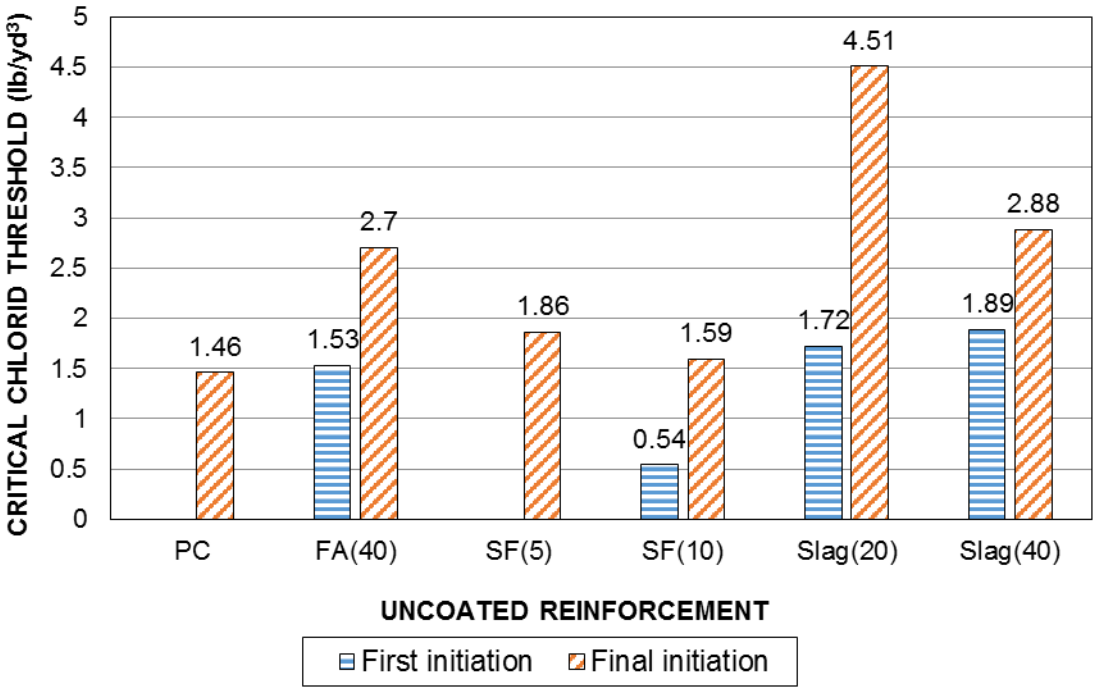

Figure 4.43—Comparison of critical chloride corrosion threshold for specimens containing uncoated conventional reinforcement

Specimens with epoxy-coated reinforcement (ECR) containing 100% ordinary portland cement showed an average CCCT value and time to corrosion initiation as 7.05 lb/yd^3 (4.17 kg/m^3) and 40 weeks, respectively, more than four times the threshold and almost three times the age of those for uncoated bars (1.46 lb/yd^3 (0.86 kg/m^3) and 15.8 weeks). This higher critical chloride threshold and time to initiation for epoxy-coated bars compared to bare bars in specimens containing 100% portland cement is due to the fact that chloride ions, oxygen and moisture do not penetrate through concrete uniformly because of a non-uniform concrete matrix, so in specimens with epoxy-coated bars it is less likely for a region of locally high chloride content to coincide exactly with the damaged site of bar. This CCCT value for ECR, is obtained for specimens without any crack; existence of crack on the surface of concrete can increase the probability for chloride ions, moisture, and oxygen to coincide with the damaged site of coating and result in the reduction of CCCT value of ECR. Similar to bare bars, most of specimens with epoxy-coated bars containing supplementary cementitious materials had re-initiation after repassivation. However, the final CCCT values for the reinforcement in specimens containing supplementary cementitious materials which initiated to date were not significantly higher than those for specimens with uncoated bars. In addition, the time to initiation for specimens with epoxy-coated and supplementary cementitious materials were close to the initiation time for the specimens with bare bars. However, not all specimens with ECR have initiated, and these values are likely to change.

The chloride content rates (lb/yd^3/week) at the top bar level of specimens containing fly ash, silica fume, slag and only ordinary portland cement are compared in Figure 4.44. Chloride concentration rates at a certain level of concrete can be used for comparing chloride ingress rates for different specimens, since these values are directly proportional; that is, higher chloride ingress rate result in higher chloride ions accumulation at a certain level of concrete. As shown, specimens

containing 40% fly ash and 40% slag with both bare and coated bars had similar chloride concentration rates at the bar level, or in other words, similar chloride ingress rates. By combining the data for bare and coated bars of each series, chloride concentration rates for specimens containing 40% fly ash and 40% slag were 0.0366 (lb/yd^3)/week and 0.0355 (lb/yd^3)/week, respectively, almost half of that for specimens containing 20% slag (0.066 lb/yd^3/week) and one-fifth of that for specimens containing 100% portland cement (0.19 lb/yd^3/week). Specimens containing silica fume showed the lowest chloride concentration rates (0.018 lb/yd^3/week for specimens containing 5% silica fume, and 0.02 lb/yd^3/week for specimens containing 10% silica fume), one order of magnitude less than that for specimens with 100% ordinary portland cement.

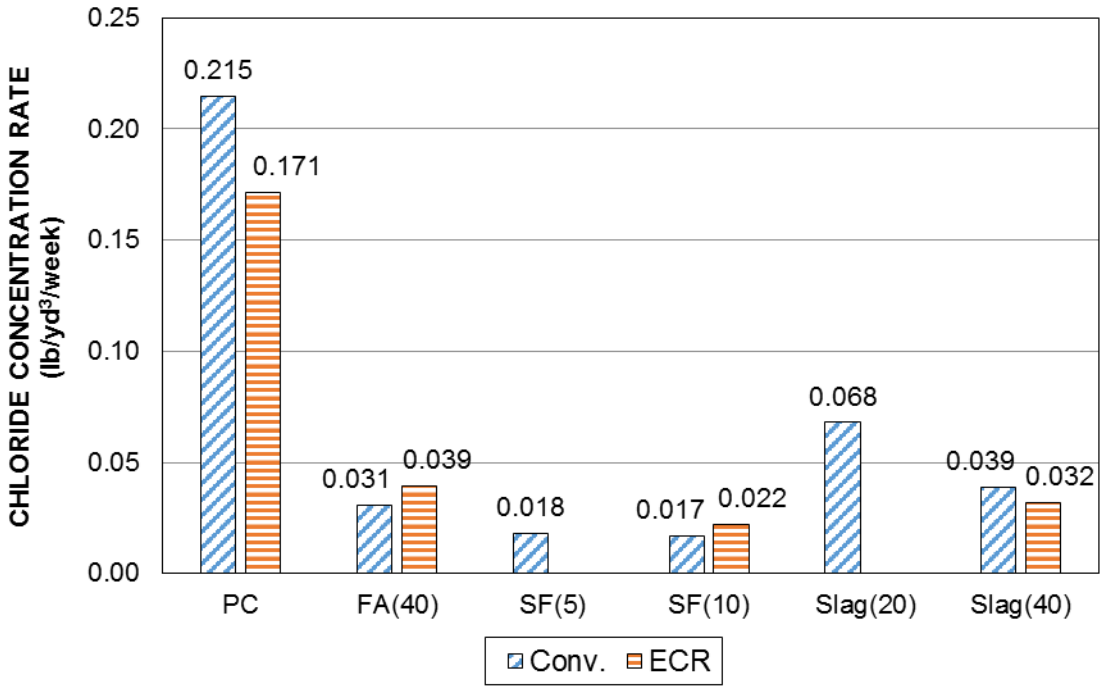

Figure 4.44—Comparison of chloride concentration rate (lb/yd^3/week) at the level of top bar for beam specimens

4.5 CONCLUSIONS

The following conclusions are drawn based on the results presented in this chapter:

1- The total corrosion losses after 96 weeks and corrosion rates for specimens with uncoated reinforcement were lowest for specimens containing silica fume following by specimens with 40% slag, 40% fly ash, 20% slag, 20% fly ash, and 100% ordinary portland cement. Increasing the amount of SCM lowered the corrosion rates and losses for all mixtures. Total corrosion losses for FA(20) and Slag(20) specimens were 25% and 10% of that for PC specimens, respectively, while for FA(40), Slag(40), SF(5), and SF(10) specimens corrosion losses were about 5% of that for PC specimens. Increasing the amount of SCM also increased the time to initiation, with the longest initiation time in mixtures containing silica fume, followed by slag cement, fly ash, and ordinary portland cement.

2- For specimens with epoxy-coated reinforcement, specimens containing 40% fly ash, 40% slag, and 10% silica fume showed corrosion loss about one tenth of that for specimens containing 100% portland cement.

3- Most specimens containing 40% fly ash, 20% slag, 40% slag, and 10% silica fume repassivated after initiation, with corrosion re-initiating at a higher chloride threshold. For fly ash and slag cement specimens, the initial CCCT value was similar to that for 100% ordinary portland cement, while the second CCCT value was significantly higher. For specimens with 10% silica fume, however, the initial CCCT value was lower than PC specimens and the second was similar to that for PC specimens. This discrepancy in two levels of CCCT values may explain the mixed results in the literature concerning the performance of SCMs.

4- Overall results show that use of fly ash and slag cement significantly decrease corrosion rate, increase the time to initiation and critical chloride threshold of concrete. The use of silica fume resulted in much greater reductions in corrosion rate and increases in time to initiation compared to slag cement or fly ash; however, the chloride threshold for specimens containing silica fume was comparable to that of specimens containing portland cement. A combination in use of ECR and supplementary cementitious materials significantly improves corrosion resistance of concrete and decreases the total corrosion loss by three orders of magnitude compared to concrete with uncoated conventional bars and 100% ordinary portland cement.

CHAPTER 5: LIFE EXPECTANCY OF CORROSION PROTECTION SYSTEMS FOR REINFORCED CONCRETE

5.1 LIFE EXPECTANCY

In this section, the life expectancy of bridge decks with the corrosion protection systems evaluated in this study is estimated. Conventional bare and epoxy-coated reinforcement are compared with alternative forms of reinforcement–galvanized steel, MMFX steel containing 9% and 4% chromium (ASTM A1035 Type CS and CM steel), and epoxy-coated MMFX steel containing 4% and 2% chromium (epoxy-coated ASTM A1035 Type CM and CL steel). Furthermore, life expectancy of reinforced concrete with partial replacement of cement by 20% fly ash, 40% fly ash, 5% silica fume, 10% silica fume, 20% slag cement, and 40% slag cement in bridge decks containing uncoated conventional steel as well as 40% fly ash, 10% silica fume, and 40% slag cement in bridge decks containing conventional epoxy-coated reinforcement are compared with concrete bridge decks containing only portland cement along with epoxy-coated and uncoated reinforcement.

The time to first repair of a concrete bridge deck (expected life) can be represented as two phases–the time to corrosion initiation of reinforcement and the time for a corroding bar to crack the concrete cover. Estimations of each of these phases are presented in the following sections.

5.1.1 Time to Corrosion Initiation

Onset of corrosion occurs when the chloride content amount at the surface of embedded bar reaches its critical chloride corrosion threshold (CCCT). The time to corrosion initiation is determined by comparing the CCCT value for each corrosion protection system with the chloride concentration at the depth of the reinforcement in concrete bridge decks. Lindquist et al. (2006)

measured the chloride content of 57 bridge decks with an average annual daily traffic (AADT) greater than 7500. Concrete was sampled in 0.75 in. (19 mm) increments up to 3.75 in. (95 mm) from the surface. Results are then interpolated to a depth of 3 in. (76.2 mm) (the cover to the top mat of steel in bridge decks) and reported at crack locations as well as away from cracks. Since existence of cracks over and parallel to the bars is common in bridge decks and can accelerate corrosion, chloride contents at crack locations are used. Figure 5.1 shows the average chloride concentration with respect to the age of the structure at crack locations at a depth of 3 in. (76.2 mm).

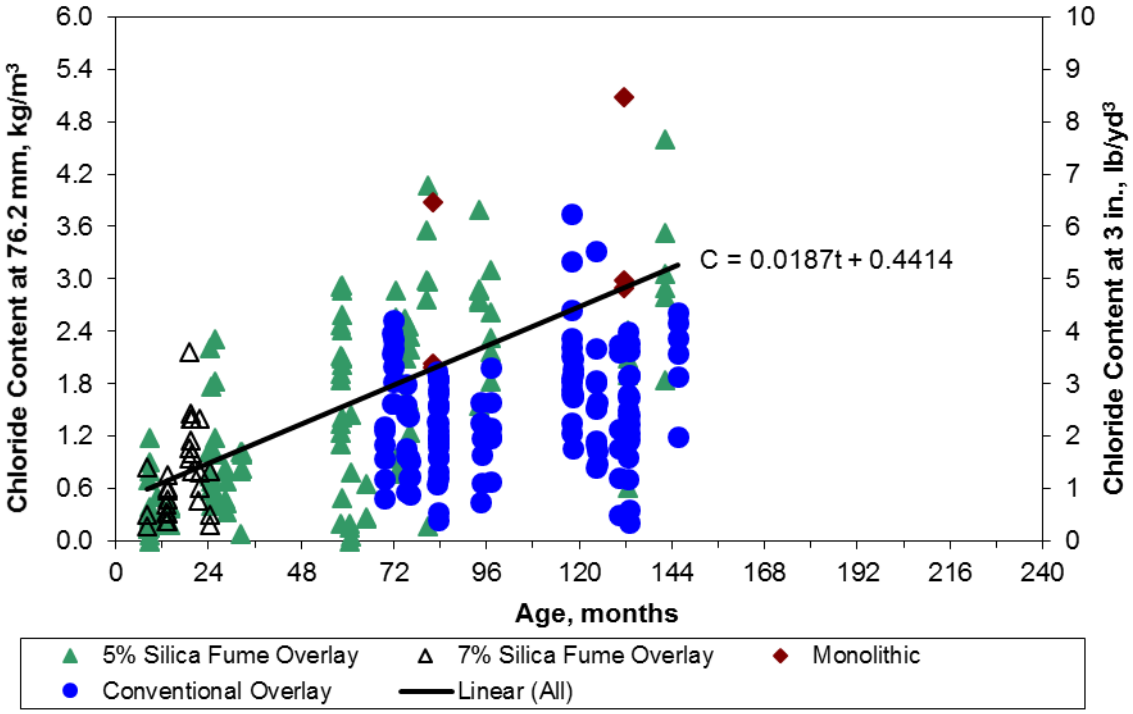

Figure 5.1— Chloride content taken on cracks interpolated at depth of 3 in. vs. placement age for bridges with an AADT > 7500 (Lindquist et al. 2006)

The trend line equation obtained from the data shows a linear relationship between chloride concentration and time at the crack locations and is independent of permeability of concrete; thus, it can be used for all specimens including specimens containing supplementary cementitious

materials. The average time to reach a specific critical chloride threshold at crack locations on the bridge decks can be expressed as:

$$t_1 = (C_{crit} - 0.4414) / 0.0187 \quad (5.1)$$

where

C_{crit} = critical chloride corrosion threshold, kg/m^3

t_1 = time to reach the critical chloride corrosion threshold, months

The critical chloride corrosion threshold (CCCT) and calculated average time to initiation based on Eq. 5.1 for each corrosion protection system in this study are tabulated in Table 5.1. The critical chloride threshold value for galvanized bars (2.57 lb/yd^3 (1.52 kg/m^3)) is obtained from a study by Darwin et al. (2009); other values are from this study. A comparison between systems with bare bars shows that conventional reinforcement in concrete without any supplementary cementitious materials has the lowest time to initiation (1.9 years). MMFX reinforcement had a time to initiation of almost 10 years, about five times greater than bridge decks with conventional bars. The use of supplementary cementitious materials (SCM) extended the time to initiation due to their higher CCCT value; however, this extension was not significant for concrete containing silica fume. Unlike systems with bare bars, for the systems with epoxy-coated reinforcement the CCCT values for concrete containing SCM were lower than that for concrete with ordinary portland cement. This can be explained by the fact that in specimens with 100% ordinary portland cement, chloride ions, oxygen, and moisture do not penetrate through concrete uniformly because of a non-uniform concrete matrix containing pores, so in specimens with epoxy-coated bars it is less likely for a region of locally high chloride content to coincide exactly with the damaged site of bar, which makes the time to initiation and CCCT value to be significantly higher for epoxy-coated bars compared to bare bars. The use of SCM's reduces the average pore size of the cement

paste, resulting in a less permeable concrete (Hooton 1986, Chindaprasirt et al. 2005), and reducing the diffusivity of ions (Bijen 1996). As a result, concrete containing SCM's has a less permeable but more uniform matrix, allowing chloride ions, oxygen and moisture to penetrate through concrete slowly but uniformly and resulting in damaged sites of ECR to initiate with a level of chloride content and time to initiation close to those for bare bars in the same concrete. There is no reason to assume, however, that ECR should have a lower threshold than a bare bar in the same concrete; cases of this occurring (such as Slag(40)) are likely due to random variation. Therefore, in cases where ECR exhibited a lower chloride threshold than bare bars in the same concrete, the value for bare bars was used for both types of reinforcement.

Table 5.1: Critical chloride threshold and time to initiation for bridge decks with different corrosion protection systems

System[a]	Critical chloride corrosion threshold		Initiation time
	lb/yd^3	kg/m^3	years
Conv.	1.46	0.86	1.9
ECR	7.05	4.17	16.4
Galvanized steel			
Zn	2.57	1.52	4.8
MMFX steel			
MMFX(4%)	4.25	2.52	9.2
MMFX(9%)	4.54	2.69	10.0
MMFX-ECR(2%)	4.11	2.43	8.9
MMFX-ECR(4%)	5.16	3.06	11.6
Supplementary cementitious materials (SCM)			
FA(20)	2.04	1.21	3.4
FA(40)	2.70	1.60	5.2
SF(5)	1.86	1.10	2.9
SF(10)	1.59	0.94	2.2
Slag(20)	4.51	2.67	9.9
Slag(40)	2.88	1.70	5.6
FA-ECR(40)	3.47	2.05	7.2
SF-ECR(10)	2.68	1.59	5.1
Slag-ECR(40)[b]	2.88	1.70	5.6

[a] Conv = concrete containing 100% portland cement and conventional bare steel
ECR = concrete containing 100% portland cement and conventional epoxy-coated steel
Zn= concrete containing galvanized steel
MMFX(4%) = concrete containing MMFX steel with 4% chromium
MMFX(9%) = concrete containing MMFX steel with 9% chromium
MMFX-ECR(2%) = concrete containing epoxy-coated MMFX steel with 2% chromium
MMFX-ECR(2%) = concrete containing epoxy-coated MMFX steel with 4% chromium
FA(20) = concrete containing 20% fly ash and conventional bare steel
FA(40) = concrete containing 40% fly ash and conventional bare steel
Slag(20) = concrete containing 20% slag cement and conventional bare steel
Slag(40) = concrete containing 40% slag cement and conventional bare steel
SF(5) = concrete containing 5% silica fume and conventional bare steel
SF(10) = concrete containing 10% silica fume and conventional bare steel
FA-ECR(40) = concrete containing 40% fly ash and conventional epoxy-coated steel
Slag-ECR(40) = concrete containing 40% slag cement and conventional epoxy-coated steel
SF-ECR(10) = concrete containing 10% silica fume and conventional epoxy-coated steel
[b]CCCT value for ECR bars was assumed equal to that for bare bars, since the measured value was lower due to random variation.

5.1.2 Corrosion Propagation Time to Crack Concrete Cover

To calculate the time to crack concrete after corrosion initiation of steel, the total corrosion loss required to crack concrete (critical corrosion loss) and the average corrosion rate of steel after initiation are necessary. By dividing the critical corrosion loss by the average corrosion rate, the time that is taken for corroded bar to crack concrete can be determined for each system.

5.1.2.1 Critical Corrosion Loss

A sufficient amount of buildup corrosion products (the critical corrosion loss) is needed to crack the concrete cover. Critical corrosion loss is estimated using an equation developed by O'Reilly et al. (2011) which represents a relationship between corrosion loss of steel at crack initiation, concrete cover, and bar diameter for localized corrosion as well as general corrosion:

$$x_{crit} = 45\left(\frac{\left[C/25.4\right]^{2-A_f}}{D^{0.38} \times L_f^{\,0.1} \times A_f^{\,0.6}} + 0.2\right) \times 3^{A_f - 1} \tag{5.2}$$

where

x_{crit} = corrosion loss at crack initiation, μm

C = cover, mm.

D = bar diameter, mm.

L_f = fractional length of bar corroding, $L_{\text{corroding}}/L_{\text{bar}}$

A_f = fractional area of bar corroding, $A_{\text{corroding}}/A_{\text{bar}}$

As shown in Chapter 2, this predictive equation rendered the critical corrosion loss for conventional steel in concrete with 1 in. clear cover as of 24 μm assuming uniform corrosion, and 21 μm considering actual corroded area of steel; these values were very close to the critical

corrosion loss, 25 μm, obtained experimentally in this study, allowing this equation to be used to predict the critical corrosion loss values needed in this section.

For conventional reinforcement, assuming uniform corrosion, fractional length (L_f) and fractional area (A_f) of corroding bar are set to 1. Thus, in a bridge deck with 3 in. (76.2 mm) clear concrete cover containing No. 5 (No. 16) uncoated steel, critical corrosion loss would be:

$$x_{crit} = 45\left(\frac{\left[{}^{76.2}\!/_{25.4}\right]^{2-1}}{16^{0.38}\times 1^{0.1}\times 1^{0.6}} + 0.2\right)\times 3^{1-1}$$

$$x_{crit} = 56\,\mu\text{m}$$

Epoxy-coated reinforcement in this report was intentionally damaged with ten holes, five on the each side of bar, with a diameter of 0.125 in. (3 mm), to simulate the damage that occurs on coated reinforcement in practice. The exposed fractional area of a bar, A_f, can be obtained by dividing the exposed area of a bar by its total embedded area in concrete:

$$A_f = \frac{A_{corroding}}{A_{bar}} = \frac{10\times\pi\left({}^{d_h}\!/_{2}\right)^2}{\pi d_b l} = \frac{10\times\pi\left({}^{3\text{mm}}\!/_{2}\right)^2}{\pi\times 16\text{ mm}\times 304.8\text{ mm}} = 0.0046$$

Exposed fractional length of a bar, L_f, is obtained as a quotient of dividing the exposed length of a bar by its total length:

$$L_f = \frac{L_{corroding}}{L_{bar}} = \frac{d_h}{l} = \frac{5\times 3\text{ mm}}{304.8\text{ mm}} = 0.049$$

By substituting the calculated A_f and L_f values in Eq. 5.2, the critical corrosion loss required to crack a 3 in. (76.2 mm) concrete cover by corrosion of a No. 5 (No. 16) epoxy-coated bar is:

$$x_{crit} = 45\left(\frac{\left[{}^{76.2}\!/_{25.4}\right]^{2-0.0046}}{16^{0.38}\times 0.049^{0.1}\times 0.0046^{0.6}} + 0.2\right)\times 3^{0.0046-1}$$

$$x_{crit} = 1610\ \mu\text{m}$$

MMFX bars were assumed to behave in a manner similar to conventional steel in terms of the corrosion losses required to crack concrete; thus, the calculated values of conventional steel were used for bare and epoxy-coated MMFX reinforcement. However, Eq. 5.2 is not applicable for concrete containing galvanized steel. Therefore, the time to cracking concrete cover for a bridge deck with galvanized bars is directly estimated in Table 5.6 by multiplying the time to cracking of conventional steel by the ratio of time to cracking of bench-scale specimens containing galvanized bars to that containing conventional reinforcement (3.76) found in Chapter 2.

5.1.2.2 Average Corrosion Rate

The average corrosion rate for each system is determined from its total corrosion loss plots obtained from LPR test results. Figure 5.2 shows corrosion loss for Specimen 1 containing 100% portland cement and conventional bare bars. Other corrosion loss plots for each system are presented in Appendices C and I. First, the corrosion initiation points and test termination points were marked, and corresponding corrosion losses (a_i) and time (t_i) for each point were determined. The average corrosion rate for individual specimen is the average slope of the line between these two points (θ), which can be calculated as the ratio of differences in corrosion losses to times ($\theta = \frac{a_2 - a_1}{t_2 - t_1}$).

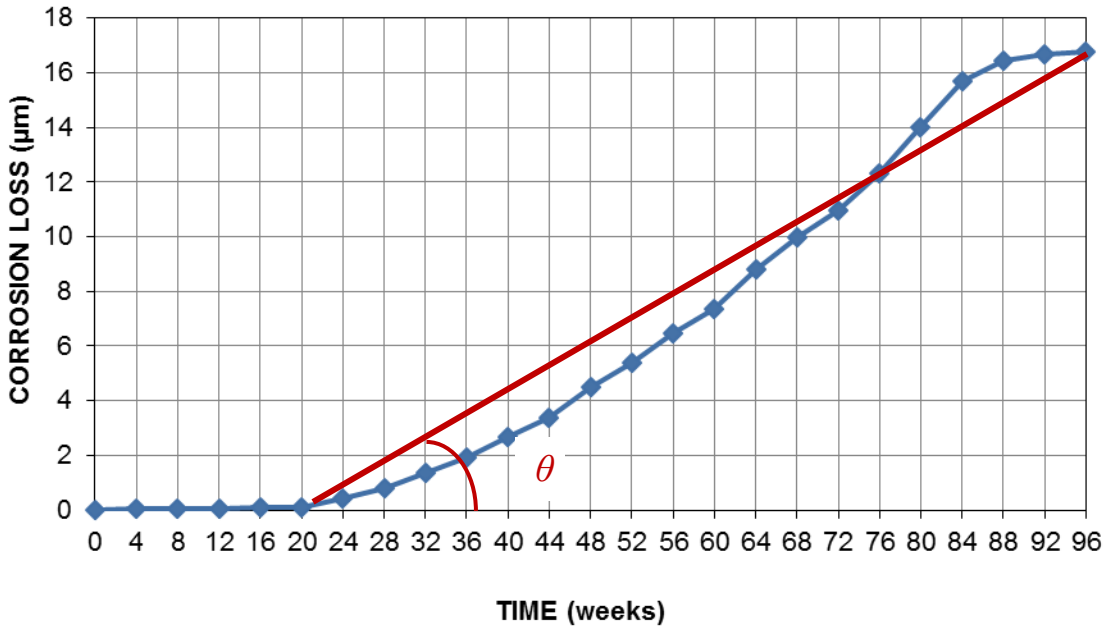

Figure 5.2— LPR test corrosion loss (µm) for Specimen 1 containing uncoated conventional reinforcement and 100% portland cement

The average corrosion rates based on LPR test results for each system in this study are tabulated in Table 5.2. Average corrosion rates are only based on specimens which have initiated corrosion. For MMFX reinforcement results are obtained from Southern Exposure specimens; for the other systems beam specimens are used. Corrosion loss plots used for all specimens with epoxy-coated bars were based on the exposed area of reinforcement. For systems with bare bars, Conv. had the highest total corrosion rate (14.5 µm/yr). Conventional epoxy-coated reinforcement in specimens with 100% portland cement showed the highest total corrosion rate based on exposed area (50.0 µm/yr) among specimens with coated bars. For specimens with supplementary cementitious materials containing bare bars, the average corrosion rate was approximately one order of magnitude less than that for specimens containing only ordinary portland cement (with the exception of specimens containing 20% fly ash, which had an average corrosion rate about a quarter of that for specimens with 100% portland cement). Specimens containing supplementary

cementitious materials along with epoxy-coated bars had an average corrosion rate one order of magnitude less than specimens containing 100% portland cement with epoxy-coated bars. Specimens with MMFX reinforcement containing 4% and 9% chromium showed approximately half the average corrosion rate (7.55 and 6.17 µm/yr, respectively) than specimens with conventional steel (14.5 µm/yr). While the average corrosion rate of MMFX-ECR(2%) specimens (40.2 µm/yr) was comparable to that of epoxy-coated conventional reinforcement (42.8 µm/yr), MMFX-ECR(4%) specimens exhibited approximately half the average corrosion rate of epoxy-coated conventional reinforcement (21.7 µm/yr).

Table 5.2: Average corrosion rate (µm/yr) after corrosion initiation based on LPR test corrosion losses

System[a,b]	Specimen								Avg.	Std. Dev.	COV
	1	2	3	4	5	6	7	8			
Conv.	10.9	16.3	15.9	15.1	14.8	13.8	-	-	14.5	1.94	0.13
ECR	39.7	59.3	38.0	42.4	86.4	34.2	-	-	50.0	19.8	0.40
Galvanized steel											
Zn	8.38	7.56	12.2	7.81	8.96	8.25	-	-	8.86	1.71	0.19
MMFX steel											
MMFX(4%)	13.0	10.9	6.18	8.97	6.44	8.21	3.74	3.03	7.55	3.40	0.45
MMFX(9%)	10.2	8.84	6.49	3.00	5.60	6.27	2.89	6.03	6.17	2.53	0.41
MMFX-ECR(2%)	27.6	45.5	49.0	24.1	51.2	43.9	-	-	40.2	11.5	0.29
MMFX-ECR(4%)	19.2	16.9	13.4	16.1	40.9	23.7	-	-	21.7	10.0	0.46
Supplementary cementitious materials (SCM)											
FA(20)	3.32	3.79	2.88	3.76	2.75	4.92	-	-	3.57	0.790	0.22
FA(40)	0.790	1.00	1.27	1.03	1.57	1.01	-	-	1.11	0.270	0.24
SF(5)	1.07	1.35	1.25	[c]	[c]	[c]	-	-	1.22	0.140	0.11
SF(10)	[c]	1.19	[c]	[c]	[c]	[c]	-	-	1.19	-	-
Slag(20)	1.17	0.410	1.11	1.31	3.34	0.670	-	-	1.42	0.970	0.68
Slag(40)	[c]	0.840	1.17	[c]	[c]	[c]	-	-	1.00	0.240	0.24
FA-ECR(40)	8.87	5.47	2.50	2.81	11.0	4.21	-	-	5.81	3.43	0.59
SF-ECR(10)	[c]	[c]	3.97	[c]	[c]	3.89	-	-	3.93	0.060	0.01
Slag-ECR(40)	3.76	5.23	3.80	[c]	7.29	[c]	-	-	5.02	1.66	0.33

[a] Corrosion losses were obtained from Southern Exposure specimens for MMFX bars and beam specimens for other systems

[b] For epoxy-coated reinforcement corrosion losses are obtained based on exposed area of bars

[c] No corrosion observed

To measure the average corrosion rate of galvanized bars, results are used from specimens in which 2% chloride by weight of cement was added to the concrete. To investigate the effect of added internal chlorides on corrosion rate, two series of specimens with and without internally mixed salt containing conventional bars are compared in Table 5.3; Conv. specimens without introduced salt to concrete mix and Conv-Salt specimens with admixed salt. No statistically significant difference was observed between the average corrosion rate for specimens with or without admixed chlorides ($p = 0.47$ with the Student's T-test); therefore, specimens with galvanized bars and admixed chlorides may be used to estimate the corrosion rate after initiation.

Table 5.3: Average corrosion rate (μm/yr) comparison for specimens with and without internally mixed chloride

System	Specimen						Avg.	Std. Dev.	COV	Student T-test
	1	2	3	4	5	6				
Conv.	10.9	16.3	15.9	15.1	14.8	13.8	14.5	1.94	0.13	0.47
Conv-Salt	14.4	15.9	16.1	14.5	15.2	13.5	14.9	0.97	0.06	

To establish the average corrosion rates for each system in bridge decks, some modification factors which represent the relationship between the tested specimens in laboratory and real bridge decks should be used. Two major differences between conditions experienced by a bridge deck and those experienced by the laboratory specimens are the severity of environment and presence of cracks on the concrete surface. Bench-scale specimens are exposed to chlorides more frequently than a real bridge deck and kept saturated for over three quarters of the time, whereas a bridge deck is saturated for a much lower percentage of time. This would result in a lower corrosion rate on bridge decks than in the lab. However, the existence of cracks on bridge decks may increase the corrosion rate compared to uncracked specimens in the lab. O'Reilly (2011), developed a coefficient relating the corrosion rate of uncracked laboratory specimens to that of field specimens

under the same exposure conditions as bridge decks in Kansas. O'Reilly found that corrosion rates from laboratory tests on bare bars could be converted to equivalent field corrosion rates in uncracked and cracked concrete by multiplying by 0.155 and 0.241, respectively. For coated bars, the conversion factors for uncracked and cracked concrete were 0.476 and 0.847. O'Reilly also noted that uncoated bars in field specimens tended to exhibit localized corrosion-only 40% of the bar area exhibited corrosion in uncracked concrete, with 33% of the bar area exhibiting corrosion in cracked concrete. This led to an additional conversion to "effective corroding area", accounting only for the percentage of bar corroding.

Using O'Reilly's coefficients, the total equivalent corrosion rate for bridge decks with and without cracks for each corrosion protection system based on exposed area of epoxy-coated reinforcement as well as total area and effective area of bare bars are calculated and tabulated in Table 5.4. Equivalent corrosion rate based on effective area of corroded bare bars in uncracked field specimens are less than but close to cracked field specimens. This can be explained by the fact that the higher corrosion rates based on total area for cracked specimens is due to their higher effective corroded area; however, the corrosion rate of an actual corroded area of a bar is very close in cracked and uncracked concrete. No field data was available for galvanized bars; based on lab results that showed uniform corrosion on galvanized bars, the total area of bar was treated as the effective area in corrosion. A coefficient of 1.8 was introduced by O'Reilly (2011) to convert corrosion rates of uncracked specimens to cracked specimens in laboratory tests. By applying this factor, equivalent corrosion rates of laboratory cracked beam specimens are calculated and shown in Table 5.4 for comparison.

Table 5.4: Equivalent total corrosion rates for bridge decks with and without cracks, and different corrosion protection systems

System[a]	Laboratory specimen corrosion rate (μm/yr)		Equivalent total corrosion rate (μm/yr)			
			Exposed area		Effective area	
	Uncracked	Cracked	Uncracked	Cracked	Uncracked	Cracked
Conv.	14.5	26.1	2.25	3.50	6.74	8.74
ECR	50.0	89.0	23.8	42.4	-	-
Galvanized steel						
Zn	8.86	16.0	1.37	2.14	-	-
MMFX steel						
MMFX(4%)	7.55	13.59	1.17	1.82	3.51	4.55
MMFX(9%)	6.17	11.1	0.96	1.49	2.87	3.72
MMFX-ECR(2%)	40.2	71.6	19.1	34.1	-	-
MMFX-ECR(4%)	21.7	38.6	10.3	18.4	-	-
Supplementary cementitious materials (SCM)						
FA(20)	3.57	6.43	0.55	0.86	1.66	2.15
FA(40)	1.11	2.01	0.17	0.27	0.52	0.67
SF(5)	1.22	2.20	0.19	0.29	0.57	0.74
SF(10)	1.19	2.15	0.18	0.29	0.56	0.72
Slag(20)	1.42	2.55	0.22	0.34	0.66	0.86
Slag(40)	1.00	1.81	0.16	0.24	0.47	0.60
FA-ECR(40)	5.81	10.3	2.76	4.92	-	-
SF-ECR(10)	3.93	7.00	1.87	3.33	-	-
Slag-ECR(40)	5.02	8.94	2.39	4.26	-	-

The time from corrosion initiation to cracking of the concrete cover for each system can be obtained by taking the critical corrosion loss from Section 5.1.2.1 and dividing by the equivalent total corrosion rates in Table 5.4 based on effective area for bare bars and exposed area for epoxy-coated reinforcement. Since it is more likely that bridge decks develop cracks over the reinforcement, corrosion rates for cracked specimens are used for comparison. The estimated times to first cracking after corrosion initiation are listed in Table 5.5. The lowest estimated time from initiation to first cracking is observed in concrete decks without any supplementary cementitious materials that contain conventional bare steel (6.4 years). For galvanized reinforcement, since no accurate critical corrosion loss for 3 in. concrete cover is available, the time from initiation to first cracking is estimated by multiplying the time from initiation to cracking of conventional steel by

the ratio of time from initiation to cracking of bench-scale specimens with galvanized bars to that with conventional reinforcement. As shown in Chapter 2, while the average time from initiation to cracking of beam specimens containing conventional bars was 21 weeks, for galvanized bars this time was 79 weeks. Therefore, the time from initiation to first cracking of bridge decks (6.4 years) is multiplied to the ratio of 79 to 21 weeks (3.76), and the time from initiation to first cracking of bridge decks with galvanized bars is estimated as 24.1 years. Bridge decks with MMFX bars containing 4% chromium have almost twice the estimated time from initiation to cracking (12.3 years) compared to conventional bare bars. Estimated time from initiation to first cracking for concrete containing MMFX bars with 9% chromium, 15.1 years, is almost triple of that for conventional reinforcement. Using supplementary cementitious materials in concrete significantly extends the estimated time from initiation to first cracking. For instance, replacing portland cement with 5% and 10% silica fume, 40% fly ash, and 40% slag would raise the estimated time to more than 75 years. The combination of using epoxy-coated bars and supplementary cementitious materials further increases estimated time from initiation to cracking (more than 300 years) about one order of magnitude more than that for ECR system alone, and four times of that for using supplementary cementitious materials along with bare bars.

Table 5.5: Estimated times to first cracking after corrosion initiation based on corrosion rate in cracked concrete

System[a]	Corrosion rate (µm/yr)	Critical corrosion loss (µm)	Cracking time (yr)
Conv.	8.74	56	6.4
ECR	42.4	1610	38.0
Galvanized steel			
Zn	2.14	-	24.1
MMFX steel			
MMFX(4%)	4.55	56	12.3
MMFX(9%)	3.72	56	15.1
MMFX-ECR(2%)	34.1	1610	47.3
MMFX-ECR(4%)	18.4	1610	87.6
Supplementary cementitious materials (SCM)			
FA(20)	2.15	56	26.0
FA(40)	0.67	56	83.3
SF(5)	0.74	56	76.0
SF(10)	0.72	56	77.7
Slag(20)	0.86	56	65.5
Slag(40)	0.60	56	92.6
FA-ECR(40)	4.92	1610	327
SF-ECR(10)	3.33	1610	483
Slag-ECR(40)	4.26	1610	378

5.1.3 Time to First Repair

The expected life of a bridge deck is the elapsed time between the construction of a bridge and the time replacement or repair of the deck is required. The time to first repair is different from the time to first crack since a bridge deck is not fully repaired at the development of the first crack, but only after significant degradation of the deck has occurred. Based on discussions with the Kansas Department of Transportation, a ten-year period is assumed between first cracking and first repair of bridge decks for all systems. The time to first cracking is the summation of the time to corrosion initiation and the time to cracking after initiation. Table 5.6 shows the initiation time, the time to first cracking after initiation, the time to first repair after cracking concrete, and the expected life of a bridge deck for each system. Conventional reinforcement in concrete without any supplementary cementitious material has the lowest expected time to first repair of 18 years,

which is within the range of 10 to 25 years predicted by KDOT and SDDOT (Darwin et al. 2002). Bridge decks with galvanized bars have an expected life of 39 years, and uncoated MMFX bars containing 4% and 9% chromium, respectively, show an expected life of 31 and 35 years in bridges, approximately twice as much as conventional reinforcement. Partial replacement of supplementary cementitious materials extended life expectancy of bride decks significantly compared to bridge decks containing only portland cement; using 20% fly ash raises the expected life of a bridge to 39 years, and replacement of cement by 40% fly ash, 5% and 10% silica fume, and 20% and 40% of slag cement increases time to first repair to more than 75 years. Decks containing ECR have an expected time to first repair of 64 years, compared to the 35 to 40 years estimated by KDOT and SDDOT (Darwin et al. 2002). In systems containing epoxy-coated MMFX bars, MMFX bars with 2% chromium had an expected life similar to that of conventional ECR; however, epoxy-coated MMFX bars with 4% chromium show an estimated life of 109 years–50% more than that for ECR. Using epoxy-coated bars in conjunction with supplementary cementitious materials increases the time to first repair to more than 300 years–almost five times of that for ECR alone.

Table 5.6: Time to first repair for corrosion protection systems based on corrosion rate in cracked concrete

System[a]	Time to initiation (yr)	Time from initiation to cracking (yr)	Time from cracking to repair (yr)	Expected time to first repair (yr)
Conv.	1.9	6.4	10	18
Zn	4.8	24.1	10	39
MMFX(4%)	9.2	12.3	10	31
MMFX(9%)	10	15.1	10	35
FA(20)	3.4	26	10	39
FA(40)	5.2	83.3	10	98
SF(5)	2.9	76	10	89
SF(10)	2.2	77.7	10	90
Slag(20)	9.9	65.5	10	85
Slag(40)	5.6	92.6	10	108
ECR	16.4	38.0	10	64
MMFX-ECR(2%)	8.9	47.3	10	66
MMFX-ECR(4%)	11.6	87.6	10	109
FA-ECR(40)	7.2	327	10	344
SF-ECR(10)	5.1	483	10	498
Slag-ECR(40)	5.6	378	10	394

5.2 COST EFFECTIVENESS

In this section, the cost effectiveness of all systems used in this study are compared. The compared systems include conventional steel, ECR, MMFX bare bars containing 9% and 4% chromium, epoxy-coated MMFX bars containing 4% and 2% chromium, conventional steel in conjunction with partial replacement of cement by 20% fly ash, 40% fly ash, 5% silica fume, 10% silica fume, 20% slag cement, and 40% slag cement, and epoxy-coated steel in conjunction with partial replacement of cement by 40% fly ash, 10% silica fume, and 40% slag cement. A 150 ft (46 m) long, 36 ft (11 m) wide, 8.5 in. (216 mm) thick bridge deck is used in the analysis. Cost estimates includes cost for initial construction of a bridge deck as well as any needed repairs to reach a target 75-year design life. Repairs are assumed to last 25 years.

5.2.1 New Bridge Construction Costs

The new bridge construction costs in this section are calculated based on the prices obtained from manufacturers and in-place costs from bids on bridge projects in Kansas. Based on 67 bridge project bids from January 2015 through September 2016 obtained from KDOT, the in-place cost of concrete, conventional steel, and ECR were \$554.43/yd^3 (\$725.20/m^3), \$0.95/lb (\$2.08/kg), and \$1.05/lb (2.32/kg), respectively. The in-place cost of reinforcement includes fabrication, transportation, and placement on the bridge decks. For galvanized bars and MMFX bare and epoxy-coated reinforcement, in-place costs are not available; therefore, the costs of fabrication [\$0.10/lb (\$0.22/kg)] and transportation and placement in Kansas [\$0.62/lb (\$1.35/kg)] are added to the mill prices of the reinforcement provided by the suppliers; the epoxy coating cost (\$0.09/lb (\$0.20/kg)) is added to bare bars to estimate the cost of epoxy-coated MMFX bars. The estimated in-place costs of MMFX bare bars containing 9% and 4% chromium are \$1.58/lb (\$3.47/kg) and \$1.21/lb (\$2.65/kg), respectively, while for epoxy-coated MMFX bars containing 4% and 2% chromium the in-place costs are \$1.30/lb (\$2.85/kg) and \$1.22/lb (\$2.67/kg), respectively. The in-place cost of galvanized bars is estimated as \$1.50/lb (\$3.29/kg).

Based on 12 monolithic bridge decks constructed in State of Kansas during the four-year period of 2004 through 2007, an average reinforcing steel quantity of 275 lb/yd^3 (163 kg/m^3) is used in estimating bridge costs (O'Reilly 2011). However, this value can be lower for the MMFX bars which have higher yielding and ultimate strength compared to conventional bars used for this estimate. For an 8.5 in. (216 mm) thick bridge deck the required amount of steel per unit surface area of deck is 64.9 lb/yd^2 (35.2 kg/m^2). The cost of required conventional steel per unit surface area of deck (\$/yd^2) is calculated below; the in-place reinforcement costs for other systems are calculated accordingly and presented in Table 5.7.

Cost of conventional steel in 8.5 in. (216 mm) thick concrete deck per square yard:

$$\frac{\$0.95}{lb} \times 64.9 \frac{lb}{yd^2} = \frac{\$61.66}{yd^2}$$

Table 5.7: In-place cost of reinforcement in an 8.5 in. (216 mm) bridge deck

Steel type	Fabricated cost $/lb ($/kg)	Placement cost $/lb ($/kg)	Total cost $/lb ($/kg)	Steel quantity lb/yd^2 (kg/m^2)	In-place cost $/yd^2 ($/m^2)
Conv.	0.33 (0.73)	0.62 (1.35)	0.95 (2.08)	64.9 (35.2)	61.66 (73.22)
Galvanized	0.88 (1.94)	0.62 (1.35)	1.50 (3.29)	64.9 (35.2)	97.35 (115.9)
MMFX(4%)	0.59 (1.30)	0.62 (1.35)	1.21 (2.65)	64.9 (35.2)	78.53 (93.40)
MMFX(9%)	0.96 (2.12)	0.62 (1.35)	1.58 (3.47)	64.9 (35.2)	102.54 (122.11)
ECR	0.42 (0.94)	0.62 (1.35)	1.05 (2.32)	64.9 (35.2)	68.15 (81.66)
MMFX-ECR(2%)	0.60 (1.32)	0.62 (1.35)	1.22 (2.67)	64.9 (35.2)	79.18 (94.17)
MMFX-ECR(4%)	0.68 (1.50)	0.62 (1.35)	1.30 (2.85)	64.9 (35.2)	84.37 (100.38)

To estimate the in-place cost of concrete with cement partially replaced by supplementary cementitious materials, the base cost of replaced cement is substituted with the base cost of the SCM. The average base cost of cement, fly ash, silica fume, and slag cement in Kansas in September 2016 were $0.06/lb ($0.14/kg), $0.03/lb (0.07/kg), $1/lb ($2.2/kg), and $0.07/lb ($0.14/kg), respectively. The in-place cost of concrete containing supplementary cementitious materials are listed in Table 5.8. The indicated percentage for each mix, for instance 20% fly ash, shows the volume portion of cement which is replaced by SCM; the volume portion then is converted to weight to estimate the material cost in Table 5.8. For an 8.5 in. (216 mm) thick bridge deck the cost of concrete containing only ordinary portland cement per unit surface area of a deck ($/yd^2) is calculated below; the in-place concrete costs for other systems is calculated accordingly and presented in Table 5.8.

The in-place cost of an 8.5 in. (216 mm) thick concrete deck containing 100% ordinary portland cement per square yard:

$$\frac{\$554.43}{yd^3} \times 8.5in. \times \frac{1yd}{36in.} = \frac{\$130.91}{yd^2}$$

Table 5.8: In-place cost of concrete containing supplementary cementitious materials

Mix type[a]	Cement lb/yd³ (kg/m³)	SCM lb/yd³ (kg/m³)	Replaced cement cost $/yd³ ($/m³)	Replacing SCM cost $/yd³ ($/m³)	Net cost difference $/yd³ ($/m³)	In-place cost $/yd³ ($/m³)	Bridge thickness in. (mm)	In-place cost $/yd² ($/m²)
100% PC	598 (355)	0	0	0	0	554.43 (725.20)	8.5 (216)	130.91 (156.64)
20% FA	506.9 (301.1)	91.1 (54.1)	5.69 (7.46)	2.73 (3.58)	-2.96 (-3.88)	551.47 (721.32)	8.5 (216)	130.21 (155.81)
40% FA	404.3 (240.2)	193.7 (115.1)	12.10 (15.86)	5.81 (7.61)	-6.30 (-8.25)	548.13 (716.95)	8.5 (216)	129.42 (154.86)
5% SF	577.1 (342.8)	20.9 (12.4)	1.31 (1.71)	20.9 (27.28)	19.60 (25.57)	574.02 (750.77)	8.5 (216)	135.53 (162.17)
10% SF	555.5 (333)	42.5 (25.4)	2.66 (3.50)	42.50 (55.88)	39.84 (52.38)	594.27 (777.58)	8.5 (216)	140.31 (167.96)
20% Slag	487.5 (290)	110.5 (65.6)	6.90 (9.04)	7.18 (9.40)	0.28 (0.36)	554.71 (725.56)	8.5 (216)	130.97 (156.72)
40% Slag	372.8 (221.4)	225.2 (133.8)	14.08 (18.44)	14.64 (19.18)	0.56 (0.74)	554.99 (725.94)	8.5 (216)	131.04 (156.80)

[a] 100% PC = Mixture paste containing 100% portland cement
20% FA = Mixture paste containing 20% fly ash and 80% portland cement by volume
40% FA = Mixture paste containing 40% fly ash and 60% portland cement by volume
20% Slag = Mixture paste containing 20% slag cement and 80% portland cement by volume
40% Slag = Mixture paste containing 40% slag cement and 60% portland cement by volume
5% SF = Mixture paste containing 5% silica fume and 95% portland cement by volume
10% SF = Mixture paste containing 10% silica fume and 90% portland cement by volume

The total cost (the sum of in-place costs of reinforcement and concrete) for each system is tabulated in Table 5.9. Comparing the systems without any supplementary cementitious materials, a new bridge deck containing conventional steel has the lowest initial cost, followed by the bridge decks containing ECR, MMFX(4%), MMFX-ECR(2%), MMFX-ECR(4%), Zn, and MMFX(9%). While systems with slag cements have comparable new bridge deck prices to systems containing only cement, the use of fly ash reduces the price and silica fume increases it.

Table 5.9: Total in-place cost for reinforced concrete per unit area of an 8.5 in. (216 mm) bridge deck

System[a]	Concrete cost $/yd^2 ($/m^2)	Reinforcement cost $/yd^2 ($/m^2)	Total cost $/yd^2 ($/m^2)
Conv.	130.91 (156.64)	61.66 (73.22)	192.56 (229.86)
Zn	130.91 (156.64)	97.35 (115.90)	228.26 (272.55)
MMFX(4%)	130.91 (156.64)	78.53 (93.40)	209.44 (250.04)
MMFX(9%)	130.91 (156.64)	102.54 (122.11)	233.45 (278.76)
FA(20)	130.21 (155.81)	61.66 (73.22)	191.86 (229.02)
FA(40)	129.42 (154.86)	61.66 (73.22)	191.08 (228.08)
SF(5)	135.53 (162.17)	61.66 (73.22)	197.19 (235.38)
SF(10)	140.31 (167.96)	61.66 (73.22)	201.97 (241.17)
Slag(20)	130.97 (156.72)	61.66 (73.22)	192.63 (229.94)
Slag(40)	131.04 (156.80)	61.66 (73.22)	192.70 (230.02)
ECR	130.91 (156.64)	68.15 (81.66)	199.05 (238.31)
MMFX-ECR(2%)	130.91 (156.64)	79.18 (94.17)	210.09 (250.82)
MMFX-ECR(4%)	130.91 (156.64)	84.37 (100.38)	215.28 (257.02)
FA-ECR(40)	129.56 (155.03)	68.15 (81.66)	197.70 (236.69)
SF-ECR(10)	140.37 (168.03)	68.15 (81.66)	208.52 (249.69)
Slag-ECR(40)	131.03 (156.79)	68.15 (81.66)	199.17 (238.45)

5.2.2 Repair Costs

A design life of 75 years is assumed for a bridge deck in the current analysis. For corrosion systems with a life expectancy greater than 75 years no repair cost is estimated; for those with time to first repair of less than 75 years, however, one or more concrete deck repairs with a 25-year design life is included. Repair costs are based on an analysis carried out by Darwin et al. (2007)

for a bridge with 8.5 in. (216 mm) thickness, 36 ft (11 m) width, and 150 ft (46 m) length. The repair costs included removing deleterious concrete and replacing with a low-slump dense concrete overlay, bridge rail modifications, approach guard rail replacement, approach pavement work, mobilization, traffic control, and other miscellaneous costs. The total repair cost was estimated as \$292/yd^2 (\$349/m^2) for a bridge deck with conventional steel; however, this estimate is used for the other kinds of reinforcement, such as ECR and MMFX, since the repair construction items are identical (no reinforcement replacement is assumed).

5.2.2.1 Present Value

To compare the cost effectiveness of different corrosion protection systems, the present value of the costs should be considered. The future repair costs are converted to present values using discount rates of 2, 4, and 6% as follows:

$$P = F \times (1+i)^{-n} \tag{5.3}$$

Where:

P = Present value

F = Future cost of repair, \$292/yd^2 (\$349/m^2)

i = Discount rate

n = Time to repair

For instance, for a bridge deck containing conventional steel, as presented in Table 5.6, the expected time to first repair is 13 years; considering a 25-year period for concrete repair over its 75-year design life, the bridge deck will require repair after 13, 38, and 63 years. The total present cost of a bridge containing conventional steel is sum of the initial cost and present values of future repairs, for which a discounted rate of 2% can be calculated as follows:

Total present cost = Initial cost + Present value of repair costs

$$= \frac{\$192.56}{yd^2} + \frac{\$292}{yd^2}\left[(1+0.02)^{-13} + (1+0.02)^{-38} + (1+0.02)^{-63}\right] = \frac{\$639.74}{yd^2}$$

For each corrosion protection system the time to repair, repair costs, and their present value are calculated and listed in Table 5.10. Present values of repair costs are calculated based on 2%, 4%, and 6% discount rates; a value of 2% is used as the primary estimate of the total cost of a bridge over a 75-year design life.

Table 5.10: Present value of repair costs for a bridge deck with different corrosion protection systems

System[a]	Time to repair (year)			Repair cost $/yd^2 ($/m^2)	Present cost $/yd^2 ($/m^2)		
	1	2	3		i=2%	i=4%	i=6%
Conv.	18	43	68	292 (349)	405.02 (484.08)	218.49 (261.14)	131.69 (157.40)
Zn	39	64	-	292 (349)	217.10 (259.50)	87.00 (104.00)	37.10 (44.35)
MMFX(4%)	31	56	-	292 (349)	254.38 (304.03)	119.04 (142.28)	59.14 (70.68)
MMFX(9%)	35	60	-	292 (349)	235.00 (280.87)	101.76 (121.62)	46.84 (55.99)
FA(20)	39	64	-	292 (349)	217.10 (259.49)	86.98 (103.96)	37.10 (44.35)
FA(40)	-	-	-	-	-	-	-
SF(5)	-	-	-	-	-	-	-
SF(10)	-	-	-	-	-	-	-
Slag(20)	-	-	-	-	-	-	-
Slag(40)	-	-	-	-	-	-	-
ECR	64	-	-	292 (349)	82.22 (98.26)	23.72 (28.35)	7.01 (8.38)
MMFX-ECR(2%)	66	-	-	292 (349)	79.03 (94.45)	21.94 (26.22)	6.26 (7.46)
MMFX-ECR(4%)	-	-	-	-	-	-	-
FA-ECR(40)	-	-	-	-	-	-	-
SF-ECR(10)	-	-	-	-	-	-	-
Slag-ECR(40)	-	-	-	-	-	-	-

By summing the initial cost and present value of repair cost considering 2% discount rate, the total costs over a 75-year design life of a bridge deck for different corrosion protection systems are calculated and listed in Table 5.11. A bridge deck containing conventional steel without any supplementary cementitious material has the highest total cost $597.58/yd^2 ($713.94/m^2) over a

75-year design life period. The Zn, MMFX(4%), and MMFX(9%) systems have comparable total costs ($445/yd^2 ($532/m^2), $464/yd^2 ($554/m^2), and $468/yd^2 ($560/m^2), respectively), lower than Conv. system, but still not as cost effective as bridge decks containing epoxy-coated bars ($281.27/yd^2 ($336.58/m^2)). Among systems with epoxy-coated MMFX bars, reinforcement MMFX-ECR(4%) has the least total cost [$215.28/yd^2 ($257.02/m^2)] and is more cost effective than epoxy-coated bars ($281.27/yd^2 ($336.58/m^2)); the MMFX-ECR(2%) system, however, has a total cost ($289.11/yd^2 ($345.27/m^2)) slightly higher than ECR system. Systems containing supplementary cementitious materials are the most cost effective systems studied. While replacing cement with 20% fly ash decreases the total cost to $408.97/yd^2 ($488.51/m^2) when using conventional reinforcement, use of 5% and 10% silica fume, 40% fly ash, and 20% and 40% slag cement reduces the total cost to about $195/yd^2 ($235/m^2), approximately one-third of what would be spent in a bridge deck with conventional reinforcement and only portland cement over a 75-year design period. A bridge deck containing silica fume has a total cost approximately 5% higher than those containing 40% slag cement and 40% fly ash. While using the combination of SCM and ECR increases the total cost over 75 years by about 5% compared to the systems with only SCM, this combination significantly increases the life expectancy and can establish a proper margin of safety to extend the design life of bridge decks over a 75-year period.

Table 5.11: Total costs over 75-year design life of a bridge deck for different corrosion protection systems

System[a]	Initial cost $/yd^2 ($/m^2)	Repair cost with i = 2% $/yd^2 ($/m^2)	Total cost $/yd^2 ($/m^2)
Conv.	192.56 (229.86)	405.02 (484.08)	597.58 (713.94)
Zn	228.26 (272.55)	217.10 (259.50)	445.36 (532.04)
MMFX(4%)	209.44 (250.04)	254.38 (304.03)	463.81 (554.07)
MMFX(9%)	233.45 (278.76)	235.00 (280.87)	468.45 (559.64)
FA(20)	191.86 (229.02)	217.10 (259.49)	408.97 (488.51)
FA(40)	191.08 (228.08)	0	191.08 (228.08)
SF(5)	197.19 (235.38)	0	197.19 (235.38)
SF(10)	201.97 (241.17)	0	201.97 (241.17)
Slag(20)	192.63 (229.94)	0	192.63 (229.94)
Slag(40)	192.70 (230.02)	0	192.70 (230.02)
ECR	199.05 (238.31)	82.22 (98.26)	281.27 (336.58)
MMFX-ECR(2%)	210.09 (250.82)	79.03 (94.45)	289.11 (345.27)
MMFX-ECR(4%)	215.28 (257.02)	0	215.28 (257.02)
FA-ECR(40)	197.57 (236.53)	0	197.57 (236.53)
SF-ECR(10)	208.46 (249.62)	0	208.46 (249.62)
Slag-ECR(40)	199.19 (238.47)	0	199.19 (238.47)

CHAPTER 6: CONCLUSIONS AND RECOMMENDATIONS

6.1 SUMMARY

The performance of several corrosion protection systems in reinforced concrete was evaluated. The investigated corrosion protections systems are:

- Conventional reinforcement and galvanized reinforcement
- Uncoated MMFX steel containing 9% and 4% chromium (ASTM A1035 Type CS and CM, respectively)
- Epoxy-coated MMFX steel containing 4% and 2% chromium (Epoxy-coated ASTM A1035 Type CM and CL steel, respectively)
- Conventional reinforcement in conjunction with ordinary portland cement as the only cementitious material as well as with volume replacements of 20% fly ash, 40% fly ash, 5% silica fume, 10% silica fume, 20% slag cement, and 40% slag cement.
- Conventional epoxy-coated reinforcement in conjunction with 100% ordinary portland cement as well as with volume replacements of 40% fly ash, 10% silica fume, and 40% slag cement as a partial replacing cementitious material.

For all specimens, corrosion potentials and macrocell corrosion rates were monitored on a weekly basis; Linear Polarization Resistance (LPR) tests were carried out for bench-scale specimens every four weeks and rapid macrocell tests every three weeks to determine total corrosion rates.

Critical corrosion loss required to crack concrete cover in specimens containing galvanized bars and conventional steel was investigated, and corrosion performance of galvanized bars and

conventional steel was compared. Admixed salt was introduced to concrete during mixing, and beam specimens were ponded with salt solution to accelerate corrosion. The average critical corrosion loss obtained for conventional steel was used to determine the accuracy of predictive equations introduced in the literature.

The corrosion performance of uncoated and epoxy-coated MMFX steel were evaluated using the rapid macrocell test, Southern Exposure, and cracked beam specimens, and compared to the performance of conventional bare and epoxy-coated bars. The critical chloride threshold of MMFX bars was measured and disbondment test was performed for specimens with epoxy-coated reinforcement.

The effect of partial replacement of cement with supplementary cementitious materials (fly ash, silica fume, and slag cement) on corrosion performance and critical chloride threshold of conventional uncoated and epoxy-coated reinforcement was investigated.

The life-expectancy and cost effectiveness of a bridge deck constructed with each system was estimated for a 75-year design period based on the results obtained from this study.

6.2 CONCLUSIONS

The following conclusions are based on the analysis and results presented in this study:

1- Galvanized rebar exhibits greater life expectancy than conventional steel against corrosion; galvanized steel requires over twice the corrosion loss, and from initiation takes almost four times as long to crack concrete as conventional steel.

2- The average critical corrosion loss to crack concrete with 1-in. cover, is found to be approximately 25 μm, very close to the value obtained by O'Reilly's (2011) predictive

equation (21 µm taking localized corrosion into account and 24 µm assuming general corrosion).

3- The average corrosion loss of MMFX bars containing 9% chromium ranges from 30% to 55% that of conventional steel, while for MMFX bars containing 4% chromium the average corrosion loss is approximately two-thirds of that for conventional steel. The average corrosion rate of MMFX bars containing 9% and 4% chromium based on LPR test were 40% and 50% of that for conventional steel, respectively.

4- The critical chloride threshold of MMFX bars containing 4% and 9% chromium (4.25 lb/yd^3 (2.52 kg/m^3) and 4.54 lb/yd^3 (2.69 kg/m^3), respectively) are about three times of that for conventional steel.

5- While the epoxy-coated MMFX bars containing 2% chromium do not show significantly better performance and cost effectiveness against corrosion compared to conventional epoxy-coated bars, epoxy-coated MMFX bars containing 4% chromium have a greater corrosion resistance and are more cost effective than MMFX-ECR(2%) and conventional epoxy-coated bars.

6- While the use of galvanized steel and uncoated MMFX bars have comparable total costs over a 75-year design life of a bridge deck and are more cost effective than conventional steel, they are not as cost effective as epoxy-coated bars.

7- Among systems containing supplementary cementitious materials along with uncoated reinforcement, the total corrosion losses and corrosion rates are lowest for specimens containing silica fume following by specimens with 40% slag, 40% fly ash, 20% slag, 20% fly ash, and 100% ordinary portland cement. Increasing the amount of SCM lowers the corrosion rates and losses for all mixtures.

8- Increasing the amount of SCM increases the time to initiation, with the longest initiation time in mixtures containing silica fume, followed by slag cement, fly ash, and ordinary portland cement.

9- Concrete containing 40% fly ash and 40% slag exposed to chloride ions show chloride ingress rates almost half of that for specimens containing 20% slag, and one-fifth of that for specimens containing 100% portland cement. Specimens containing silica fume shows the lowest chloride diffusivity rates, one order of magnitude less than that for specimens with 100% ordinary portland cement.

10- While using epoxy-coated bars reduces corrosion losses by two orders of magnitude, using a combination of epoxy-coated bars and supplementary cementitious materials decreases corrosion loss by three orders of magnitude compared to a system containing conventional bare steel without any supplementary cementitious material.

11- Most specimens containing 40% fly ash, 20% slag, 40% slag, and 10% silica fume repassivate after initiation, with corrosion re-initiating at a higher chloride threshold.

12- The initial critical chloride thresholds for slag cement and 40% fly ash specimens are similar to that for 100% ordinary portland cement, but the secondary CCCT values are significantly higher.

13- For 10% silica fume specimens, the initial CCCT value are lower, but the secondary CCCT values are similar to the critical chloride threshold of conventional steel in specimens with 100% portland cement.

14- Based on economic analysis, corrosion protection systems containing supplementary cementitious materials are the most cost-effective systems. The combination of SCM

and ECR will result in the greatest life-expectancy, with costs only slightly higher than systems with SCM and conventional uncoated steel.

6.3 RECOMMENDATIONS

1- Although galvanized steel shows better performance than conventional bars against corrosion, no equation that relates critical corrosion loss to concrete cover and bar diameter was introduced in the literature for galvanized reinforcement. Further investigation with various concrete covers and bar diameters is needed to provide a predictive equation for evaluating critical corrosion loss of galvanized bars in bridge decks.

2- Although epoxy-coated bars are the most cost-effective reinforcement studied, the effect of disbondment of epoxy coating on long-term corrosion resistance and its effect on cost effectiveness is not known. Further investigation is needed to account for possible negative impacts of coating disbondment on corrosion resistance and cost effectiveness of these reinforcement.

3- In future studies, accounting for negative coating disbondment effects in comparing the cost effectiveness of epoxy-coated MMFX bars and conventional ECR, especially for epoxy-coated MMFX bars containing 4% chromium (which shows less disbondment and better performance than conventional ECR), can further exhibit greater cost-effectiveness of these bars against conventional ECR.

4- Since pickling is effective on improving corrosion resistance of MMFX bars containing 9% chromium in the rapid macrocell test, pickled MMFX bars should be evaluated in

the bench-scale tests to further investigate the effectiveness of pickled MMFX bars containing 9% chromium.

5- Additional research is needed to determine why most specimens containing 40% fly ash, 20% slag, 40% slag, and 10% silica fume repassivated after corrosion initiation, and then re-initiated at a higher chloride threshold.

6- Systems with supplementary cementitious materials are the most cost effective systems studied. While a combination of using epoxy-coated bars and SCM increases the cost slightly, it raises the life-expectancy of bridge decks significantly; therefore, using SCM along with ECR is found to be the most effective system studied, and is recommended for construction of bridge decks.

REFERENCES

Akhoondan, M., & Sagüés, A. A. (2012). "Comparative Cathodic Behavior of ~9% Cr and Plain Steel Reinforcement in Concrete," *Corrosion,*Vol. 68, No. 4, 10 pp.

Alonso, C., Andrade, C., Rodrigues, J., & Diez, J. M. (1998). "Factors Controlling Cracking of Concrete Affected by Reinforcement Corrosion," *Materials and Structures,*Vol. 31, No. 211, pp. 435-441.

Andrade, M. C., & Macias, A. (1988). "Galvanized Reinforcements in Concrete," *Surface Coatings-2, A. D. Wilson, J. W. Nicolson, and H. J. Prosser, eds. Elsevier Applied Science publications*, pp. 137-182.

Angst, U. M., Elsener, B., Larsen, C. K., & Vennesland, Ø. (2011). "Chloride Induced Reinforcement Corrosion: Electrochemical Monitoring of Initiation Stage and Chloride Threshold Values," *Corrosion Science,* Vol. 53, No. 4, pp. 1451-1464.

Ann, K. Y., & Song, H.-W. (2007). "Chloride Threshold Level for Corrosion of Steel in Concrete," *Corrosion Science,*Vol. 49, No. 11, pp. 4113-4133.

Arya, C., & Wood, L. A. (1995). "The Relevance of Cracking in Concrete to Corrosion of Reinforcement," *Concrete Society, Slough*, 32 pp.

Arya, C., & Xu, Y. (1995). "Effect of Cement Type on Chloride Binding and Corrosion of Steel in Concrete," *Cement and Concrete Research,*Vol. 25, No. 4, pp. 893-902.

ASTM A955/A955M (2014). "Standard Specification for Deformed and Plain Stainless-Steel Reinforcing Bars for Concrete Reinforcement," ASTM International, West Conshohocken, PA. 13 pp.

Balma, J., Darwin, D., Browning, J. P., and Locke, C. E., (2005) "Evaluation of Corrosion Protection Systems and Corrosion Testing Methods for Reinforcing Steel in Concrete," *SM Report* No. 76, University of Kansas Center for Research, Inc., Lawrence, Kansas, 517 pp.

Beeby, A. (1983). "Cracking, Cover and Corrosion of Reinforcement," *Concrete International,*Vol. 5, No. 2, pp. 35-40.

Bentur, A., Berke, N., & Diamond, S. (1997). "Steel Corrosion in Concrete: Fundamentals and Civil Engineering Practice," London: *E & FN Spon*, 197 pp.

Bertolini, L., Bolzoni, F., Pastore, T., & Pedeferri, P. (2004). "Effectiveness of a Conductive Cementitious Cortar Anode for Cathodic Protection of Steel in Concrete," *Cement and Concrete Research,*Vol. 34, No. 4, pp. 681-694.

Bijen, J. (1996). "Benefits of Slag and Fly Ash," *Construction and Building Materials,*Vol. 10, No. 5, pp. 309-314.

Bouteiller, V., Cremona, C., Baroghel-Bouny, V., & Maloula, A. (2012). "Corrosion Initiation of Reinforced Concretes Based on Portland or GGBS Cements: Chloride Contents and Electrochemical Characterizations versus Time," *Cement and Concrete Research*, Vol. 42, No.11, pp. 1456-1467.

Breit, W., & Schiessl, P. (1997). "Investigation on the Threshold Value of the Critical Chloride Content," Paper presented at the *Fourth CANMET/ACI Conference on Durability of Concrete,* Detroit USA. Vol 2., pp. 363-372.

Browne, R. D. (1980). "Mechanisms of Corrosion of Steel in Concrete in Relation to Design, Inspection, and Repair of Offshore and Coastal Structures," *ACI Special Publication* 65, pp. 169-204.

Cady, P. D., & Weyers, R. E. (1992). "Predicting Service Life of Concrete Bridge Decks Subject to Reinforcement Corrosion," *Corrosion Forms and Control for Infrastructure,* 328 pp.

Castel, A., Vidal, T., Francois, R., & Arliguie, G. (2003). "Influence of Steel-Concrete Interface Quality on Reinforcement Corrosion Induced by Chlorides," *Magazine of Concrete Research,*Vol. 55, No. 2, pp. 151-159.

Chindaprasirt, P., Chotithanorm, C., Cao, H.T., & Sirivivatnanon, V. (2007). "Influence of Fly Ash Fineness on the Chloride Penetration of Concrete," *Construction and Building Materials,*Vol. 21, No. 2, pp. 356-361.

Clemena, G. G., & Virmani, Y. P. (2004). "Comparing the Chloride Resistances of Reinforcing Bars," *Concrete International,*Vol. 26, No. 11, pp. 39-49.

Clifton, J. R., Beeghly, H. F., & Mathey, R. G. (1994). "Non-Metallic Coatings for Concrete Reinforcing Bars," *National Bureau of Standards,* pp. 236-424

Cody, R. D., Cody, A. M., Spry, P. G., & Gan, G.-L. (1996). "Concrete Deterioration by Deicing Salts: an Experimental Study," Paper presented at the *1996 Semisesquicentennial Transportation Conference Proceedings.* pp. 4-7

Darwin, D., Browning, J., Gong, L., & Hughes, S. R. (2007). "Effects of Deicers on Concrete Deterioration," *ACI Materials Journal,*Vol. 105, No. 6, pp. 622-627.

Darwin, D., Browning, J., Nguyen, T.V., and Locke, C.E., Jr. (2002). "Mechanical and Corrosion Properties of a High-Strength, High Chromium Reinforcing Steel for Concrete," *SM Report* No. 66, University of Kansas Center for Research, Inc., Lawrence, Kansas, pp. 142; also South Dakota Department of Transportation Report, SD2001-05-F.

Darwin, D., Browning, J., Nguyen, T., & Locke, C.E. (2007). "Evaluation of Metallized Stainless Steel Clad Reinforcement," *South Dakota Department of Transportation Report, SM Report* No. 90, University of Kansas Center for Research, Inc., Lawrence, Kansas, 156 pp.

Darwin, D., Browning, J , O'Reilly, M, & Lihua Xing, a. J. J. (2009). "Critical Chloride Corrosion Threshold of Galvanized Reinforcing Bars," *ACI Materials Journal,*Vol. 106, No. 2, pp. 176-183.

Darwin, D., Browning, J., O'Reilly, M., Locke, C.E., and Virmani, Y. P. (2011) "Multiple Corrosion Protection Systems for Reinforced Concrete Bridge Components," Publication No. FHWA-HRT-11-060, Federal Highway Administration, *SM Report No.* 101, University of Kansas Center for Research, Inc., Lawrence, Kansas, 255 pp.

Darwin, D., O'Reilly, M., Somogie, I., Sperry, J., Lafikes, J., Storm, S., Browning, J. (2013) "Stainless Steel Reinforcement as a Replacement for Epoxy-Coated Steel in Bridge Decks," *SM Report* No. 105, The University of Kansas Center for Research, Inc., Lawrence, Kansas, 205 pp.

Draper, J., Darwin, D., Browning, J. P., Locke, C. E. (2009), "Evaluation of Multiple Corrosion Protection Systems for Reinforced Concrete Bridge Decks," *SM Report* 96, University of Kansas Center for Research, Inc., Lawrence, Kansas, 429 pp.

El Maaddawy, T. A., & Soudki, K. A. (2003). "Effectiveness of Impressed Current Technique to Simulate Corrosion of Steel Reinforcement in Concrete," *Journal of Materials in Civil Engineering*,Vol. 15, No. 1, pp. 41-47.

Erdoğdu, Ş., Bremner, T., & Kondratova, I. (2001). "Accelerated Testing of Plain and Epoxy-Coated Reinforcement in Simulated Seawater and Chloride Solutions," *Cement and Concrete Research*,Vol. 31, No. 6, pp. 861-867.

Fanous, F., & Wu, H. (2005). "Performance of Coated Reinforcing Bars in Cracked Bridge Decks," *Journal of Bridge Engineering*,Vol. 10, No. 3, pp. 255-261.

FHWA. (2014). "Deficient Bridges by State and Highway Systems," http://www.fhwa.dot.gov/bridge/nbi/no10/defbr14.cfm. Accessed 12/30/2015.

Francois, R., & Arliguie, G. (1999). "Effect of Microcracking and Cracking on the Development of Corrosion in Reinforced Concrete Members," *Magazine of Concrete Research*,Vol. 51, No. 2, pp. 143-150.

Glass, G. K. (2000). "The Participation of Bound Chloride in Passive Film Breakdown on Steel in Concrete," *Corrosion Science*,Vol. 42, No. 11, pp. 2013-2021.

Garcia, V., François, R., Carcasses, M., & Gegout, P. (2014). "Potential Measurement to Determine the Chloride Threshold Concentration that Initiates Corrosion of Reinforcing Steel Bar in Slag Concretes," *Materials and Structures*, Vol. 47, No. 9, pp. 1483-1499.

Gong, L., Darwin, D., Browning, J. P., & Carl E. Locke, J. (2003). "Evaluation of Mechanical and Corrosion Properties of MMFX Reinforcing Steel for Concrete," *Kansas Department of Transportation, Report FHWA-KS-02-8*, 114 pp.

Gu, P., & Beaudoin, J. J. (1998). "Obtaining Effective Half-Cell Potential Measurements in Reinforced Concrete Structures," *Institute for Research in Construction, National Research Council of Canada*, No. 18, 4 pp.

Haran, B. S., N., B., Popov, M. F., Ralph, P., & White, E. (2000). "Studies on Galvanized Carbon Steel in $Ca(OH)_2$ Solutions," *Materials Journal*,Vol. 97, No. 4, pp 425-431.

Hime, W. G., & Machin, M. (1993). "Performance Variances of Galvanized Steel in Mortar and Concrete," *Corrosion*,Vol. 49, No. 10, pp. 858-860.

Holloway, M., & Sykes, J. M. (2005). "Studies of the Corrosion of Mild Steel in Alkali-Activated Slag Cement Mortars with Sodium Chloride Admixtures by a Galvanostatic Pulse Method," *Corrosion science*, Vol. 47, No. 12, pp. 3097-3110.

Hooton, R. D. (1986). "Permeability and Pore Structure of Cement Pastes Containing Fly Ash, Slag, and Silica Fume" *Blended Cements, ASTM STP 897*, G. Frohnsdorff, Ed., American Society for Testing and Materials, Philadelphia, pp. 128-143.

Hong, K., & Hooton, R. D. (1999). "Effects of Cyclic Chloride Exposure on Penetration of Concrete Cover," *Cement and Concrete Research,*Vol. 29, No. 9, pp. 1379-1386.

Hussain, S. E., Al-musallam, A., & Al-ghahtani, A. S. (1995). "Factors Affecting Threshold Chloride for Reinforcement Corrosion in Concrete," *Cement and Concrete Research,*Vol. 25, No. 7, pp. 1543-1555.

Hussain, S. E., & Rasheeduzzafar. (1994). "Corrosion Resistance Performance of Fly Ash Blended Cement Concrete," *Materials Journal,*Vol. 91, No. 3, pp. 264-272.

Ji, J., Darwin, D., and Browning, J. P. (2005). "Corrosion Resistance of Duplex Stainless Steels and MMFX Microcomposite Steel for Reinforced Concrete Bridge Decks," *SM Report* 80, University of Kansas Center for Research, Inc., Lawrence, Kansas, 507 pp.

Jones, D. A. (1996). "Principles and Prevention of Corrosion,*"* New York: *Macmillan Publising Co.* 500 pp.

Kepler, J.L., Darwin, D., and Locke, C.E., Jr. (2000) "Evaluation of Corrosion Protection Methods for Reinforced Concrete Highway Structures," *SM Report* No. 58, University of Kansas Center for Research, Inc., Lawrence, Kansas, 221 pp

Koch, G. H., Brongers, M. P., Thompson, N. G., Virmani, Y. P., & Payer, J. H. (2002). "Corrosion Cost and Preventive Strategies in the United States," *Federal Highay Administration,* FHWA-RD-01-156, 784 pp.

Kranc, S. C., Sagues, A. A., Francisco, J., & Presuel-Moreno. (2002). "Decreased Corrosion Initiation Time of Steel in Concrete due to Reinforcing Bar Obstruction of Diffusional Flow," ACI *Materials Journal,*Vol. 99, No. 1, pp 51-53.

Lambert, P., Page, C., & Vassie, P. (1991). "Investigations of Reinforcement Corrosion. 2. Electrochemical Monitoring of Steel in Chloride-Contaminated Concrete," *Materials and Structures,*Vol. 24, No. 5, pp. 351-358.

Lee, H., Cody, R. D., Cody, A. M., & Spry, P. G. (2000). "Effects of Various Deicing Chemicals on Pavement Concrete Deterioration," Paper presented at the *Mid-Continente Transportation Symposium Proceedings*. pp. 151-155

Lindquist, W. D., Darwin, D., Browning, J., & Miller, G. (2006). "Effect of Cracking on Chloride Content in Concrete Bridge Decks," *ACI Materials Journal,*Vol. 103, No. 6, 467 pp.

Mackechnie, J. R., & Alexander, M. G. (1996). "Marine Exposure of Concrete under Selected South African Conditions," *ACI Special Publication* 163, pp. 201-214.

Mangat, P., Khatib, J., & Molloy, B. (1994). "Microstructure, Chloride Diffusion and Reinforcement Corrosion in Blended Cement Paste and Concrete," *Cement and Concrete Composites,*Vol. 16, No. 2, pp. 73-81.

Mangat, P., & Molloy, B. (1992). "Factors Influencing Chloride-Induced Corrosion of Reinforcement in Concrete," *Materials and Structures,*Vol. 25, No. 7, pp. 404-411.

Manning, D. G. (1996). "Corrosion Performance of Epoxy-Coated Reinforcing Steel: North American Experience," *Construction and Building Materials,*Vol. 10, No. 5, pp. 349-365.

McDonald, D. B., Pfeifer, D. W., & Sherman, M. R. (1998). "Corrosion Evaluation of Epoxy-Coated, Metallic-Clad and Solid Metallic Reinforcing Bars in Concrete," *Federal Highay Administration*, No. FHWA-RD-98-153, 140 pp.

McDonald, D. B., Pfeifer, D. W., Sherman, M. R., & Blake, G. T. (1996). "Slowing Corrosion Damage in Concrete: The Use of Organic-Coated, Ceramic-Clad, Metallic-Clad and Solid Metallic Reinforcing Bars," Paper presented at the *Materials for the New Millennium*, pp. 1266-1275

McHattie, J., Perez, I., & Kehr, J. (1996). "Factors Affecting Cathodic Disbondment of Epoxy Coatings for Steel Reinforcing Bars," *Cement and Concrete Composites,*Vol. 18, No. 2, pp. 93-103.

Mindess, S., Young, J. F., & Darwin;, D. (2002). "Concrete,*"* (second ed.): *Prentice Hall*. 644 pp.

Monticelli, C., Natali, M. E., Balbo, A., Chiavari, C., Zanotto, F., Manzi, S., & Bignozzi, M. C. (2016). "Corrosion Behavior of Steel in Alkali-Activated Fly Ash Mortars in the Light of their Microstructural, Mechanical and Chemical Characterization," *Cement and Concrete Research*, VoL. 80, pp. 60-68.

O'Reilly, M., Darwin, D., Browning, J.P., and Locke, Jr., C. E. (2011), "Evaluation of Multiple Corrosion Protection Systems for Reinforced Concrete Bridge Decks," *SM Report 100*, University of Kansas Center for Research, Inc., Lawrence, Kansas, 535 pp.

Oh, B. H., & Jang, S. Y. (2003). "Experimental Investigation of the Threshold Chloride Concentration for Corrosion Initiation in Reinforced Concrete Structures," *Magazine of Concrete Research,*Vol. 55, No. 2, pp. 117-124.

Oh, B. H., Kim, K. H., & Bong Seok, J. (2009). "Critical Corrosion Amount to Cause Cracking of Reinforced Concrete Structures," *ACI Materials Journal,*Vol. 106, No. 4, pp. 333-339.

Otieno, M. B., Alexander, M. G., & BeushausenOtieno, H.-D. (2010). "Corrosion in Cracked and Uncracked Concrete – Influence of Crack Width, Concrete Quality and Crack Reopening," *Magazine of Concrete Research,*Vol. 62, No. 6, pp. 393-404.

Page, C., & Vennesland, Ø. (1983). "Pore Solution Composition and Chloride Binding Capacity of Silica-Fume Cement Pastes," *Matériaux et Construction,*Vol. 16, No. 1, pp. 19-25.

Pettersson, K., Jorgenson, O., & FidjestolI, P. (1996). "The Effect of Cracks on Reinforcement Corrosion in High-Performance Concrete in a Marine Environment," *ACI Special Publication* 163, pp. 185-200.

Presuel-Moreno, F., Scully, J. R., & Sharp, S. R. (2010). "Literature Review of Commercially Available Alloys That Have Potential as Low-Cost, Corrosion-Resistant Concrete Reinforcement," *Corrosion,*Vol. 66, 13 pp.

Presuel-Moreno, F. J., & Moreno, E. I. (2016). Effect of Fly Ash and Silica Fume on Time to Corrosion Initiation for Specimens Exposed Long Term to Seawater," *ACI Special Publication* 308, pp. 1-20.

Rasheeduzzafar, Al-saadoun, S. S., & Al-gahtani, A. S. (1992). "Corrosion Cracking in Relation to Bar Diameter, Cover, and Concrete Quality," *Journal of Materials in Civil Engineering,*Vol. 4, No. 4, pp. 327-342.

Rasheeduzzafar, Dakhil, F. H., Bader, M. A., & Mukarram Khan, M. (1992). "Performance of Corrosion-Resisting Steels in Chloride-Bearing Concrete," *ACI Materials Journal,*Vol. 89, No. 5, pp. 439-448.

Rasheeduzzafar, Ehtesham Hussain, S., & Al-Gahtani, A. S. (1991). "Pore Solution Composition and Reinforcement Corrosion Characteristics of Microsilica Blended Cement Concrete," *Cement and Concrete Research,*Vol. 21, No. 6, pp. 1035-1048.

Redaelli, E., Bertolini, L., & Elsener, B. (2013). "Corrosion of Steel in Concrete : Prevention, Diagnosis, Repair (2nd Edition),*" John Wiley & Sons*. 414 pp.

Rodriguez, O. G., & Hooton, R. D. (2003). "Influence of Cracks on Chloride Ingress into Concrete," *ACI Materials Journal,*Vol. 100, No. 2, pp. 120-126.

Roventi, G., Bellezze, T., Giuliani, G., & Conti, C. (2014). "Corrosion Resistance of Galvanized Steel Reinforcements in Carbonated Concrete: Effect of Wet–Dry Cycles in Tap Water and in Chloride Solution on the Passivating Layer," *Cement and Concrete Research,*Vol. 65, pp. 76-84.

Samples, L. M. (1998). "Durability of Concrete Bridge Decks with Emphasis on Epoxy-Coated Bars," (Ph.D), *Purdue University*. 271 pp.

Saraswathy, V., & Song, H.-W. (2005). "Performance of Galvanized and Stainless Steel Rebars in Concrete under Macrocell Corrosion Conditions," *Materials and Corrosion,*Vol. 56, No. 10, pp. 685-691.

Schiegg, Y., Büchler, M., & Brem, M. (2009). "Potential Mapping Technique for the Detection of Corrosion in Reinforced Concrete Structures: Investigation of Parameters Influencing the Measurement and Determination of the Reliability of the Method," *Materials and Corrosion,*Vol. 60, No. 2, pp. 79-86.

Scott, A., & Alexander, M. (2007). "The influence of Binder Type, Cracking and Cover on Corrosion Rates of Steel in Chloride-Contaminated Concrete," *Magazine of Concrete Research,*Vol. 59, No. 7, pp. 495-505.

Sirivivatnanon, V., Bucea, L., Meck, E., Yozghatlian, S., & C ao, H. (1994). "Influence of Fly Ash, Ground Granulated Blast Furnace Slag and Silica Fume on Chloride Induced Corrosion of Steel Reinforcement [Keynote paper]," Paper presented at the *Second International Symposium on Blended Cements, Malaysia*., pp. 114-120

Smith, L., Kessler, R., & Powers, R. G. (1993). "Corrosion of Epoxy-Coated Rebar in a Marine Environment," *Transportation Research Circular*, No. 403, pp. 36-45.

Soylev, T. A., & Francois, R. (2003). "Quality of Steel–Concrete Interface and Corrosion of Reinforcing Steel," *Cement and Concrete Research,*Vol. 33, No. 9, pp. 1407-1415.

Suda, K., Misra, S., & Motohashi, K. (1993). "Corrosion Products of Reinforcing Bars Embedded in Concrete," *Corrosion Science,*Vol. 35, No. 5–8, pp. 1543-1549.

Thomas, M. (1996). "Chloride Thresholds in Marine Concrete," *Cement and Concrete Research,*Vol. 26, No. 4, pp. 513-519.

Thomas, M. D. A., & Matthews, J. D. (2004). "Performance of PFA Concrete in a Marine Environment—10-Year Results," *Cement & Concrete Composites,*Vol. 26, No. 1, pp. 5-20.

Torres-Acosta, A. A., & Sagues, A. A. (2004). "Concrete Cracking by Localized Steel Corrosion--Geometric Effects," *ACI Materials Journal,*Vol. 101, No. 6, pp. 501-507.

Treadaway, K., & Davies, H. (1989). "Performance of Fusion-Bonded Epoxy-Coated Steel Reinforcement," *Structural Engineer,*Vol. 67, No. 6, pp. 99-108.

Trejo, D., & Pillai, R. G. (2004). "Accelerated Chloride Threshold Testing? Part II: Corrosion-Resistant Reinforcement," *ACI Materials Journal,*Vol. 101, No. 1, pp. 57-64.

Tromans, D. (1980). "Anodic Polarization Behavior of Mild Steel in Hot Alkaline Sulfide Solutions," *Journal of the Electrochemical Society,*Vol. 127, No. 6, pp. 1253-1256.

Tuutti, K. (1980). "Service life of Structures with Regard to Corrosion of Embedded Steel," *ACI Special Publication,*Vol. 65, pp. 223-236.

Verbeck, G. (1975). "Mechanisms of Corrosion of Steel in Concrete," *American Concrete Institute, Farmington Hills, MI,* 17 pp.

Virmani, Y. P., & Clemeña, G. G. (1998). "Corrosion Protection Concrete Bridges," *Federal Highway Administration,*Vol. Report No. FHWA-RD-98-099, 72 pp.

Weyers, R. E., Pyc, W., & Sprinkel, M. M. (1998). "Estimating the Service Life of Epoxy-Coated Reinforcing Steel," *ACI Materials Journal,*Vol. 95, No. 5, pp. 546-557.

Wipf, T. J., Phares, B. M., & Fanous, F. (2006). "Evaluation of Corrosion Resistance of Different Steel Reinforcement Types," *Center for Transportation Research and Education, Iowa State University,* 75 pp.

Xu, A., & Shayan, A. (2016). "Relation between Reinforcing Bar Corrosion and Concrete Cracking," *ACI Materials Journal,*Vol. 113, No. 1, pp. 3-12.

Yeomans, S. R. (1994). "Performance of Black, Galvanized, and Epoxy-Coated Reinforcing Steels in Chloride-Contaminated Concrete," *Corrosion,*Vol. 50, No. 1, pp. 72-81.

Yonezawa, T. (1988). "Pore Solution Composition and Chloride Effects on the Corrosion of Steel in Concrete," *Corrosion,*Vol. 44, No. 7, pp. 489-499.

Youping, L., & Richard, E. W. (1998). "Modeling the Time-to-Corrosion Cracking in Chloride Contaminated Reinforced Concrete Structures," ACI *Materials Journal,*Vol. 95, No. 6, pp. 675-680.

Yu, H. (2007a). "Effects of Reinforcement and Coarse Aggregates on Chloride Ingress into Concrete and Time-to-Corrosion: Part 1 - Spatial Chloride Distribution and Implications," *Corrosion,*Vol. 63, No. 9, pp. 843-849.

Yu, H. (2007b). "Effects of Reinforcement and Coarse Aggregates on Chloride Ingress into Concrete and Time-to-Corrosion: Part 2 - Spatial Aggregates Distribution of Coarse," *Corrosion*,Vol. 63, No. 10, pp. 924-931.

Zayed, A. M., & Sagues, A. (1989). "Corrosion of Epoxy-Coated Reinforcing Steel in Concrete," *Corrosion*, pp. 89-379.

APPENDIX A

AVERAGE MACROCELL AND LPR CORROSION RATE AND LOSS, AND CORROSION POTENTIAL OF TOP AND BOTTOM MATS OF BEAM SPECIMENS CONTAINING CONVENTIONAL AND GALVANIZED STEEL

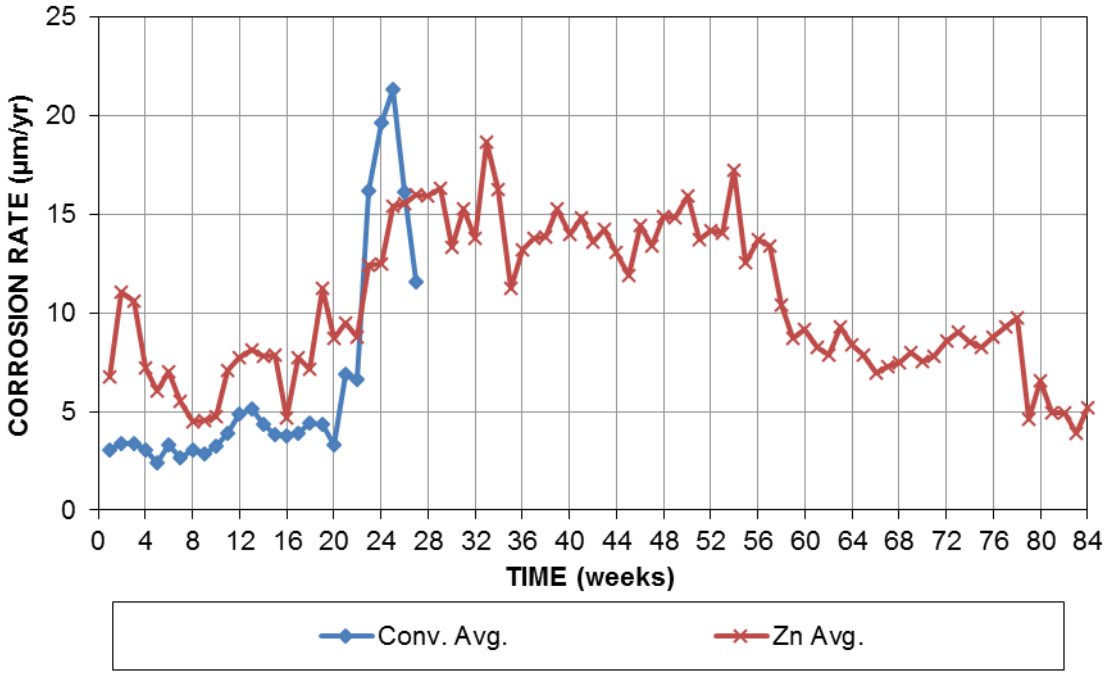

Figure A.1— Average macrocell corrosion rates (µm/yr) for beam specimens containing conventional and galvanized steel

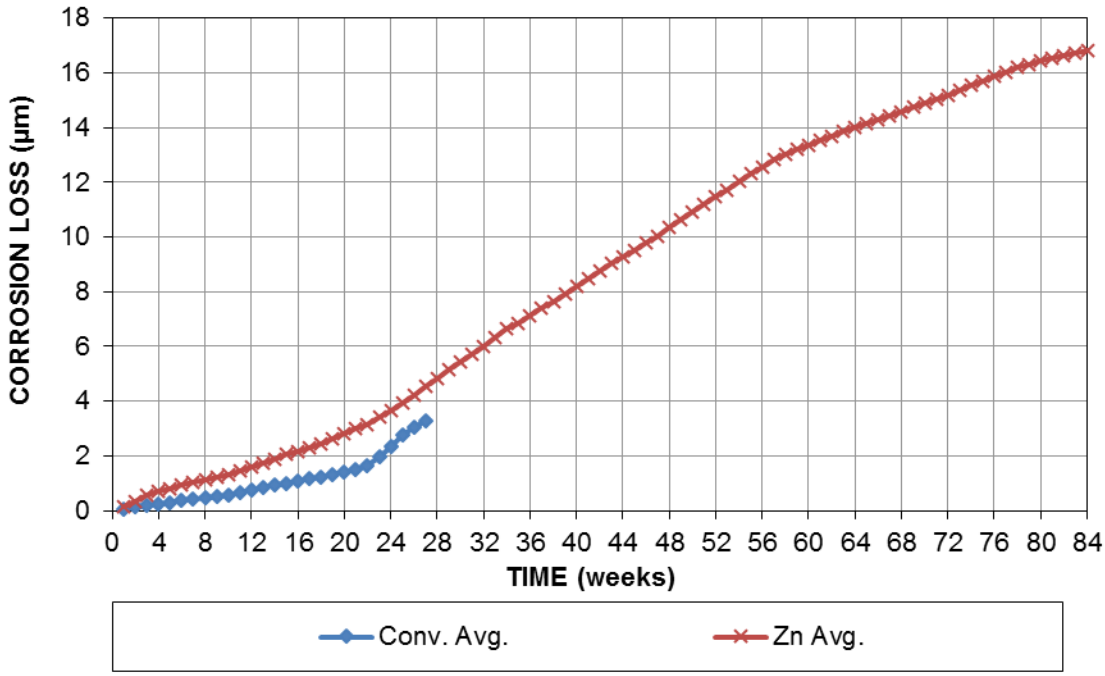

Figure A.2— Average macrocell corrosion losses (µm) for beam specimens containing conventional and galvanized steel

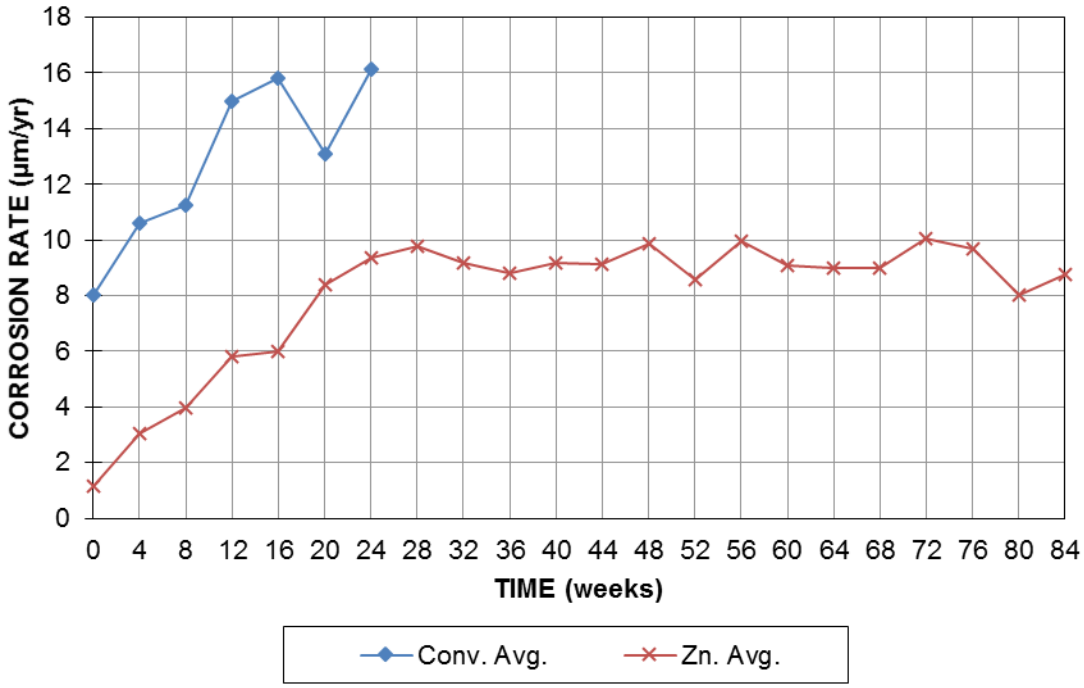

Figure A.3— Average LPR test corrosion rates (µm/yr) for beam specimens containing conventional and galvanized steel

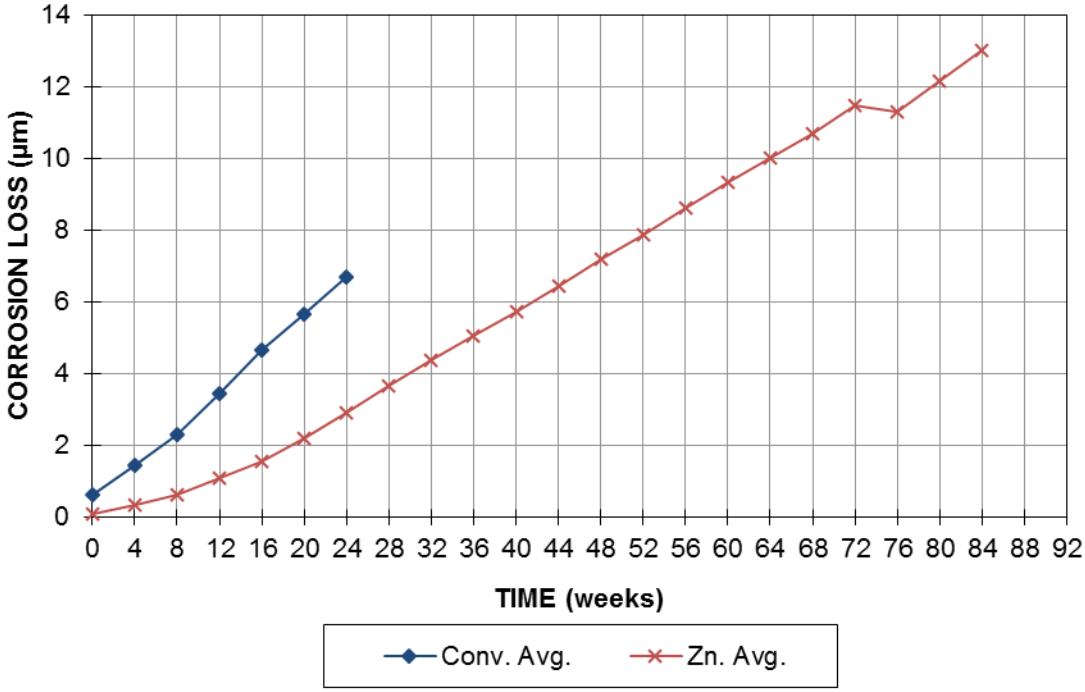

Figure A.4— Average LPR test corrosion losses (µm) for beam specimens containing conventional and galvanized steel

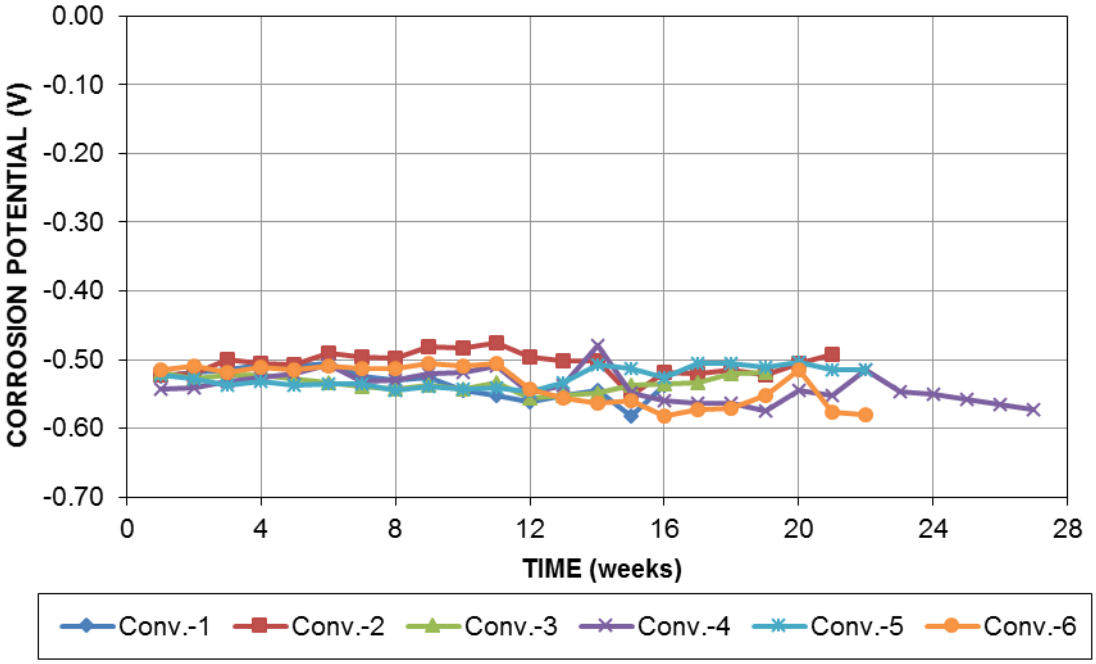

Figure A.5— Corrosion potentials (V) versus CSE for top mat of beam specimens containing conventional steel

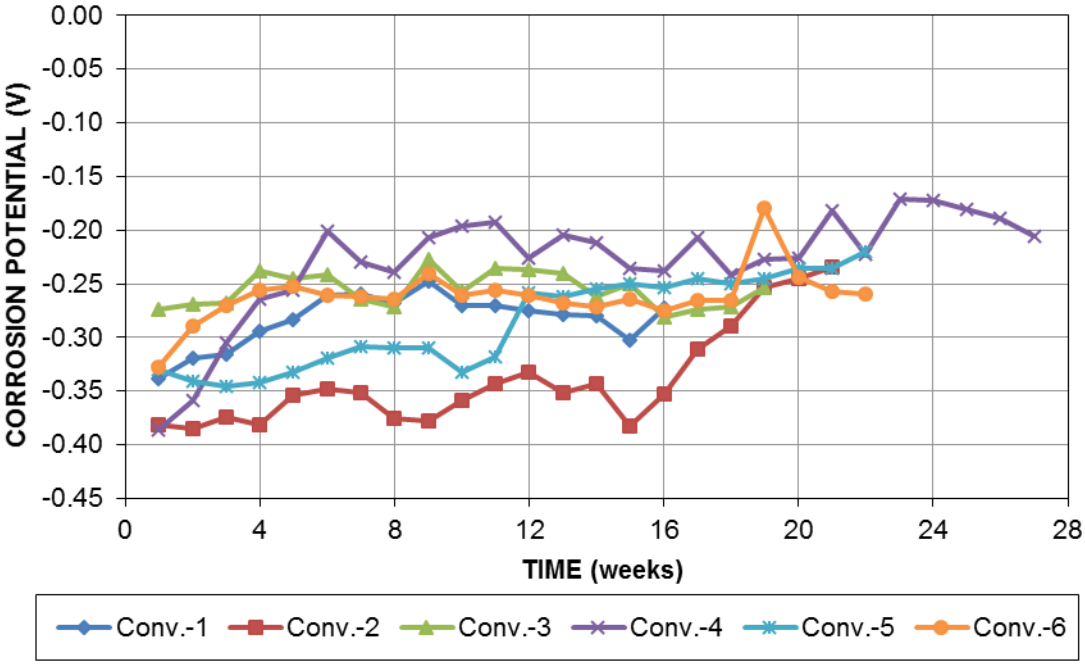

Figure A.6—Corrosion potentials (V) versus CSE for bottom mat of beam specimens containing conventional steel

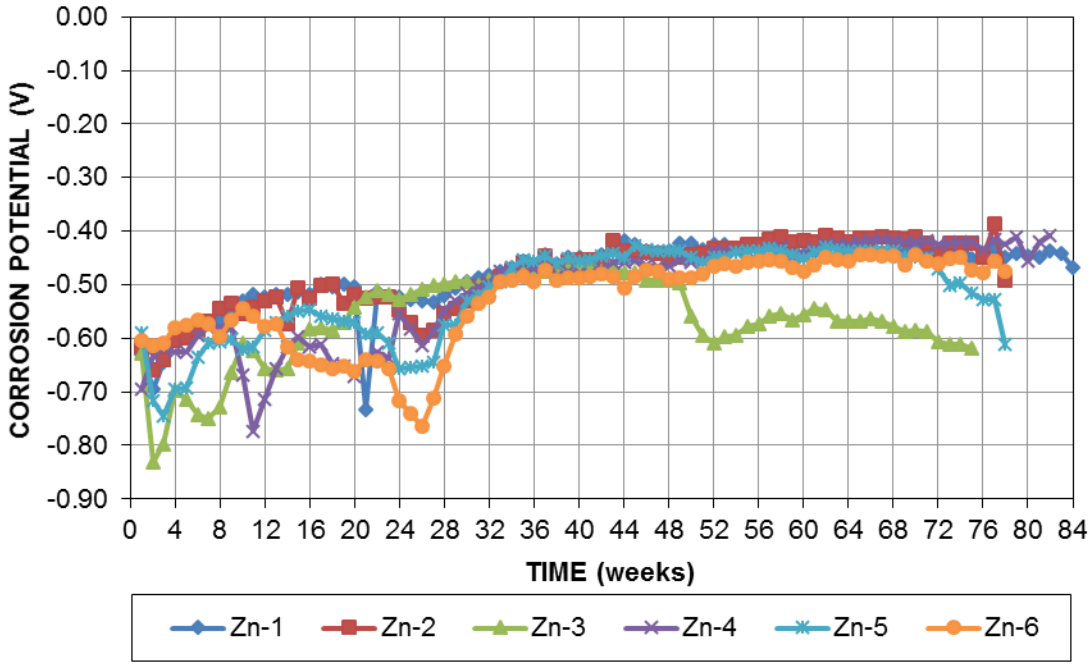

Figure A.7— Corrosion potentials (V) versus CSE for top mat of beam specimens containing galvanized steel

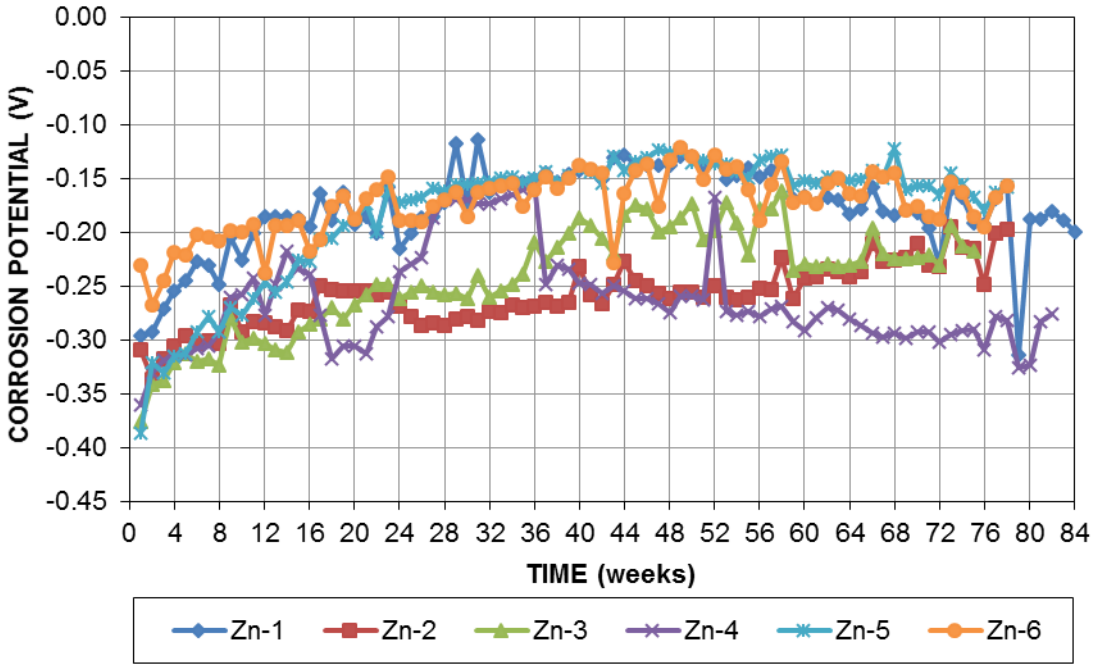

Figure A.8— Corrosion potentials (V) versus CSE for bottom mat of beam specimens containing galvanized steel

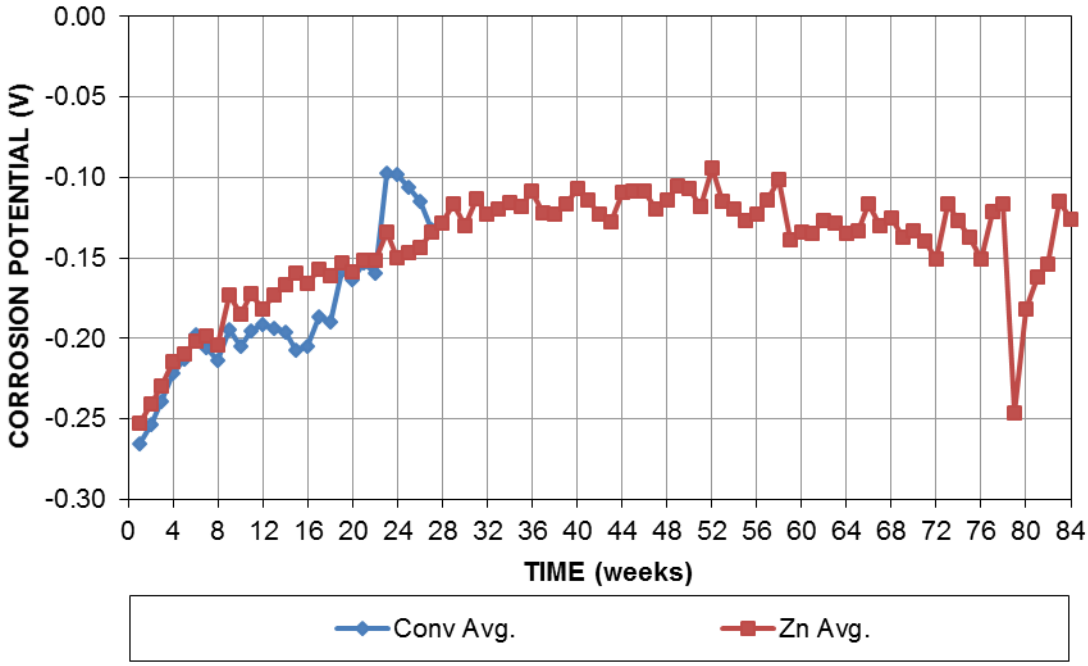

Figure A.9— Average corrosion potentials versus CSE (V) for bottom mat of beam specimens containing conventional and galvanized steel

APPENDIX B

MACROCELL LOSS OF SOUTHERN EXPOSURE AND CRACKED BEAM SPECIMENS CONTAINING BARE AND EPOXY-COATED MMFX REINFORCEMENT

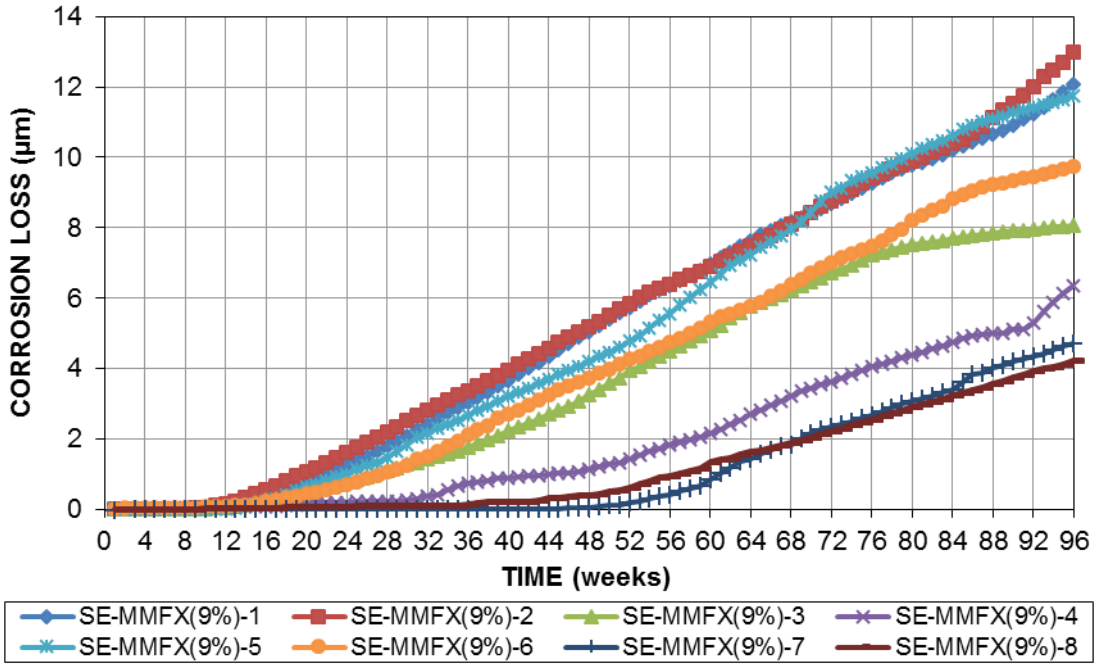

Figure B.1— Macrocell corrosion losses (µm) for Southern Exposure specimens containing MMFX(9%) bars

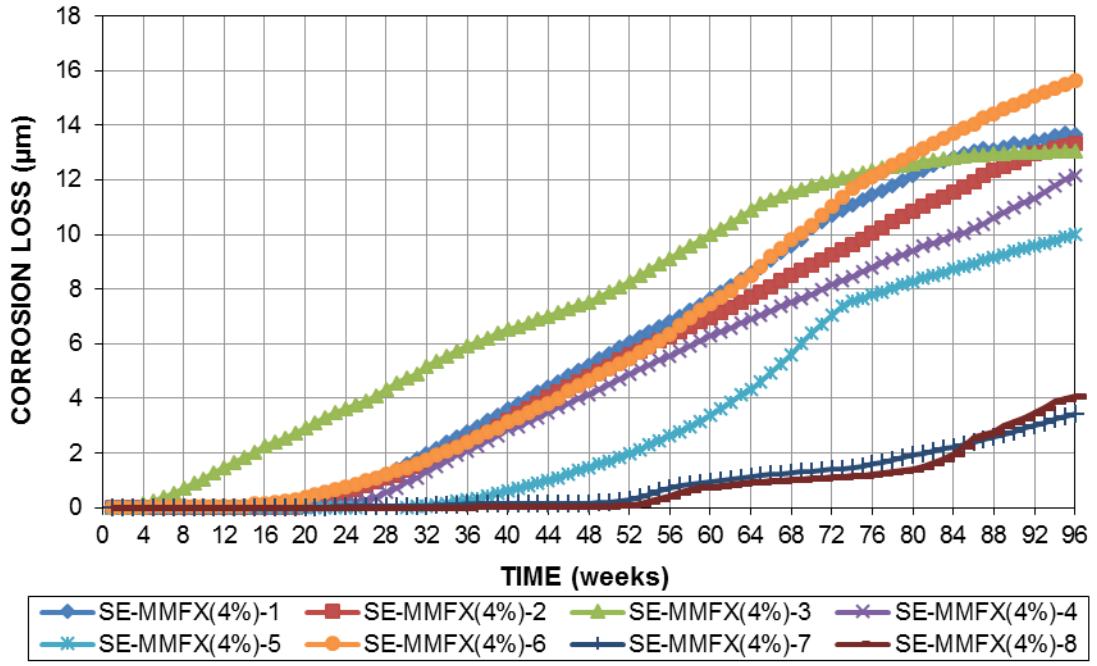

Figure B.2— Macrocell corrosion losses (µm) for Southern Exposure specimens containing MMFX(4%) bars

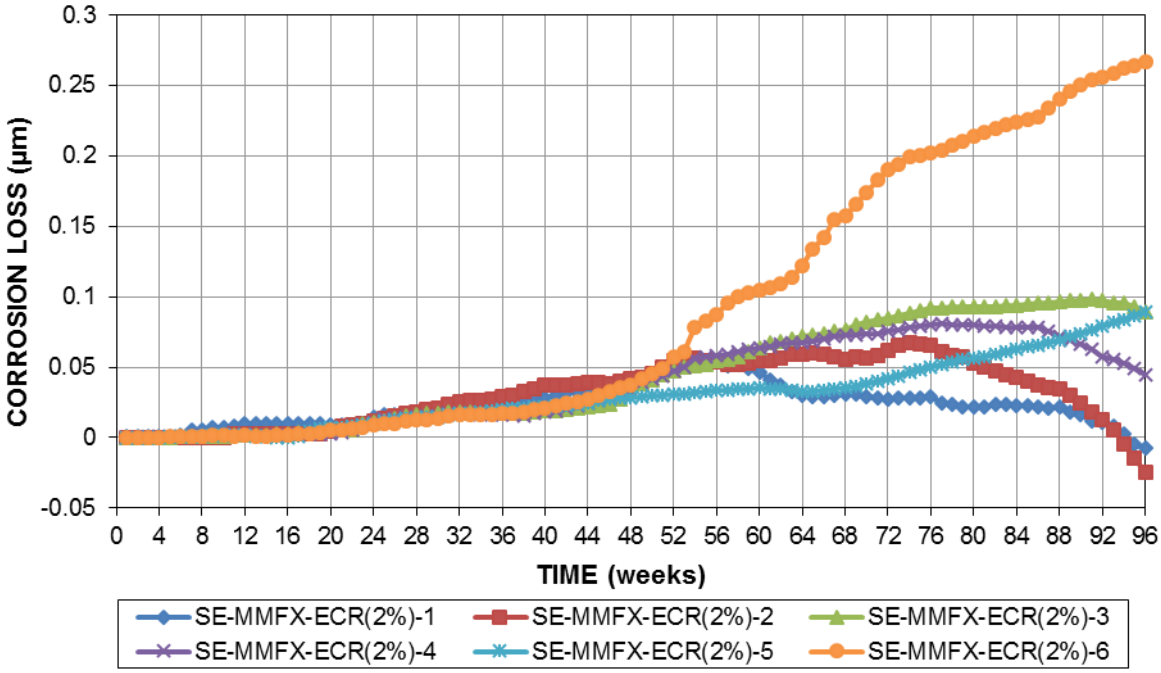

Figure B.3— Macrocell corrosion losses (µm) based on total area of reinforcement for Southern Exposure specimens containing MMFX-ECR(2%) bars

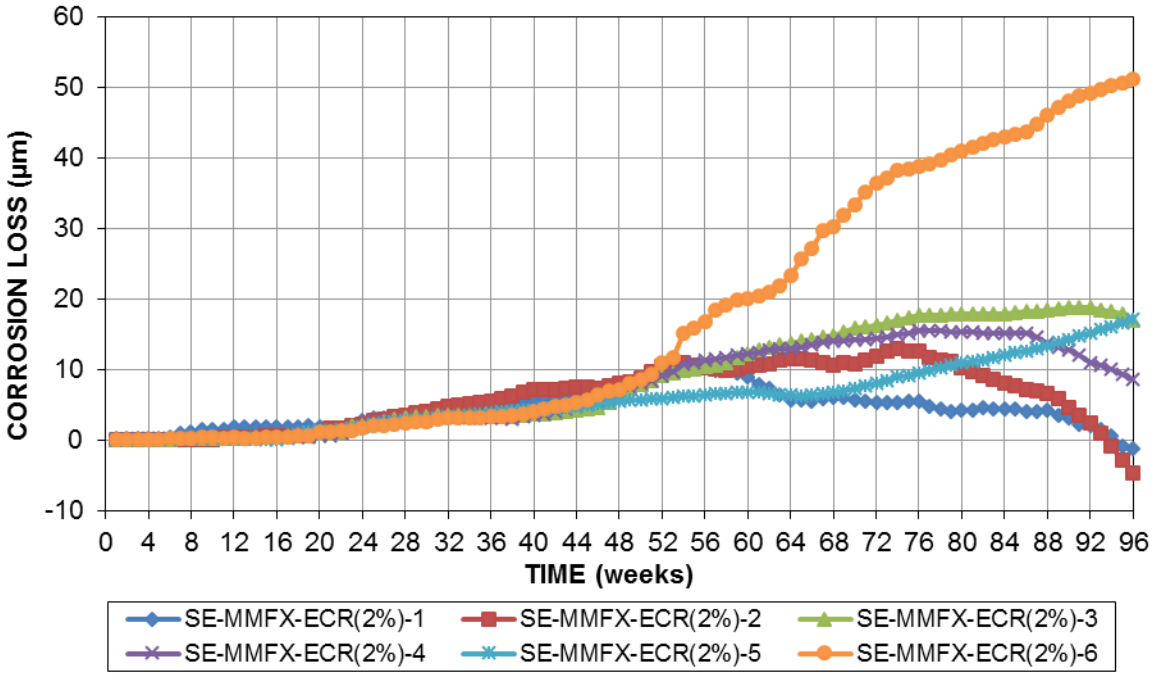

Figure B.4— Macrocell corrosion losses (µm) based on exposed area of reinforcement for Southern Exposure specimens containing MMFX-ECR(2%) bars

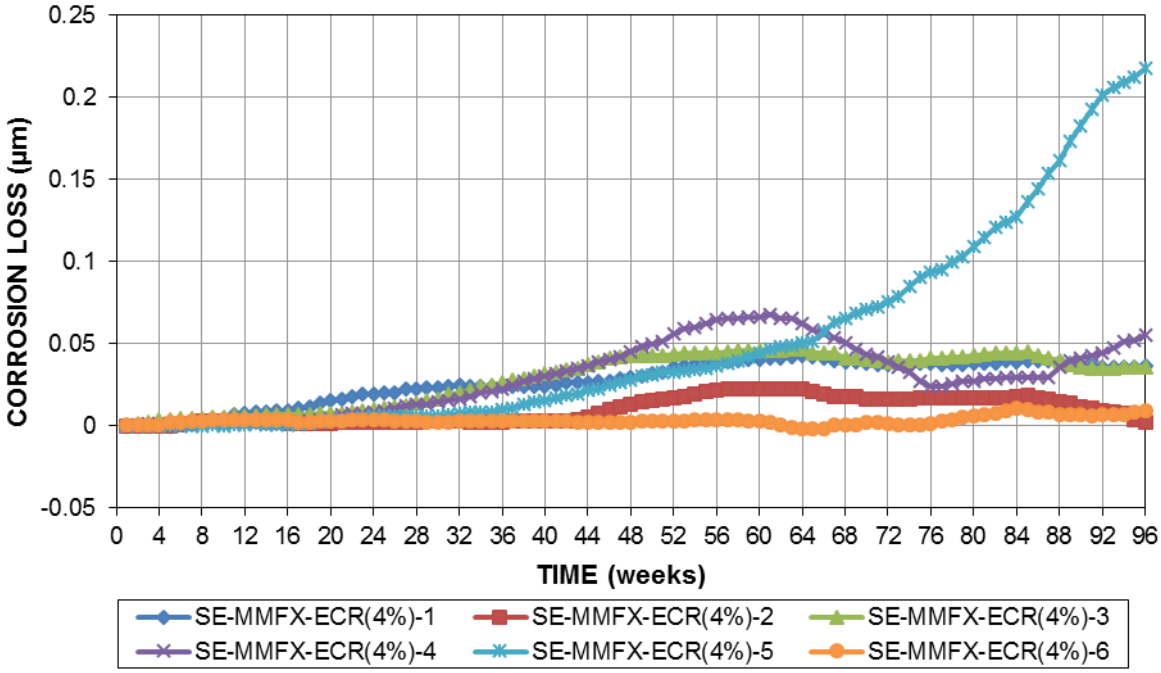

Figure B.5— Macrocell corrosion losses (µm) based on total area of reinforcement for Southern Exposure specimens containing MMFX-ECR(4%) bars

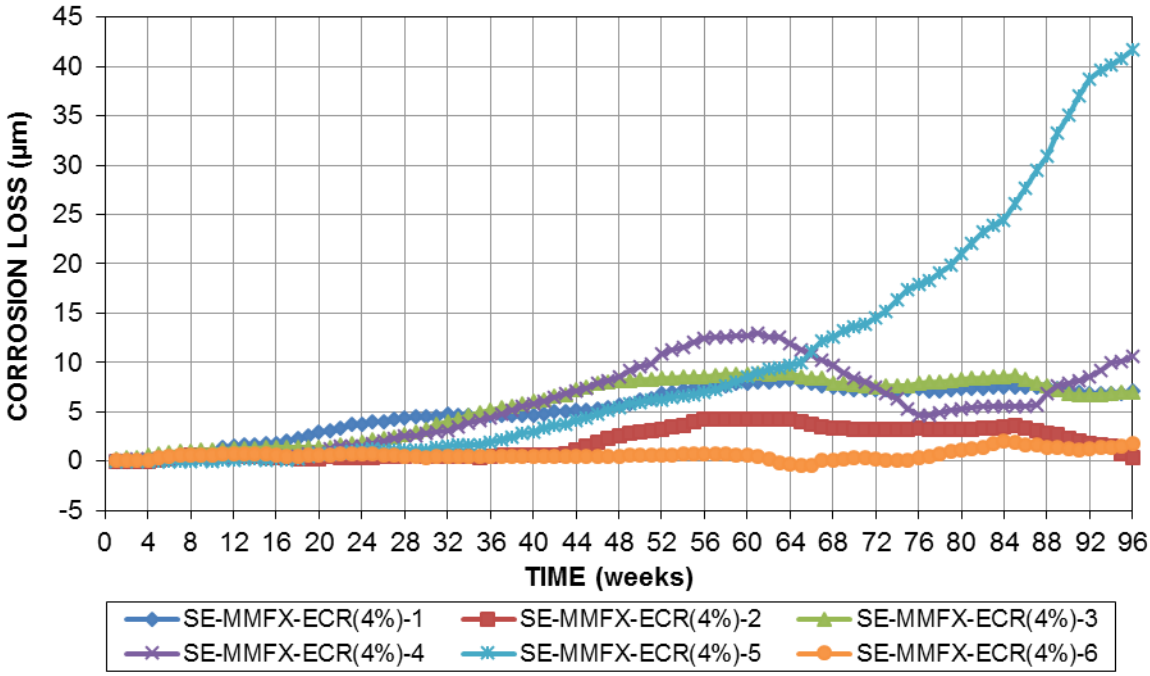

Figure B.6— Macrocell corrosion losses (µm) based on exposed area of reinforcement for Southern Exposure specimens containing MMFX-ECR(4%) bars

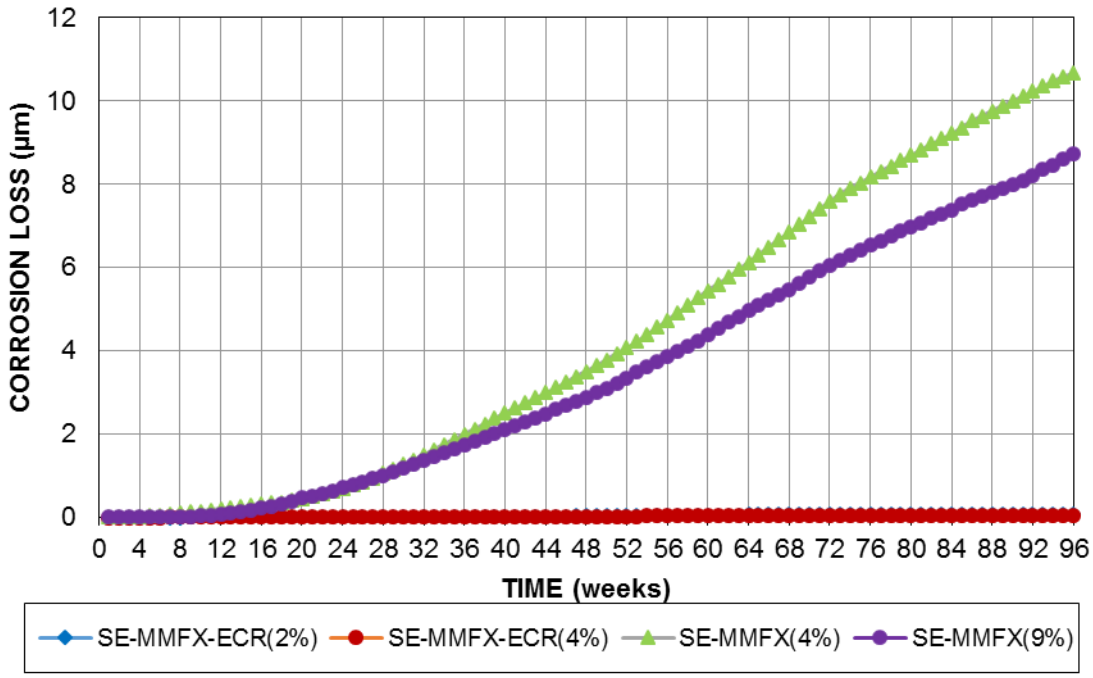

Figure B.7— Average corrosion loss (µm) based on total area versus time for Southern Exposure specimens

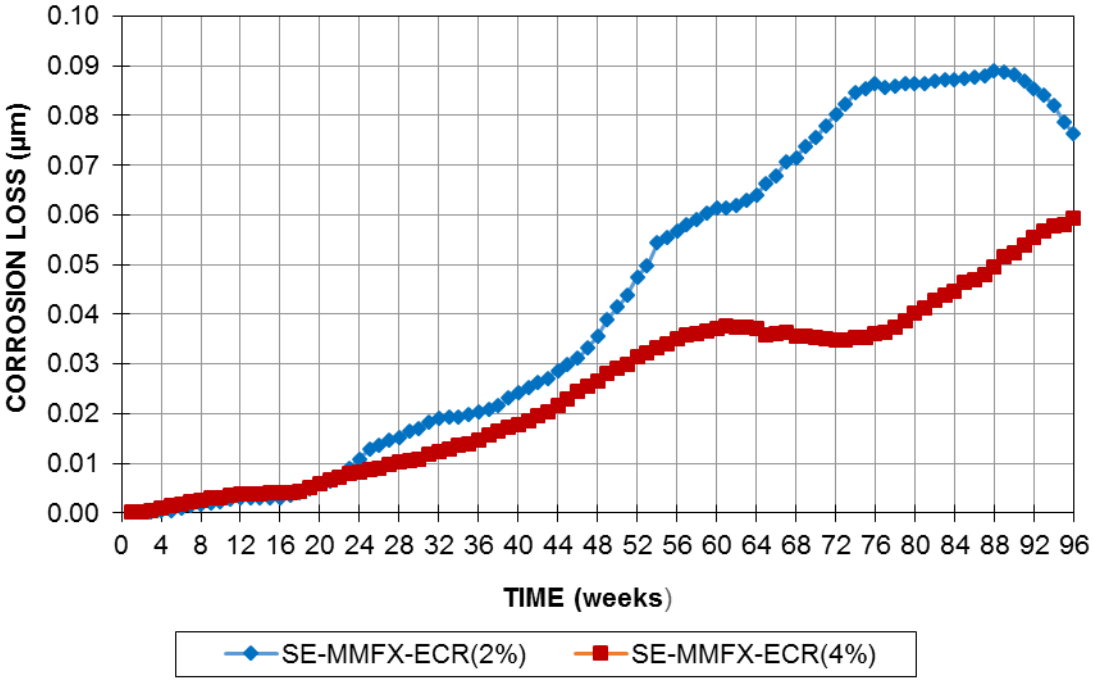

Figure B.8— Average corrosion loss (µm) based on total area versus time for Southern Exposure specimens with epoxy-coated reinforcement

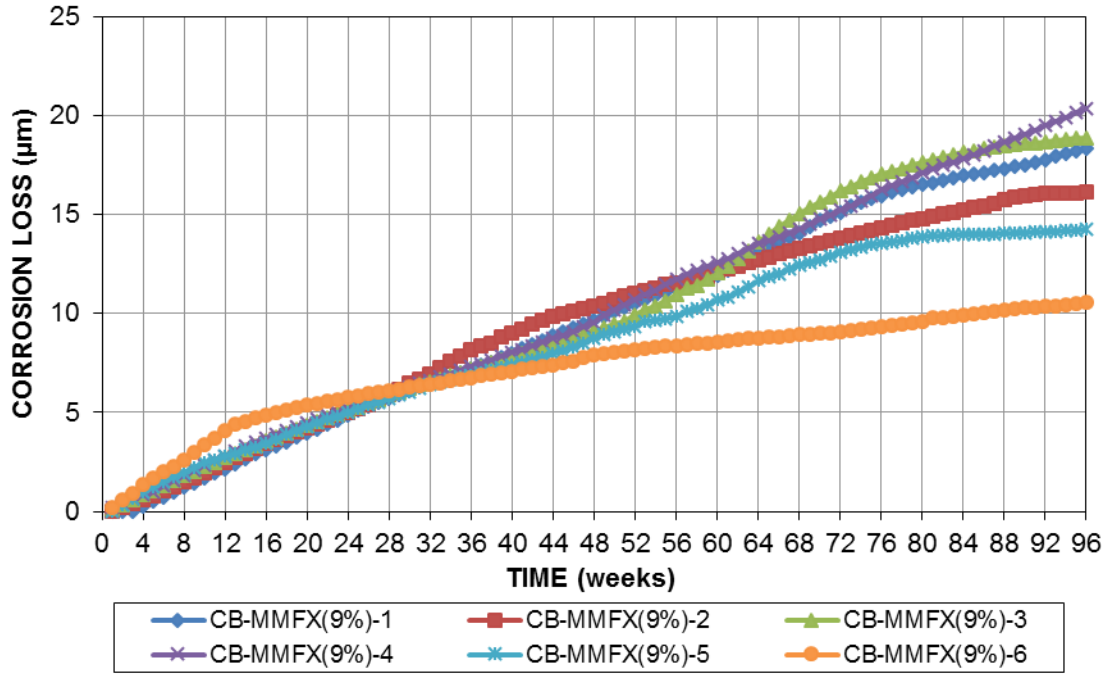

Figure B.9— Macrocell corrosion losses (µm) for cracked beam specimens containing MMFX(9%) bars

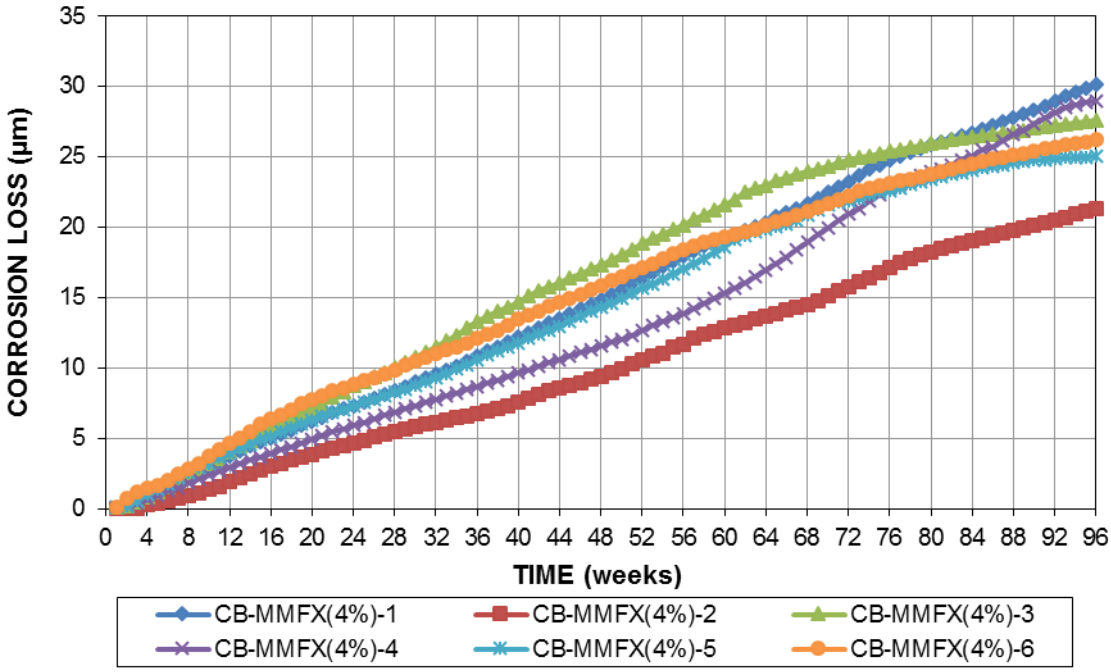

Figure B.10— Macrocell corrosion losses (µm) for cracked beam specimens containing MMFX(4%) bars

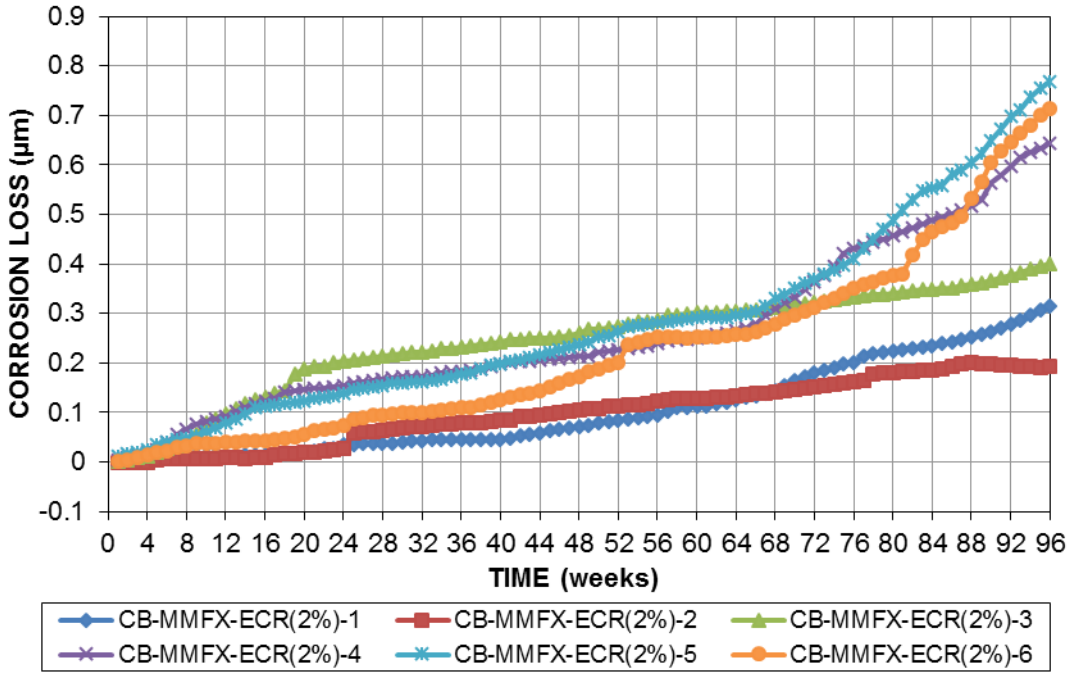

Figure B.11— Macrocell corrosion losses (µm) based on total area of reinforcement for cracked beam specimens containing MMFX-ECR(2%) bars

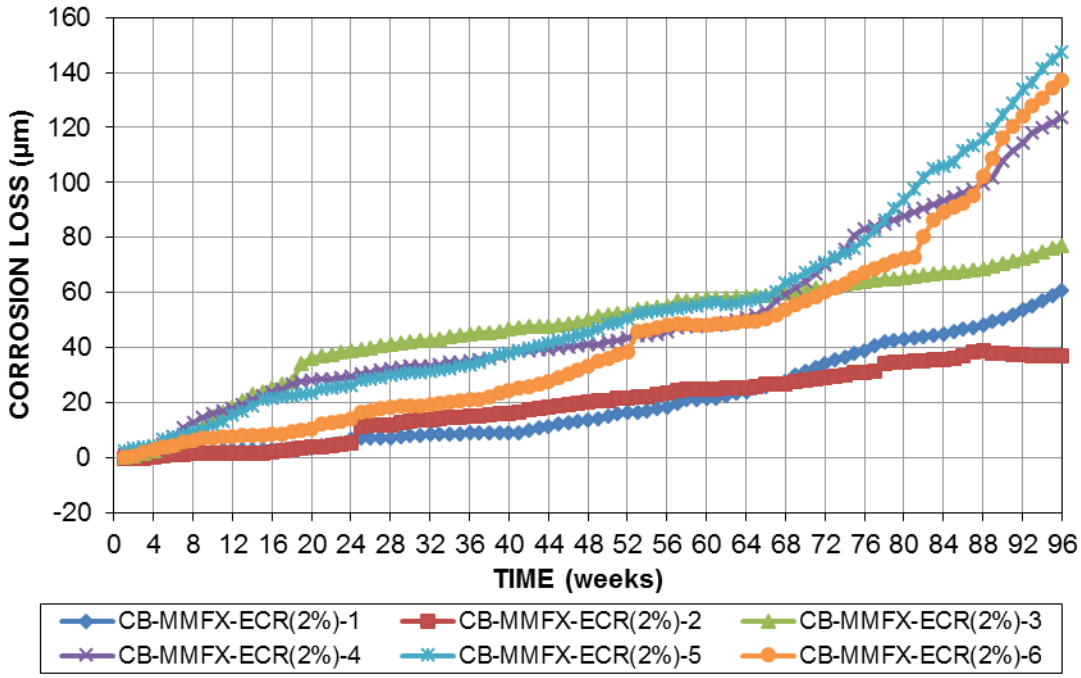

Figure B.12— Macrocell corrosion losses (µm) based on exposedl area of reinforcement for cracked beam specimens containing MMFX-ECR(2%) bars

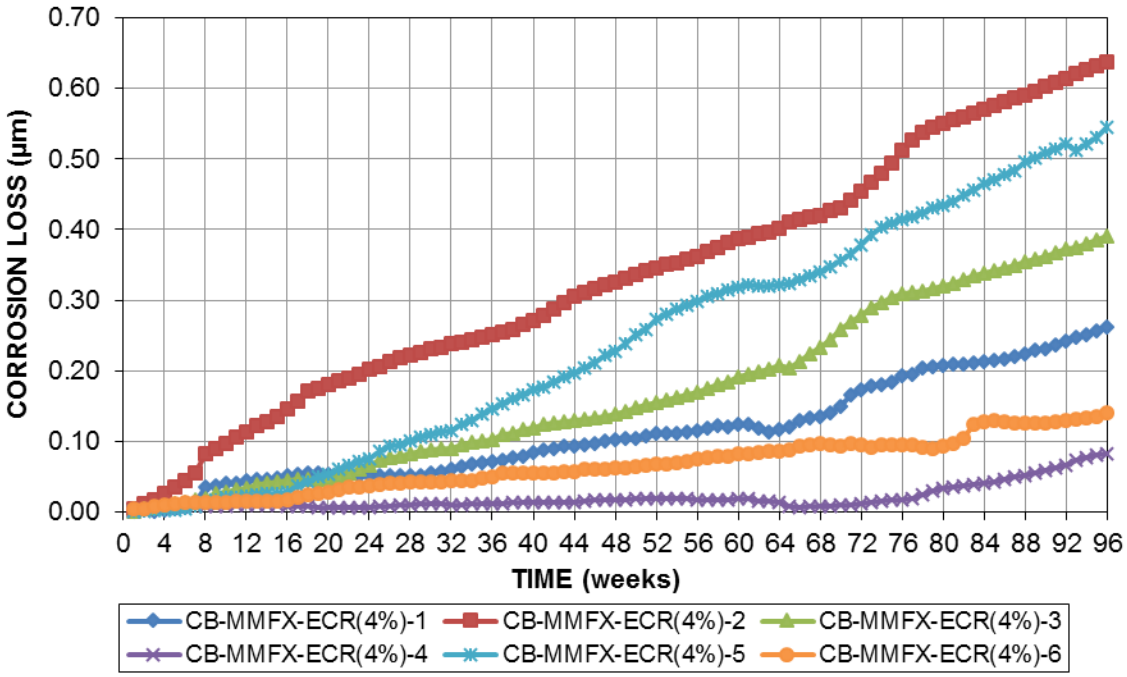

Figure B.13— Macrocell corrosion losses (µm) based on total area of reinforcement for cracked beam specimens containing MMFX-ECR(4%) bars

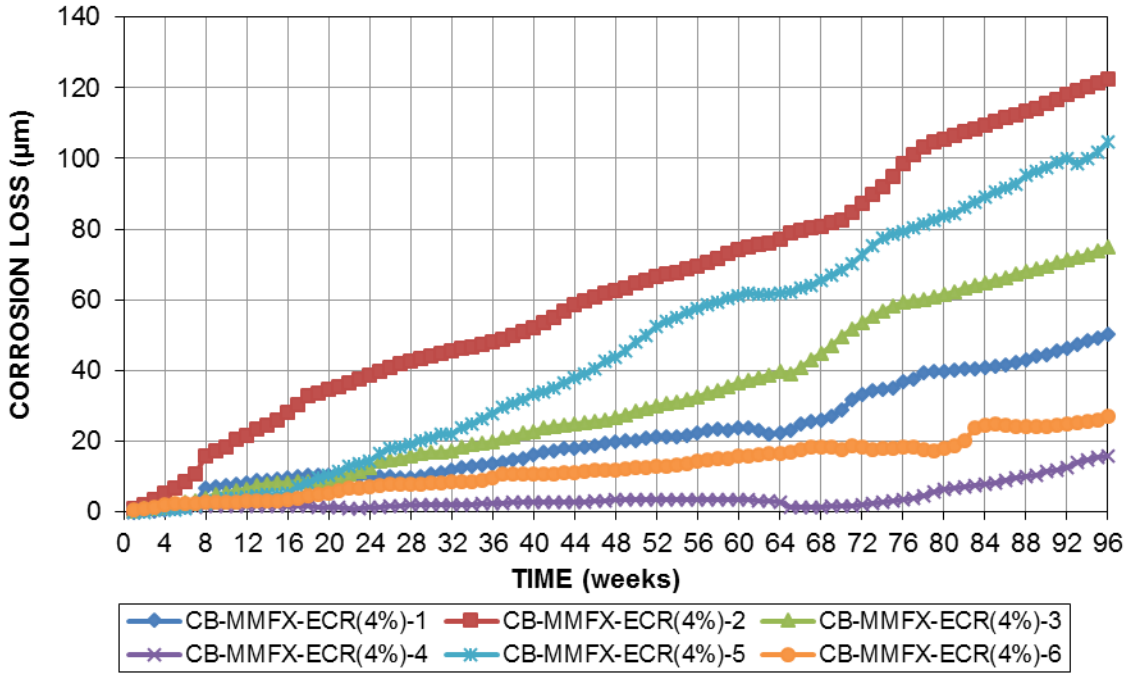

Figure B.14— Macrocell corrosion losses (µm) based on exposedl area of reinforcement for cracked beam specimens containing MMFX-ECR(4%) bars

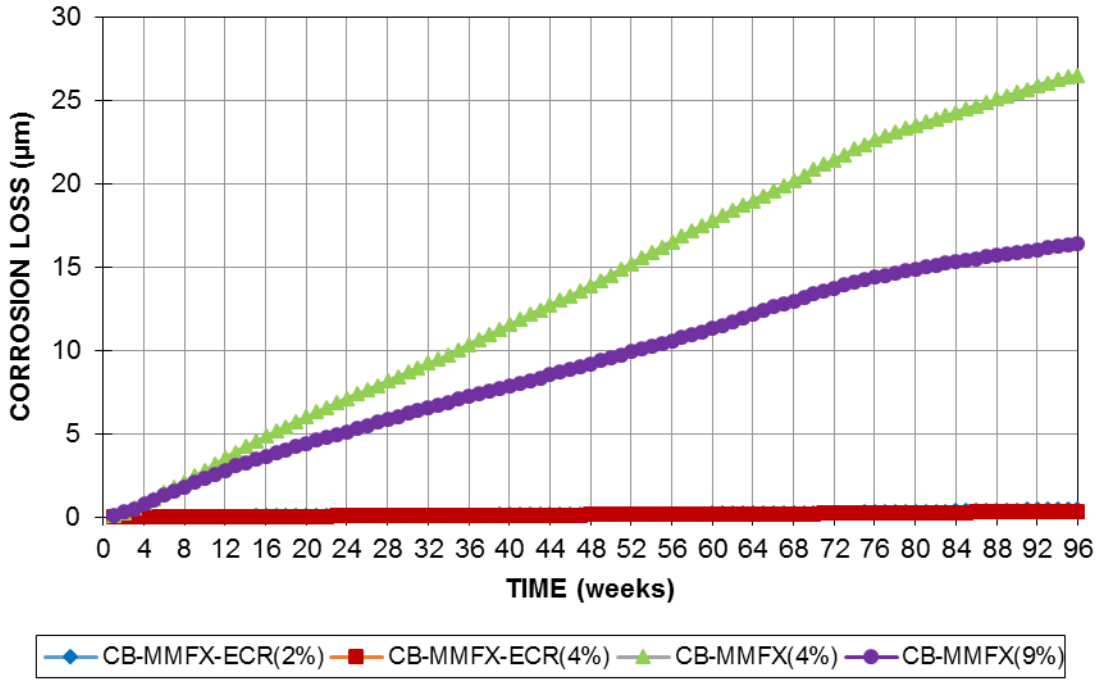

Figure B.15— Average corrosion loss (µm) based on total area versus time for cracked beam specimens

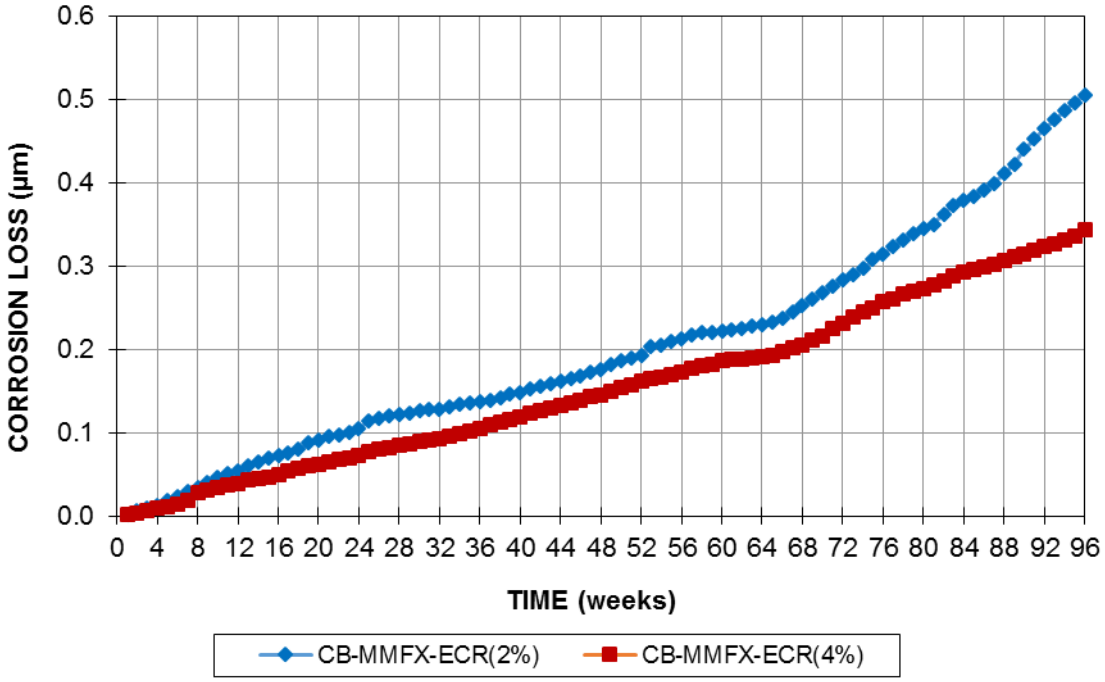

Figure B.16— Average corrosion loss (µm) based on total area versus time for cracked beam specimens with epoxy-coated reinforcement

APPENDIX C

LPR CORROSION LOSS OF SOUTHERN EXPOSURE AND CRACKED BEAM SPECIMENS CONTAINING BARE AND EPOXY-COATED MMFX REINFORCEMENT

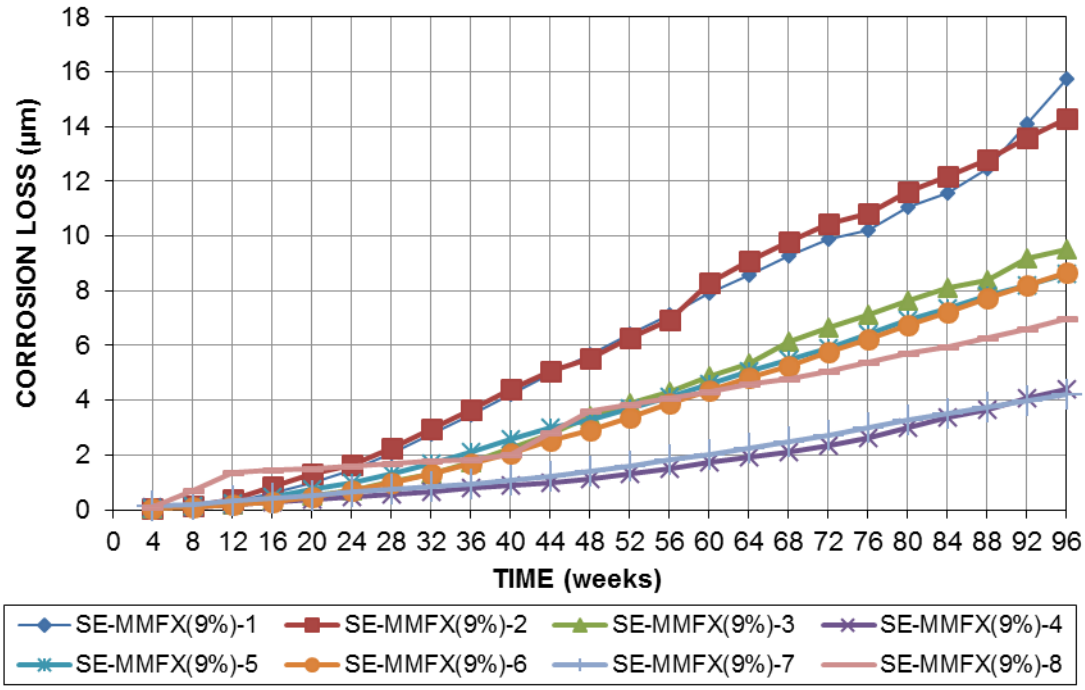

Figure C.1— LPR test corrosion losses (µm) for Southern Exposure specimens containing MMFX(9%) bars

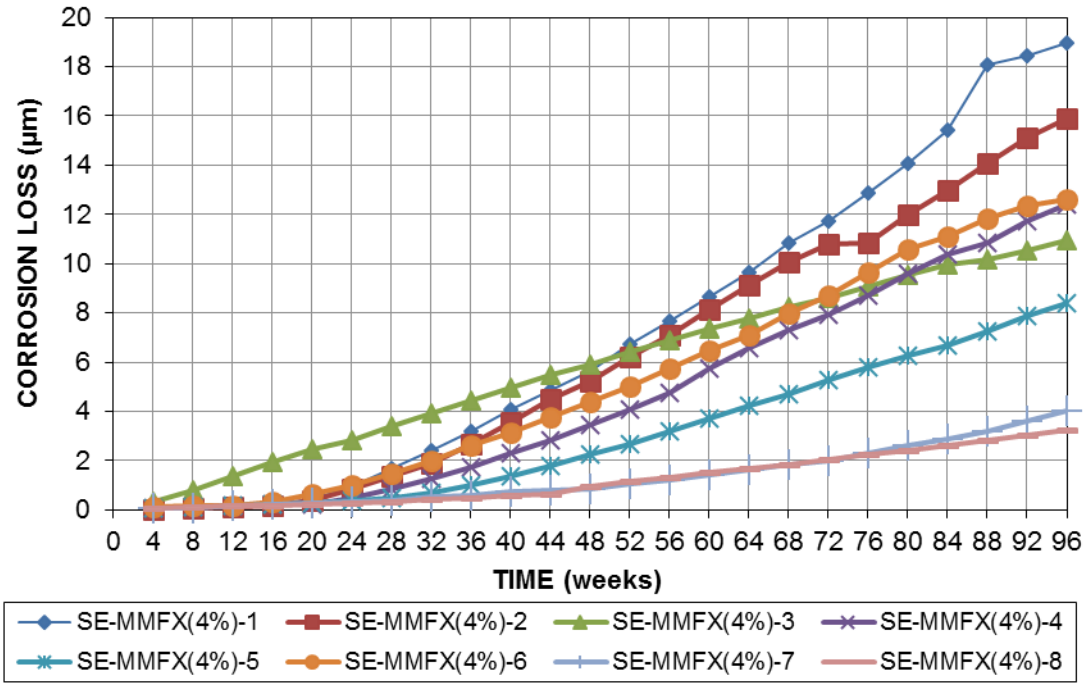

Figure C.2— LPR test corrosion losses (µm) for Southern Exposure specimens containing MMFX(4%) bars

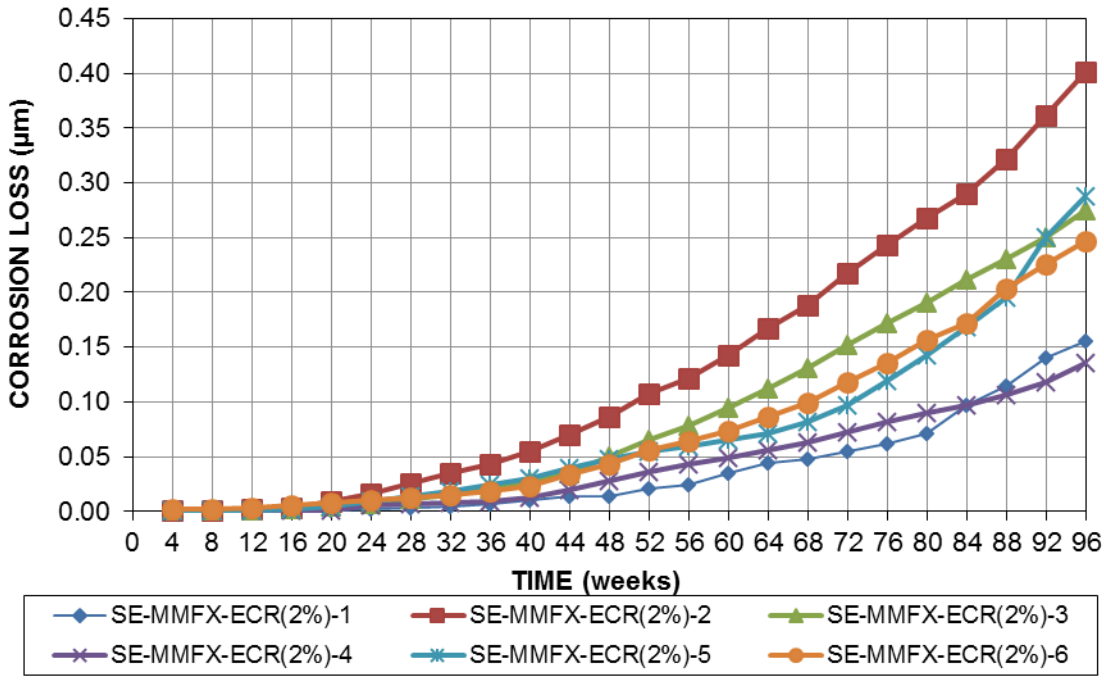

Figure C.3— LPR test corrosion losses (µm) based on total area of reinforcement for Southern Exposure specimens containing MMFX-ECR(2%) bars

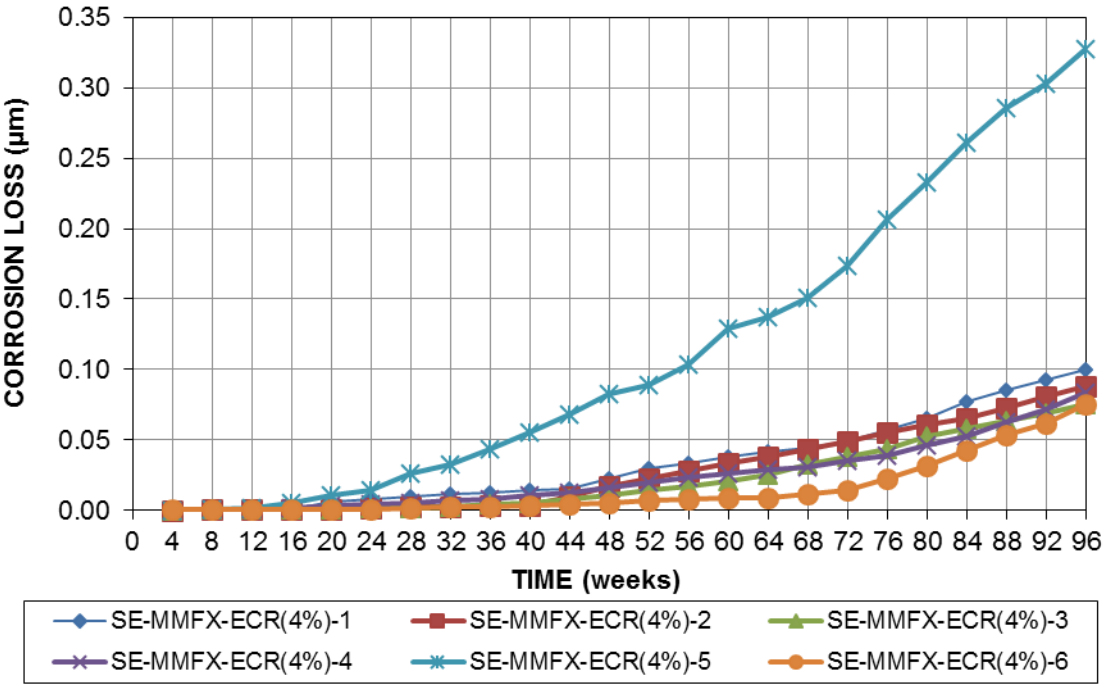

Figure C.4— LPR test corrosion losses (µm) based on total area of reinforcement for Southern Exposure specimens containing MMFX-ECR(4%) bars

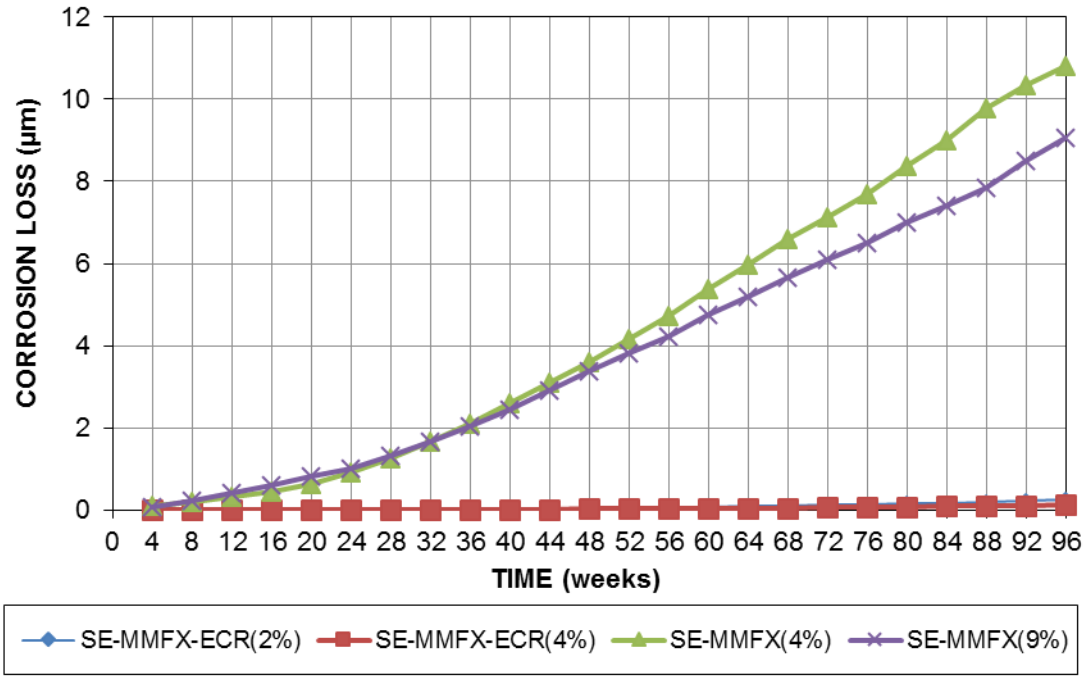

Figure C.5— Average LPR test corrosion loss (µm/yr) based on total area versus time for Southern Exposure specimens

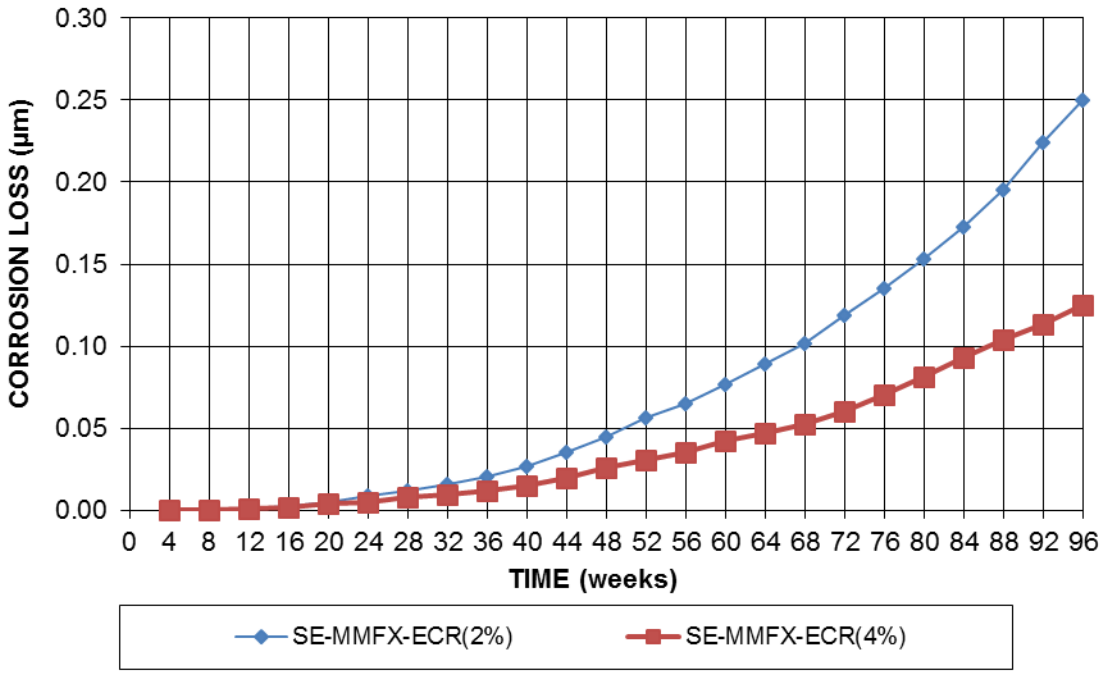

Figure C.6— Average LPR test corrosion loss (µm/yr) based on total area versus time for Southern Exposure specimens containing epoxy-coated reinforcement

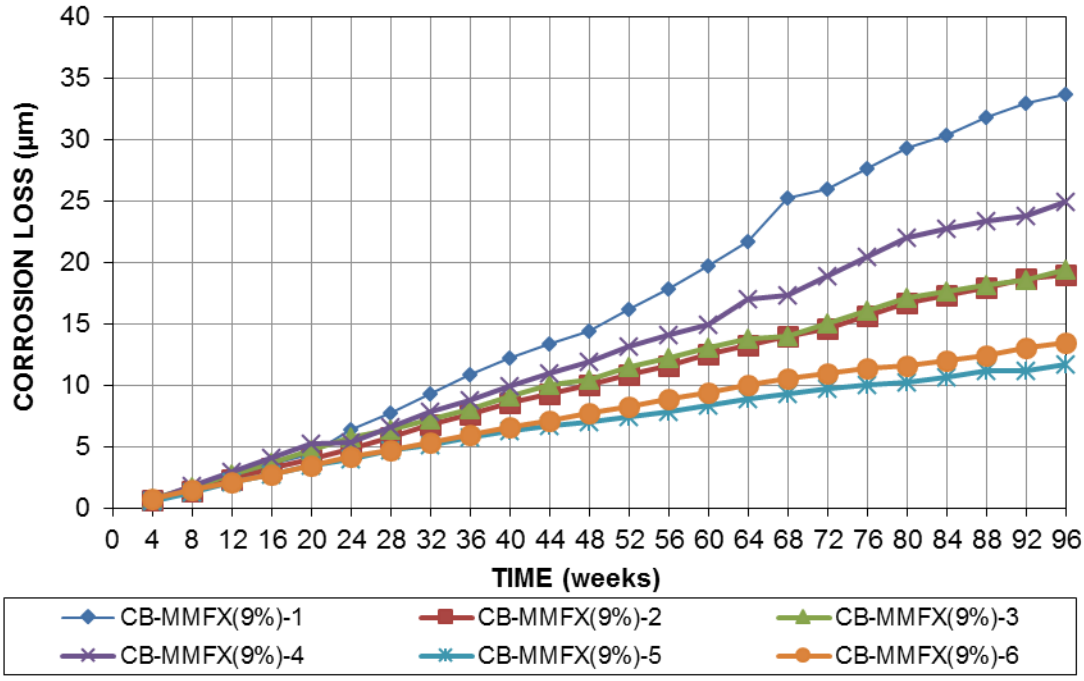

Figure C.7— LPR test corrosion losses (µm) for cracked beam specimens containing MMFX(9%) bars

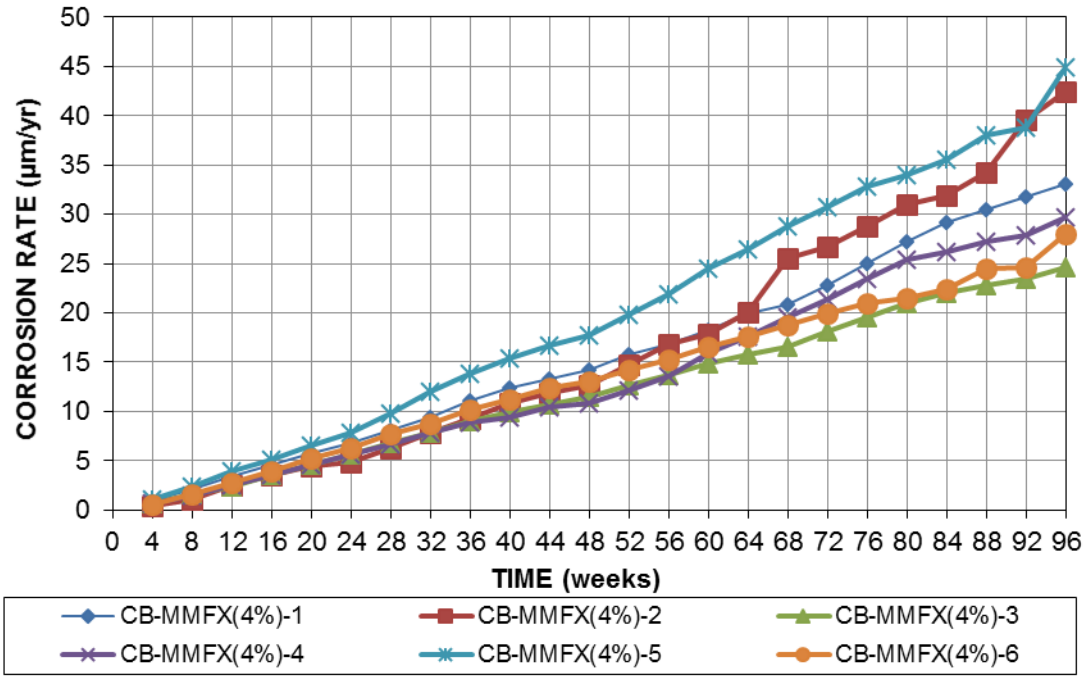

Figure C.8— LPR test corrosion losses (µm) for cracked beam specimens containing MMFX(4%) bars

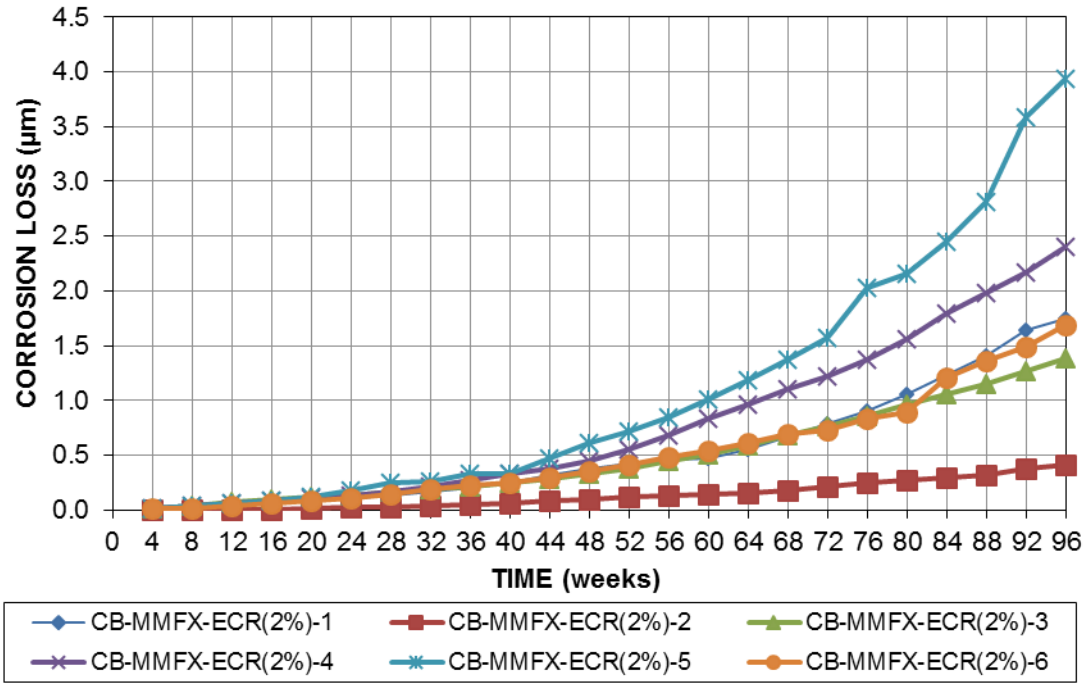

Figure C.9— LPR test corrosion losses (µm) based on total area of reinforcement for cracked beam specimens containing MMFX-ECR(2%) bars

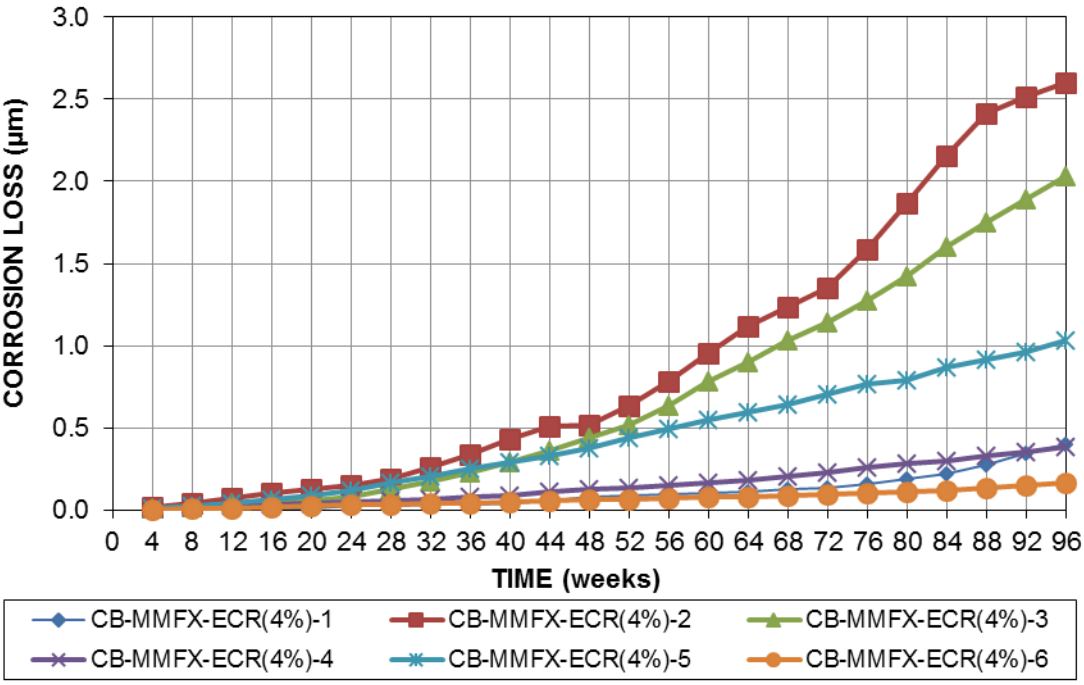

Figure C.10— LPR test corrosion losses (µm) based on total area of reinforcement for cracked beam specimens containing MMFX-ECR(2%) bars

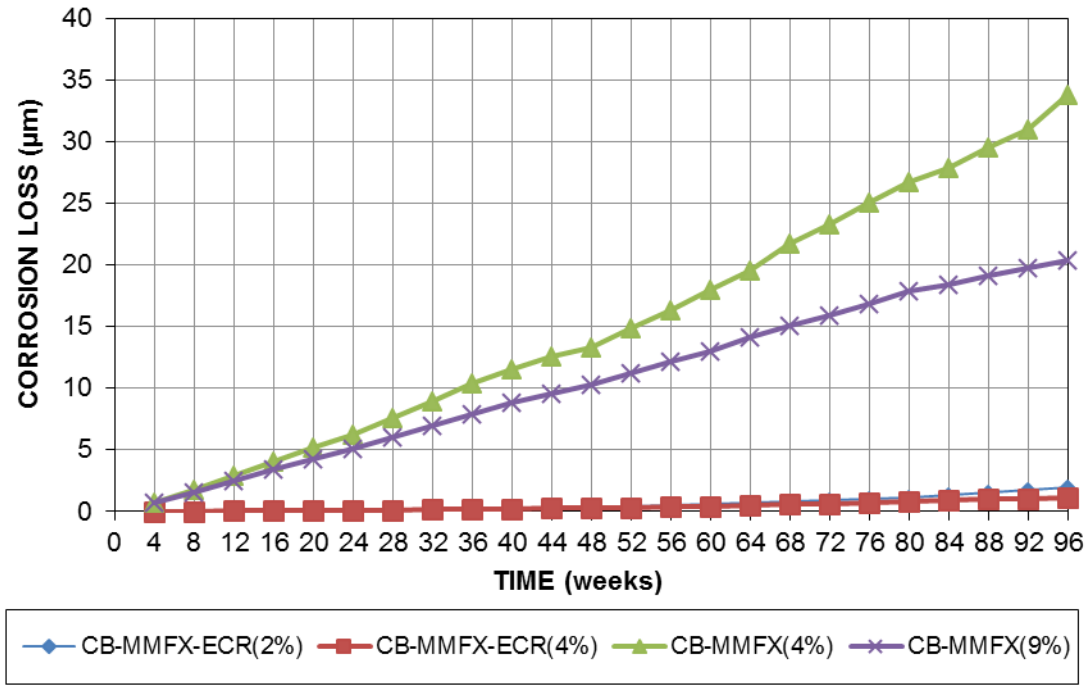

Figure C.11— Average LPR test corrosion loss (µm/yr) based on total area versus time for cracked beam specimens

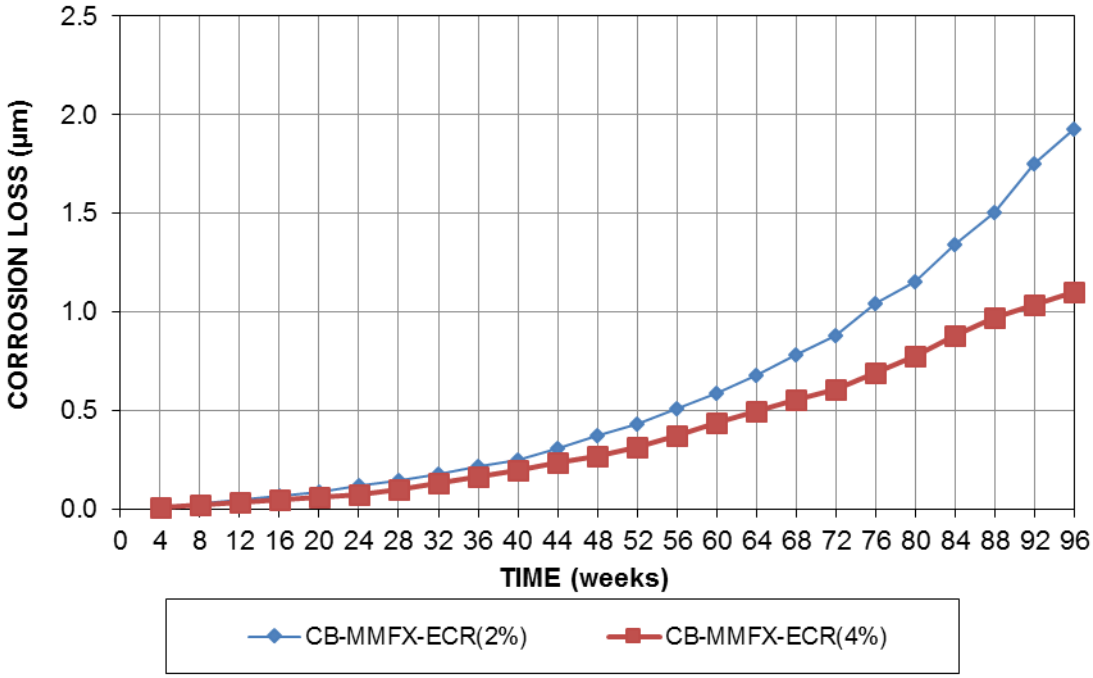

Figure C.12— Average LPR test corrosion loss (µm/yr) based on total area versus time for cracked beam specimens containing epoxy-coated reinforcement

APPENDIX D

TOP AND BOTTOM MAT CORROSION POTENTIAL OF SOUTHERN EXPOSURE AND CRACKED BEAM SPECIMENS CONTAINING BARE AND EPOXY-COATED MMFX REINFORCEMENT

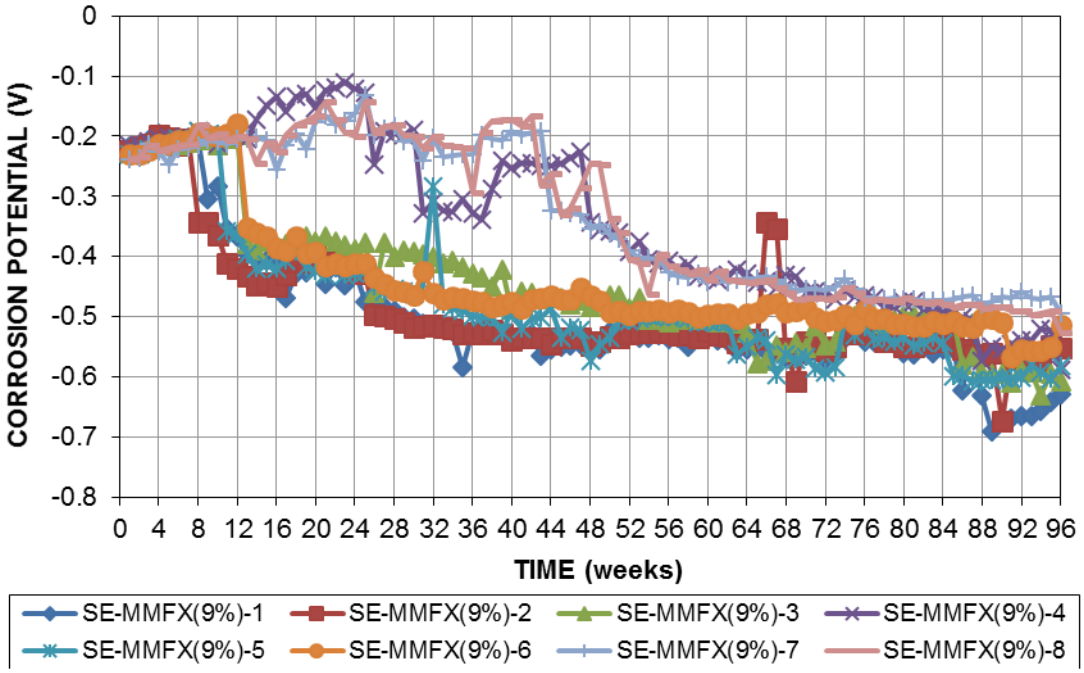

Figure D.1—Top mat (anode) corrosion potential (CSE) versus time for Southern Exposure specimens containing MMFX(9%) bars

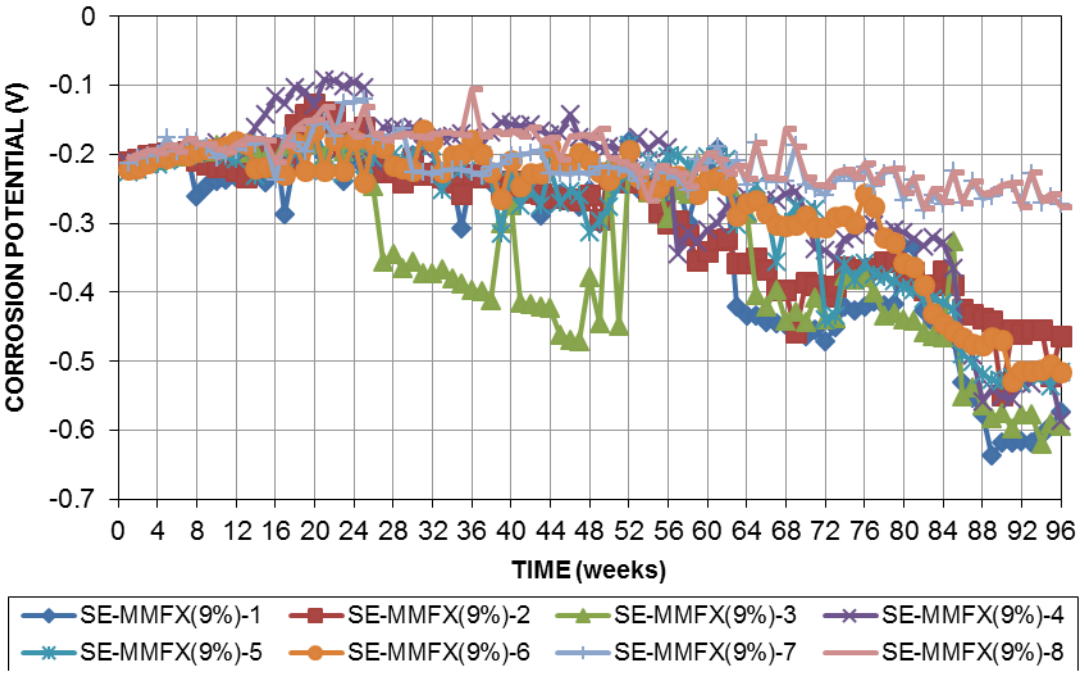

Figure D.2—Bottom mat (cathode) corrosion potential (CSE) versus time for Southern Exposure specimens containing MMFX(9%) bars

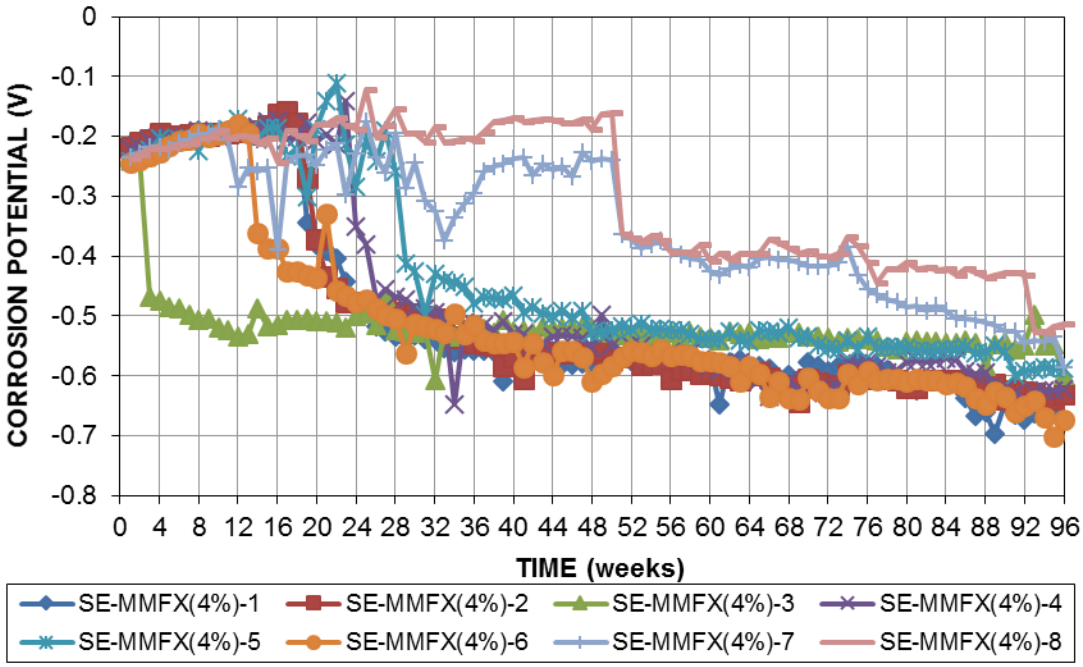

Figure D.3—Top mat (anode) corrosion potential (CSE) versus time for Southern Exposure specimens containing MMFX(4%) bars

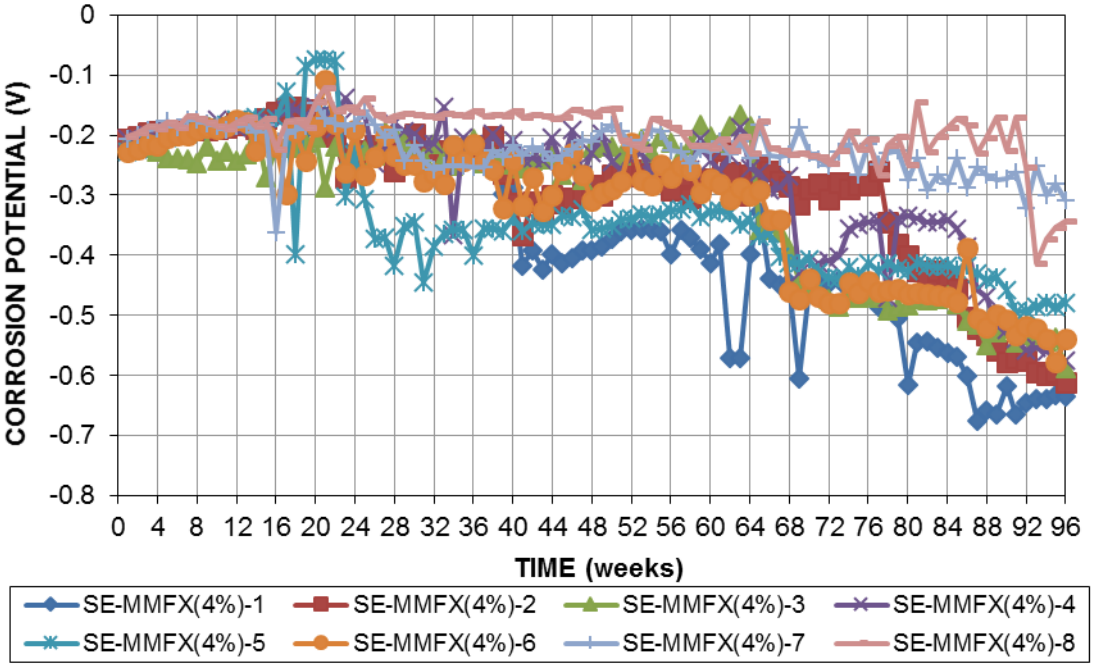

Figure D.4—Bottom mat (cathode) corrosion potential (CSE) versus time for Southern Exposure specimens containing MMFX(4%) bars

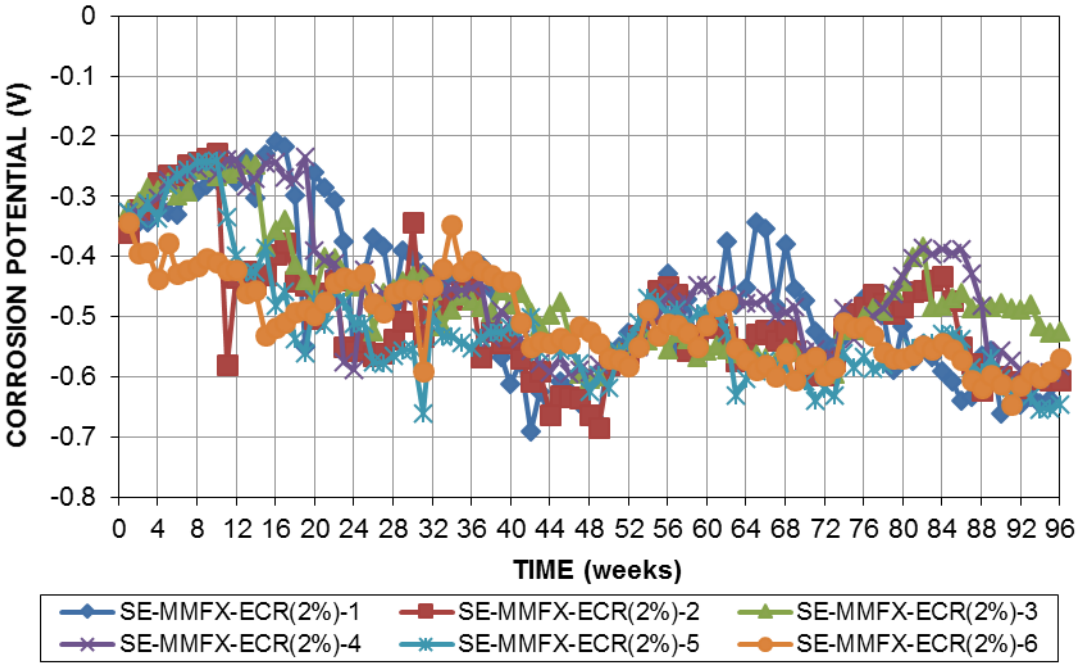

Figure D.5—Top mat (anode) corrosion potential (CSE) versus time for Southern Exposure specimens containing MMFX-ECR(2%) bars

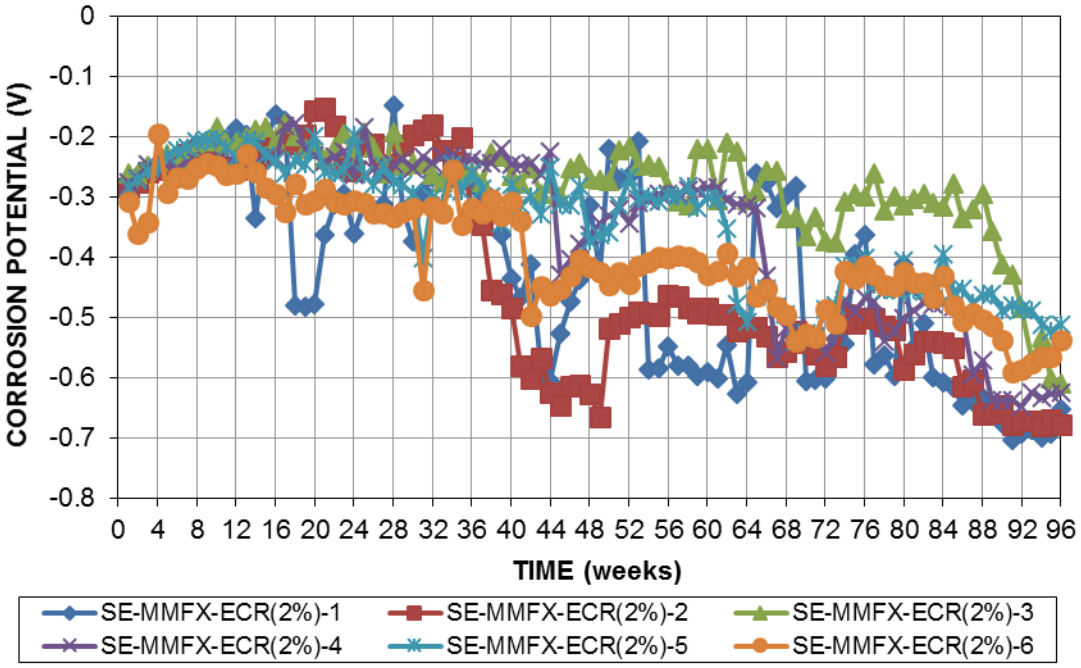

Figure D.6—Bottom mat (cathode) corrosion potential (CSE) versus time for Southern Exposure specimens containing MMFX-ECR(2%) bars

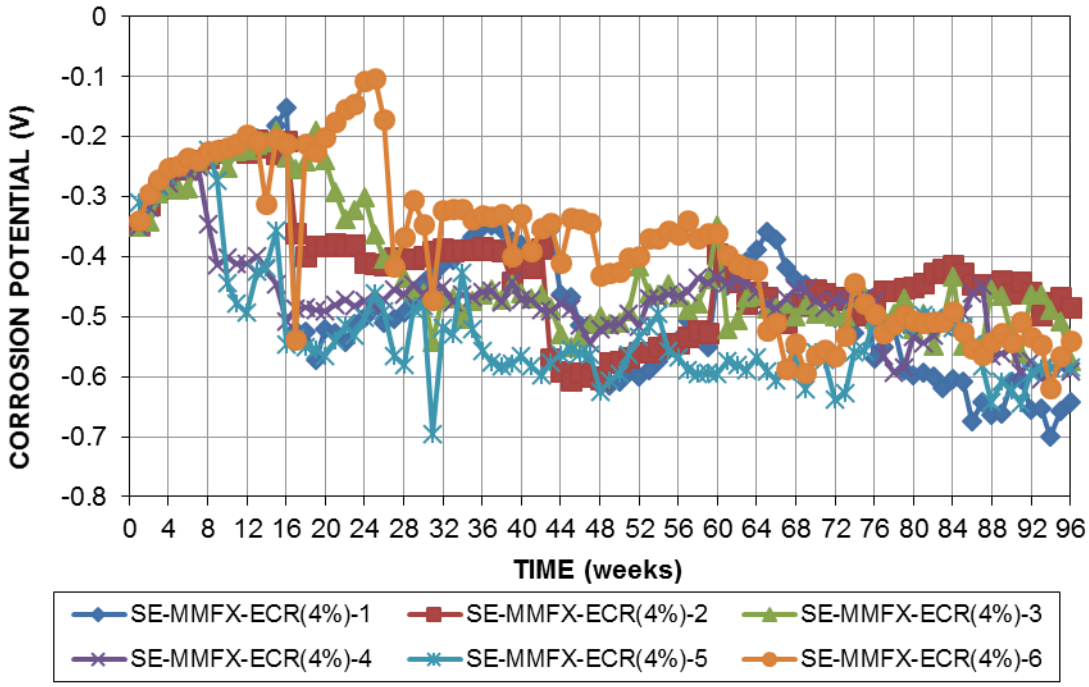

Figure D.7—Top mat (anode) corrosion potential (CSE) versus time for Southern Exposure specimens containing MMFX-ECR(4%) bars

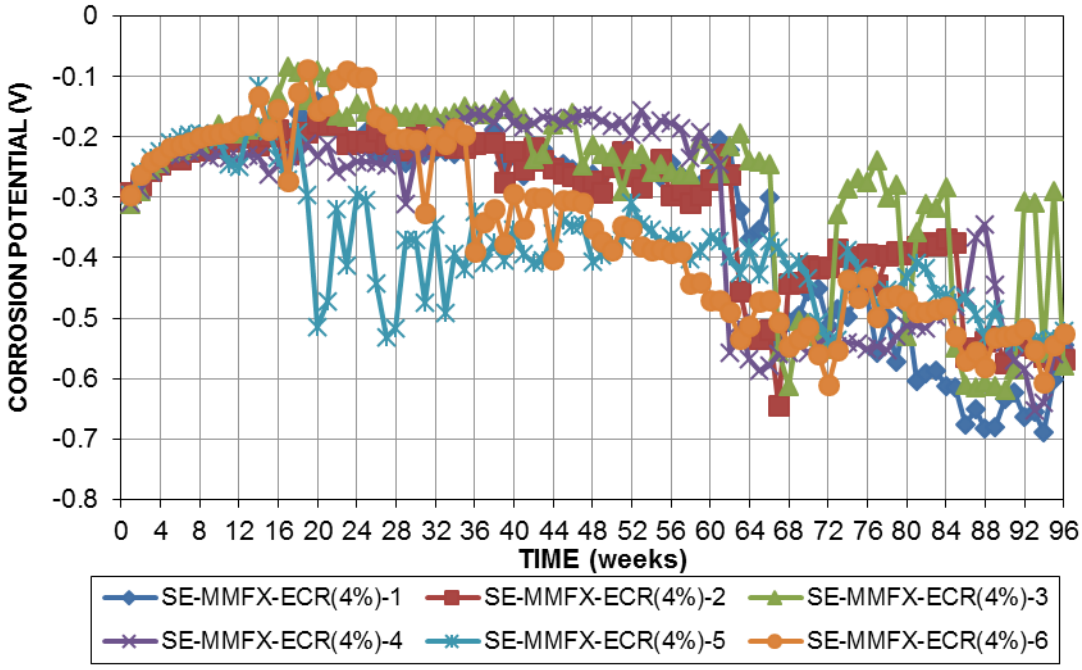

Figure D.8—Bottom mat (cathode) corrosion potential (CSE) versus time for Southern Exposure specimens containing MMFX-ECR(4%) bars

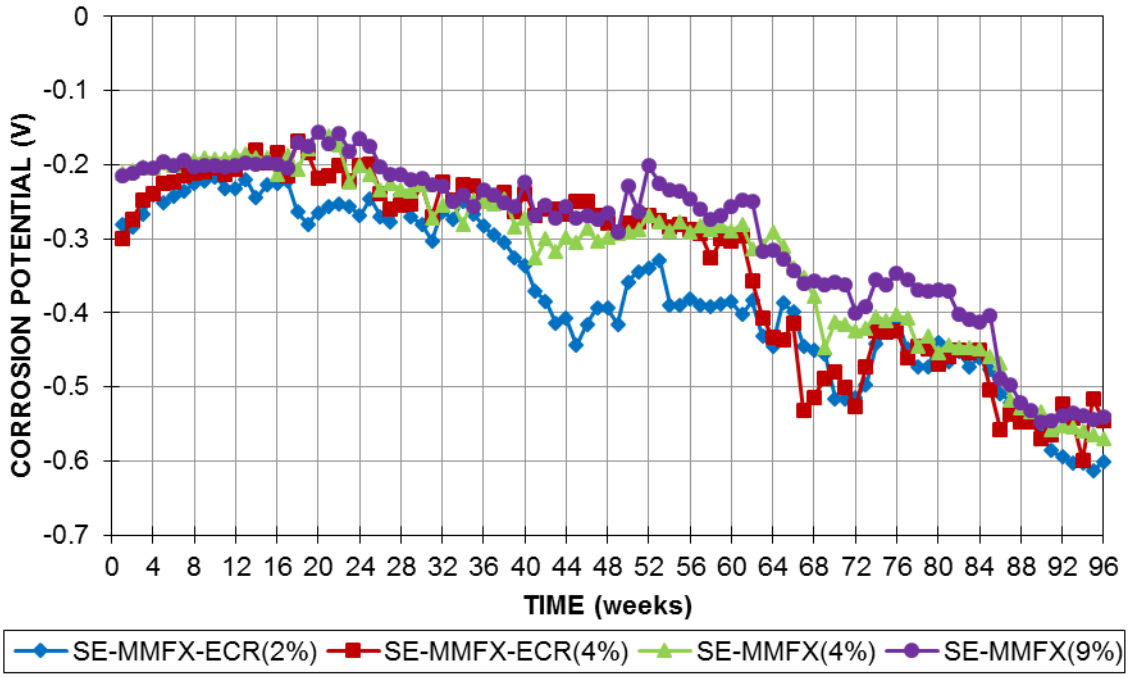

Figure D.9—Bottom mat (cathode) corrosion potential (CSE) versus time for Southern Exposure specimens

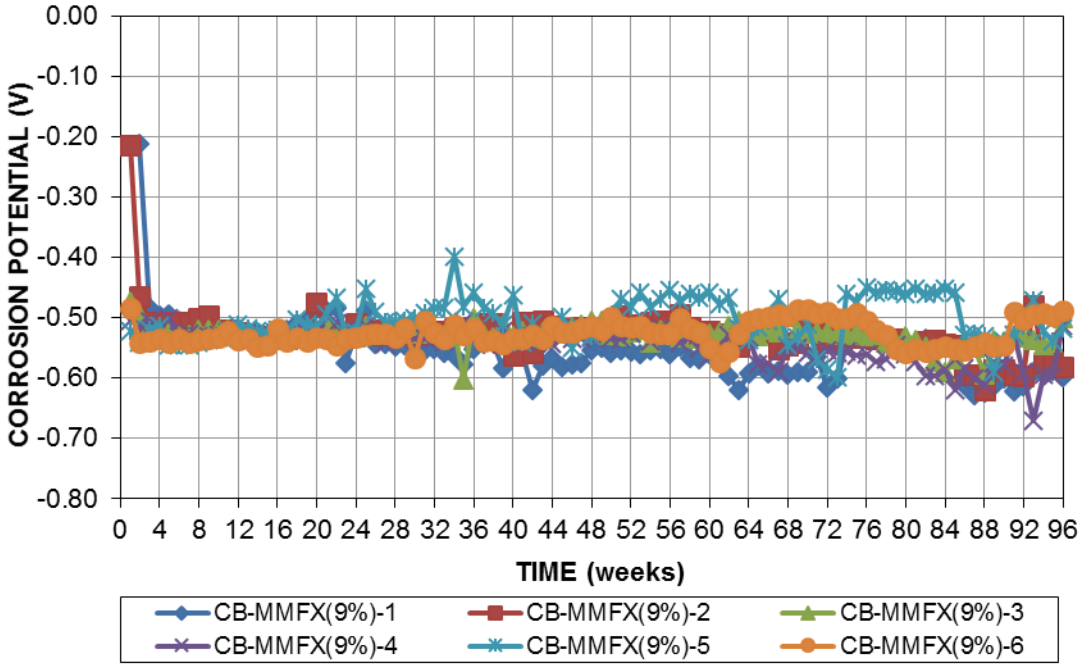

Figure D.10—Top mat (anode) corrosion potential (CSE) versus time for cracked beam specimens containing MMFX(9%) bars

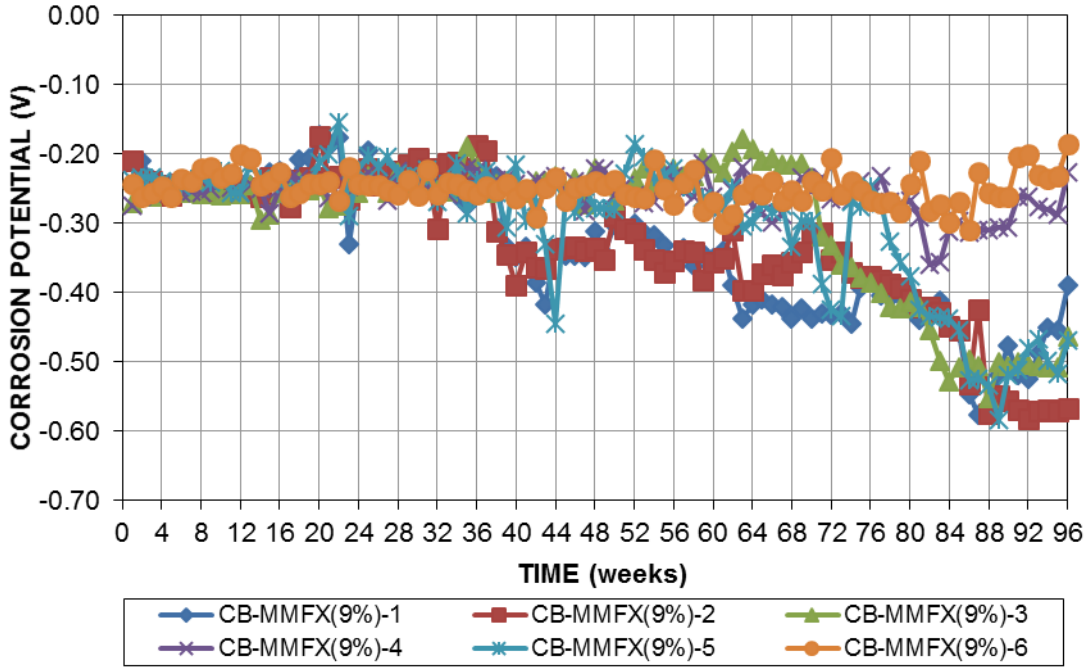

Figure D.11—Bottom mat (cathode) corrosion potential (CSE) versus time for cracked beam specimens containing MMFX(9%) bars

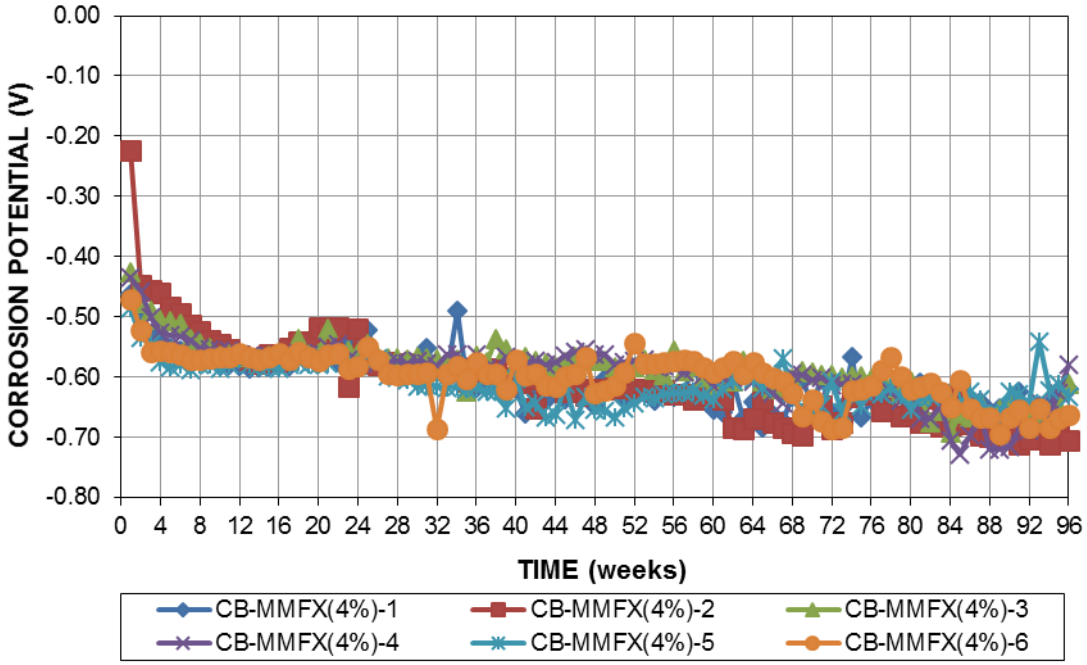

Figure D.12—Top mat (anode) corrosion potential (CSE) versus time for cracked beam specimens containing MMFX(4%) bars

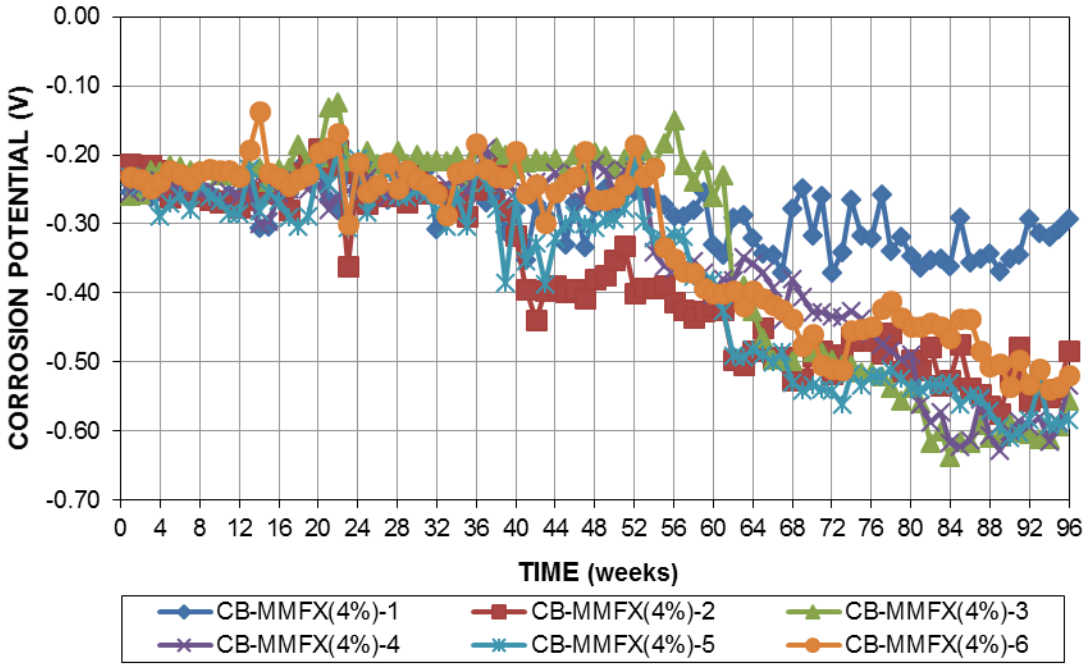

Figure D.13—Bottom mat (cathode) corrosion potential (CSE) versus time for cracked beam specimens containing MMFX(4%) bars

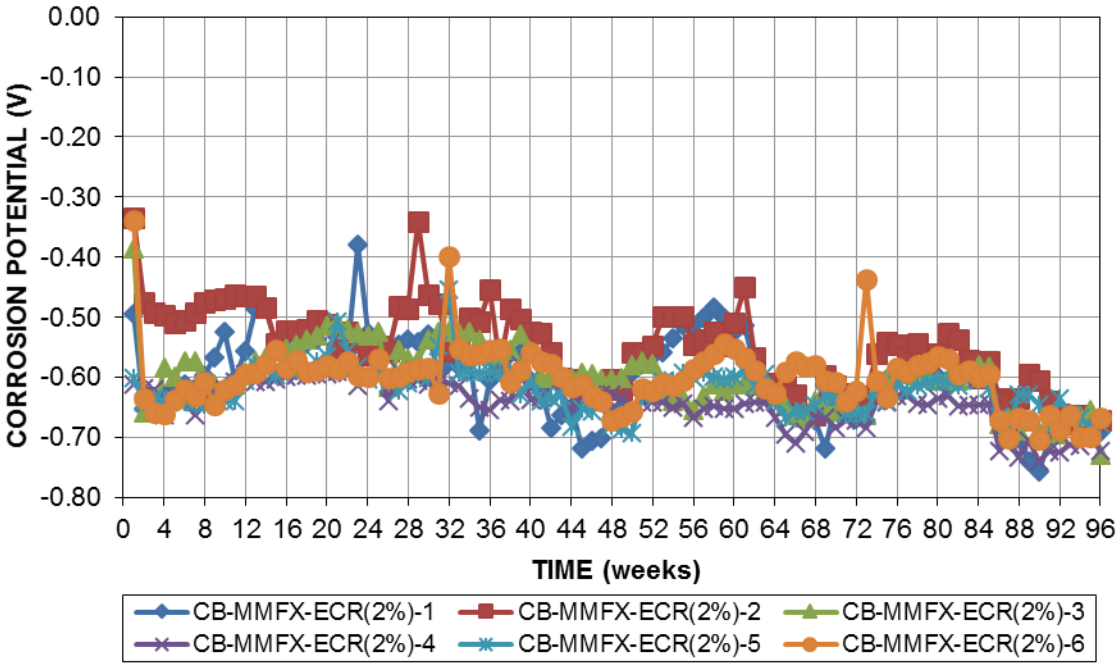

Figure D.14—Top mat (anode) corrosion potential (CSE) versus time for cracked beam specimens containing MMFX-ECR(2%) bars

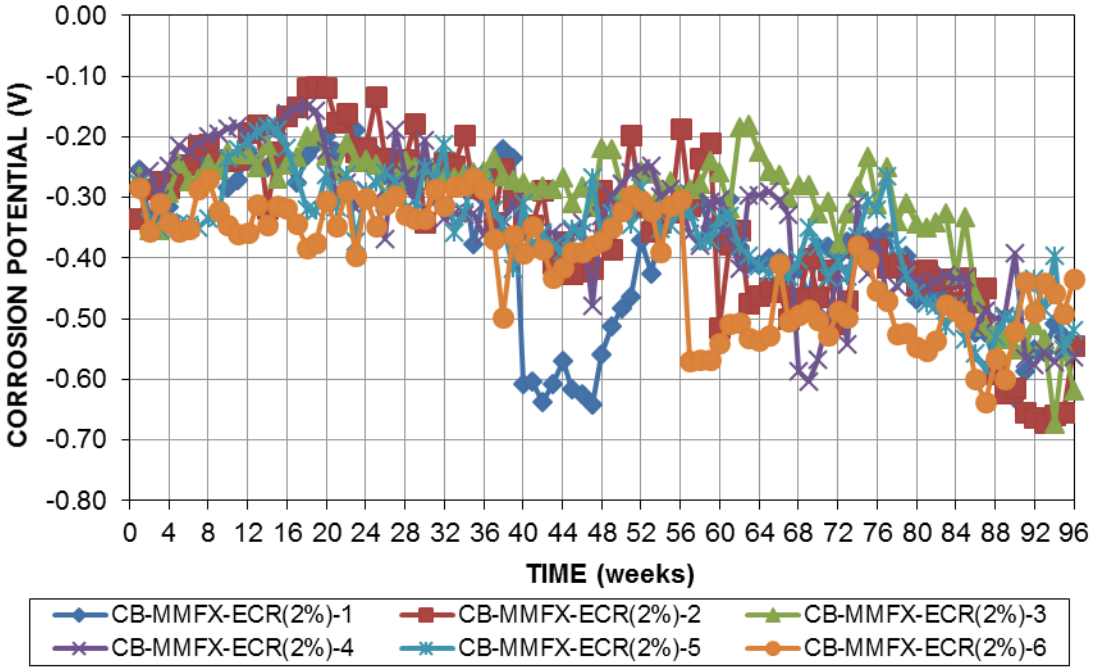

Figure D.15—Bottom mat (cathode) corrosion potential (CSE) versus time for cracked beam specimens containing MMFX-ECR(2%) bars

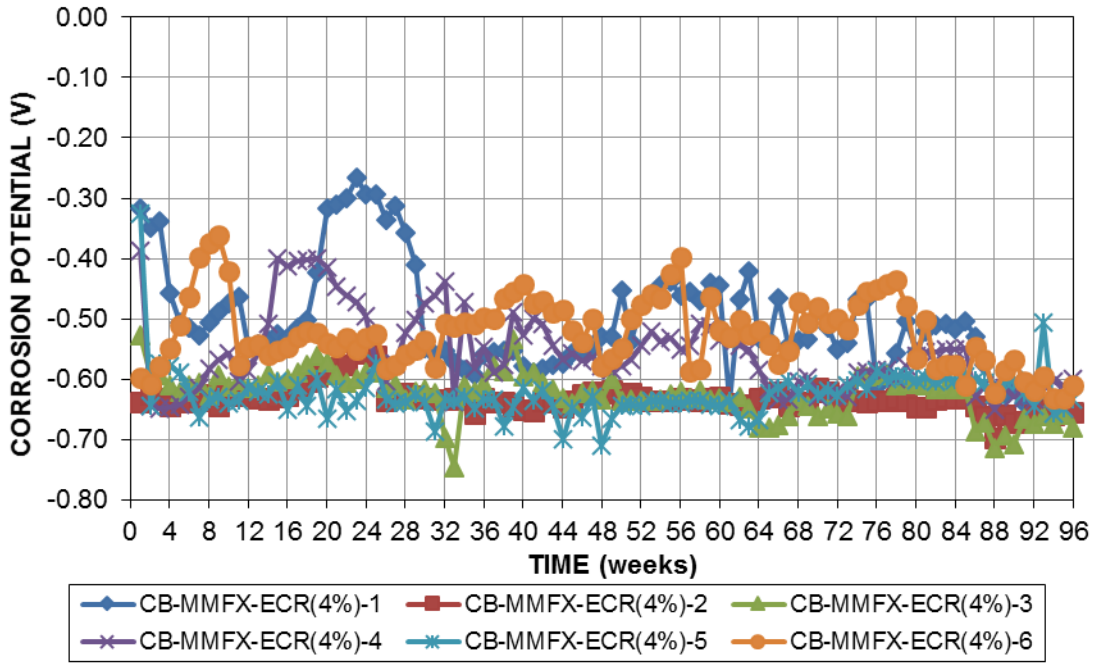

Figure D.16—Top mat (anode) corrosion potential (CSE) versus time for cracked beam specimens containing MMFX-ECR(4%) bars

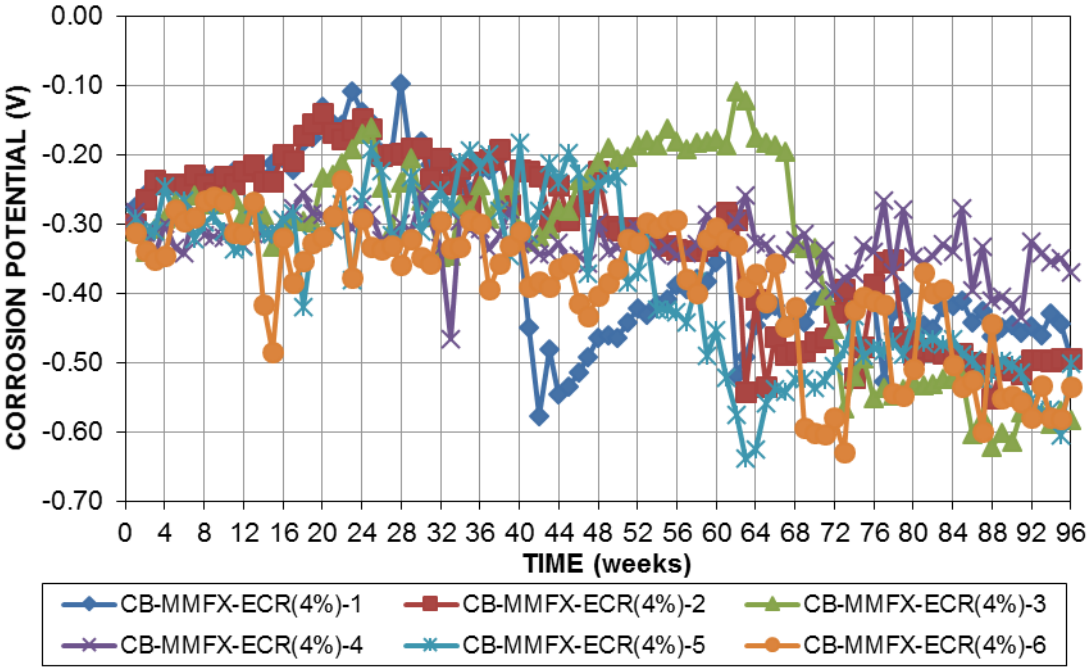

Figure D.17—Bottom mat (cathode) corrosion potential (CSE) versus time for cracked beam specimens containing MMFX-ECR(4%) bars

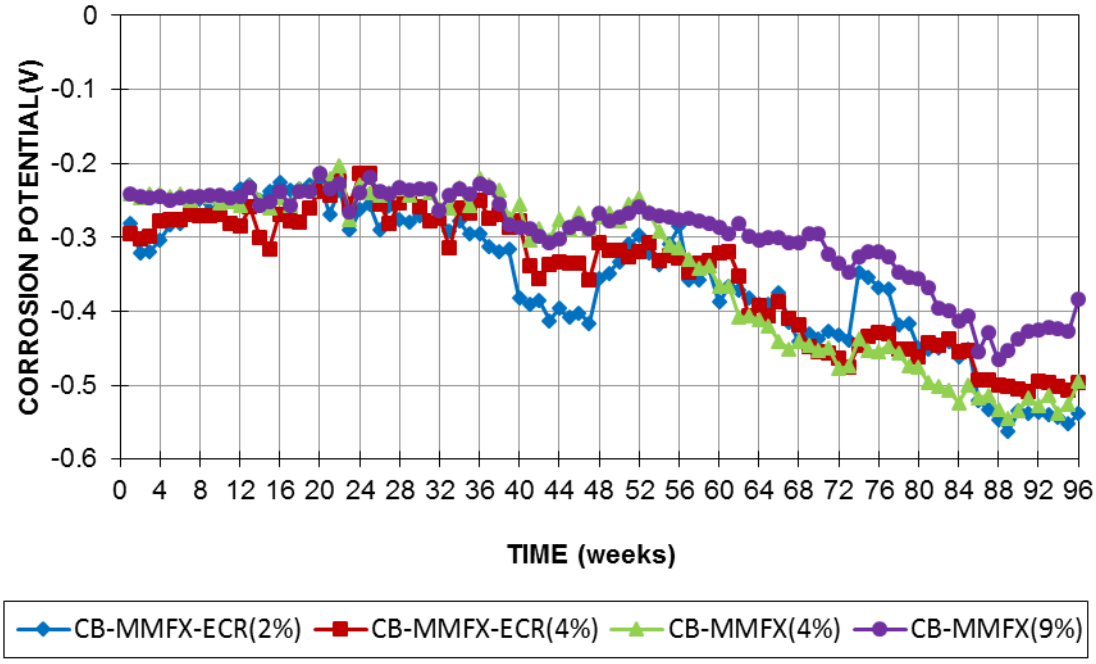

Figure D.18—Bottom mat (cathode) corrosion potential (CSE) versus time for cracked beam specimens

APPENDIX E

MACROCELL AND LPR CORROSION RATE, AND CORROSION POTENTIAL OF TOP AND BOTTOM MATS OF BEAM SPECIMENS CONTAINING EPOXY-COATED MMFX BARS WITH 2% AND 4% CHROMIUM

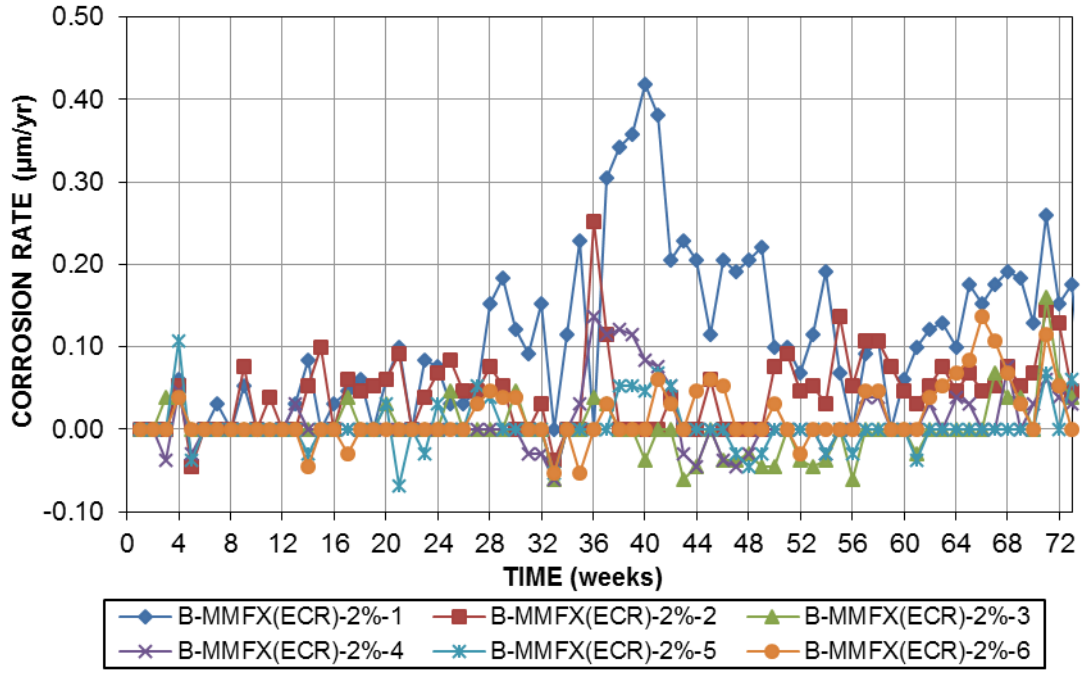

Figure E.1— Macrocell corrosion rates (µm) based on total area of reinforcement for beam specimens containing MMFX-ECR(2%) bars

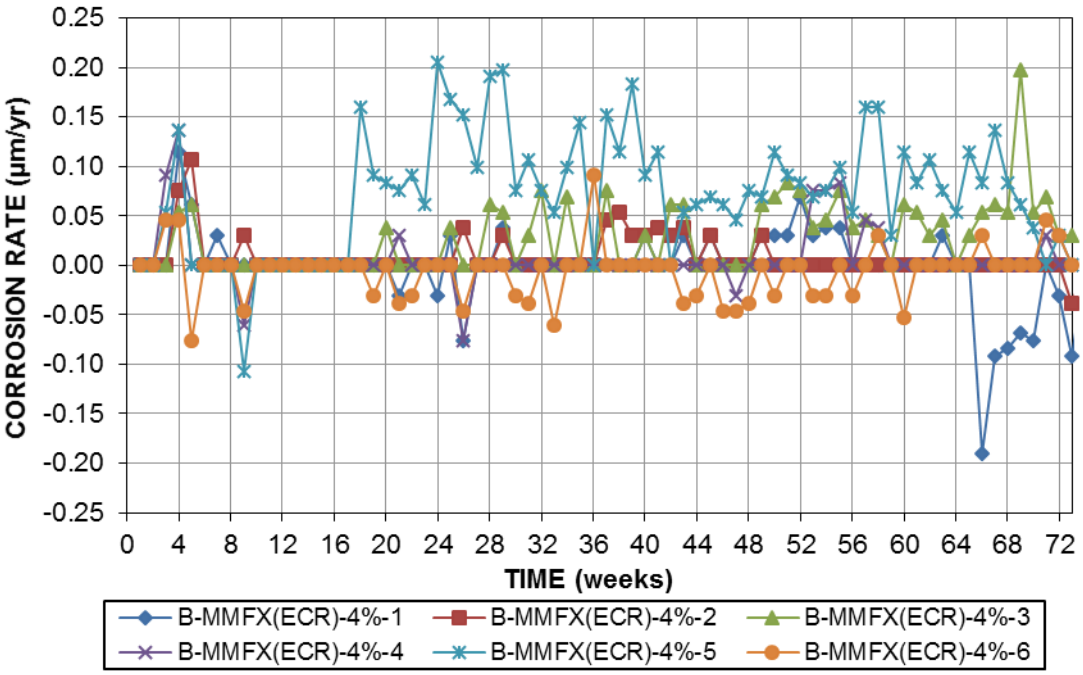

Figure E.2— Macrocell corrosion rates (µm) based on total area of reinforcement for beam specimens containing MMFX-ECR(4%) bars

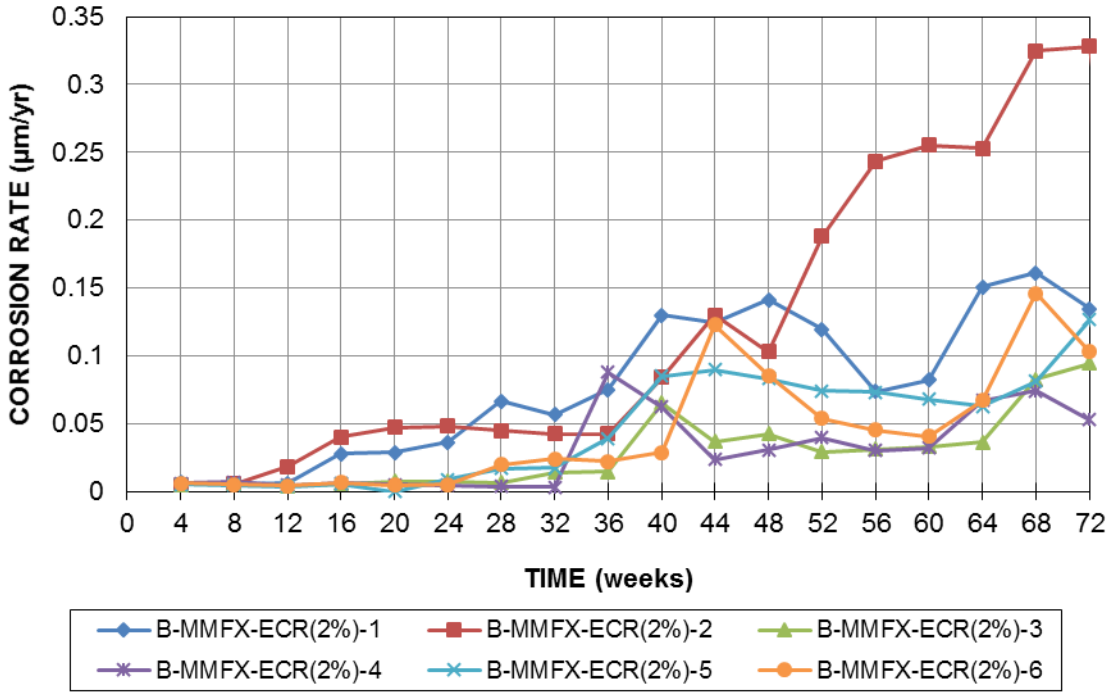

Figure E.3— LPR test corrosion rates (µm) based on total area of reinforcement for beam specimens containing MMFX-ECR(2%) bars

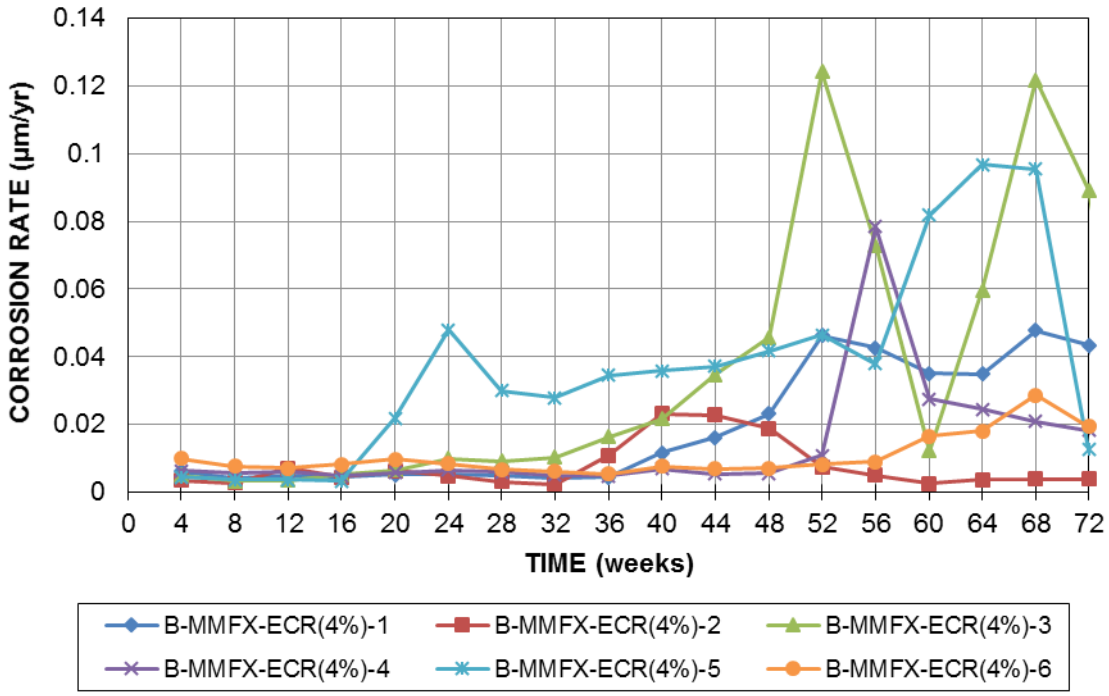

Figure E.4— LPR test corrosion rates (µm) based on total area of reinforcement for beam specimens containing MMFX-ECR(4%) bars

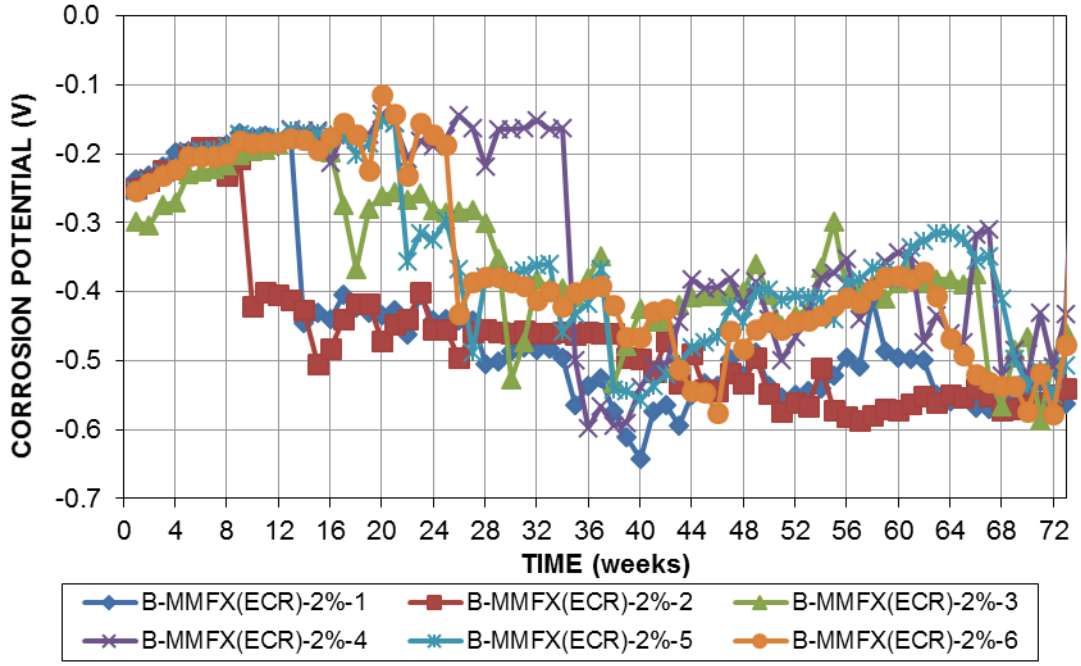

Figure E.5—Top mat (anode) corrosion potential (CSE) versus time for beam specimens containing MMFX-ECR(2%) bars

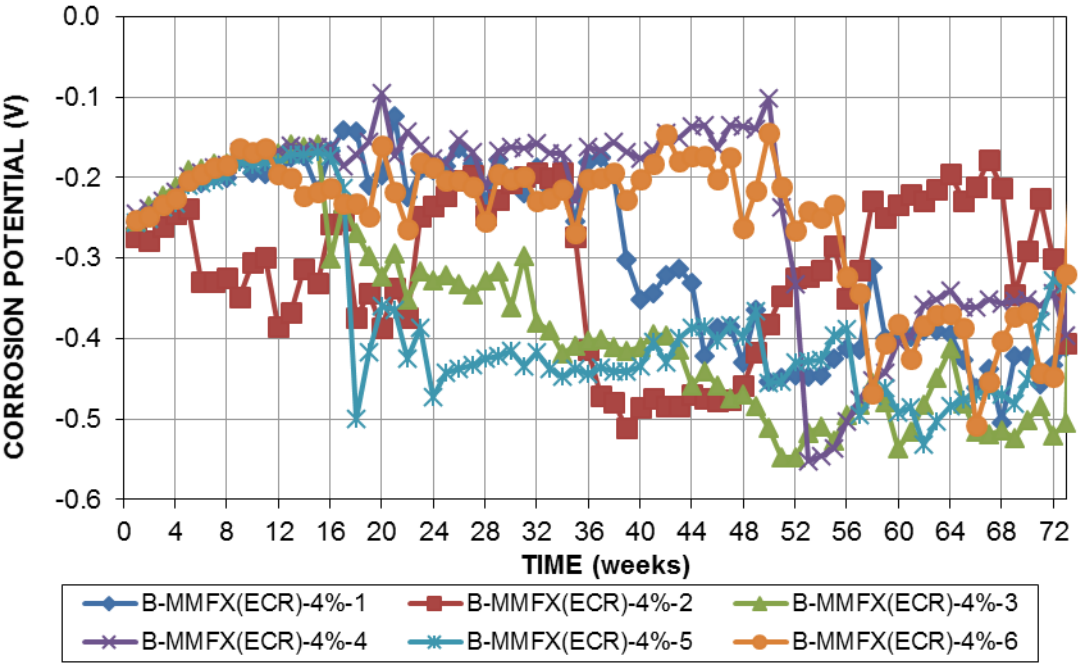

Figure E.6—Top mat (anode) corrosion potential (CSE) versus time for beam specimens containing MMFX-ECR(4%) bars

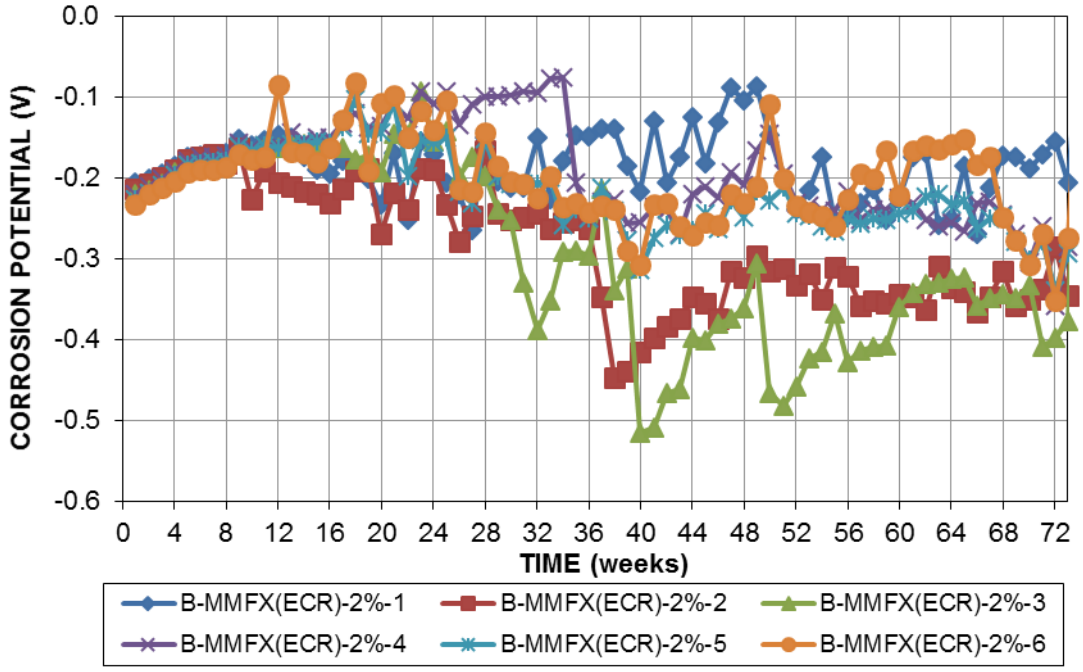

Figure E.7—Bottom mat (cathode) corrosion potential (CSE) versus time for beam specimens containing MMFX-ECR(2%) bars

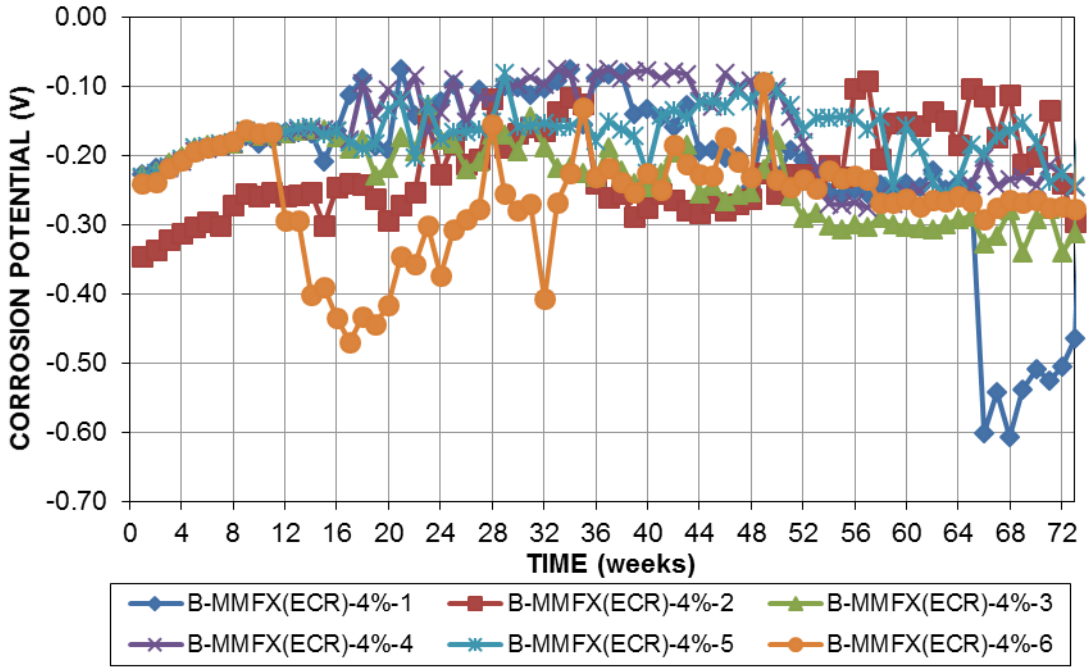

Figure E.8—Bottom mat (cathode) corrosion potential (CSE) versus time for beam specimens containing MMFX-ECR(4%) bars

APPENDIX F

DISBONDMENT TEST FOR THE BOTTOM MATS OF SOUTHERN EXPOSURE AND CRACKED BEAM SPECIMENS CONTAINING EPOXY-COATED MMFX BARS WITH 2% AND 4% CHROMIUM

Table F.1: Disbonded area at week 96 for the MMFX-ECR(4%) bottom bar in Southern Exposure specimens

Specimen	Site 1 (in^2)	Site 2 (in^2)	Site 3 (in^2)	Average ($in.^2$)
1	0.14	0.14	0.29	0.19
2	0.61	0.32	0.15	0.36
3	0.17	0.19	0.09	0.15
4	0.23	0.15	0.03	0.14
5	0.41	0.61	0.42	0.48
6	0.14	1.05	0.11	0.43
Average				0.29

Table F.2: Disbonded area at week 96 for the MMFX-ECR(2%) bottom bar in Southern Exposure specimens

Specimen	Site 1 (in^2)	Site 2 (in^2)	Site 3 (in^2)	Average ($in.^2$)
1	0.28	0.62	0.10	0.33
2	0.71	0.19	0.16	0.35
3	0.77	0.39	0.04	0.40
4	0.32	0.14	0.06	0.17
5	0.12	0.35	0.17	0.21
6	0.17	0.49	0.07	0.24
Average				0.29

Table F.3: Disbonded area at week 96 for the MMFX-ECR(4%) bottom bar in cracked beam specimens

Specimen	Site 1 (in^2)	Site 2 (in^2)	Site 3 (in^2)	Average (mm^2)
1	0.24	1.05	0.15	0.48
2	0.27	0.17	0.13	0.19
3	0.60	0.23	0.24	0.36
4	0.33	0.27	0.21	0.27
5	0.78	0.30	0.27	0.45
6	0.23	0.15	0.12	0.17
Average				0.32

Table F.4: Disbonded area at week 96 for the MMFX-ECR(2%) bottom bar in cracked beam specimens

Specimen	Site 1 (in^2)	Site 2 (in^2)	Site 3 (in^2)	Average (mm^2)
1	0.43	0.31	0.17	0.30
2	0.12	0.14	0.15	0.14
3	0.22	0.73	0.95	0.63
4	1.03	1.04	0.08	0.72
5	1.05	0.80	0.64	0.83
6	0.11	0.40	0.37	0.29
Average				0.49

APPENDIX G

MACROCELL CORROSION LOSS OF BEAM SPECIMENS CONTAINING SUPPLEMENTARY CEMENTITIOUS MATERIALS WITH BARE AND EPOXY-COATED REINFORCEMENT

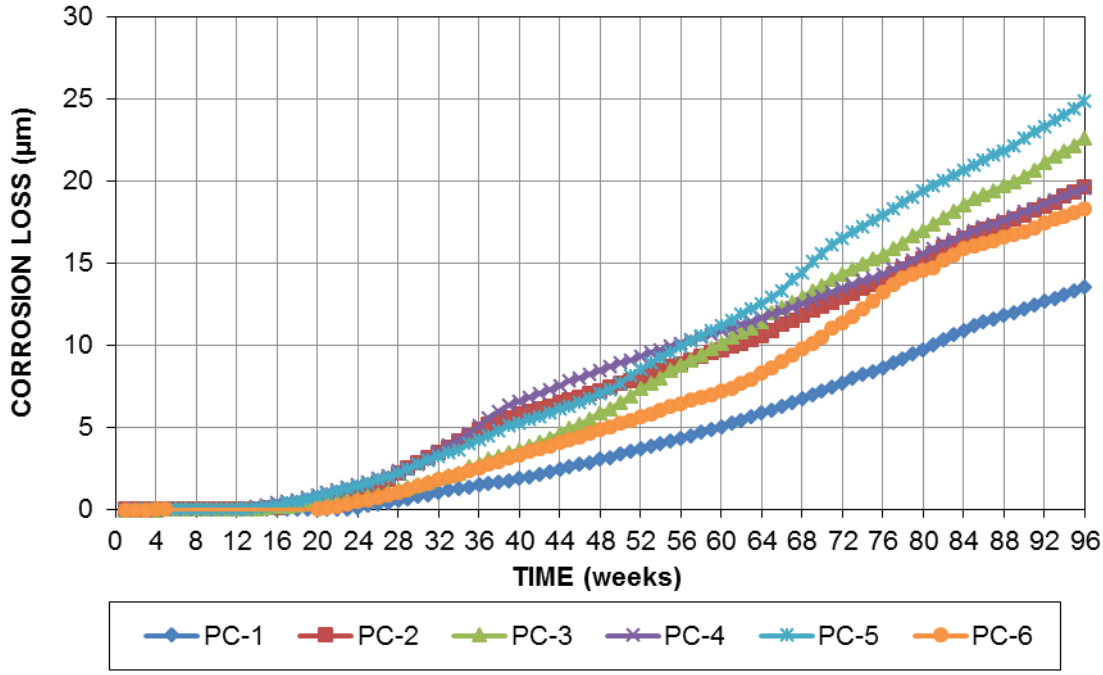

Figure G.1— Macrocell corrosion losses (µm) for specimens containing uncoated conventional reinforcement and 100% portland cement

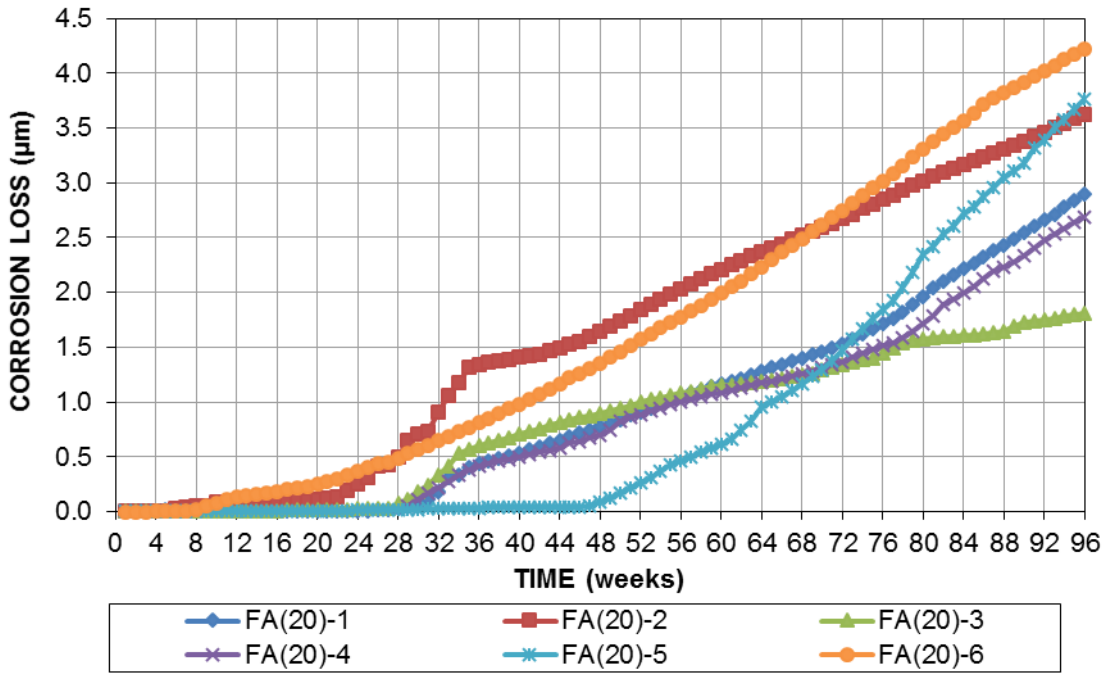

Figure G.2— Macrocell corrosion losses (µm) for specimens containing uncoated conventional reinforcement and 20% fly ash

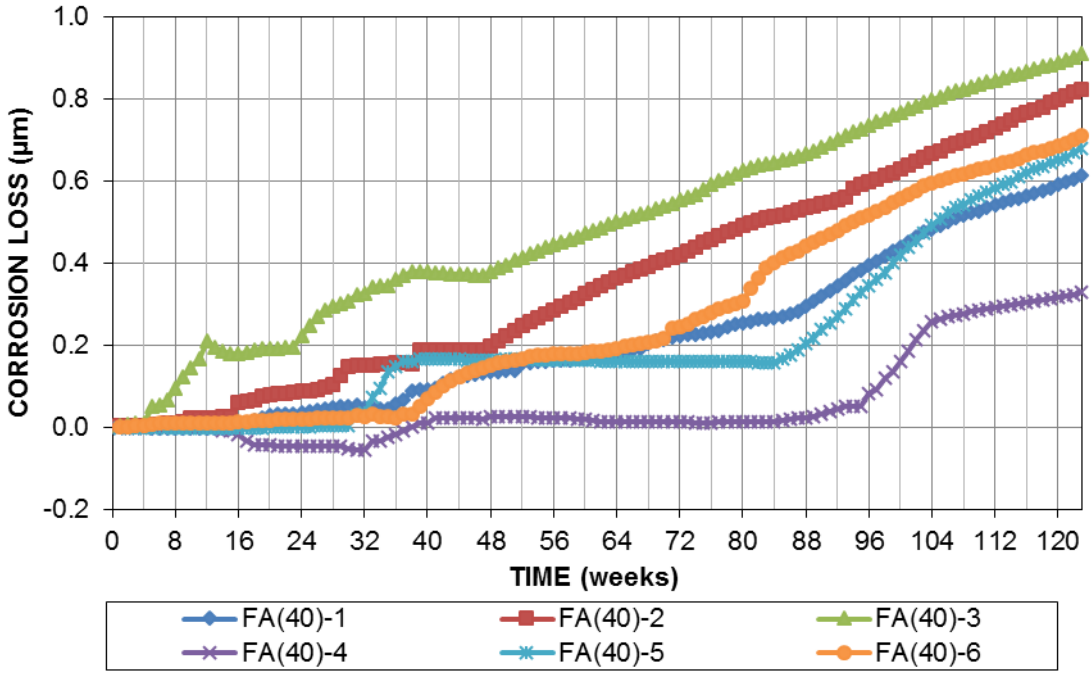

Figure G.3— Macrocell corrosion losses (µm) for specimens containing uncoated conventional reinforcement and 40% fly ash

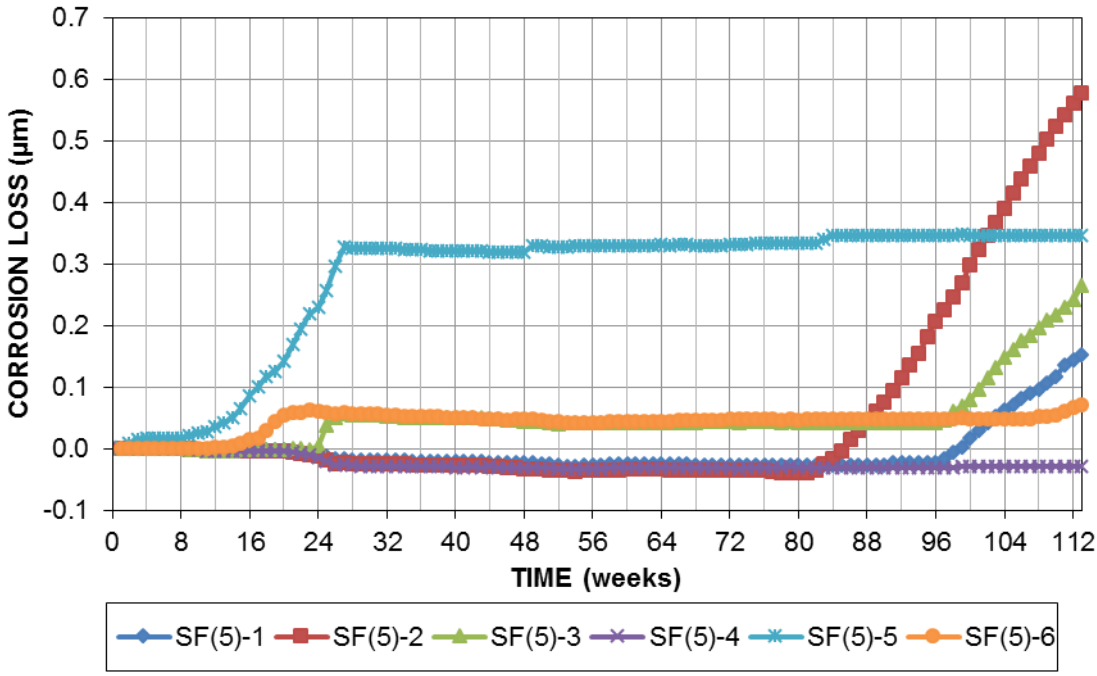

Figure G.4— Macrocell corrosion losses (µm) for specimens containing uncoated conventional reinforcement and 5% silica fume

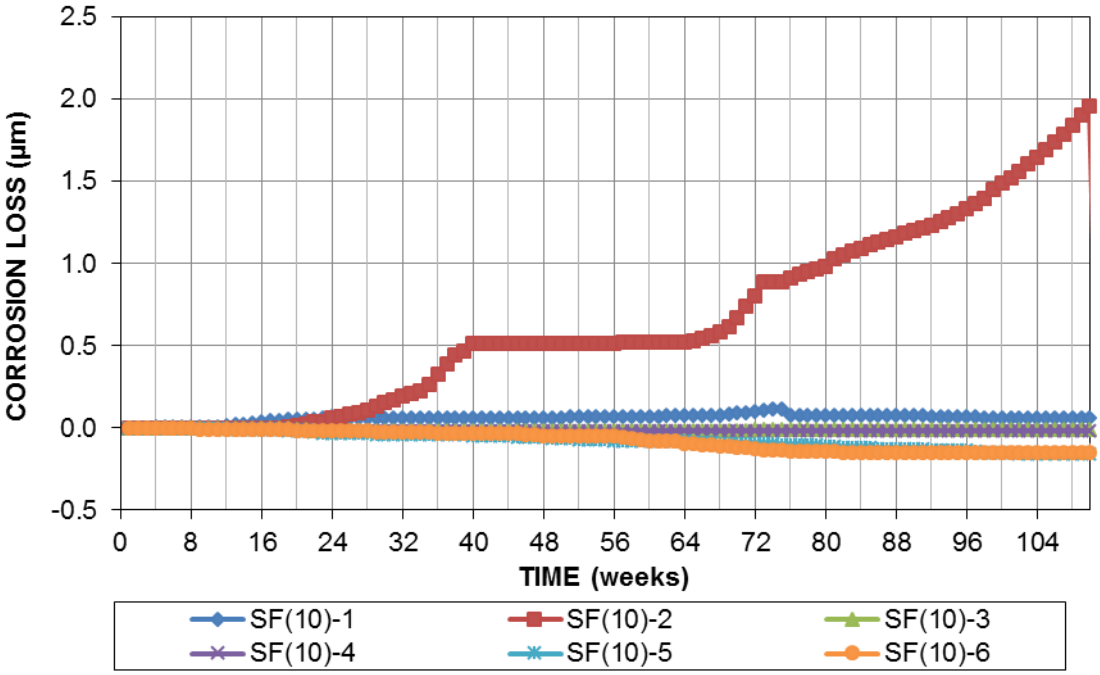

Figure G.5— Macrocell corrosion losses (µm) for specimens containing uncoated conventional reinforcement and 5% silica fume

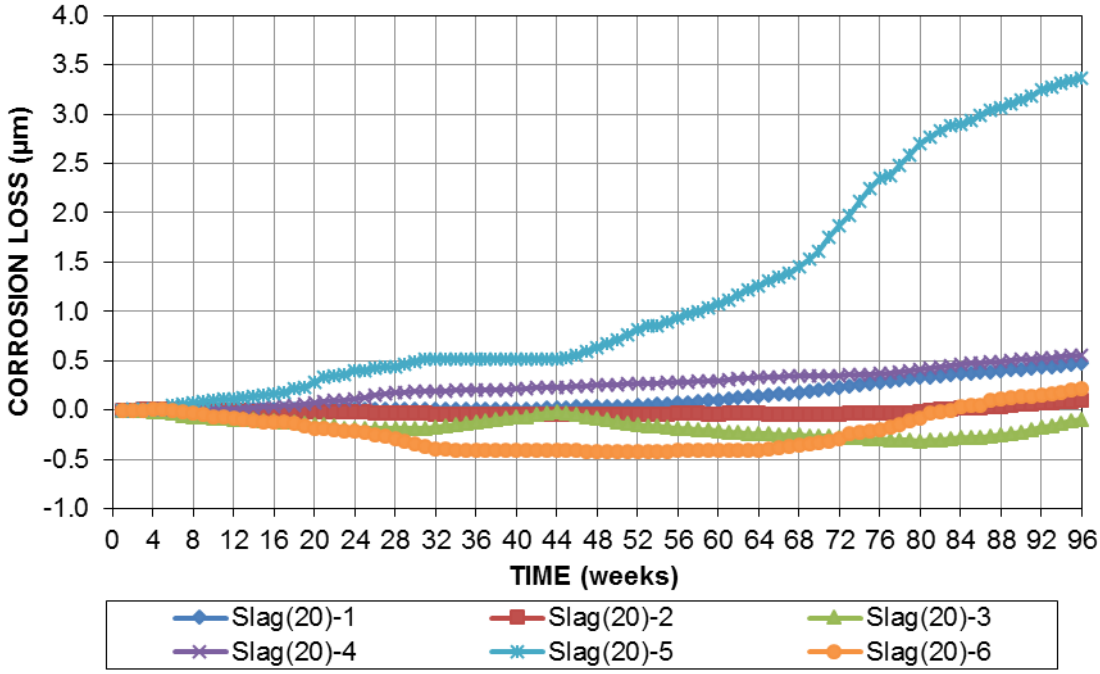

Figure G.6— Macrocell corrosion losses (µm) for specimens containing uncoated conventional reinforcement and 20% slag cement

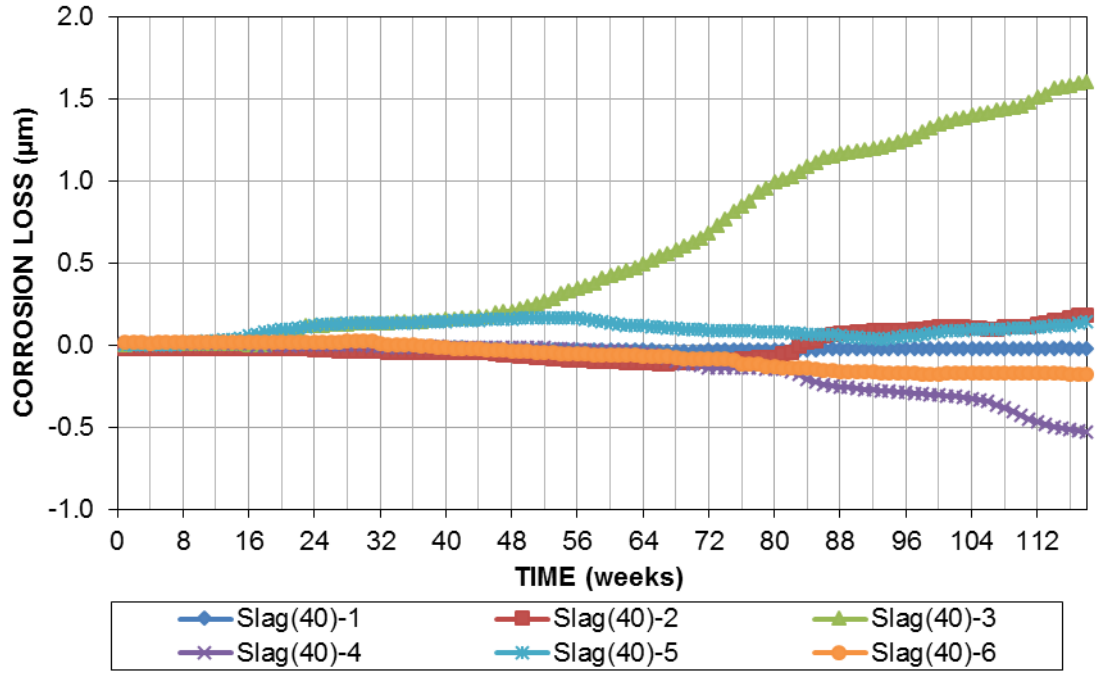

Figure G.7— Macrocell corrosion losses (µm) for specimens containing uncoated conventional reinforcement and 40% slag cement

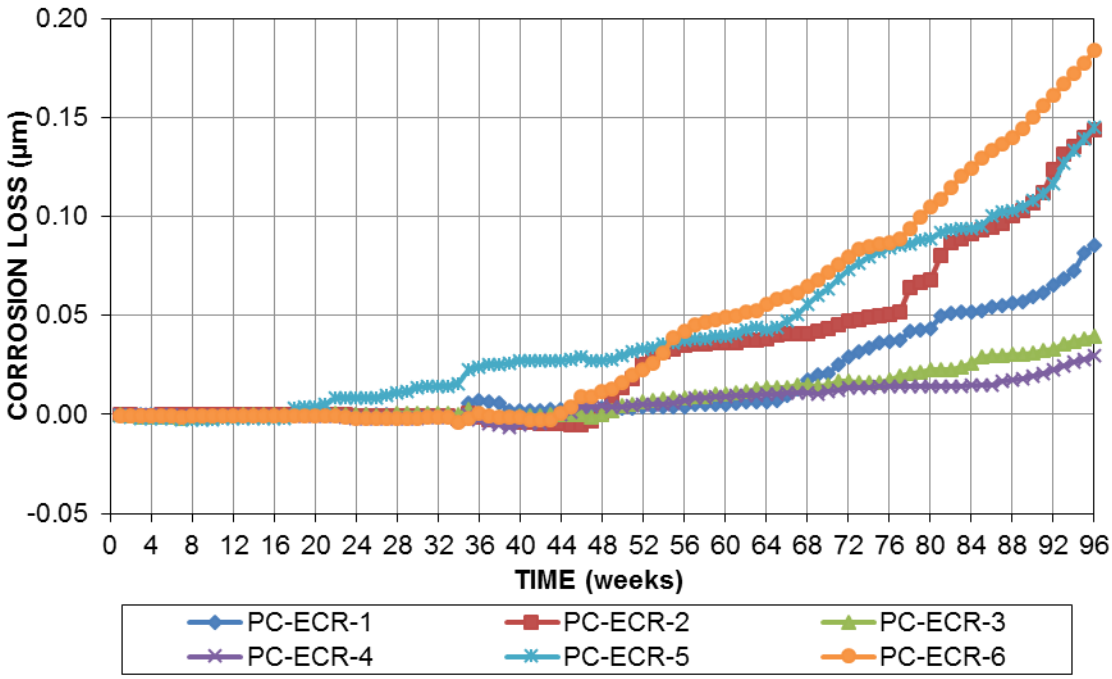

Figure G.8— Macrocell corrosion losses (µm) for specimens containing epoxy-coated conventional reinforcement and 100% portland cement

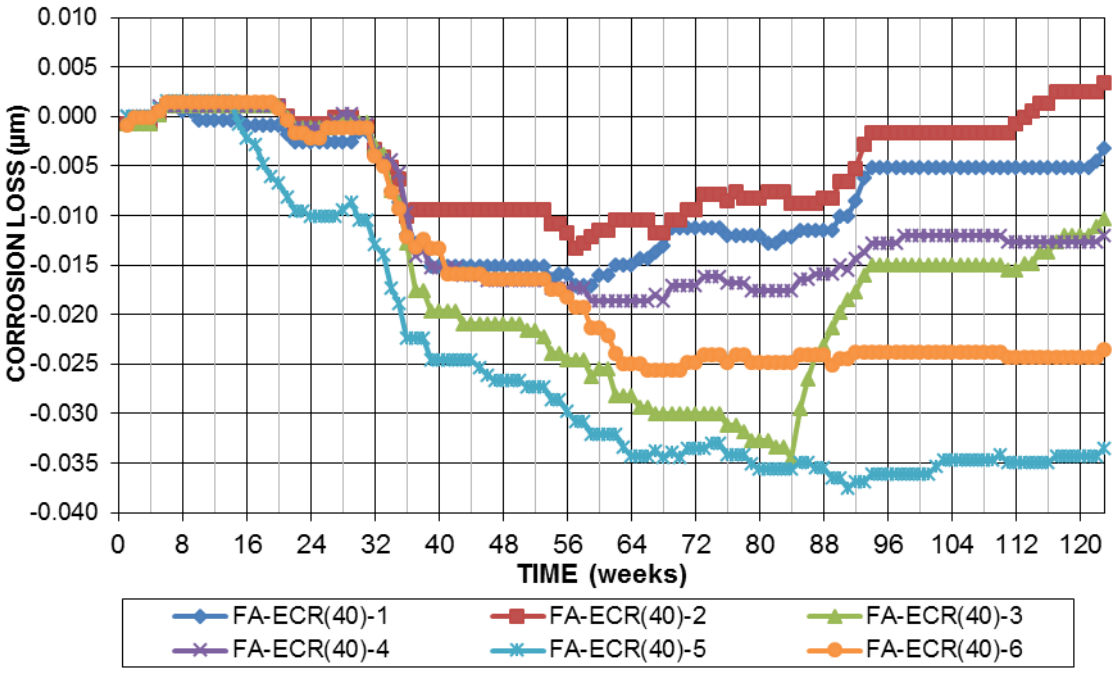

Figure G.9— Macrocell corrosion losses (µm) for specimens containing epoxy-coated conventional reinforcement and 40% fly ash

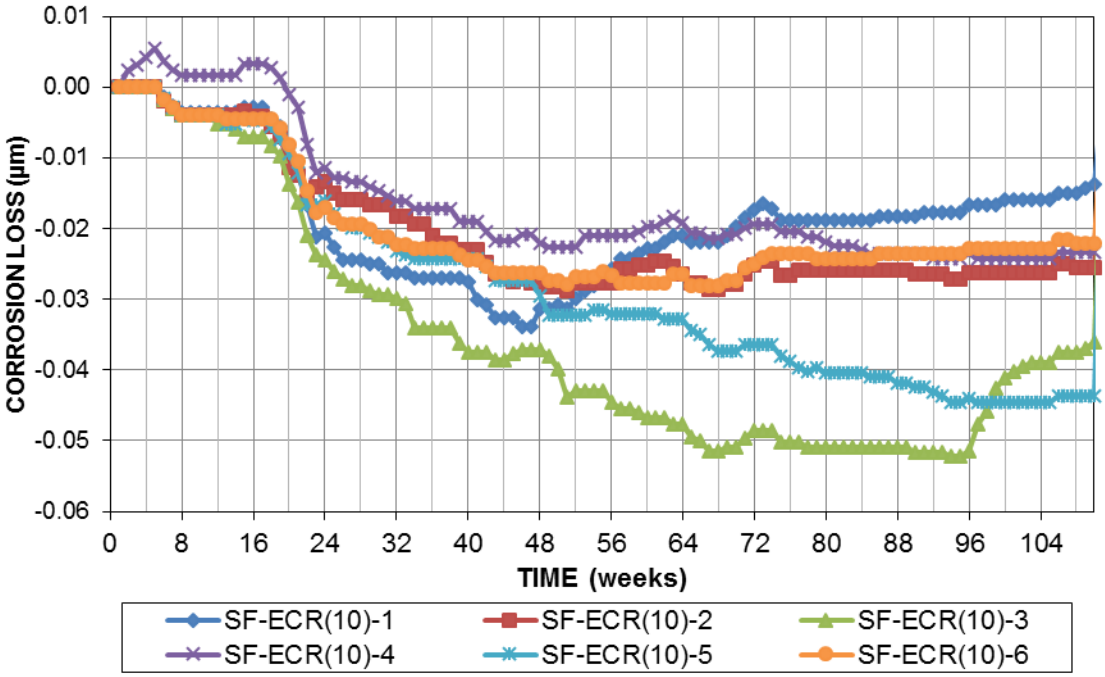

Figure G.10— Macrocell corrosion losses (µm) for specimens containing epoxy-coated conventional reinforcement and 10% silica fume

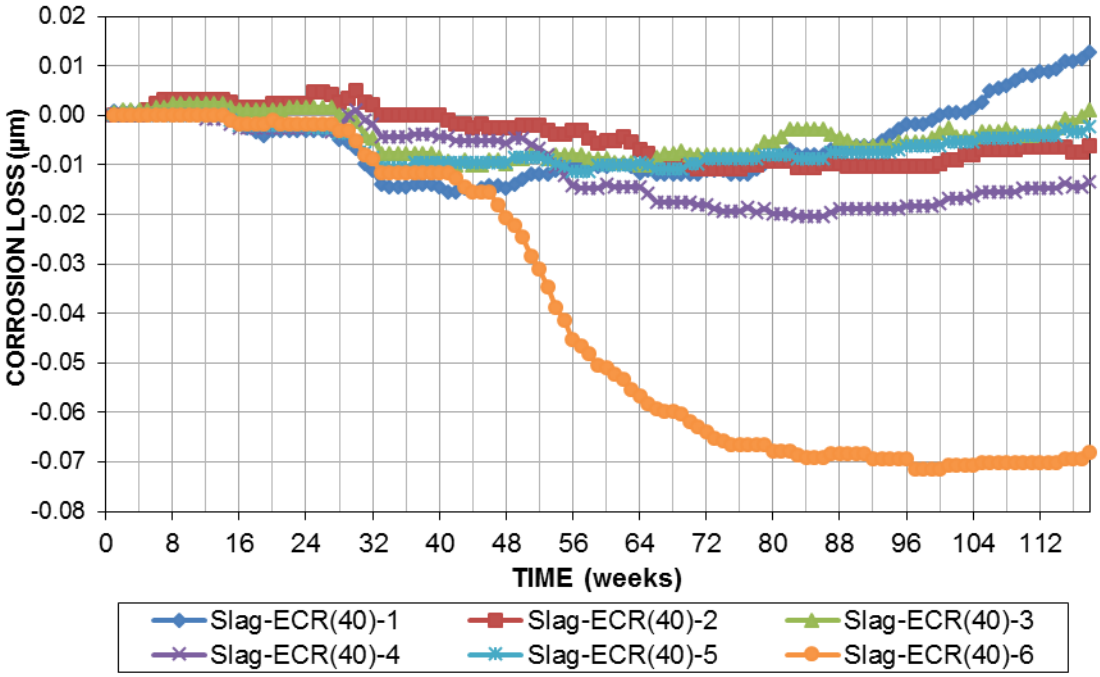

Figure G.11— Macrocell corrosion losses (µm) for specimens containing epoxy-coated conventional reinforcement and 10% silica fume

APPENDIX H

LPR CORROSION RATE OF BEAM SPECIMENS CONTAINING SUPPLEMENTARY CEMENTITIOUS MATERIALS WITH BARE AND EPOXY-COATED REINFORCEMENT

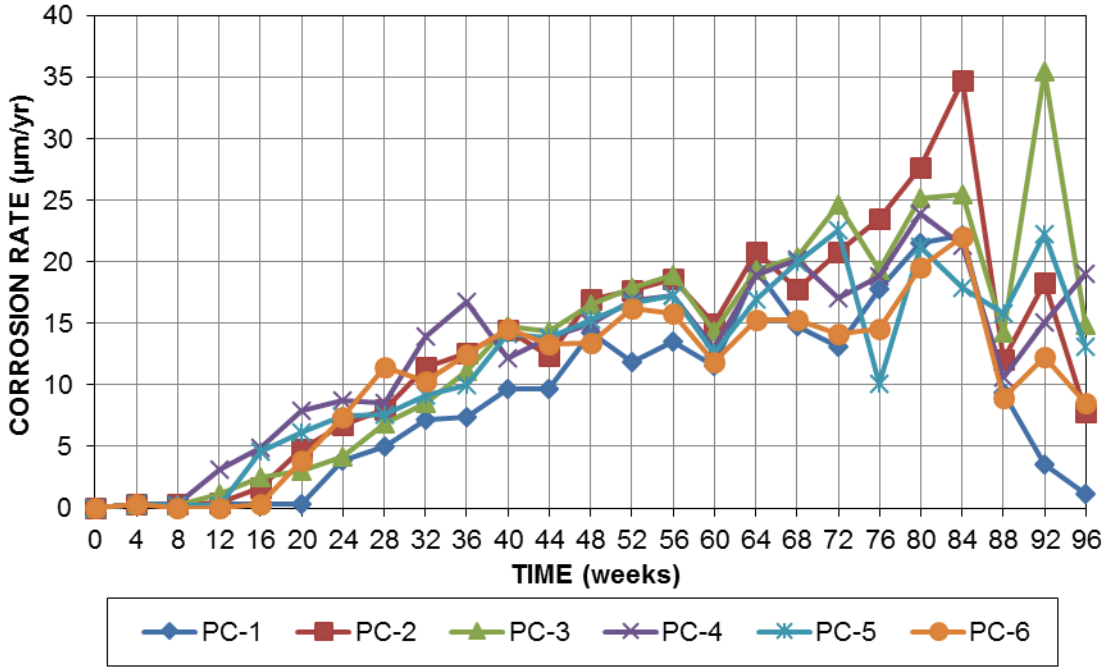

Figure H.1— LPR test corrosion rates (µm/yr) for specimens containing uncoated conventional reinforcement and 100% portland cement

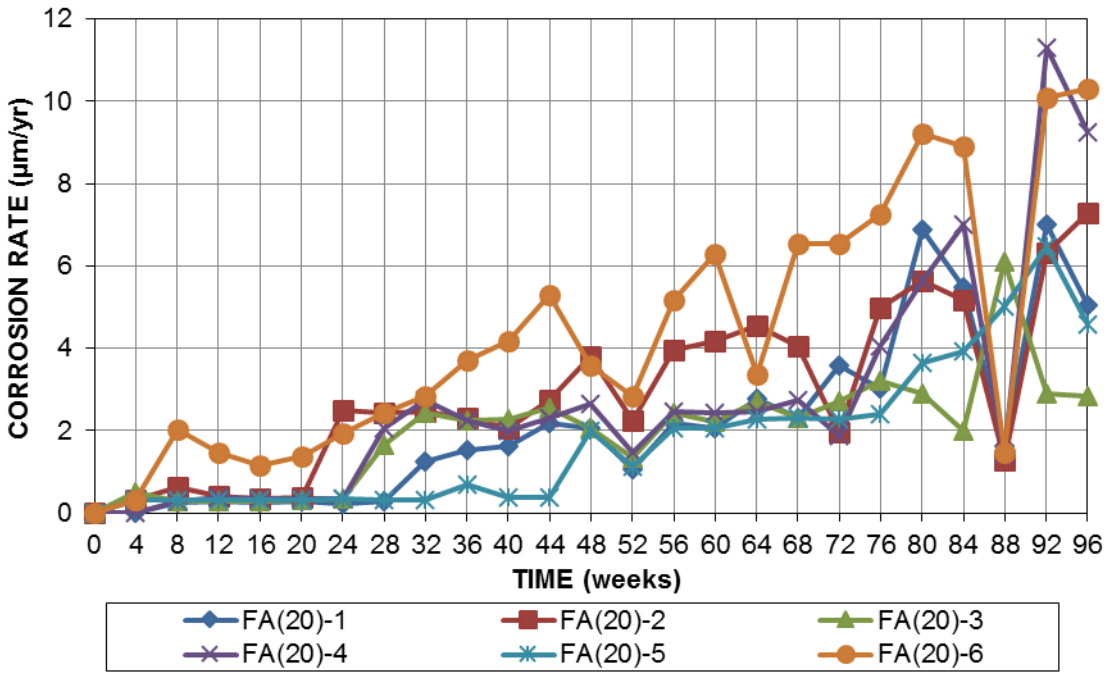

Figure H.2— LPR test corrosion rates (µm/yr) for specimens containing uncoated conventional reinforcement and 20% fly ash

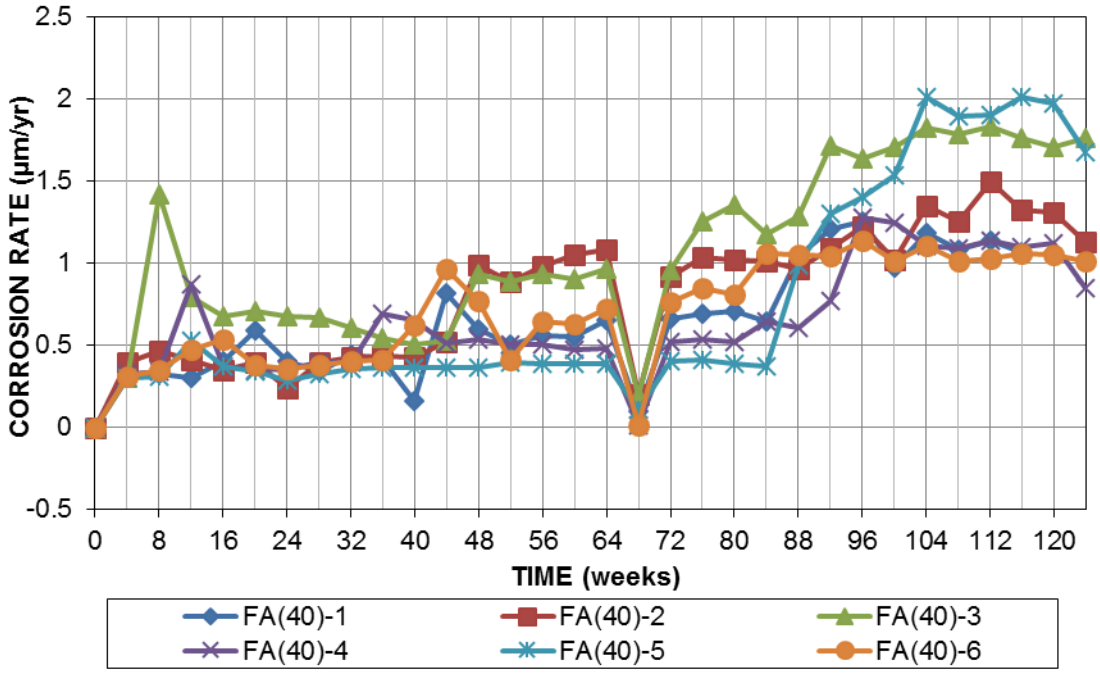

Figure H.3— LPR test corrosion rates (µm/yr) for specimens containing uncoated conventional reinforcement and 40% fly ash

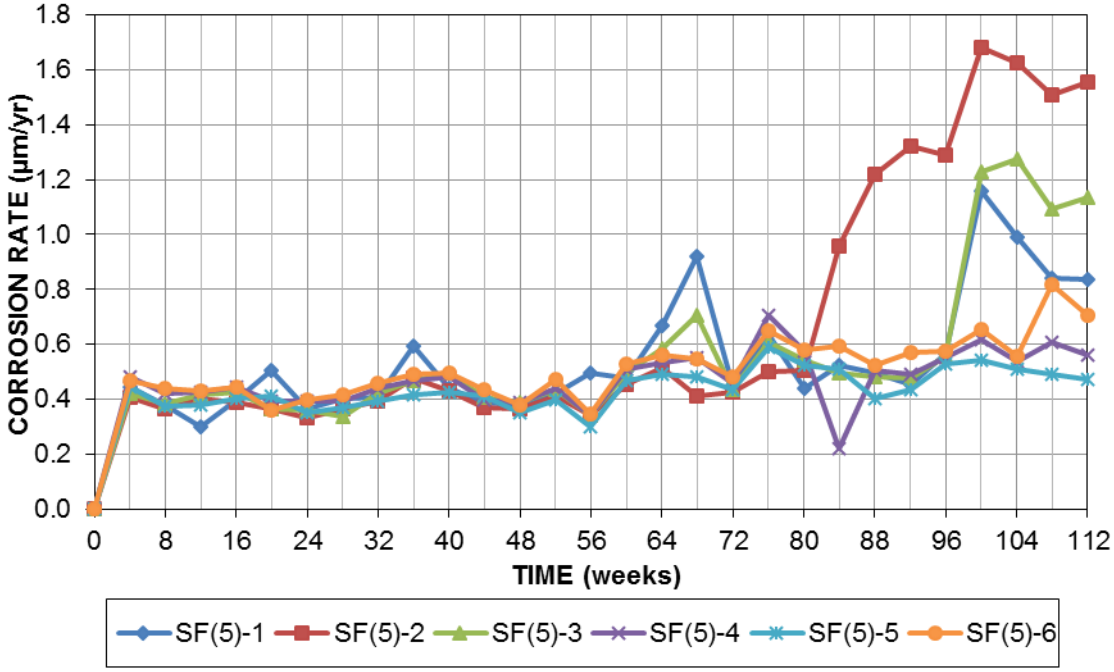

Figure H.4— LPR test corrosion rates (µm/yr) for specimens containing uncoated conventional reinforcement and 5% silica fume

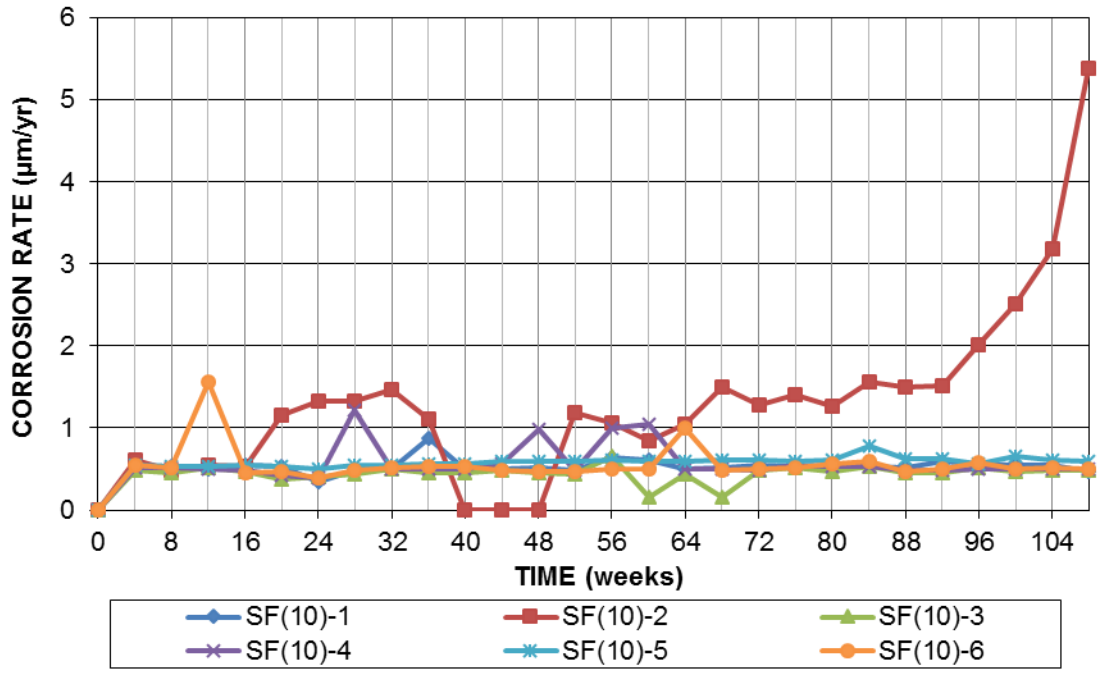

Figure H.5— LPR test corrosion rates (µm/yr) for specimens containing uncoated conventional reinforcement and 10% silica fume

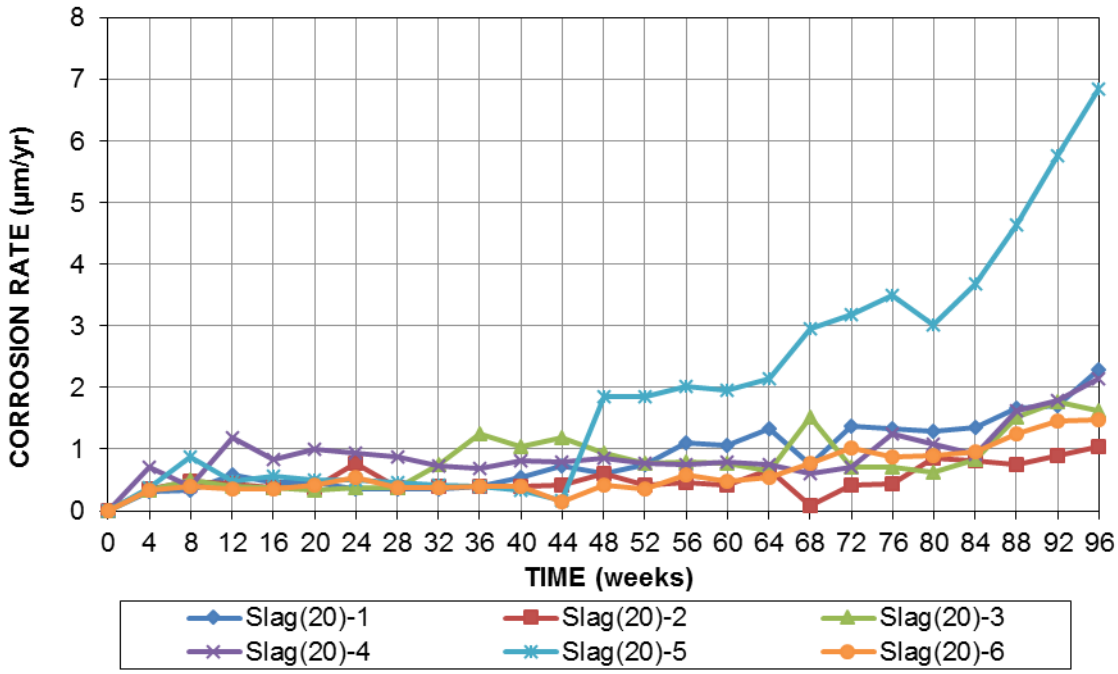

Figure H.6— LPR test corrosion rates (µm/yr) for specimens containing uncoated conventional reinforcement and 20% slag cement

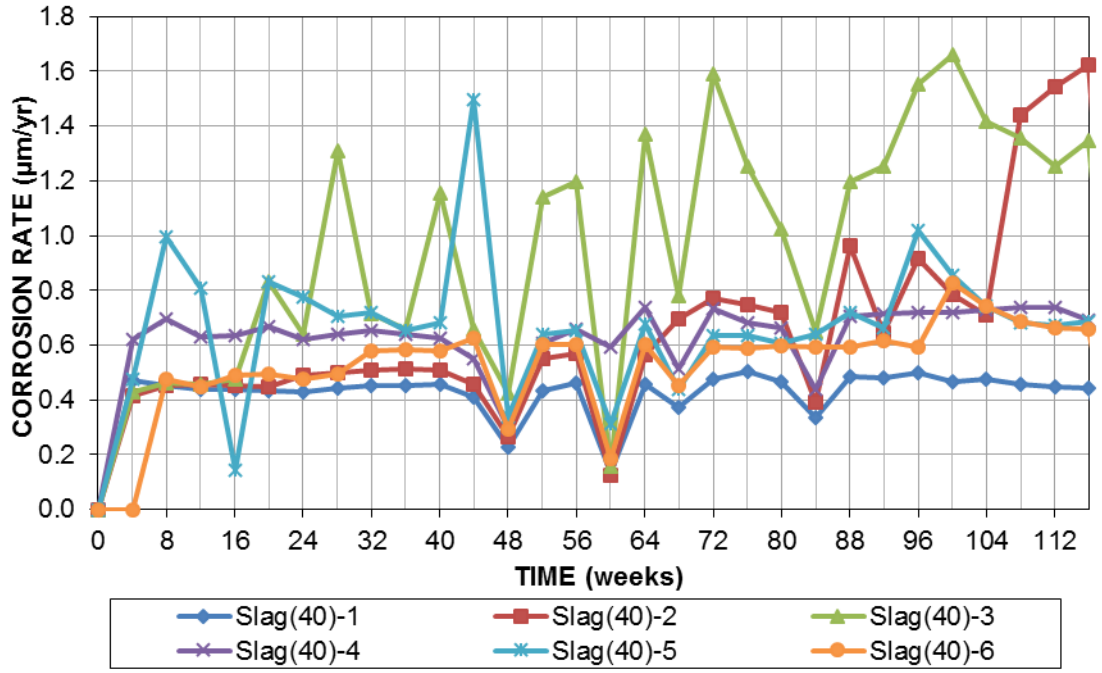

Figure H.7— LPR test corrosion rates (µm/yr) for specimens containing uncoated conventional reinforcement and 40% slag cement

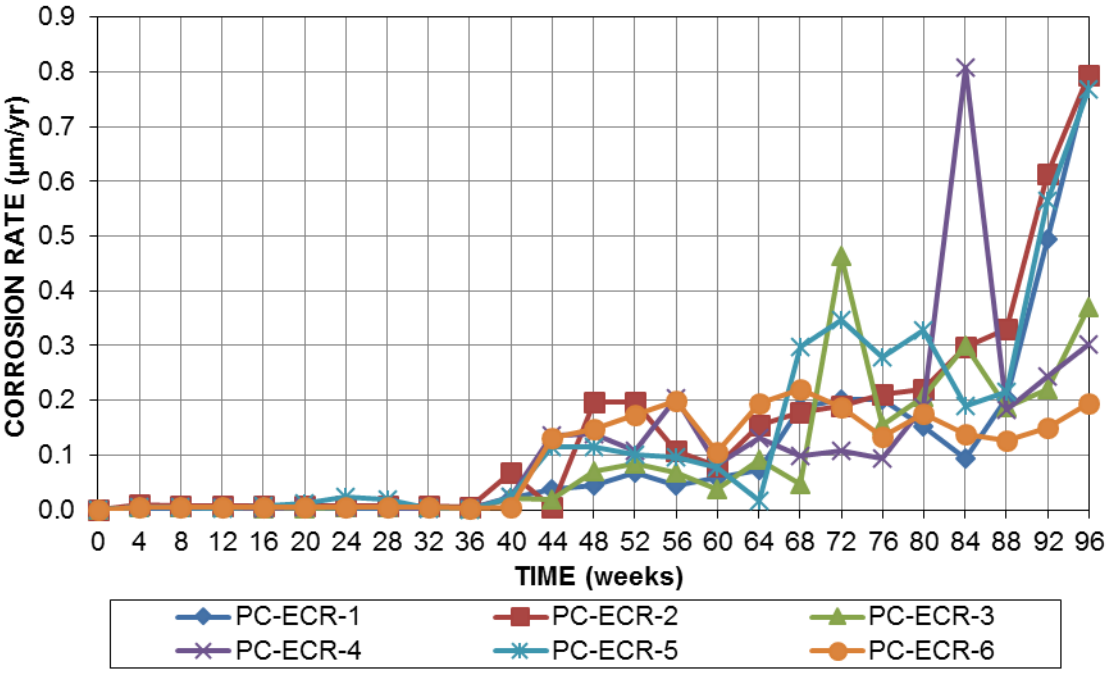

Figure H.8— LPR test corrosion rates (µm/yr) for specimens containing epoxy-coated reinforcement and 100% portland cement

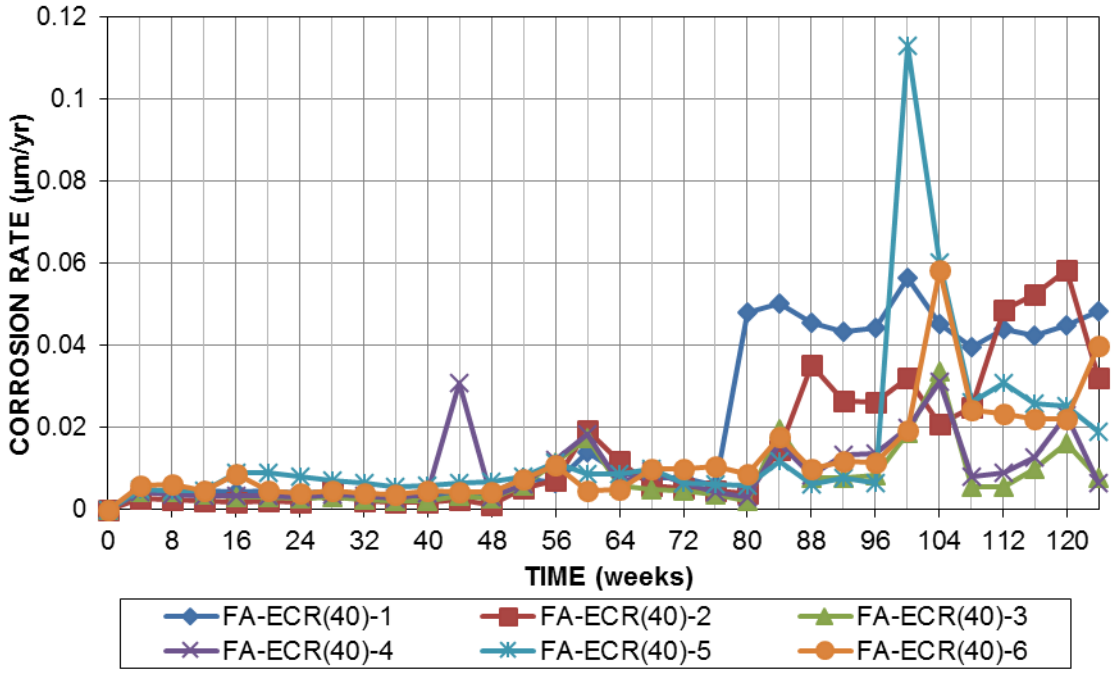

Figure H.9— LPR test corrosion rates (µm/yr) for specimens containing epoxy-coated reinforcement and 40% fly ash

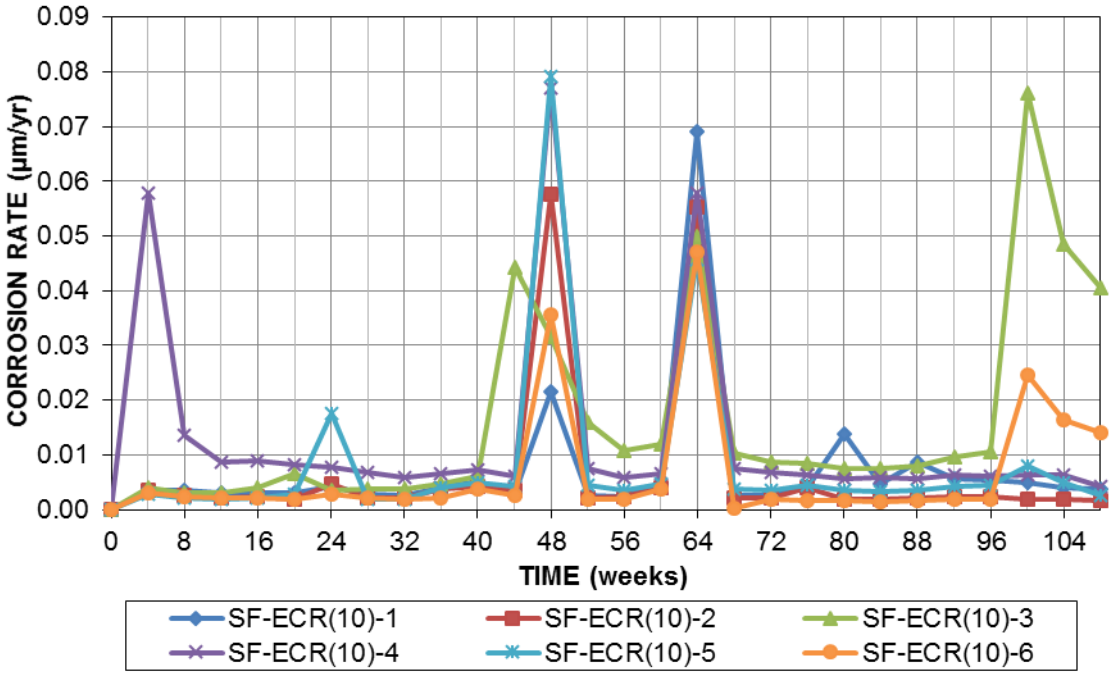

Figure H.10— LPR test corrosion rates (µm/yr) for specimens containing epoxy-coated reinforcement and 10% silica fume

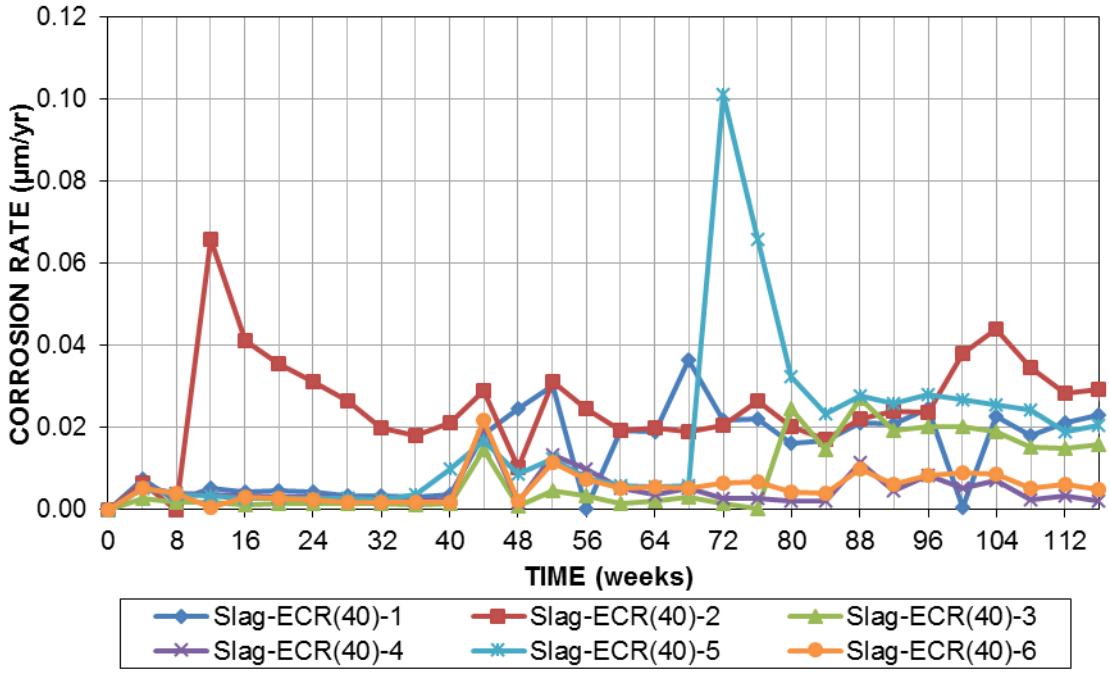

Figure H.11— LPR test corrosion rates (µm/yr) for specimens containing epoxy-coated reinforcement and 40% slag cement

APPENDIX I

LPR CORROSION LOSS OF BEAM SPECIMENS CONTAINING SUPPLEMENTARY CEMENTITIOUS MATERIALS WITH BARE AND EPOXY-COATED REINFORCEMENT

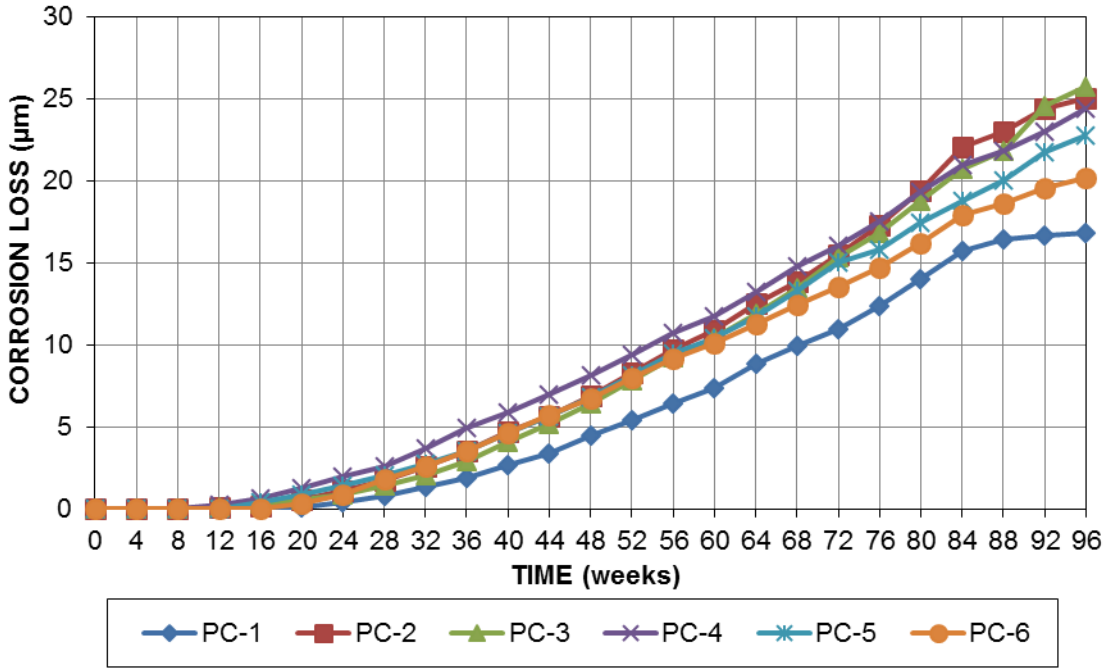

Figure I.1— LPR test corrosion losses (µm) for specimens containing uncoated conventional reinforcement and 100% portland cement

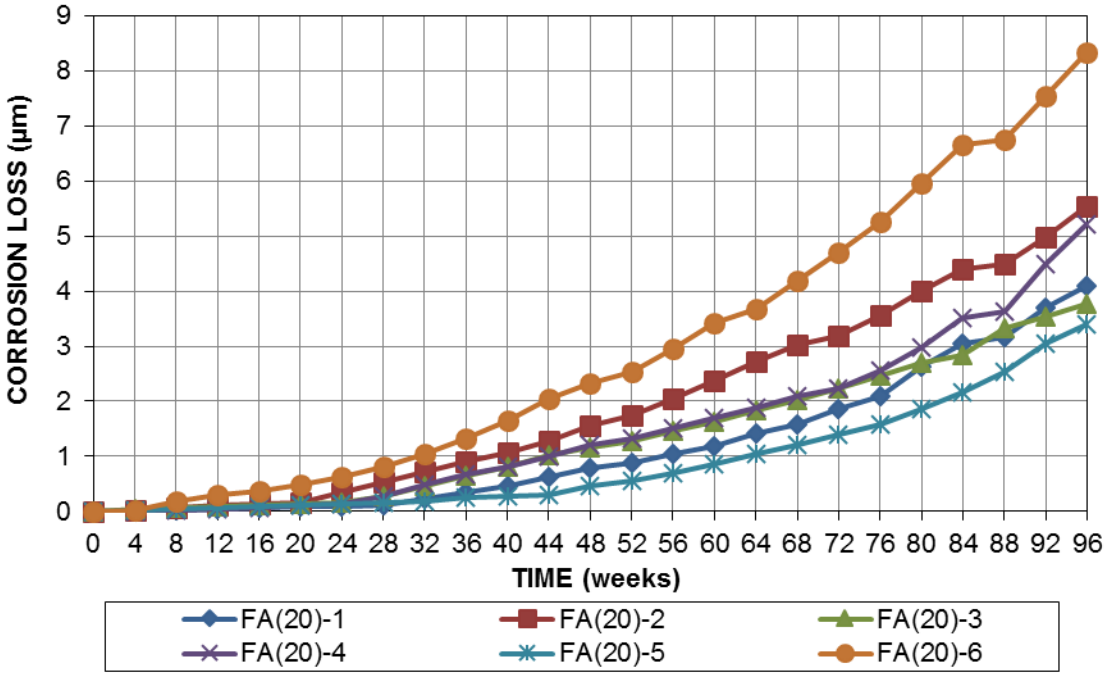

Figure I.2— LPR test corrosion losses (µm) for specimens containing uncoated conventional reinforcement and 20% fly ash

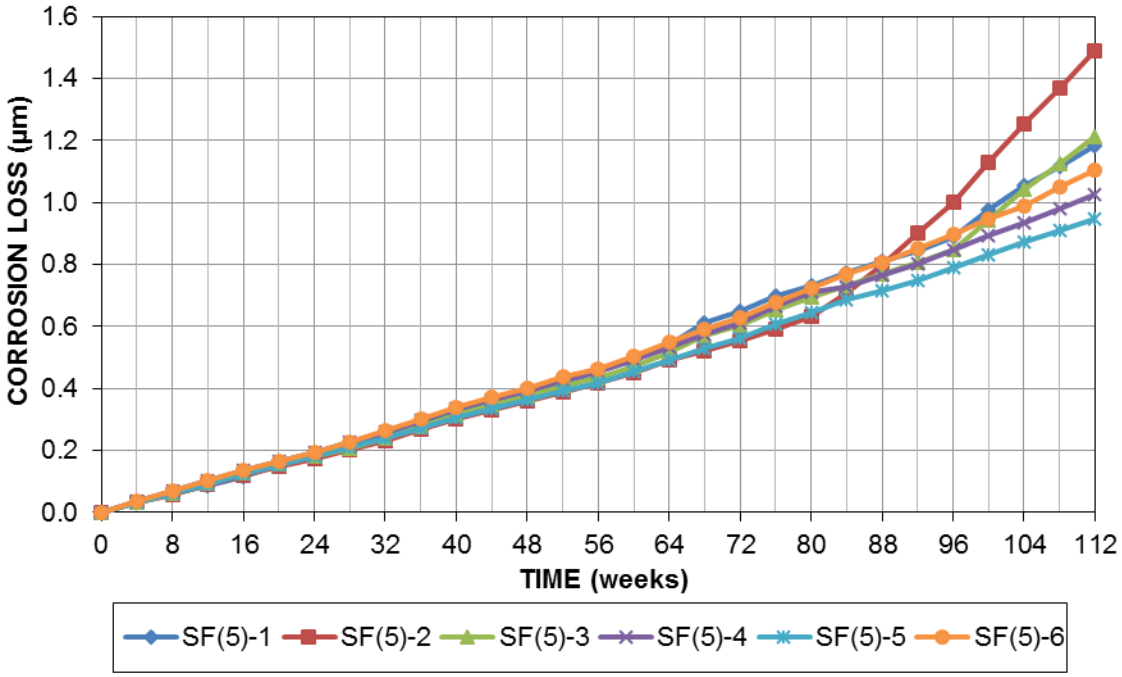

Figure I.3— LPR test corrosion losses (µm) for specimens containing uncoated conventional reinforcement and 5% silica fume

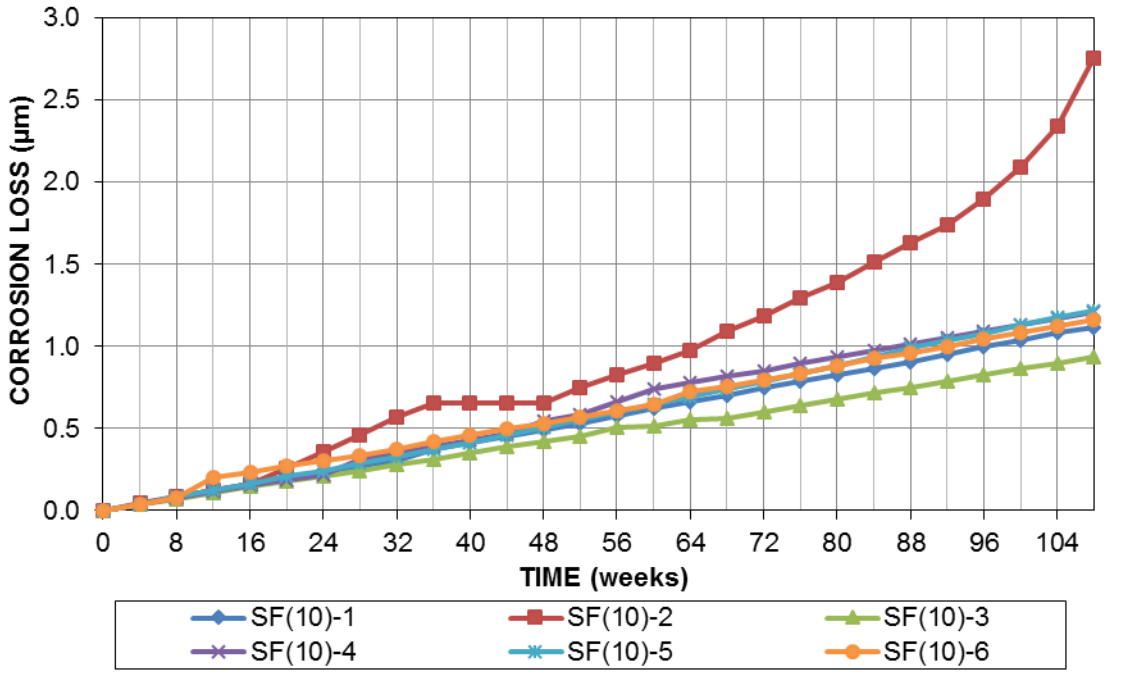

Figure I.4— LPR test corrosion losses (µm) for specimens containing uncoated conventional reinforcement and 10% silica fume

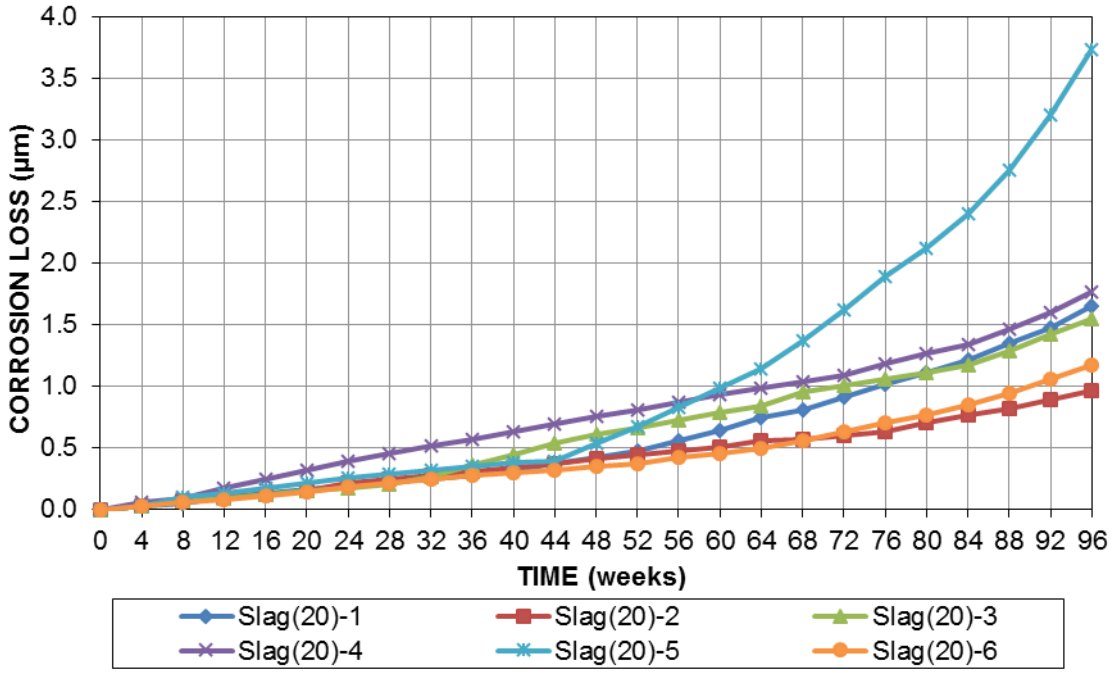

Figure I.5— LPR test corrosion losses (µm) for specimens containing uncoated conventional reinforcement and 20% slag cement

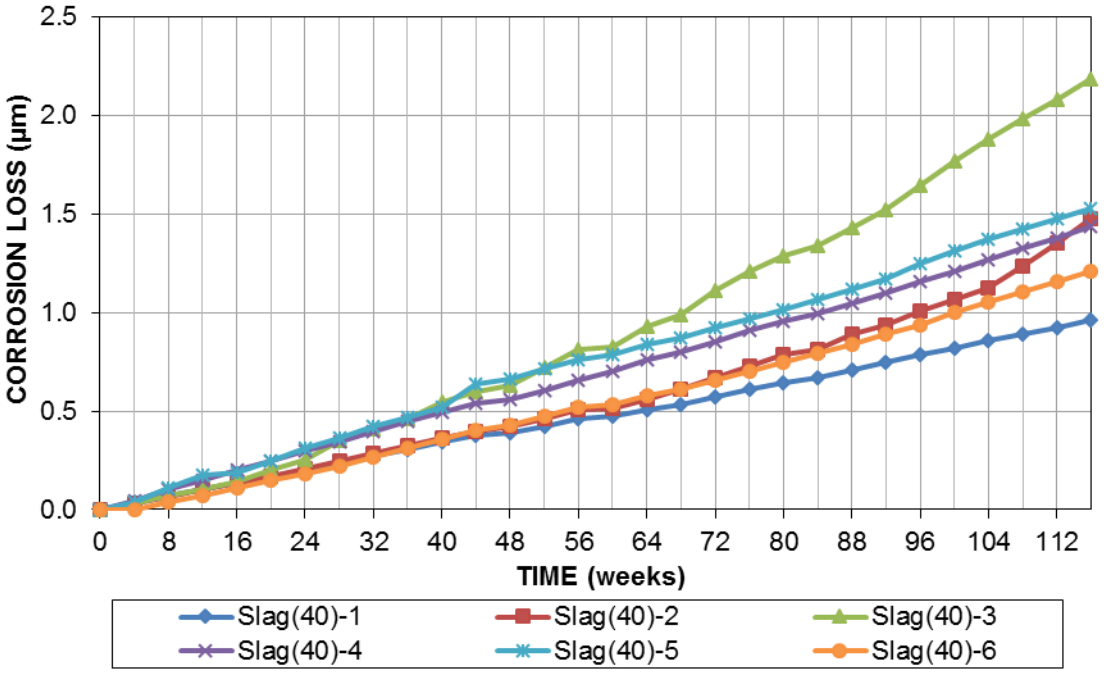

Figure I.6— LPR test corrosion losses (µm) for specimens containing uncoated conventional reinforcement and 40% slag cement

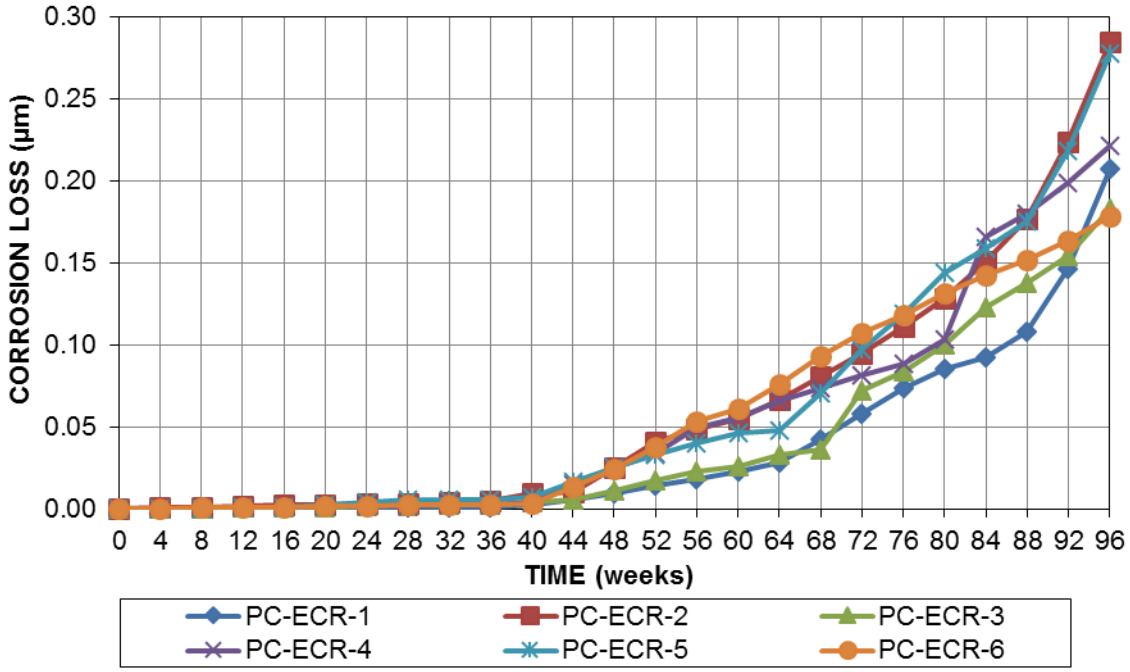

Figure I.7— LPR test corrosion losses (µm) for specimens containing epoxy-coated conventional reinforcement and 100% portland cement

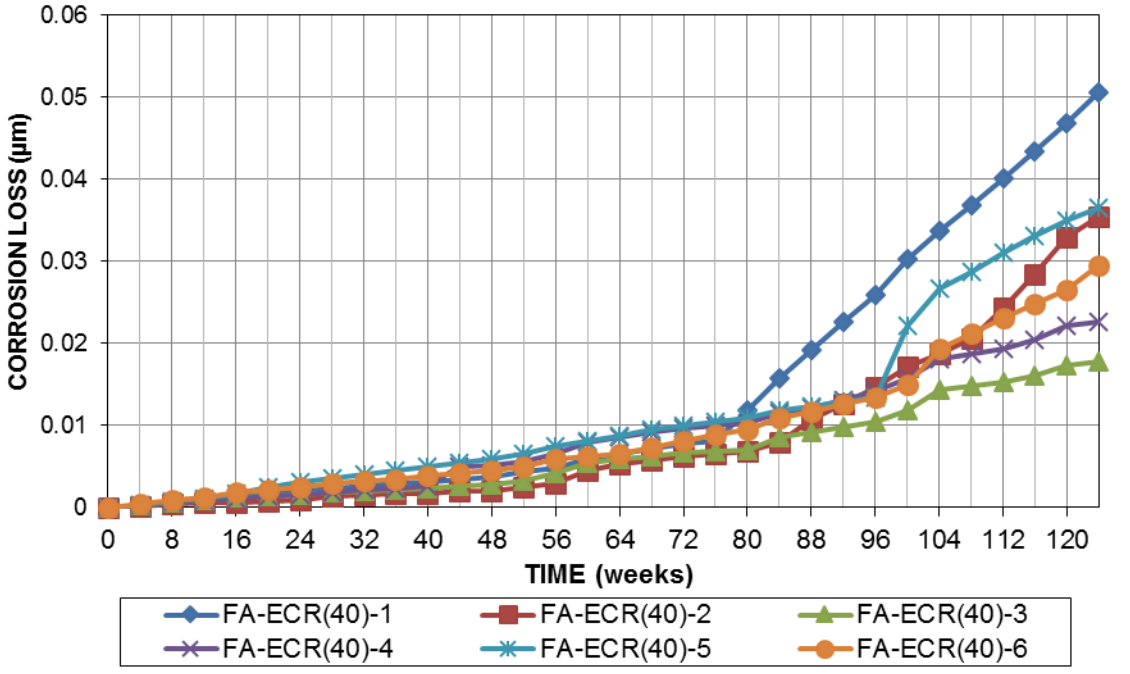

Figure I.8— LPR test corrosion losses (µm) for specimens containing epoxy-coated conventional reinforcement and 40% fly ash

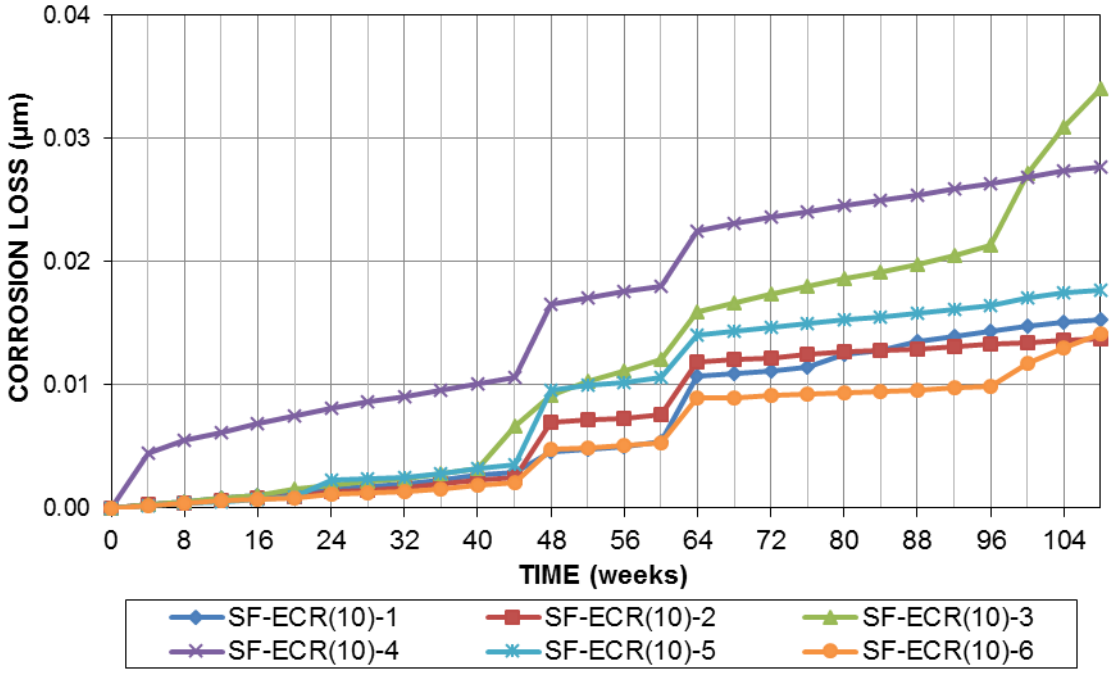

Figure I.9— LPR test corrosion losses (µm) for specimens containing epoxy-coated conventional reinforcement and 10% silica fume

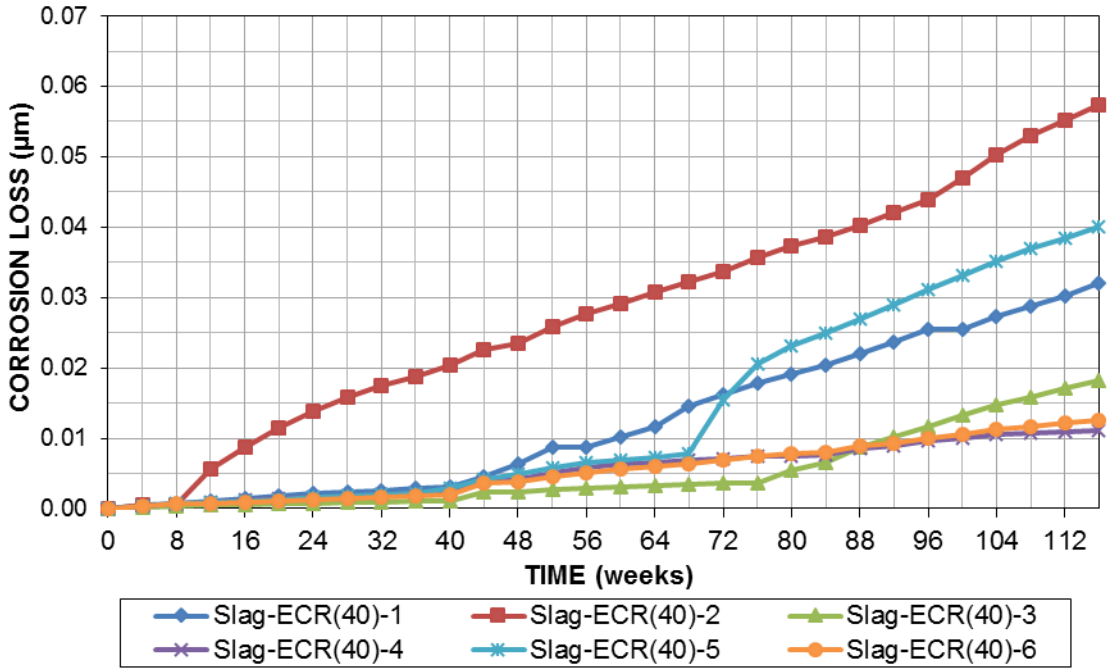

Figure I.10— LPR test corrosion losses (µm) for specimens containing epoxy-coated conventional reinforcement and 40% slag cement

APPENDIX J

BOTTOM MAT CORROSION POTENTIAL OF BEAM SPECIMENS CONTAINING SUPPLEMENTARY CEMENTITIOUS MATERIALS WITH BARE AND EPOXY-COATED REINFORCEMENT

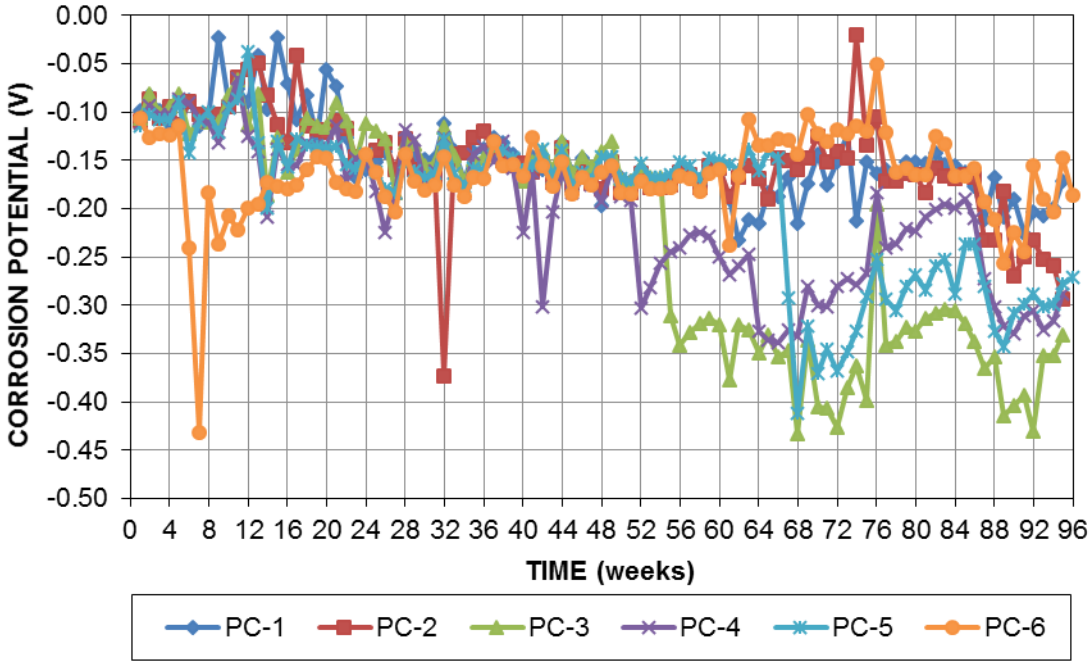

Figure J.1—Bottom mat (cathode) corrosion potential (SCE) versus time for beam specimens containing conventional reinforcement and 100% portland cement

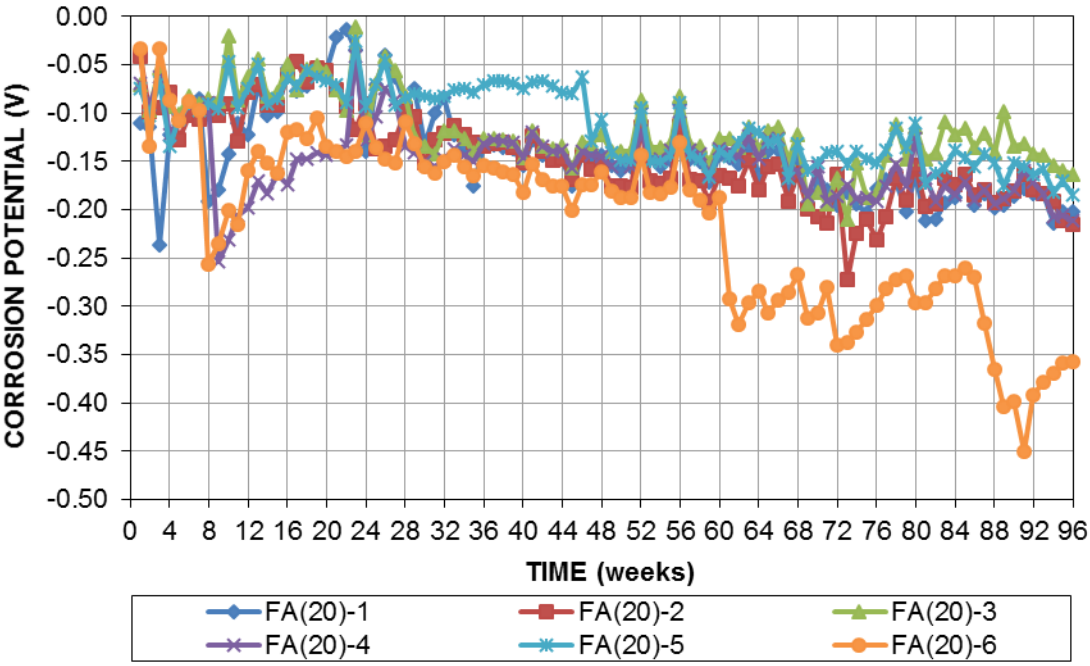

Figure J.2—Bottom mat (cathode) corrosion potential (SCE) versus time for beam specimens containing conventional reinforcement and 20% fly ash

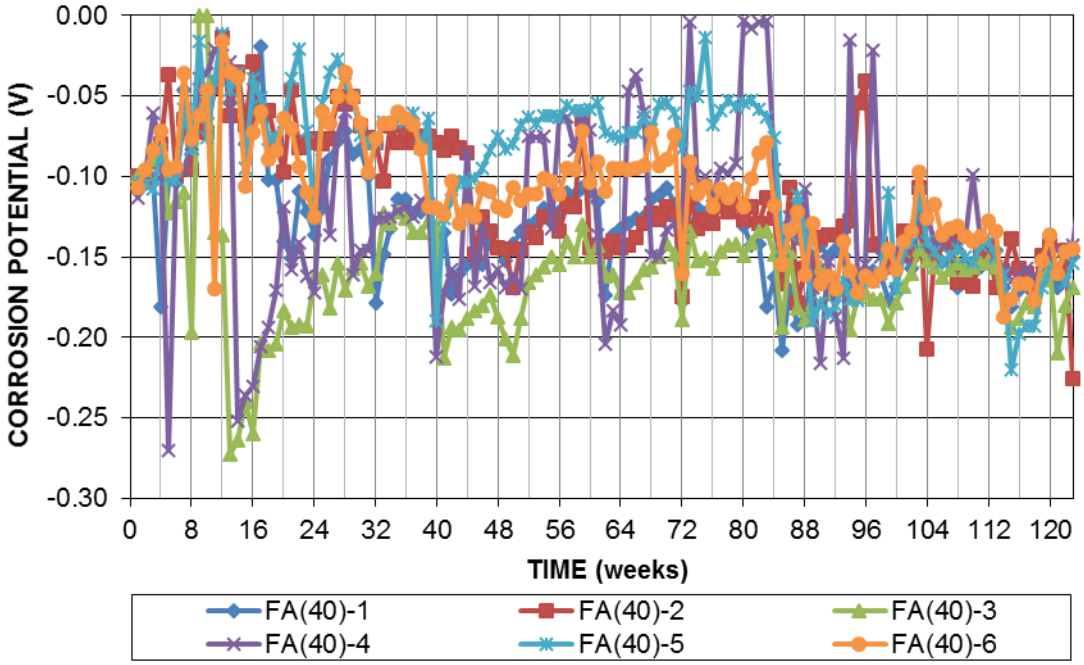

Figure J.3—Bottom mat (cathode) corrosion potential (SCE) versus time for beam specimens containing conventional reinforcement and 40% fly ash

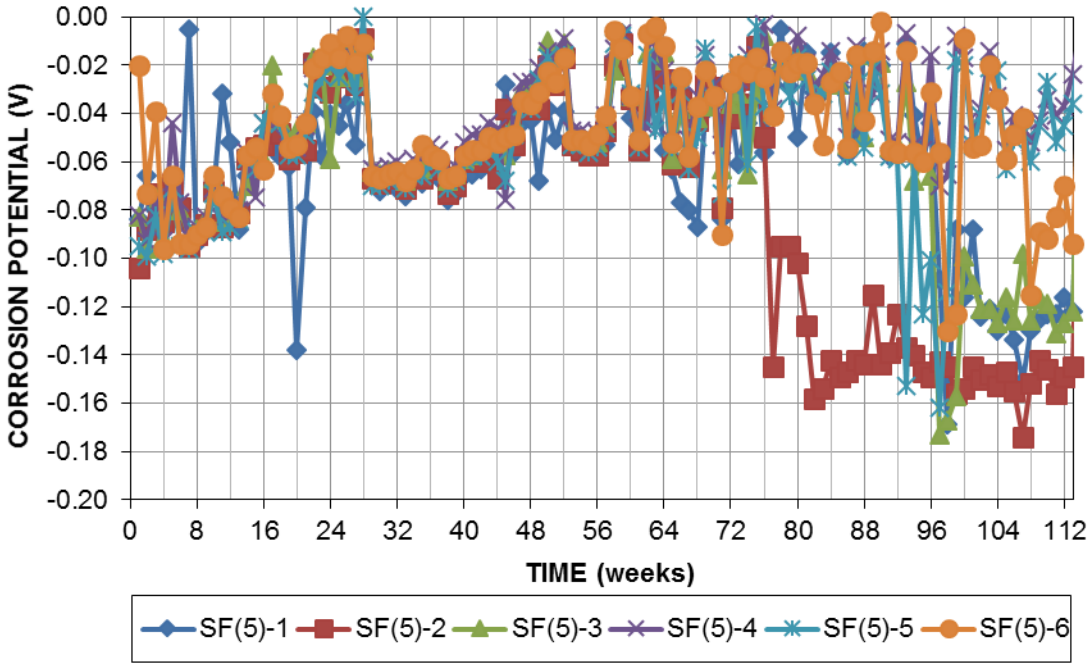

Figure J.4—Bottom mat (cathode) corrosion potential (SCE) versus time for beam specimens containing conventional reinforcement and 5% silica fume

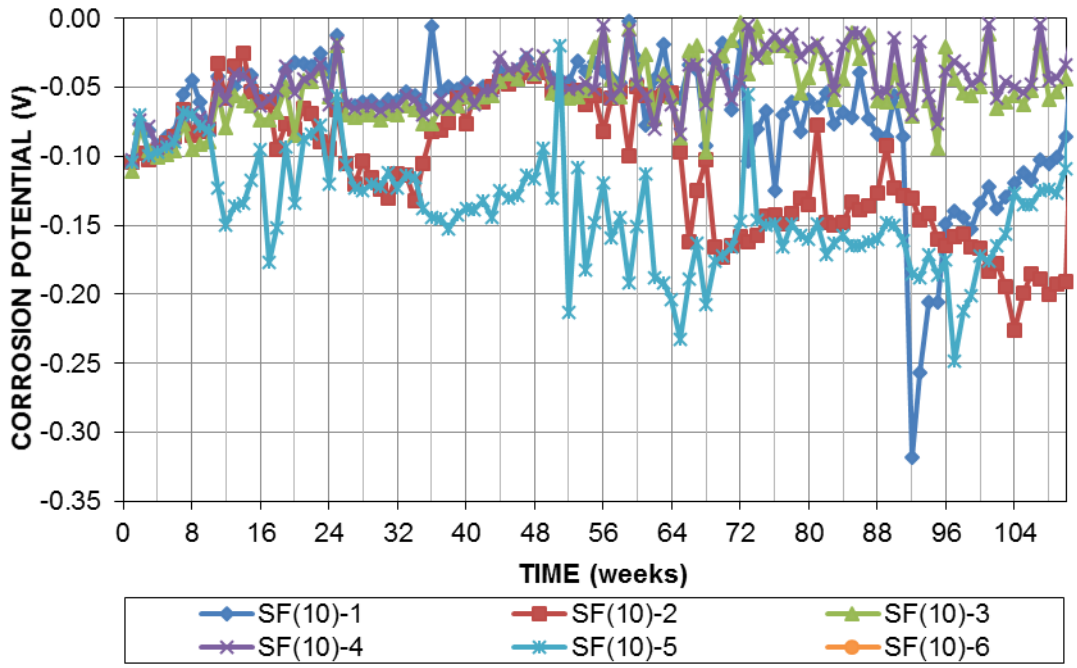

Figure J.5—Bottom mat (cathode) corrosion potential (SCE) versus time for beam specimens containing conventional reinforcement and 10% silica fume

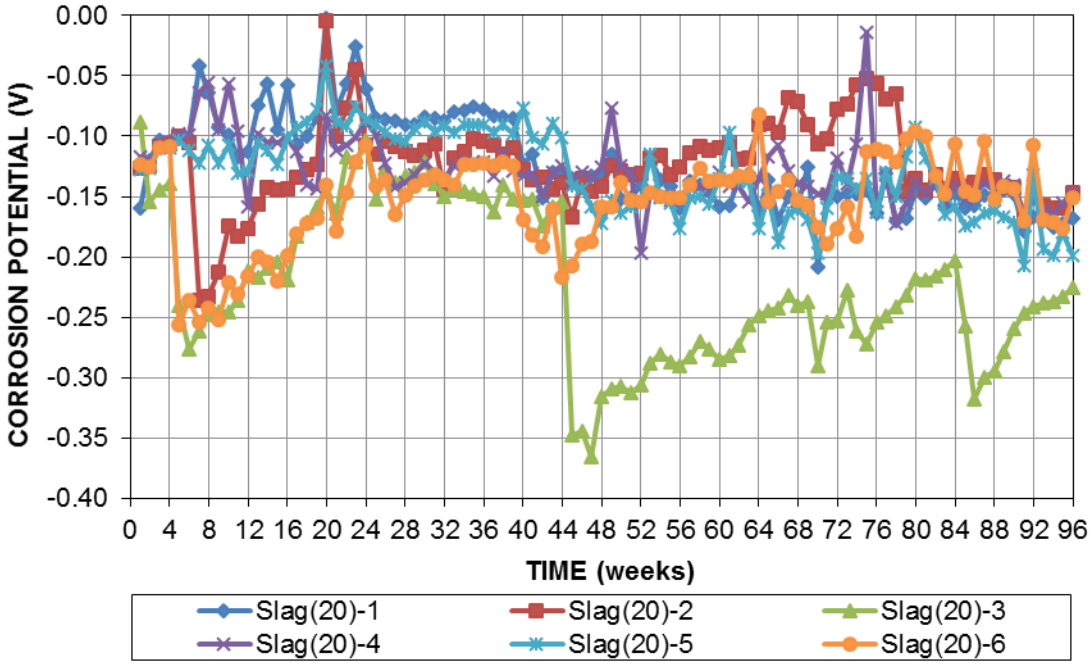

Figure J.6—Bottom mat (cathode) corrosion potential (SCE) versus time for beam specimens containing conventional reinforcement and 20% slag cement

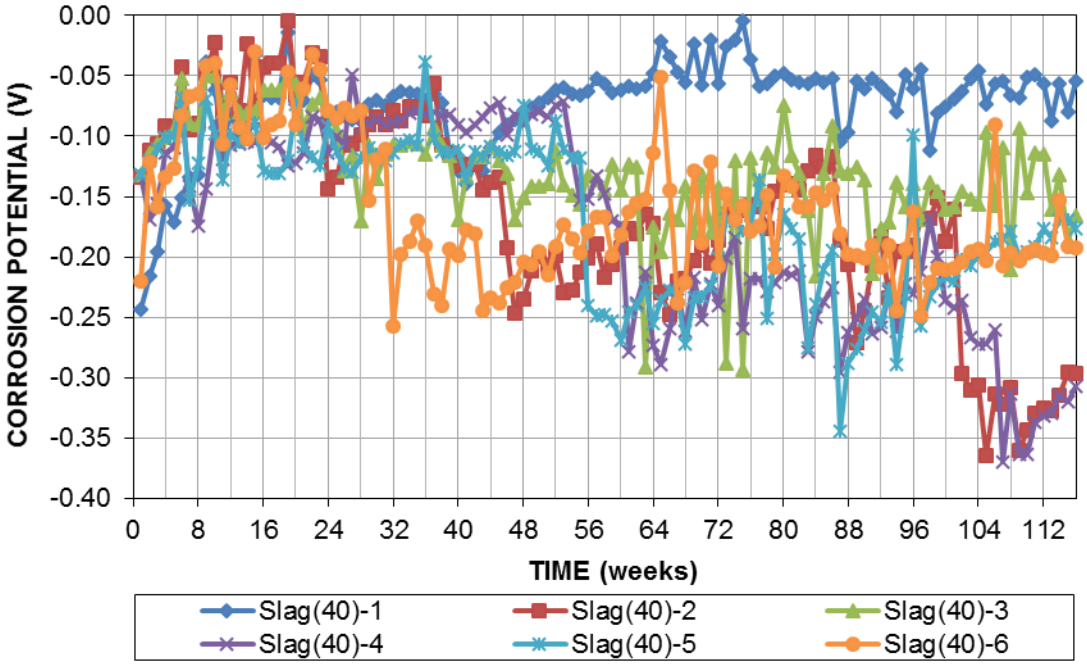

Figure J.7—Bottom mat (cathode) corrosion potential (SCE) versus time for beam specimens containing conventional reinforcement and 40% slag cement

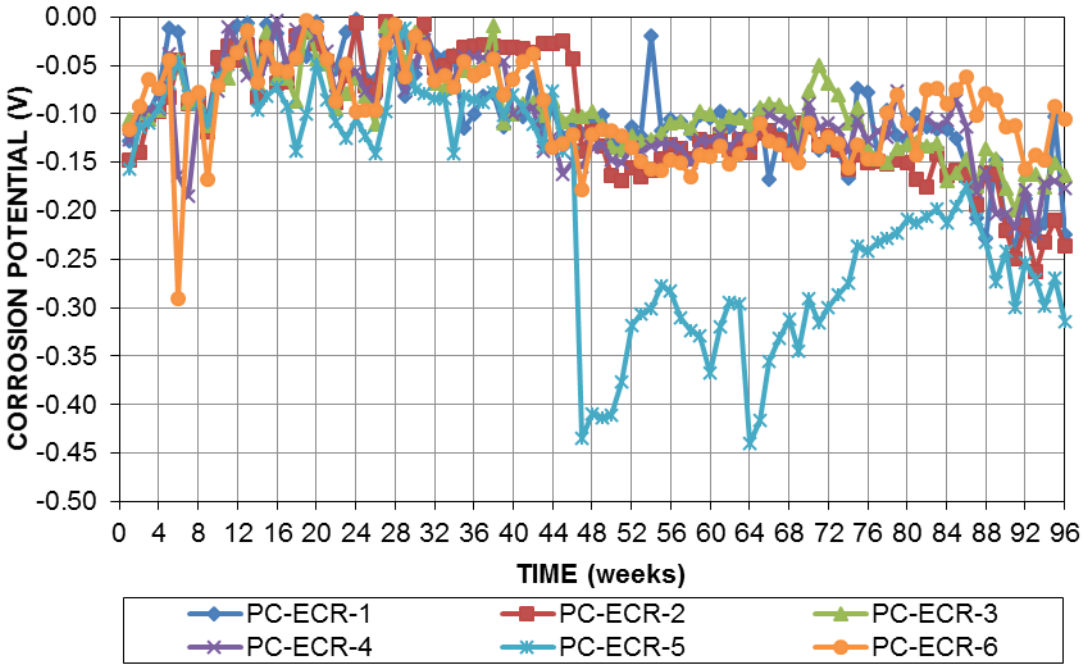

Figure J.8—Bottom mat (cathode) corrosion potential (SCE) versus time for beam specimens containing epoxy-coated reinforcement and 100% portland cement

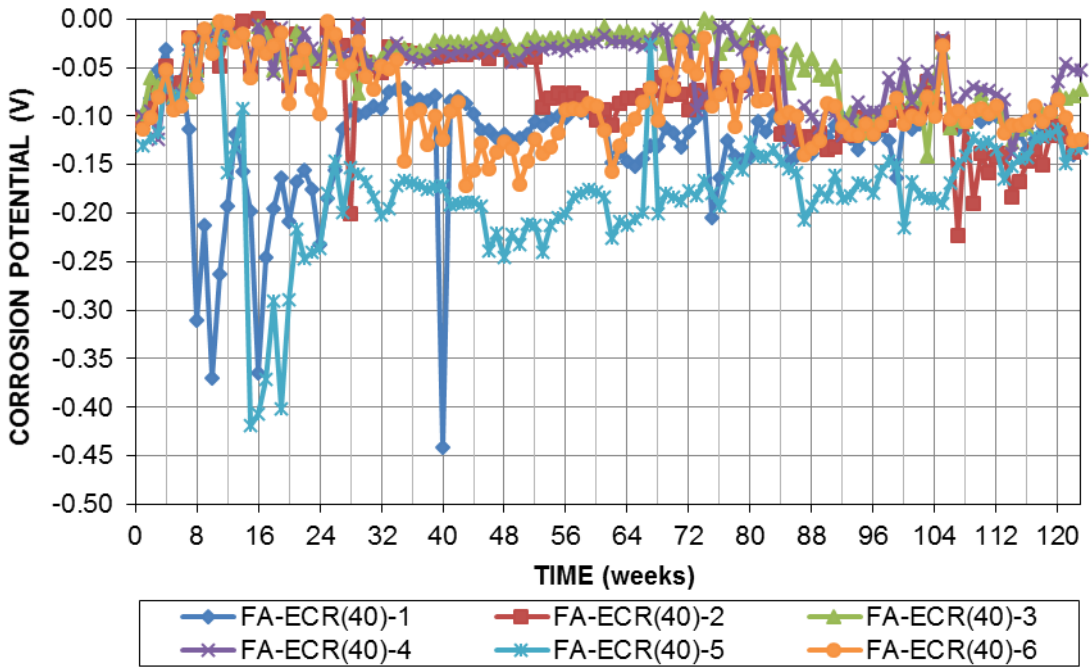

Figure J.9—Bottom mat (cathode) corrosion potential (SCE) versus time for beam specimens containing epoxy-coated reinforcement and 40% fly ash

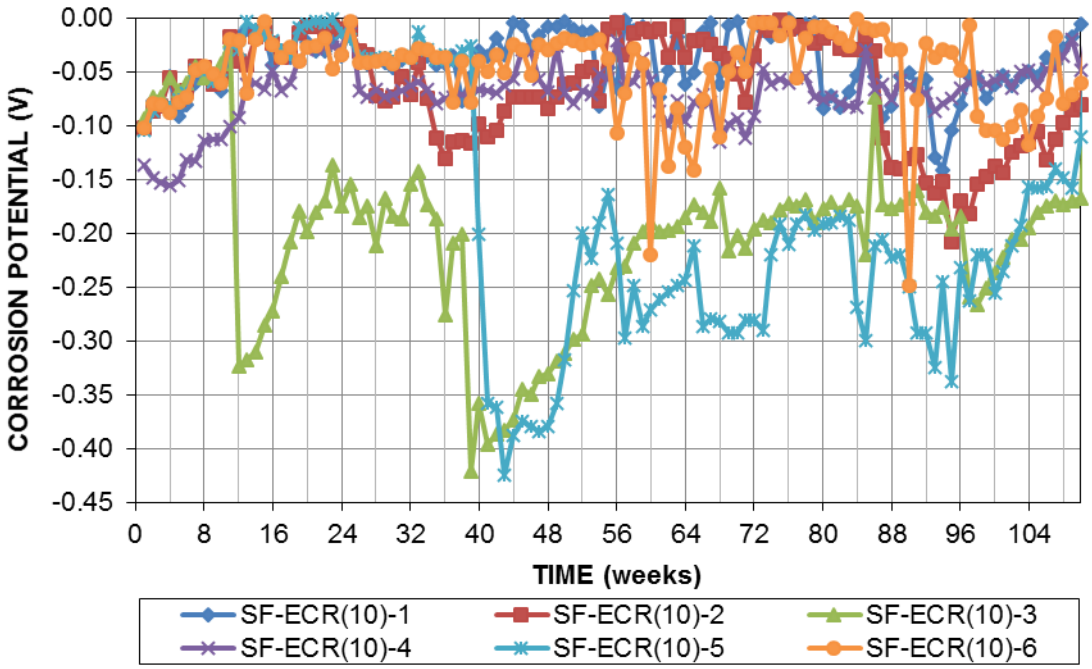

Figure J.10—Bottom mat (cathode) corrosion potential (SCE) versus time for beam specimens containing epoxy-coated reinforcement and 10% silica fume

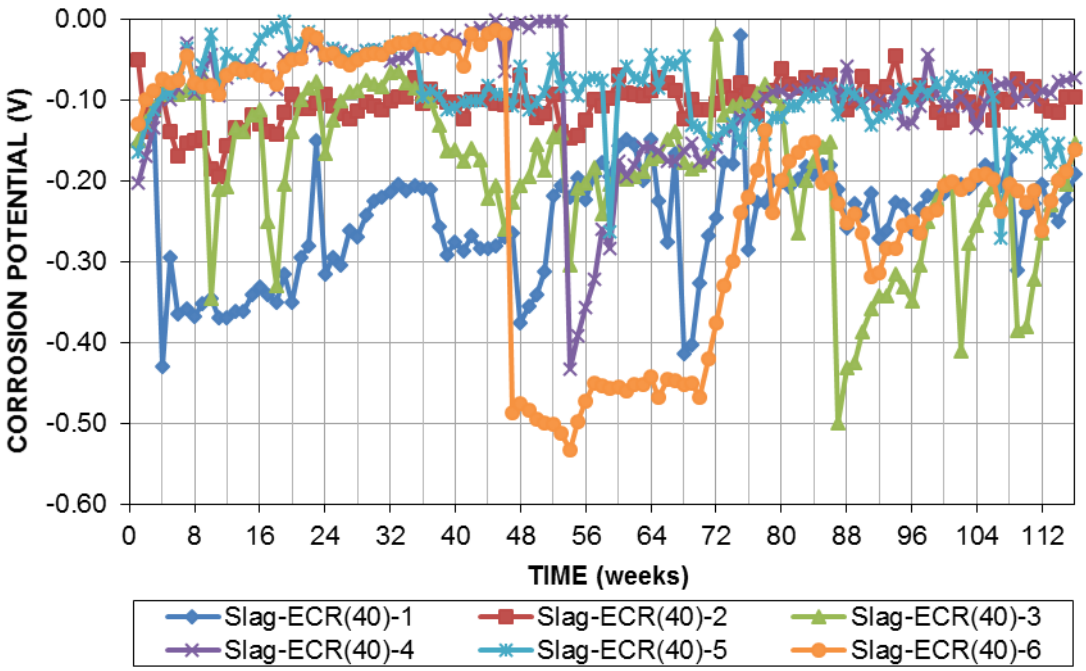

Figure J.11—Bottom mat (cathode) corrosion potential (SCE) versus time for beam specimens containing epoxy-coated reinforcement and 40% slag cement

APPENDIX K

CHLORIDE CONCENTRATION DATA OF SPECIMENS CONTAINING MMFX BARS

Table K.1: Critical chloride threshold for Southern Exposure specimens with MMFX uncoated bars containing 9% chromium

Specimen	Chloride Content (lb/yd^3)[a]						Avg.	Std. Dev.
	1	2	3	4	5	6		
MMFX(9%)-1	4.16	4.84	4.48	2.61	4.35	5.00	4.24	0.85
MMFX(9%)-2	5.74	6.18	5.22	6.04	6.08	4.28	5.59	0.73
MMFX(9%)-3	2.56	2.21	1.74	1.87	3.00	5.17	2.76	1.27
MMFX(9%)-4	6.67	4.50	2.99	3.50	4.04	3.01	4.12	1.38
MMFX(9%)-5	2.01	1.48	2.16	1.96	1.90	1.73	1.87	0.24
MMFX(9%)-6	1.45	1.57	1.57	1.56	1.50	1.90	1.59	0.16
MMFX(9%)-7	4.75	4.88	10.23	4.52	4.62	3.71	5.45	2.38
MMFX(9%)-8	5.74	7.82	8.55	16.5	8.78	16.8	10.7	4.73
							4.54	**1.47**

[a]1 (lb/yd^3) = 0.592 (kg/m^3)

Table K.2: Critical chloride threshold for Southern Exposure specimens with MMFX uncoated bars containing 4% chromium

Specimen	Chloride Content (lb/yd^3)[a]						Avg.	Std. Dev.
	1	2	3	4	5	6		
MMFX(4%)-1	1.75	3.45	2.73	3.28	4.71	2.38	3.05	1.02
MMFX(4%)-2	3.17	2.74	2.28	2.65	4.80	5.14	3.46	1.21
MMFX(4%)-3	0.44	2.65	3.97	11.92	8.83	5.24	5.51	4.21
MMFX(4%)-4	0.45	2.18	4.02	2.57	3.80	5.17	3.03	1.66
MMFX(4%)-5	5.77	5.03	3.94	2.14	2.66	3.11	3.78	1.41
MMFX(4%)-6	-	3.53	2.39	1.67	1.96	2.12	2.34	0.72
MMFX(4%)-7	7.55	5.66	5.03	4.43	5.63	3.79	5.35	1.30
MMFX(4%)-8	7.59	5.18	5.62	12.67	5.00	8.70	7.46	2.94
							4.25	**1.81**

[a]1 (lb/yd^3) = 0.592 (kg/m^3)

Table K.3: Critical chloride threshold for beam specimens with MMFX epoxy-coated bars containing 2% chromium

Specimen	Chloride Content (lb/yd^3)[a]								Avg.	Std. Dev.
	1	2	3	4	5	6	7	8		
MMFX-ECR(2%)-1	8.24	3.48	3.52	2.63	4.00	4.75	-	-	4.44	1.99
MMFX-ECR(2%)-2	2.72	2.18	5.72	8.09	9.96	5.37	3.83	-	5.41	2.83
MMFX-ECR(2%)-3	2.33	4.49	7.27	3.15	3.99	2.39	-	-	3.93	2.06
MMFX-ECR(2%)-4	2.43	4.01	2.68	4.31	4.83	4.04	7.41	4.34	4.26	1.52
MMFX-ECR(2%)-5	9.14	2.07	1.76	6.00	1.59	1.59	-	-	3.69	3.17
MMFX-ECR(2%)-6	2.57	2.94	1.69	6.33	1.04	3.20	-	-	2.96	1.84
									4.11	**1.94**

[a]1 (lb/yd^3) = 0.592 (kg/m^3)

Table K.4: Critical chloride threshold for beam specimens with MMFX epoxy-coated bars containing 4% chromium

Specimen	Chloride Content (lb/yd^3)[a]						Avg.	Std. Dev.
	1	2	3	4	5	6		
MMFX-ECR(4%)-1	5.33	5.12	9.05	5.23	3.18	2.76	5.11	2.23
MMFX-ECR(4%)-2	2.42	2.05	3.56	2.28	5.14	5.10	3.42	1.41
MMFX-ECR(4%)-3	8.92	5.65	5.30	7.00	7.79	5.34	6.67	1.49
MMFX-ECR(4%)-4	6.72	6.92	6.42	2.13	4.25	4.52	5.16	1.88
MMFX-ECR(4%)-5	6.42	3.69	4.54	2.77	3.12	4.37	4.15	1.31
MMFX-ECR(4%)-6	8.52	7.15	6.12	7.17	4.00	5.56	6.42	1.56
							5.16	**1.66**

[a]1 (lb/yd^3) = 0.592 (kg/m^3)